[redacted]

WADC TECHNICAL REPORT 55-305, PART II

(Title Unclassified)

STRUCTURAL DESIGN FOR AERODYNAMIC HEATING

PART II

ANALYTICAL STUDIES

W. H. Dukes and A. Schnitt

Bell Aircraft Corporation
Buffalo, New York

October 1955

Aircraft Laboratory
Contract No. AF33(616)-2581
Task No. 13719

Wright Air Development Center
Air Research and Development Command
United States Air Force
Wright-Patterson Air Force Base, Ohio

[redacted]

FOREWORD

On 23 August 1954, Bell Aircraft Corporation initiated a program for WADC in accordance with USAF Contract No. AF 33(616)-2581, Project No. 1368, "Construction Techniques and Application of New Materials," to study structural design for aerodynamic heating with range of investigation to extend to Mach 20. The contract was administered under the direction of the Structures Branch, Aircraft Laboratory, Directorate of Development, Wright Air Development Center, with Lt. Roger Brislawn acting as Technical Project Officer.

Messrs. W. H. Dukes and A. Schnitt were responsible for the study organization and for the technical direction of the work accomplished. The editing of the manuscript for this volume was performed by Mr. H. Stafford.

[redacted]

ABSTRACT

Problems confronting the structural designer of hypersonic aircraft are explained; a generalized study of many future vehicles has revealed the boundary values of these problems in terms such as temperatures and heating rates. A comprehensive survey of available structural materials has defined mechanical properties, physical characteristics, probable applications, and an introduction to the metallurgical aspects of high temperature. The fundamentals of insulation are explained, methods of analysis are given, and representative weights and thicknesses are shown for many applications. A survey of structural cooling systems and cooling materials has been made and, by rationalization and approximate design, the most suitable cooling systems have been selected. The temperature gradients and thermal stresses in airframes have been analyzed, and the results of computer calculations are presented graphically for design purposes. Methods are given for estimating the strength of various structural elements under a variety of temperature-loading conditions. Parameters have been developed for the comparison of various structural configurations on the basis of weight-strength. Using these parameters, optimum stresses are given for the structural configurations considering a variety of materials, temperatures, and times of loading, including the effect of insulation and cooling.

PUBLICATION REVIEW

This report has been reviewed and is approved.

FOR THE COMMANDER

Leigh W. Linnman

D. D. McKee
Colonel, USAF
Chief of Aircraft Laboratory
Directorate of Development

[redacted]

PREFACE

With the current development of turbojet engines with sufficient thrust to maintain flight in excess of Mach 3 and 100,000 feet altitude, ramjet engines with even greater capabilities, and rocket engines rated at more than 100,000 pounds thrust, aircraft could be designed to operate at a wide range of Mach numbers, flight times, and altitudes. In fact, the size and specific impulse of present-day rocket engines are such that launching a satellite of considerable weight is possible. These power plant developments lead to aircraft having many variations in size and shape, the structural designs of which are greatly complicated by the effects of aerodynamic heating. This one complication has so many ramifications, and so many projected and uncertain forms of solution, that it can be stated that structural design is the foremost problem of supersonic and hypersonic flight.

To resolve the problems introduced by flight at such speeds, the structures engineer must first acquire a sound knowledge of the ramifications of aerodynamic heating as it affects aircraft structure. The engineer must learn the properties and uses of new materials, especially those with properties heretofore considered undesirable for aircraft applications. He may find that the thermal properties of materials are more significant than the mechanical properties; however, the mechanical properties must be considered since the engineer must compare materials on a mechanical-thermal basis. Because aerodynamics and structures are now more closely interrelated, the structures engineer must possess some knowledge of the aerodynamics of aerodynamic heating. Also, cursory knowledge in certain branches of thermodynamics, metallurgy, physics, and chemistry is essential. Structural design at the higher Mach numbers requires invention, and it is not at all obvious as to when a particular type of structural arrangement is the most efficient.

Since the stress-strain relations of materials are time dependent, and stress and strain vary nonlinearly with time, the engineer is confronted with the "fourth dimension." Most theoretical work has either not been devised or not been checked experimentally. Because existing methods of analysis are generally quite complex, the structures engineer must acquire a knowledge for using them, and on occasion even devise his own methods. At the outset, he has no "feel" for the problems, no backlog of experience by which he can judge the severity of aerodynamic heating, few or no appropriate methods of analysis, and no means of determining the degree of accuracy of existing methods. An example is the problem of thermal stresses in airframe components, the magnitude of which can only be computed more accurately and expeditiously be automatic computing machines. Another example of a problem that the structures engineer has not been able to fully grasp is that of creep which is a function of the time-temperature-loading cycle to which the structure will be subjected, or how creep relieves internal stresses, or the permissible amount of creep for a given structural component. In fact, the creep criteria are only part of a new set of essential criteria that varies widely from aircraft to aircraft. In developing criteria, the structures engineer must resolve, for instance, differences in characteristics for a "one-shot" missile and a repeatedly used airplane. Since most high-speed aircraft contain large volumes of fuel, the engineer must learn to design and to apply a new type of structure – pressure vessels. He must consider, among the many problems associated with pressure vessels, the fatigue strength of the structure and the corrosive action of some propellants.

An avenue of solution to some of the problems is found in the use of insulation or cooling, or a combination of both. Although these systems have been in use for many years in other fields, the structures engineer does not know their applicability to modern aircraft. Nor does he know which of the myriad of arrangements and materials hold the greatest potential for a given set of aerodynamic heating conditions. Moreover, new methods of cooling specifically for aircraft use are being devised, such as transpiration and film cooling, and the structures to accommodate these systems are not at all obvious. The structures engineer may be called upon to establish and maintain an internal environment for propellants, crew, and equipment, in addition to the usual functions of providing a structure of a given shape which is capable of carrying specified aerodynamic and ground loads.

The necessity for knowing the sequence of time-temperature-loading combination to which the structure is subjected (a design problem analogous to but more complex than the derivation of the fatigue load-frequency spectrum) has resulted in carrying this problem to the laboratory to devise methods of reproducing these sequences. The testing of structural elements and components at elevated temperatures is far from a simple matter compared with room temperature testing, since new testing techniques must be developed and employed; moreover, there are more than a few methods of producing the correct environmental heating conditions, and each method has limitations regarding temperature, time at temperature, and heat flux. All this must be learned and checked experimentally. Since the cost of structural testing becomes prohibitive, the structures engineer must learn to tailor his testing program and the size of the test specimens. Accordingly, it is equally difficult and costly to perform design work by use of the "cut-and-try" testing approach.

The foregoing discussion explains in part the meaning of the "thermal problem" from the standpoint of the structures engineer; it also reveals the need for a systemized study of the solutions to many aerodynamic heating problems.

Generally, the objective of this study was to obtain and to gather preliminary structural design information applicable to all design phases of the thermal problem, so as to furnish the structures engineer with a sound base of systematic methods by which he may conduct his work. The objectives of the study were:

(1) To collect, analyze, and report data which provide solutions to thermal problems considered to be of most general interest.

(2) To perform original work in design and analysis wherever required.

(3) To prepare such data for ready understanding and use by the stress analyst and by those performing preliminary design and analysis.

(4) To show suggested and projected methods of supersonic and hypersonic aircraft construction and their attendant problems.

(5) To establish a framework of reports for future additions and revisions.

In satisfying the objectives of this study, the following approach was assumed. First, it was established, as well as possible, what information should be accumulated and, later, presented in the study. It is understandable that the subsequent literature survey, in a field of study as broad and as novel as this one, revealed that much data were missing and that some available information was preliminary, unverified, and complex. Nevertheless, in keeping with the purposes of the study, preliminary information was employed and only the simpler methods available were adopted, provided that they showed conservativeness and not an intolerable degree of error. An attempt was made to perform the analytical work required and heretofore nonexistent; furthermore, each problem was approached and presented from the viewpoint of the structures engineer, particularly those problems not directly associated with the field of structures.

This volume is Part II of a three-part final report which presents the results of a comprehensive study of the structural design of airframes subjected to aerodynamic heating as a result of flight up to Mach 20. Part II is considered the principal volume since it contains fundamental treatments of the subject matter. Essentially, the volumes are organized in the following manner:

[redacted]

PART I, DESIGN INFORMATION

This volume contains a compilation of data resulting from the study which would serve particularly as a ready reference to the stress analyst. The format, presentation, and contents of Part I are similar to the usual structures manual of airframe manufacturers. Data from the study are presented graphically and have been derived, in most cases, from the work presented in Part II. To facilitate the rapid analysis of structures subjected to aerodynamic heating, the graphical presentations are preceded by concise discussions of each subject and by practical examples of their use. Although Part I is not considered complete in terms of present-day manuals devoted to room-temperature structures, it does present data by which one can (1) readily estimate stagnation, transient, and equilibrium temperatures; (2) obtain pertinent information on the mechanical and physical properties of the more established structural, insulating, and cooling materials; (3) rapidly estimate thermal gradients and stresses in stiffened structures; (4) obtain critical stresses for columns and plates at uniform temperature and under short- and long-time loading, and for columns under linear temperature gradients; (5) estimate the weights and gages of pressure vessels for a variety of materials; (6) obtain buckling coefficients for unstiffened and ring-stiffened cylinders with and without internal pressure; and (7) readily determine structural temperatures or insulation requirements for the design of insulated structures. Since a portion of the material contained in Part I is of a classified nature, the entire volume is classified CONFIDENTIAL.

PART II, ANALYTICAL STUDIES

This volume presents the bulk of the analytical results of the study. It is designed for use by structures engineers engaged in preliminary analysis of aircraft, and by stress analysts who wish to consult theoretical derivations or learn methods of analysis. Part II, furthermore, presents data that are not amenable to graphical presentation suitable for Part I, or are considered limited in the number of times the data might be referred to in practice, or are considered somewhat approximate or preliminary. Part II contains a brief discussion of structural problems of high-speed aircraft and thereby forms the framework of the study. The practical limits of significant aerodynamic heating parameters are then determined for study of structures within this framework. To help deal with many of the problems that are defined quantitatively, systematic studies are presented of (1) suitable materials of construction, including insulating and cooling materials; (2) the analysis of many types and configurations of insulation and cooling systems; (3) the theoretical derivations and methods for computing temperature gradients, stresses, and deflections in stiffened structures; (4) the theory and methods of strength analysis; (5) the derivation of parameters by which materials, structural arrangements, and insulating and cooling materials can be compared on the basis of efficiency; and (6) the actual comparison of these efficiencies in terms of allowable stress level and weight for protected and unprotected structure. The contents of Part II is discussed more fully in the Introduction. Since most of the material contained in Part II is of a classified nature, the entire volume is classified CONFIDENTIAL.

PART III, STRUCTURAL DESIGN

This volume is concerned exclusively with the subject of structural design and, therefore, should be most useful to those engaged in preliminary design and analysis. Generally, the work is based upon the analytical studies reportedin Part II.Methods of construction are proposed that meet the maximum thermal environmental conditions derived for the future aircraft considered, one of which operates at Mach 20. Furthermore, methods of construction for intermediate thermal flight conditions proposed (and under development) by others and proposed herein are examined and discussed. Proposed constructional methods are presented for those portions of aircraft which experience relatively higher temperatures and heat inputs, such as leading edges; the re-entry missile is included in this category. The advantages, disadvantages, and developmental problems connected with each type of construction are included in the discussions. The security classification of Part III is SECRET.

[redacted]

TABLE OF CONTENTS

INTRODUCTION

Presented in this volume are the results of analytical investigations, newly derived methods of analysis, and compilations of data considered necessary for the study of the structural design of airframes subjected to aerodynamic heating as a result of flight up to Mach 20. The information herein not only serves in the preliminary and detail design of airframes proposed and discussed in Part III, but may possibly aid in the development of other structural configurations.

This volume is separated into nine sections. Because of the over-all size of the volume, each section is preceded by a table of contents and lists of illustrations and tables where applicable; references are found at the end of each section.

Section I presents a general discussion that defines the scope of the problem and delineates the subjects which should be investigated and considered in the design of high-speed aircraft.

In Section II, typical flight paths of various types of vehicles are studied to determine the most severe thermal conditions likely to be encountered with each aircraft. In particular, approximate analytical solutions are obtained for the boost, glide, cruise, and re-entry portions of typical flight paths by means of which the maximum thermal conditions are evaluated.

Section III presents an extensive survey of the structural materials that are available for high-temperature applications. The behavior of materials at elevated temperatures is treated briefly from both a metallurgical standpoint and on an individual material basis; a discussion of creep is included. The thermal properties of materials are also presented. The information gathered in this section, especially the short- and long-time stress-strain curves presented in Part I, Section 2.0, are used throughout Part II.

In Section IV, the principles of heat transfer through insulating materials are explained, and analytical solutions are developed for the design of various insulating arrangements. Results from studies of insulating materials are presented to select materials of highest efficiency, and curves are included to give insulation weights and thicknesses for many practical applications.

In Section V is a review of all known methods suitable for cooling airframes and, by rationalization and preliminary design to obtain system weights, the most promising systems are shown.

Section VI presents solutions for the transient temperature gradients, thermal stresses, and thermal deflections in typical aircraft structures. Analytical solutions are derived and followed by special formulation of the problem suitable for use with automatic computation devices.

Presented in Section VII are various methods for resolving the strength of structural elements in the presence of certain specific temperature effects. Topics included are buckling of columns with nonuniform material properties; determination of buckling and ultimate load of plates under variable edge loading; creep buckling; buckling of cylinders; and pressure vessel design.

In Section VIII, parameters are developed by which materials and structural configurations may be compared on the basis of minimum weight-strength. Methods of obtaining optimum stress curves for various configurations under steady-state or transient heating conditions are developed. Parameters for the comparison of unprotected and protected structures are included.

[redacted]

In Section IX, the methods of Section VIII are used to obtain curves of optimum compressive stress for wide columns, multiweb beams, and unstiffened cylinders, for a range of temperatures and materials. Both short-time and long-time loadings are considered. The use of this information is illustrated by means of typical examples. Calculations of structural weight are presented for various elements for unprotected structures, and for structures protected by insulation and cooling.

SECTION I

THE STRUCTURAL PROBLEMS OF HIGH-SPEED FLIGHT

By A. Schnitt

[redacted]

TABLE OF CONTENTS

SECTION I
THE STRUCTURAL PROBLEMS OF HIGH-SPEED FLIGHT

A. GENERAL

The purpose of this section is to explain the many problems influencing the structural design and analysis of high-speed aircraft. These problems are categorized under aerodynamic, materials, structural, aeroelastic, and propellant tanks. Some of the problems have already been experienced in flight, while others have been experienced only in the study stage of high-speed aircraft, or are pure conjecture. Not all the problems would be experienced with any one aircraft. After explaining the mechanisms and the structural implications, the degree of data available, exclusive of that in this study, is mentioned when considered to add depth to understanding the problem.

It should be recognized that the use of insulation on the outside of the structure, or the use of internal systems for cooling the surface of the aircraft, will alleviate many of the problems discussed; however, additional problems arise from the use of these systems.

The unconventional high-speed structures proposed in this study have problems of their own; these are discussed in detail in Part III of the report.

B. AERODYNAMIC

There are three groups of aerodynamic problems with which the structures engineer should be acquainted because they can directly influence design and analysis. These problems require compromise between aerodynamics and structures in order to obtain an optimized weapon system. Since the problems are actually more complex than stated, the discussion should in no way be interpreted as being complete; the problems may be altered by variables such as Mach number, Reynolds number, and altitude.

1. Accuracy of Aerodynamic Heating Information

Theoretical aerodynamic heating information such as heat transfer coefficients, recovery temperatures, and the type of boundary layer (i. e., laminar, mixed, or turbulent) have been checked experimentally in wind tunnels, free flight models, and missiles for a number of configurations up to approximately Mach 10; however, experimental verification up to this Mach number is not yet complete. Exceeding this velocity and at very high altitudes, as in the slip-flow region, theory is considered less accurate. Moreover, the accuracy of aerodynamic heating information decreases at the leading edges and the nose of the bodies; little or no information is available on heat transfer to control surfaces, at the junction of wings and fuselage, and at other areas of disturbances caused by shock waves, noise, and wakes.

2. Skin Roughness

It may not be possible with high-speed aircraft to maintain a skin surface as smooth as that achieved with transonic aircraft; for this reason, some effects of skin roughness are given.

One effect of surface roughness is the reduction in the transition Reynolds number; the height of the roughness to cause this transition is related to the boundary layer thickness. Therefore, for an increased surface roughness, transition from laminar to turbulent flow occurs farther upstream. Since the frictional coefficients are substantially greater in turbulent flow than in laminar flow, the aircraft performance is adversely affected. Heat transfer coefficients, furthermore, are increased in nearly the same proportion as the friction drag coefficients.

Skin roughness increases skin friction drag in both the laminar and turbulent flow; however, in turbulent flow there is a permissible height of skin roughness for which no drag increase would result. This permissible height is a function of Reynolds number per foot, and the allowable roughness, therefore, decreases with increasing velocity and increases with increasing altitude.

[redacted]

3. Means of Reducing Heat Transfer Rate

Various means have been suggested for reducing the over-all heat transfer rate. These deal with methods of stabilizing the laminar boundary layer. The first method, described previously, deals with minimizing skin roughness. Another method is to have a favorable external shape for which the surface pressure gradients decrease with distance aft of the vehicle nose. Tests at Mach 1.61 show the effect of shape on the length of the laminar flow region: a parabolic body experiences laminar flow for the first half of its length, the ogive-cylinder for one-quarter of its length, and the cone-cylinder for one-eighth of its length. A third method is to cool the surface of the vehicle below the recovery temperature; tests on a parabolic body at Mach 1.61 show a doubling of the laminar length for a 10% decrease in the surface temperature.

The design of leading edges are most difficult because of the much higher heat transfer rate in this area. These rates, however, can be reduced by increasing the leading edge radius; the heat transfer coefficients vary INVERSELY as the square root of the radius. The pressure drag incurred by blunting the leading edge can be reduced by sweepback.

A promising approach to lessen the heat transfer rate is with the use of transpiration or porous wall cooling. Here, a liquid or gas if forced through pores in the surface of the aircraft. If a fluid is used, it will vaporize near or at the surface of the skin. Theoretical calculations borne out by a number of experiments show that not only does the heat capacity of the coolant reduce the temperature of the skin, but the expelled gas appreciably reduces the heat transfer rate by keeping the boundary layer away from the skin.

C. MATERIALS

The behavior of materials at elevated temperatures is the cause of the major structural problems of high-speed flight. Significant generalizations are made regarding mechanical and thermal properties, the action of creep, material oxidation, erosion and ablation, and the failure of materials under thermal shock and fatigue.

1. Mechanical Properties

Metallic materials that are heat-treated or work-hardened gradually lose their strength as the annealing temperature is reached. Annealed materials lose their strength as the melting temperatures are approached. The same deterioration of mechanical properties is true for ceramic materials (such as oxides and carbides) and for cermets (combined ceramics and metals). Moduli of elasticity do not fall off as rapidly as the strengths until melting temperatures are approached. Strengths, moreover, decrease with exposure time to elevated temperatures. All materials are affected by rates of loading in both the elastic and plastic regimes; the slower the rate of loading, the lower the yield and ultimate strengths and the greater the elongation at failure. This phenomenon implies the existence of creep, and this is further described in the following.

In addition, the room-temperature properties are adversely affected after materials have been exposed to elevated temperatures and the effect increases with time of exposure. Since high-speed aircraft may be required to sustain higher loads at lower or subsonic speeds, this behavior becomes significant.

From the afore-mentioned, it becomes apparent that the properties of the material at a given instant are influenced by its prior history of loading, temperature, and time at temperature. This fact becomes most significant when attempting the stress analysis of an aircraft which experiences significant aerodynamic heating; this is discussed further in the following.

2. Thermal Properties

The thermal properties of structural materials may contribute more to producing (thermal) stress than externally applied loads. The properties of concern are (a) coefficient of thermal expansion, (b) coefficient of conductivity, (c) heat capacity, (d) emissivity, and (e) absorptivity. Chiefly, properties a, b, and c affect the magnitude of thermal stresses and distortions, while c, d, and e determine temperature rise. Emissivity becomes important when the surface temperature approaches approximately 800°F and appreciable heat is radiated by the skin; absorptivity becomes important when solar radiation is considered at very high altitudes (50 miles or higher).

While properties b and c are required in the study of insulating materials, the study of coolants must include pressure-volume and temperature-entropy diagrams, and heat transfer characteristics in the liquid and vapor states.

Much of the required data are already available; however, an appreciation of the amount missing and the bibliographic scatter of data is first realized when attempting design and analysis. Generally, it is not simple to determine many of the physical properties. Moreover, some properties have a wide scatter of values like the coefficients of thermal expansion which, for some materials, are greatly affected by small variations in heat treatment. Little thermodynamic data exist for promising metal coolant materials in the vaporized condition.

3. Creep

The creep of some of the common structural materials in the plastic range (static fatigue) has been observed as a slight reduction in ultimate strength proportional to the time during which load is applied, and as an increase in elongation at failure. At elevated temperatures, this phenomenon is exaggerated and creep occurs in the upper portion of the elastic range as well.

Creep data for materials are usually obtained by heating a specimen to a given temperature and then loading it at a constant nominal stress until failure. The strain is plotted vs. time and a characteristic curve is obtained. The initial portion of the curve shows a parabolic increase in strain rate (primary phase), then a linearly increasing strain rate (secondary phase), and finally, an ever-increasing strain rate (tertiary phase) ending in failure (stress rupture). The creep rates vary nonlinearly with stress level and temperature. Recently, means of creep testing in compression have been developed and, for some wrought materials, the creep rate at a given stress proved to be about twice that in tension.

Since high-speed aircraft fly at various Mach numbers and altitudes for various lengths of time, and experience maneuvers and gust loadings of various magnitudes, an infinite amount of creep data are apparently required. In appreciation of this problem, creep tests have been conducted for the more simplified conditions of constant temperature-alternating stress, constant temperature-cyclic stress, and cyclic temperature and stress; attempts at correlating these test results to predict creep action under arbitrary time-temperature-loading sequences require further study and further experimental verification. Good correlation of creep data under constant temperature-load conditions has been made and this contribution has proved to be valuable.

4. Erosion

Materials, including the aluminum alloys and carbon steels, are damaged by rain erosion at subsonic speeds, and it is probable that the rate of erosion increases at supersonic speeds. A simplified explanation of this phenomenon is that part of the energy of the water droplet is imparted to the material and the cohesive strength of the material is exceeded locally causing it to chip. At HYPERSONIC SPEEDS AND LOW DENSITIES air molecules may have sufficient energy to cause significant erosion, especially at leading edges and noses of bodies; so far, there is no known test information to verify this.

5. Oxidation

Metals exposed to air at elevated temperatures oxidize more rapidly. The oxides of some metals are tenacious and further rapid oxidation is prevented; the oxides of others are flaky or easily abraded. While an aircraft is airborne, there should be sufficient amounts of air for oxidation (at least at the leading edge and on the underside of the vehicle), and the erosive action of the air may cause the rapid oxidation and reduction of surface material thickness for some materials; this action has not been explored experimentally. There is sufficient concern for the oxidation of metals to make the development of protective ceramic coatings a rapidly increasing field.

6. Ablation

Ablation is the removal of material by melting. This occurs when the aerodynamic heat transfer rates are greater than the capacity of the material to absorb and transfer heat through the surface thickness of the metal. Such heating rates can be experienced by a re-entry missile. Since heat is absorbed in melting, ablation can be thought of as a cooling mechanism. Tests have been performed in a wind tunnel to observe this phenomenon.

[redacted]

7. Thermal Shock

When suddenly exposed to high temperatures, materials having little or no ductility experience thermal stresses greater than their strength, and fracture occurs. Although materials such as ceramics have higher strengths at extremely high temperatures, they have no ductility and generally low coefficients of thermal conductivity, and are prone to thermal shock. Recently, extensive work has been performed in this field and it is possible to predict the thermal shock resistance of materials from a given set of test conditions.

8. Thermal Fatigue

Some materials may not fail upon the first exposure to heat, but may fail upon cyclic heating and cooling. Fracture may occur in only a few cycles, or after many thousands of cycles; creep and the reversal of stress upon cooling may be part of the mechanism involved. Tests to determine the thermal fatigue characteristics of a material should reproduce, as closely as possible, the particular time-temperature cycle under consideration.

D. STRUCTURAL

In the analysis of room-temperature structures, the material stress-strain curve fundamentally furnishes all the material property information required, and methods based upon the theories of elasticity and plasticity are adequate. For structures subjected to aerodynamic heating, two effects complicate design and analysis: the existence of thermal gradients and stresses, and the time-dependent stress-strain relation of materials. To date, only a description of the mechanisms involved in the more complex cases have been explained; however, some work has been performed in devising methods of analysis for simple structural elements under simplified heating conditions.

A review of the structural problems and methods of analysis are discussed further in this section. Consideration is given to reduction in strength, thermal gradients and stresses, analysis in the presence of thermal stresses and creep, and thermal distortions. Since some of the structural problems can be minimized by the use of insulation and cooling, the problems associated with the use of these systems are also reviewed briefly.

1. Reduction in Strength

The obvious effect of a reduction in mechanical properties is an increase in structural weight. If the structure is designed on a stiffness basis, and this may occur more often in supersonic than in subsonic aircraft, an increase in weight may also be expected.

For the simple condition of constant and uniform temperature and under short-time loading, the critical, yield, and ultimate stresses of structural elements can be computed using the material stress-strain curve obtained at the given temperature and methods of analysis based upon the theories of elasticity and plasticity. The use of such methods has been checked by tests on columns, plates, and multiweb beams, and it seems reasonable to assume that all structure can be analyzed in this fashion. Nevertheless, in the design of structure at uniform temperature and short-time loading, there are no comprehensive methods by which to select the optimum material, structural arrangement, and attainable stress for a particular loading condition.

It is equally obvious that a further increase in weight results when the loading is applied for a long time and creep takes place. The stability of elements under creep has received wide experimental and theoretical investigation, particularly for columns. Also, tests have been conducted to determine the stability of plates and shells. An accurate method of analysis for columns has been developed, but it is quite complex and time-consuming. Since it would be expeditious if short-time methods of analysis could be applied to structure in the presence of creep, a synthetic "isochronous" stress-strain curve derived from creep data has been proposed for the stability analysis of columns; this method of analysis has been shown to be fairly accurate and always conservative, and it may prove to be sufficiently accurate for the prediction of the critical and ultimate strengths of plates, shells, and stiffened structure. Here again, in the design it is equally important to be able to select the optimum material, structural arrangement, and attainable stress for a given loading condition, and such methods have not yet been devised.

2. Thermal Gradients and Stresses

There are two distinct types of thermal gradients to which high-speed aircraft are subjected. The first type exists in long-time stabilized flight; the second type is produced under conditions of acceleration or deceleration, and by maneuver or gust or change in altitude.

Thermal gradients arise in long-time stabilized flight because of the differences in heat transfer coefficients which vary from point to point on the surface of an aircraft. These differences are a result of (1) transition from laminar to turbulent flow at some point aft of the leading edge of wings or the nose of bodies, (2) increasing Reynolds number which decreases heat transfer coefficients, (3) decreasing local angles of incidence which decrease heat transfer coefficients, and (4) disturbances which locally increase heat transfer coefficients. Thus, an airplane of conventional structure in long, steady flight will have its aerodynamic surfaces deflected upward and swept either forward or aft depending upon the existence and length of a laminar flow region. Similarly, the fuselage will become concave upward. Since these gradients will be nonlinear, stabilized flight conditions will result in thermal stresses.

The second type of thermal gradients, produced by accelerated or nonsteady flight, are obliterated after a sufficiently long time at stabilized flight; nevertheless, it is this type which is more difficult to handle analytically or to minimize from a design standpoint. These thermal gradients occur wherever there is a local thickening of the surface skin as at stiffeners, ribs, beams, or doublers, or wherever there is a change in skin thickness. During acceleration, skin temperatures are maximum at the center of supporting structure and gradually decrease toward a stiffening element. Again, the temperature continues to drop through the stiffening element and into the interior; the skin will be in compression, usually biaxially, and the cooler portions of the structure will be in tension. Upon decelerating, the skin cools faster than the interior structure and the stress conditions become reversed.

There are numerical and analytical procedures for computing thermal gradients, but these methods, naturally, are tedious. They become more tedious at higher temperatures when, in a wing for example, consideration should be given both to convection within the wing and to radiation from the lower surface to the beam webs and upper surface. The need exists, however, for the general solution of a skin-stiffener element by which a structures engineer can rapidly determine temperature gradients and stresses as a function of material and geometry.

A further complication arises when the stiffening element is not an integral part of the skin, but is attached mechanically. The thermal conductance of riveted joints is receiving attention; test results show that the conductance has a wide range of values and many parameters, among which is the number of times the joint has been heated.

3. Analysis in the Presence of Thermal Stress

The inclusion of thermal stresses in stress analysis is quite complex since thermal gradients produce stress without strain, and strain without stress. The predominant effect of thermal stresses is that they can produce buckling. A stiffened panel will buckle when the thermal stresses exceed the critical stress of the panel at the given temperature. The temperature or stress distribution across a panel is rarely uniform, and it has been suggested that the average stress be used in predicting the critical stress; however, a more precise approach appears desirable. Since thermal stresses are transient, it is unlikely that a material would be used that has such poor heat resistant qualities that creep buckling would occur.

Thermal stresses are directly additive to applied stresses in determining the plate buckling characteristics of a structure under load. When thermal buckling occurs, and application of the external load is continued, thermal stresses gradually reduced by the deformation and the post-buckling strength of the stiffened structure is not materially lowered. Tests on multiweb beams with thermal stresses show no appreciable reduction in ultimate strength, although the load at which skin buckling occurs is reduced proportionately by the thermal stresses. Further analytical and experimental work is required in predicting stress redistribution after buckling and the ultimate stress of stiffened structures in the presence of thermal stresses.

Thermal stresses complicate the attachment requirements of supported skin because the thermal loads are concentrated at the ends of panels. Although not verified experimentally, it is

reasonable to predict that thermal buckling of skin panels will produce added "roughness" which may increase drag and heat transfer coefficients and, in turn, further increase buckling. Design means have been proposed for reducing thermal stresses, such as the use of corrugated or trussed webs. These devices cannot be applied throughout an aircraft structure and do not remove all the important thermal stresses.

4. Analysis in the Presence of Creep

The stress analysis of aircraft structures subject to creep and having a time-temperature-loading spectrum has not received much study; this is perhaps due to its complexity. Some of the factors that add to the complexity are (1) the lack of methods to predict the action of materials under arbitrary time-temperature-loading history, (2) the presence of residual stresses upon removal of load, resulting in repeated changes in stress distribution, (3) the reduction in shear lag due to creep, (4) the fact that creep takes place in local areas of high stress levels, and (5) the lack of knowledge relative to the creep of joints and attachments.

5. Thermal Distortions

Many causes of thermal distortion have already been described. These distortions may become permanent if creep occurs; for example, a buckled panel may experience local stresses in the troughs and crests of buckles great enough to permit creep in these areas, and this may result in the buckles becoming permanent. Over-all distortions of wings, which may increase with time if creep exists, change the loading and heat transfer distributions; pressure distributions on warped and twisted wings may best be determined in a wind tunnel.

The heating of structure results in considerable geometric growth which may cause, among other things, control surface jamming and may necessitate remote actuation of aerodynamic controls.

6. Insulation and Cooling

It has been shown that a small thickness of insulation over the surface of an aircraft can materially reduce thermal stresses, although not the maximum temperatures unless the flight time is significantly short. The special requirements for this insulating material, such as low conductivity, low density, high elasticity, adhesion, and ability to resist erosion, do not make for imminent development. A thicker layer of insulation would also reduce maximum temperatures, and would probably save weight for many aircraft having short flight times; however, the requirements for the development of this material are obviously more stringent. Other means of insulating aircraft using existing materials are being studied.

Internal cooling systems for directly cooling the surface skin can only be used for short times of flight, otherwise the coolant weight becomes excessive. Cooling systems, the skin design to accommodate cooling systems, and the selection of the optimum coolant are also being studied.

The use of propellants as a coolant has been suggested and studied, but the stringent limitations on temperature rise permitted for each propellant makes this solution problematical.

E. AEROELASTIC

Aerodynamic heating may produce serious aeroelastic problems. The flutter and aileron reversal speeds may be appreciably reduced and the flutter of skin panels may be precipitated by the reduction of panel stiffness, thermal stresses, and buckling.

1. Reduced Bending and Torsional Stiffness

It has been noted previously that both bending and torsional stiffnesses of wings will be reduced by the lowering of elastic modulus and by the contribution of thermal stresses in producing panel buckling. However, there is an additional reduction in torsional stiffness resulting from the over-all thermal stresses sustained by a wing; that is, those stresses due to the nonuniform temperature distribution along the chord which produce compression in the leading and trailing edges.

The reduction in torsional stiffness is an apparent one. When the wing is twisted, the vertical components of the compressive loads in the leading and trailing edges act in the same direction as the twisting moment and, in effect, reduce torsional stiffness. The seriousness of this situation is apparent considering that supersonic wings may likely be of thin design to optimize aircraft performance.

2. Panel Flutter

It has been shown theoretically that supersonic flow can incite vertical oscillations of a panel without the presence of aerodynamic heating. Aerodynamic heating reduces the stiffness of a panel progressively by the reduction in modulus of elasticity, by the presence of thermal stresses, and by buckling. Failure occurs as a result of fatigue. A slight pressure differential on the panel may prevent flutter.

F. PROPELLANT TANKS

An inherent characteristic of high-speed aircraft is the large volumes of propellants. Since it is often more efficient to design propellant tanks as integral parts of the airframe (basic load-carrying parts of the structure), the cylindrical portions of the tanks are exposed to the airstream, and the tanks and their contents are subjected to aerodynamic heating. The resulting problems are different from those previously described.

1. Thermal Stresses

With the cylindrical portion of propellant tanks exposed to aerodynamic heating, the temperature of the fuel will increase exponentially as the tanks are emptied in flight. That portion of the tank wall not in contact with the fuel will more quickly approach the equilibrium temperature. Consequently, sizable thermal stresses can result; furthermore, any stiffening of the tank wall, which is usually required, would also produce thermal stresses. Localized and transient thermal stresses can be caused by a splash of fuel against the heated portions of the tank walls, and rapid boil-off of fuel might result causing a momentary increase in the working pressure.

2. Working Pressures

Heated fuels require increased tank working pressures to lessen fuel boil-off losses. Higher working pressures are required for propellants such as liquid oxygen to ensure that the propellant pumps do not cavitate. For these propellants, the working pressure must be held to some incremental pressure above the boiling point of the propellant; this is commonly referred to as the "hot lox" problem in the case of liquid oxygen.

3. Creep

Propellant tanks operate at fairly high stress levels. If a small evidence of creep exists, the tank radius and, hence, the stress level will increase. Since the creep rate increases exponentially with stress, instability will occur in time. A theoretical or experimental treatment of this problem apparently has not yet been conducted.

4. Explosion Hazard

Aerodynamic heating may greatly increase the explosion hazard. Small amounts of fuel leakage into a compartment, which may for some reason be filled with ram air, may form a fuel-air mixture sufficient to support combustion. If the stagnation temperature of the air is at or above the ignition temperature of the mixture, an explosion will occur. It seems necessary, therefore, to ensure propellant tanks against minute leakages, especially for high Mach number flight, and to seal effectively all compartments against ram-air leakage.

Most of the previous discussion is based upon information that can be found in the extensive literature already published on the subject of aerodynamic heating, particularly the numerous NACA publications on experimental and theoretical developments. Out of this extensive literature, those publications to which specific reference has been made in the course of the work presented in this report are listed in the bibliographies appended to Sections II through IX.

[redacted]

SECTION II

PROBLEM BOUNDARIES

By W. H. Dukes, C. M. Schmidt,
A. Hanawalt, and R. Postle

[redacted]

[redacted]

TABLE OF CONTENTS

LIST OF ILLUSTRATIONS

LIST OF TABLES

[redacted]

NOMENCLATURE

A = frontal area of re-entry missile (ft^2)

C_D = drag coefficient (dimensionless)

C_L = lift coefficient (dimensionless)

h = altitude (ft)

h_c = heat transfer coefficient (BTU/ft^2hr)

h_f = re-entry altitude (ft)

I = specific impulse of propellant

L/D = lift to drag ratio (dimensionless)

M = Mach number

P/P_o = ratio of atmospheric pressure at altitude to the value at sea level (dimensionless)

R = range of vehicle (mi.)

R_f = ratio of propellant weight to total weight at beginning of stage being considered $= W_f / W_o$

R_T = ratio of thrust to total weight at beginning of stage being considered $= T/W_o$

r = base radius of cone (ft)

r_o = radius of the earth (mi.)

T = thrust (lb)

T_a = ambient temperature (°R)

T_r = recovery temperature (°R)

T_w = structural wall temperature (°R)

V = velocity (ft/sec)

V_f = velocity at beginning of unpowered flight, also re-entry velocity (ft/sec)

V_o = initial velocity at beginning of stage (ft/sec)

V_s = satellite velocity at sea level (ft/sec)

NOMENCLATURE (cont)

$\overline{V}$ = velocity of glide vehicle, expressed in terms of sea level satellite velocity (dimensionless)

$\overline{V}_f$ = velocity at beginning of impowered flight, expressed in terms of sea level, satellite velocity (dimensionless)

W = instantaneous weight of vehicle (lb)

W_f = total weight of fuel carried in the stage being considered (lb)

W_o = total vehicle weight at beginning of stage under consideration (lb)

$\frac{W}{S}$ = wing loading (lb/ft^2)

x = distance behind vehicle nose (ft)

α = a constant defining the density variation with altitude (1/ft)

β = semivertex angle of cone (degrees)

γ = angle of inclination of climb during boost (degrees)

θ = time (sec)

θ_1 = dimensionless time $R_T\theta/I$

ρ_{SL} = air density at sea level ($slugs/ft^3$)

σ = ratio of density at altitude to density at sea level (dimensionless)

Φ = total range of vehicle, expressed in terms of the earth's radius = R/r_o (dimensionless)

ζ = distance from beginning of flight, expressed in terms of the earth's radius (dimensionless)

ψ = distance from the end of glide flight, expressed in terms of the earth's radius (dimensionless)

[redacted]

SECTION II

PROBLEM BOUNDARIES

A. GENERAL

During the design of an airframe for subsonic or low supersonic speeds, the structure can be studied on the basis of local loading and section shape; other parameters generally have a secondary effect. Since the number of section shapes is quite limited, being usually flat or near flat panels, cylinders, or combinations of both, a general structural study can be made in simple terms.

When speeds are sufficient to cause aerodynamic heating, however, many new parameters are introduced, since the heating is a function of the complete flight history, the body shape, and the nature of the structure itself. The problem is broadened further because the presence of heating increases the number of possible types of structure, and the variety of structural materials, that must be considered.

If a comprehensive study of supersonic and hypersonic structure is to be made, with consideration of the many variables involved and the possible aircraft types and flight plans, structural arrangements and associated thermal parameters must be examined in a systematic manner. It is the purpose of this section of the report to make such an examination. In this way, only the practical range of thermal parameter values will be included in the structural study to follow and, conversely, the results of the study can be related to specific aircraft types.

By following this procedure, if it is possible to indicate the most suitable type of construction, the structural materials, the type of heat protection, and the unit structural weights for various types of future aircraft, the information will be of considerable assistance in preliminary structural design, and will also give direction to future research. In particular, it may avoid wasteful research directed at the attainment of impractical combinations of thermal parameter values.

This section begins with a discussion of probable future types of supersonic aircraft and the type of flight path each may use. The limitation of air-breathing engines and the efficient use of rocket power plants are discussed, since these form important practical limitations to the range of variables that must be considered. It is shown that each flight path may be divided generally into phases such as boost, glide, and cruise, and that considerations given to each phase are reasonably independent of the remainder of the flight. The factors controlling and limiting each phase of flight, such as required range, minimum energy expenditure during climb, and boost accelerations as limited by the crew, are proposed as the basis for computation of flight path relationships. The significant thermal parameters required for structural design at elevated temperatures are then given for each type of flight path and structural arrangement.

Theoretical methods of obtaining numerical values for the relationships between speed, altitude, time, and range for each flight path phase are developed on the basis of a number of simplifying assumptions. Such assumptions are necessary because the number of possible variables is large. To include all effects is unnecessary for the purposes of this study, since they would only serve to obscure the important factors. Graphical results of the various flight path relationships are presented, based upon the theoretical considerations, and, from these, additional curves are produced to give values of the thermal parameters.

Because of the necessary simplifying assumptions made in the theoretical work discussed previously, additional support has been given to the calculated boundary values of the aerodynamic heating problem by the collection of statistical data from progress reports and final reports on existing and projected aircraft. Because much of this statistical information has a SECRET security classification, it is not included in this part of the report, but instead the comparisons with theory are made in the summary of problem boundaries in Section I of Part III.

B. FUTURE VEHICLE TYPES

Table II-1 summarizes those vehicles in the supersonic and hypersonic speed range to which it is expected that most attention will be directed in the next phase of airframe development. The table has been subdivided on the basis of the vehicle characteristics which are most significant in their effect on the vehicle design. These characteristics are the presence or absence of a crew, the type of power plant, and the particular flight path to be flown.

In selecting these vehicles it was presumed that for a considerable future time, the cost and complexity of high-speed flight could only be justified for the delivery of costly high-energy warheads. Such warheads would be used against large, important ground targets so that the primary vehicle for hypersonic flight is the medium or long-range bomber. Prestrike and poststrike reconnaissance is a necessary part of such a mission, and it is assumed that hypersonic reconnaissance vehicles will also be built. Finally, the use of such bombardment vehicles leads directly to interceptors of similar speed capabilities, as a countermeasure.

The presence of a crew within a vehicle generally requires that the vehicle be nonexpendable and that it be designed for repeated flights. The feature of recoverability usually requires low-speed flight characteristics and sufficient wing area to support the aircraft during landing. A crew limits accelerations, particularly longitudinal, and may also necessitate larger safety factors for structural design.

The effects of power plant and flight path on the elevated temperature aspects of structural design are closely related, since the power plant is probably the most significant factor to be considered in establishing the flight path. Power plants considered in this study are the turbojet, the ramjet, and both liquid- and solid-propellant rockets. Each of these engines has its own characteristics and is best suited for a particular flight path.

Present-day turbojet engines are relatively limited in thrust, so that only moderate longitudinal accelerations are achieved. The use of solid-propellant rocket boosters does not materially change this situation, since their thrust duration is usually short. Optimistic extensions of present turbojet developments suggest that considerations should be limited to encompass velocities up to approximately Mach 3.0, and, since air-breathing engines are limited by air density and the requirement of flame propagation, maximum altitudes of approximately 65,000 feet. Hydrogen has the ability to sustain a flame under conditions of very low pressure, and its use as a fuel promises to raise altitude limitations of turbojet engines. For the present, 100,000 feet will be considered a maximum. These characteristics, together with its relatively high efficiency, make the turbojet engine most suitable for cruising-type paths at speeds less than Mach 3.0.

Since the ramjet has no rotating machinery, the speed limitation is raised arbitrarily to approximately Mach 5.0. At this speed, the ram air entering the engine would be at approximately 2000 °F before the addition of combustion heat. Therefore, to achieve this speed, extensive development of existing materials or the addition of a complex cooling system to the engine would be necessary. Such a cooling system would require an expendable cooling material since ram-air cooling is, evidently, ineffective because of the air temperature. Because of the speed limitation, the ramjet requires a cruise-type flight path to achieve range, but rocket boost is also necessary to achieve the speed (approximately Mach 1.0 to 2.0) at which ram compression is sufficient to operate the engine; hence, the boost-cruise flight.

Present rocket engine designs are such that large thrusts are obtainable with a small engine weight, so that large longitudinal accelerations of the rocket propelled vehicle are possible. Since this is not an air-breathing engine, it is unlimited in altitude and speed, but this characteristic is also its most serious restriction. The rocket-propelled vehicle must carry its own supply of oxidizer, of generally three times the weight of fuel. When this fact is combined with the low efficiency of the rocket, it is evident that such vehicles will carry large quantities of propellants. In a Mach 20 vehicle, for instance, 80% of the take-off weight may be propellants, while the corresponding value for a conventional subsonic fighter is approximately 20%.

[redacted]

For large rocket-propelled vehicles, therefore, it becomes important, in the achievement of minimum take-off weight, to minimize the energy used in accelerating propellant to the maximum speed. Evidently, all propellants should be exhausted at the instant that maximum speed is achieved, so that the propulsive effort should be used entirely in accelerating. The necessary range is then attained either by gliding or by following a ballistic trajectory in which aerodynamic forces are essentially absent. A "skip" path is also possible, in which the vehicle descends quite rapidly into the atmosphere and then climbs above the atmosphere again by exchanging some kinetic energy for altitude. This process is repeated several times with a net loss of velocity at each "skip." The energy loss appears as aerodynamic heating, but the airframe has an opportunity to dissipate this heat by radiation while the vehicle is in the ballistic part of the projection outside the atmosphere. This flight path is complex for a generalized analysis, and is neglected in the present work since it has already been shown (Reference 1) to give more severe aerodynamic heating problems than the glide path.

For reasons discussed previously, cruising flight at constant speed and altitude is usually inefficient with rocket propulsion, unless the range is less than approximately 100 nautical miles.

The following is a more detailed description of the vehicles summarized in Table II-1.

1. Ballistic Missile

Since this vehicle follows a ballistic trajectory, it does not depend upon aerodynamic forces for lift. Some aerodynamic control may be provided during the initial stages of launch but, for most operations, the range will require a maximum altitude well beyond the earth's atmosphere where the only control is from rocket engines mounted on gimbals, auxiliary rockets, or vanes in the engine exhaust. Since only auxiliary rockets could be used after the boost phase, all guidance functions would generally be performed during boost.

Because this vehicle has no wings, it is not recoverable and, of course, is unmanned. The speeds and altitudes required to achieve range are generally such that only the rocket-type power plant is suitable. The principle of expending propellants as rapidly as possible is invariably followed in the design of these vehicles, with the rate of expulsion being a compromise between propulsion efficiency, power plant size and weight, and acceleration forces on the structure and equipment.

To minimize further the energy used in accelerating, these vehicles are usually constructed in stages; a small vehicle contains the payload, to which is attached one or more boosters. As propellant tanks are emptied, they can then be jettisoned, together with some of the engines, so that propellant is not used unnecessarily to accelerate structural weight.

Maximum velocities are generally achieved after the vehicle has left the atmosphere; at this point, aerodynamic heating does not exist. The booster stages are then subjected only to moderate heating for short times. The stage containing the payload, however, re-enters the atmosphere at maximum speed and thus experiences severe heating. The time of this heating is short because the vehicle traverses only the thickness of the atmosphere under heating conditions. For aerodynamic heating considerations, this flight path may be divided into the booster phase and re-entry phase.

2. Long-Range Bombardment - Bomber - Boost Glide

As explained previously, the use of rocket propulsion for this vehicle requires a boost-glide flight path, probably using a multistage vehicle from which propellant tanks and engines are jettisoned after the propellants are used. Considerable speed is required to achieve range by gliding, and this speed permits sufficient lift to be obtained at altitudes beyond the limits of air-breathing engines. Thus, the high altitude tends to reduce the severity of aerodynamic heating and to compensate somewhat for the high speed.

The manned boost-glide bomber must have range beyond the target so that it may return to friendly territory; this can only be achieved by speed. The manned boost-glide airplane will thus be larger and faster than the unmanned expendable missile having the same operational radius.

The final stage of this airplane must also have low-speed flight characteristics and a wing area sufficient for landing.

This type of flight path may be divided into a boost phase applying to booster and the final stage vehicle, and a glide phase in which only the final stage participates. Heating conditions are moderate and of short duration for the booster, and moderate to severe for the final stage, depending on speed. Heating will exist for an extended time on the final stage vehicles.

3. Long-Range Bombardment - Bomber - Cruise

Air-breathing engines will be used in a long-range cruising vehicle so that speed and altitude will be limited as mentioned previously. Heating conditions will be moderate, but may persist for a number of hours, particularly with the manned bomber where extra range is required for return to base.

If turbojets are used with or without afterburners, the climb and acceleration is unlikely to be critical for thermal effects. If the ramjet is used, speeds may be greater, and the necessary rocket boost at launch may produce significant thermal transients. The flight path should thus be considered in two phases, boost and cruise.

4. Long-Range Bombardment - Bomb

Manned recoverable bombers will continue to carry the warhead in a separate bomb which will be released into the airstream with the same velocity as the bomber. Aerodynamic heating must, therefore, be considered in the bomb design.

For bombers using air-breathing engines, the bomb may be of a conventional gravity-type or a powered and winged missile. Considering the speed and altitude limitations of air-breathing engines, it is unlikely that the gravity bombs will give critical heating conditions. The powered missile bombs should be treated as a bomber having the same power plant and flight path characteristics.

When launched from rocket-powered bombers, the bomb should have sufficient range potential from its launch velocity to make power or wings unnecessary. The bomb, therefore, enters a ballistic path. It descends into dense atmosphere at high speed so that heating conditions range from moderate to extreme, but exposure-time is short.

5. Reconnaissance

The remarks made previously for the bomber apply equally to reconnaissance vehicles, except that such vehicles generally will be manned. Reconnaissance information transmitted by radio from an expendable missile is unlikely to equal the quality of photographic data, except by the use of equipment too costly to be expended after one flight. Since photographic results necessitate a recoverable vehicle, it will be advantageous to include a crew in order to minimize the unreliabilities and inaccuracies of presently developed automatic guidance, and to facilitate recovery.

6. Short-Range Interceptor - Rocket-Propelled

The unmanned version of this vehicle may be air or ground launched, with air-launching being reserved for the smaller short-range missiles that can be carried to altitude rapidly in larger high-speed aircraft. Interception missiles of long-range (more than 20 nautical miles), or of high speed, will be large enough to make ground-launching more practical; the same is true of the manned interceptor.

The unmanned rocket-powered interceptor may be expected to use power for its complete flight to the attack, since most of this time will be consumed in climbing. Thus, the flight is entirely boost, with temperatures and heating rates reaching high values if the speed is sufficient, but the total flight time is of short duration.

The manned rocket-powered interceptor, while also using power up to and including combat so that speed and altitude can be achieved and maintained, will then glide back to base. The flight

would be boost-glide with heating rates and temperatures reaching high values, depending on final speed, and with short exposure times but considerably longer than those of the unmanned interceptor.

7. Short-Range Interceptor – Air-Breathing Engines

Whether manned or unmanned this vehicle may be expected to be rocket-boosted for rapid acceleration to altitude. The manned vehicle may also use boost for combat. The flight path is thus divided into boost and cruise phases. Heating rates and temperatures will be moderate because of the limited speed capability of the air-breathing engine. Times during which heating is present will be short for the unmanned vehicle, extending to moderate for the manned vehicle.

From the previous discussions it is evident that the flight paths of future high-speed vehicles can be divided generally into one or more of the following phases:

(1) Boost, with increasing speed and either constant or increasing altitude

(2) Cruise at constant speed and altitude.

(3) Glide at decreasing speed and/or altitude.

(4) Ballistic re-entry, decreasing speed and altitude.

Each phase has peculiar characteristics with regard to the effects of aerodynamic heating, and these are discussed in more detail in the following paragraphs.

The boost phase of flight is characterized by increasing speed with or without increasing altitude, so that the aerodynamic conditions are changing. This leads to temperature gradients within the structure with corresponding thermal stresses or deformation. Except for the re-entry missile, the boost phase can be expected to be the primary cause of temperature gradients and thermal stresses in a structure. Other causes, such as change in angle of attack during maneuver or deceleration prior to landing, are comparatively unimportant.

Changes in angle of attack or altitude, for instance, result only in changing the heat transfer coefficient, and this produces a change in structural temperature only to the extent that radiation from the surface is present. Radiation will be significant if the speed is high so that surface temperature is high, or if the altitude is considerable so that convective heat transfer to the structure is small. In either case, it is clear that to achieve these conditions severe boosting will be required, so that boost will probably still give the critical thermal stresses. The deceleration prior to landing can presumably be performed so that, here too, the thermal stresses are no more critical than during boost; it should be noted that in this case the thermal stresses are of opposite sign from those produced by the boost. Since the rate of change of speed, without power, is dependent upon drag, it may be necessary to limit the rate of descent to lower altitude so that speed can be lost more gradually under conditions of low drag.

For the boost-glide or boost-cruise flight paths, the boost phase will have no significance other than to produce maximum transient conditions. The reason for this is that the maximum structural temperatures will almost always be reached shortly after completion of boost due to the thermal inertia of the structure.

For the unmanned rocket-powered interceptor, which is powered continuously to the target, the entire flight may be considered as boost so that this phase produces not only maximum thermal stresses, but also maximum temperatures. Similarly, the boost phase of the ballistic flight path will generally continue until the missile is beyond the atmosphere; aerodynamic heating is then reduced to zero and maximum temperatures will have been passed.

During boost flight, maximum acceleration for a manned vehicle will be determined by the physical limitations of the crew, while the rate of climb will probably be such that minimum energy is expended. For an unmanned vehicle, the maximum acceleration is obtained by optimizing between an increasing power plant weight and a reducing propellant weight (due to increased efficiency by more rapid useage), as the thrust is increased. Rates of change in altitude for an unmanned vehicle probably will be chosen for minimum energy expenditure if the vehicle is intended for cruise or glide, but for interception the criteria may well be minimum time to altitude.

In view of these complexities, the boost flight will be studied analytically by assuming a constant angle of climb and by expressing the results in terms of the ratios of thrust to take-off weight, and propellant weight to take-off weight. With these variables, any required combinations of velocity and altitude can be obtained for the start of a glide or cruise flight; the boost required to achieve the necessary range with a ballistic missile is included, since velocity and climb angle at the end of boost are related to the required range.

While the assumption of a constant angle of climb is only approximate, it permits the development of generalized relationships between speed, altitude, and time in terms of few parameters. Such generalization is the objective of this section of the report. In using the data to be presented, it is suggested that the flight path angle be selected to give the desired combination of speed and altitude at the end of boost.

This approach also permits a limiting acceleration to be used as a criterion for a manned vehicle, since maximum acceleration is related to thrust and propellant weight ratios. The altitude-time relationships will also show the climb angle to reach altitude in minimum time, and, if no other requirements are specified, this may be used as the criterion for the boost of an unmanned interceptor.

As previously explained, most cruising will be done with air-breathing engines and these have definite altitude and speed limitations. Relationships exist between speed, altitude, required range, lift-drag ratio, and fuel weight, but these are not simple. They depend closely upon vehicle configuration and engine performance (particularly as affected by intake duct shape).

Because of this difficulty, the thermal parameter values for cruise flight will be based upon arbitrary combinations of speed and altitude values which will be representative of both present and anticipated future practice.

The glide phase of a flight path is similar to the cruise phase except that speed and altitude change gradually, but usually not sufficiently fast to cause transient heating effects within the structure.

For glide flight, maximum values of speed are limited only by orbital speed, but attention during this study will be confined to values not exceeding Mach 20. Speed, altitude, and range, however, are related in a manner that depends primarily upon lift-drag ratio; consequently, when values of this ratio are assumed, a relationship exists between the temperatures or heating rates and the time of application.

The re-entry phase of a ballistic missile involves a decreasing altitude, and a decreasing speed due to drag. Re-entry speed and angle are related to the required range, but the deceleration after entry into the atmosphere depends upon body shape and is therefore arbitrary.

A ballistic missile is usually required to strike with the maximum possible velocity, but this must be accomplished with a body shape that has stability about the pitch and yaw axes, and also with heating rates that can be dealt with structurally. Many combinations of expendable drag-brake surfaces are possible to reduce speed at high altitudes where heating rates are low, but to establish the boundaries of the problem it will be assumed that these devices are undesirable and that a constant drag coefficient applies throughout re-entry. The drag coefficient can then be obtained from a specified striking velocity, and the resulting velocity-time-altitude relationships are readily calculated from the equations of motion. Maximum values of temperature, heating rate, and total heat will then follow.

[redacted]

C. THERMAL PARAMETERS

Before the boundaries of the thermal problems can be established, it is necessary to discuss the thermal parameters that control structural design, and the factors affecting their numerical values.

The thermal parameters involved in a particular design problem will depend upon the type of structure and flight path, and the effect of the structure being a function of the ability of its outer surface to absorb heat from the boundary layer. Three classifications can be recognized:

(1) Infinite heat capacity – surface maintained at constant temperature

(2) Zero heat capacity – surface rises instantaneously to equilibrium temperature

(3) Finite heat capacity – surface temperature a function of time

Condition (1) is realized with any form of structural cooling system, including methods of structural protection in which the heat is absorbed by melting of an exterior coating, and methods in which the heat is absorbed by endothermic chemical reactions.

For any type of flight path, the thermal parameters associated with this condition are the heat flux rate and the time during which the flux acts. The heat flux is dependent upon boundary layer temperature, which is a function of speed, and the heat transfer coefficient, which is a function of local pressure, velocity, type of boundary layer flow, and boundary layer thickness. Since these external aerodynamic conditions may vary during flight, the heat flux may also vary. Numerical values of the heat flux are independent of all structural characteristics, except the constant wall temperature as established by the particular cooling system.

Condition (2) is produced by the use of a perfect insulation around the structure, and it is closely approached by existing practical insulators. The thermal parameters controlling the design of such a system are equilibrium temperatures of the outer surface and the length of time during which they act. Equilibrium temperatures depend upon the boundary layer temperature and the local heat transfer coefficient; therefore, they may change numerically with a change in external aerodynamic conditions. Equilibrium temperatures are independent of the structure except for the emissivity of the outer surface. For the present study, it is sufficient to consider a constant value of emissivity since some control can be exercised over the surface condition.

Condition (3) occurs in a structure unprotected from the hot boundary layer, so that the heat transferred causes a rise in structural temperature. Also included is the case in which the skin is designed primarily for the function of absorbing heat, with an acceptable temperature rise. In this latter case, the skin either will be much thicker than is necessary for load carrying, or will be of material selected for heat absorbing ability, but having low structural efficiency.

The choice of thermal parameters for the design of unprotected structure will closely depend upon the particular flight path being considered. For the most practical boost-glide or boost-cruise flights, unprotected structure will attain an equilibrium temperature shortly after entering the glide or cruise phases. Since aerodynamic conditions are reasonably constant during glide or cruise, the only important thermal parameter for these phases of flight is maximum equilibrium temperature.

During the boost phase of flight, the changing aerodynamic conditions cause temperature gradients within an unprotected structure, and these result in thermal stresses or deformations or both, depending upon the internal structural restraints. Unfortunately, the controlling thermal parameters are complex. The shape of the temperature gradient through the structure depends upon the value of the heat transfer coefficient between the boundary layer and the structural surface, while the absolute magnitude of the gradient is set by the boundary layer temperature. The problem is further complicated because, in general, both boundary layer temperature and heat transfer coefficient will vary with time; however, for the simple, generalized comparisons to be made in this section, it is considered sufficient to neglect this complexity by using suitable average or mean values.

[redacted]

The methods developed in Section 3.0 of Part I are extended only to the case of varying boundary layer temperature and constant heat transfer coefficient. It will therefore be necessary to take an arithmetical mean value of heat transfer coefficient, but the varying boundary layer temperature can be dealt with by the method in Section VI of this part of the report, where a correction factor is developed by which the maximum thermal stresses produced during a boost of constant thrust can be related to the boundary layer temperature at the end of boost.

The thermal parameters required for the design of unprotected structure for the boost phase of a flight are, therefore, an average value of heat transfer coefficient, and the value of boundary layer temperature at the end of boost. If the flight is entirely boost, as the case may be with an unmanned interceptor, then the additional parameter of surface temperature at the end of boost is required.

The use of an unprotected skin for the primary purpose of absorbing heat rather than carrying load will usually be an inefficient technique because of the small specific heat of most metals in the solid state. However, since it offers the advantages of convenience and simplicity, this type of skin is expected to be applied in the re-entry portion of ballistic missiles. In order to design the skin for such a function, the most useful thermal parameter is the total heat input to the skin during the flight.

These thermal parameters are summarized for various flight paths and structure in Table II-2.

It will be noted that numerical values of the thermal parameters described previously always depend upon boundary layer temperature and heat transfer coefficient. Boundary layer temperature depends only upon speed and altitude, both of which are given by the flight path; the heat transfer coefficient varies, as previously mentioned, with local pressure, boundary layer thickness, and type of flow. Among the factors affecting local pressure are the body shape and the angle of attack. For the purposes of this section, these two items are considered by choosing typical values of the angle of tangency between the surface, at the point being considered, and the air stream.

Boundary layer thickness is a function of distance behind the leading edge or fuselage nose. The effect of this factor on the value of thermal parameters is included by presenting values for a number of representative distances behind the leading edges.

D. ANALYSIS OF FLIGHT PATHS

1. Boost Flight

Assuming (1) constant angle of climb, (2) zero drag, and (3) fuel expended only during boost so that arguments apply to one stage of a multistage vehicle, then the equation of motion for the vehicle is

$$T - W \sin\gamma = \frac{W}{g}\frac{dV}{d\theta},$$

where W is the instantaneous value of weight at time θ. If the stage under consideration begins boost with a fuel weight W_f, having a specific impulse I, then the duration of boost is

$$W_f\left(\frac{I}{T}\right).$$

Therefore, propellant is used at the rate of

$$\frac{W_f \times T}{W_f \times I} = \frac{T}{I} \text{ lb/sec.}$$

Then $W = W_o\left(1 - \frac{T\theta}{IW_o}\right)$, where W_o is the total vehicle weight at the beginning of the stage firing. The equation of motion then becomes

[redacted]

$$\frac{dV}{d\theta} = \frac{gT}{W_o\left(1-\frac{T\theta}{IW_o}\right)} - g\sin\gamma .$$

It will be convenient to make the following substitutions:

R_T = ratio of thrust to total vehicle weight at beginning of stage = $\frac{T}{W_o}$.

R_f = ratio of propellant weight to total vehicle weight at beginning of stage = $\frac{W_f}{W_o}$.

θ_1 = dimensionless time = $\frac{R_T\theta}{I}$.

Making these substitutions reduces the equation of motion to $\frac{R_T}{I}\frac{dV}{d\theta_1} = g\left\{\frac{R_T}{(1-\theta_1)} - \sin\gamma\right\}$.

Integrating this equation gives $V = gI\left[-\ln(1-\theta_1) - \theta_1\frac{\sin\gamma}{R_T}\right] + C_1$.

Initial conditions are $\theta = \theta_1 = 0$, $V = V_c$ giving $C_1 = V_o$,

so that

$$V = gI\left[\ln\left(\frac{1}{1-\theta_1}\right) - \left(\frac{\sin\gamma}{R_T}\right)\theta_1\right] + V_o . \qquad (1)$$

The altitude is

$$h = \int \sin\gamma V d\theta_1 = \frac{I}{R_T}\sin\gamma\int V d\theta_1$$

$$= g\frac{I^2}{R_T}\sin\gamma\left[\int\ln\left(\frac{1}{1-\theta_1}\right) - \left(\frac{\sin\gamma}{R_T}\right)\int\theta_1 d\theta_1\right] + \frac{I}{R_T}\sin\gamma\int V_o d\theta_1$$

$$= g\frac{I^2}{R_T}\sin\gamma\left\{(1-\theta_1)\left[-1+\ln(1-\theta_1)\right] - \frac{\sin\gamma}{R_T}\frac{\theta_1^2}{2}\right\} + V_o I\frac{\theta_1}{R_T}\sin\gamma + C_2 .$$

At $\theta_1 = 0$, $h = h_o$, so that $C_2 = g\frac{I^2}{R_T}\sin\gamma + h_o$

Therefore,

$$h = gI^2\frac{\sin\gamma}{R_T}\left[\theta_1 + (1-\theta_1)\ln(1-\theta_1)\right] - gI^2\left(\frac{\sin\gamma}{R_T}\right)^2\frac{\theta_1^2}{2} + V_o I\left(\frac{\sin\gamma}{R_T}\right)\theta_1 + h_o . \qquad (2)$$

Using Equations (1) and (2), velocities and altitudes have been calculated and plotted against the dimensionless time parameter θ_1 in Figure II-1. The curves are presented for the complete range of values of the parameter $\frac{\sin\gamma}{R_T}$. The maximum value of this parameter is 1.0 since the maximum value of $\sin\gamma$ is equal to 1.0, and for a vertical climb the minimum value of R_T

also equals 1.0. The curves are presented in carpet form to permit simple and accurate interpolation for intermediate values of $\frac{\sin\gamma}{R_T}$.

Figure II-1 gives values for boost flight starting at zero velocity and altitude, so that the values are only applicable to the first stage of a multistage vehicle. Multistage vehicles may be necessary for extreme speeds (> 6000 ft/sec); for the second and later stages of such vehicles, Equations (1) and (2) must be applied directly. The maximum value of θ_1 for any stage is equal to R_f for that stage.

Based upon the values given in Figure II-1, Figure II-2 shows corresponding recovery or boundary layer temperatures and equilibrium temperatures. Both plots have been prepared using the methods and charts given in Section I of Part I, so that recovery temperatures include the effect of specific heat change in the boundary layer air and are generally smaller values than are given by the simple expression $T_0(1+0.18\,M^2)$. In preparing the curves, a flat plate at an angle of attack of 7° has been assumed, since this is considered typical of lower surfaces of wings. Such assumptions will generally give conservative values for bodies and fuselages. Turbulent flow was assumed in computing equilibrium temperatures, and values are given at three chordwise stations.

Figure II-3 gives heat transfer coefficients at three chordwise stations and for four values of $\frac{\sin\gamma}{R_T}$ based upon the assumptions discussed previously. Heat transfer coefficients depend upon structural temperature which will vary during the boost period if the structure is unprotected; in calculating the coefficients of Figure II-3, a constant and typical value of 400°F has been used for the surface temperature. This value is sufficiently close to the 200°F wall temperature of a water-cooled structure so that the coefficients can be used to calculate fluxes into a cooling system. The wall temperature of 400°F also gives heat transfer coefficients suitable for the discussion of thermal stresses for unprotected structures, since maximum stresses generally occur early in boost when wall temperatures are low. If the heat transfer coefficients are used to obtain transient skin temperatures, they will be conservative since wall temperatures will generally exceed 400°F at the end of boost.

The second graph of Figure II-3 gives heat flux into a structure that is water cooled to 200°F. Three chordwise stations are considered for various values of $\frac{\sin\gamma}{R_T}$. The heat flux values were computed from the heat transfer coefficients discussed previously, and from the recovery temperatures of Figure II-2.

2. Glide Flight

In Reference 1 the equations of motion of glide flight are developed, including the effects of centrifugal force, and assuming a constant lift-to-drag ratio, $\frac{L}{D}$. Equation (30) of Reference 1 gives the velocity of a glide vehicle as

$$\bar{V}^2 = 1-(1-\bar{V}_f^2)\,e^{2\zeta/(\frac{L}{D})},$$

where $\bar{V}_f$ is the velocity at beginning of glide and the bars over both $\bar{V}$ and $\bar{V}_f$ signify that these velocities are expressed in terms of satellite velocity at sea level. The value of satellite velocity is taken as 25,930 ft/sec. Similarly, the term ζ is the distance from the beginning of the flight expressed in dimensionless form by dividing by the earth's radius. This radius is taken as 3955 statute miles.

From the same reference, Equation (33) gives the total range possible with a glide vehicle, starting the glide with the dimensionless velocity $\bar{V}_f$, as

$$\Phi = \frac{1}{2}\left(\frac{L}{D}\right)\ln\left(\frac{1}{1-\bar{V}_f^2}\right).$$

From this equation, the initial glide velocity, $\bar{V}_f$ necessary to achieve a given range is given by

$$\left(1-\bar{V}_f^2\right)=e^{-2\Phi/\left(\frac{L}{D}\right)}.$$

Combining this with the equation for velocity gives

$$\bar{V}^2=1-e^{-2\Phi/\left(\frac{L}{D}\right)}e^{2\zeta/\left(\frac{L}{D}\right)},$$

or

$$\bar{V}^2=1-e^{-2(\Phi-\zeta)/\left(\frac{L}{D}\right)}$$

If a new parameter, ψ, is defined as the distance from the end of flight, or range-to-go, at the time velocity $\bar{V}$ is achieved, then the equation for $\bar{V}$ becomes

$$\bar{V}^2=1-e^{-2\psi/\left(\frac{L}{D}\right)}. \tag{3}$$

Again, the term ψ is expressed in terms of the earth's radius so that it is dimensionless. Equation (3) shows that the velocity at any point in the glide is a function of only the distance to go, and is independent of the previous history of the flight. Thus, a single curve of velocity against distance shows both the maximum velocity for any range and the velocity at any point along the glide flight.

In order to determine altitude corresponding with this velocity, it is appropriate to assume that the glide vehicle, since it expends no fuel, flies at constant wing loading, $\frac{W}{S}$. Then at any speed, the altitude must be selected so that the following equation is satisfied:

$$\frac{W}{S}\left[1-\left(\frac{V}{V_s}\right)^2\right]=\frac{C_L\rho V^2}{2}.$$

This equation is more conveniently written as

$$\frac{W}{S}\left[1-\left(\frac{V}{V_s}\right)^2\right]=1481\,\frac{P}{P_0}\left(C_L M^2\right), \tag{4}$$

since C_L will generally vary with Mach number. Both the C_L vs. M variation and the minimum $\frac{L}{D}$ are functions of the vehicle shape and, for the purpose of a general study, typical values must be assumed.

The term in parenthesis to the left-hand side of Equation (4) corrects the lift for centrifugal effects.

Using Equations (3) and (4), velocities and altitudes have been calculated and plotted against range in Figure II-4 for two values of $\frac{L}{D}$ and $\frac{W}{S}$. Note that the horizontal axis may be read as range, giving maximum and initial values of velocity and altitude; or as range to go, in which case the velocity and altitude is appropriate to the particular stage of the flight. Lift-drag values of 5.0 and 2.0, and wing loadings of 25 and 50 lb/ft^2, are intended to cover the range of values expected for hypersonic vehicles.

Figure II-4 also shows time-to-go for any value of remaining range; this curve was obtained by graphical differentiation of the velocity curve.

In order to calculate values of altitude, an angle of attack of 7° has been assumed, giving the C_L vs. M curve shown in Figure II-5. This curve, taken from the results of a design study of a hypersonic vehicle, is considered representative. Combining the C_L vs. M curve with properties of the NACA standard atmosphere, permitted curves of the right-hand side of Equation (4) to be drawn for various altitudes. Curves of the left-hand side of Equation (4) were then super-

imposed for the two values of $\frac{W}{S}$, and the intersections gave the altitude velocity relationships appearing in the second curve of Figure II-5.

With the velocities and altitudes of Figure II-4, equilibrium temperatures have been calculated using the methods of Section 1.0, Part I; the results are presented in Figure II-6. Temperatures are given for three chordwise stations assuming turbulent flow conditions and a flat plate at an angle of attack of 7°. Figure II-7 gives heat fluxes into a structure having a surface maintained at 200°F by water cooling, all other conditions being the same as for the equilibrium temperature curves.

3. Cruise Flight

It was explained in Section II, B, that, for cruise flight conditions, an arbitrary relationship between velocity and altitude would be selected to reflect present and anticipated future practice. Therefore, no theoretical treatment of the problem is necessary except for the simple relation between flight time and range $\theta = \frac{R}{V}$.

Figure I-7 of Section I, Part III, gives statistical data from many supersonic missile and airplane projects, and illustrates current trends in the relationship between speed and altitude for cruise-type vehicles. Since most severe heating conditions will occur at the lowest altitude appropriate to each speed, a minimum altitude of 45,000 feet will be assumed at Mach 2.0, increasing to 62,000 feet at Mach 5.0. As explained previously, a speed of Mach 5.0 is a reasonable maximum for air-breathing engines. Cruising with rockets is not included because it is generally inefficient. Figure II-8 shows the speed-altitude relationship assumed for cruise flight, and also the corresponding flight time for various ranges.

Based upon the speed-altitude curves of Figure II-8 and the methods given in Section 1.0, Part I, the curves of Figure II-9 show not only equilibrium temperatures for the cruise flight conditions, but also heat fluxes into a structure with its surface water-cooled to 200°F. Values are given at three chordwise stations, assuming turbulent flow and a flat plate inclined at an angle of attack of 7°. These assumptions are not significant at speeds less than Mach 4.0.

4. Re-entry Flight

Equation (12) of Reference 1 gives the following equations for the velocity and angle of climb of a ballistic missile at power cutoff, with the angle chosen for maximum range for a given velocity:

$$\bar{V}_f^2 = 1 - \tan^2 \gamma, \text{ and } \Phi = \pi - 4\gamma.$$

Assumptions made in developing these expressions are (1) the distance covered during powered flight is negligible compared with the total range, (2) neglect of earth's atmosphere during boost and re-entry, and (3) neglect of earth's rotation. With these assumptions, the ballistic trajectory becomes a planetary ellipse and the vehicle leaves and returns to the earth's surface with the same magnitudes of velocity and flight path inclination. Thus, $\bar{V}_f$ can be considered as the re-entry velocity appropriate to the range Φ.

Substituting the second equation mentioned previously into the first gives

$$\bar{V}_f^2 = 1 - \tan^2\left(\frac{\pi - \frac{R}{r_o}}{4}\right). \qquad (5)$$

To compute velocities within the atmosphere, during re-entry, Reference 2 makes additional assumptions: (1) constant drag coefficient, C_D, (2) constant path angle, γ, (3) gravity small compared with drag, and (4) isothermal atmosphere.

The last assumption, (4), leads to the expression for density at any altitude, in terms of the density at sea level $\sigma = e^{-ah}$. With these assumptions, Reference 2

[redacted]

expresses the velocity at any point during re-entry as

$$V = V_s \bar{V}_f \, e^{-\frac{C_D A}{W \sin\gamma} \frac{\rho_{SL}}{2\alpha} \sigma} . \qquad (6)$$

Equation (6) gives the velocity-altitude relationship during re-entry but for analysis of the thermal problems the variation of velocity and altitude with time is required.

$$\text{Vertical velocity} = V \sin\gamma = \frac{dh}{d\theta} ,$$

therefore, $d\theta = dh / V \sin\gamma$

and $\theta = \int_{h_f}^{h} \frac{dh}{V \sin\gamma} .$

The lower limit for this integral is an arbitrarily assigned value of re-entry altitude. It will be obvious from the curves which follow that any value above 200,000 feet will give the same results.

Substituting the expression for V in the equation for time gives

$$\theta = \frac{1}{V_s \bar{V}_f \sin\gamma} \int_{h_f}^{h} e^{B\sigma} \, dh ,$$

where $B = \frac{C_D A}{W \sin\gamma} \frac{\rho_{SL}}{2\alpha}$ and $\sigma = e^{-\alpha h}$.

Writing the integral in terms of σ, so that it becomes $-\frac{1}{\alpha} \int \frac{e^{B\sigma} \, d\sigma}{\sigma}$,

this expression may now be expanded by a Taylor series to give $\ln \sigma + \sum_{m=1}^{\alpha} \frac{B^n \sigma^n}{n(n!)}$.

Then $\theta = \frac{1}{V_s \bar{V}_f \sin\gamma} \left[(h - h_f) - \frac{1}{\alpha} \left\{ B\left(e^{-\alpha h} - e^{-\alpha h_f}\right) + \frac{B^2}{4}\left(e^{-2\alpha h} - e^{-2\alpha h_f}\right) \right.\right.$

$\left.\left. + \frac{B^3}{18}\left(e^{-3\alpha h} - e^{-3\alpha h_f}\right) f \text{-------} \right\}\right] . \qquad (7)$

Using a value for r_o of 3955 mi, and V_s equal to 25,930 ft/sec, then values of V_f, calculated from Equation (5) for various ranges, are

Range (statute mi)	500	1000	2000	3000	4000	6000
Re-entry Velocity (ft/sec)	8900	12240	16390	19100	20950	23400

From Equations (6) and (7), the velocity variation during re-entry depends upon the drag-weight parameter, $\frac{C_D A}{W}$, for which a practical range of values must be assigned. The important criterion, one that is relatively easy to establish, is striking velocity which is obtained from Equation (6) with a value for h of zero. Two extreme values of striking velocity are considered to be Mach 1.0 and 5.0, representing a minimum acceptable value and a maximum practical value, respectively. Various devices and refinements, such as drag brakes and two-stage re-entry vehicles, have been proposed to achieve high striking velocities, with most of the deceleration occurring

at high altitudes where heating conditions are minimized. However, it is considered that these complexities are undesirable if the heating rates of a vehicle striking at high velocity, and having constant drag characteristics, can be met. This condition thus forms the boundary of the heating problem for re-entry vehicles.

From Equation (6) with an altitude of zero, the required values of $\frac{C_D A}{W}$ for striking velocities of Mach 1.0 and 5.0, and for various values of range, are

	Range (statute mi)	500	1000	3000	6000
$\frac{C_D A}{W}$	M = 1.0 at h = 0	0.00150	0.00170	0.00170	0.00130
	M = 5.0 at h = 0	0.00034	0.00056	0.00074	0.00061

Using these values for $\frac{C_D A}{W}$ Figures II-10 and II-11 show values of velocity, altitude, and time during re-entry for various ranges, calculated from Equations (6) and (7).

From the velocities and altitudes of Figures II-10 and II-11, the recovery temperatures (or boundary layer temperatures) shown in Figure II-12 have been calculated using the methods of Section 1.0, Part I. For this curve and those which follow, a cone having a semivertex angle of 7° was assumed, with turbulent boundary layer conditions. Also, following the principle that thermal boundaries are sought, only the case of striking at Mach 5.0 has been carried further.

Figure II-13 shows heat transfer coefficients for the 7° cone, also calculated from the data of Section 1.0, Part I. Three vertical scales are provided to give coefficients at three positions aft of the nose. Coefficients at any position can be obtained by dividing the values for the one foot-station by the factor: (Distance behind nose) 0.2. Based upon the heat transfer coefficients from Figure II-13 and the recovery temperatures from Figure II-12, Figure II-14 gives heat fluxes into the 7° cone, assuming that the structure is held at constant temperature by means of a cooling system. To obtain conservative values, it was assumed that a water cooling system would be used, thus setting the wall temperature at approximately 200°F. Again, the three vertical scales give the flux at three positions on the cone.

To obtain the total flux during re-entry, the flux per unit area can be integrated over the cone surface and throughout the re-entry flight as

$$\text{Total flux} = \int \left[(T_r - T_w) \int h_c \, dA \right] d\theta .$$

For turbulent flow, heat transfer coefficient varies as $x^{0.2}$, so that in terms of the coefficient at the one foot station

$$h_c = \frac{h_{c1}}{x^{0.2}} .$$

For a cone of semiangle β, the surface area of an element cut parallel to the base is

$$dA = 2\pi x \tan\beta \, dx ,$$

thus $$\int_0^{r/\tan\beta} h_c dA = h_{c1} \int_0^{r/\tan\beta} \frac{2\pi x \tan\beta \, dx}{x^{0.2}} = \frac{2\pi}{1.8} h_{c1} \frac{r^{1.8}}{(\tan\beta)^{0.8}} ,$$

where r is the base radius of the cone.

Therefore, total flux becomes $\frac{2\pi}{1.8} \frac{r^{1.8}}{(\tan\beta)^{0.8}} \int h_{c1} (T_r - T_w) \, d\theta .$

[redacted]

To minimize the absolute size term in this expression, the total flux is given in terms of unit base area

$$\frac{\text{Total flux}}{\text{Base area}} = \frac{1.11}{(\tan\beta)^{0.8}\, r^{0.2}} \int h_{cl}\,(T_r - T_w)\,d\theta, \left(BTU/ft^2\right). \tag{8}$$

For a practical range of values of r, say from one to five feet, the term $r^{0.2}$ varies only from 1.0 to 1.38; consequently, to eliminate absolute size as a parameter, an average value of 1.20 will give values sufficiently accurate for present purposes.

Note that the integral $\int h_{cl}\,(T_r - T_w)\,d\theta$ is the area under the curves of Figure II-14. Using Equation (8) and Figure II-14, total fluxes per unit area were obtained and are presented in Figure II-15.

Also shown in Figure II-14 is the total flux for a 14° cone, and this was obtained from the curve for the 7° cone by assuming that the only important effect on cone angle change is the change in pressure. If the pressure change is known, then the heat transfer coefficient, and hence the heat flux, is in proportion to $(\text{pressure})^{0.8}$. Unfortunately, the pressure ratio change due to a cone angle change varies slightly with speed and, of course, the speed varies during re-entry. To eliminate this difficulty, the effects of cone angle change were evaluated at the speed corresponding with maximum flux intensity, this in turn being obtained from the time given by Figure II-14.

The flux intensities given in Figure II-14 are satisfactory over most of the vehicle surface, but the methods used are not suitable for extrapolation to the vehicle nose where intensities are greatest. Accordingly, flux intensities at the nose have been calculated independently by the methods of Reference 3, and are presented in Figure II-15 for various values of nose radius and missile range. In selecting the values of velocity and altitude appropriate to each range, the times of maximum flux at the one-foot station, as shown in Figure II-14, were considered critical.

Figure II-16 gives equilibrium temperatures at two stations for the 7° cone, assuming turbulent flow. These values have also been calculated by the methods of Section 1.0, Part I, using velocities and altitude from Figure II-11. Equilibrium temperatures have been cut off at 2800°F, since this is considered a maximum value of interest at present.

REFERENCES

(1) Eggers, A. J., Allen, H. J., and Neice, S. E., "A Comparative Analysis of the Performance of Long-Range Hypervelocity Vehicles," NACA RM A54L10, March 1955.

(2) Gazley, C. (Jr.), "The Re-entry of Long-Range Ballistic Missiles," Rand Report S-20, June 1954.

(3) Sibulkin, M., "Heat Transfer Near the Forward Stagnation Point of a Body of Revolution," Journal of Aeronautical Sciences, Volume 19, 1952, Page 570.

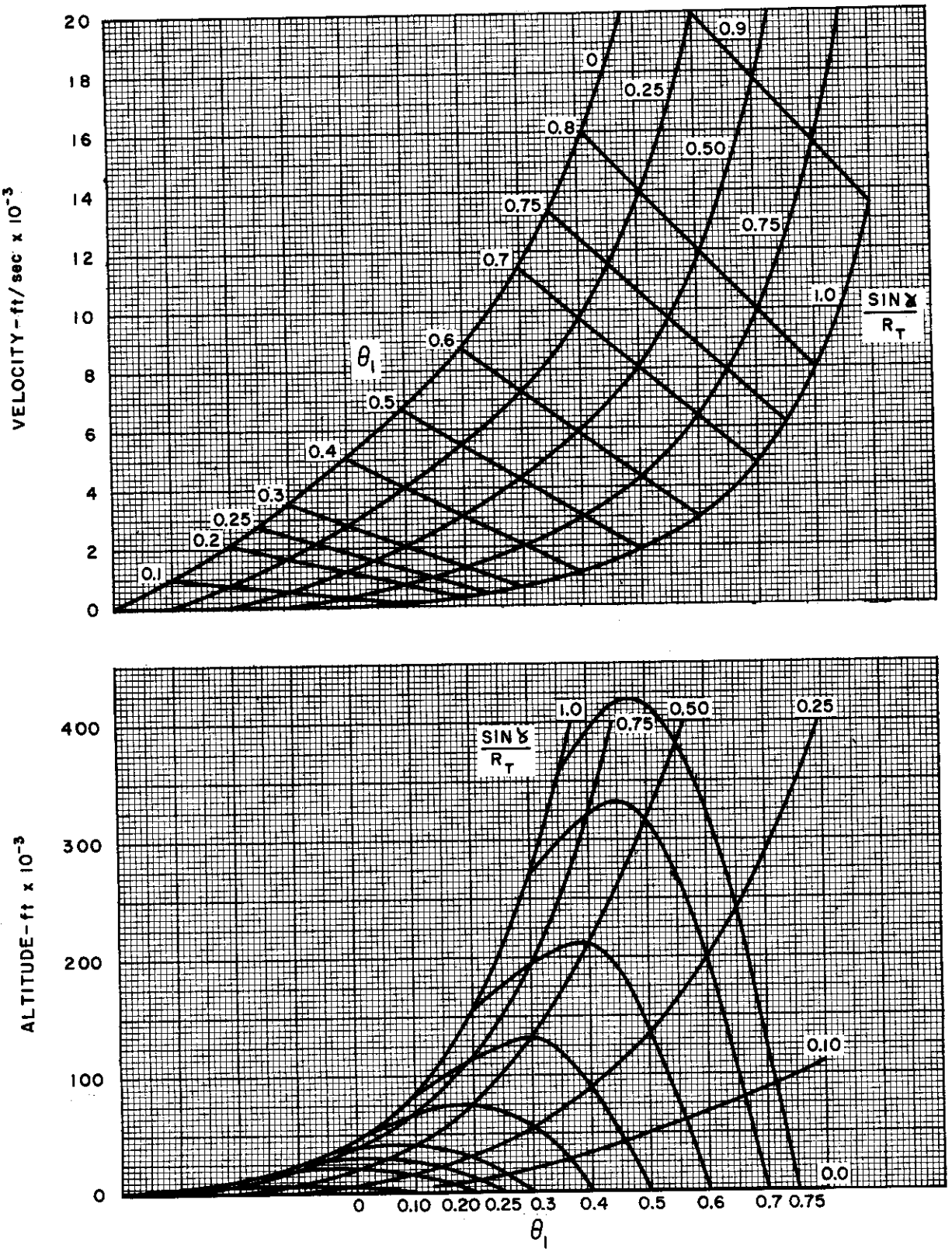

Figure II-1. Velocity and Altitude for Boost Flight

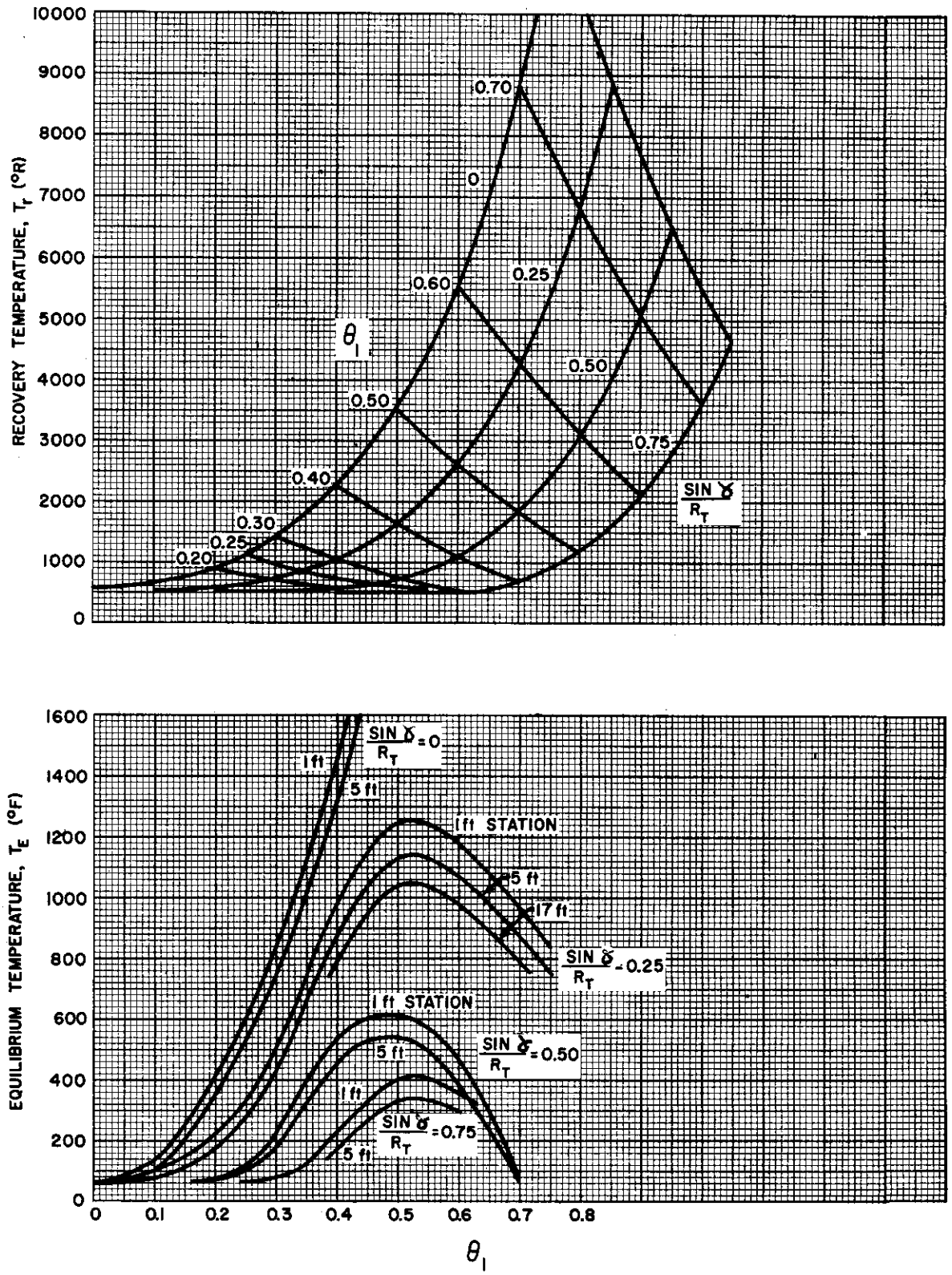

Figure II-2. Equilibrium and Recovery Temperatures for Boost Flight

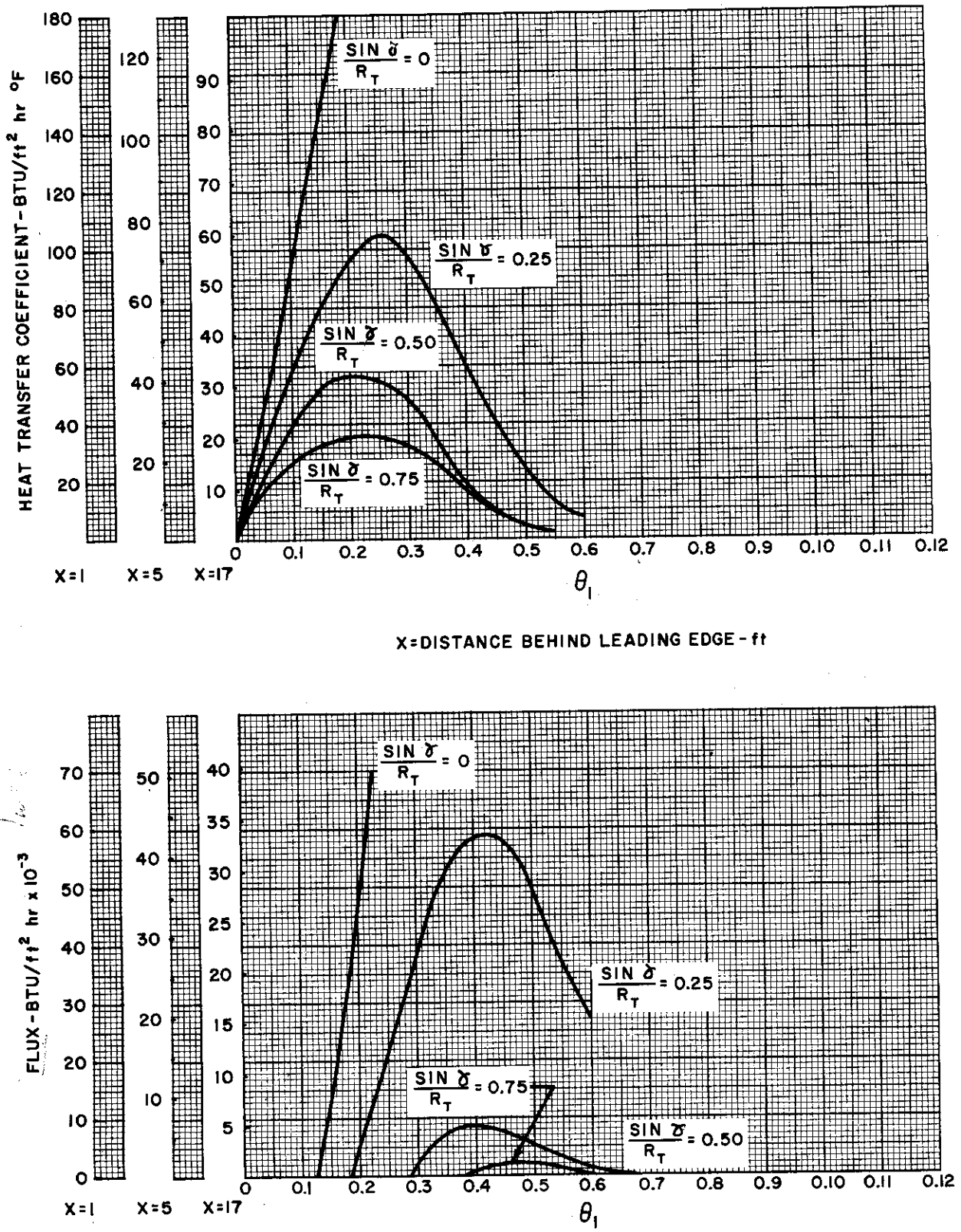

Figure II-3. Heat Transfer Coefficient and Heat Flux for Boost Flight

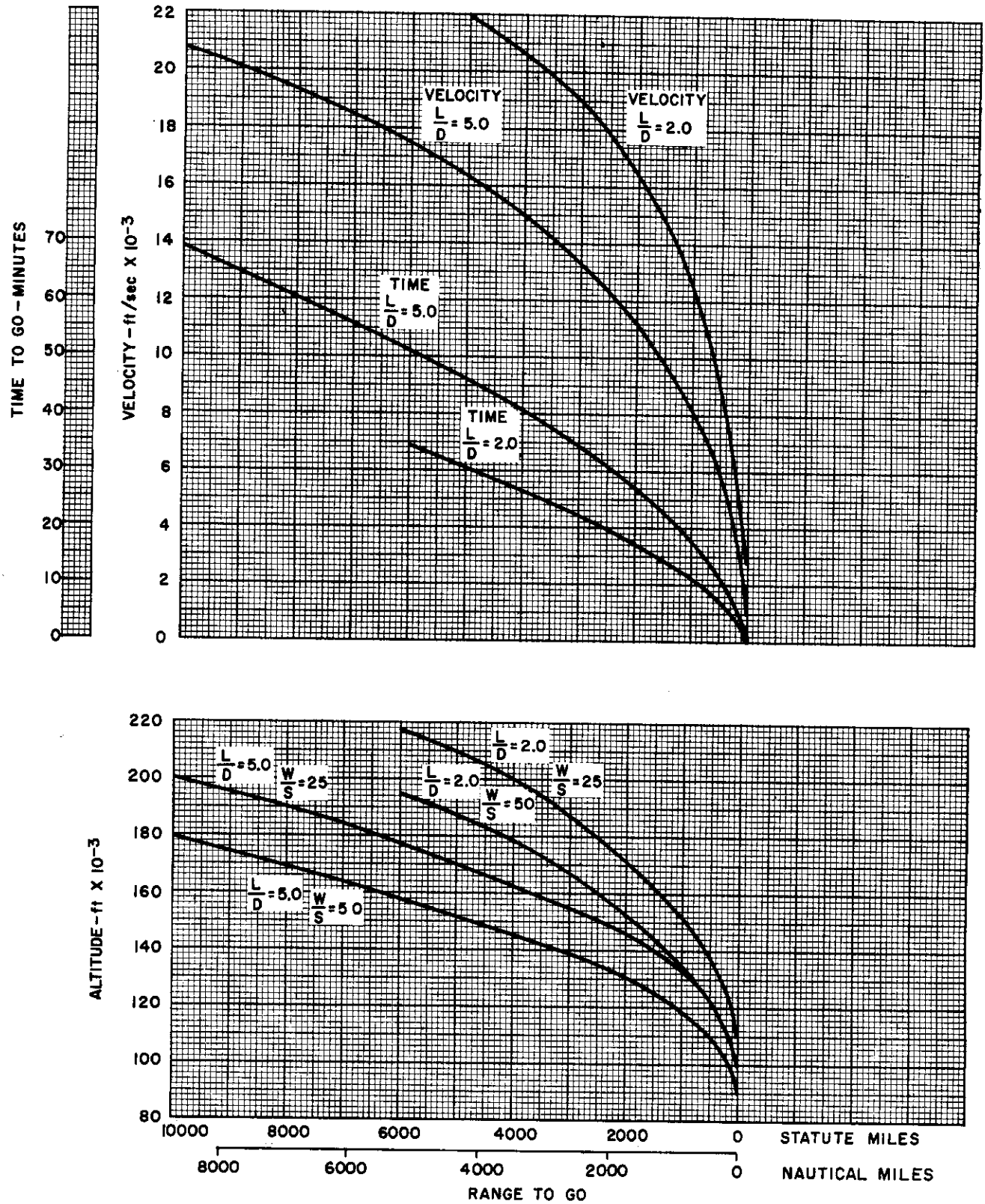

Figure II-4. Velocity, Altitude, and Time for Glide Flight

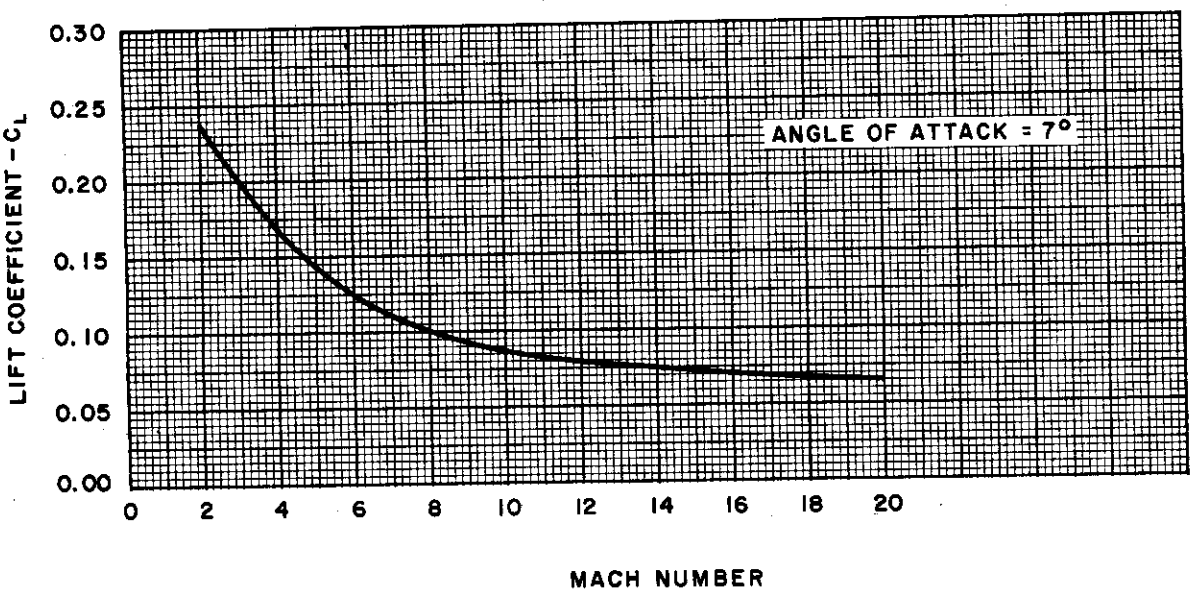

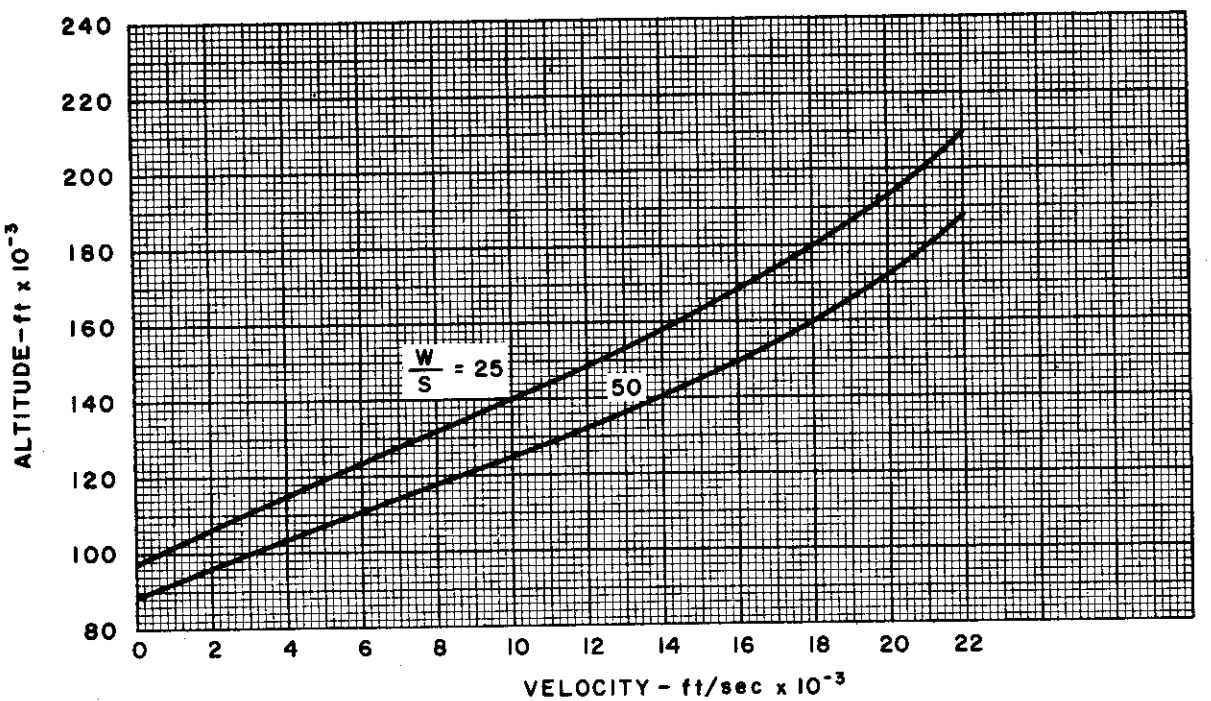

Figure II-5. Lift Coefficient and Altitude-Velocity Relationship for Glide Flight

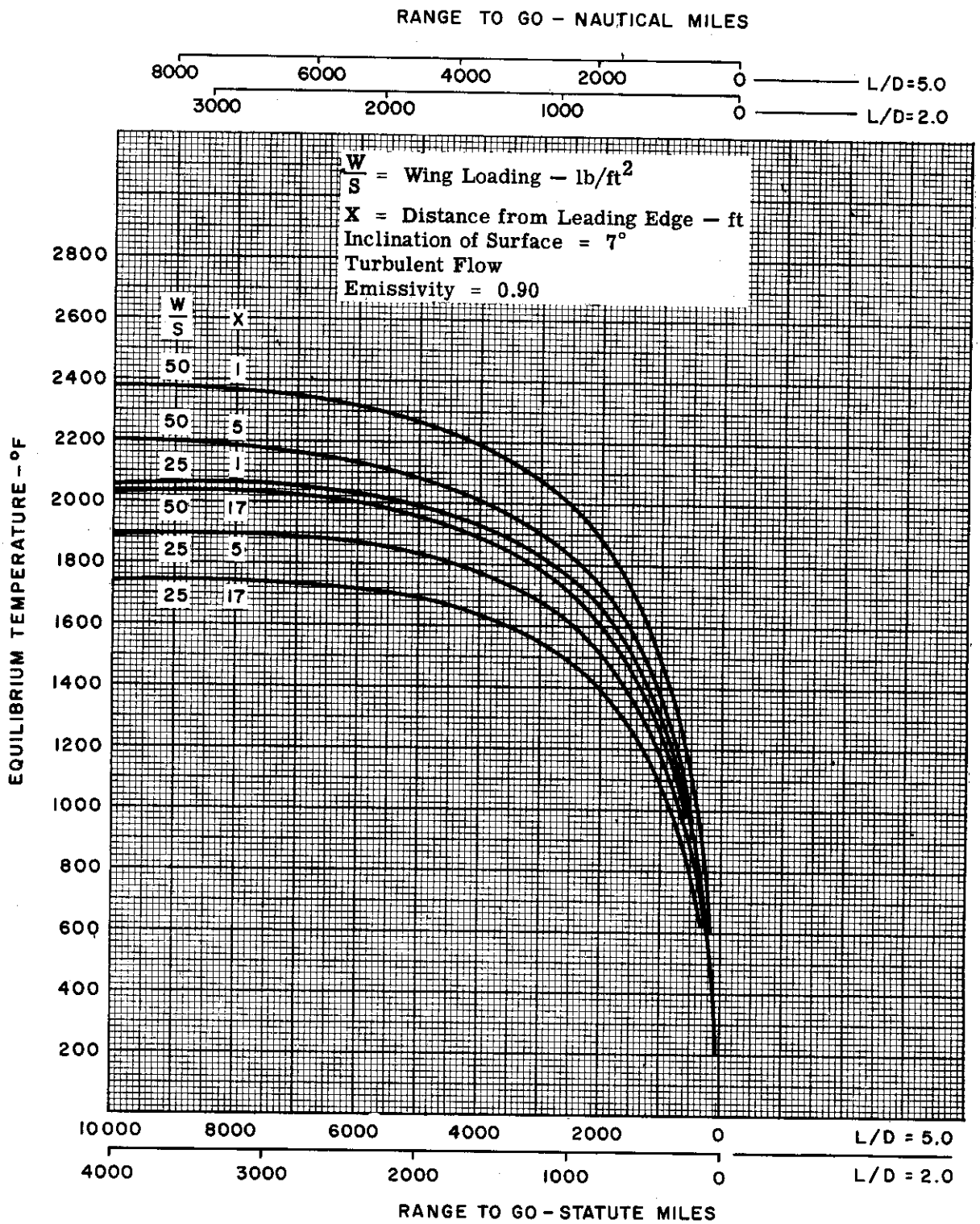

Figure II-6. Equilibrium Temperatures for Glide Flight

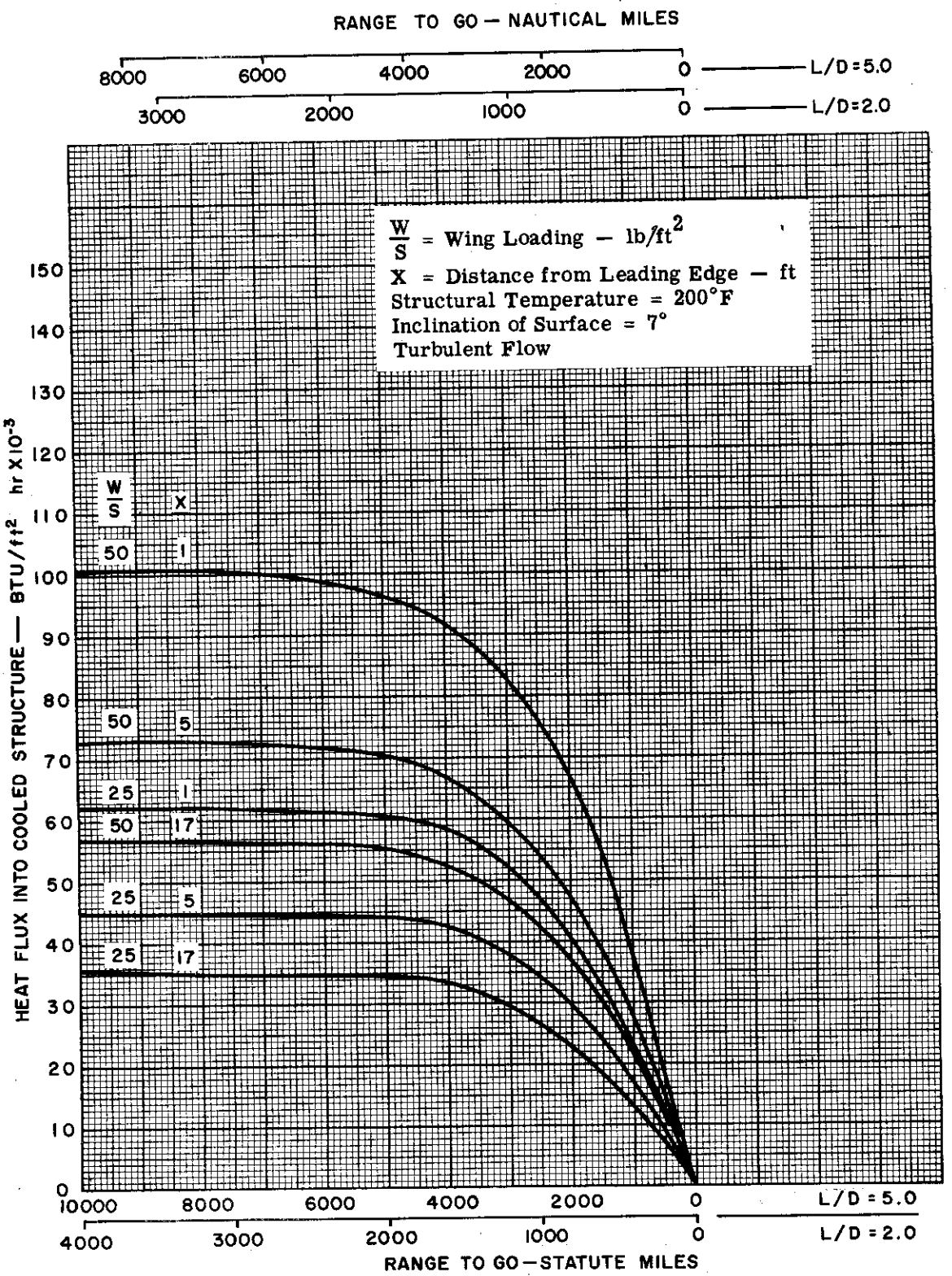

Figure II-7. Heat Flux into Cooled Structure for Glide Flight

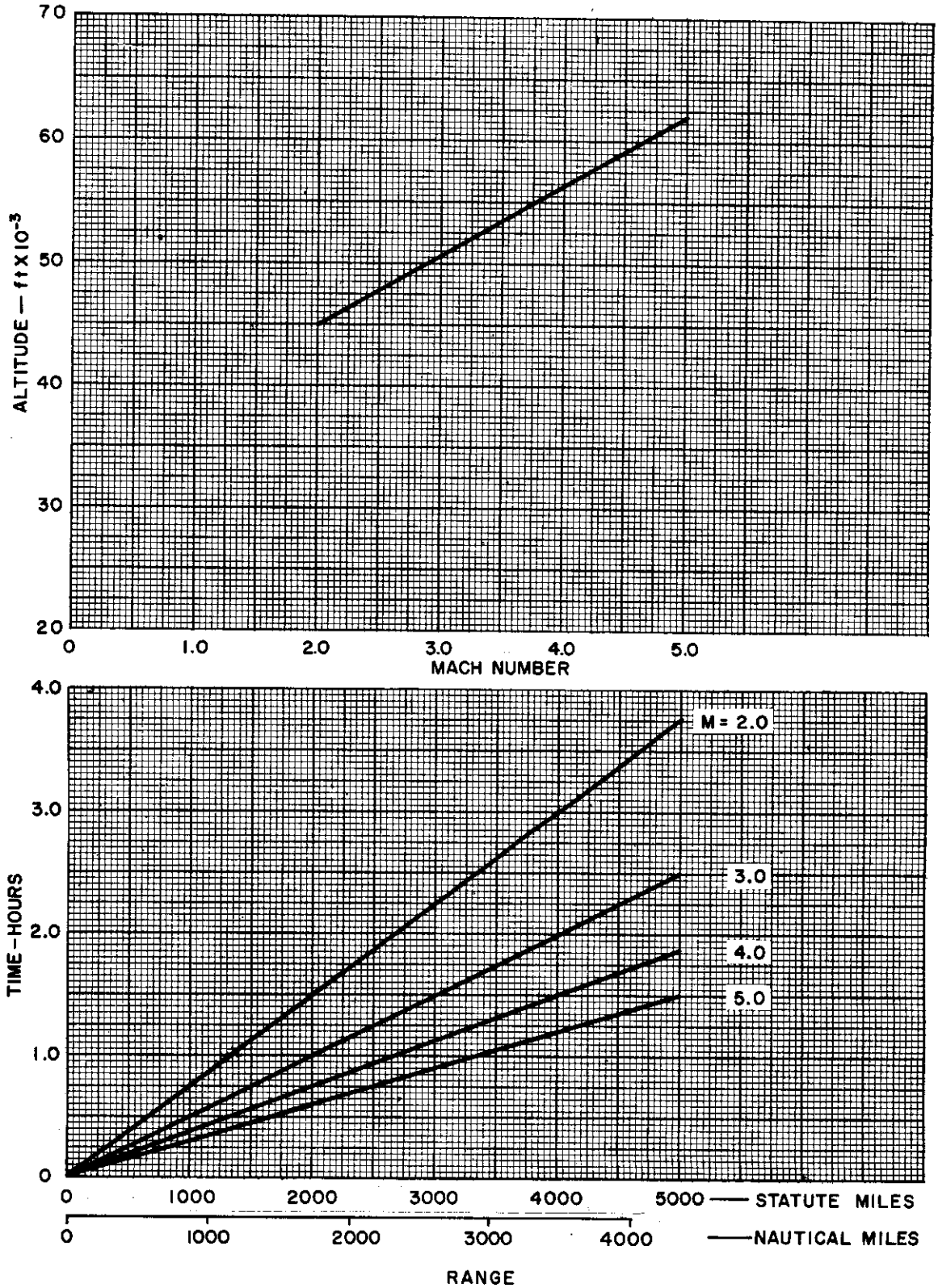

Figure II-8. Velocity, Altitude, and Time for Cruise Flight

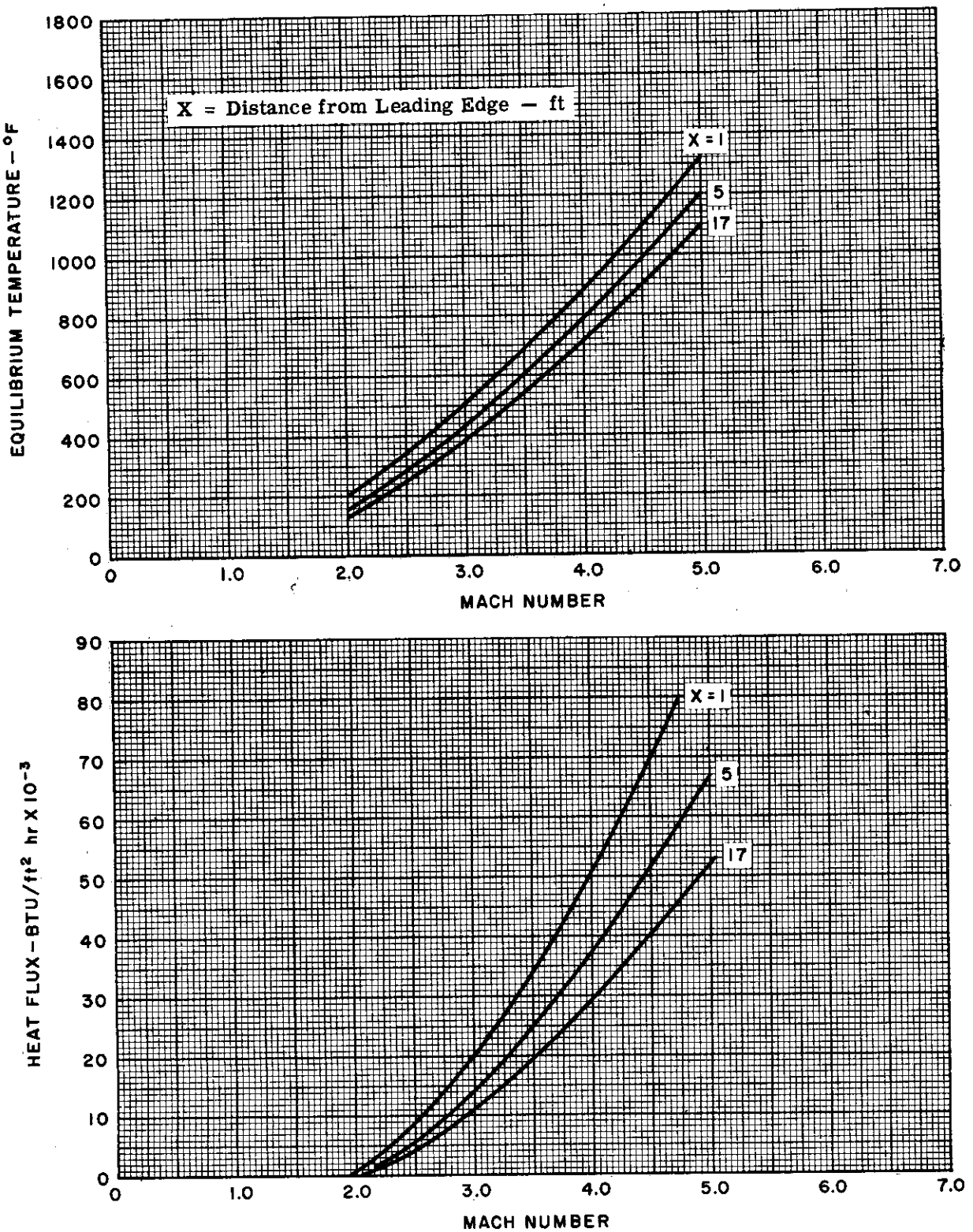

Figure II-9. Equilibrium Temperatures and Heat Fluxes for Cruise Flight

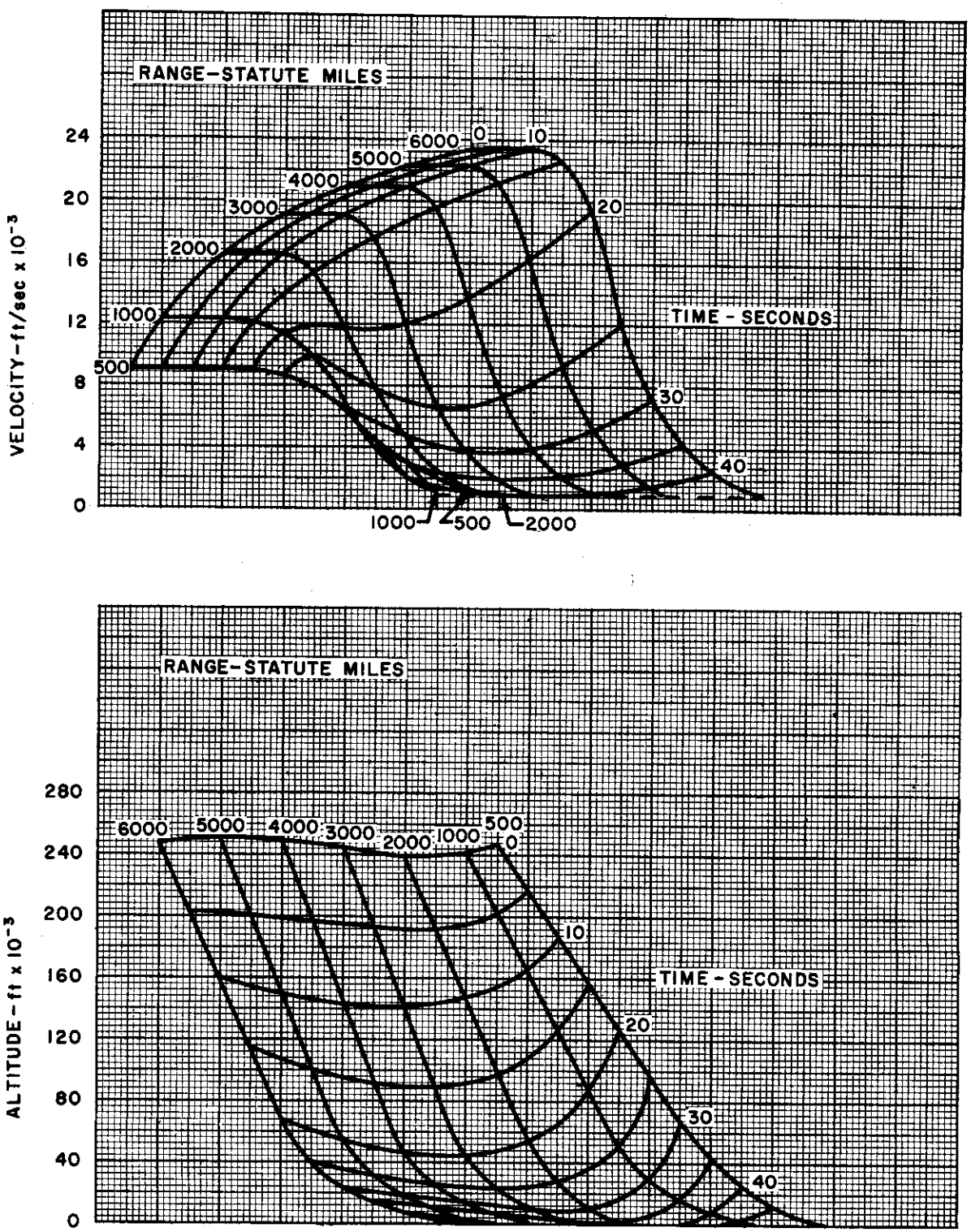

Figure II-10. Velocity and Altitude for Re-entry Flight, Mach 1.0 Striking Velocity

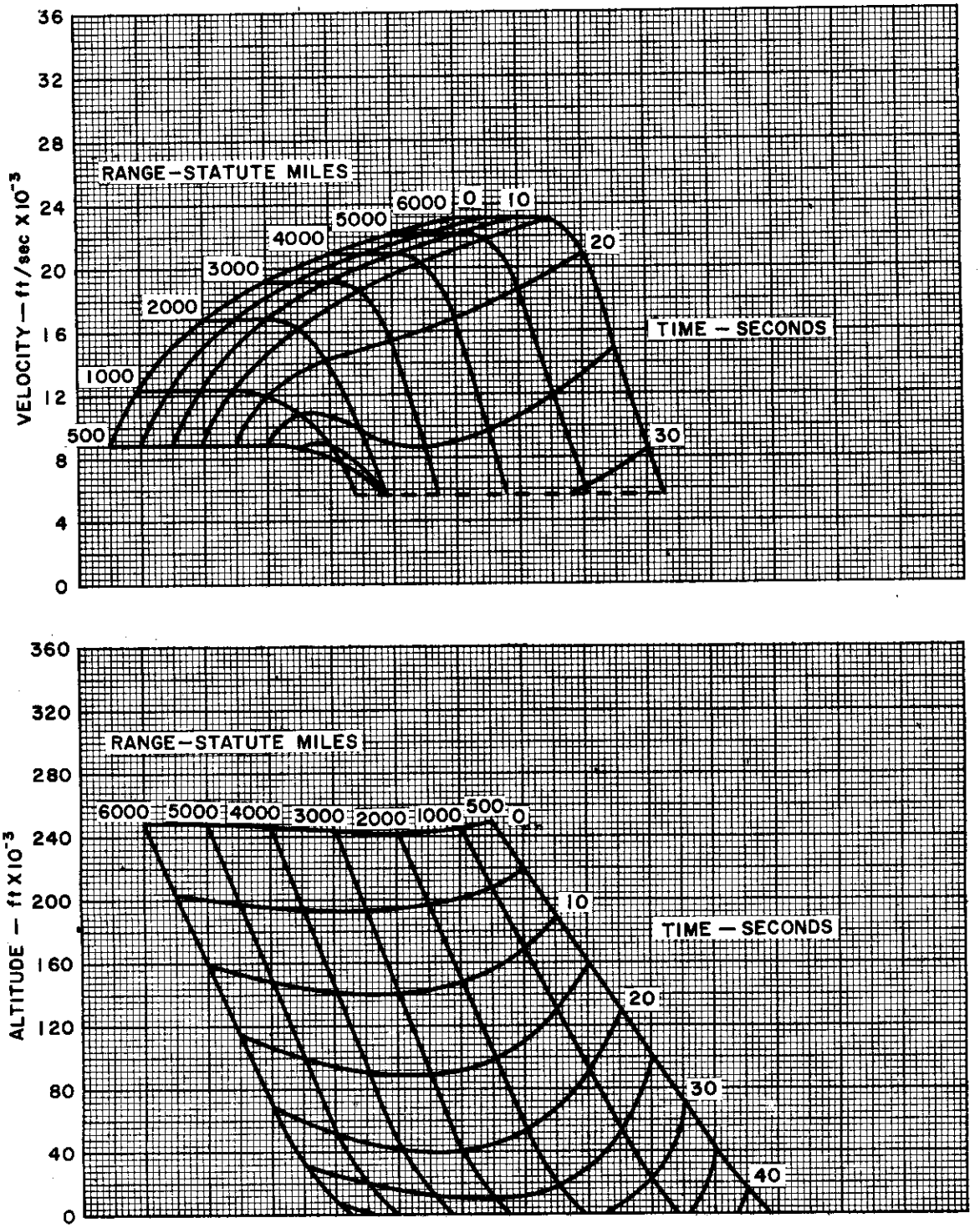

Figure II-11. Velocity and Altitude for Re-entry Flight, Mach 5.0 Striking Velocity

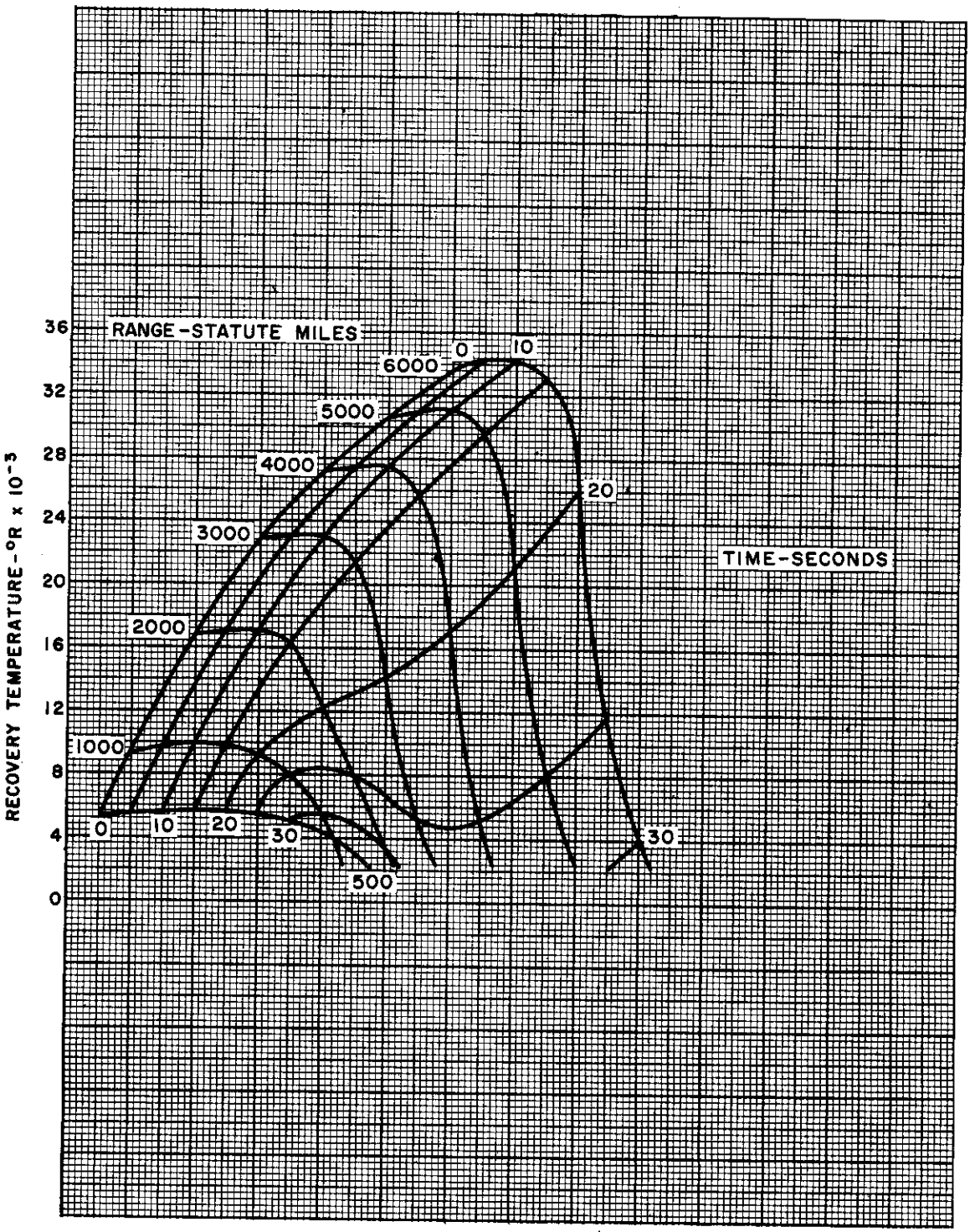

Figure II-12. Recovery Temperature for Re-entry Flight, Mach 5.0 Striking Velocity

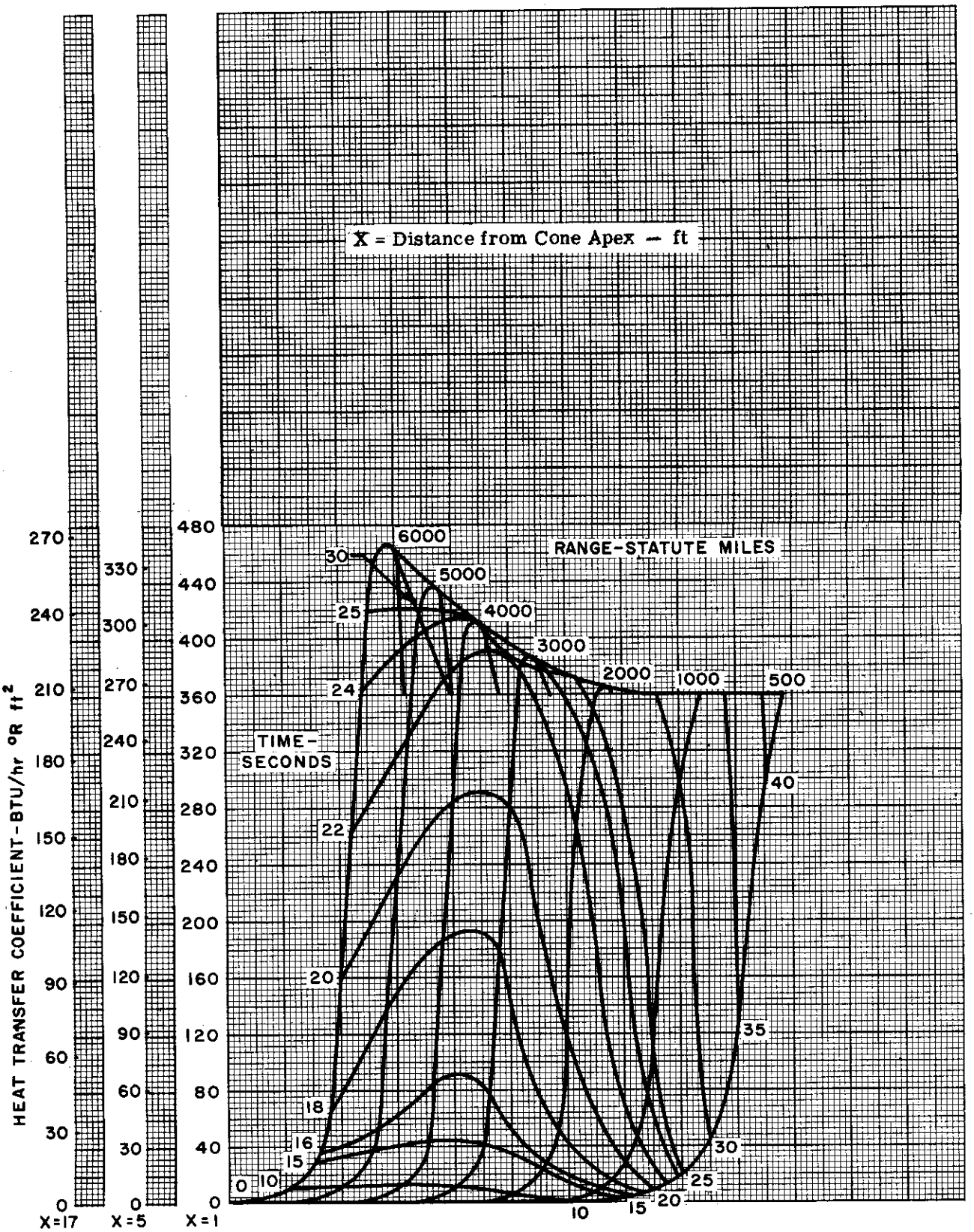

Figure II-13. Heat Transfer Coefficient for Re-entry Flight, Mach 5.0 Striking Velocity

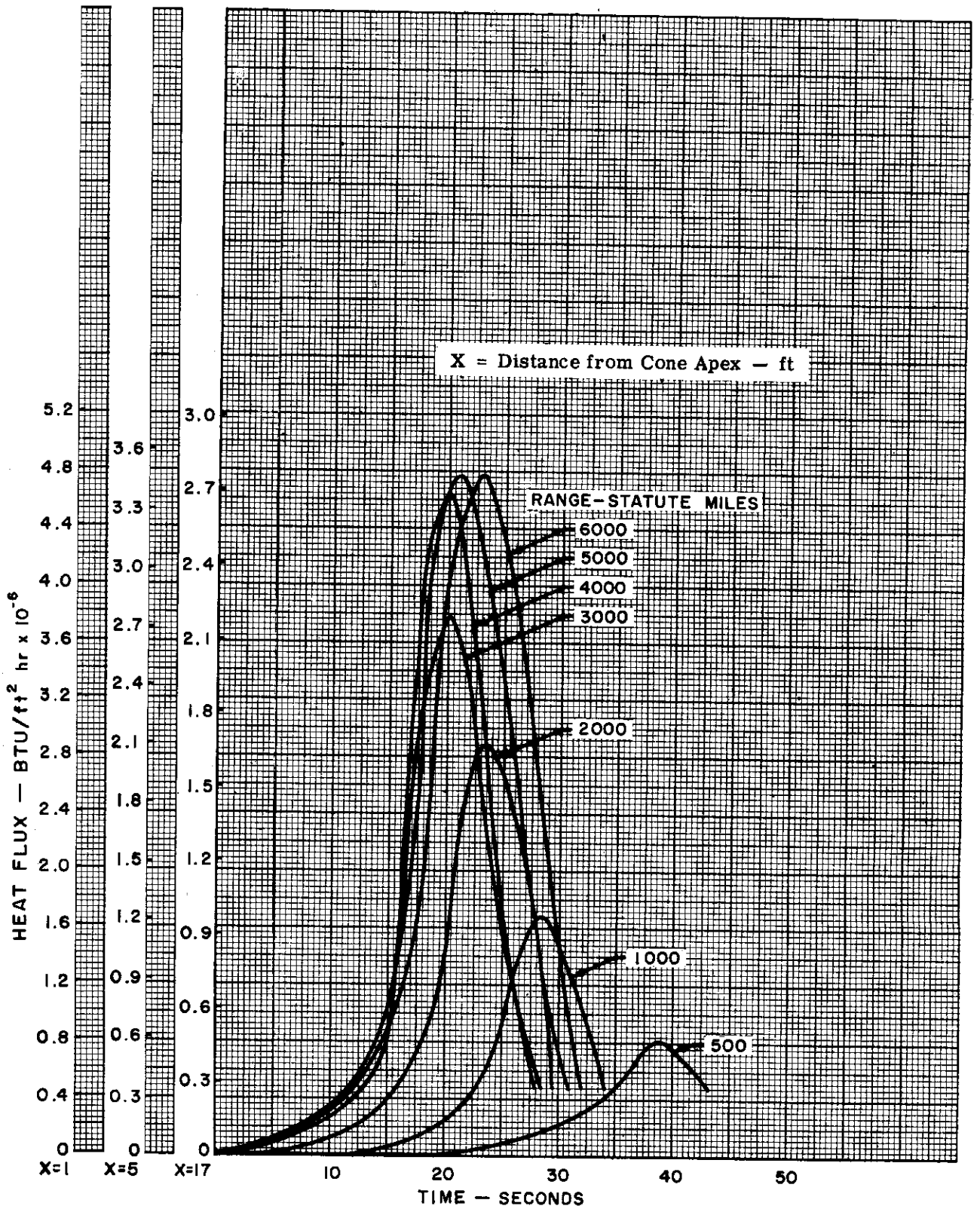

Figure II-14. Heat Flux Into Cooled Structure for Re-entry Flight, Mach 5.0 Stiking Velocity

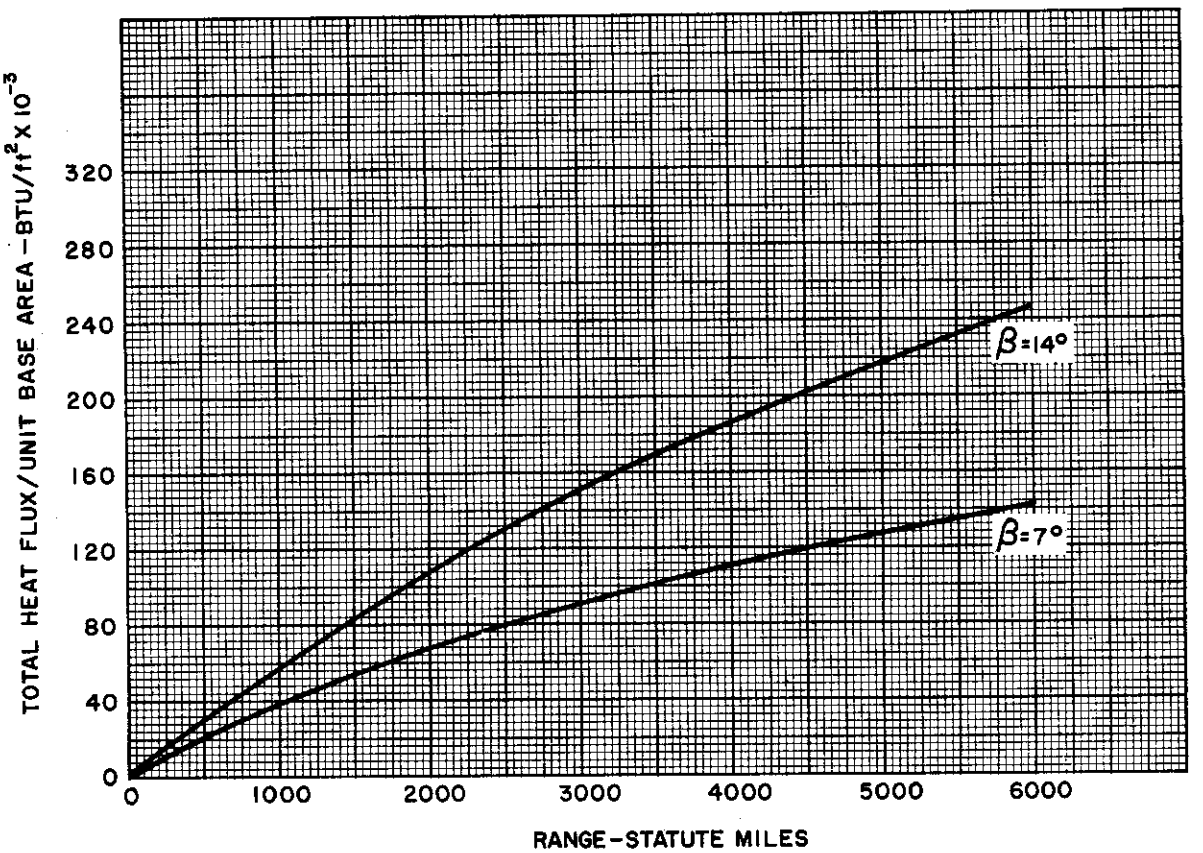

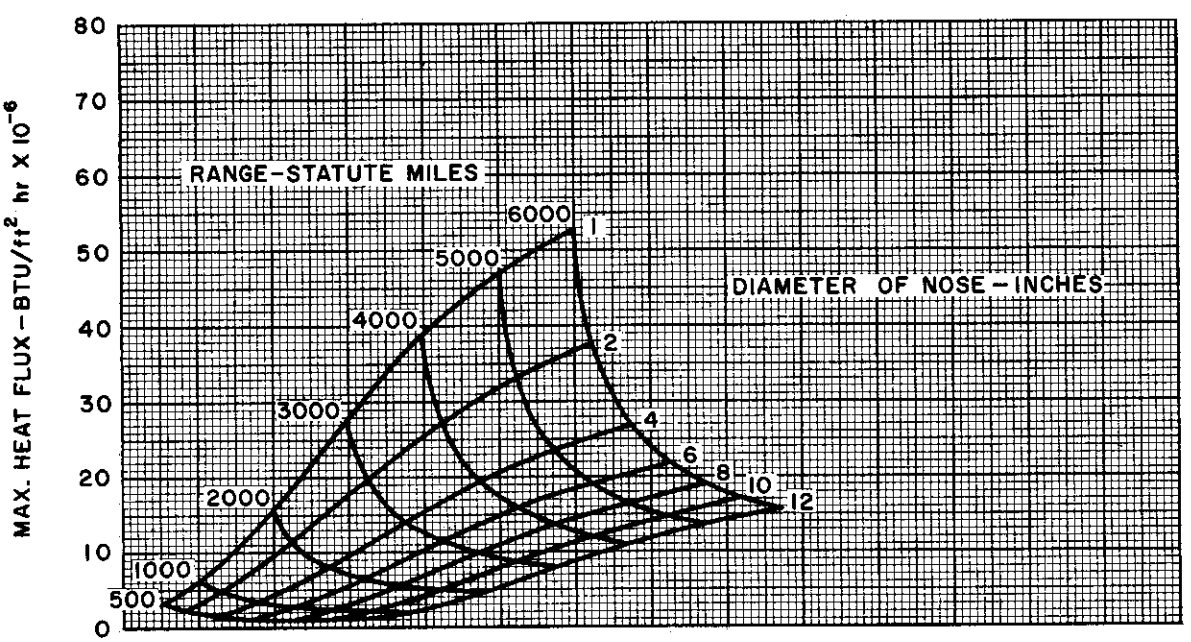

Figure II-15. Total Flux and Maximum Flux Intensity for Re-entry Flight, Mach 5.0 Striking Velocity

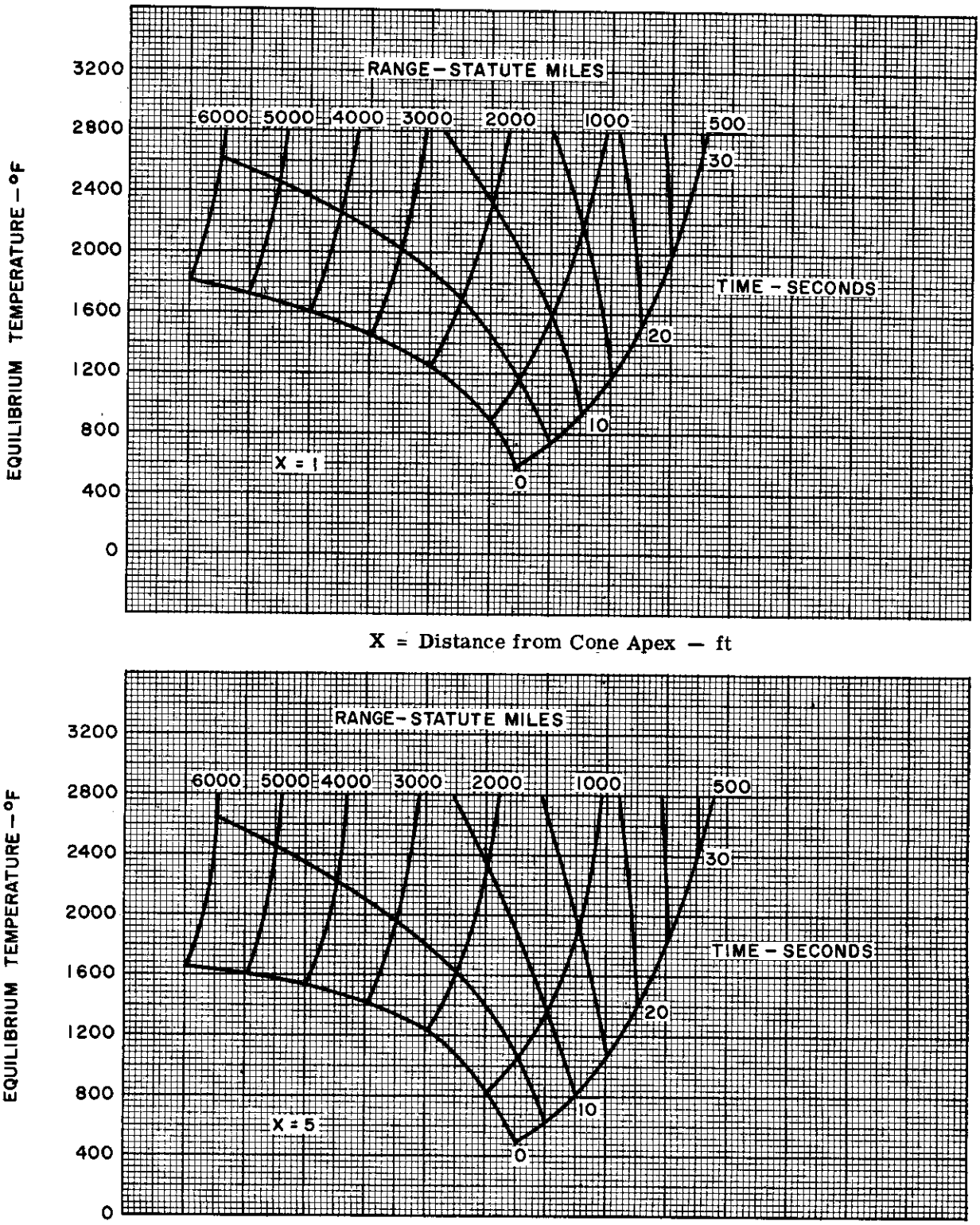

Figure II-16. Equilibrium Temperatures for Re-entry Flight, Mach 5.0 Striking Velocity

TABLE II-1

SUMMARY OF VEHICLES DEFINING MAXIMUM ENVIRONMENTAL CONDITIONS

Vehicle Type		Unmanned Vehicles — Expendable — High Longitudinal Accelerations		Manned Vehicles — Repeated Flights — Limited Accelerations	
		Power Plant		Power Plant	
		Rocket	Air-breathing	Rocket	Air-breathing
Long-and Medium-Range Bombardment	Re-entry Vehicle	Ballistic trajectory. Extreme temperatures and heating rates. Very short exposure time.			
	Booster Vehicles	Moderate temperatures and heating rates. Very short exposure time.			
	Bomber	Boost-glide flight path. High temperatures and heating rates. Moderate exposure time (max. 1-1/2 hours).	Climb-cruise flight path with turbojets. Low Mach numbers (3.0). Moderate temperatures and heating rates. Long exposure time (to 2-1/2 hours).	Similar to unmanned vehicles, except speeds will be higher for same radius since range is required for return.	Same as for unmanned vehicles, except exposure times may be doubled for same radius.
Long- and Medium-Range Bombardment			Boost-cruise with ram-jets. Moderate Mach numbers (3.0 to 5.0) Moderate exposure time (1 to 1-1/2 hours).		
	Bomb			Ballistic or glide flight path. High temperatures and heating rates. Short exposure time.	Conventional gravity bombs or a powered missile.

[redacted]

TABLE II-1 (cont)

Vehicle Type	Unmanned Vehicles — Expendable — High Longitudinal Accelerations		Manned Vehicles — Repeated Flights — Limited Accelerations	
	Power Plant		Power Plant	
	Rocket	Air-breathing	Rocket	Air-breathing
Reconnaissance			Same as for bomber, but no bomb.	Same as for bomber.
Short-Range Interceptor	Air or ground launch. Boost throughout flight. High temperatures. Short exposure time.	Air or ground launch. Cruise flight path, possibly with rocket boost for combat. Ram-jets may have rocket boost after launch. Moderate temperatures. Moderate exposure time.	Ground launch. Boost and possibly powered combat. Glide return. High temperatures and heating rates. Short exposure time.	Ground launch. Cruise flight path with rocket boost for combat. Ram-jet may have rocket boost at launch. Moderate temperatures. Short exposure time.

TABLE II-2

THERMAL INFORMATION REQUIRED FOR STRUCTURAL DESIGN

Flight Path	Type of Structure			
	Cooled	Insulated	Unprotected	
			Designed for Load	Designed as Heat Sink
Glide	Variation of heat flux with time.	Variation of equilibrium temperature with time.	Maximum equilibrium temperature.	Not practical.
Cruise	Heat flux (constant) and length of time acting.	Equilibrium temperature (constant) and length of time acting.	Maximum equilibrium temperature.	Not practical.
Boost	Variation of heat flux with time.	Variation of equilibrium temperature with time.	Average heat transfer coefficient. Maximum boundary layer temperature. Time of boost.	
Ballistic Reentry	Variation of heat flux with time.	Variation of equilibrium temperature with time.	Loadings expected to be less critical than heating	Total heat input.

[redacted]

NOTES

SECTION III

STRUCTURAL MATERIALS

By J. Padlog and A. Schnitt

TABLE OF CONTENTS

LIST OF TABLES

[redacted]

SECTION III

STRUCTURAL MATERIALS

A. GENERAL

With minor exceptions, all or some portion of the structure of high-speed aircraft must be capable of carrying load at elevated temperatures. As shown in Section II, the temperature ranges are greater than the melting point of the most heat-resistant alloy; consequently, for the design of efficient structures, the entire field of available materials requires investigation. Even materials heretofore disregarded because of high cost, low ductility, or low strength at room temperatures must be considered if they show promising characteristics at elevated temperatures; thus, the range of material types is greatly increased as well.

The amount of information required for the proper selection and use of materials at elevated temperatures is many times that required for room-temperature design. The thermal properties of specific heat, and the coefficients of thermal expansion and conductivity, are required because they are, in many cases, more important than mechanical properties. Thermal properties, moreover, change with temperature. The required information on mechanical properties is multiplied because of the following specific responses of materials to elevated temperature:

(1) Mechanical properties deteriorate with temperature and further deteriorate with time at temperature.

(2) At elevated temperature, materials may continue to exhibit both elastic and plastic properties under normal testing speeds.

(3) When the load is sustained for a period of time at stress levels even within the elastic range, the material may elongate or creep with no additional applied load.

(4) The creep rate increases nonlinearly with increase in temperature or stress, ending in failure or stress rupture in the case of tension.

(5) Materials exposed to elevated temperatures may lose part of their room and intermediate temperature strengths, and the loss may be influenced by the length of exposure time at elevated temperatures.

The time-temperature-loading conditions just described are quite simple compared with the temperature-loading history which a particular aircraft might experience. Since the variations in such histories are likely to be innumerable, such information on materials must be learned, for the time being, on an individual basis. The most important aspect of such histories is the cumulative effect of creep; many investigations are under way to devise methods for converting arbitrary sequences of intermittent temperature, time, and loading into a set of constant conditions of temperature, time, and loading.

The surface stability of materials is affected by the length of time at temperature. When surface instability exists, two solutions are possible. Additional material may be added to allow for the reduction in thicknesses expected for the life of the aircraft, or a protective, ceramic coating may be applied to the material. The latter approach introduces another branch of materials study for structures operating at elevated temperatures.

In this section is a general survey, a critical evaluation, and specific data on suitable materials that are available commercially. Most of the data that are considered more reliable are presented graphically in Part I, Section 2.0, in the form of stress-strain curves. Portions of the data on insulating and cooling materials are presented in Sections IV and V of this volume, which are devoted exclusively to the treatment of insulation and cooling; the remaining data are contained in Part I, Section 2.0.

[redacted]

Since a background of metallurgy is desirable for an understanding of the behavior of materials at elevated temperatures, brief discussions are given of the structure of metallic materials and the manner by which alloying, heat treatment, and work hardening raise the mechanical properties. Following this, the effects of elevated temperature on the structural and surface stability of materials are discussed, especially the phenomenon of creep. A critical review is presented of the recent attempts at correlating creep data under cyclic temperature, time, and stress, with creep data under constant temperature and stress.

Next, the general behavior, limitations, and suitability of available materials for service at elevated temperatures are discussed. The groups of materials considered are aluminum, magnesium, and titanium alloys; alloy steels; stainless steels; highly alloyed austenitic steels; nickel, cobalt, and chromium base alloys; molybdenum; tungsten; ceramics; and cermets. Summary tables are presented (supplemental to data shown in Section 2. 0 of Part I) to give the significant mechanical and thermal properties of these materials.

Finally, the cost and the fabrication methods that can be employed with the more uncommon materials are presented.

The data presented have been compiled from various reports of the NACA, reports of tests performed by other institutions, brochures and catalogs of other contractors, and unpublished test data. Many of these sources of information are mentioned in the bibliography at the end of this section.

B. BEHAVIOR OF MATERIALS AT ELEVATED TEMPERATURES

It is believed that a knowledge of the mechanisms that govern the behavior of materials at elevated temperatures is important for the proper application of such materials. In understanding the principles of material behavior, the engineer may make a reasonable prediction of the response of materials where previous test results are unavailable, and may also be in a position to evaluate his own test results more correctly.

First, the basic structure of metallic materials, and the microstructural changes that occur during exposure at different temperature levels, are reviewed briefly. Explanations are then given for the metallurgical changes obtained by cold working and heat treatment, so that the subsequent alteration in initial properties during exposure at elevated temperatures may be understood.

The suitability of a material for service at a given temperature, or in a given temperature range, will be governed by its structural stability; the importance of this fact and the factors influencing the stability of a material are discussed. The importance of the lack of surface stability as reflected by the ability of a material to resist oxidation and corrosion in various media is emphasized.

Because of the incidence of creep during elevated temperature service for most materials, it is important for design purposes to predict the life expectancy of a structural element subjected to complex heating and stressing spectrums. As an aid to predicting the life expectancy of a structural element, corresponding to rupture or a specified deformation, the mechanism and factors influencing the creep and stress rupture properties of metallic materials are discussed. In addition, the methods proposed for calculating the life expectancy of a structural part subjected to intermittent heating and stressing are reviewed.

For design purposes, the available creep and rupture data for various materials are compiled and correlated with the time-temperature parameter proposed by Larson and Miller. While the results of this correlation are presented as design curves in Part I, Section 2. 0, the procedure by which these curves are derived is explained herein.

1. Structure of Metallic Materials

The following is a general discussion of the structure of metallic materials. Although the treatment is by no means exhaustive, it attempts to explain the structural changes in materials resulting from heating and cooling, and to define such terms as critical temperatures and phases.

[redacted]Al

In the solid state, all metallic materials consist of minute crystals. These crystals, in turn, are composed of atoms arranged in a geometric pattern. The size and shape of the crystal formations, referred to as grains, depend upon the nature of the metal and its processing; for example, at room temperature, the elements iron, chromium, and molybdenum crystallize into a body-centered cubic lattice structure, and the elements aluminum and nickel crystallize into a face-centered cubic lattice.

In the molten state, the atoms are disordered, and upon cooling, crystals begin to grow at random points or nuclei. Because of the discontinuity at the grain boundaries, the material in the grain boundaries will be somewhat strained and will have properties different from those of the grains.

Alloys are formed by mixing two or more elements in the molten state to form a liquid solution. On cooling to the solid state, the alloy components may remain dissolved in each other forming a solid solution, or they may separate out wholly or partly, forming distinct crystals of each element and their combined forms. The combination of constituents that form a homogeneous material is called a phase, and this has a definite atomic arrangement and a unique set of characteristics.

Metals in solid solution form entirely new compounds and have properties completely different from those of the constituent elements. In solid solution, furthermore, the proportions of the elements are not fixed but may vary over a wide range, whereas the proportions of elements forming compounds are fixed. In alloys where the elements do not form solid solutions, they separate out into individual crystals forming a mechanical mixture.

Some of the elements crystallize into different space structures depending upon the temperature or pressure conditions. Representative of the so-called allotropic metals which behave in this way are iron, chromium, cobalt, manganese, nickel, tin, and tungsten. The ability of these metals and their alloys to transform or recrystallize from one crystal structure to another is important in controlling their properties by heat treatment. The temperatures at which changes in the crystal structure occur are called critical points. As an example of the way in which this phenomenon occurs, the element iron will be discussed.

On cooling from the molten state, pure iron crystallizes into a body-centered cubic structure, termed delta iron, and remains in this form until the temperature drops to 2570° F. Below this temperature, the crystal structure changes spontaneously to a face-centered cubic form, known as gamma iron, which remains stable until about 1670° F. Again, below 1670° F, the crystal structure changes back to a body-centered cubic structure called alpha iron. Between these critical temperatures, the crystalline structure or phase remains stable.

The addition of alloying elements changes the characteristics of the principal metallic element. Thus, the addition of small amounts of carbon to iron, for example, may alter the critical temperature at which phase changes take place. As an aid to understanding the metallurgical changes that occur in alloys when cooled or heated slowly, the iron-carbon alloys will be discussed.

When heated to the molten state, the carbon combines with a portion of the iron to form iron carbide. Upon cooling slowly, the alloy goes through various phases depending upon the carbon content. For example, when slowly cooling, an iron-carbon alloy containing 0.25% carbon forms a solid solution of carbon in gamma iron; this phase, called austenite, exists down to about 1500°F. Upon further cooling, the austenite decomposes and the ferrite phase forms, resulting in an austenite and ferrite mixture. Ferrite is pure iron and is soft. Between 1500° and 1350°F, the ferrite separating out is in the form of beta iron; below 1350°F, the beta iron transforms to alpha iron and the ferrite separating from the austenite in this temperature range goes directly into the alpha form. Below 1290° F, the remaining austenite breaks up into ferrite and cementite (iron carbide) forming a laminated structure called pearlite. The final structure at room temperature consists of pearlite and free ferrite. The ratio of pearlite to ferrite depends upon the percentage of carbon present. Thus, by altering the carbon content, the hardness of the material can be controlled. In general, the microstructure will transform in reverse order upon slow heating, but the critical points (or temperatures) at which phase changes occur will be slightly different.

[redacted]

2. Heat Treatment

The properties of a material exposed to elevated temperatures in service are influenced critically by the previous heat treatment of the material. The heat treatment process and the metallurgical changes incurred by the process are discussed briefly in an effort to explain the behavior of heat treated materials at all temperatures.

The purpose of heat treating metals is to relieve or balance internal stresses, or to change the structure so that a certain desired microstructure is obtained; depending upon the composition of the material, the chemical, mechanical, and physical properties may be altered. The common methods of heat treatment involve a crystal transformation process. This means that upon heating to a solid solution temperature, the structure of the metal undergoes crystal changes, and these changes may or may not be the same as those encountered previously on cooling.

The metallurgical changes that take place during heat treatment are a function of temperature and time. The temperature usually governs the rate at which structural changes take place, and the time determines the extent to which these changes progress. The changes that take place in any alloy, ferrous or nonferrous, depend upon the dominant material in the alloy. The response to the heat treatment process of the dominant material is affected by alloying elements.

The mechanism of strengthening or hardening an alloy susceptible to an allotropic transformation process by heat treatment can be explained, in general, as follows. In alloy steels, austenite is unstable at subcritical temperatures. Rapid cooling or quenching of the alloy steel from a temperature exceeding the critical point at which it is austenitic prevents its decomposition, and a structure known as martensite results at room temperature. Martensite, the hardest constituent in heat-treated steels, forms at a temperature that is dependent upon the alloy content. Slower cooling from the critical temperature permits the austenite to transform partially at subcritical temperatures, until at room temperature, weaker transformation products such as pearlite and bainite are present in addition to martensite. Since martensite is unstable, heating the martensitic steel to temperatures even below the critical temperature adds mobility to the molecules and starts decomposition. If the heating is controlled carefully (tempering), the brittleness of the hardened steel can be reduced by coalescing a definite amount of the carbon dissolved in the martensite. Heating beyond the critical point, followed by slow cooling, results in complete decomposition or transformation of the austenite, yielding a soft material of ferrite plus pearlite. Upon heating the hardened material, the constituents remain essentially stable below the tempering temperature, provided that the alloy was initially held long enough at the tempering temperature to allow the transformation reaction to go to completion. Thus, a steel hardened by tempering at a given temperature, for a time less than that required to give complete transformation, will not be stable when reheated to this or to lower temperatures. The degree of structural instability, and corresponding loss in strength and hardness, is dependent not only on the service temperature and exposure time, but also on the heat treatment. In general, commercially heat-treated alloy steels will be stable for fairly long times when operating at temperatures approximately 100° to 150° F below the tempering temperatures.

In addition to lowering the critical points, the presence of alloying elements tends to slow down the rate at which austenite transforms into pearlite, and into either ferrite or cementite. This decrease in transformation rate permits better control of heat treatment. Furthermore, with increasing alloy content, the temperature at which martensite begins to precipitate out of solid solution is decreased. If sufficient amounts of alloying elements are added, an austenitic structure (referred to as austenitic metal) will result at room temperature. The austenitic alloys thus formed are not affected materially by cooling or heating (because no phase changes occur), and consequently cannot be hardened by heat treatment. Most austenitic steels can be cold-worked to high strengths and, because of their high alloy content, have good resistance to corrosion and oxidation at elevated temperatures.

Many alloys attain high strength and hardness by an age-hardening or precipitation-hardening heat treatment process. The principle of precipitation hardening is based primarily upon the ability of the solute metals to be more soluble at higher temperatures than at lower temperatures. The process and mechanism involved is explained briefly as follows.

Complex compounds are formed by the addition of precipitation-hardening elements, such as titanium, columbium, or copper, to the base metal. When the alloy is heated to an elevated temperature for a period of time (solution treatment), temperature and time being dependent upon the alloy, the constituents form a solid solution. Cooling rapidly enough (quenching) leaves the solute in solid solution (supersaturated solution). Since the solid solution state is unstable at temperatures below the solution temperature, controlled heating or aging is then performed at the proper temperature. This causes the precipitation of the solute phase, and the complex compounds tend to grow from nuclei appearing at the grain boundaries and in strained regions. The hardening that results from this process is believed to be produced by the distortion of the lattice structure during the first stages of precipitation. The aging temperature and time have a marked influence on the resulting properties; to obtain optimum properties, these factors must be controlled within narrow limits.

The structure of the precipitation-hardened material is unstable at temperatures that are slightly less than or greater than the aging temperature. Additional heating in the vicinity of, or above, the aging temperature causes an agglomeration of precipitation particles; consequently, a decrease in the optimum properties (overaging) results. The higher the temperature and the longer the exposure time, the more rapidly will the alloy approach the annealed condition. For some age-hardenable materials, the loss in initial properties from overaging can be recovered by additional exposure at the aging temperature.

3. Work Hardening

The work hardening process by which the strength of metals is increased is described herein. The response of such metals to elevated temperatures is discussed in terms of the metallurgical aspects of the work-hardening process, mainly recrystallization. The equicohesive temperature is defined.

Work hardening is a process in which a metal or alloy is hardened and strengthened by permanent deformation performed within certain temperature ranges. Work hardening, a rather complex phenomenon, is not yet entirely or satisfactorily explained; however, it is believed that during work hardening, a complex process of slip takes place within and between the grains and this results in a strained crystal structure.

The effects of work hardening on mechanical properties are well known. Work hardening is influenced by factors such as (1) the dominant metal in the alloy, (2) the alloying element or elements and their concentration, (3) the temperature and time, and (4) the type, rate, and amount of deformation.

When a cold-worked or work-hardened material is heated below a certain temperature or range of temperatures, the properties obtained by cold working will not be altered and the locked-in stresses due to cold work will not be relieved. However, for another particular temperature or range of temperatures and time, the internal stresses will be decreased or balanced. In this process, known as stress relief or recovery, there will be little change in the crystal structure or mechanical properties, except that the yield stress may be increased. When the material is heated above the temperature to produce stress relief, the strained crystal structure in the cold-worked metal will start to recrystallize as the metal structure approaches its unstressed condition. Since recrystallization is a rate process, the temperature at which it occurs will depend upon the degree of cold work and the time of heating. For a given heating time, the temperature to cause recrystallization generally becomes less with increasing amounts of cold work; for a constant amount of cold work, the recrystallization temperature falls off with increasing time at temperature. If a material is heated after it has recrystallized, its grain size increases at a rate depending upon the temperature until an equilibrium grain size, also dependent upon the temperature, is attained.

It seems appropriate to discuss the equicohesive temperature for any given metal or alloy. The lowest temperature at which recrystallization occurs corresponds with the equicohesive temperature of the material. In passing through the equicohesive temperature from a lower to a higher temperature, the mode of fracture within the material changes from a transcrystalline fracture (failure through the grains) to an intercrystalline fracture (failure around the grains). Since this

[redacted]

change in mode of failure is significant in the understanding of creep, the implications of the equicohesive strength is discussed further in Section III, B.

4. Structural Stability

The term structural stability is used to define the retention of some specific material property such as strength, ductility, or shock resistance during exposure to stress or temperature, or both stress and temperature. Structural instability may manifest itself by carbide precipitation, spheroidization, sigma-phase formation, temper embrittlement, structural transformation, and precipitation-aging effects (discussed previously). The effects of stress, time, and temperature on the properties of materials are complicated by the lack of stability. Usually, instability is clearly indicated in short-time tests.

In obtaining short-time strength properties at elevated temperatures, a specimen is heated for a predetermined time, usually for 30 minutes or less, and then loaded at a normal strain rate until failure occurs. By conducting short-time tensile strength tests at various temperatures, an indication of the stability of the material is obtained. In general, by plotting tensile strength vs. temperature, a flat curve indicates stability and good long-time (creep) properties at elevated temperatures, while a curve that slopes downward with increasing temperature indicates a relatively unstable material; the degree of instability increases with increasing slope.

For a given temperature range, a material may show stability, or no loss in strength, under long-time temperature exposure and short-time loading. This indicates that the properties of the material are independent of time of exposure. Heating above this temperature range results in a loss in strength with increasing time of exposure. To illustrate the effect of exposure time at elevated temperatures on the short-time tensile properties, Inconel X sheet age-hardened at 1300° F for 20 hours is examined. The effect of exposure time of approximately 2 hours at various temperatures ranging from 1300° to 1700° F on the short-time tensile properties of this material at all temperatures is given in Figure 2.2-40 of Part I; the reduction in tensile strength indicated in this figure at any temperature is based upon room temperature hardness. The data, although approximate, indicate the sharp reduction in the short-time tensile strength of Inconel X when exposed to temperatures above the aging temperature of the metal.

5. Surface Stability

Surface stability is one of the most important properties to look for when selecting materials for use at elevated temperatures. When corrosion or oxidation is severe, the material thickness may be reduced enough to warrant its allowance in design. Not only oxidation, the result of oxygen combining with the material constituents, but corrosion, the result of attack by other media are generally increased with increasing temperature. The three types of attack are defined as:

(1) General - a uniformly scaled or corroded surface

(2) Pitting - a nonuniform attack of scaling or corrosion

(3) Intergranular - an attack in the grain boundaries

Intergranular oxidation or corrosion is the most dangerous since it is not evident on the surface.

Since oxidation and corrosion are time-dependent, a material may be satisfactory for short-time use at temperatures higher than the maximum temperature at which attack is considered negligible for continuous service.

Intermittent stressing and heating is generally more severe because the protective scale may crack or separate from the material, exposing new surfaces to attack.

6. Creep

The application of a constant load to a material at a stress below the proportional limit or yield stress, and at room temperature and relatively low temperatures, results in a deformation which remains constant and independent of time. For the purposes of analysis, this is assumed to be true in the plastic region although increased straining with time is known to take place. At

[redacted]

sufficiently high temperatures, the material will deform plastically (creep) with time even at stresses below the proportional limit as determined by normal straining rates. The many factors influencing the creep and rupture properties of metallic materials are discussed briefly. In addition, the methods for extending the conventional constant stress-constant temperature creep and rupture data to the more complex condition of random loading and stressing are reviewed. The method used to develop the master creep and rupture curves presented in Part I, Section 2.0 for various materials is explained.

a. Creep Under Constant Temperature and Load

Typical creep data as obtained in a constant tension load-constant temperature test are shown in the following diagram. The initial extension that occurs with loading represents the elastic strain. Creep which follows generally portrays three stages, and these are known as primary, secondary, and tertiary creep. During the primary stage, strain hardening overcomes creep at an accelerating rate; in the secondary stage, the creep rate is constant; and in the tertiary stage, the creep rate increases exponentially ending in fracture. The accelerated creep rate during the third stage is believed to be caused primarily by a reduction in the cross-sectional area either by necking or by localized intercrystalline fissures.

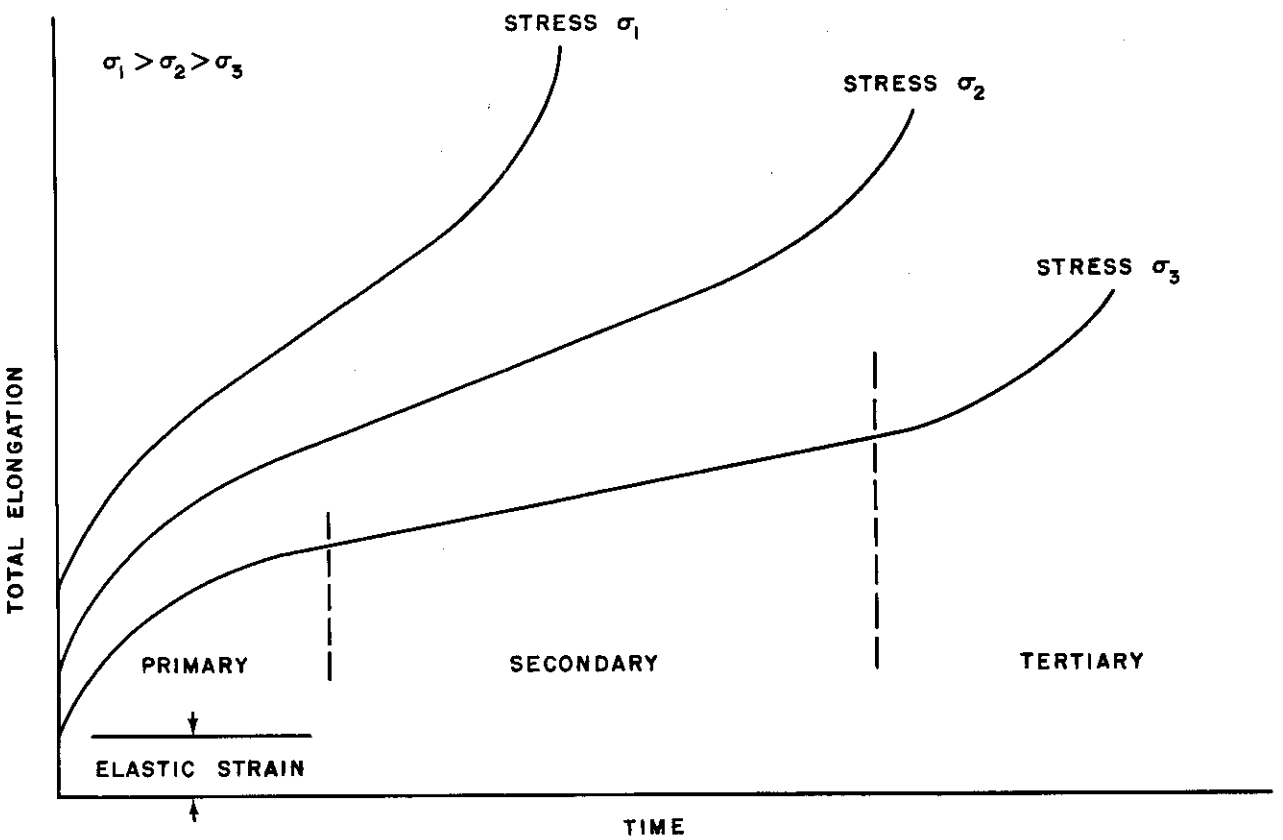

The equicohesive temperature, as noted previously, is significant regarding the creep of materials. The creep deformation of a material subjected to stress and to temperatures exceeding its equicohesive temperature, or lowest temperature of recrystallization, depends upon the rate at which strain-hardening caused by yielding is recovered by the recrystallization process. At or below the equicohesive temperature, strain-hardening predominates, and continuous creep does not occur except when the stresses are great enough to overcome the resistance produced by strain-hardening. Above this temperature, the rate of recrystallization governs, resulting in continuous creep even at low stresses.

Creep properties are more sensitive to minor variations in the metallurgical structure of a metal than are the other commonly measured strength properties. Test samples obtained from the same heat or from the same stock may show large variations in creep rate, although not as large a variation as samples obtained from different heats or sources.

There are numerous variables which have a marked influence on the creep properties of materials; many of these have not been investigated completely. Some of the important factors affecting creep strength yet to be discussed are structural stability, heat treatment, cold work or previous deformation, surface stability, and grain size.

The structural stability of a material either heat-treated or cold-worked has an important effect on creep resistance at elevated temperatures. Operating at temperatures above which the alloy is stable, ultimately reduces the constituents to the annealed form. For a given operating temperature, there is a particular heat treatment or cold work process that will result in maximum stability and minimum creep at the operating temperature. The optimum hardness process may not result in maximum strength properties at room temperature; consequently, a material should have different heat treatments specified depending upon the range of the operating temperature. Moreover, when comparing the short-time strength properties of materials at the operating temperature, the higher strength material does not, in general, represent greater creep resistance.

In some instances, structural instability in a material occurring at the operating temperature will have little effect on the creep strength. For example, carbide precipitation occurring in the grain boundaries of the austenitic chromium-nickel steels at 900° F and higher have little if any effect on the creep strength. However, the formation of the sigma phase in certain steels has a pronounced weakening influence on the high-temperature creep resistance of the steel.

Tests indicate that a material having a coarse grain has higher creep resistance than one having a fine grain. The explanation for this phenomenon is that, at temperatures above the equicohesive temperature, the material in the grain boundary is weaker than the grains; consequently, larger grains will result in less grain boundary material and higher creep strength.

The decrease in load-carrying area caused by oxidation or corrosion increases true stress and, consequently, decreases creep strength. The magnitude of the scaling or surface instability depends upon the factors discussed previously. If the oxides or other compounds flake off under creep deformation, an accelerated process will result including decreased material thickness, increased stress, and increased creep.

b. Intermittent Stressing and Heating

It is more probable that the structural components of the airframe of a high-speed aircraft will be subjected to complex conditions of heating and stressing, rather than to the simple conditions of constant stress and temperature for which most of the creep and rupture data have been obtained. Depending upon service conditions, each structural element will be subjected to variations in stress and temperature level during the life of the structure; furthermore, for design purposes, the life expectancy of the structural element must be determined, corresponding to a particular failure criterion such as time to rupture, time to a specified total deformation, or time for creep buckling. The intent here is to review and present the methods available for determining the life expectancy of structural materials subjected to random temperature and stressing conditions.

Many investigations have been and are being performed to determine the creep deformation and strength properties of materials under intermittent stressing at constant temperature, intermittent heating at constant stress, and combined intermittent stressing and heating. Preliminary results indicate that, for some materials, conventional creep and rupture data from constant load-constant temperature tests can be used to predict creep deformation and rupture under arbitrary sequences.

c. Intermittent Stressing at Constant Temperature

From cyclic stressing or periodic overstressing tests it was found that, for a given ratio of overload time to normal time, the creep characteristics of various materials were not affected

significantly by various timing patterns of overload application. Also, the application of overloads for relatively small percentages of the total time produced increases in creep deformation and reduced time to rupture. The test results for these two conditions of intermittent stressing indicated that the total creep is equivalent to the net time spent at each stress level. This suggested the following formula to predict rupture time, or time to produce a given total creep deformation, for randomly applied loads and constant temperature:

$$\sum \frac{\theta_i}{\theta_{L_i}} = \frac{\theta_i}{\theta_{L_i}} + \frac{\theta_2}{\theta_{L_2}} + \frac{\theta_3}{\theta_{L_3}} + --+ \frac{\theta_n}{\theta_{L_n}} = 1 , \qquad (1)$$

where θ_i equals total time in service that the metal will be subjected to stress σ_i and temperature T_i ; and θ_{L_i} equals time to rupture, or time to obtain a specific total creep deformation under stress σ_i and temperature T_i corresponding with constant load-constant temperature creep and rupture data.

In comparing data obtained from cyclic stress-constant temperature tests, the discrepancies between the calculated times for specified amounts of creep deformation or times to fracture were generally of the order of 25 to 50%. A few discrepancies as high as 100% were found; however, on a basis of stress rather than time, these amounted to a difference of only 5 to 10%.

d. Intermittent Heating at Constant Stress

The cumulative creep hypothesis upon which Equation (1) is based was applied to the case of constant stress and intermittent rectangular, saw tooth, and special (impulse-type) temperature cycles to determine analytically the time to rupture. The test rupture lives obtained for the various tests fell substantially between the calculated value and one-half the calculated value; however, the maximum difference between the experimental and calculated life time corresponded with a discrepancy in stress of only 10%. It was presumed that for some of the materials tested, the error was due to metallurgical instability, as discussed previously.

e. Combined Intermittent Stressing and Heating

This type of loading, a much more complicated case than those discussed previously, has not as yet been investigated sufficiently. It appears plausible, however, that Equation (1) can be extended to this case as well by computing fractions of stress rupture life or creep deformation life obtained under various conditions of stressing and heating. This equation, however, may yield large errors if the applied stress and temperature combinations cause significant metallurgical changes that greatly affect the strength of the material. In general, when the microstructure or external surface is not altered by temperature, stress, time, and environment, creep and rupture behavior may be expected to be the same for constant and intermittent stressing and heating conditions.

f. Correlation of Creep and Rupture Data

The constant-temperature, constant-load creep and rupture data from available literature for materials of interest are not usually complete for all deformations, stresses, temperatures, and times desirable in practice. Therefore, methods forcorrelating the data irrespective of material are required to permit interpolation or extrapolation. Of the many attempts to accomplish this, the parameter derived from the rate-process theory by Larson and Miller performs this correlation satisfactorily for a wide range of times and temperatures, and for such materials as steels, high-temperature alloys, and aluminum alloys.

Although the Larson-Miller parameter was correlated both for large strains of the order of 1 to 2% total deformation and for rupture, it is desirable, for the purposes of stress analysis, to determine the time-temperature-stress-deformation relationship for materials where total deformations are much smaller. Therefore, the use of this parameter was extended to the low deformation range of materials in this study and, for reasons discussed later, is considered satisfactory.

The simple Larson-Miller time-temperature parameter used to correlate creep and stress rupture data has the form

$$(T + 460)(C + \log_{10}\theta), \tag{2}$$

where T is the temperature in degrees Fahrenheit, θ is the time in hours to rupture or to a specified strain, and C is a constant. When this parameter is plotted against stress, a master stress-rupture or creep curve is obtained.

A value of C equal to 20 was found to be satisfactory for many materials when correlating rupture and creep data; however, there are indications that C is not a constant. In the correlation of data in this report, a constant of 20 is used for all materials because it was found that the spread in creep data overshadowed this assumption.

Because of the lack of creep data for small strains, the short-time compressive stress-strain curves were used to extend the master creep curves to smaller total strains. This was done with the conservative assumption that the stress at a particular strain on the short-time stress-strain curve was constant for a time equal to the strain divided by the test strain rate belonging to the stress-strain curve. In this way, master creep curves were obtained matching the compressive stress-strain curves. Since the stress-strain curves correspond with standard yield stress, the possible contradiction of creep and short-time data is eliminated.

The creep data were obtained from tensile constant-load creep tests and were assumed to be equal to the compression creep properties; however, these data may prove somewhat inaccurate when results of compressive creep tests become available.

In addition, this method of correlating creep properties of a material assumes that creep takes place at all stress levels and temperatures. This assumption is valid at the higher temperatures, but is not necessarily correct at the lower temperatures, especially at the lower stress levels.

The master creep and rupture curves present in Part I, Section 2. 0, were prepared from creep test data corresponding with times less than or slightly greater than 200 hours. Because the master creep curves are based upon the short-time compressive properties corresponding with an exposure time at temperature of one-half hour, they should be used with caution if temperature exposure times are less than one-half hour.

C. DISCUSSION OF MATERIALS FOR USE AT ELEVATED TEMPERATURES

Since the temperatures developed during high-speed flight will vary in magnitude throughout the airframe as a result of location or controlled cooling, it becomes necessary for optimum design to investigate all structural materials. There is a wide range of materials that may meet the requirements of service condition.

The materials discussed in this section include the ferrous and nonferrous metals, ceramics, and cermets.

In general, the heat-resistant alloys that are available commercially lose their strength appreciably beyond 1600° F, and have little usable strength aboe 1800° F for service times greater than 1000 hours. However, many of these alloys can be used for intermittent short-time service at temperatures as high as 2400° F. The recently developed cermets have long-time strengths that are, in general, more than double that of the best commercial high-temperature alloy at temperatures of 1600° and 1800° F; however, above 2000° F their strength and oxidation resistance is comparable to the best high-temperature alloys. For temperatures of 2000° F and above, ceramic materials have great superiority over all other materials since they retain their strength and are oxidation resistant.

The various available materials suitable for elevated temperature service are discussed with emphasis on (1) the manner in which the material attains optimum strength, (2) material behavior at elevated temperatures, and (3) material limitations.

1. Aluminum Alloys

The commonly used high-strength aluminum alloys are based upon alloy systems containing copper, magnesium, silicon, zinc, etc. Wrought aluminum alloys based upon copper contain from 2.5 to 5.5% copper and small quantities of other elements such as magnesium and manganese. Examples of such aluminum, copper-bearing alloys are 2017 (4% Cu) and 2024 (4.5% Cu). A typical high-strength aluminum alloy based upon magnesium and silicon is 6061. The aluminum alloys having the highest room-temperature strength are based upon zinc; such an alloy is 7075 (5.6% Zn).

These commercial aluminum alloys attain high room-temperature strengths after being given a precipitation-hardening or age-hardening heat treatment. The precipitation-hardening heat treatment process for these alloys consists of a solution heat treatment in the range of 825° to 980° F, followed by aging at lower temperatures. Aluminum alloy 2024 attains 90% of its full room-temperature strength when naturally aged at room temperature for 24 hours, and its full strength when artificially aged at 350° F for 6 hours. For optimum room-temperature strengths, aluminum alloy 6061 is aged at 320° F for 16 to 20 hours and alloy 7075 is aged at 250° F for 24 to 28 hours. When initially underaged, these alloys may be strengthened by additional aging at elevated temperatures, but with consequent decrease in ductility. Such is usually the case for alloy 2024 when solution heat-treated and aged (T6 and T4 conditions). The strength of these alloys can be increased by additional cold work, but with a consequent decrease in ductility and formability.

The precipitation-hardened aluminum alloys become structurally unstable when exposed to temperature in the vicinity or above the aging temperature with subsequent loss in strength. Heating to temperatures 100° F below the aging temperature for a sufficient time will eventually anneal these alloys. The temperature at which the materials will maintain their original properties depends critically upon the time of exposure at temperature. Prolonged heating of 2024-T4 aluminum alloy at temperatures above 200° F will result in a decrease in room-temperature ultimate strength, but the room-temperature tensile yield stress will not be decreased when exposure is for long times at temperatures up to 300° F. The room-temperature properties of 7075-T6 aluminum alloy are greatly decreased after exposure for long times at temperatures above 150° F, but for short-time exposures of approximately 30 minutes, this alloy will remain structurally stable under exposure temperatures up to 250° F.

In general, the short-time strength of the aluminum alloys decrease with temperature; however, at temperatures above the aging temperature, the decrease becomes more rapid. At lower temperatures, 7075-T6 has superior short-time properties; at higher temperatures 2024-T3 is superior.

Creep becomes significant for 7075 aluminum alloy at temperatures above approximately 150° F for exposure times greater than 100 hours; creep becomes important for 2024 aluminum at approximately 250° F. For temperatures above 300° F, 2024 aluminum alloy has superior creep strength as compared with other sheet aluminum alloys.

2. Magnesium Alloys

Magnesium yields alloys with excellent properties and high ratios of strength-to-weight when alloyed with small amounts of other metals such as aluminum, manganese, zirconium, zinc, rare earth metals, and thorium. Proper combinations of these alloying constituents provide alloys with valuable high-temperature properties. Unfortunately, the casting alloys have the best elevated-temperature properties; however, future developments may make these alloys available in wrought products.

The common commercial magnesium alloys that are available in sheet form and may be considered for elevated temperature application are FS1 alloy (2.5 to 3.5% Al, 1.2% Mn) and M

alloy (0.7 to 1.3% Zn, 0.08 to 0.14% Cu). These alloys cannot be heat treated, but obtain their optimum properties when strain-hardened and partly annealed (the H24 condition). The FS1 alloy shows superior strength properties to the M alloy at all temperatures. Both alloys become unstable at approximately 300° F. They experience little effect on strength at temperature for exposure times up to 1000 hours; however, exposure at temperatures above approximately 250° F decreases room-temperature properties appreciably. At approximately 150° F, these alloys start to lose their short-time strength rapidly. Creep and stress-rupture strength become important for design at approximately 150° F; at temperatures above 300° F, creep and rupture strengths are reduced considerably.

A recently developed high-temperature magnesium-thorium alloy, HK-31 (3% Th and 0.5 to 0.7% Zr), has greater short-time and creep strength than the aluminum alloys at and above approximately 450° F. To obtain optimum strength properties in the range of 300° F to 700° F, HK-31 is either strain-hardened or heat-treated. The T6 heat treat condition (solution heat-treated at 1050° F and aged at 850° F for 1/2 hour) appears to give the best short-time and creep properties above 300° F, although complete test results are not available. The short-time strength of this material begins to decrease rapidly at 600° F. Its creep properties become an important consideration for design at temperatures above approximately 300° F.

3. Titanium Alloys

The favorable atomic size of titanium and its other fundamental properties make alloying possible with nearly all other useful metals. Because of the relatively high melting point of titanium, approximately 3150° F, its alloys show promise of application above 1000° F. However, this high melting point limits its alloying to those metals having low volatilization rates.

The principal metals added to commercial titanium alloys are aluminum, molybdenum, tin, chromium, vanadium, and manganese. The three types of crystal structures obtained from alloying additions are alpha, beta, and combined alpha-beta. The general properties inherent in each are (1) alpha-good weldability, tough and strong both hot and cold, resistant to oxidation, fair formability, (2) beta-excellent ductility, strong both hot and cold, vulnerable to contamination with hydrogen, oxygen, and nitrogen, and (3) combined alpha-beta-strong both cold and warm, but weak hot, good weldability, excellent forgeability.

The titanium alloys available in sheet form are C-110M (8% Mn), 6 Al-4 V, and A-110AT (6% Al, 2.5% Sn). These alloys are used in the annealed condition, but recent investigations on the 6 Al-4 V alloy show an improvement in properties by heat treatment.

Titanium and its alloys have unique creep properties. At temperatures from 80° F to 400° F, these materials creep at stresses below the yield stress. At temperatures between 400° and 600° F, creep is negligible; above 600° F, the creep rate increases to a point where the creep strength falls below the yield stress. Between room temperature and 600° F, C-110M alloy shows a much greater resistance to creep than A-110AT alloy; at 800° F, the A-110AT shows a substantial increase in resistance over C-110M alloy. These two alloys have the same room-temperature strength properties and yet show marked differences in creep properties.

The commercial titanium alloys lose their short-time strength rapidly from room temperature to 400° F. Only a slight loss of strength is noted between 400° F and 600° F, but the strength drops rapidly above 600° F. The stability of these alloys has not been investigated fully, but recent results on 6 Al-4 V alloy show it to be stable up to temperatures of 800° F after 200 hours exposure.

One characteristic of titanium is its excellent corrosion resistance in oxidizing liquid media, but poor resistance in reducing liquid media. The reaction of titanium to oxygen, nitrogen, or hydrogen gas at moderate temperatures is one of its undesirable features; the resultant oxides, nitrides, and hydrides are soluble in titanium and their solution causes a rapid strengthening and embrittling of the base metal. Hydrogen and nitrogen diffuse directly into the titanium, and oxygen forms a scale at approximately 500° F. No data are available to establish a maximum

service temperature below which contamination in air will be insignificant. In general, a maximum service temperature between 800° and 1000° F seems practical for long-time service in air.

The welding technique employed with titanium alloys is critical because of its susceptibility to absorb gases. The titanium alloys A-110AT and 6 Al-4 V can be fusion-welded or resistance-welded easily with resulting good ductility and strength, provided that approved welding procedures are followed.

4. Alloy Steels

Alloy steels consist of iron to which is added carbon and small percentages of other elements that modify the properties of the steel. The added elements may be divided into two classes, carbide-forming and noncarbide-forming. Those that form carbides will remove some of the carbon from the iron and will introduce the effects of their own carbides in place of iron carbide. Elements that form carbides are manganese, chromium, titanium, vanadium, molybdenum, tungsten, and columbium. Elements that do not form carbides are copper, nickel, cobalt, silicon, aluminum, and zinc.

Molybdenum or tungsten are present in small percentages primarily to improve strength. Chromium is added in quantities up to 10% to increase corrosion and oxidation resistance; when present in small amounts, it increases hardness and strength. The addition of small amounts of nickel improves strength and increases corrosion resistance, especially when in the presence of other elements such as chromium.

The alloy steels discussed thus far are martensitic and can be heat-treated to high room-temperature strengths. The higher chromium content steels (4 to 10% Cr) have good oxidation resistance up to approximately 1300° F, but lose their high strength obtained by heat treatment at approximately the same temperatures as do the steels containing less than 3% chromium. The latter alloys are oxidation-resistant up to approximately 1100° F. Consequently, steels containing more than 3% chromium are of value at elevated temperatures when corrosion or oxidation resistance governs design.

Aircraft quality alloy steels such as AISI 4140, 4340, 8630, and HY-Tuf contain small percentages of alloy elements (less than 3% chromium) and offer high strength in the heat-treated condition. However, the desirability of using these steels repeatedly at elevated temperatures depends upon the temperature and time of exposure. Once the tempering temperature for any given room-temperature strength is exceeded, or exposure times increased beyond a predetermined period, these steels lose their stability. The SAE 4340 nickel-chromium alloy steel can be heat-treated to over 300,000 psi room-temperature ultimate tensile strength, but for exposure temperatures approximately at and above 400° F, this strength will be lost. When this alloy is heat treated to 200,000 psi room-temperature ultimate tensile strength by tempering at 800° F, it becomes metallurgically unstable when subjected to temperatures above approximately 600° F, thereby resulting in loss of the original room-temperature strength.

The advantages of alloy steels are ease of forming, welding, and high strength at the lower temperatures. By proper alloying any desired set of properties may be obtained at a relatively low cost.

5. Stainless Steels

The stainless steels may be divided into three main groups: (1) the straight chromium stainless steels (AISI 400 series, martensitic and ferritic), (2) the austenitic stainless steels (AISI 300 series), and (3) the age- or precipitation-hardening stainless steels of the 18-8 type.

The straight chromium stainless steels contain from 11 to 27% chromium and small amounts of nickel (about 0.5%). Types 403 (12% Cr), 410 (12% Cr), 416 (14% Cr), 420 (14% Cr), and 431 (17% Cr) are martensitic and can be hardened by heat treatment. Types 405 (13% Cr) and 446 (27% Cr) are ferritic and can not be hardened by heat treatment. Depending upon the chromium content, type 430 may be either martensitic or ferritic. At temperatures above 800° F, the strength of these steels drops off rapidly; beyond 1200° F, their strength is relatively low. These stainless steels are used at elevated temperatures primarily because of

[redacted]

their oxidation and corrosion resistance which increases with chromium content. The martensitic grades are fully oxidation-resistant below the temperature range 1300° to 1400° F, and the ferritic grades below the temperature range 1500° to 2000° F.

The martensitic grades can be heat-treated to room-temperature ultimate strengths above 200,000 psi when quenched and tempered from between about 300° and 1300° F, depending upon the composition. The tempering temperatures in the range of 700° to 1000° F should be avoided since these temperatures result in poor impact strength. In thin sections, the martensitic grades are air-hardening and this is a disadvantage where annealed material must be welded.

The austenitic stainless steels contain more than 7% nickel in addition to high percentages of chromium (11 to 25%). These steels may be divided broadly into three groups according to the percentage of chromium and nickel content. These groups are (1) 18-8 type: AISI 302 and 304, and the modified grades AISI 316, 321, and 347; (2) 25-12 type: AISI 309; and (3) 25-20 type: AISI 310 and 314.

These steels are used commercially because of their high resistance to oxidation at elevated temperatures and their low corrosion rate in various media. The 18-8 types are fully oxidation-resistant up to about 1600° F, and the other grades are fully oxidation-resistant up to about 2000° F.

When heated in the range from about 900° to 1300° F, all the austenitic grades except the modified 18-8 types are susceptable to carbide precipitation in the grain boundaries, and this can lead to intergranular corrosion or oxidation.

The austenitic grades have greater strength than the martensitic or ferritic grades at elevated temperatures. The 18-8 types have good strength up to 1500° F, and type 316 exceeds the other grades in creep and rupture strength because of its m[redacted]um content. The austenitic steels can be hardened only by cold-working. The cold-worked [redacted]s in which strengths are attained up to and including 300,000 psi offer little to increasing the high-temperature properties; when heated to temperatures above about 800° F, the cold-worked material will recrystallize and assume, in time, the elevated temperature properties of annealed material.

The higher chromium grades 25-12 and 25-20 are used above 1500° F since their high alloy content prevents excessive scaling; such temperatures would lead to early failure for the 18-8 type.

The precipitation-hardening stainless steels are primarily modifications of the austenitic 18-8 chromium-nickel stainless steels. Their age-hardening characteristics are obtained by the addition of small percentages of titanium, aluminum, copper, and beryllium. Representative commercial alloys in this class are 17-7 PH, Stainless W, and Allegheny metal 350. They can be age-hardened to a room-temperature tensile strength ranging from 200,000 to 225,000 psi without appreciable loss in ductility. In addition, their room-temperature tensile strength can be increased to more than 250,000 psi by suitable cold work and aging treatments, but with a corresponding loss in ductility. These materials are aged at temperatures from 900° to 1200° F, the higher strength being obtained at the lower aging temperatures. Their short-time properties begin to drop off rapidly between 600° and 800° F, depending upon the aging temperature; however, most of their strength is maintained up to 1000° F. Above approximately 900° F, these alloys become metallurgically unstable and have little advantage over the ordinary austenitic stainless steels.

6. Highly Alloyed Austenitic Steels

The highly alloyed austenitic steels may be divided into two groups according to the way they obtain their high strength at elevated temperatures: (1) cold- or hot-worked austenitic steels, and (2) precipitation-hardening austenitic steels.

The first group of alloys are primarily chromium-nickel-iron alloys containing small amounts of one or more other elements such as molybdenum, tungsten, titanium, and columbium. The optimum strengths are obtained primarily by cold working at room temperature or hot

working at temperatures ranging from 1200° to 1400° F, depending upon the service temperature. Optimum creep and rupture properties are obtained by hot working. Although their creep strength is higher than the austenitic stainless steels, their good forming properties are retained. They are readily welded by existing processes and are fully oxidation-resistant up to approximately 1600° F. Some representative alloys in this group are 19-9 DL, 16-25-6, and Haynes alloy 88. The short-time strength of these materials begins to decrease rapidly between 1000° and 1200° F; for temperatures above approximately 950° F, their creep properties can govern design. At temperatures above approximately 1500° F, their creep and rupture strengths are comparatively low.

In the precipitation-hardening austenitic steels, higher amounts of cobalt, chromium, and nickel are added, decreasing the iron content to as low as 15%. These alloys are stabilized by small amounts of tungsten, molybdenum, and columbium, and attribute their aging properties to elements such as aluminum, titanium, and molybdenum. In general, these alloys have superior strength at the higher temperatures than the highly alloyed steels that canot be heat treated. They are usually age-hardened between 1200° and 1500° F and, since they soften slowly by over-aging, they retain a large percentage of their strength for long periods of time at these temperatures. For continuous service, their maximum oxidation-resistant temperature is between 1600° and 1900° F, depending upon the nickel and chromium content. Generally, above 1200° F, the cobalt-chromium-nickel-iron alloys have better creep and rupture strengths at the elevated temperature than the chromium-nickel-iron alloys, mainly because of the addition of cobalt. Examples of commercial alloys of this type containing cobalt are H-155, S-590, S-816, V-36, K-42-B, and Refracataloy 26. These alloys are fully oxidation-resistant at temperatures ranging from 1800° to 1900° F. They have relatively good strength up to 1600° F and usable strength up to 2000° F for short times. Alloys S-816 and V-36 have the best strength properties at higher temperatures. Alloy V-36, a modification of alloy S-816, contains less of the critical element columbium.

Some commercial alloys of the chromium-nickel-iron type are A-286, Discaloy, and S-495. These alloys have good strength up to about 1350° F and relatively little usable strength above 1600° F.

7. Nickel Base Alloys

The nickel base alloys contain between 45 and 80% nickel to increase stability at high temperatures without loss of good forming properties. Their oxidation resistance is excellent up to 2100° F.

Some of these alloys, such as Inconel X, M-252, Waspaloy, and the Nimonic series 75, 80, and 90, contain titanium and aluminum, and are capable of age-hardening. In general, these alloys have high strength up to 1600° F, and high temperature properties comparable to the less available cobalt alloys at temperatures up to 1800° F. They are usually age-hardened at about 1300° F. Inconel X has the highest long-time strength up to 1600° F when properly heat treated. The Nimonic alloys are similar to Inconel X in composition and strength.

Another group of nickel base alloys containing high percentages of molybdenum and having high strength up to 1800° F are Hastelloy B, Hastelloy C, and Hastelloy X. Hastelley C has no chromium and is not as resistant to oxidation as the other alloys that contain about 16 to 22% chromium. Hastelloy C has high strength up to and above 1800° F. These alloys are used in the annealed condition.

The creep and rupture strengths of all nickel base alloys are important for long-time service at temperatures above approximately 1200° F.

8. Cobalt Base Alloys

The cobalt base alloys contain up to 65% cobalt, not more than 3% iron, 17 to 30% chromium, and between 3 to 20% nickel. By adding molybdenum or tungsten in quantities of about 5 to 15%,

their high-temperature stability is greatly increased. These alloys have high hardness and excellent long-time oxidation and corrosion resistance up to about 2100° F. Most of these materials are casting alloys. A commercial sheet alloy, L-605 (Haynes alloy 25), is the strongest of all considered high-temperature alloys above 1600° F. Because of its high critical alloy content, it is used only in the temperature range of 1700° to 2200° F when high strength is required. This alloy is used in the annealed condition at these high temperatures.

9. Chromium, Tungsten, and Molybdenum

Alloys that are based upon the higher melting point metals such as chromium, tungsten, and molybdenum are being developed for applications at temperatures above 1600° F.

Chromium base alloys show promise because of their good oxidation resistance, high elevated-temperature strength, and low density compared with the cobalt base alloys. Cast chromium base alloys have been produced with strengths (at 1600° F) twice that of the cobalt base alloys. Their principle disadvantage is lack of ductility at room temperature.

Tungsten has the highest melting point of all metals, 6152° F, and is produced by powder metallurgy techniques. At temperatures between 750° to 930° F, tungsten will oxidize in air. At room temperature, tungsten in sheet form can attain short-time tensile strength above 300,000 psi depending upon the thickness of the metal. Tungsten base alloys containing theoria have usable strength at temperatures even above 5000° F. At 5000° F, a tungsten base alloy in wire form containing 2% thoria has a short-time tensile strength of about 10,000 psi. A pure tungsten wire has been shown to have a short-time tensile strength of about 10,000 psi at 3500° F.

Molybdenum melts at about 4730° F and is produced either by an arc-casting process or by the powder metallurgy process. The commercial molybdenum base alloys contain small quantities of elements such as titanium, columbium, vanadium, and tungsten. These alloys are stronger than pure molybdenum which has a higher strength at temperatures above 1600° F than all the heat-resistant alloys.

Molybdenum starts to oxidize in air at temperatures between 750° and 930° F and evaporates at appreciable rates above 1400° F. Ceramic and metallic coatings have been developed which provide oxidation resistance at temperatures above 2000° F.

The elevated temperature strength of molybdenum and its alloys is greatly improved by cold working. The recrystallization temperature of the molybdenum alloys exceeds about 2150° F (corresponds to high degree of cold work). The short-time tensile properties of these materials drop off rapidly between temperatures of about 1600° to 1800° F; for service temperature above approximately 1600° F, creep and stress rupture properties become important considerations in design. At 2600° F, these alloys still have usable strength. The molybdenum alloy containing 0.45% titanium is claimed to have the best strength properties of all those available commercially.

The advantages of molybdenum base alloys are high modulus of elasticity at all temperatures, good shock resistance, high resistance to corrosion in many media, high temperature strength, and an ample supply. Their disadvantages are lack of oxidation resistance requiring a protective coating, high density, and low ductility at room and lower temperatures. Molybdenum and its alloys may be welded and brazed, but with some loss in initial properties.

10. Ceramics

Ceramic materials have been used successfully in many commercial high-temperature applications such as the linings of rocket combustion chambers, jet engine turbine parts, and high-temperature furnaces. These materials are being considered for application in the hotter portions of high-speed aircraft because of their high refractory characteristics at temperatures above 1800° F, the temperature at which metals deteriorate rapidly.

Ceramics are nonmetallic materials composed primarily of fluxes and refractories. The fluxes have lower melting points and are used to fuse or melt the pure refractories in the ceramic composition. Typical fluxes include materials such as borax and the oxides of lead, magnesium, barium, and calcium. Refractories include the oxides of elements such as aluminum, beryllium,

[redacted]

zirconium, thorium, and magnesium, and include the so-called refractory hard metals, borides, nitrides, carbides, and silicides. Graphite can also be classified as a ceramic.

The pure oxide refractories are crystalline and self-bonded, and will withstand higher temperatures than the oxide compositions which are not free from the fluxing effects of low-temperature melting oxides. The high purity oxide refractories are difficult to produce and this results in high costs. The commercial high-temperature oxide refractories contain impurities and small quantities of other oxides which facilitate ease of fabrication and increase microstructural stability at elevated temperatures for longer periods of time. The commercial high-temperature oxide ceramics comprise combinations of the pure refractory oxides such as alumina (Al_2O_3), zirconia (ZrO_2), beryllia (BeO), magnesia (MgO), thoria (ThO_2), and silica (SiO_2).

Oxide compositions are limited by their brittleness and low resistance to thermal shock. When compared with metals, they have low coefficients of expansion and low thermal conductivities. Their compressive strength is much higher than their tensile strength; for the same material, a room-temperature strength of 400,000 psi and a tensile strength of 30,000 psi is not uncommon.

The refractory hard metals are primarily carbon, silicon, boron, or nitrogen compounds of the transition metals of the fourth to sixth groups of the periodic table, such as titanium, tungsten, molybdenum, and zirconium. These refractories show metallic luster and thermal and electrical conductivities comparable to the metals. Their melting points, hardness, modulus of elasticity, and strength properties are excellent at elevated temperatures. The usefulness of most of these materials in the pure form is limited by their susceptibility to oxidation at low temperatures and by their brittleness.

There are many refractory hard metals on the market with suitable oxidation resistance and strength above 1800° F. Those based upon zirconium boride, titanium boride, chromium boride, titanium carbide, boron carbide, zirconium carbide, and silica carbide are being used in many high-temperature applications. By mixing the borides and carbides, a compressive strength of 600,000 psi and a bending strength of 55,000 psi at 2200° F have been obtained. The oxidation resistance of these materials is improved by the use of special bonding materials. For example, silicon carbide readily oxidizes above 1475° F and, by properly bonding it with silicon nitride, oxidation resistance may be obtained up to 2200° F.

Graphite sublimes at approximately 8500° F and does not lose its strength below 4500° F. At temperatures above 700° F, this material oxidizes rapidly; however, protective coatings are being developed which may eliminate this disadvantage. The advantages of graphite are inertness to chemical action, good high-temperature strength, excellent resistance to thermal shock, high subliming point, good heat conductivity, low coefficient of expansion, and low density.

Oxide ceramic compositions have been developed for use as protective coatings for metals and refractory hard metals exposed to high temperatures in an oxidizing atmosphere. Such coatings as A-418 composition, which was developed by the National Bureau of Standards, contain chromium oxide, zirconia, and alumina, and withstand temperatures up to 1700° F for long periods of time. There are many other special coatings designed for particular metals such as Inconel, L-605, 18-8 stainless steel, and N155. The best high-temperature coating is generally believed to be useful up to 2100° F, but claims for some coatings indicate that they are useful up to the melting temperatures of highly heat-resistant alloys. The coatings available have good shock and fatigue resistance.

11. Cermets

Cermets are metal bonded refractory compounds fabricated by powder metallurgy methods. The oxide, boride, carbide, nitride, and silicide compounds are, in effect, cemented together by either one or more metals such as nickel, cobalt, chromium, tungsten, and molybdenum, or by the high-temperature alloys such as the nickel or cobalt base alloys and the stainless steels. The proportion of refractory material to metal is varied to produce materials with properties most suitable for a given application; increasing the quantity of binder metal will increase the room-temperature strength and thermal shock resistance, but will decrease high-temperature strength. The commercial cermets have higher strength at elevated temperatures than the high-temperature alloys. They also have high thermal conductivity and good thermal shock resistance, and are oxidation-

resistant to temperatures as high as 2000° F for short periods of time. Their primary disadvantage is poor impact resistance.

The best available cermets having suitable oxidation-resistance and strength at temperatures up to 2000° F are based upon titanium carbide and alumium oxide. Titanium base compositions such as Kentanium and WZ contain from 35 to 90% titanium carbide with either nickel, nickel-chromium, or nickel-cobalt-chromium alloys as the binder. They can attain short-time strengths of more than 30,000 psi at 2000° F. The rupture strength of one of the better cermets, K161B, is about 3200 psi for 100 hours at 2000° F.

Cermets based upon oxides have become increasingly important because of their high resistance to oxidation. A commercial cermet containing 77% chromium and 23% aluminum oxide, Metanic LT-1, resists oxidation in air up to 2200° F.

The heat-resistant cermets, based upon oxides, have been developed for application as protective coatings for most of the heat-resistant metals. Some of these cermet coatings can withstand temperatures of 2000° F above the melting point of the metals they protect. A typical cermet coating containing 66% nickel and 33.3% molybdenum oxide can be applied to mild steel, Inconel, and the Hastelloys. This coating is claimed to offer low thermal conductivity and excellent resistance to hot gas errosion, shock, and high-temperature oxidation.

D. SUMMARIES OF MATERIAL PROPERTIES

For design at room temperature, it has been the practice to use material mechanical properties which are computed on a probability basis. Mechanical properties at elevated temperatures for the commonly used materials, such as the aluminum alloys, are given in Reference 109 as a percentage of the room-temperature probability strengths. For the remainder of the materials suitable for elevated temperature service, insufficient tests have been performed from which reliable data can be obtained. For this reason, material properties presented herein for the newer materials should be considered as typical or representative data. Tables III-1, III-2, and III-3 summarize the mechanical, physical, and thermal properties of many materials considered suitable for elevated temperature use and for which data are available in the literature. These tables are supplemented by data presented in Part I, Section 2.0.

E. FABRICATION AND COST

The newer high-temperature materials are generally more difficult to fabricate than the conventional aluminum alloys and stainless steels. With few exceptions, most high-temperature alloys can be welded or formed by one or more available technique, although additional precautions are required.

Most high-temperature alloys have been fusion-welded and spot-welded satisfactorily; inert-gas shielded arc-welding is recommended for most of the alloys. The properties of the welds, especially in sheet materials, are influenced appreciably by their configuration; for satisfactory welded joints, a tight butt weld followed by rolling is recommended.

Because of their high alloy content, the high-temperature materials tend to work-harden rapidly and to require additional intermediate annealing during forming operations. Annealing requires temperatures above 2000° F and necessitates the use of both high-temperature furnaces and special equipment for removing scale.

The refractory materials are difficult to fabricate because of brittleness and high softening temperatures. Most of these materials cannot be welded, but some can be brazed. Although the ceramic and cermet materials can be fabricated for only relatively small part applications, they are finding many applications as protective coatings.

Because of their high alloy content and special fabrication techniques, most high-temperature alloy parts cost considerably more than parts fabricated from low-temperature alloys and stainless steels. High-temperature alloys contain relatively large proportions of nickel, cobalt, columbium,

molybdenum, chromium, and tungsten; these elements are considered critical either because they are scarce in the earth, or because they are not available in this country, or both.

The high-temperature ceramic and cermets that require specialized fabrication techniques are costly, especially since the few types that are of interest are still in the experimental stages of development.

Typical costs have been summarized in Table III-4 for some of the available materials.

REFERENCES

(1) "Metals Handbook," The American Society for Metals, 1948 Edition.

(2) "Metals Handbook," The American Society for Metals, 1954 Supplement.

(3) Schwarzkoff, P. and Kieffer, R., "Refractory Hard Metals," The Macmillian Company, New York, 1953.

(4) Everhart, J. L., Lindlief, W. E., Kanegas, J., Weissler, P. G., and Siegel, F., "Mechanical Properties of Metals and Alloys," U. S. Department of Commerce, National Bureau of Standards, Circular C447, December 1943.

(5) Clark, Claude L., "High-Temperature Alloys," Pitman Publishing Corporation, New York, 1953.

(6) Samans, C. H., "Engineering Metals and Their Alloys," The Macmillian Company, New York, 1950.

(7) Clark, F. H., "Metals at High Temperatures," Reinhold Publishing Corporation, New York, 1950

(8) "High-Temperature Steels and Alloys for Gas Turbines," The Iron and Steel Institute, London Special Report No. 43, July 1952.

(9) Freudenthal, A. M., "The Inelastic Behavior of Engineering Materials and Structures," John Wiley & Sons, Inc., New York, 1950.

(10) "Designing with Magnesium," American Magnesium Corporation, 1947.

(11) Hoyt, Samuel L., "Metal Data," Reinhold Publishing Corporation, New York, 1952.

(12) "Haynes Alloys for High-Temperature Service," Haynes Stellite Division, Union Carbide and Carbon Corporation, 1950.

(13) Leach, A. E. and Lundstrom, H. M., "Evaluation of Titanium and Titanium-Base Alloys at Bell Aircraft Corporation," Bell Aircraft Corporation, BLR 51-57, Revised October 1954.

(14) Preston, D., "Exploratory Investigation of High-Temperature Sheet Materials," ASTM Preprint 85, 1952.

(15) Krivobok, V. N. and Talbot, A. M., "Effect of Temperatures on the Mechanical Properties, Characteristics, and Processing of Austenitic Stainless Steels," Proceeding of ASTM, 1950, Vol. 50.

(16) "Heat Treating of Republic Enduro Stainless Steels," Republic Steel Corporation, 1952.

(17) "Heat Treatment and Physical Properties of the Austenitic Chromium-Nickel Stainless Steels," The International Nickel Company, Inc., 1947.

(18) Hughes, P. J., Inge, J. E., and Prosser, S. B., "Tensile and Compressive Stress-Strain Properties of Some High-Strength Sheet Alloys at Elevated Temperatures," NACA TN 3315, November 1954.

(19) "Steels for Elevated Temperature Service," United States Steel Corporation, 1949.

(20) "Haynes Alloys for High-Temperature Service," Haynes Stellite Company, Kokomo, Indiana, 1950.

(21) "Hastelloy Alloy X," Union Carbide and Carbon Corporation, 1955.

(22) "Inconel X - A High Strength, High Temperature Alloy," The International Nickel Company, Inc., January 1949.

(23) "Engineering Properties of Inconel and Inconel X," Technical Bulletin T-7, The International Nickel Company, Inc., June 1953.

(24) Simmons, W. F. and Cross, H. C., "The Elevated Temperature Properties of Selected Super-Strength Alloys," ASTM Special Technical Publication No. 160, 1954.

(25) Frey, D. N., Freeman, J. W., and White, A. E., "Fundamental Aging Effects Influencing High-Temperature Properties of Solution-Treated Inconel X," NACA TN 2385, June 1951.

(26) Flanigan, A. E., Tedsen, L. F., and Dorn, J. E., "Stress Rupture and Creep Tests on Aluminum-Alloy Sheet at Elevated Temperatures," Technical Publication Number 2033, American Institute of Mining and Metallurgical Engineering, September 1946.

(27) Manson, S. S. and Haferd, A. M., "A Linear Time-Temperature Relation for Extrapolation of Creep and Stress-Rupture Data," NACA TN 2890, March 1953.

(28) Guarnieri, G. J. and Salvaggi, J., "Limiting High Temperature Creep and Rupture Stress of Sheet Alloys for Jet Applications," USAF, USN, Project Squid, Technical Memorandum Number CAL. -39, September 1951.

(29) Johnston, G. S., "A Study of Materials Operating at Elevated Temperatures," Bell Aircraft Corporation, Report 02-941-024, Revised April 1952.

(30) "HK-31 New Thorium Alloy," Brooks and Perkins, Inc., Detroit, Michigan.

(31) "Magnesium Data," Brooks and Perkins, Inc., Detroit, Michigan.

(32) Krebs, C. V., "A Survey of the Titanium Field," Airframe and Equipment Engineering Report Number 3, U. S. Civil Aeronautics Administration, August 1954.

(33) Heimerl, G. J. and Roberts, W. M., "Determination of Plate Compressive Strengths at Elevated Temperatures," NACA TN 1806, February 1949.

(34) Heimerl, G. J. and Hughes, P. J., "Structural Efficiencies of Various Aluminum, Titanium, and Steel Alloys at Elevated Temperatures," NACA TN 2975, July 1953.

(35) Roberts, W. M. and Heimerl, G. J., "Elevated-Temperature Compressive Stress-Strain Data for 24S-T3 Aluminum Alloy Sheet and Comparisons with Extruded 75S-T6 Aluminum Alloy," NACA TN 1837, March 1949.

(36) Adenstedt, H. K., "Handbook on Titanium," WADC Technical Report 54-305, Part I, August 1954.

(37) Craighead, C. M., Grube, K. P., Eatwood, L. W., and Lorig, C. H., "The Effects of Temperature on the Mechanical Properties of Magnesium Alloys," Battelle Memorial Institute, R-146, October 1949.

(38) Guarnieri, G. J. and Gillig, F. J., "A Study of the Tensile and Creep-Rupture Properties of Fifteen Heats of C-100M Titanium Alloy Sheet," Cornell Aeronautical Laboratory, Inc., WADC Technical Report 55-164, September 1955.

(39) Vawter, F. J., Guarnieri, G. J., Yerkovich, L. A., and Derrick, G., "Investigation of the Compressive, Bearing, and Shear Creep-Rupture Properties of Aircraft Structural Metals and Joints at Elevated Temperatures," Cornell Aeronautical Laboratory, Inc., WADC Technical Report 54-270, Part I, June 1954.

(40) Miller, D. E., "Determination of the Physical Properties of Ferrous and Nonferrous Structural Sheet Materials at Elevated Temperatures," Armour Research Foundation, AFTR 6517, Part 4, December 1954.

(41) Simmons, W. F., Vanecho, J. A., and Cross, H. C., "Short-Time, High-Temperature Properties of Heat-Resisting Alloy Sheet," Battelle Memorial Institute, R-147, June 1949.

(42) Doerr, D. D., "Determination of Physical Properties of Nonferrous Structural Sheet Materials at Elevated Temperatures," Armour Research Foundation, AFTR 6517, Part 1, December 1951. "Typical Stress vs. Strain and Stress vs. Deformation Curves," Supplement 1, 1953.

(43) Doerr, D. D., "Determination of Physical Properties of Ferrous and Nonferrous Structural Sheet Materials," Armour Research Foundation, AFTR 6517, Part 2, April 1954.

(44) Miller, Donald E., "Determination of Physical Properties of Ferrous and Nonferrous Structural Sheet Materials at Elevated Temperatures, Armour Research Foundation, AFTR 6517, Part 3, June 1954.

(45) Jackson, L. R., Schwope, A. D., and Shober, F. R., "Information on the Plastic Properties of Aircraft Materials and Plastic Stability of Aircraft Structures at High Temperatures," Battelle Memorial Institute, RM-333, December 1949.

(46) Craighead, C. M., Eastwood, L. W., and Lorig, C. H., "An Appraisal of the Usefulness of Aluminum Alloys for Supersonic Aircraft and Guided Missile Construction," Battelle Memorial Institute, R-104, August 1948.

(47) Templin, R. L. and Hartman, E. C., "The Elastic Constants for Wrought Aluminum Alloys," NACA TN 966, January 1945.

(48) Jenkins, D. R., Wenk, S. A., and McMaster, R. C., "Basic Studies for the Development of Methods for Laboratory Investigations of Structures Which Must Operate at Elevated Temperatures," Battelle Memorial Institute, G-1273, June 1950.

(49) Rowley, L. N. and Skrotzki, G. A., "High-Temperature Metals," Power, October 1947.

(50) Cross, H. C., McMaster, R. C., Simmons, W. F., and Vanecho, J. A., "Short-Time High-Temperature Properties of Heat-Resisting Alloy Sheet," Battelle Memorial Institute, RA-15077, February 1948.

(51) Lucks, C. F., Thompson, H. B., and Smith, A. R., "Thermal Properties of Certain Materials," Battelle Memorial Institute, Progress Reports G-1364, October 1949-October 1950.

(52) "Magnesium Design Notes," The Dow Chemical Company, 1954.

(53) Krebs, C. V., "A Survey of the Titanium Field," U. S. Civil Aeronautics Administration, Report No. 53, August 1954.

(54) "Digest of Steels for High Temperature Service," The Timken Roller Bearing Company, 1946.

(55) Simmons, W. F. and Cross, H. C., "Report on the Elevated Temperature Properties of Stainless Steels," ASTM Special Technical Publication No. 124, 1952.

(56) Miller, R. F. and Heger, J. J., "The Strength of Wrought Steels at Elevated Temperatures," ASTM Special Technical Publication No. 100, 1950.

(57) Garofalo, F., Malenock, P. R., and Smith, G. V., "The Influence of Temperature on the Elastic Constants of Some Commercial Steels," ASTM Special Technical Publication No. 129, June 1952, Pages 10-27.

(58) Furman, D. E., "Thermal Expansion Characteristics of Stainless Steels Between -300° and +1000° F," Journal of Metals, April 1950.

(59) Simmons, W. F. and Cross, H. C., "The Elevated-Temperature Properties of Chromium-Molybdenum Steels," ASTM Special Technical Publication No. 151, 1953.

(60) Frey, D. N., Freeman, J. W., and White, A. E., "Fundamental Effects of Aging on Creep Properties of Solution-Treated Low-Carbon N-155 Alloy," NACA Report No. 1001, 1950.

(61) Frey, D. N. and White, A. E., "Fundamental Effects of Cold-Work on Some Cobalt-Chromium-Nickel-Iron Base Creep-Resistance Alloys," NACA TN 2586, January 1952.

(62) Simmons, W. F., "V-36 Alloy, Determination of Design Data," AFTR No. 5949, May 1950.

(63) Evans, Jr., J. E., "Thermal Conductivity of 14 Metals and Alloys up to 1100° F," NACA RM E 50L07, March 1951.

(64) Guarnieri, G. J. and Yerkovich, L. A., "The Influence of Periodic Overstressing on the Creep Properties of Several Heat-Resistant Alloys," ASTM Proceeding, 1952, Vol. 52, Pages 934-950.

(65) Miller, J., "Effect of Temperature Cycling on the Rupture Strength of Some High-Temperature Alloys," ASTM Special Technical Publication No. 165, 1954.

(66) Guarnieri, G. J., "The Creep-Rupture Properties of Aircraft Sheet Alloys Subjected to Intermittent Load and Temperature," ASTM Special Technical Publication No. 165, 1954.

(67) Simmons, W. F. and Cross, H. C., "Constant and Cyclic-Load Creep Tests of Several Materials," ASTM Special Technical Publication No. 165, 1954.

(68) "Symposium on Effect of Cyclic Heating and Stressing on Metals at Elevated Temperatures," ASTM Special Technical Publication No. 165, 1954.

(69) "Symposium on Strength and Ductivity of Metals at Elevated Temperatures," ASTM Special Technical Publication No. 128, 1952.

70) Gerard, G., "Life Expectancy of Aircraft Under Thermal Flight Conditions," Journal of Aeronautical Sciences, October 1954, Vol. 21, No. 10, Pages 675-680.

(71) Guarnieri, G. J., "Intermittent Stressing and Heating of Aircraft Structural Metals," WADC TR 53-24, Parts I & II, 1954.

(72) Shepard, L. A., Dean, S. C., Wiseman, C. D., and Dorn, J. E., "The Creep Properties of Metals Under Intermittent Stressing and Heating Conditions," WADC TR 53-336, Part I, "Intermittent Stressing," September 1953; Part II, "Intermittent Heating," July 1954; Part III, "Combined Intermittent Stressing and Heating," July 1954.

(73) Guarnieri, G. J., "Intermittent Stressing and Heating of Aircraft Structural Metals," WADC Technical Report 53-24, Part 2, September 1954.

(74) Perlmutter, I., "Stress Rupture Tests on Sheet Alloys for High Temperature Applications," AFTR No. 6188, July 1950.

(75) Bruchart, W. L., Jaffee, R. J., Whalen, S. J., and Gonser, B. W., "Molybdenum Alloys and Protection by Cladding," Battelle Memorial Institute, R-200, April 1950.

(76) Frahme, H., "Design Properties of a New Sintered Metallic Oxide," Design News, February 1955.

(77) International Critical Tables II, McGraw Hill Book Company, New York City, 1942.

(78) Wilkes, G. B., "The Specific Heats of Magnesium and Aluminum Oxides at High Temperatures," Journal of American Ceramic Society, 1932, Vol. 15, No. 1, Pages 72-77.

(79) "Ceramic Data Book," Industrial Publications, Inc., 1951 - 1952.

(80) Maxwell, W. A. and Smith, R. W., "Thermal Shock Resistance and High-Temperature Strength of a Molybdenum Disilicide-Aluminum Oxide Ceramic," NACA RM E 53F26, October 1953.

(81) Brinkman, Robert J., "Ceramic Coating Conference, 27 and 28 May 1952," WADC TR 53-37, September 1954.

(82) "Ceramics," A Selected Report Bibliography, U. S. Armed Services Technical Information Agency, April 1951.

(83) Duckworth, W. H., Johnston, J. K., Jackson, L. R., and Schofield, H. Z., "Mechanical Properties of Ceramic Bodies," Project Rand, R 209, August 1950.

(84) Fowler, E., Ferrel, E., Quirk, J., King, B. W., and Harman, C, G., "Investigation of High-Temperature Thermal Properties of Ceramic Heat Insulators," Battelle Memorial Institute, Progress Reports, November 1951 - February 1952.

(85) Glasser, F. W., et al., "Cemented Borides," Summary Progress Report, Contract NG-ONR-256, American Electro Metal Corporation, New York, July 1954.

(86) Knudsen, F. P., Moreland, R. E., and Geller, R. F., "Physical Characteristics in Titanium-Carbide-Base Cermets at Elevated Temperatures," WADC TR 54-1, May 1954.

(87) Maxwell, W. A., "Some Stress-Rupture and Creep Properties of Molybdenum Disilicide in the Range 1600° to 2000° F," NACA RM E53D09, June 1952.

(88) Long, A. R., "Fabrication and Properties of Hot-Pressed Molybdenum Disilicide," NACA RM E50F22, August 1950.

(89) West, E. D., Ditmars, D. A., and Ginnings, D. C., "Thermal Conductivity and Heat Capacity of Molten Materials," Part 5, "The Thermal Conductivity of Molybdenum Disilicide From 300° to 800° C," WADC TR 53-201, August 1954.

(90) Heimerl, G. J., "Time-Temperature Parameters and an Application to Rupture and Creep of Aluminum Alloys," NACA TN 3195, June 1954.

(91) Sachs, G., "Survey of Low-Alloy Aircraft Steels Heat Treated to High-Strength Levels," Part 4, "High Strength Steels and Their General Static Properties," WADC Technical Report 53-254, Part 4, August 1954.

(92) Guarnieri, G. J. and Salvaggi, J., "Limiting High Temperature Creep and Rupture Stresses of Sheet Alloys for Jet Applications," Cornell Aeronautical Laboratory, Inc., Technical Memorandum No. CAL-39, September 1951.

(93) Huffman, J. W., "Application of Metallic Materials for Aircraft Structures in the Temperature Range 600° to 1100° F," Society of Automotive Engineers, Presented at Aircraft Research Seminar, December 1954.

(94) Levy, Alan, "Metals for Short Time Service at High Temperatures," Material & Methods, April 1955, Pages 117-132.

(95) Clauser, H. R., "Materials For High Temperature Service," Materials & Methods, April 1955, Pages 117-132.

(96) O'Keefe, P., "Carbon and Graphite Materials and Parts," Materials & Methods, April 1952, Pages 119-134.

(97) Everhart, J. L., "Age-Hardenable Metals," Materials & Methods, October 1954, Pages 121-136.

(98) Everhart, J., "New Refractory Hard Metals," Materials & Methods, August 1954.

(99) Graham, John W., "Sintered Titanium Carbides Open New Industrial Horizons," The Iron Age, 13 August 1953.

(100) Johnson, B. M., Turner, A. A., and Schroeder, H. S., "Super Refractories Give Operators Unique Range of Properties," Journal of Metals, May 1955.

(101) Caldwell, V., "Beyond the Metals," Steel, 1 and 8 August 1955.

(102) Redmond, J. C. and Graham, J. W., "Field of Cemented Carbides Expanded by Titanium Compositions," Metal Progress, April 1952, Pages 67-70.

(103) Smiley, W. D., "Literature Search on the Properties and Fabrication of Carbon Base Materials," Stanford Research Institute, SRI Project CU-824, August 1954.

(104) Pfaffinger, K., Blumenthal, H., and Glaser, F. W., "Titanium-Carbide-Base Cermets for High-Temperature Service," ASTM Paper 94B.

(105) Shevlin, T. S. and Hauck, C. A., "Alumina-Base Cermets," WADC TR 54-173, Part I, March 1954.

(106) Maxwell, W. A., "Oxidation-Resistance Mechanism and Properties of Molybdenum Disilicide," NACA RM E52A04, March 1952.

(107) "Symposium on Porcelain Enamels and Ceramic Coatings as Engineering Materials," ASTM Special Technical Publication No. 153, 1954.

(108) Guarnieri, G. J., "Intermittent Stressing and Heating Tests of Aircraft Structural Metals," Cornell Aeronautical Laboratory, Inc., WADC TR 53-24, Part 3, June 1955.

(109) "Strength of Metal Aircraft Elements," ANC-5, March 1955.

[redacted]

TABLE III-1

SUMMARY OF MECHANICAL PROPERTIES OF STRUCTURAL MATERIALS

Material	Short-Time Ultimate Tensile Strength (psi x 10^{-3}*)	Short-Time Tensile Yield Stress (psi x 10^{-3}*)	Elongation (%)	Modulus of Elasticity Tension (psi x 10^{-6})	Modulus of Rigidity (psi x 10^{-6})	Poisson's Ratio	Stress for 0.5% Total Deformation in 100 Hours (psi x 10^{-3})	Stress for Rupture in 100 Hours (psi x 10^{-3})
2024-T3 Clad Aluminum Alloy	Fig. 2.2-1	Fig. 2.2-1	Fig. 2.2-1	Fig. 2.2-1	R.T. 4.0	R.T. 0.32	Fig. 2.2-4	Fig. 2.2-5
7075-T6 Aluminum Alloy	Fig. 2.2-7	Fig. 2.2-7	Fig. 2.2-7	Fig. 2.2-7	R.T. 3.9	R.T. 0.32	Fig. 2.2-10	Fig. 2.2-11
6061-T6 Aluminum Alloy	R.T. 42.0 200° 38.5 300° 34.4 400° 27.6 600° 9.0 700° 4.0	R.T. 35.0 300° 30.1 400° 24.0 600° 6.8 700° 3.0	R.T. 10.2 300° 10.3 400° 13.5 600° 15.0 700° 25.5	R.T. 9.9 300° 8.7 400° 7.8 600° 4.95	R.T. 3.85	R.T. 0.32	300° 27.5 400° 16	300° 32 400° 18
FSI-H24 Magnesium Alloy.	Fig. 2.2-13	Fig. 2.2-13	Fig. 2.2-13	Fig. 2.2-13			Fig. 2.2-16 300° 2.4 400° 1.1	Fig. 2.2-17
M-H24 Magnesium Alloy	R.T. 32 200° 25.5 300° 19.2 400° 13.5 600° 5.5 700° 3.2	R.T. 22 200° 18.5 300° 10.2 400° 6 600° 1.8 700° 1	R.T. 3 200° 7.7 300° 14 400° 22 600° 47.5 700° 64	R.T. 6.4 200° 5.92 300° 5.1 400° 3.7 600° 1.93	R.T. 2.4	R.T. 0.35	200° 11.5 250° 5.7 300° 3.0	
HK31-T6 Magnesium Alloy	R.T. 37.3 200° 30 300° 25 400° 22 600° 19.4 700° 14.8	R.T. 18.3 200° 17.5 300° 16 400° 14 600° 12.6 650° 10.4	R.T. 13.3 500° 18.5 600° 17.5 650° 22	R.T. 6.4 300° 5.8 400° 5.75 500° 5.5 600° 5.4		R.T. 0.35	400° 14 500° 8.2 600° 2.2 650° 1.3	
C-110M Titanium Alloy	Fig. 2.2-19	Fig. 2.2-19	Fig. 2.2-19	Fig. 2.2-19			Fig. 2.2-22	Fig. 2.2-23
A-110AT Titanium Alloy	R.T. 115 200° 98.5 600° 66.0 1000° 56.0 1200° 37.5	R.T. 108.5 200° 93.0 600° 53.6 1000° 45.0 1200° 25	R.T. 18.0 200° 19.0 600° 16.0 1000° 18.0 1200° 35.0				400° 60 800° 40	200° 85 400° 70 600° 58.6 800° 54 1000° 31 1200° 14

NOTES: *Exposed approximately 1/2 hour at test temperature.

R.T. = room temperature.
All temperatures in °F.

All figure numbers pertain to Part I.

[redacted]

[redacted]

TABLE III-1 (cont)

Material	Short-Time Ultimate Tensile Strength (psi x 10^{-3}*)	Short-Time Tensile Yield Stress (psi x 10^{-3}*)	Elongation (%)	Modulus of Elasticity Tension (psi x 10^{-6})	Modulus of Rigidity (psi x 10^{-6})	Poisson's Ratio	Stress for 0.5% Total Deformation in 100 Hours (psi x 10^{-3})	Stress for Rupture in 100 Hours (psi x 10^{-3})
6AL-4V Titanium Alloy	R.T. 130 200° 125 400° 110 600° 105 800° 95 1000° 76	R.T. 120 200° 118 400° 105 600° 92 800° 80 1000° 65	R.T. 10 200° 15 400° 15 600° 15 800° 17 1000° 30	R.T. 16.9 200° 10.6 400° 16.2 600° 14.7 800° 13.2 1000° 10.1				
Alloy Steels 4140, 8630, 4340 H.T. to 200,000 psi	Fig. 2.2-25	Fig. 2.2-25	Fig. 2.2-25	Fig. 2.2-25	Fig. 2.2-25	R.T. 0.292 300° 0.294 600° 0.3 1000° 0.308		
Hy-Tuff, Annealed at 1600°F; Tempered at 600°F, 1/2 Hr	R.T. 220 200° 220 400° 218.5 600° 206 800° 160 1000° 88	R.T. 181 200° 174 400° 159 600° 140 800° 112 1000° 70	R.T. 11 200° 10.5 400° 10 600° 11 800° 16 1000° 25	R.T. 28 200° 27.3 400° 26 600° 23.8				
Stainless Steel 18-8 Types 3/4-Hard	Fig. 2.2-29	Fig. 2.2-29	Fig. 2.2-29	Fig. 2.2-29	Fig. 2.2-29	R.T. 0.3 400° 0.31 1000° 0.32 1500° 0.336		
Stainless Steel AISI Type 316 Annealed	R.T. 85.5 1000° 69 1200° 57 1400° 25 1600° 22 1800° 14 2000° 8	R.T. 38.5 1000° 32 1200° 20 1400° 19 1500° 18.5	R.T. 60 1000° 44 1200° 43 1400° 42 1500° 42	Fig. 2.2-29	Fig. 2.2-29			1200° 28 1400° 14 1500° 9.3 1600° 6 1800° 3.6
Stainless Steel AISI Type 310 Annealed	R.T. 92 1000° 78 1200° 62 1400° 41 1600° 25 1800° 14 2000° 8 2100° 6 2300° 4.5	R.T. 40 1000° 25 1200° 24 1400° 20 1500° 19	R.T. 47 1000° 33 1200° 34 1400° 38 1600° 45 1800° 54 2000° 63 2100° 66	Fig. 2.2-29	Fig. 2.2-29			1200° 27 1500° 9.5

NOTES:

*Exposed approximately 1/2 hour at test temperature.

R.T. = room temperature.
All temperatures in °F.

All figure numbers pertain to Part I.

[redacted]

TABLE III-1 (cont)

Material	Short-Time Ultimate Tensile Strength (psi x 10^{-3}*)	Short-Time Tensile Yield Stress (psi x 10^{-3}*)	Elongation (%)	Modulus of Elasticity Tension (psi x 10^{-6})	Modulus of Rigidity (psi x 10^{-6})	Poisson's Ratio	Stress for 0-5% Total Deformation in 100 Hours (psi x 10^{-3})	Stress for Rupture in 100 Hours (psi x 10^{-3})
Stainless Steel AISI Type 410 Annealed	R.T. 89 1000° 48 1200° 22 1400° 11 1600° 9 1800° 7 2000° 4 2300° 1.5	R.T. 62 1000° 48 1200° 18 1400° 8	R.T. 30 1000° 30 1200° 51 1400° 67 1500° 74					
17-7PH Stainless Steel	Fig. 2.2-33	Fig. 2.2-33	Fig. 2.2-33	Fig. 2.2-33		R.T. 0.27-0.28		600° 162 700° 141 800° 124 900° 73
16-25-6 Iron-Chromium-Nickel Alloy	R.T. 125 1000° 103 1200° 90 1400° 61 1600° 36 1800° 22	R.T. 150 1000° 73 1200° 68 1400° 52 1600° 36 1800° 19	R.T. 25 1000° 28 1200° 20 1400° 31 1600° 31 1800° 38	R.T. 28.5 1000° 23.4 1200° 22.4 1400° 21.6 1500° 21.3	R.T. 11 1000° 8.5 1200° 7.9 1400° 7.7 1500° 7.3	R.T. 0.286 1000° 0.326 1400° 0.340		1000° 81 1200° 50 1350° 28
19-9DL Iron-Chromium-Nickel Alloy	R.T. 129 1000° 92 1200° 72 1300° 58 1400° 40 1600° 18 1800° 10	R.T. 108 1000° 82 1200° 66 1300° 52 1400° 36 1500° 17	R.T. 22 1000° 8 1200° 10 1300° 19 1400° 28 1600° 46 1800° 68	R.T. 29.5 200° 28.5 600° 25.9 1000° 23.3 1200° 22 1400° 20.7 1500° 20	R.T. 11.4 600° 9.9 1000° 8.8 1200° 8.2 1500° 7.5	R.T. 0.286 1000° 0.318 1500° 0.336		1000° 78 1200° 37 1350° 12
N-155 Cobalt-Nickel-Chromium-Iron Alloy	R.T. 118 1000° 93 1200° 79 1400° 60 1600° 35 1800° 19 2000° 9 2200° 4.6 2400° 0	R.T. 57 1000° 48 1200° 43 1400° 35 1600° 25 1800° 14 2000° 9	R.T. 40 1000° 33 1200° 32 1400° 32 1600° 34 1800° 37 2000° 51 2200° 27	R.T. 29.3 1000° 24.2 1500° 20.8			1350° 17 1500° 11	1200° 60 1350° 28 1500° 17 1600° 15 1800° 3.3

NOTES:

*Exposed approximately 1/2 hour at test temperature.

R.T. = room temperature.

All temperatures in °F.

All figure numbers pertain to Part I.

TABLE III-I (cont)

Material	Short-Time Ultimate Tensile Strength (psi x 10^{-3}*)	Short-Time Tensile Yield Stress (psi x 10^{-3}*)	Elongation (%)	Modulus of Elasticity Tension (psi x 10^{-6})	Modulus of Rigidity (psi x 10^{-6})	Poisson's Ratio	Stress for 0-5% Total Deformation in 100 Hours (psi x 10^{-3})	Stress for Rupture in 100 Hours (psi x 10^{-3})
S-590 Cobalt-Nickel-Chromium-Iron Alloy	R.T. 140 1000° 128 1200° 100 1400° 67 1600° 40 1800° 21 2000° 13	R.T. 74 1000° 79 1200° 71 1400 56 1600° 36 1800° 20 2000° 14	R.T. 20	R.T. 31.1 600° 28 1000° 26 1200° 24.6 1500° 22.9	R.T. 11.9 600° 11.6 1050° 9.45	R.T. 0.31 600° 0.324 1050° 0.339	1000° 55 1100° 41 1200° 33 1350° 21 1500° 17.5	1000° 90 1100° 65 1200° 48 1350° 30 1500° 22
S-816 Cobalt-Nickel-Chromium-Iron Alloy	R.T. 148 1000° 121 1200° 110 1400° 88 1600° 51 1800° 26 2000° 12 2200° 6	R.T. 63 1000° 46 1200° 42 1400° 40 1600° 34 1800° 24 2000° 12	R.T. 31 1000° 27 1200° 22 1400° 25 1600° 17 1800° 20 2000° 24	R.T. 35.2 600° 31.7 1050° 28.7 1200° 27.6 1500° 25.4 1600° 25.1	R.T. 13.6 600° 12.2 1050 10.8 1200° 10.5 1500° 9.6	R.T. 0.294 600° 0.304 1050° 0.315 1500° 0.316	1200° 42 1350° 23 1500° 14	1200° 60 1350° 36 1500° 24 1600° 15 1800° 5.5 1900° 3.2
Refractoloy 26 Cobalt-Nickel-Chromium-Iron Alloy	R.T. 153 1000° 142 1200° 134 1400° 108 1600° 48	R.T. 96 1000° 91 1200° 94 1400° 90 1600° 48	R.T. 18 1000° 17 1200° 14 1400° 13 1600° 49		70° 31.4 1000° 27.5 1500° 20			1200° 80 1350° 50 1500° 27
A-286 Iron-Chromium-Nickel Alloy	R.T. 144 1000° 128 1200° 106 1400° 65 1600° 28 1800° 10 2000° 6	R.T. 93 1000° 90 1200° 85 1400° 56 1500° 23	R.T. 25 1000° 18.5 1300° 11 1500° 68.5	70° 29.1 1000° 23.5 1200° 22.2 1400° 20.6 1600° 18.9	70° 10.4 1000° 8.4 1200° 7.95 1400° 7.53 1500° 7.3	R.T. 0.306 1000° 0.328 1200° 0.336 1500° 0.344	1000° 84 1100° 76 1200° 53 1300° 30	1000° 99 1100° 81.5 1200° 64 1300° 44.5 3500° 35 1500° 13.8
V-36 Cobalt-Nickel-Chromium-Iron Alloy	R.T. 150	R.T. 76	R.T. 22				1350° 24.5 1500° 17 1700° 11 1800° 7.5	1350° 35 1500° 23 1700° 13 1800° 8.5
M-252 Nickel-Base	R.T. 162 1000° 156 1200° 143 1400° 121 1600° 62	R.T. 99 1000° 83 1200° 88 1400° 80 1600° 60						1350° 52 1500° 29 1600° 16

NOTES: *Exposed approximately 1/2 hour at test temperature. R.T. = room temperature. All temperatures in °F.

[redacted]

TABLE III-1 (cont)

Material	Short-Time Ultimate Tensile Strength (psi x 10^{-3}*)	Short-Time Tensile Yield Stress (psi x 10^{-3}*)	Elongation (%)	Modulus of Elasticity Tension (psi x 10^{-6})	Modulus of Rigidity (psi x 10^{-6})	Poisson's Ratio	Stress for 0-5% Total Deformation in 100 Hours (psi x 10^{-3})	Stress for Rupture in 100 Hours (psi x 10^{-3})
Inconel X Nickel-Base	Fig. 2.2-37	Fig. 2.2-37	Fig. 2.2-37	Fig. 2.2-37	Fig. 2.2-37	R.T. 0.29	Fig. 2.2-43	Fig. 2.2-44 1900° 2.7
Hastelloy C Nickel-Base	R.T. 130 1000° 97 1200° 86 1400° 63 1600° 38 1800° 19 2000° 12	R.T. 54 1000° 55 1200° 50 1400° 47 1600° 36	R.T. 38 1000° 22 1200° 23 1400° 32 1600° 39 1800° 38 2000° 30	R.T. 28.5 1200° 26.8 1500° 22 1800° 18.7				
Hastelloy X Nickel-Base	R.T. 113.2 1000° 94 1200° 83 1400° 63.1 1600° 36.5 1800° 21 2000° 9.5 2200° 4.6 2350° 2.6	R.T. 55.8 1000° 41.5 1200° 40.7 1400° 37.8 1600° 25.7 1800° 17.0	R.T. 43 1000° 45 1200° 37 1400° 37 1800° 43 2000° 39 2200° 40 2350° 5	400° 23.8 600° 25.5 1000° 24.3 1400° 20.1 1600° 18.7			1200° 25 1350° 13 1500° 9 1650° 4.5 1800° 2.0 1900° 1.4 (73.9 hr)	1200° 42 1350° 26 1500° 14 1650° 8.3 1800° 3.4
Haynes Alloy No. 25 (L-605) Cobalt-Base	Fig. 2.2-46	Fig. 2.2.46	Fig. 2.2-46	Fig. 2.2-46			Fig. 2.2-47 1500° 13 1600° 8 1800° 3	Fig. 2.2-47

NOTES:

*Exposed approximately 1/2 hour at test temperature.

R.T. = room temperature.

All temperatures in °F.

All figure numbers pertain to Part I.

[redacted]

TABLE III-2

SUMMARY OF PHYSICAL PROPERTIES OF STRUCTURAL MATERIALS

Material	Density ($lb/in.^3$)	Melting Point (°F)	Specific Heat (BTU/°F/lb)	Thermal Conductivity (BTU-in./ft^2 hr in.)	Mean Coefficient Of Thermal Expansion (in./in./°F x 10^6)	Oxidation Resistance Scaling(°F)
2024-T3 Clad Aluminum Alloy	0.1	935-1180°	Figure 2.2-6	Figure 2.2-6	Figure 2.2-6	
7075-T6 Aluminum Alloy	0.1	890-1180°	Figure 2.2-12	Figure 2.2-12	Figure 2.2-12	
6061-T6 Aluminum Alloy	0.1	1250°				
FSI-H24 Magnesium Alloy	0.064	1160°	Figure 2.2-18	Figure 2.2-18	Figure 2.2-18	
M-H24 Magnesium Alloy	0.064	1200°	68-212° 0.249	212-482° 871	60-212° 14 60-750° 16	
HK31-T6 Magnesium Alloy	0.064					
C-110M Titanium Alloy	0.171	2730-2910°	Figure 2.2-24	Figure 2.2-24	Figure 2.2-24	500-1000°
A-110AT Titanium Alloy	0.161	2800°	32° 0.126 600° 0.145 1200° 0.170 1500° 0.188	32° 51.8 600° 75.6 1200° 107.3 1500° 125.0	300° 5.2* 1000° 5.8* 1300° 6.25*	500-1000°
6AL-4V Titanium Alloy	0.160	2800°			90-932° 5.2 932-1652° 5.8	500-1000°
Refractoloy 26 Cobalt-Nickel-Chromium-Iron Alloy				200° 104 600° 136 800° 151 1100° 173		
A-286 Iron-Chromium-Nickel Alloy	0.286	2550°	79-304° 0.1 82-577° 0.11 86-1004° 0.11 104-1299° 0.11	70° 88 572° 124 800° 140 932° 151 1200° 172	70-200° 9.2 70-600° 9.5 70-1000° 9.9 70-1500° 10.3	1850°
V-36 Cobalt-Nickel-Chromium-Iron Alloy	0.313	2400°	Same as S-816		Same as S-816	
Inconel X Nickel-Base	0.298	2540°	Figure 2.2-45	Figure 2.2-45	Figure 2.2-45	1600°
M-252 Nickel-Base	0.298	2485°		70° 79 800° 115 1200° 135	70-200° 7.8 70-600° 8.0 70-1000° 8.2 70-1500° 8.8	1800°
Waspaloy Nickel-Base	0.298	2500°				
Hastelloy C Nickel-Base	0.323	2350°	R.T. 0.092	392° 78 572° 88 752° 98 932° 108 1112° 118	70-600° 7.02 70-800° 7.35 70-1000° 7.44 70-1200° 7.73 70-1500° 8.07 70-1600° 8.20	2000°
Hastelloy X Nickel-Base	0.297	2400°		R.T. 67.3 572° 102 932° 127 1292° 158 1652° 190	79-200° 7.7 79-600° 7.9 79-800° 8.15 79-1000° 8.39 79-1200° 8.56 79-1650° 9.07 79-1800° 9.20	
Haynes Alloy 25 (L-605) Cobalt-Base	0.33	2570°	R.T. 0.0925	Figure 2.2-48	Figure 2.2-48	1900°
Alloy Steels 4140, 8630, 4340 H.T. to 200,000 psi	0.281	2500°	Figure 2.2-28	Figure 2.2-28	Figure 2.2-28	1000°
Hy-Tuff Annealed at 1600°F; Tempered at 600°F, 1/2 hr	0.281	2500°	Same as 8630	Same as 8630	-100° to -200° 6.4	1000°
18-8 Type Stainless Steels 3/4-Hard	0.29	2550-2650°	Figure 2.2-32	Figure 2.2-32	Figure 2.2-32	1650°
AISI Type 316 Stainless Steel Annealed	0.29	2500-2550°	Figure 2.2-32	Figure 2.2-32	Figure 2.2-32	1600°

NOTES: *Instantaneous coefficient of thermal expansion. All figure numbers pertain to Part I.
R.T. = room temperature.

TABLE III-2 (cont)

SUMMARY OF PHYSICAL PROPERTIES OF STRUCTURAL MATERIALS

Material	Density, ($lb/in.^3$)	Melting Point (°F)	Specific Heat (BTU/°F/lb)	Thermal Conductivity (BTU-in./ft^2 hr in.)	Mean Coefficient Of Thermal Expansion (in./in./°F x 10^6)	Oxidation Resistance Scaling(°F)
AISI Type 310 Stainless Steel Annealed	0.29	2550-2650°	32-212° 0.12	212° 90 392° 98.4 572° 105 752° 114 932° 120	32-212° 8 32-572° 9 32-932° 9.4 32-1112° 9.7 32-1832° 10.6	2000°
AISI Type 410 Stainless Steel Annealed	0.28	2700-2790°	32-212° 0.11	212° 173 392° 180 572° 186 752° 193	32-212° 6.1 32-1000° 7.2 32-1832° 7.6	1200°
17-17 PH Stainless Steel	0.276	2550-2650°	Figure 2.2-36	Figure 2.2-36	Figure 2.2-36	1650°
16-25-6 Iron-Chromium-Nickel Alloy					70-200° 8.4 70-400° 8.7 70-600° 8.85 70-800° 9.05 70-1000° 9.2 70-1200° 9.4 70-1400° 9.5	
19-9 DL Iron-Chromium-Nickel Alloy	0.287	2600°		70° 94 200° 101 600° 117 1000° 134 1200° 143 1400° 150 1600° 163	70-212° 8.5 70-600° 9.31 70-1000° 9.78 70-1200° 9.97 70-1500° 10.1 70-1600° 10.2	1750°
H-155 Cobalt-Nickel-Chromium-Iron Alloy	0.3	2400°		392° 101 572° 110 752° 120 932° 129 1112° 139 1200° 154	70-200° 7.8 70-600° 8.0 70-1000° 8.5 70-1500° 9.0	1900°
S-590 Cobalt-Nickel-Chromium-Iron Alloy	0.301	2450°	77-572° 0.1 77-932° 0.1 77-1292° 0.11	70° 82 800° 125 1200° 150 1292° 155	70-200° 7.5 70-600° 7.6 70-1000° 8.0 70-1200° 8.0 70-1400° 8.3 70-1600° 8.4 70-1800° 8.4	1850°
S-816 Cobalt-Nickel-Chromium-Iron Alloy	0.313	2400°	77-572° 0.095 77-932° 0.10 77-1292° 0.12	70° 82 300° 101 800° 125 1200° 150 1292° 155	70-200° 6.5 70-600° 6.6 70-1000° 7.1 70-1200° 7.4 70-1400° 7.7 70-1600° 8.0 70-1800° 8.3	1850°

All figure numbers pertain to Part I.

[redacted]

TABLE III-3

PROPERTIES OF HIGH-TEMPERATURE REFRACTORY-TYPE MATERIALS

Material	Melting Point (°F)	Density ($lb/in.^3$)	Oxidization Resistance (°F)	Short-Time Tensile Strength (psi x 10^{-3})	Short-Time Compressive Strength (psi x 10^{-3})	Transverse Rupture Strength (psi x 10^{-3})	Modulus of Elasticity (psi x 10^{-6})	Specific Heat (BTU/lb/°F)	Thermal Conductivity (BTU-in./ ft^2 hr in.)	Coefficient of Thermal Expansion (in./in./°F x 10^6)	Stress for Rupture in 100 Hours (psi x 10^{-3})
Molybdenum	4710°	0.369	700° (932° Max.)	Fig. 2.2-49			Fig. 2.2-49	Fig. 2.2-50	Fig. 2.2-50	Fig. 2.2-50	1600° 35 1800° 29 2000° 8.4
Tungsten	6120°	0.697	750-930°	2500° 25 3000° 15 4000° 6.0 4500° 2.0 (For Wire)			R.T. 50	70-212° 0.034 70-1832° 0.0365	70° 1060	32-932° 2.5 1112-1832° 2.88	
Aluminum Oxide Alite 212	3720°	0.131	2912°*	Fig. 2.2-51	R.T. 285 Alumina R.T. 420 1830° 125 2730° 14	R.T. 48	Fig. 2.2-51	Fig. 2.2-52	Fig. 2.2-52	Fig. 2.2-52	
Beryllia Beryllium Oxide	4500°	0.113		R.T. 20	R.T. 110 1830° 35 2910° 7		R.T. 43	257-1870° 0.071	2012° 70-122	R.T.-1800° 5	
Zirconia Zirconium Oxide	4900°	0.212		R.T. 21 1830° 13 2730° 22	R.T. 290 1830° 170 2730° 2.8		R.T. 24 1830° 16	70-1832° 0.157	2400° 14.3	R.T.-1800° 3-6	
Graphite	8550°	0.0556-0.0596	700°	R.T. 3.5 1000° 3.7 2000° 4.2 3000° 4.6 4000° 5.6 4500° 6.7	R.T. 10	R.T. 4.8	0.6-1.9	100° 0.178 400° 0.28 800° 0.364 1000° 0.392	100° 985 400° 815 800° 635 1000° 575 2000° 220	R.T. 1.5-0.94	
Zirconium Boride	5400°	0.18-0.191	> 2000°	1800° 35-40		60° 66 1800° 63 2200° 55	60° 31.6 1800° 24	60° 0.115 1800° 0.25	110° 191	75-1000° 2.7 75-2200° 3.2	1800° 18.5
Chromium Boride 300 Series	3200-3450°	0.223-0.225	> 1800°			1800° 80-138				70-1800° 5.45	1800° 12-28 2000° 3.5
Chromium Boride 400 Series	3400-3600°	0.225-0.260	< 2000°			1800° 90-140				70-1800° 5.5	1800° 14-24 2000° 15

NOTES:

*Maximum working temperature.
R.T. = room temperature.

All figure numbers pertain to Part I.

[redacted]

[redacted]

TABLE III-3 (cont)

Material	Melting Point (°F)	Density ($lb/in.^3$)	Oxidization Resistance (°F)	Short-Time Tensile Strength (psi x 10^{-3})	Short-Time Compressive Strength (psi x 10^{-3})	Transverse Rupture Strength (psi x 10^{-3})	Modulus of Elasticity (psi x 10^{-6})	Specific Heat (BTU/lb/°F)	Thermal Conductivity (BTU-in./ ft^2 hr in.)	Coefficient of Thermal Expansion (in./in./°F x 10^6)	Stress for Rupture in 100 Hours (psi x 10^{-3})
Silicon Carbide	3990°	0.183	1475°			2460° 2.0-5.6		70-1832° 0.186 32-2550° 0.285	2000° 66 2200° 109-113	70-2000° 2.5 70-2550° 2.44	
Nickel Aluminide (Ni, Al)	3000-3050°	0.205-0.210	> 2000°			1800° 65-145 2000° 60-150				70-1800° 8.0	1800°<12
Molybdenum Dicilicide	3400°	0.22	3090°	R.T. 25 1000° 31 1400° 35 1800° 40 2000° 41 2200° 37-42 2400° 22-41	R.T. 350	1800° 67 2000° 85 2200° 54			300° 385 1000° 240 1400° 220	R.T.-2732° 5.1	1600° 35.5 1800° 28.5 200° 8.2
Titanium Carbide +10 to 40% Ni or Ni Alloy Kentanium	5800°	0.198-0.234	> 1800°	R.T. 80-155 1500° 55 1800° 40 2000° 30 2200° 12 2400° 3	R.T. 550	R.T. 175	R.T. 35-60		R.T. 206-247	70-1200° 4.5-6.2	1600° 29.2 1800° 15.5 2000° 3.2 (K 161 B)
Metamic Lt-1 Chromium (70%) & Aluminum Oxide	3360°	0.216	2190°	1800° 17.5 2000° 12.0 2200° 7.0 2400° 3.2		R.T. 50 1830° 38 2550° 15			58.1	32-1830° 4.66	
WZ-1 Titanium Carbide & Nickel-Chromium		0.216-0.249	> 2000°			R.T. 175-225 1832° 125-150				70-1832° 5.6-7.0	1800° 14.0
WZ-12 Titanium Carbide & Nickel-Chromium -Cobalt		0.216-0.249	> 2000°	R.T. 120-150 752° 118-135 1112° 110-120 1472° 76-90 1832° 33-48 2000° -30		R.T. 175-225 1832° 125-150				70-1832° 5.5-6.6	1800° 9.5

NOTE:

R.T. = room temperature.

[redacted]

[redacted]

TABLE III-4

APPROXIMATE COST OF STRUCTURAL MATERIALS (1955)

Materials	Cost (per lb)
Aluminum Alloys	$ .51
Magnesium Alloys	.59
Titanium Alloys	15.00
Alloy Steels	
4130, 8630, 4340	.06
Stainless Steels	
18-8	.36
310	.60
430, 446	.60
17-7 PH	.36
Highly Alloyed Austenitic Steels	
19-9 DL	.75
N-155	4.00
S-590	3.43
S-816	6.14
A-286	1.87
Nickel-Base Alloys	
Inconel X	2.00
Hastelloy X	2.50
Hastelloy C	3.50
Cobalt-Base Alloys	
H. S. 25 (L-605)	5.50

[redacted]

NOTES

SECTION IV

INSULATION

By W.H. Dukes, M.A. Goldberg and M.A. Brull

TABLE OF CONTENTS

[redacted]

LIST OF ILLUSTRATIONS

LIST OF TABLES

[redacted]

NOMENCLATURE

a = a constant defined in the text

B = constant defined in the text

$C = \left(T_o - T_{mi}\right) / \left(T_o - T_m^*\right)$

c_i = specific heat of insulation (BTU/lb °F)

c_m = specific heat of metal (BTU/lb °F)

D = fiber diameter

f = fraction of total insulation volume which is fiber

g = gravity constant (ft/sec^2)

h = heat transfer coefficient (BTU/ft^2 hr °F)

h_e = effective heat transfer coefficient which includes the thermal resistance of the insulation (BTU/ft^2 hr °F)

$K = k_m / k_i$

k = conductivity (BTU-in./ft^2 hr °F)

k_a = conductivity of air (BTU-in./ft^2 hr °F)

k_c = thermal conductivity of air including convection (BTU-in./ft^2 hr °F)

k_g = thermal conductivity of a free gas

k_i = conductivity of insulation (BTU-in./ft^2 hr °F)

k_m = conductivity of metal skin (BTU-in./ft^2 hr °F)

k_r = equivalent conductivity for radiation (BTU-in./ft^2 hr °F)

L = thickness of gas layer (ft)

L_f = average spacing between fibers (microns)

L_g = mean free path of a molecule in a free gas

(N_{Gr}) = Grashof number

n = number of intermediate radiation foils in an air space

Q_o = total heat flux (BTU/hr)

r = distance from point source of heat (in.), or $t / (t + x_i)$

$R^2 = \alpha_m / \alpha_i = K\delta^2$

$S = \bar{s}/x$

$\bar{s}$ = variable in the thickness direction through an insulated slab (in.)

T = structural temperature (°F or °R)

T_i = temperature of insulation (°F)

T_m = temperature of metal skin (°F), or mean temperature (°R)

T_{mi} = initial metal temperature (°F)

NOMENCLATURE (cont)

T_m^* = metal temperature having the maximum value through the thickness (°F)

T_o = temperature at outer surface of insulation (°R or °F)

T_{oj} = equilibrium temperature at the end of the j^{th} time interval (°F)

T_r = boundary layer recovery temperature (°F or °R)

T' = temperature in structural skin, neglecting thermal leakage through insulation (°F)

ΔT = temperature difference across an air space (°F)

T_I = initial temperature (°R)

t = metal skin thickness (in.)

$u_m = T/T_o$

$u_i = T_I/T_o$

v = ratio of temperature rise (due to thermal leakage) to the structural temperature without leakage

x,y,z = mutually perpendicular coordinate axes

X = total thickness of insulation plus skin (in.)

x_i = insulation thickness (in.)

Y = temperature concentration factor due to thermal leakage through insulation

q = heat flux per unit area (BTU/ft^2 hr)

α = fraction of incident radiant energy absorbed by a fiber

α_m = diffusivity of metal (in.^{2}/sec)

α_I = diffusivity of insulation (in.^{2}/sec)

β = coefficient of cubic expansion of gas

γ = a constant defined in the text

$\delta^2 = \rho_i c_i / \rho_m c_m$

ϵ = surface emissivity

ϵ_e = effective emissivity between two parallel walls

η = a constant defined in the text

θ = time (sec)

ν = kinematic viscosity of gas

ρ_i = density of insulation (lb/ft^3)

ρ_m = density of metal skin (lb/ft^3)

$\tau = \alpha_m \theta / x^2$

[redacted]

SECTION IV

INSULATION

A. GENERAL

Since the use of insulation as a means of protection against heat is a successful and well-established practice in many branches of engineering, it is necessary to inquire into its possibilities when applied to high-speed aircraft structures. The objective of this section is to make such an inquiry to establish (1) the types of insulation that are most suited for airframe applications, (2) the purposes insulation might serve, and (3) the properties such as weights and thicknesses that are involved in the various applications. Insulation is one more subject, introduced by aerodynamic heating, in which the structures engineer has little or no previous experience. An attempt will be made in this section to develop some of the "feel" for the subject that is usually the result of such experience.

This section begins with a discussion of the mechanics of heat transfer through various types of insulation, the effect of various factors such as temperature and pressure, and the directions which should be followed in developing improved insulating materials. Although this material development is primarily a matter for the manufacturer rather than the airframe designer, since it is closely associated with manufacturing processes, an understanding of the principles will be of assistance in devising superior combinations of existing materials.

Analytical methods are given for the design of insulation for specific applications and these include a compilation of existing work together with some original analyses. These methods cover all insulation types that are presently used and, in most cases, both steady-state and transient conditions are included. The transient condition will arise often in the design of high-speed airframes, since it is the case where heat passing through the insulation is absorbed only by the structure beneath, leading to a constantly changing structural temperature.

A survey of available insulating materials and combinations of materials is given, and sufficient comparisons are made to demonstrate those arrangements that are most efficient and should be included in studies of insulated structure. Such studies are made in a limited manner in Section IX where insulated structures are compared with other types. It has been found that only a limited number of insulating systems justify continued consideration.

Presented in the final part of this section is a discussion of the various structural applications for which insulation is expected to be used. Curves and tables are included to show weights and thicknesses involved in these applications. These data are intended for developing a "feel" for the use of insulation; when used in conjunction with Sections II and IX, these data should enable the design engineer to evaluate insulation for any particular problem, at an early stage of his work.

B. HEAT TRANSFER THROUGH INSULATION

Transfer of heat through a medium occurs by one or more of the following mechanisms:

(1) Conduction – energy transfer by molecular agitation.

(2) Radiation – an electromagnetic form of energy transmission.

(3) Convection – energy transfer by mass displacement of the medium.

Conduction is predominant in solids, while liquids and particularly gases transmit relatively small quantities of heat by conduction. Since radiation can exist only through a nonabsorbing medium, it is an important form of heat transfer through gases and is the only method of transferring heat through a vacuum. Convection, since it requires circulation and mixing of the medium to effect heat transfer, can exist only in liquids and gases.

A comparison of the thermal conductivities of air, water, and aluminum typifies the relative conductivity of gases, liquids, and solids. Water is 300 times more conductive than still air, whereas the conductivity of aluminum is 30 times greater than that of water.

Because of the low conductivity of gases, the most efficient methods of insulating concern the use of a blanket of air as the heat-resisting means, with arrangements for minimizing heat transmission by convection and radiation. In the fibrous, powdered, and other loose fill-type insulations, the material breaks up the air space into small cells so that convection is prevented, and the fill also blocks most of the radiation. Some additional conduction is provided by the fibers or powder granules, but again this is minimized by the small contact areas between any two fibers or grains. Since the heat transfer through such a material is complex, an over-all conductivity is usually determined experimentally and the material is treated theoretically as if it had only conduction characteristics. Generally, such a conductivity will vary widely with temperature.

Similar results are obtained in a slightly different manner with cellular materials. These are a continuous rather than a loose fill-type material in which numerous bubbles or cells are formed during manufacture. The percentage of volume occupied by these pockets controls the density and the conductivity, the large cell volume giving low values of both. If the cell volume is small, so that density and conductivity are relatively high, some mechanical strength is achieved. The mechanism of heat transfer is similar to that occurring in fibrous materials; conduction along the cell walls, and conduction, convection, and radiation across the cells. Again, the object is to achieve a large number of small cells. This will generally stop convection completely, provide a long conduction path along the cell walls, and interpose the maximum number of planes to radiation. The significance of this latter point will be demonstrated later.

A third method of utilizing the low conductivity of air is to omit the fill material, with a consequent saving in weight, and to provide the two parallel walls bounding the air space with highly reflective surfaces to minimize radiant heat transfer. Convection effects must then be included, so that this system is effective when the air pressure is low and convection is small.

At high temperatures, the heat transmission by radiation may still be significant in the insulating arrangement described in the previous paragraph despite the reflective surfaces of the bounding walls. Additional highly reflective metal foils can then be introduced into the air space, parallel with the bounding walls, and separated from each other. In this manner, radiation is reduced further by the multiplicity of reflective surfaces, but at the cost of additional weight and increased conduction through the foil separating means. Such an arrangement of metal foils has been termed a radiation barrier.

Since these insulations are based upon the low conductivities of gas, they are relatively efficient from the thermal point of view. None of the materials, however, have mechanical strength; their use around the outside of an airframe requires an additional structural shell for protection from aerodynamic forces, and to maintain the airframe shape.

To avoid this complexity, it is natural to seek materials having both mechanical strength and insulating value together with resistance to high temperature. The combination of these three requirements has narrowed the field of interest to the ceramics (primarily the metal oxides), but the best ceramic is inferior in insulating value and heavier in weight when compared with fibrous materials.

It is now appropriate to consider in detail the effect of various factors on the heat transfer through each of these material types.

1. Fill- and Cellular-Type Insulators

a. Temperature Effects

The various modes of heat transfer through fibrous and cellular insulators have already been described. In discussing temperature effects on the insulation, it is convenient to consider the effects on the individual modes of heat transfer. In Reference 1, Vershoor and

[redacted]

Greebler have shown that the contribution of radiation to the apparent conductivity of a fibrous material is given by

$$k_r = 2.74 \times 10^{-13} \frac{T_m^3 L_f}{a^2} ,$$

where the quantity a is the fraction of incident radiant energy absorbed by a single fiber, L_f is the average spacing between fibers, and T_m is the average temperature of the insulator. This equation shows that radiation effects in fibrous insulators increase rapidly with temperature; the effect is illustrated for a typical material in Figure IV-1. This figure shows the contribution to total conductivity of the various forms of heat transmission at three temperature levels, 500°, 1000°, and 1500°F. The curves are taken from Reference 2.

The variation of thermal conductivity of air with temperature is shown in Figure 2.3-1 of Part I, and significant increases are apparent as the temperature increases. Since air is an important component of a fibrous insulator, increases in its conductivity contribute to the total as shown in Figure IV-1. These increases are much more moderate than those that are due to radiation, as is to be expected from the cubic term in the expression for k_r.

Fiber conduction increases only slightly with temperature so that, from the equation for k_r, the most promising approach to minimizing conductivity increases with temperature is to increase fiber opacity and decrease the average spacing. A reduction of average spacing without change in density requires smaller fiber diameter, which is probably controlled by the manufacturing process and the type of material. Occasional attempts have been made to increase fiber opacity by techniques such as dusting with aluminum powder, but the results are not conclusive.

The data with respect to fibrous materials apply equally to cellular materials where again a material of high opacity is desirable, with cells of small size.

b. Density Effects

The density of fill-type insulating materials is indicative of the quantity of solid material present, so that as density increases the conduction through this material increases. Radiation transmission through the insulation is, however, reduced by increased density, and at very low densities, where radiation is important, this effect predominates. Figure IV-1 illustrates these trends.

For this type of insulating material, therefore, the effect of increasing density is first to decrease conductivity and then to increase it. Total conductivity curves for a number of materials have the characteristic shape shown in Figure IV-2, and this shape is more pronounced as temperatures are increased.

Evidently, from Figure IV-2, fill-type materials have a density, at each temperature, at which conductivity is a minimum, and for some applications this may be the optimum condition. For airframe design, it may be expected that weight is the criterion, indicating that maximum thermal resistance is required for each pound of insulation. Optimum conditions are then reached at a minimum value of the quantity (conductivity x density), and this condition generally exists at a density below that of minimum conductivity.

c. Pressure Effects

Since pressure changes in an insulating material can affect only the gas characteristics, it is necessary to consider the effect of pressure on the conductivity of a gas.

The kinetic theory shows that the thermal conductivity of a gas is proportional both to the density of the gas and to the mean free path of its molecules. The density is directly proportional to pressure, and the mean free path is inversely proportional to pressure so that conductivity remains constant. This independence of conductivity and pressure persists until the pressure is low enough that the mean free path of the molecules is of the same order as the fiber spacing or

pore size in the insulation. Further reductions in pressure can affect only density, so that conductivity decreases proportionately.

From Reference 1, if the fibers of an insulation are assumed to be randomly oriented but in planes normal to the heat flow, the average distance between fibers is

$$L_f = 0.785\ D/f,$$

where D is the fiber diameter and f is the fraction of total volume constituted by fiber. If L_g is the mean free path of a molecule in free gas, for a fibrous material containing a gas, the mean free path of a molecule is

$$L = L_g \Big/ \left(1 + \frac{L_g}{L_f}\right).$$

Then the thermal conductivity of a gas in a fibrous insulation is

$$k = k_g \frac{L_g}{\left(1 + \frac{L_g}{L_f}\right)},$$

where k_g is the thermal conductivity of the free gas.

This analysis shows another reduction in conductivity which is possible with fine fibers that are closely spaced, if the spacing is reduced to the same order as the mean free-path lengths. Although this has not been accomplished generally with commercial materials in the usual range of pressures, successful tests are reported in Reference 3 in which conductivity reductions were obtained by adding a fine powder to the insulation to fill the spaces between fibers.

At pressures below 10 mm of mercury, existing insulating materials are apparently sufficiently fine to show reductions in conductivity as the pressure is reduced further. The results of tests in Reference 1 are given in Figure IV-2. From the figure it will be seen that very low conductivities are possible by the method of Reference 1. Also shown are results of calculations based upon the formulas presented previously. Of particular significance are the low values of conductivity at the higher densities where radiation effects are small.

Except in pressurized areas, the interior of an airframe is generally at a pressure close to ambient, so that the venting of an insulation to ambient pressures should not impose a structural weight penalty. With this condition, the reductions in conductivity discussed previously may have application to aircraft flying at the extreme altitudes considered in Section II. At 200,000 feet, for example, ambient pressure is 0.0044 psi or 0.228 mm of mercury. At this pressure, Figure IV-2 shows a 70% reduction in conductivity for the 4.63 lb/ft^3 material.

d. Fiber Orientation

In fibrous insulators, the orientation of the fibers has an effect on the direct conduction; the most desirable condition is for fibers to cross normal to each other so that only point contacts are made. Standard insulating materials presumably satisfy this requirement sufficiently since, from Figure IV-1, the direct fiber conduction is very small over the density range of interest (2 to 6 lb/ft^3).

2. Air Space Insulation

The principal factors affecting the conductivity of air, as described for fill-type materials, apply equally when the air is used alone, as an insulator. In this application, however, the air space will be much larger than those existing within fill-type materials, so that heat transfer by natural convection will probably exist. Although convection is a mechanical process and as such is treated analytically in Section IV, C, it depends upon air characteristics which are in turn affected by pressure and temperature. Consequently, some discussion is justified here.

As shown in Section IV, C, the quantity of heat transferred by convection between horizontal plates depends upon the ratio between the coefficient of cubic expansion and the square of kinematic viscosity. Heat transferred by convection increases as the square root of this ratio increases. The ratio increases rapidly with pressure and decreases, also at a high rate, with temperature. An increase in pressure from 200 to 2000 lb/ft^2 produces a tenfold increase in the ratio which is increased by a further factor of 5.0 if the pressure is increased to 4000 lb/ft^2. Conversely, a temperature rise from 0° to 900°F reduces the ratio by a factor of 100.

These changes are large, but two factors exist that appreciably reduce their significance. The first factor is that convection is easily stopped by mechanical means, and this is one of the functions of the fibers or granules in a fill-type insulation. More important is the fact that applications for insulation involve aircraft which fly at high altitude where pressures are low, and at high speed involving high temperature. Conditions are therefore correct for minimizing natural convection in air spaces used as insulation, provided only that dynamic pressures can be kept out of the insulating element.

It has been explained that the use of an air space as insulation may permit significant heat transfer by radiation, depending upon the temperature levels. The heat transferred by radiation is a function of the emissivities of the surfaces bounding the air space, and emissivity, in turn, is critically dependent upon surface condition.

Low values of surface emissivity in the temperature range of interest are achieved with polished metallic surfaces; the factors affecting this surface condition are primarily temperature and corrosion.

Temperature produces a direct increase in emissivity, but it is also the cause of surface oxidation in most materials. An oxidized surface will usually have an emissivity between five and ten times that of a polished surface. Only one material, platinum, seems to be completely free of oxidation at temperature; gold possibly has a similar characteristic. Economic considerations will probably prevent the use of these materials directly. Their use as a plating or cladding is difficult because the surface has porosity and oxidation of the base material still occurs.

Fortunately, this problem is not too important because the effective emissivity is a function of the condition of both facing surfaces, and its value can not exceed the lower emissivity of either face. This will be evident from the analysis in Section IV, C. Since the use of insulation is generally to delay structural temperature rise, the structural wall bounding the air space will be cool and not be subjected to significant oxidation. Corrosion and oxidation that occurs under normal low-temperature conditions, then, becomes the important consideration.

Here again, the highly polished condition which achieves low emissivity values cannot be maintained for any length of time, as is common experience except in one important case. This exception to the general rule involves pure aluminum which forms a thin, impervious oxide coating after which further corrosion ceases. Samples of aluminum foil subjected to room-temperature atmospheric conditions for a number of years have shown negligible increases in emissivity, and some evidence exists that the initial formation of oxide slightly reduces the emissivity.

It should be noted that the reflectivity of surfaces to visible light is not necessarily a criterion by which to judge their performance with lower frequency radiation. Transparent lacquers, for instance, which may effectively prevent corrosion and have no effect on the visible reflectivity of a surface, nevertheless produce high values of emissivity when applied to thermal insulation.

3. Radiation Barrier Insulation

Since this type of insulation is compounded of reflective foils with air between, it is subject to all the effects discussed previously. Generally, the foils will be sufficiently close that convection will not be important and, if an aluminum structure is involved, as is usually the case, there will be a sufficient number of cool aluminum foils to avoid the problems of oxidation. The most important factor affecting the over-all conductivity of radiation barrier insulation is, therefore, the effect of temperature on the conductivity of air.

4. Solid-Type Insulation

The only consideration with a solid-type insulation is the effect of temperature which tends to increase conductivity. Since the importance of this effect varies considerably between different materials, actual values must be taken from material properties.

C. ANALYTICAL METHODS

The discussions of the previous section have described the various mechanisms by which insulating materials retard the flow of heat. From the number of insulation methods that have been mentioned, it is apparent that an analytical treatment of the subject required the solution of three problems:

(1) Transfer of heat to a skin protected by a layer of low conductivity material.

(2) Transfer of heat to a skin protected by radiation foils, including the effect of air between the foils.

(3) Transfer of heat across an air space, including the effect of convection.

Item (1), the first problem, is applicable not only to solid insulation-type materials, but also to fibrous, granular, and cellular materials because the thermal properties of the latter three are generally expressed by an over-all conductivity that has been determined experimentally. The problem is solved only for the transient condition where the inside skin acts as the heat sink and thus experiences a continuous temperature rise. The steady state condition, such as may be applied to the insulation of a cooling system, is extremely simple and may be found in text books on heat transfer.

Item (2), applicable to radiation barriers, considers in this case both transient and steady state conditions. Item (3) required consideration of all modes of heat transfer in the analysis and, since each mode depends upon different parameters, the generalized analytical approach is not practical. Therefore, only the steady-state condition is considered since, with this simplification, the various modes of heat transfer can be treated separately and the total obtained by summing.

The discussions in Section IV, B emphasized the efficiency of gases and loose fill-type insulating materials; obviously, the use of such materials requires an outer structural wall capable of carrying aerodynamic pressure loads. It is also evident that load-carrying attachments will be necessary for such an outer wall and that these attachments may provide a path of thermal leakage through the insulation. Analytical solutions are therefore included for the two cases of a point and a line type of leakage path. The former represents a single bolt or pin type of outer wall attachment, while the latter is equivalent to an angle or channel.

1. Transfer of Heat Through a Low-Conductivity Material

To estimate the insulation required to maintain a structure below a given temperature, the problem of heat conduction through a composite slab will be considered. Such a slab is shown in the following sketch, together with the coordinate system used.

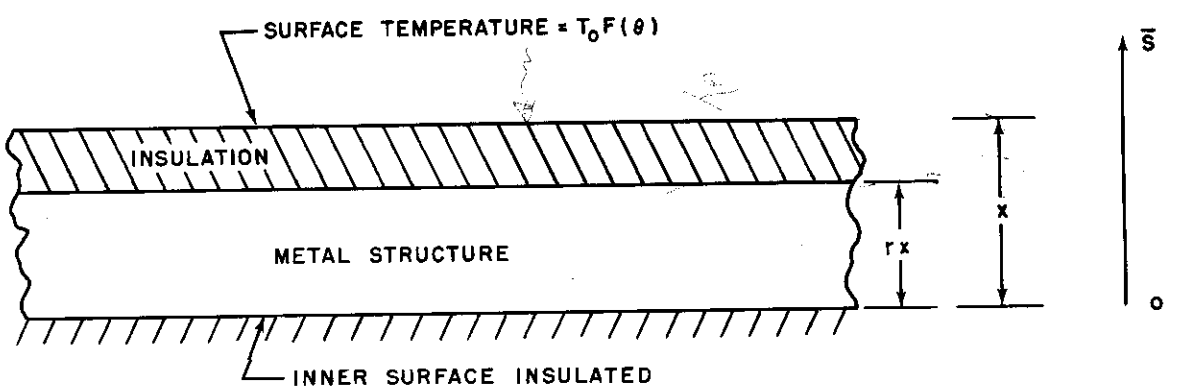

By writing heat balance equations for an element of insulation and an element of metal, it is found (Reference 3) that the temperature in the slab must satisfy the differential equations

$$\frac{\partial^2 T_m}{\partial \bar{s}^2} = \frac{1}{\alpha_m} \frac{\partial T_m}{\partial \theta}, \quad 0 \leq \bar{s} \leq rX, \text{ and} \tag{1}$$

$$\frac{\partial^2 T_i}{\partial \bar{s}^2} = \frac{1}{\alpha_i} \frac{\partial T_i}{\partial \theta}, \quad rx \leq \bar{s} \leq X, \tag{2}$$

with the boundary conditions

$$\left.\begin{aligned} &\frac{\partial T_m}{\partial \bar{s}} = 0 \text{ at } \bar{s} = 0, \\ &T_m = T_i \text{ and } k_m \frac{\partial T_m}{\partial \bar{s}} = k_i \frac{\partial T_i}{\partial \bar{s}} \text{ at } \bar{s} = rX, \text{ and} \\ &T_i = T_o F(\theta) \text{ at } \bar{s} = x, \end{aligned}\right\} \tag{3}$$

and the initial condition

$$T(S, \theta) = T_o f(\bar{s}). \tag{4}$$

The subscript m denotes the metal and the subscript i denotes the insulator. It is convenient to define the following dimensionless variables

$$S = \bar{s}/X, \quad \tau = \alpha_m \theta / X^2, \quad u = T/T_o, \quad K = k_m/k_i,$$

$$R^2 = \alpha_m/\alpha_i = K\delta^2, \text{ and } \delta^2 = \rho_i c_i / \rho_m c_m.$$

Introducing these variables in equations (1) through (4) gives

$$\left.\begin{aligned} &\frac{\partial u_m}{\partial S^2} = \frac{\partial u_m}{\partial \tau}, \quad 0 < S < r, \text{ and} \\ &\frac{\partial u_i}{\partial S^2} = R^2 \frac{\partial u_i}{\partial \tau}, \quad r < S < 1. \end{aligned}\right\} \tag{5}$$

$$\left.\begin{aligned} &\frac{\partial u_m}{\partial S} = 0 \text{ at } S = 0, \\ &u_m = u_i \text{ and } K \frac{\partial u_m}{\partial S} = \frac{\partial u_i}{\partial S} \text{ at } S = r, \text{ and} \\ &u_i = F(\tau) \text{ at } S = 1. \end{aligned}\right\} \tag{6}$$

$$u(S, 0) = f(S). \tag{7}$$

Since the last of the boundary conditions, equation (6), is time dependent, this boundary-value problem is not amenable to separation of variables. It is possible, however, to obtain a solution by assuming u_i and u_m in the form

$$u(S, \tau) = F(\tau) + v(S, \tau). \tag{8}$$

Substitution of equation (8) in equations (5), (6), and (7) will yield a set of equations in $v(s, \tau)$ which may be solved by the usual technique. The solution is (see Reference 3)

[redacted]

$$u(S,\tau) = F(\tau) + \sum_{n=1}^{\infty} \Phi_n(S) \left[A_n e^{-\lambda_n^2 \tau} - B_n \int_0^{\tau} e^{-\lambda_n^2 (\tau - \sigma)} F'(\sigma)\, d\sigma \right], \tag{9}$$

where $\Phi_n(S) = \begin{cases} \cos \lambda_n S, & 0 \le S \le r \\ \beta_n \sin R\lambda_n (1-S), & r \le S \le 1 \end{cases}$, (10)

$$\beta_n = \frac{\cos \lambda_n r}{\sin R\lambda_n (1-r)} ,$$

$$A_n = 2 \frac{\int_0^r y(S) \cos \lambda_n S\, ds + \delta^2 \int_r^1 g(S) \beta_n \sin R\lambda_n (1-S)\, ds}{\int_0^r \cos^2 \lambda_n S\, ds + \delta^2 \int_r^1 \beta_n^2 \sin^2 R\lambda_n (1-S)\, ds} ,$$

$$g(S) = f(S) - F(0) ,$$

and the eigenvalues λ_n are the positive roots of the equation

$$\tan \lambda_n r \tan R\lambda_n (1-r) = \frac{R}{K} . \tag{11}$$

The maximum temperature in the structure is $u(r,\tau)$, at the junction of the metal and the insulation. For the purpose of developing a simple method of estimating the required insulation thickness, this temperature is approximated by taking the first term of the infinite series of equation (9) and adjusting its coefficient so that the initial condition remains satisfied. For simplicity, the equilibrium temperature of the outer skin is also assumed constant, so that $F(\tau) = 1$ and $F'(\tau) = 0$. The approximate expression for the maximum metal temperature, then, is

$$\frac{T_m^*}{T_o} = 1 + \left(\frac{T_{mi}}{T_o} - 1 \right) e^{(\lambda_1^2 \alpha_m \theta)/x^2} , \tag{12}$$

where T_{mi} is the initial temperature of the metal.

Equation (12) may easily be put in the form

$$\lambda_1 = \frac{x_i}{\sqrt{\alpha_m}} \sqrt{\frac{\ln C}{\theta}} , \tag{13}$$

where x_i is the insulation thickness, and C is defined as

$$C = \frac{T_o - T_{mi}}{T_o - T_m^*} . \tag{14}$$

Since the metal thickness will generally be small compared with the insulation thickness for fibrous insulations, equation (11) may be approximated by

$$R\lambda_1 (1-r) = \tan^{-1} \frac{R}{K\lambda_1 r} . \tag{15}$$

From equation (13) and the definition of r, it is possible to obtain the relations

$$\lambda_1 r = \frac{t}{\alpha_m}\sqrt{\frac{\ln C}{\theta}}$$

$$R\lambda_1 (1-r) = \sqrt{\frac{x_i}{\alpha_i}}\sqrt{\frac{\ln C}{\theta}},$$

where t is the thickness of the metal. Making use of these expressions in equation (15) gives

$$\sqrt{\frac{x_i}{\alpha_1}} = \frac{\sqrt{\theta}}{\ln C}\tan^{-1}\left[\frac{\sqrt{\theta}}{\ln C}\,\frac{k_i}{\sqrt{\alpha_i}\,\rho_m c_m t}\right]. \tag{16}$$

Equation (16) is in a convenient form to calculate the insulation thickness required for a given case. Graphical representatives of this equation are shown in Part I, Section 6.0.

The temperature function for the case of variable equilibrium temperatures may be obtained from equation (9), or an approximation may be calculated by applying the Duhamel theorem to equation (12). The Duhamel formula may be written (see Reference 4)

$$\bar{u}(x,\theta) = \int_0^\theta F(\theta-\tau)\,\frac{\partial u}{\partial \tau}\,d\tau, \tag{17}$$

where $\bar{u}$ is the temperature corresponding with variable equilibrium temperature equal to $T_0 F(\theta)$, and T_0 is a reference value for the equilibrium temperature. In equation (17), u denotes the structural temperature in the case of constant equilibrium temperature at the outer surface. If the integral of equation (17) is approximated by a finite summation, and the time elapsed is divided into j increments, the temperature at the end of the jth time increment becomes

$$T_j = \left(1-\frac{1}{C}\right)\left[T_{oj} + \frac{1}{C}\,T_{o,j-1} + \frac{1}{C^2}\,T_{o,j-2} + \cdots + \frac{1}{C^{j-1}}\,T_{o1}\right] + \frac{1}{C^j}\,T_{mi}, \tag{18}$$

where T_{oj} equals the equilibrium temperature at the end of the jth time interval, T_{mi} equals the initial structure temperature, and C is defined in equation (14) in terms of the temperature at the beginning and at the end of a given time interval when the equilibrium temperature is constant. The use of this expression is explained in detail together with examples in Section VI of this report.

2. Transfer of Heat to a Skin Protected by Radiation Foils

From Reference 5, the radiant heat transfer per unit area between two parallel surfaces having temperatures T_0 and T_1 and surface emissivities of ϵ_0 and ϵ_1, respectively, is given by

$$q_{0-1} = \sigma\,\epsilon_{0-1}\left(T_0^4 - T_1^4\right),$$

where ϵ_{0-1} is an effective emissivity between the two surfaces, and

$$\epsilon_{0-1} = \frac{1}{\frac{1}{\epsilon_0} + \frac{1}{\epsilon_1} - 1}.$$

If a gas, such as air, is present between the foils, then an additional conduction term must be included to give the total heat transfer

$$q_{o-1} = \sigma \epsilon_{o-1} \left(T_o^4 - T_1^4\right) + \left[k_i \Big/ \left(x_i \Big/ (n+1)\right)\right]\left(T_o - T_1\right).$$

In this equation, x_i is the total thickness of the air space and n is the number of intermediate foils, so that the space is divided into $(n+1)$ elements all assumed equal. Convection is neglected since it will generally be possible to place the foils sufficiently close together to prevent it.

In a manner similar to the afore-mentioned, the heat transferred between foils 1 and 2 is

$$q_{1-2} = \sigma \epsilon_{1-2} \left(T_1^4 - T_2^4\right) + \left[k_i \Big/ \left(x_i \Big/ (n+1)\right)\right]\left(T_1 - T_2\right),$$

and similarly for foils 2 and 3, 3 and 4, etc. Note that, since the heat capacities are neglected,

$$q_{o-s} = q_{01} = q_{12} = q_{23} = \cdots\cdots = q_{n-s}.$$

Then, summing the heat fluxes through the various foils gives

$$\begin{aligned}(n+1)\, q_{o-s} &= q_{o-1} + q_{1-2} + q_{2-3} + q_{3-4} + \text{----} q_{n-s} \\ &= \sigma\left[\epsilon_{o-1}\left(T_o^4 - T_1^4\right) + \epsilon_{1-2}\left(T_1^4 - T_2^4\right) + \text{----} + \epsilon_{n-s}\left(T_n^4 - T^4\right)\right] \\ &\quad + \left[k_i \Big/ \left(x_i \Big/ (n+1)\right)\right]\left[\left(T_o - T_1\right) + \left(T_1 - T_2\right) + \text{----} \left(T_n - T\right)\right].\end{aligned}$$

If all values of ϵ are assumed equal and given by ϵ_e, the equation reduces to

$$q_{o-s} = \frac{\sigma \epsilon_e}{(n+1)}\left(T_o^4 - T^4\right) + \frac{k_i}{x_i}\left(T_o - T\right).$$

This equation gives the heat flux across a radiation barrier, including the effect of air between the foils, and is therefore the complete solution for the case when the structure is maintained at constant temperature, such as by cooling.

In the transient condition, with all heat absorbed by the structural skin, the heat flux is equated to the rate of structural temperature rise, giving

$$\rho_m C_m t \frac{dT}{d\theta} = \frac{\sigma \epsilon_e}{(n+1)}\left(T_o^4 - T^4\right) + \frac{k_i}{x_i}\left(T_o - T\right).$$

It is not practical to solve this equation exactly, but two useful solutions can be obtained by making certain assumptions. First, consider the case when the presence of air is neglected so that $k_i = 0$. Then, by separating the variables and integrating both sides of the equation, the solution is

$$\frac{\sigma \epsilon_e \theta}{(n+1)(\rho_m C_m t)} = \frac{1}{4T_o^3}\left[2\left(\tan^{-1}\frac{T}{T_o} - \tan^{-1}\frac{T_1}{T_o}\right) + \ln\left(\frac{T_o + T}{T_o - T}\,\frac{T_o - T_1}{T_o + T_1}\right)\right],$$

[redacted]

where T_1 is the initial structural temperature. Curves to facilitate the evaluation of this equation are given in Section 6.4 of Part I.

In order to include the effect of conduction through the air, it is noted that T_o will generally be large ($>1500°R$), otherwise radiation will not be important and radiation barriers will not be required. It is also found from Section IX that, if insulation is used, it is generally advantageous to use the insulation with an aluminum structure. This is doubly true when radiation barriers are used as insulation because of the added difficulty of maintaining low emissivity values at higher temperatures. Accordingly, the structural temperature T will vary through a small range, possibly from 560° to 760°R, and the T^4 term in the differential equation can be replaced by the approximation

$$T^4 \approx 4a^3T - 3a^4,$$

where a is a constant temperature selected from the midpoint of the range of T.

Making this substitution reduces the differential equation to

$$\rho_m C_m t \frac{dT}{d\theta} = \frac{\sigma \epsilon_e}{(n+1)}\left(T_o^4 - 4a^3T + 3a^4\right) + \frac{k_i}{x_i}\left(T_o - T\right).$$

This equation can be reduced to

$$\frac{dT}{d\theta} = B - \gamma T,$$

where

$$B = \frac{k_i}{x_i}\left(\frac{1}{\rho_m C_m t}\right)\left[T_o + \frac{\sigma \epsilon_e}{(n+1)}\frac{x_i}{k_i}\left(T_o^4 + 3a^4\right)\right], \quad \text{and}$$

$$\gamma = \frac{k_i}{x_i}\left(1 + 4\frac{a^3 x_i}{k_i}\frac{\sigma \epsilon_e}{(n+1)}\right)\frac{1}{\rho_m C_m t}.$$

The solution to the differential equation is

$$T = \frac{B}{\gamma} - e^{-\gamma\theta}\left(\frac{B}{\gamma} - T_1\right).$$

This last expression may be written as

$$e^{\gamma\theta} = \frac{\frac{B}{\gamma} - T_1}{\frac{B}{\gamma} - T},$$

or

$$\gamma\theta = \ln\left[\frac{\frac{B}{\gamma} - T_1}{\frac{B}{\gamma} - T}\right] = \ln\left(\frac{B - \gamma T_1}{B - \gamma T}\right).$$

Now, let $\eta = \frac{\sigma \epsilon_e}{(n+1)}\frac{x_i}{k_i}$ and, according to the afore-mentioned explanation, a may be expressed as $a = \frac{1}{2}(T_1 + T)$.

[redacted]

Then $\frac{B-\gamma T_1}{B-\gamma T} = \frac{T_o+\eta T_o^4+3\eta\frac{1}{16}(T_1+T)^4-T_1-4\eta\frac{1}{8}(T_1+T)^3 T_1}{T_o+\eta T_o^4+3\eta\frac{1}{16}(T_1+T)^4-T-4\eta\frac{1}{8}(T_1+T)^3 T}$ and

$$\gamma\theta = \frac{1}{\rho_m C_m t}\ \frac{\sigma\epsilon_e}{(n+1)}\ \frac{1}{\eta}\left[1+\frac{1}{2}\eta(T_1+T)^3\right]\theta ,$$

so that the final solution is

$$\frac{1}{\rho_m C_m t}\left[1+\frac{1}{2}\eta(T_1+T)^3\right]\theta = \left(\frac{x_i}{k_i}\right)\ln\left[\frac{T_o-T_1+\eta T_o^4+\frac{3}{16}\eta(T_1+T)^4-\frac{1}{2}\eta(T_1+T)^3 T_1}{T_o-T+\eta T_o^4+\frac{3}{16}\eta(T_1+T)^4-\frac{1}{2}\eta(T_1+T)^3 T}\right] .$$

As explained previously, T may range from 560° to 760°R approximately, and over this range of values the last two terms of both denominator and numerator of the $\ln$ term are small when compared with $\eta\ T_o^4$.

Similarly, it can be shown by substitution of values that $\frac{1}{2}\eta(T_1+T)^3$ is small when compared with unity for the practical range of values of ϵ_e, η, x_i, and k_i, and for T_i equals 560°R and T equals 760°R.

With these simplifications, the expression reduces to

$$\frac{\theta}{\rho_m C_m t} = \frac{x_i}{k_i}\ \ln\left(\frac{T_o - T_1 + \eta\ T_o^4}{T_o - T + \eta\ T_o^4}\right) .$$

This equation is presented graphically in Section 6.0 of Part I.

3. Transfer of Heat Across an Air Space

Heat transferred by conduction across an air space, under steady state conditions, is given by

$$q_c = \frac{k_a}{x_i}\ \Delta\ T .$$

Values of thermal conductivity for air, k_a, are given for various temperatures in Figure 2.3-1 of Part I. Figure 6.3-1 of Part I gives values of the heat transfer by conduction for a range of values of air-space depth and mean temperature.

Heat transferred by radiation can be obtained by simplification of the expressions given in Section IV. Making n equal to zero and neglecting the air conduction terms gives

$$q_r = \theta\ \epsilon_e\ \left(T_o^4 - T^4\right) .$$

If the two facing surfaces are identified by the subscripts 1 and 2, the effective emissivity for infinite parallel surfaces is

$$\epsilon_e = \frac{1}{\frac{1}{\epsilon_1}+\frac{1}{\epsilon_2}-1} .$$

Values of surface emissivity for various materials, surface conditions, and temperatures are given by Figures 2.3-5 through 2.3-12 of Part I, and the total heat transfer by radiation for a number of practical cases is shown in Figure 6.3-4 of Part I.

[redacted]

From page 534 of Reference 9, the heat transfer between two horizontal plane surfaces separated by air can be represented by

$$q_k = \frac{k_c}{L} \Delta T ,$$

where k_c is a conductivity which includes both conduction and natural convection effects. Reference 9 also shows that $k_c / k_a = \Phi (N_{Gr})$, where (N_{Gr}) is the dimensionless Grashof number and, for heat flow upwards, is equal to

$$\frac{\beta g}{\nu^2} L^3 \Delta T .$$

This condition occurs when a horizontal air space is used as insulation on the lower surface of a wing or fuselage. If the hot wall is on top, such as occurs on the top surface of a wing, convection will not exist.

On page 536 of Reference 9, a curve is given of k_c / k_a plotted against (N_{Gr}) and this curve applies when the value of (N_{Gr}) is between 2000 and 10 million. When this value is less than 2000, k_c / k_a equals 1.0, indicating that convection does not exist.

Within the range of application, the curve of Reference 9 can be closely approximated by the linear equation

$$\log (k_c / k_a) = \frac{1}{3} \log (N_{Gr}) = 1.10 .$$

Thus, $k_c / k_a = 0.080 \sqrt[3]{(N_{Gr})}$,

from which $q_k = 0.080 \; k_a \sqrt[3]{\frac{\beta g}{\nu^2}} \; (\Delta T)^{1.333}$.

Values of q_k as given by this equation are presented graphically for many values of air pressures, temperature difference, and mean air temperature in Figure 6.3-3 of Part I.

Before the afore-mentioned equation can be used, it is necessary to check that convection exists by ensuring that the Grashof number exceeds 2000. Therefore, convection exists if

$$\frac{\beta g}{\nu^2} L^3 \Delta T > 2000 .$$

If, for convenience, L is considered in inch units, the condition for convection becomes

$$\frac{\beta g}{\nu^2} L^3 \Delta T > 3.456 \times 10^6 .$$

This condition is easily reduced to

$$\log L > \frac{1}{3} \log \frac{3.45 \times 10^6}{\left(\frac{\beta g}{\nu^2}\right)} - \frac{1}{3} \log \Delta T .$$

For a gas such as air, the factor $\frac{\beta g}{\nu^2}$ depends only upon mean temperature and pressure. This equation indicates, therefore, that a plot of L against ΔT on log-log graph paper for various values of mean temperature and pressure will give a series of straight lines. If, for a particular example, the values of L and ΔT give a point which lies above the

corresponding temperature-pressure line, then convection exists. Figure 6.3-2 of Part I presents such a plot.

4. Thermal Leakage Through Insulation

Outer wall and insulation attachments provide paths of relatively high conductivity through the insulation material; as a result, structural temperature increases locally and thermal stress follows. The thermal gradients due to such conductive "short circuits" are, in general, of a secondary nature and may be expressed in the form of "temperature concentration factors" to be applied to the local temperatures in the protected structure. In practice, two types of attachments are encountered; each requires development of an analytical method for the evaluation of short-circuit effects.

The first type of attachment consists of rivets or bolts separated sufficiently that they may be treated as point sources of heat. It can be shown (see Reference 6) that the dimensionless temperature rise, v, is determined from

$$v = -\frac{Q_o \times 144}{4\pi k_m t T'} E_i\left(-\frac{r^2}{4\alpha_m \theta}\right), \tag{19}$$

where $v = \Delta T/T'$, the ratio of the temperature rise due to thermal short circuit to the structural temperature without short circuit, and $-E_i(-x)$ is the exponential integral as plotted in Reference 7. It is convenient to write equation (19) as

$$\frac{v k_m t T'}{144 Q_o} = -\frac{1}{4\pi} E_i\left(-\frac{r^2}{4\alpha_m \theta}\right). \tag{20}$$

This relation is presented graphically in Section 6.0 of Part I. It should be noted that for small values of the argument $-\frac{r^2}{4\alpha_m\theta}$, the function $E_i\left(-\frac{r^2}{4\alpha_m\theta}\right)$ may be represented approximately (see Reference 6) by

$$E_i\left(-\frac{r^2}{4\alpha_m\theta}\right) = 0.5772 + \ln\left(\frac{r^2}{4\alpha_m\theta}\right),$$

so that equation (2) becomes

$$\frac{v k_m t T'}{144 Q_o} = \frac{1}{4\pi}\left[\ln\left(\frac{4\alpha_m\theta}{r^2}\right) - 0.5772\right].$$

It is clear from the definition of v that the temperature at any point of structure is given by

$$T = (1+v)\,T',$$

so that the quantity $(1+v)$ can be considered a "temperature concentration factor." The effects of any number of attachments on the temperature at one point may be obtained by successive application of the proper concentration factors. The influence of one attachment dies out rapidly, however, with distance.

The second type of attachment to be investigated is a continuous strip which may be considered to act as a line source of heat. In this case, the temperature in the structure can be obtained by applying Newman's method (see Reference 8). Briefly, Newman shows that the solution of heat conduction problems within three-dimensional finite slabs may be obtained from one-dimensional solutions if (1) no heat is generated within the slab, (2) all boundary conditions are symmetric, and (3) the external temperature is uniform over the entire body so that the equations can be put in homogeneous form. With these assumptions, it can be shown that the dimensionless temperature in the three-dimensional slab is

[redacted]

$$v(x,y,z,\theta) = v_x(x,\theta)\, v_y(y,\theta)\, v_z(z,\theta)\,,$$

where

$$v(x,y,z,\theta) = \frac{T_o - T}{T_o - T_i}\,,$$

$$v_x = \frac{T_o - t_x}{T_o - T_i}\,,$$

$$v_y = \frac{T_o - t_y}{T_o - T_i}\,,$$

$$v_z = \frac{T_o - t_z}{T_o - T_i}\,,$$

and t_x, t_y, and t_z are the temperature solutions for one-dimensional slab problems with the proper boundary conditions.

In the case of a line attachment acting as a conductive short circuit, in view of the aforementioned remarks, the temperature may be expressed as

$$\frac{T_o - T}{T_o - T_i} = \frac{T_o - T'}{T_o - T_i}\, Y(y,\theta)\,,$$

where $Y(y,\theta)$ is the dimensionless temperature rise for a rod subjected to convection at both ends from a medium at temperature T_o. The heat transfer coefficient at the ends of the rod must be chosen so as to represent the effect of the line attachment. The solution for $v_y(y,\theta)$ is a classical problem which is treated in Reference 6.

The temperature concentration factor may now be defined as

$$Y = \frac{T_o - T}{T_o - T'}\,.$$

Values for this quantity are presented in the curves of Part I, Section 6.0. These curves are based upon the solution for Y given in Reference 6.

D. EFFICIENCIES OF INSULATING MATERIAL

In this section, a comparison is made of the insulating efficiency of many products that are available commercially, and also of material arrangements and combinations which have been devised to produce high resistance to heat transfer.

The first consideration in the choice of insulation is presumably weight; the requirement is for the maximum thermal resistance per pound of insulation, per unit area. Resistance is the inverse of conductivity so that the parameter for insulation comparison becomes: thermal conductivity x density. While this parameter serves well for the comparison of standard insulating materials, there are many cases where it cannot be used. Air is an excellent insulator, but its effective weight at ambient pressure is zero. Heat transmission is not only governed by conduction, but also may include convection and radiation. In this case, the insulation thickness would form a better basis for comparison. Similarly with the use of radiation foils, the weight will depend upon foil thickness which is, in turn, dependent upon the details of foil spacing arrangements. These cases will be treated individually in the following.

1. Low-Conductivity Materials

Figure IV-3 compares, on the basis of the conductivity times density parameter, a number of low-conductivity insulating materials that are available commercially. Comparisons are made

over a range of temperatures since temperature effects differ depending upon the mechanical construction of the material. These materials are of low density, compared with the metals, and have either zero mechanical strength or a small amount that is unimportant for airframe use. Only materials having high-temperature resistance are included; this excludes all organic materials, some of which are efficient insulators at low temperatures.

From Figure IV-3, three materials consisting of fine mineral fibers deserve most attention. Commercial names for these materials are Thermoflex, Refrasil, and Fiberfrax. More detailed curves of conductivity at various densities and temperatures are given in Section 2.0 of Part I. Thermoflex at 3 lb/ft^3 is the most promising of these materials and will be used as the basis of comparison for the remainder of this section. In cases where an excessive thickness of this low-density material becomes necessary, it should be noted from the curves in Section 2.0 of Part I that reductions in conductivity as a result of increased density will not result in significant thickness reduction. The corresponding weight penalty, however, can become large.

Low-conductivity ceramic coatings have a value of (conductivity x density) approximately 100; this is much higher than that of any material shown in Figure IV-3. Minimum values of conductivity are approximately 10 BTU-in./ft^2 hr °F with densities of approximately 125 lb/ft^3. Despite this comparison, however, this type of material has an application, as a thin coating, where heat fluxes are large. A conductivity of 10 BTU-in./ft^2 hr °F, for instance, will produce a temperature drop of 1000°F across a thickness of 0.01 inch if the flux is one-million BTU/hr ft^2. Section II shows that such values of flux are easily achieved with re-entry vehicles.

2. Radiation Shields

The significance of emissivity in radiant heat transfer and the effect of various factors on emissivity has been discussed in Section IV, B. Values of emissivity for a number of materials and a range of surface conditions and temperatures are given in Section 2.3 of Part I.

The efficiency of radiation barriers, using thin foils of these materials, cannot be directly compared with the low-conductivity insulators since the weight of the foil depends upon its method of support. Each application must therefore be considered individually.

One significant fact that can be illustrated and applied generally is shown in Figure IV-4. This figure shows heat transfer across a 1/2-inch air space with gold radiation shields interposed. The number of shields is limited to three because the reduction in heat transfer does not justify the added weight.

3. Air Space

The conductivity of air is presented graphically in Section 2.3 of Part I, and a comparison of its usefulness, compared with Thermoflex, is given in Figure IV-5. These curves of equivalent conductivity are obtained by dividing the total heat transferred by the air-space depth and the temperature difference. Radiation is included in the heat transferred across the air space and typical wall surfaces of Inconel X on the hot side and aluminum on the cold side have been assumed. Convection has been neglected on the assumption of high-altitude, low-pressure conditions. From this graph, it is evidently beneficial to use the air space as insulation if the insulating requirements are small so that the air blanket is thin. As the required thickness increases, the fibrous material gives lower conductivity, although at a small penalty in weight. This conclusion is emphasized if convection is involved, and the possibility of convection increases as the thickness of the air blanket is increased.

4. Insulation Combinations

Figure IV-6 (taken from Reference 10) gives the results of tests on a number of combinations of insulating materials such as foils and screens. These results are again presented as conductivity times density, so that the comparison is directly one of efficiency. Thermoflex, included on the curve in Figure IV-6, is shown to be superior at all temperatures.

[redacted]

E. APPLICATION OF INSULATION

Previous parts of this section have explained the mechanics of insulation, have compared the various insulating materials and combinations of materials, and have shown the development of analytical methods for insulation design. The most promising type of insulation discussed within this section is used in Section IX. Here, comparisons are made of unprotected, insulated, and insulated and cooled structures to show where insulation is most advantageously used, and the structure weights that result. Although this essentially gives all that is required for the design of insulation, the equations and curves of Section IX do not give general ideas of insulation weights and thicknesses. It is the purpose of this section to present curves which may give a sense of "feel" for the use of insulation, and which show the usefulness of insulation as a thermal-stress-reducing means, an item not covered in Section IX.

In considering the use of insulation in hypersonic aircraft structures, three principal applications are evident:

(1) Delay of temperature rise in structure so that materials of higher specific strength can be used.

(2) Reduction of heat flux into structural cooling systems.

(3) Reduction of thermal gradients in a structure, to reduce thermal stresses.

An indication of the ability of insulation to delay structural temperature rise is presented in Figures IV-7 through IV-11 which represent various typical combinations of structural material, structural temperature, flight time, and temperature at the outer face of the insulation. Aluminum and Inconel X are included as structural materials, and their maximum structural temperatures are assumed to be 350° and 1200°F, respectively. These temperatures are approximate values where the respective material properties begin to drop rapidly, and may be expected to give optimum weight of the structure-insulation combination.

Thermoflex of 3 lb/ft^3 density, the most efficient single insulating material available, has been assumed in preparing Figures IV-7 through IV-10; where insulating requirements are small, additional curves are given using a ceramic coating. At the cost of decreased efficiency, the use of ceramic coating has the merit of simplicity, if small thicknesses are required. A moderately dense ceramic of 125 lb/ft^3 has been assumed, with a typical conductivity of 10 BTU-in./ft^2hr°F. Average values, with respect to both time and position within the insulating material, have been taken for the insulation conductivity.

The additional scale along the bottom of each plot shows the Mach numbers corresponding with each temperature, assuming that 90% of stagnation temperature is reached on the outer surface. This is approximately true at 50,000 feet altitude for turbulent flow conditions, neglecting radiation.

Where insulation is used as structural protection, one of its advantages is that some protection from aerodynamic heating is provided automatically for the crew, equipment, propellant tanks, and engines. The extent of this protection depends upon the final structural temperature. Generally, if these temperatures are selected only on a structural basis, they will be too high for equipment compartments even if aluminum is used. It may therefore be necessary to know the additional insulation required to keep wall temperatures at a level suitable for equipment.

Present equipment specifications require operation under maximum temperature conditions of 160°F, and the crew can apparently function for a short time with cabin walls at such a temperature. If 160°F is selected as a maximum wall temperature in these areas of the airframe, therefore, equipment cooling is required only to the extent of removing heat generated within the equipment, as with present-day aircraft. Attempts to reduce maximum wall temperatures below 160°F result in rapidly increasing insulation requirements as the initial temperature is approached.

The use of a maximum cabin-wall temperature of 160°F implies an aluminum structure. Figure IV-11 shows the insulation requirements for such conditions for two typical values of wall thickness and for a range of equilibrium temperatures at the outer face of the insulation. Ther-

moflex insulation at a density of 3 lb/ft^3 is assumed, and the initial wall temperature is taken as 70°F. The wall thicknesses chosen are intended to be representative of the more lightly loaded areas of the airframe, since this is where equipment is often located, and the thin wall increases the insulation requirements. Again, for convenience, a Mach number scale for 50,000 feet altitude, turbulent flow conditions, and no radiation is added to the plot.

For prolonged flight at high speeds, the use of insulation alone as a means of maintaining low structural temperatures may be impractical, and it may be necessary to cool the structural surface. Under these circumstances, it will generally be economical to use a layer of insulation around the structure, since a comparatively small weight of such material can effect large reductions of the heat flux into the cooling system. Such an arrangement may be used provided that the equilibrium temperatures at the outer surface of the insulation are not beyond the range of usefulness of available materials.

If the structure is maintained at a constant temperature by cooling, a simple steady-state condition exists, and the relationship between insulation thickness and the heat flux that is passed into the cooling system is

$$q = \frac{k}{x_i} (T_o - T) \cdot$$

If it is assumed that the heat conducted through the insulation is a small quantity, then the insulation surface temperature may be identified with the equilibrium temperature which is readily obtained from Section 1.0 of Part I. The error involved in this assumption is only significant at high Mach numbers with very thin layers of insulation; under such circumstances, the heat flux into the cooling system is conservatively overestimated.

Cooling fluids for the systems being considered are discussed in Section V where it is shown that water is generally the most suitable. A typical system pressure at altitude is 6.0 psi which gives a boiling point, and hence a structural temperature, of 170°F.

As shown in Part C of this section, the most efficient insulation available for elevated temperature use is the fiberous material Thermoflex, having a density of 3 lb/ft^3. The conductivity of this material over a range of mean temperatures is given in Part D of this section.

Using Thermoflex insulation, and a structural temperature of 170°F, the relationship between heat flux and insulation thickness is presented graphically in Figure IV-12. In preparing this illustration, the insulation conductivity appropriate to the mean temperature was used.

To permit reliable interpolation, and also to indicate the significance of using insulation with a cooling system, Figure IV-12 includes curves of heat flux for zero insulation thickness. A number of curves are necessary for zero insulation thickness because the flux cannot be reduced to a point where it is dependent upon only one variable. These curves are plotted against T_o, although an actual equilibrium temperature will not be achieved on a cooled uninsulated surface. This device, however, is a convenient method of including the effect of heat transfer coefficient, since equilibrium temperatures are easily obtained from Section 1.0 of Part I.

The curves of heat flux with zero insulation thickness are calculated from the approximate equation

$$q = 0.154 \left(\frac{T_o}{100}\right)^4 \left[\frac{T_r - 630}{T_r - T_o}\right] \cdot$$

All temperatures are expressed in degrees Rankine. This equation is developed by solving the heat balance equation under equilibrium conditions for the value of the heat transfer coefficient, and applying this value to obtain flux into the cooled surface. The assumptions involved are that the heat transfer coefficient is unchanged by the reduction of surface temperature to 170°F; T_o is associated with a surface emissivity of 0.90, recovery factor is 0.90, and surface temperature is 170°F.

Immediately apparent from Figure IV-12 is the large reduction in heat flux, and hence coolant weight, that can be produced by moderate amounts of insulation. A one-inch thickness, weighing 0.25 lb/ft^2, will reduce the flux by 95% or more, bringing coolant weights down to practical levels. This fact is developed more fully in Section V where it forms an important step in the rationalization of cooling system studies.

It is significant that convective heat input from the boundary layer is reduced only slightly by the presence of insulation, since this input is a function only of boundary layer temperature, outer surface temperature, and heat transfer coefficient. Reduction of flux into the structure will result because the insulation resistance permits the outer surface temperature to rise, so that most of the convective heat input is dissipated by radiation.

Figure IV-12 can also be used to optimize the distribution of weight between coolant and insulation for any particular cooling problem. The following example illustrates the procedure.

Find the optimum thickness of Thermoflex insulation, of 3 lb/ft^3 density, for use in conjunction with a structural cooling system for an aircraft flying at Mach 5.0. The altitude is 105,000 feet, flight time is 15 minutes, and a typical value of equilibrium temperature at the outer surface of the insulation is 950°F. Water is used as the coolant.

Total heat of water is approximately 1100 BTU/lb so that a flux into the cooling system of 1000 BTU/hr ft^2 requires 0.227 lb/ft^2 of water for the 15-minute flight.

From Figure IV-12 at T_o equals 950°F;

Insulation thickness (in.)	0.25	0.50	0.75	1.0	1.5
Insulation weight (lb/ft^2)	0.062	0.125	0.187	0.250	0.375
Heat flux (BTU/hr ft^2) x 10^{-6}	1.91	0.97	0.65	0.48	0.32
Water weight (lb/ft^2)	0.434	0.220	0.148	0.109	0.073
Total weight (lb/ft^2)	0.496	0.345	0.335	0.359	0.448

Therefore, an insulation thickness of approximately 0.75 inch should be used. It can be shown, in fact, that minimum total weight will occur when insulation and coolant weights are equal, but it is obvious from this example that the total weight is quite insensitive to the precise insulation thickness. This fact is important because in many cases it will be found that nonoptimum insulation thicknesses must be used to keep these thicknesses within practical limits.

This optimization process should consider only the factors affected by heat flux. Such items as the cooling system and the outer structural cover for the insulation are not involved.

The problem of thermal stresses in structures unprotected from the effects of aerodynamic heating has been discussed adequately in other sections of this report. It will be apparent from these discussions that the problem is acute and not readily solved. One obvious approach, however, is to insulate the structure, probably using only sufficient insulation to reduce temperature gradients and making no attempt to reduce the maximum temperatures. This approach is particularly attractive if it can be shown that a thin coating of a readily applied, low-conductivity material is sufficient. It therefore becomes desirable to demonstrate the benefits that can be obtained from the use of insulation for this purpose.

Unfortunately, the calculation of thermal gradients and stresses is extremely complex since it includes parameters of the structural geometry, structural material, and the boundary layer aerodynamics. To this is added the insulation characteristics. It is, therefore, not practical to attempt a generalization of this subject, but a few examples, investigated systematically, will be sufficient to establish an appreciation of the values involved.

A multiweb wing is considered in which web spacing is made equal to web depth, since this arrangement generally approaches optimum proportions; the width-to-thickness ratio for the skin panels is equal to 30. Computations have been made, using the method and curves of Section 3.0

of Part I, to give thermal stresses in the skin for two values of web spacing and three values of heat transfer coefficient. Results are presented in Table IV-1.

In order to use the curves in Section 3.0 of Part I, an effective value of heat transfer coefficient is computed, and this includes the thermal resistance of the insulation. Thermal resistance is the inverse of conductivity, and the resistances of insulation and boundary layer are in series, therefore

$$\frac{1}{h_e} = \frac{1}{h} + \frac{1}{k/x} ,$$

where h_e is an effective heat transfer coefficient. Manipulating this equation gives

$$h_e = h\left(\frac{1}{1+\frac{hx}{k}}\right).$$

Two structural materials are considered, aluminum and Inconel X; these represent the extremes that might be used in structures designed to operate at elevated temperatures. Similarly, two insulating materials are included. Thermoflex is an efficient low-density fiberous material, but it has no mechanical strength, and its use would require an outer shell capable of carrying aerodynamic pressures. The ceramic coating noted in Table IV-1 is representative of materials having sufficient mechanical strength to form the outer surface of the airframe, except that the value of conductivity is the lowest that could be found. Note that the thicknesses of ceramic used in Table IV-1 are large for application as a coating. Such thicknesses probably would not absorb structural strains without cracking, but these factors only emphasize the conclusions to be drawn from the table. It should be noted also that the stresses are calculated for a boundary layer temperature rise of 1000°F, this rise occurring instantaneously. Stresses may be proportioned directly for any other value of temperature rise.

By inspection of Table IV-1, it will be seen immediately that ceramic coatings are of no practical value in reducing thermal stresses, since a 0.10-inch thickness, weighing 1.5 lb/ft^2, produces negligible reduction of stress level. At such a thickness, some error is involved in the calculations by neglecting heat capacity within the ceramic insulation, but the conclusions are unchanged since the fiberous insulation is much more effective. As mentioned elsewhere in this report, an outer wall for the protection of fiberous insulation can be produced for approximately 1.0 lb/ft^2, so that for the 1.5 lb/ft^2, much lower thermal stresses can be achieved by using a 1.0-inch thickness of this material.

[redacted]

REFERENCES

(1) Vershoor, J. D. and Greebler, P., "Heat Transfer by Gas Conduction and Radiation," Transactions of ASME, Volume 74; No. 6, August 1952.

(2) Greebler, P., "Thermal Properties and Applications of High Temperature Aircraft Insulations," Paper presented at ASME semiannual meeting, 24 June 1954.

(3) Brull, M. A., "Transient Temperature Distribution in Insulated Aircraft Structures," Bell Aircraft Corporation, Report 02-984-034, 1955.

(4) Churchill, R. V., "Modern Operational Mathematics in Engineering," McGraw-Hill Book Company, 1944, Page 142.

(5) McAdams, "Heat Transmission," McGraw-Hill Book Company, Second Edition, 1942, Page 59.

(6) Carslaw, H. S. and Jaeger, J. C., "Conduction of Heat in Solids," Oxford Clarendon Press, 1948.

(7) Jahnke and Ende, "Tables of Functions."

(8) Newman, A. B., "Heating and Cooling of Rectangular and Cylindrical Solids," Industrial and Engineering Chemistry, Volume 28, 1936.

(9) Jakob, Max, "Heat Transfer," John Wiley & Sons, Inc., Volume 1, 1949.

(10) Jelinek, D., "The Development of a High-Temperature Lightweight Insulation for Jet Aircraft," North American Aviation, Inc., January 1946.

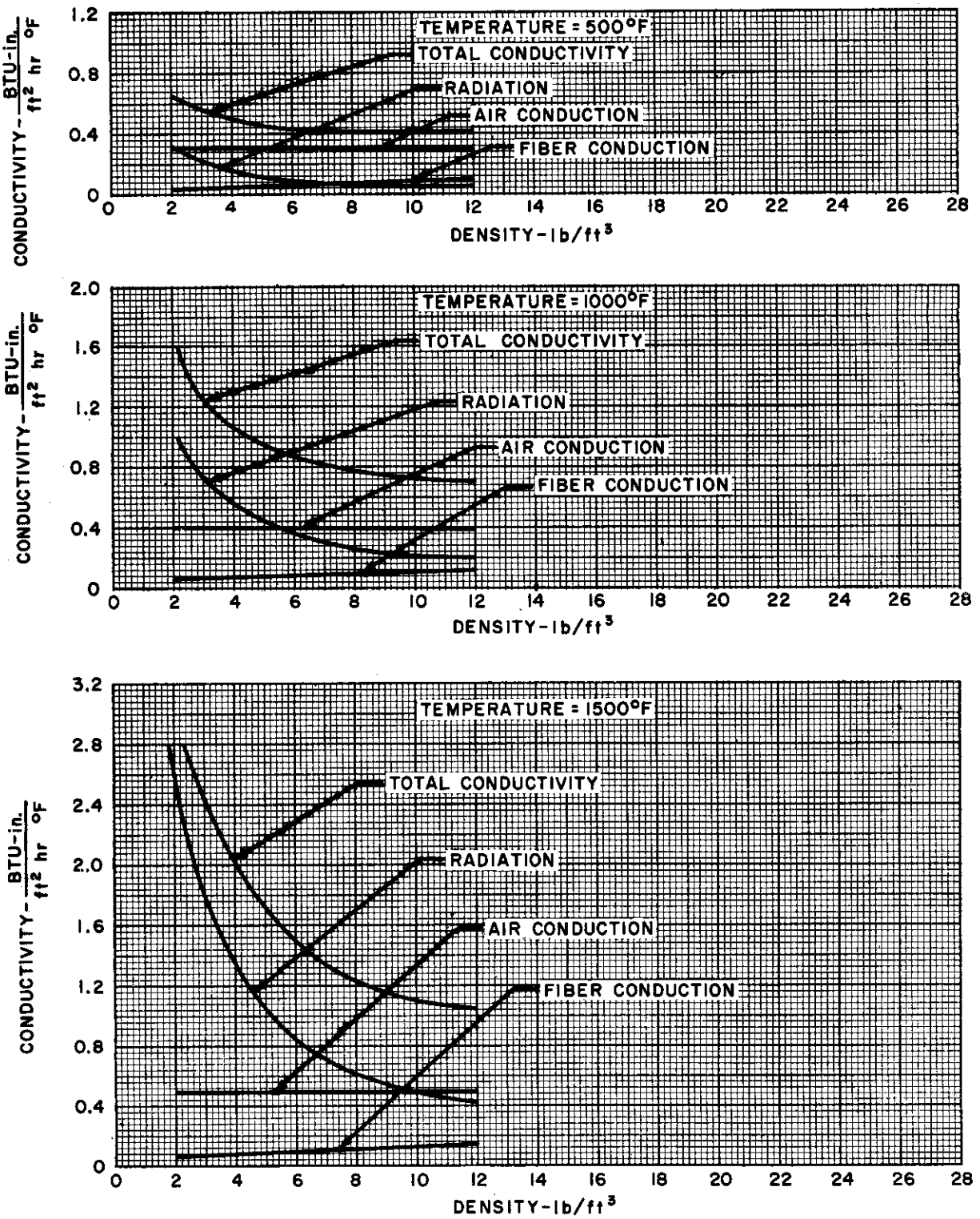

Figure IV-1. Temperature and Density Effects on Thermal Conductivity — Typical Aircraft Felt

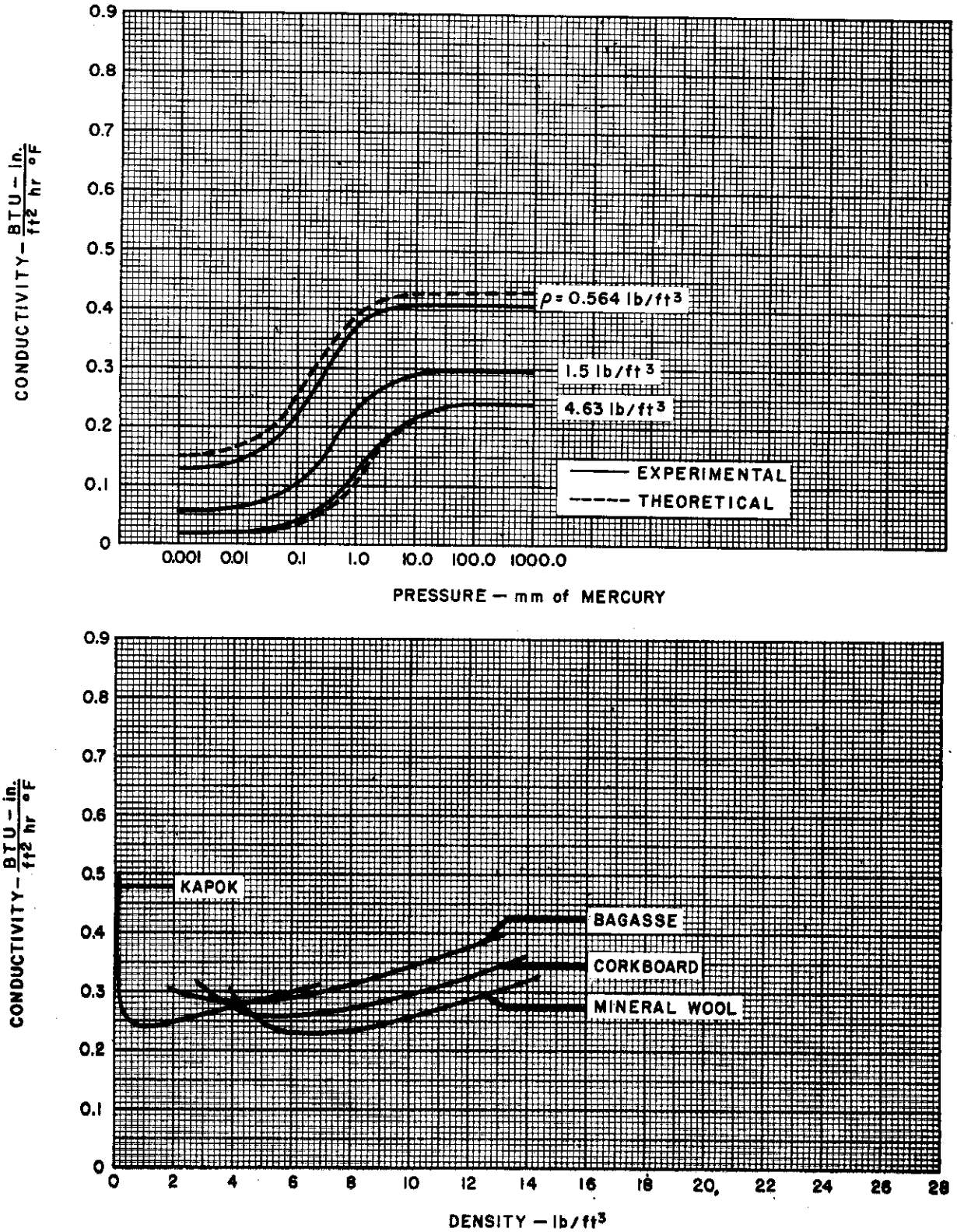

Figure IV-2. Pressure and Density Effects on Thermal Conductivity — Typical Fibrous Insulation

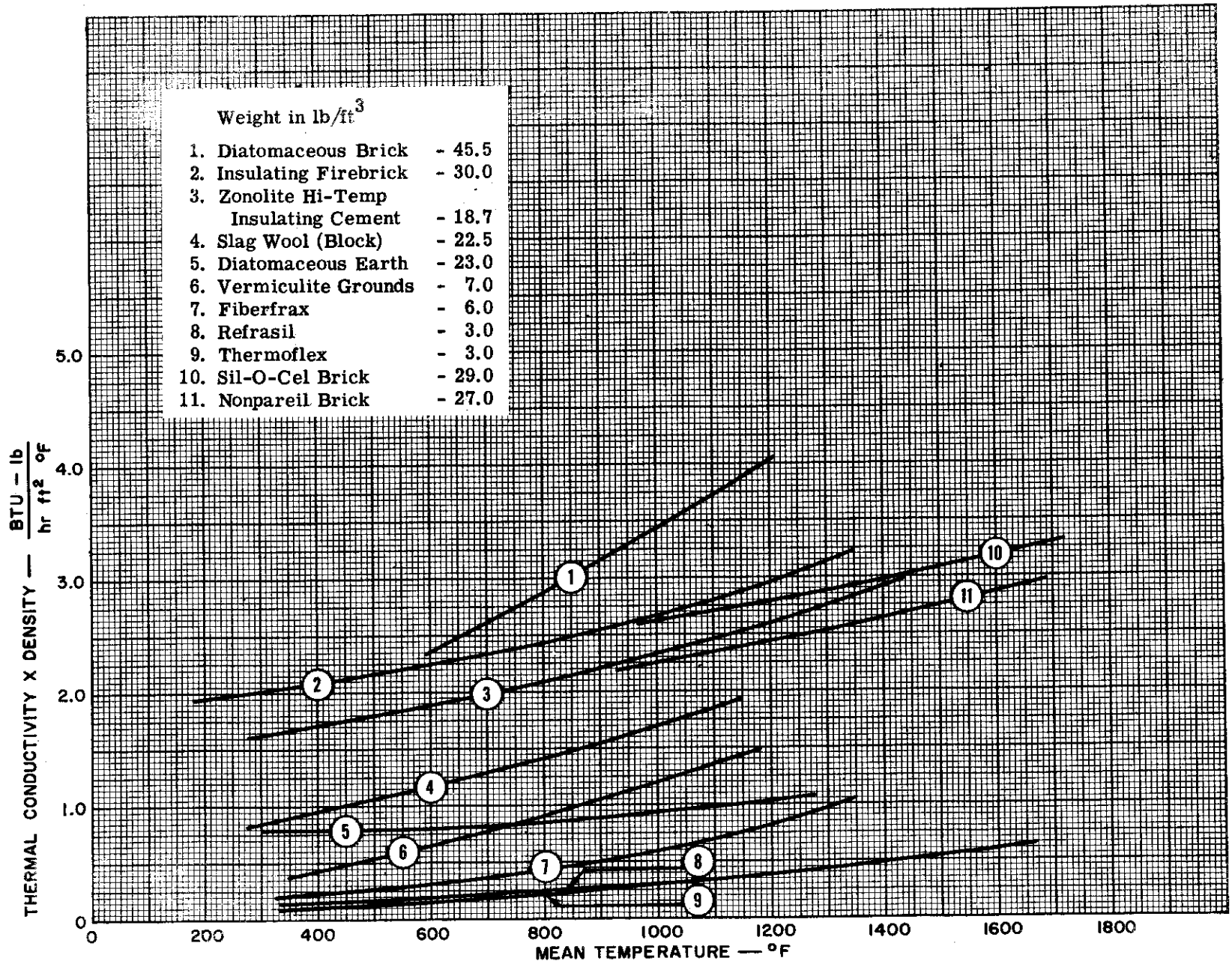

Figure IV-3. Efficiency of Various Insulating Materials

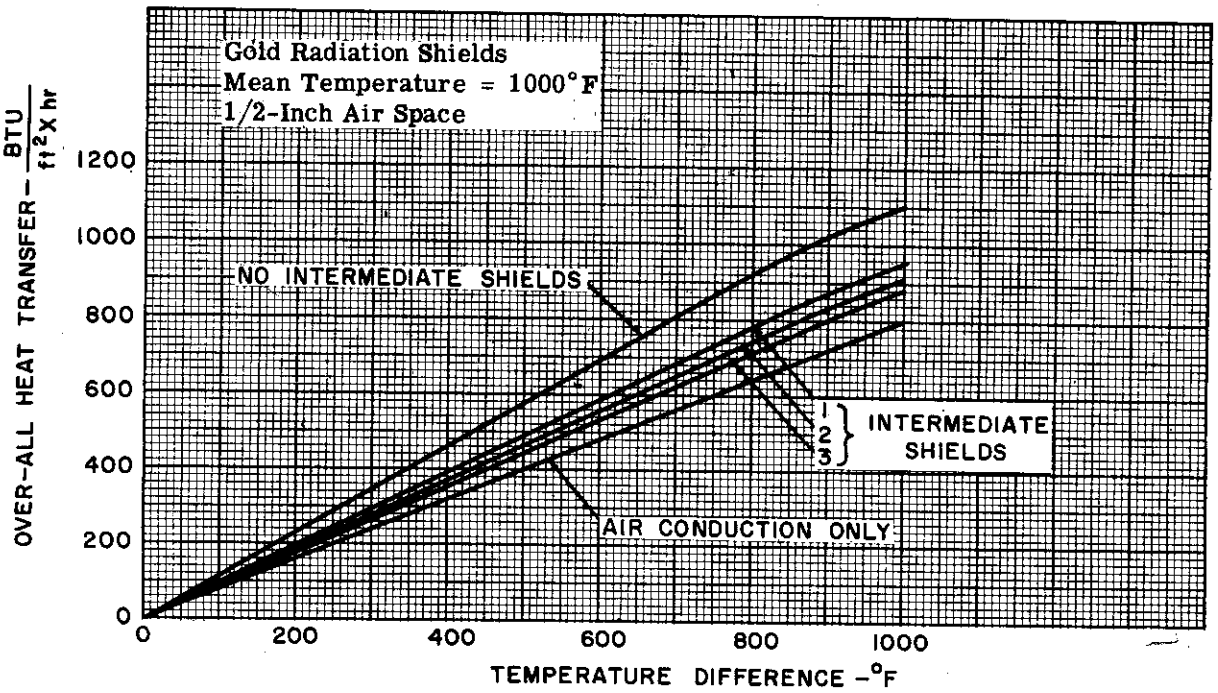

Figure IV-4. Effect of Radiation Shields on Heat Transmission Across an Air Space

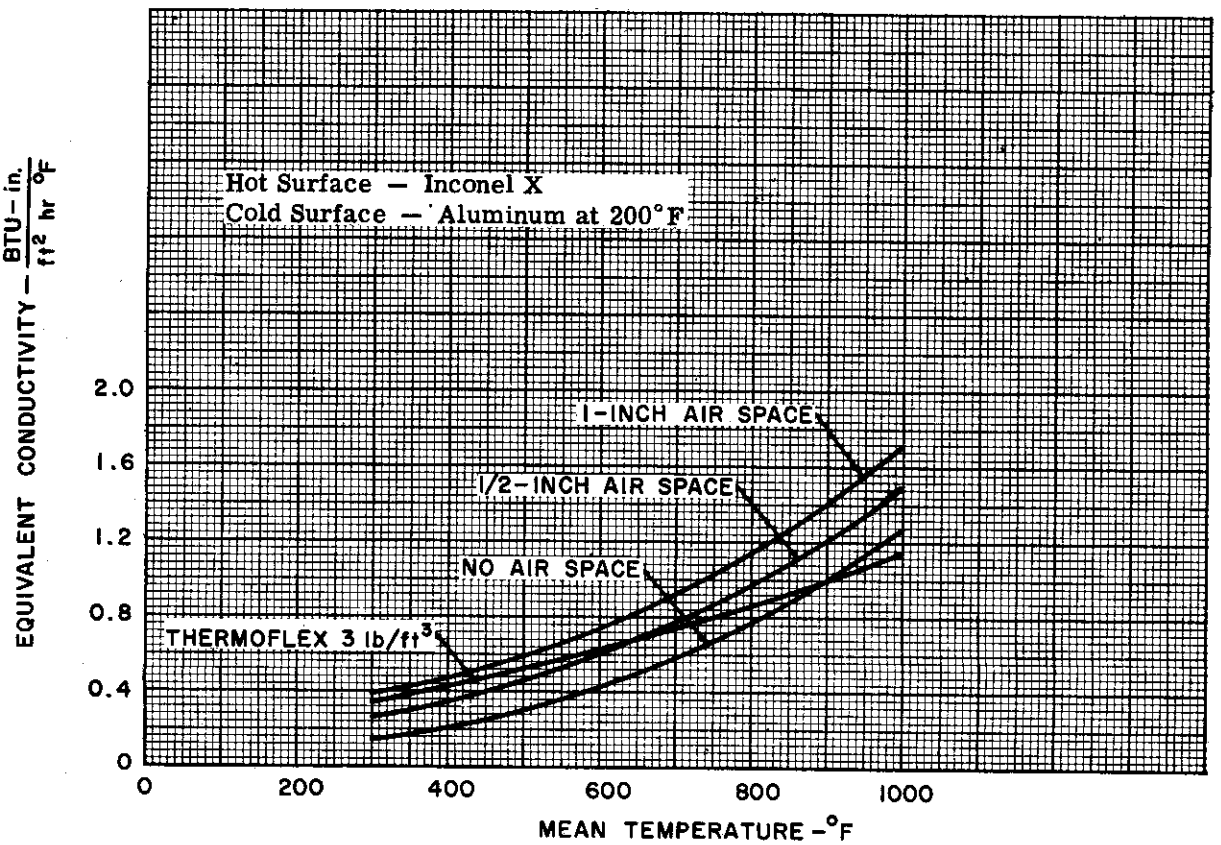

Figure IV-5. Comparison of Heat Transfer – Air Space and Thermoflex

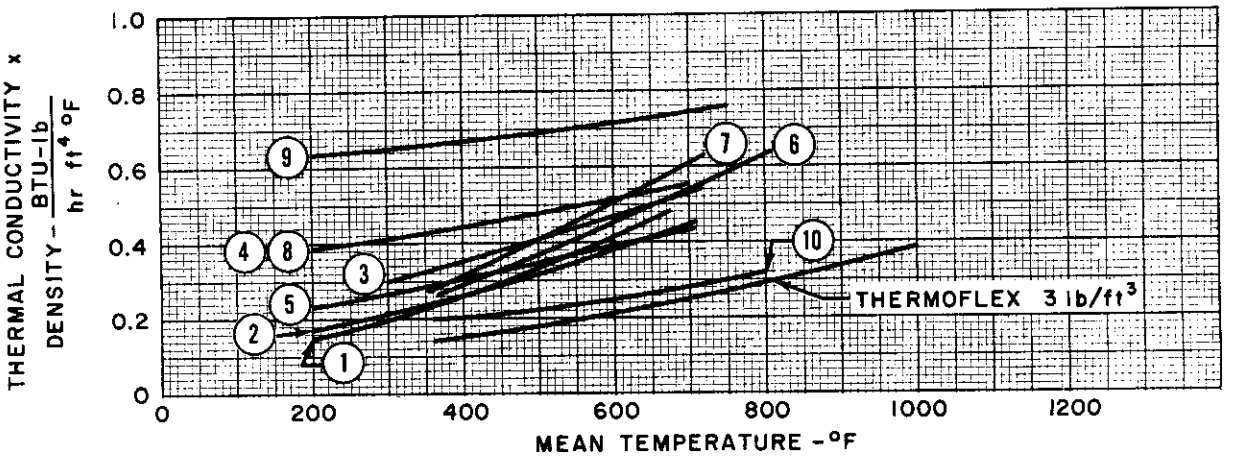

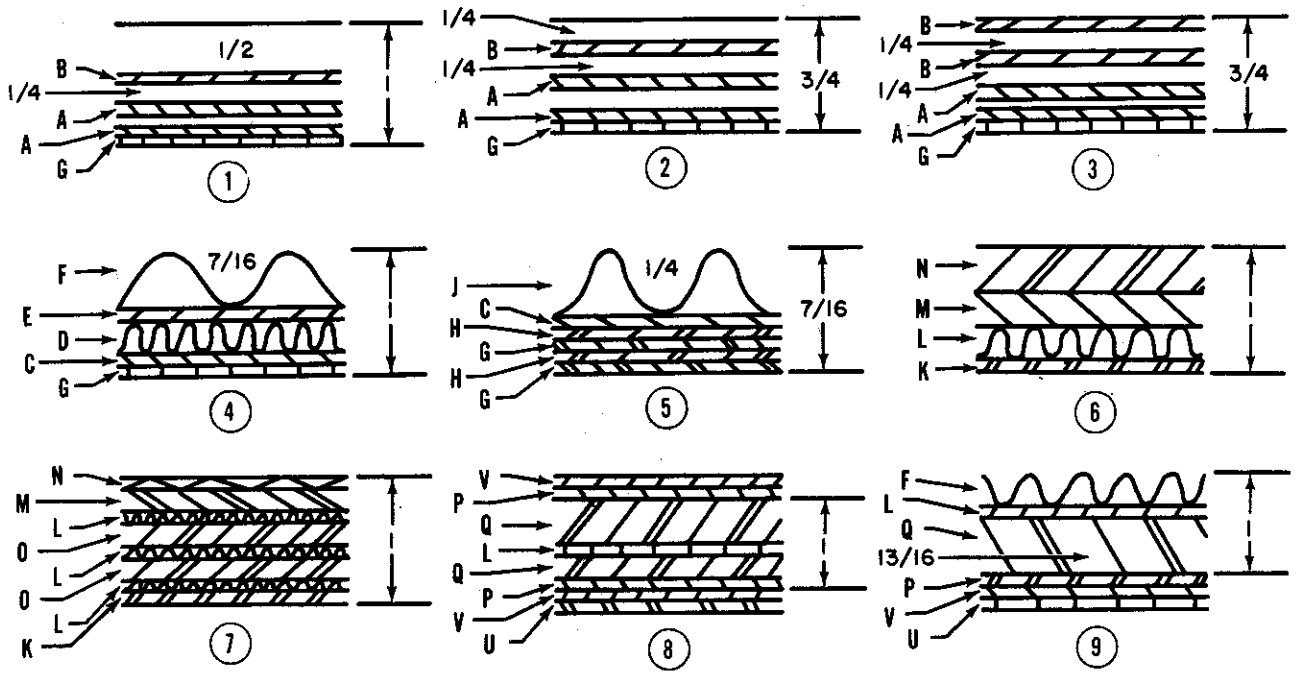

A. 0.003 Aluminum Foil
B. 0.005 Silver Foil
C. 0.002 Aluminum Foil
D. 0.5625 Crumpled Foil
E. 0.002 Silver Foil
F. Stainless Steel Screen (14-Mesh)
G. Aluminum Screen
H. 0.035 Aluminum Wire
J. Stainless Steel Screen
K. Aluminized Neoprene Glass Cloth

Note: All dimensions in inches.

L. 0.00045 Crumpled Alfol
M. 0.25 Santocel "O" Packet
N. Asbestos Glass Cloth
O. 0.25 AA-PF Fiberglass
P. Asbestos Millboard
Q. 5 lb/ft^3 Amosite
R. 0.125 Leach Fiberglass
S. 0.00045 Alfol
T. 0.0005 Silver Foil
U. Aluminum Screen, Silicone Impregnated
V. Knitted Inconel Screen

Figure IV-6. Efficiency of Insulation Combinations

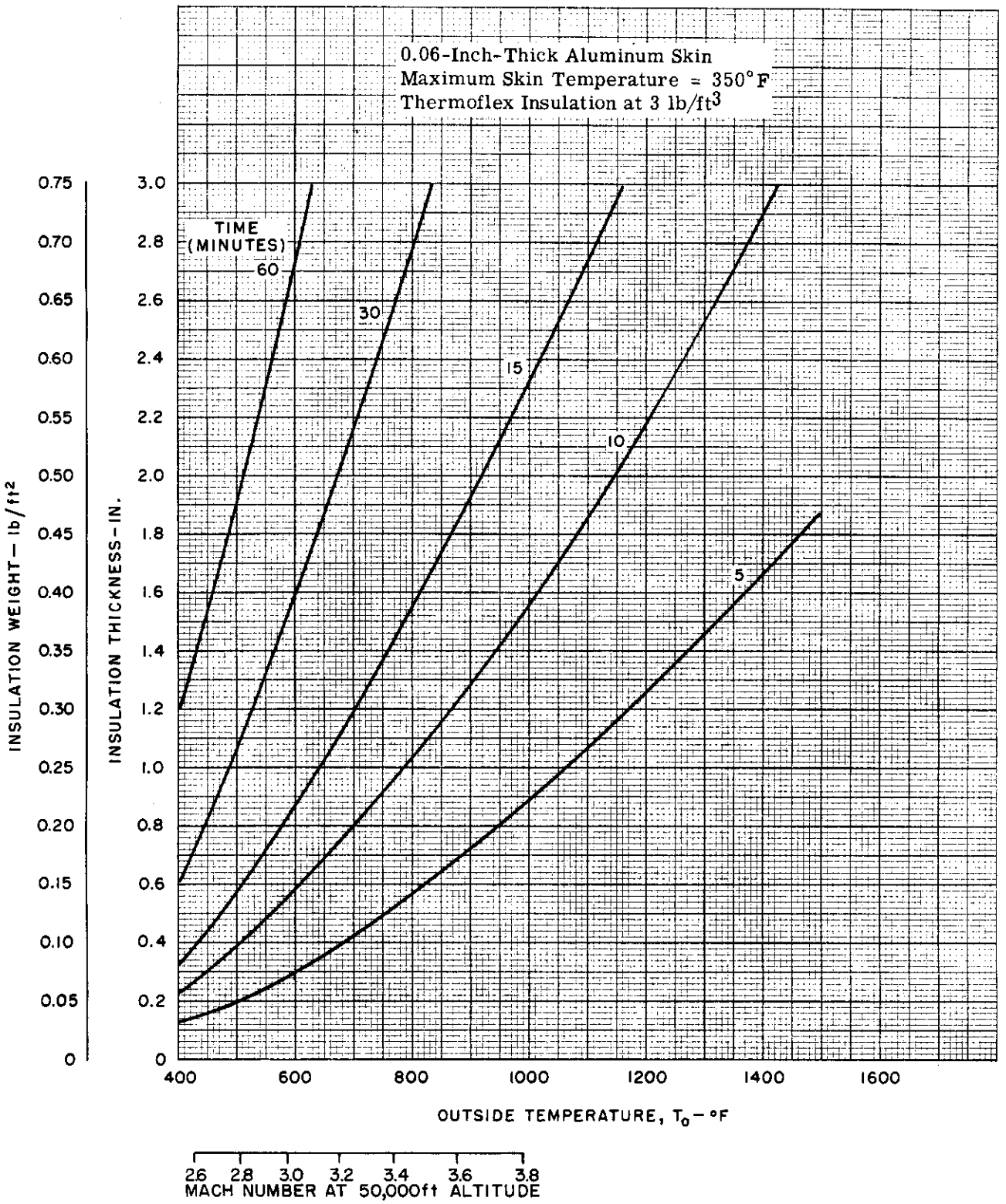

Figure IV-7. Insulation Requirements to Delay Structural Temperature Rise — 0.06-Thick Aluminum Skin with Thermoflex

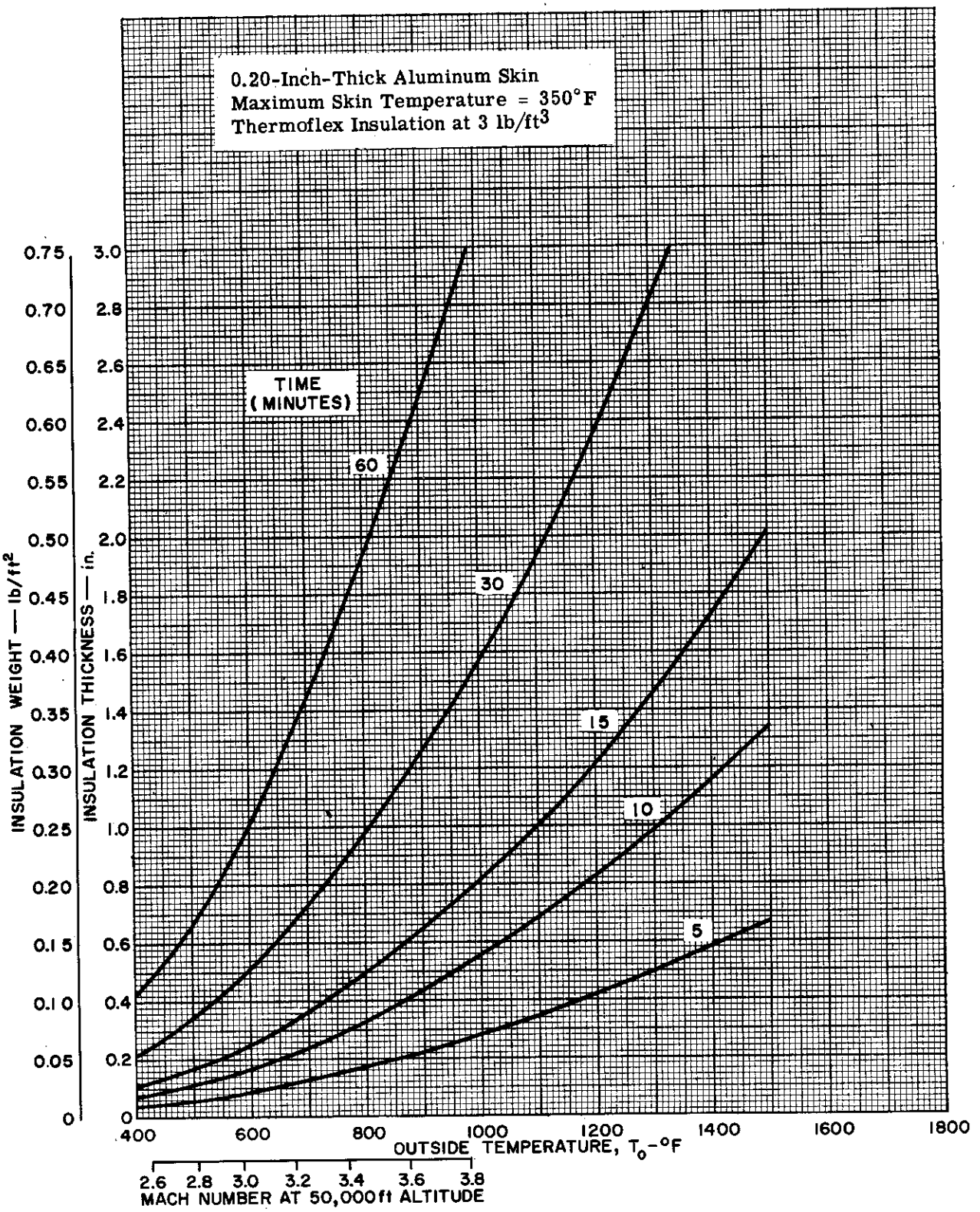

Figure IV-8. Insulation Requirements to Delay Structural Temperature Rise — 0.20-Thick Aluminum Skin with Thermoflex

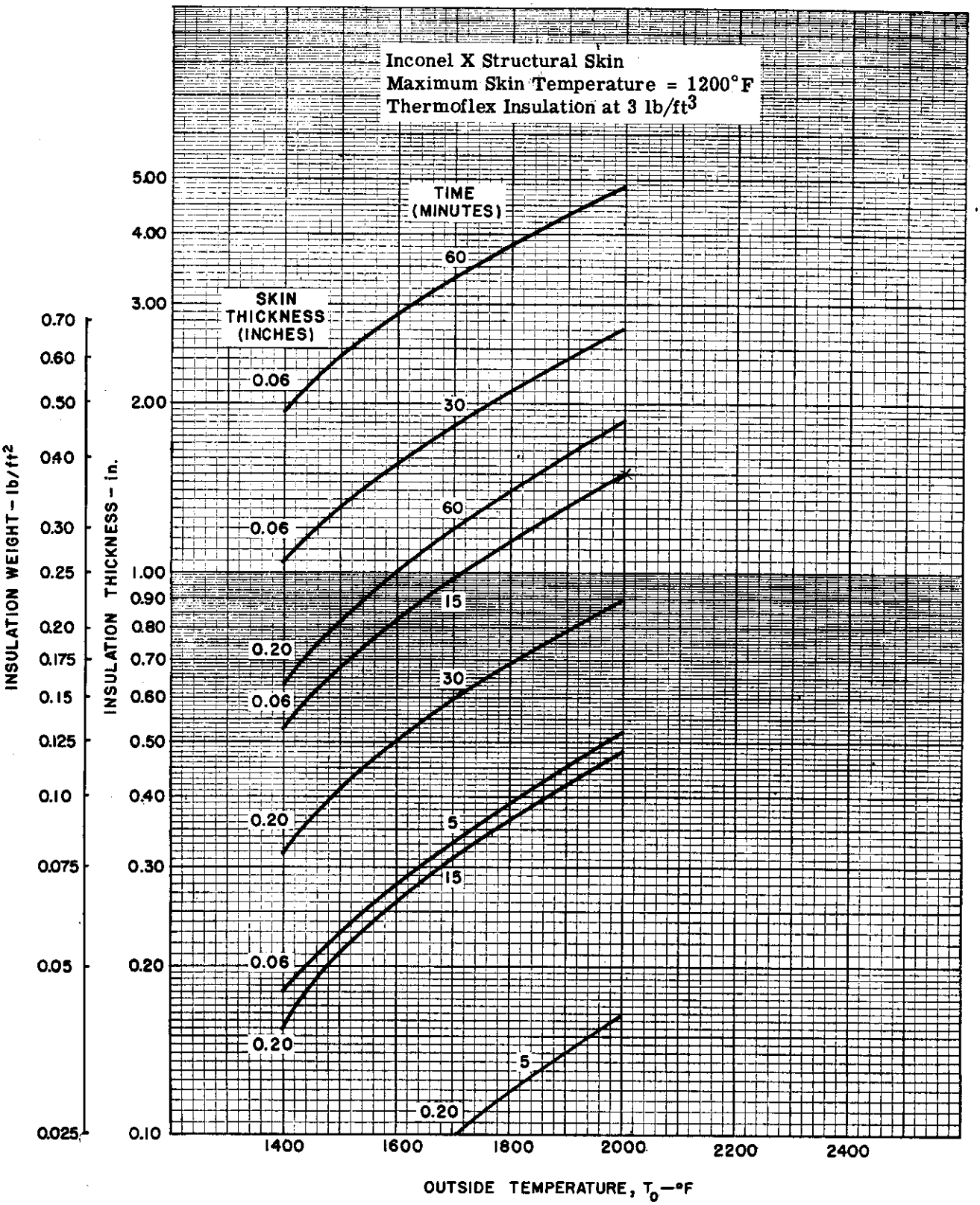

Figure IV-9. Insulation Requirements to Delay Structural Temperature Rise — Inconel X Structural Skin with Thermoflex

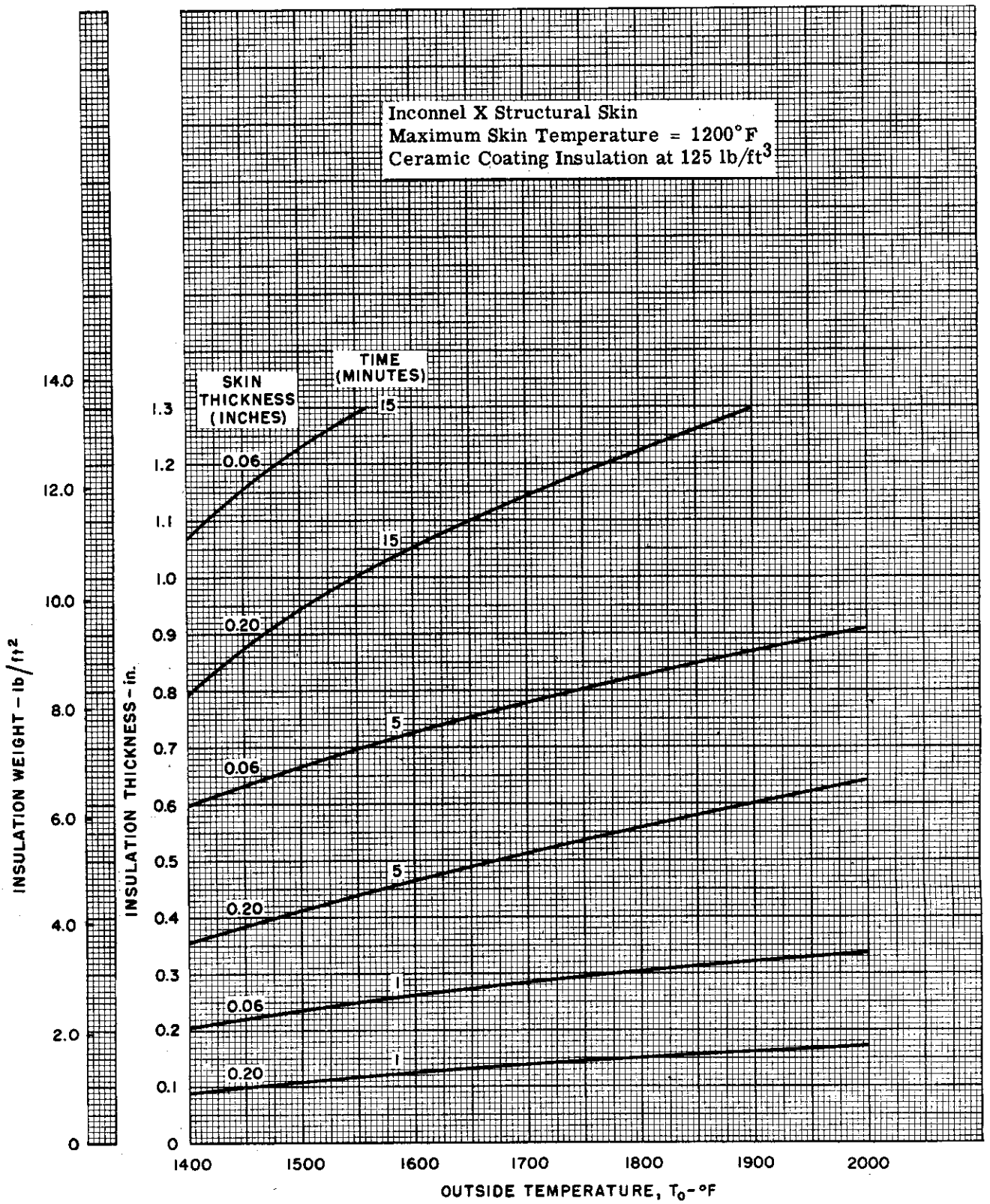

Figure IV-10. Insulation Requirements to Delay Structural Temperature Rise — Inconel X Structural Skin with Ceramic Coating

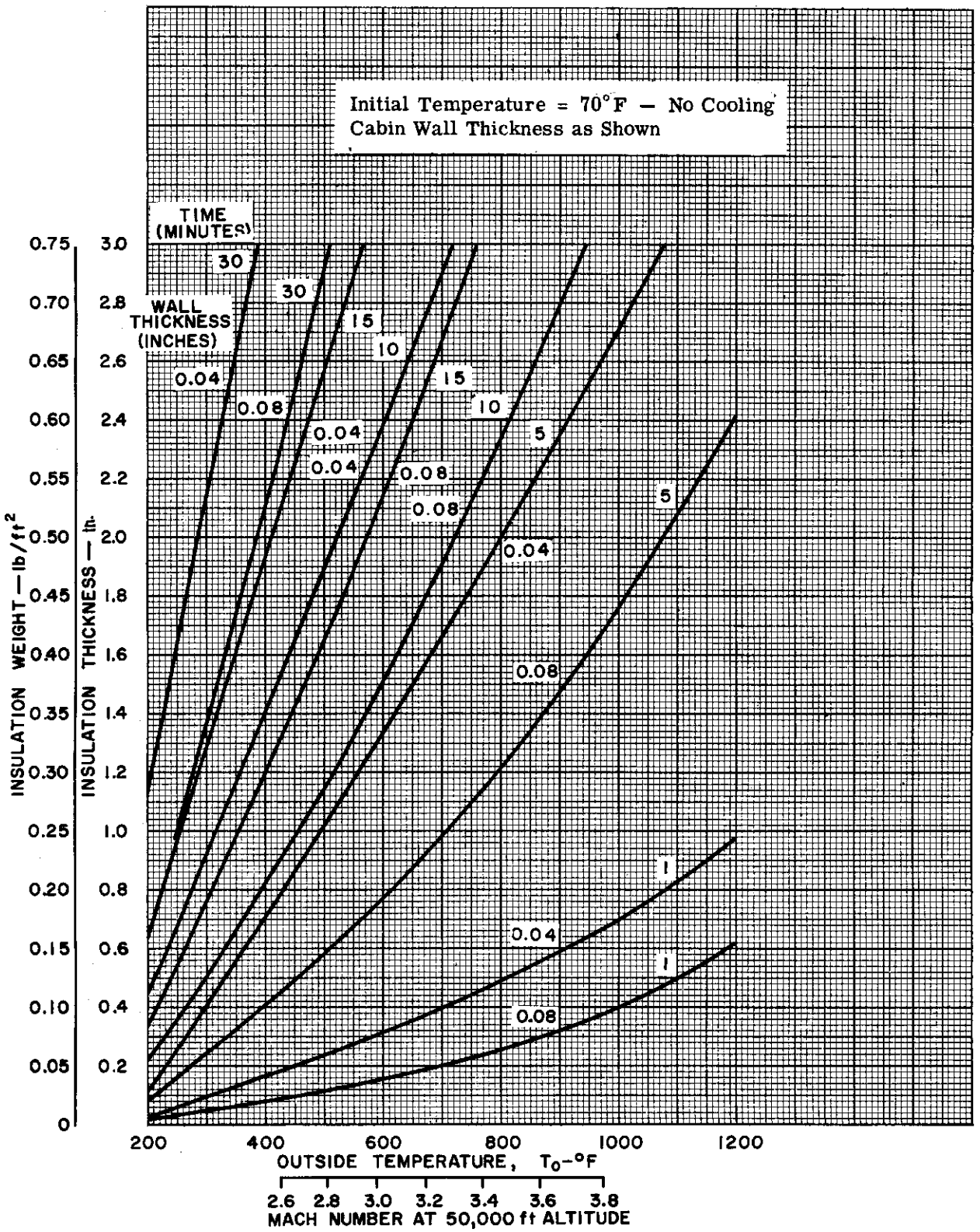

Figure IV-11. Insulation Requirements for Maximum Wall Temperature of 160°F

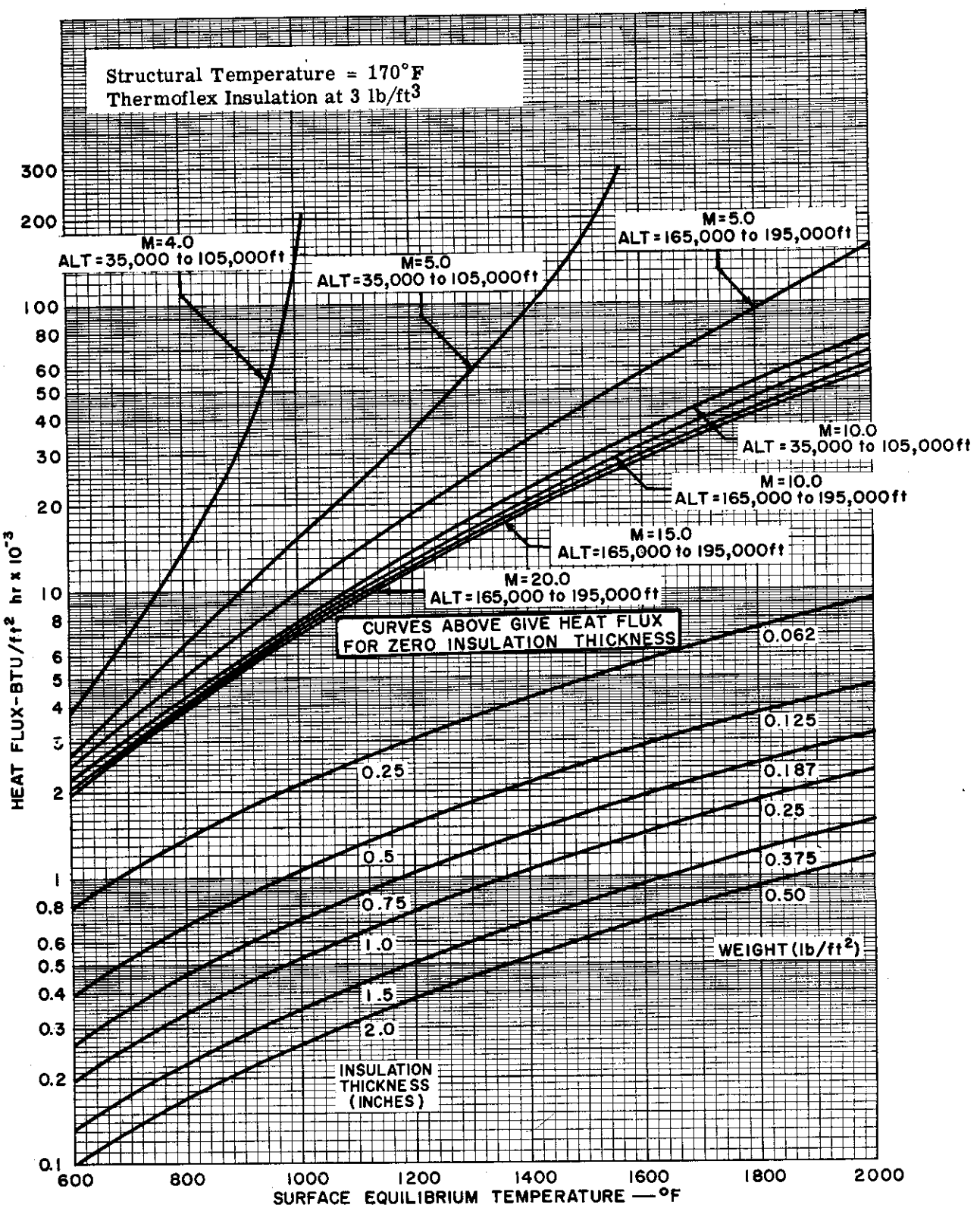

Figure IV-12. Heat Flux into Structural Cooling Systems

[redacted]

TABLE IV-1

REDUCTION OF THERMAL STRESS IN SKIN BY THE USE OF INSULATION

Web Spacing (inches)			5.0			10.0		
Heat Transfer Coefficient (BTU/ft^2 hr °F)			10	20	50	10	20	50
Structural Material	Insulation Material	Insulation Thickness (inches)						
Aluminum k = 840	No Insulation	0	9,600	13,550	21,000	13,550	19,200	26,500
	Thermoflex ρ = 3 lb/ft^3 k = 0.50	0.25	3,910	4,100	4,200	5,650	5,810	5,960
		0.50	2,890	2,960	3,010	4,100	4,200	4,260
		1.00	2,080	2,110	2,140	2,940	3,000	3,010
	Ceramic Coating ρ = 125 lb/ft^3 k = 10	0.05	9,350	12,950	19,200	13,250	18,250	25,200
		0.10	9,140	12,400	17,500	12,950	17,520	24,600
Inconel X k = 110	No Insulation	0	49,300	60,500	70,700	60,700	69,200	74,900
	Thermoflex ρ = 3 lb/ft^3 k = 0.50	0.25	21,600	22,700	23,200	30,500	32,000	32,900
		0.50	16,000	16,400	16,650	22,700	23,100	23,500
		1.00	11,450	11,700	11,800	16,200	16,600	16,450
	Ceramic Coating ρ = 125 lb/ft^3 k = 10	0.05	48,000	59,800	69,200	60,000	68,000	73,500
		0.10	47,500	58,100	67,400	59,700	67,400	72,000

Multiweb wing; web depth-to-spacing ratio of 1.0.
Stresses expressed in psi for a boundary layer temperature of 1000°F.

[redacted]

NOTES

[redacted]

SECTION V

COOLING

By M.I. Weinberg and E.J. Norwich

[redacted]

[redacted]

TABLE OF CONTENTS

LIST OF TABLES

[redacted]

NOMENCLATURE

A = area to be cooled (ft^2)

A_x = heat exchanger area (ft^2)

C_p = specific heat at constant pressure

d = depth of duct (ft)

F''' = friction factor

h_c = heat transfer coefficient ($BTU/ft^2hr^\circ F$)

h_x = heat transfer coefficient in heat exchanger ($BTU/ft^2hr^\circ F$)

h_s = heat transfer coefficient in structure ($BTU/ft^2hr^\circ F$)

k_f = coefficient of thermal conductivity ($BTU\text{-}ft/ft^2hr^\circ F$)

N = length of duct (ft)

N_r = number of rows in heat exchanger bank

P_1 = pressure before compression or expansion (lb/ft^2)

P_2 = pressure after compression or expansion (lb/ft^2)

q = heat flux (BTU/ft^2hr)

T_o = ambient temperature ($^\circ R$)

T_1 = temperature before compression or expansion ($^\circ R$)

T_2 = temperature after compression or expansion ($^\circ R$)

T_f = coolant outlet temperature ($^\circ R$)

T_l = coolant inlet temperature ($^\circ R$)

T_s = structural temperature ($^\circ R$)

T_x = heat exchanger temperature ($^\circ R$)

T_B = boiling temperature of expended coolant ($^\circ R$)

V = coolant velocity (ft/sec)

W = total mass flow (lb/hr)

w = local mass flow ($lb/hr/sq\ ft^2$)

γ = specific heat ratio

μ_f = absolute viscosity (lb/hr/ft)

ρ = density (lb/ft^3)

[redacted]

SECTION V

COOLING

A. GENERAL

Cooling as a method of heat protection is so widely used that no study of structure subjected to an elevated temperature environment could be complete without its inclusion. Cooling also has certain characteristics not possessed by other protection methods such as insulation, but which may be necessary in certain applications. The most important of these characteristics of a cooling system is its ability to hold a surface at a fixed temperature, almost without regard to the heat flux entering the surface and for an indefinite length of time. The purpose of this section is to study briefly all conceivable cooling systems in an attempt to isolate those which may have useful applications to airframe cooling.

Cooling as applied to aircraft has been under study for a number of years, but it has been confined largely to cooling in the proximity of turbojet engine tail pipes, and the cooling of electrical equipment. In these systems, ram air was used as a coolant because flight speeds were subsonic and ram temperature rise was negligible. For the general structural cooling of airframes subjected to aerodynamic heating, the investigations have been relatively sparse. The reports mentioned in References 15, 16, and 17 are typical of the work that has been done, but a review of these reveals little consideration for design problems. Reference 18, although more detailed, is confined to only one type of system.

Owing to the large number of cooling arrangements to be studied, this section offers only a little more detail than has been written by previous authors. However, an attempt is made to be comprehensive in the range of systems studied. Because of this wide range of possibilities, the method of approach has been to use rationalization wherever possible, and then to calculate approximate system weights for final comparison. To avoid the need for design of innumerable heat exchangers, turbines, and pumps, use has been made of components already designed and weights have been obtained by suitable proportioning.

Since the subject of airframe structural cooling is relatively new, this section begins with a comprehensive survey and compilation of all known cooling methods that may have application to the problem. The method of operating each system is described, its advantages and disadvantages are discussed, and possible applications are given.

Many of the more promising systems cool the structure by absorbing heat into a material carried specifically for the purpose; this material is then expended overboard. Since the weight of such a cooling system is largely a function of the weight of the expendable coolant, part of this section is devoted to the selection of the more efficient coolant materials.

In the final portion of this section, rationalization is employed to reduce the cooling problem to the consideration of high and low flux systems, and to eliminate many of the possibilities advanced previously. Approximate weights are calculated for those systems which remain, and the result is a clear indication of the most suitable system for each level of heat intensity.

B. DESCRIPTION OF COOLING SYSTEMS

The ultimate purpose of all structural cooling systems is to absorb heat entering the structure and to dissipate this heat to the surrounding atmosphere. This can be accomplished either by rejecting the heat directly to the atmosphere, or indirectly to the atmosphere by transferring the heat to a material which is then expended overboard. The method by which the heat is transferred to the atmosphere is one means of classifying structural cooling systems, but it is equally appropriate to consider common mechanical characteristics of the systems as the basis for classification. Systems may be grouped, therefore, depending upon whether or not the working fluid experiences a change of state; also, they may be grouped as closed-cycle or open-cycle systems.

[redacted]

Table V-1 is a list of all structural cooling methods presently conceived. These are classified first by the method in which the heat is transferred to the atmosphere, and then by the mechanics of the systems. Each of these systems is treated in some detail in the following paragraphs to explain its method of operation, as well as its significant characteristics, limitations, and applications.

1. Direct Open-Cycle Cooling - Heat Sink Carried in Vehicle

An open-cycle cooling system is one in which the heat-absorbing fluid passes out of the system and is expended overboard after performing its cooling function. The term "direct" implies that the expendable material takes heat directly from the structure or surface to be cooled, without the use of an intermediate fluid. As will be shown in a later part of this section, where comparisons are made of the heat-absorbing ability of various coolants, it is always efficient to absorb much of the heat by a change of state, so that the coolants are generally carried in the liquid form and are expended as vapor or gas. An exception occurs when fuel is used as a coolant because of the requirements of the power plant which uses the fuel.

Open-cycle expendable coolants may be used in four system configurations to control structural temperatures, but all coolants are not necessarily amenable to each system. The four are convection cooling, transpiration or "sweat" cooling, film cooling, and surface melting or sublimation (ablation) cooling.

a. Convection Cooling

This is the simplest form of cooling in which the coolant circulates in passages within the structure and absorbs heat by convective heat transfer between the passage walls and the flowing coolant. If the coolant is not to change state, such as may be the case with fuel, then the influx of heat merely produces a temperature rise. Mass flow rates must be adjusted so that sufficient heat can be accepted without boiling, and the passage lengths must be arranged so as to control within limits the wall temperatures at the outlet where the coolant is hottest. Heat transfer rates to liquids are good, with a result that flow velocities are generally within conventional engineering practice.

The distribution of ducting must be such that local hot spots will not occur in the structure where stresses are high; it will usually be possible to route the ducts so that the higher-stressed portions of the structure can be controlled at low temperatures, while the less critical areas are permitted to reach higher temperatures.

If a change of state of the coolant is permissible, then boiling occurs in the coolant passages and, characteristic of the boiling process, the entire system operates at a temperature which is a function only of the pressure and which can therefore be closely controlled. Owing to the large volumetric changes that occur when a liquid is boiled, it will not generally be possible to evaporate the coolant completely as it passes through the duct because this would result in the passages being almost entirely filled with vapor. Since vapors and gases have small coefficients of heat transfer when compared with the liquid, and since the vapor can absorb heat only by further temperature rise, the lack of liquid in the ducts will usually result in excessive temperatures or burnout. To avoid this difficulty, the flow rates are arranged so that the heat absorbed is able to boil only a small fraction of the total flow, and thus a considerable quantity of liquid remains in the passages. The liquid-vapor mixture is then returned to the supply tank where the vapor is separated and expended, and the liquid is returned for further circulation.

Cooling by convection requires a finite temperature difference between the coolant and the structure, but during boiling very large heat fluxes can be transferred for small temperature differences, provided that the boiling is not of the "film" type. As is characteristic of many liquids, particularly water, at a particular value of heat flux which depends on surface conditions, flow velocity and pressure, and duct shape, the production of vapor is sufficiently fast that a continuous film is formed between the hot wall and the liquid. This film acts as an

insulator and, when it forms, much greater temperature differences are required between the wall and the liquid; this results in a significant rise in wall temperature which generally is disastrous.

Included as a ramification of a convection cooling system is one in which the expendable coolant is both retained adjacent to, and transported into direct contact with, the structure to be cooled by the capillarity of a suitable material rather than by passages and ducts. The system therefore functions as a "blotter" which is kept moist as the coolant is evaporated, either by being fed with coolant at appropriately spaced points, or by the ability of the "blotter" to retain sufficient liquid for the complete flight. The object of such an arrangement is to eliminate the mechanical equipment necessary for the functioning of a true convection system.

Convection cooling with liquids has the merits of simple operating principles, relatively simple mechanical equipment, small power requirements, and ability to deal with a wide range of heat fluxes. If the coolant changes in state, the system is tolerant of inaccuracies in the control of flow rates because of the constant temperature characteristic of the boiling phenomenon. Since the external aerodynamic surface is not disturbed by a convective cooling system, there is no increase in drag or heat transfer coefficient as a result of surface roughness. As mentioned previously, the systems in which the coolant is retained adjacent to the structure in a blotter type of material offer the advantage of a reduced, or even a zero, mechanical complexity and weight, but there is evidence that the capillary action is seriously affected by gravity.

Because convective cooling can be adapted to a wide range of heat fluxes, it can be used in most cooling applications. Its use is not limited by large boundary layer temperatures since the wall temperature of the cooling passages is controlled only by the coolant. For instance, if water cooling is used, with boiling at approximately 200° F, then the structure can be of aluminum, although the surface may be in contact with a boundary layer of extreme temperature.

The use of convective cooling with liquids is limited only at extreme values of heat flux. Under such conditions, film boiling of the liquid may result so that it is not possible to transfer the heat flux without an unacceptable temperature difference between the passage wall and the coolant. Moreover, the gradient established by the flux through the wall thickness of the passage may be sufficiently severe that the outside will melt while the inside remains at the coolant temperature. Such severe conditions are encountered with ballistic re-entry vehicles.

An additional advantage of convective cooling is that it offers excellent opportunity for the efficient use of small amounts of surface insulation. When insulation is used around a cooled structure, the outer surface temperature will rise to a level near the equilibrium temperature which is established when the convective heat input from the boundary layer is balanced by radiant heat output from the surface. If this outer surface temperature is low enough to permit the use of insulation, then large reductions of heat flux into the cooling system and, hence, of cooling fluid requirements will result. This point is demonstrated in Section IV.

The weight of an open-cycle convective cooling system employing liquid coolant is dependent primarily upon the total heat to be absorbed and the type of coolant. Since heat capacity of unit weight of coolant is obviously the important criterion, comparisons of various coolants are made on this bases in a subsequent part of this section. Some weight penalty may result from cooling ducts and passages, although much of this material can usually be used as structure. The weight of ducting is affected by the choice of coolant since the coolant, together with the operating pressure, establishes the working temperature and hence the required duct material. As will be shown later, pumping machinery weights for open-cycle convective cooling systems are relatively small if the coolants are liquids.

b. Transpiration Cooling

Transpiration cooling indicates a coolant flow outwardly through a "porous" external surface, issuing as a gas into the boundary layer. If the dispersion of the flow passages is fine enough, the exit temperature of the coolant gas may be identified as that of the wall, indicating

that the heat capacity of the coolant has been used internally to its fullest extent. Initially, the coolant may be either liquid or gas, but the liquid state is preferred in order to take advantage of latent heat of vaporization.

Methods of construction applicable to the use of sweat cooling, and materials to implement these methods, are not resolved as yet. Large porous metal skins have been produced, but light-weight ducting of adequate coverage appears to be an elusive design problem. Since temperature control and flow control are synonymous in this case, and the flow path is parallel for the entire sweat-cooled surface, the metering problem becomes complex.

Compared with the convective cooling system, transpiration cooling offers greater efficiency and the ability to deal with a flux of any magnitude. The greater efficiency arises partly because (1) the latent heat of vaporization of the coolant is used fully within the structural wall and superheat of the vapor is achieved as the coolant issued into the high-temperature boundary layer, and (2) a gas flow normal to the aerodynamic surface reduces the heat fluxes significantly. There is a possibility, however, that this latter advantage is offset partly by the tendency of the emerging gas to destabilize a laminar boundary layer. Large heat fluxes impose no limit on the use of transpiration cooling, since the cooling action occurs through the wall thickness so that gradients in the wall can be controlled.

The disadvantages of transpiration cooling are (1) an apparent difficulty in developing a porous surface that is not blocked by impurities in the coolant, (2) the large pressures necessary to force coolant through the wall, with the resulting requirements of powerful pumping machinery and a heavy structural wall to sustain the pressure, (3) the difficult metering problem already discussed, and (4) the difficulty of using the system in conjunction with insulation.

Considering all these characteristics, it is evident that transpiration cooling is most suited to areas of extreme heat flux, such as leading edges and body noses.

c. Film Cooling

Film cooling also employs an outward flow of coolant through openings or orifices in the external surface, but here the passages are comparatively widely spaced and the coolant issued in the liquid phase. Each passage is associated with an area of surface over which the liquid film is attached; the degree of attachment is dependent upon the volatility of the coolant, stream static pressure, coolant flow rate, and stream velocity. The fluid is ultimately lost by evaporation into the boundary layer.

Film cooling is similar in principle and mechanics to transpiration cooling, has the same applications, and has similar advantages and disadvantages with respect to convection cooling. Compared with transpiration cooling, film cooling shows lower efficiency in that some of the latent heat of evaporation is used to cool the boundary layer and part of the ambient stream, rather than only the structure. However, construction and metering problems appear to be somewhat less difficult, and operating pressures can be lower.

d. Ablation Cooling

With ablation cooling, the coolant is carried in solid form on the external surface, in direct contact with the boundary layer. Heat is absorbed by melting and perhaps vaporizing the material, with the resultant liquid or gas being carried away by the stream. Analysis of such a system is evidently complex since it involves mechanical forces between the boundary layer and the liquid or gaseous products, heat transfer to a molten surface, considerations of possible sublimation or other molecular activity at the surface, and the effects of changing body profile. Neither empirical nor theoretical approaches to the problem exist in sufficient quantity to provide any realistic basis for comparison with other systems, but the heat capacities of materials, covered in the next section, will show its maximum potential.

The advantage to be expected from ablation cooling is the simplicity of the system since only the coolant is required, with no mechanical devices, passages, or valves. The weight saving from this advantage may be offset, however, unless the full latent heat of evaporation can be utilized before the material is carried away by the air stream.

[redacted]

With almost all coolants, the heat capacity per unit volume is such that it is impractical to place the required volume on the outside of a vehicle unless the flight is of short duration. Ablation cooling is obviously suitable for areas of high heat flux, and this, together with the short-time requirement, makes it particularly appropriate for the cooling of re-entry vehicles.

2. Indirect Open-Cycle Cooling – Heat Sink Carried in Vehicle

Indirect open-cyle cooling differs from direct cooling only in that an intermediate nonexpendable fluid is used to transport heat between the surface to be cooled and the heat sink material. Obviously, such a system can be used only with convective cooling and, therefore, it has the advantages, disadvantages, and limitations explained previously for the convective system.

A number of reasons exist for the use of an indirect system and these will be considered individually. An indirect system may have the advantage of convenience; for instance, when water is used as the final heat sink, it may be more convenient to circulate air in a close circuit and to include a heat exchanger to transfer heat to the water. This arrangement would avoid problems of fluid leakage at innumerable points over the airframe surface.

This example also serves to indicate how an indirect system may save weight by minimizing the residual weight of liquid which must be retained in the system to ensure satisfactory functioning at the end of flight. In an area directly cooled by water, for instance, it is not practical to attempt to boil all water out of the system, since temperature control cannot then be maintained. With the indirect system, however, it is necessary only that the heat exchanger be water-covered to ensure satisfactory functioning. Note that this weight advantage can be expected only when the intermediate fluid is a gas.

An indirect cooling system has application where material problems exist at very high temperatures. For instance, since many light metals have considerable heat capacity when vaporized, they are desirable coolants. However, light metals are corrosive to most structural materials and there is an oxidation problem with the structural materials at the necessary boiling temperatures. An intermediate coolant, more compatible with structural materials, might be used therefore with the more troublesome heat sink material confined to an expendable and readily replaceable tank.

The indirect system is also the means by which a structure may be cooled to a low temperature, such as required for the use of aluminum, but with the heat being absorbed by a high-capacity material of high boiling temperature. This is accomplished by a suitable refrigeration system in which the intermediate coolant temperature is raised by compression to the boiling temperature of the primary coolant.

It will be evident that indirect cooling systems can be classified into two groups depending upon whether the intermediate coolant is merely circulated as a heat-transporting medium, or is compressed and expanded to dissipate heat at a higher temperature level than that at which it is taken from the structure. This latter group will be termed a refrigerating system.

3. Endothermic Reactions – Heat Sink Carried in Vehicle

Certain chemical compounds are available which, when subjected to heat exceeding certain temperatures, react chemically to form other compounds, and in so doing absorb heat. Such reaction is called endothermic and is a possible means of cooling. The system has the attractions of ablation cooling in that it is free of mechanical devices, but its usefulness primarily depends upon the heat that can be absorbed per pound of material, and whether a compound can be found with a reaction temperature suitable for the particular application. Mechanical properties of the material will determine whether it can be used externally, as is usually convenient, or whether it must be positioned inside the structure adjacent to the skin. If the vehicle is recoverable and reuseable, structural corrosion following the chemical reaction may be a factor for consideration.

[redacted]

4. Open-Cycle Atmospheric Cooling – Atmosphere Used as a Heat Sink

Cooling arrangements of this nature have been in general use since the inception of the airplane. In brief, a direct open-cycle atmospheric cooling system is one that intercepts a portion of the free air stream, routes it internally through suitable ducting to absorb heat, and then rejects the heated air overboard.

Engine cooling, cabin cooling and ventilation, and equipment cooling have been accomplished in this fashion by the use of simple routing ducts. However, if the air stream is fast enough to heat the structure, it is incapable then of cooling in such a simple fashion. In fact, the use of a supersonic air stream for cooling required a turbine to extract the kinetic energy from the stream so that its velocity relative to the airframe is lost without excessive temperature rise.

The turbine output must, of course, be converted by some utilizer into heat or work. If the conversion is into heat, either directly or indirectly, no gain has been made; if the conversion is into work that will not appear internally as heat, it must be performed on the external stream. It would appear that recompression of the internal cooling stream, after it has absorbed structural heat, would be the most convenient way of absorbing the work, and this is the procedure usually followed. The open-cycle atmospheric cooling system, therefore, consists of an inlet and diffuser, an air turbine, a heat exchanger (structure), a mechanical utilizer (compressor) and an exit.

At first glance, open-cycle atmospheric cooling is an attractive cooling system because it requires no weight in heat sink material within the vehicle. This is particularly convenient for long flight times since the cooling system weight will be independent of time. Air is also a convenient fluid to circulate around the structure because it has no particular hazards, ducting leakage is unimportant, there is no system maintenance except for the turbine and compressor, and no logistic problems are involved.

However, there are serious limitations to this system and, while these are discussed later in this section, the most important should be obvious here. The entire inlet duct and the first nozzle stage of the turbine would be subjected to recovery temperatures and would operate at these temperatures, unless cooled, since these areas experience the same boundary layer conditions as the external surface. Temperatures are near stagnation because no relief by radiation is possible in an internal duct; each hot wall merely radiates to all others and the effect is canceled. A glance at Section II will show the large values of recovery temperature that are attained at low supersonic speeds.

Recompression, to absorb the work removed from the air stream, means raising the temperature of the stream that already contains the entire net influx of heat to the structure. Thus, it must be expelled at approximately the original velocity, but at a much higher "ambient" temperature, so that boundary layer temperatures on some of the compressor blades and along the exit duct exceed those on the inlet side.

Other problems are introduced by the large volumes involved when the air is expanded to a temperature low enough to be useful, and by relatively small heat transfer coefficients that are obtained between the slow-moving internal air and the structure.

As will be shown later in this section, the net result of these difficulties is to limit open-cycle atmospheric cooling, for all practical purposes, to speeds below which cooling is not required.

The system just described was direct cooling by means of air; the term "direct" signifies that the final coolant (air) is used in contact with the structure to be cooled. An indirect system is possible in which a secondary fluid is circulated, in a closed system, through the structure and a heat exchanger. The air passes only over the heat exchanger.

The indirect system was not considered seriously during the present study because its only advantage lies in overcoming the difficulty of circulating large volumes of air through the structure. This is done, of course, at the cost of added weight and extra machinery. Both the

turbine and the compressor for the main air flow are still required and the extreme temperature problems of the inlet and exit systems are not reduced.

If the turbine and compressor are not used, the heat must be forced into the stream across the high-temperature boundary layer. This requires a compression-expansion phase in the secondary coolant, but it then becomes unnecessary to take the high-velocity air stream into the vehicle, and the arrangement is better considered as a closed cycle system.

5. Closed Cycle Atmospheric Cooling – Atmosphere Used as a Heat Sink

These systems involve a coolant circulating within a closed circuit, absorbing heat from the hot areas of the airframe, transporting it to a preselected cooler area, and there dissipating it. Thus, the coolant performs the same function as the secondary coolants in the indirect systems described previously, but it is now considered the primary coolant since no other exists within the system.

In order to dissipate heat to the atmosphere from an airframe subjected to aerodynamic heating, it must be possible for the coolant to raise the temperature of the area selected for dissipation to a point at least above the local equilibrium temperature. If this is done, heat will be dissipated by radiation at an intensity proportional to the difference between the fourth powers of the operating temperature and the normal equilibrium temperatures. The area required will then follow from the total flux to be dissipated and, naturally, the area will be minimized by selecting the coolest part of the airframe surface.

If the operating temperature can be raised further until it exceeds the boundary layer temperature, then heat will also be dissipated by convection; from the recovery temperatures presented in Section II, it will be obvious that this can be achieved only at low speeds.

The two possible variations of the closed cycle atmospheric cooling system are the circulation system and the refrigeration system. The difference between these two variants has already been explained in connection with indirect open-cycle cooling. The circulation system is only a means of transporting heat, and no mechanical work is performed on the cooling fluid except the action of the circulating pump in overcoming flow resistance. Heat is absorbed by a temperature difference between the hot structure and the fluid, and heat is expended when the coolant arrives in an area where its temperature is at least above the normal equilibrium temperature.

Obviously, such a system is limited to applications where a considerable variation of equilibrium temperature occures across the wing chord or along the body; such a situation arises at high altitude and high speed. For the same reason, this system cannot be expected to cool large areas because, as more area is included in the "hot" side of the cycle, the total flux is increased but less area remains for dissipation. The circulation system also has the restriction that structural temperatures in the cooled area cannot be below equilibrium temperature in the dissipation area.

The refrigeration system overcomes these difficulties, but only at the expense of pumping machinery and a substantial power requirement. By means of a compressor, the coolant temperature is raised after leaving the structure so that the dissipation may occur at a temperature limited only by materials available for construction of the area and the compressor. After loosing some of its heat, the coolant is expanded to a lower temperature before re-entering the structure.

Obviously, this system has flexibility and a wider range of application than the circulation system, provided that suitable materials can be found. Such a material must possess the necessary relationship between phase change temperature and pressure, must have a high specific-heat ratio and a high critical temperature, and must not cause corrosion of the structure.

Since the closed cycle systems require no heat sink within the aircraft, they are independent of flight time and are free of logistic problems. System weights will depend upon the type of coolant used, which in turn depends upon the temperature levels required and whether or not the system uses the refrigeration principle. The refrigeration system, by raising the final temperature, re-

duces the area required for heat dissipation, but it may increase the structural problems of this area and necessitate extra machinery and power for the compression.

C. COMPARISON OF EXPENDABLE COOLING MATERIALS

Some of the desirable characteristics of expendable coolants are:

(1) High bulk density

(2) Phase change (or chemical change) from initial to jettisoned state

(3) High total heat in jettisoned state

(4) Low suppression pressures throughout the useable temperature range

(5) Chemical compatibility with structural materials

This section reviews those materials that comply with one or more of these requirements. Comparisons are presented on the basis of the most significant factor, item (3), and recommendations are made regarding the materials that should be considered in future studies. In making these comparisons, water is used as a basis because of its outstanding combination of desirable characteristics. It has high specific heat and high latent heat of vaporization, and it is plentiful, easily handled, nontoxic, essentially noncorrosive to materials of construction, and nonflammable. Furthermore, water boils at a reasonable pressure at the limiting operating temperature of the most efficient structural material, aluminum alloy.

Expendable coolants fall into two general classifications; those in which an endothermic chemical change plus sensible heat are involved, and those in which the changes are physical only, namely, change of state and sensible heat. The nature of chemical substances quickly defines the area in which fruitful values for endothermal reactions may be found, but the search for high values of specific heats and latent heats of fusion and vaporization must be more comprehensive.

Using water as the basis for comparison, the only endothermic reactions considered worthy of mention are those in which the heat absorbtion exceeds the total heat of steam at 200° F, and in which the reaction temperature occurs in a suitable range. Only lithium hydroxide, lithium hydroxide monohydrate, and boric acid conform with these requirements.

Up to 1000° F, the heat absorbed by each of these materials is:

Lithium hydroxide	1480 BTU/lb
Lithium hydroxide monohydrate	1593 BTU/lb
Boric acid	1360 BTU/lb

The lithium compounds are extremely corrosive to all structural materials, to the degree that it is impractical to use them except for short periods of time. It is apparent from the afore-mentioned values that the small saving in coolant weight that might result from the use of these materials, as compared with water, will generally be eliminated by the fact that an aluminum alloy structure cannot be used. Further consideration of endothermic reactions is therefore unnecessary.

In the search for expendable coolants that depend upon physical characteristics for their total heat capacities, water is again used as a basis and the initial choice is made by considering the total heat per pound of material at a temperature between 200° and 2000° F. Principal sources for this information are References 2 through 5. Only the alkali metals, hydrogen and helium, and of course water, merit further consideration. Total heats of these materials at various temperatures within the afore-mentioned range, are shown in Figures 2.4-1 and 2.4-2 of Section 2.0, Part I.

Helium is eliminated immediately because, in order to show a greater heat capacity than water, it must receive a temperature rise of at least 800° F. The critical temperature of helium is so low that practically all of its heat capacity is sensible heat in the gaseous phase. If helium is introduced into the structure in the liquid phase, the low-temperature storage problem must be considered and the structure will operate at approximately 800° F. If it is stored as a gas, a high-pressure storage vessel is required to keep volumes practical, and structural temperatures will be higher than 800° F.

Helium must be circulated through the structure as a gas and, as will be shown later, the resulting cooling system is heavier than one circulating a liquid. The provision of liquid helium also involves logistic problems. Evidently, water is more convenient in every respect; for the same weight of coolant, water will result in a lighter (aluminum) structure. Helium is therefore not considered further.

The total heat of hydrogen at 200° F when measured from absolute zero is approximately double that obtained in raising water from 32° F to saturated steam. Nevertheless, many of the reasons that eliminate helium as a useful coolant also apply to hydrogen. The weight of coolant that might be saved by using hydrogen is offset by the increased equipment weight of a gaseous system, and the weight involved in storing the liquid.

The critical temperature of hydrogen is so low that it is impractical to maintain it as a liquid by the application of pressure; instead heat must be kept away from the storage tank, presumably by insulation. Some relief to the problem of loss by boiling in the tank can be obtained by a pressure of 40 to 60 psi, but this raises the boiling point some 15° F. Thus, some heat can then be absorbed in raising the hydrogen temperature by this amount before boiling begins. Obviously, an optimization is required between tank weight to carry the pressure, insulation weight, and hydrogen loss, but the arrangement will be heavier than the corresponding storage system for water because the latter requires neither insulation or pressure.

Another difficulty with the use of hydrogen is its volume. Assuming that for the same heat capacity the weight is one-half that of water, the volume will be seven times as great. Space is generally at a premium in any aircraft, but even if it were not, the larger volume implies a much heavier tank, a particularly significant item with a pressurized and insulated tank.

An additional difficulty with hydrogen, the fire and explosion hazard, necessitates that the entire structure be perfectly sealed against leaks. The question of flammability when the hydrogen is expended overboard is avoided because little is known about ignition and flame front stability at the low pressures and high velocities that would exist. Reference 3 (volume II, page 172) indicates that the ignition lag for hydrogen is 0.5 second when it is heated 513° C at 75 mm of mercury and mixed with air at the same temperature and pressure. At supersonic speeds for which heating is important, the flame would not propagate closer than 2000 feet behind the aircraft.

On the basis of these facts, hydrogen is not considered further as a structural coolant, but it is possible that suitable applications may arise.

Nearly all alkali metals have a higher latent heat of evaporation than that of water. Potassium is the exception. The alkali metals have boiling points at low pressure that exceed the temperature limits for aluminum and titanium alloys. The only metals that boil at temperatures within the tolerance limits of any present-day high-temperature alloys are lithium, magnesium, and sodium.

Lithium metal, in both solid and liquid phases, has the highest specific heat of any known element or compound. It has the highest latent heat of vaporization, with the single exception of carbon (graphite). However, graphite exhibits its superior heat capacity at a temperature of 4200° C, which makes it useless for anything but surface evaporation (ablation) cooling. Lithium also presents a difficulty, since in the molten state it is nearly indiscriminate in its attack on any substance. Pure iron, as well as molybdenum, appears to be reasonably resistant to rapid destruction by lithium. But pure iron, at the temperature of boiling lithium, cannot be considered a structural material. Molybdenum, while retaining good physical characteristics at temperatures of nearly 2000° F (lithium boils at 1983° F at 100 mm of mercury), is seriously affected by oxidation. Its use, therefore, would be contingent upon the successful development of coatings that would prevent, or satisfactorily delay, its oxidation at the noted temperature.

Despite these difficulties, the heat capacity of lithium is so much greater than all other materials that it must be considered for cooling areas of high heat flux, such as leading edges, where the outer surface must be cooled because equilibrium temperatures are too high for any known material.

Magnesium, having a heat capacity less than one-third that of lithium, is not much more docile in the company of present-day high-temperature service alloys (Reference 14). Iron, tungsten,

[redacted]

molybdenum, and chromium are satisfactory for use at low-pressure boiling temperatures of magnesium (1450° F), but other metals appearing in the alloys are not. In particular this would affect the nickel, copper, and cobalt in materials such as Inconel X and S-816. Because of this difficulty, magnesium offers less promise than sodium as a coolant.

Sodium has a specific heat approximately equal to that of magnesium, but a latent heat of vaporization only 75% as great. Thus, it is somewhat less effective than magnesium as a heat sink, but it has a long record of successful use as a molten coolant in exhaust valves of internal combustion engines. Also, sodium has a small-to-negligible effect on all accepted high-temperature service alloys.

Because of its high boiling point, and hence the need for a dense high-temperature structural material, it is doubtful if sodium would be competitive with water as a coolant for primary structure despite its much larger heat capacity. Applications can be imagined in which structural loading is low, but flight time is long.

Sodium lends itself, however, to the direct surface cooling of areas where equilibrium temperatures are too high for the use of insulation, but its efficiency can never approach that of lithium. It may, therefore, be expected to have application in the interim period during which the more difficult problems of lithium are being resolved.

Heat capacities of the light metals, lithium, magnesium, and sodium, are compared over a wide range of temperatures and pressures in Figure 2.4-2 of Section 2.0, Part I. These values are summarized, together with the values for water, in the following tabulation.

SUMMARY OF EXPENDABLE COOLANTS

Material	Pressure (mm of mercury)	Heat Capacity per Unit Weight (BTU/lb)	Heat Capacity per Unit Volume (BTU/ft^3)	Boiling Temperature (°F)
Water		1,100	68,200	
Lithium	1.0	10,000	330,000	1,370
	1,122	11,000	364,000	2,500
Magnesium	10.0	2,880	311,000	1,370
	5,408	3,250	351,000	2,500
Sodium	100.0	2,300	140,000	1,285
	3,866	2,500	152,500	2,000

In addition to these coolants, there is the possibility, as explained in Section V, B, of using fuel as a coolant by circulating it through the structure before it is consumed in the engine. This is feasible only on aircraft propelled by air-breathing engines, since with rocket propulsion the fuel or propellant is expended shortly after the start of flight. Consideration is, therefore, limited to JP-4 fuel, and since it is not permissible to vaporize the fuel before it enters the engine, only its specific heat and permissible temperature rise are of interest. For purposes of cooling system design, the specific heat may be taken as 0.45 BTU/lb° F, while the temperature limits are -20° and +250° F (Reference 12). If the fuel is precooled before flight, therefore, the maximum available heat capacity is 0.121 BTU/lb.

D. COOLING SYSTEM ANALYSIS

1. Problem Rationalization

In Section V, B, many structural cooling systems have been described. Each system may use a variety of coolants and may operate at various temperature levels. A large number of com-

[redacted]

[redacted]

binations is thus possible, but a complete numerical analysis of all these possibilities is impractical and unnecessary because it can be shown by argument alone that only a few combinations justify detailed study.

For the purpose of cooling system design, structures can be divided into two groups on the basis of the equilibrium temperature that can be realized on an insulated surface at the point being considered. The significance of this division is that it defines whether or not insulation can be used in conjunction with the structural cooling, the importance of insulation being that moderate amounts can produce large reductions of flux into the cooling system. Reductions in heat flux by factors of 10 to 50 are easily achieved with a small weight of insulation, so that its use with a cooling system is necessary.

As shown in Figure IV-12, a one-inch thickness of Thermoflex insulation weighing 0.25 lb/ft^2 will reduce the heat flux, for a wide range of applications, to a level of approximately 1000 BTU/ft^2hr which requires approximately one pound of water per hour for the cooling of one square foot. As shown elsewhere, an outer wall is required to protect the nonstructural insulation and this can be constructed for a weight of approximately one pound per square foot. Thus, by using insulation, most structural cooling can be accomplished for a weight of 2 1/2 to 3 lb/ft^2. To this must be added the weight of the cooling system.

These weights should be contrasted with the coolant weights required for direct cooling of the outer surface. Values for this latter case can be obtained by taking the heat flux values given in Section II for various flight paths and aircraft types, multiplying by the flight time in hours, and dividing by 1000, to represent approximately the heat capacity of water. The result is the coolant weight in pounds per square foot. Only for extremely short flight-times or for low speeds will the weight approach that of the insulated system. In making this comparison, allowance should also be made for the shorter flight time in the weight of the insulated system; for 0.1 hour, for instance, its weight is decreased to approximately 1.5 lb/ft^2.

This comparison is only slightly improved in favor of direct surface cooling if the higher heat capacities of the light metals are used, rather than water. Because of the high boiling point of the light metals, their use also requires either a high-temperature structural material, or an intermediate cooling system to carry heat from the structure to the heat sink.

From these arguments it is clear that insulation should be used in conjunction with cooling wherever possible, and the limit is actually imposed by the equilibrium temperature reached on the outer surface of the insulation. The outer protective wall around the insulation needs only sufficient strength to carry aerodynamic pressure loads, and for this purpose low stress levels can be tolerated. Thus, with present-day materials, outer wall temperatures of 1800° to 2000° F are permissible. From the curves of Section II, it will be seen that this permits the use of insulation with cooling, over all areas considered as primary structure, for all future aircraft types except the re-entry portion of the ballistic missile. This latter vehicle is not considered to have primary structure in the usual sense, because any such structure will be lightweight since no surfaces are involved. The re-entry missile is therefore considered a heat problem rather than a structural problem; as such, its cooling systems belong in the high flux category.

Transpiration cooling, as discussed in Section V, B, is expected to give large reductions in heat transfer, in many applications, but this system can be applied only to the cooling of the outer surface. Therefore, if an optimistic heat flux reduction factor of 5.0 is assumed, the result does not generally approach the performance of insulation.

There are two classes of cooling problems to be considered:

(1) Cooling systems for primary structure; insulation used in conjunction with cooling; heat flux of the order of 1000 BTU/ft^2hr; maximum equilibrium temperature on outer surface approximately 1800° F.

(2) Cooling systems for secondary structure, such as leading edges, body nose, re-entry missiles, and drag brakes; outer surface cooled directly; heat fluxes much greater than 1000 BTU/ft^2hr, and may reach a peak on the nose of the re-entry missile of

[redacted]

20 to 30 x 10^6 BTU/ft^2hr. Equilibrium temperatures will generally be sufficient, if the cooling system fails, to render the structural material useless.

Item (1) is primarily a problem of finding the system having minimum weight; item (2) has in addition the important question of feasibility.

The result of this rationalization is to eliminate, for primary structural cooling, the systems that function only if the outer surface is cooled. These systems are film, transpiration, and ablation cooling. From the discussions and values presented in Section V, C, the use of endothermic reaction cooling is eliminated for primary structure, and expendable coolants to be considered can be reduced to water, sodium, and lithium.

A search for refrigerants having a liquid-vapor phase within a useful range of temperatures and pressures produced only mercury as a possibility. This problem is discussed more fully in Reference 1, where the requirements of a refrigerant are explained. In particular, a high specific heat ratio is required to minimize pressures and pumping power. The kinetic theory of gases shows that highest values of specific heat ratio are associated with the monatomic gases and that decreasing values accompany increasing molecular complexity. This fact eliminates many organic and inorganic liquids with boiling points in the acceptable range. Detailed computations for a mercury refrigeration system are given in Reference 1 for a cooling system handling a moderate heat flux, and excessive weights are shown.

For these reasons, consideration of the refrigeration cycle has been limited in this section to the use of air, with no phase change.

It is now possible to summarize the cooling systems listed in Table V-1 which are applied to the cooling of primary structure in this section:

(1) Direct, open-cycle convective cooling with heat sink carried in vehicle.
   (a) Coolant circulated through structural passages in the structure.
   (b) Coolant retained in a blotter-type material.

(2) Indirect, open-cycle convective cooling with heat sink carried in vehicle.
   (a) Air or steam circulated, water as heat sink, structures of aluminum, titanium, and stainless steel.
   (b) Air circulated, sodium and lithium as heat sink, structures of aluminum and titanium.

(3) Direct, open-cycle cooling with air.

(4) Direct, closed-cycle cooling with atmosphere as heat sink.
   (a) Circulation system.
   (b) Refrigeration system using air as the working fluid.

The study of these systems will show that, except for a few special cases, the cooling of primary structure is accomplished with the least weight by open-cycle convective cooling in which water is circulated through passages within the structure. This system not only has minimum weight, but also offers the greatest convenience since it uses conventional aluminum alloy structure and there are no logistic problems involved with water. Protection of crew, equipment, and engines is achieved at no extra cost in system weight. Moreover, the system has the uniformity of temperature and the safety factor against unexpected flux differences that are inherent in the constant-temperature characteristic of the boiling phenomenon.

Following the consideration of cooling for primary structure, some attention is given to the more difficult problem of cooling secondary areas of high heat flux. These investigations are somewhat limited by the lack of experimental data, but it is possible to show which systems have the most promise and to indicate some of the more important problems involved in their development. Again, direct cooling of the hot surface is shown as the most simple system and, generally,

the one having least weight. Until the development of transpiration cooling systems is complete, the use of the light metals, particularly lithium, in a convective system appears to be the best approach.

2. Cooling Systems for Primary Structure

a. Direct, Open-Cycle Convective Cooling – Heat Sink Carried in Vehicle

Section V, B, describes this system of cooling and explains the advantages to be expected from its use. Two variants of the system are discussed: (1) coolant circulated through passages within the structure, and (2) coolant retained adjacent to the structure in a blotter-type material.

Both variants will be considered in the following examples which are concerned only with heat absorption by boiling. The case of fuel cooling is not considered since its range of applicability is small, and factors such as power plant and flight path are involved.

From Section V, C, the only coolants worthy of consideration are water, sodium, and lithium. Lithium boils at a temperature (approximately 1900° to 2000° F) which is greater than temperatures experienced over most areas of primary structure (see Section II), and therefore can not be used for direct convective cooling in such areas. Similar restrictions apply to the use of sodium, to a smaller degree, but a structure operating at 1200° to 1400° F would be necessary for direct sodium cooling, and the resulting increase in structural weight easily offsets the saving in coolant weight. For the flux of 1000 BTU/ft^2hr, a typical value for an insulated water-cooled aluminum structure, the saving in coolant cannot exceed 1 lb/ft^2 of cooled surface. Only a structure of extremely light loading could be changed from aluminum to a 1200° F material, with a weight increase of less than 1 lb/ft^2. It remains therefore to consider direct, open-cycle convective cooling using water as the coolant and aluminum as the structural material. The structure is limited to 200° F and the heat flux to be absorbed will be taken as 1000 BTU/ft^2hr.

(1) Coolant Circulated Through Passages Within the Structure

Passages within the structure are assumed to be formed by attaching a second skin, containing flat corrugations, to the outside of the primary structural skin. A value of 2000 ft^2 has been chosen arbitrarily as a suitable total surface area and it is visualized that such an aircraft may have a wing span of 30 feet. Each corrugation may therefore be 15 feet long, without a break or section change, so that it is able to carry compression or tension loads. Hence, the corrugated skin is considered fully effective structurally, and no weight penalty is included.

Although the size and shape of the corrugation may vary considerably, an average width of 1.375 in. is used for one complete corrugation. Velocity of the coolant at the exit end of each tube is arbitrarily chosen at 25 ft/sec and the coolant "quality" at this point is assumed to be 10%. The "quality" refers to the percentage of mass flow that is present as a vapor or gas. The complete system is under 12 psia pressure for a steady-state condition so that at 200° F, 1 lb of 10% quality mixture occupies 3.25 ft^3. The average specific volume in a tube (5% quality) is 1.634 ft^3/lb. At a saturation temperature of 200° F, 976.6 BTU are required to evaporate fully one pound of water.

For one corrugation 15 ft long, the area to be cooled is 1.72 ft^2 and the amount of heat absorbed equals 1.72 x 1000/3600 = 0.478 BTU/sec.

The flow required to produce 10% quality at the end of one corrugation is 0.478/(10 x 976.6) = 0.0049 lb/sec. The required cross-sectional area necessary for the velocity to be 25 ft/sec and the mixture to be of 10% quality at the end of the duct is (0.0049 x 3.25)/25 = 0.000637 ft^2. The flow of 0.0049 lb/sec is equivalent to (0.0049 x 60)/8 = 0.03675 gpm for one corrugation, or (0.03675 x 2000)/1.72 = 42.8 gpm for the complete airplane.

Typical weight for a pump rated at 200 gpm is 120 lb, so that by direct ratio, a 42.8 gpm unit should weigh 25.7 lb or a unit weight of 0.0128 lb/ft^2.

This pump weight is considered conservative, but no weight is included for a power unit. A steam turbine is assumed, and this unit would be small and weigh only 4 to 5 lb. Steam would be produced by a small high-pressure circuit in the cooling system.

[redacted]

Actual conditions of coolant flow are unknown because of continuous quality change; for this reason, no attempt has been made to determine pressure loss of the system. Weight of turbine and pump is therefore based upon flow alone with neglect of head requirements. Flow velocities are low and no difficulties are expected from pressure loss, but the velocities can easily be reduced with only an added weight due to residual water in the ducts.

Weight of water required to fill the tubes (considered to be unuseable as the system must never become dry) equals $(0.000637 \times 15)/(1.72 \times 1.634) = 0.0034$ lb/ft^2.

Taking 1.5 hr as a conservative flight time, tank capacity is required for $2000 \times 1000/976.6 = 2050$ lb of water, or 33 ft^3. This requires approximately 60 ft^2 of tank shell area, or, assuming a 0.050 aluminum shell, plus 50% for stiffening, plus 10% for excess capacity, gives a tank weight of $60 \times 144 \times 0.05 \times 0.1 \times 1.6 = 69$ lb.

Adding 30 lb for steam trap, relief valve, and tank supports gives a total tank weight, per unit of cooled area, of 0.05 lb/ft^2. This will be used conservatively for any flight time.

Total weight of equipment is, therefore, $0.0128 + 0.0034 + 0.0500 = 0.0662$ lb/ft^2. This weight is very low, and it may be preferable to take a weight of 0.10 lb/ft^2 to include such incidentals as metering values, controls, exhaust steam line, and short lengths of internal pipes. Total weight of this system, therefore, including water for a flight time of one hour, is 1.10 lb/ft^2.

Weights for this system have been investigated for a wide range of flight times and heat fluxes and the results are presented in Appendix B of Reference 1.

In Section V, B, a ramification of the direct, open-cycle convective cooling system is described in which the expendable coolant is retained adjacent to and in direct contact with the structure by means of the capillarity of a suitable retentive material. As mentioned in Section V, B, there is evidence that the capillary action is seriously affected by gravity, but, nevertheless, typical weights will be calculated. Again, two forms of this system are possible. The first uses sufficient retaining material to store all of the coolant for the flight so that no supply system, pump, or storage tank is required. The second system has a much thinner layer of retaining material, but each point is supplied with coolant from a central source. In both cases, water is the only coolant to be considered both for the reasons advanced in connection with the previous water circulating system, and because no material is known which might act as a blotter with liquid metal.

(a) Retention Cooling Without a Supply System

A material having apparently satisfactory characteristics for the entrainment of water is Vermiculite, and exfoliated mica. The vermiculite is loaded permanently inside the airplane structure, being supported by a light metal screening and suitable reinforcing braces.

Before flight, the required amount of water is introduced into the Vermiculite by subjecting it to saturated steam. Under these conditions, it has been found that the Vermiculite absorbs at least three times its own weight (Reference 8). Total heat of water, including the sensible heat to reach boiling, is approximately 1110 BTU/lb so that for the same heat flux of 1000 BTU/ft^{2}hr:

$$\text{Water weight for one-hour flight} = 1000/1110 = 0.90 \text{ lb/ft}^2$$

$$\text{Weight of Vermiculite} = 0.90/3 = 0.30 \text{ lb/ft}^2$$

For an aluminum metal screening and supports, allow 0.110 lb/ft^2; this gives a total weight of 1.31 lb/ft^2. Although this weight is greater than that given for the water circulating system, for shorter flight times, the two weights will approach each other, since with the retention system both water and Vermiculite weights are reduced by reduced time.

Curves of retention system weights for a range of flight times and heat fluxes are included in Appendix B of Reference 1.

[redacted]

(b) Retention Cooling With a Supply System

From Reference 8, a woven fiberglass-type fabric with the trade name Refrasil is suggested as the most suitable water retainer for the system which is supplied at individual points. A thickness of 0.017 in. is given, having a weight of 0.10 lb/ft^2.

Again in Reference 8, it is shown that very small feed lines are sufficient to supply the water, assuming that feed points are spaced 9 in. apart in both directions, and that these lines, together with residual water and connectors, can be expected to weigh approximately 0.044 lb/ft^2. Small lines are sufficient in this case, since the quantity to be supplied is only that which is evaporated and there is no volumetric change by boiling in the feed lines.

Pump and water tank weight is assumed to be the same as for the circulating system, although the pump might be smaller because flow rates are smaller. Weight for these two items is 0.0128 + 0.050 = 0.0628 lb/ft^2.

The final item required in this system is a small sensing and metering valve at each feed point. Following the suggestion of Reference 8, a weight of 0.10 lb/ft^2 is allowed. Total weight of this system for one hour of flight is, therefore, 0.10 + 0.044 + 0.0628 + 0.10 + 0.90 = 1.207 lb/ft^2. This system weighs approximately the same as the circulation system. However, no residual water in the blotter insulation has been considered, so it is assumed that the water supply is stopped before the end of the flight, and the blotters are boiled dry. To keep the entire system wet would require an additional 0.19 lb/ft^2.

This fact, together with the problems of gravity effects on the water and the design of a sensing-metering valve, is considered sufficient to discard the system in favor of the direct circulation of water.

b. Indirect, Open-Cycle Convective Cooling - Heat Sink Carried in Vehicle

In Section V, B, the possible merits of this cooling system are explained, and it is shown that two arrangements are possible: (1) circulating an intermediate coolant, in which case the temperature of the structure must exceed the final temperature of the expended material, and (2) compressing and expanding the intermediate coolant to expel heat at a higher temperature than the structure. Both systems are considered in the examples that follow.

In Section V, C, it is shown that only water and light metals have sufficient heat capacity to justify their use as expendable coolants. Since the lowest boiling point that can be achieved, with reasonable pressures, in any of the light metals exceeds the level at which an efficient structure can work, the indirect system, using only a circulating intermediate coolant, can only be used with water. In the following examples, therefore, aluminum, titanium, and stainless steel structures are studied using water as the final heat sink, and a vapor as the intermediate coolant. The vapor is air for the aluminum structure, and steam for the titanium and stainless steel structures. Steam is used in the latter cases because the structural temperatures are much higher than the boiling point of water. Moreover, by using the steam produced as an intermediate coolant, it is possible to superheat and thus increase the total capacity of the expended material.

For the second system mentioned previously, in which the intermediate coolant is compressed and expanded through the cycle, only the light metals are used as expendable coolants since the added complexity of a compressor and power unit is unnecessary for water. The example is thus confined to the use of sodium as the final coolant, air as the intermediate coolant, and aluminum, titanium, and stainless steel structures.

The reason for the consideration of aluminum, titanium, and stainless steel structures is to reduce heat flux by operating at higher temperature. The reduced heat flux should result in reduced weight of both equipment and expendable coolant, these effects being offset by the increased weight of the higher temperature structure. Final weight comparisons cannot be made in general terms since they obviously depend upon structural loading and flight time. This section of the report is therefore concerned primarily with the development of system weights. The comparative structural weights, at the respective temperatures, can be obtained from Section IX.

All structures considered here are insulated with a one-inch thickness of low-density mineral wool felt with a suitable protective outer wall, as described elsewhere in the report. Structures of aluminum, titanium, and stainless steel are maintained at 200°, 600°, and 1000° F, respectively. Heat flux is taken as 1000 BTU/hr ft^2 for the aluminum structure; corresponding values for the titanium and stainless steel structures are 700 and 254 BTU/hr ft^2, respectively. Weights are based upon an airplane of 250 ft^2 wing area and 2000 ft^2 of external surface area to be cooled.

To facilitate this work, it was desirable to avoid the detail design of numerous heat exchangers, blowers, and motors, merely to obtain weight. The weights used were therefore suitably proportioned from known weights for particular designs which, it may be assumed, are already optimized for minimum weight. A summary of these typical weights and relevant information is given in the following; the source of the information is References 7, 9, and 10.

Weight of heat exchanger = 2.0 lb

Fuel side heat-transfer coefficient = 315 BTU/hr $ft^{2\circ}$ F

Air side heat-transfer coefficient = 63.0 BTU/hr $ft^{2\circ}$ F

Over-all heat-transfer coefficient = 55.4 BTU/hr $ft^{2\circ}$ F

Heat-transfer surface area = 3.68 ft^2 (see Figure 6 of Reference 9 for arrangement)

Air mass flow = 2360 lb/hr

Weight of blower = 2.25 lb

Weight of motor = 8.28 lb

Power required = 875 watts

Fundamental to the discussion of cooling systems, in which a vapor or gas is used, is the heat transfer coefficient.

Heat transfer coefficients between the structure and the circulating vapor were derived from data for thermal de-icing systems. Practically no other experimental information has been found for duct configurations suitable for cooling the structure. The major source is Reference 6. The equation used is well known (Reference 7):

$$h_c \frac{d}{k} = 0.0225 \left(\frac{dG}{\mu_f}\right)^{0.8} \left(\frac{c_p \mu_f}{k_f}\right)^{0.4}.$$

This equation applies to the heating of fluids in circular tubes in turbulent flow. In this case, the value of d is the depth of the duct along the outer surface (about 1/4 inch).

Tests on the model showed the values of h_c to be about 50% higher than predicted by the afore-mentioned equation (Figure 7 of Reference 6) for any given Reynolds number. This would indicate that the degree of turbulence in a flat duct is higher than that in a circular duct; in effect, a higher Reynolds number. No statements were made that would substantiate this conjecture; in fact, the discussion of results is relatively meager.

By inserting values for $c_p \mu_f / k_f$ in the afore-mentioned equation, for air in the temperature range in which it is expected to be used, and simplifying the term dG/μ_f, the equation is reduced to

$$h_c = 1.5 \left[0.02 \frac{k}{d} \left(\frac{w}{\mu_f}\right)^{0.8}\right].$$

The factor 1.5 has been shown separately since it is not derived from theory, but rather from the empirical results. The remainder of the equation appears in Reference 6. Heat transfer coefficients between the vapor and the heat exchanger are derived by extrapolation of the data mentioned.

[redacted]

From these data, the heat transfer coefficient is 63.0 BTU/hr ft^2° F, with a mass flow of 2360 lb/hr. From Reference 7, the heat transfer coefficient for a tubular heat exchanger varies as the 0.6 power of the mass flow; thus, the heat transfer coefficient can be written approximately as

$$h_x = 63.0\left(\frac{W}{2360}\right)^{0.6} = 0.596\, W^{0.6}.$$

This expression for h_x holds, provided that the area of the heat exchanger, normal to the vapor stream, is not changed. If it is changed, then h_x is also changed for the same mass flow. For the heat exchanger being used as an example, the reference area upon which heat transfer is based is 3.68 ft^2. The value of h_x will be affected inversely as the area, so that

$$h_x = 0.596\left(W\frac{3.68}{A_x}\right)^{0.6} = 1.307\left(\frac{W}{A_x}\right)^{0.6}.$$

The weight of the heat exchanger is proportional to the area A_x. In the exchanger used as a reference, the area is 3.68 ft^2 and the weight is 2.0 lb. Therefore, heat exchanger weight is

$$\frac{2.00 \times A_x}{3.68} = 0.542\ A_x \text{ lb.}$$

(1) Indirect, Circulation-Type Cooling Systems

Significant weight items in this system, apart from the coolant material, are the vapor-to-water heat exchanger and the air-circulating blower and its power supply. To obtain these weights, it is necessary primarily to find the mass flow of the vapor and its temperature rise through the structure. These quantities are corrected by the equations expressing the convective heat transfer from structure to vapor, and the temperature rise in the vapor during its passage through the structure.

If the vapor enters the structure at temperature T_i and leaves at temperature T_f the mean temperature is $1/2(T_f+T_i)$, so that the average temperature difference between structure and vapor is

$$\left(T_s - \frac{T_f + T_i}{2}\right).$$

To absorb a heat flux per unit area of q, the heat transfer coefficient that must be achieved is

$$h_s = q/\left(T_s - \frac{T_f+T_i}{2}\right).$$

Therefore, by transposing the expression given previously for heat transfer coefficient, the necessary mass flow passing any point on the structure is

$$(w)^{0.8} = \frac{h_s\, d(\mu_f)^{0.8}}{0.03 k_f}.$$

The total mass flow from the entire surface area being cooled is

$$W = Aq/c_p(T_f - T_i),$$

so that W/w is the number of circuits in cooling system. Now T_i is also the temperature at which the vapor leaves the heat exchanger while T_f is the entering temperature. Therefore, the average temperature difference between the vapor and the water in the heat exchanger is $\left(T_x - \frac{T_f+T_i}{2}\right)$. Heat exchanger heat-transfer coefficient, based upon the total mass flow W, is h_x and the total heat to be absorbed is Aq. The necessary heat exchanger area is therefore

$$A_x = Aq/h_x\left(T_x - \frac{T_f + T_i}{2}\right).$$

[redacted]

[redacted]

But $h_x = 1.307 \left(\frac{W}{A_x}\right)^{0.6}$, so that $A_x = Aq \,/\, 1.307 \left(\frac{W}{A_x}\right)^{0.6} \left(T_x - \frac{(T_f + T_i)}{2}\right)$;

but $w^{0.8} = \mu_f^{0.8} \quad \frac{h_s d}{0.03 k_f} = \mu_f^{0.8} \frac{g d}{\left(T_s - \frac{T_f + T_i}{2}\right)} \, 0.03 k_f$,

therefore $\left(T_s - \frac{T_f + T_i}{2}\right) = \frac{q d}{0.03 k_f} \left(\frac{\mu}{w}\right)^{0.8}$.

Now $\left(T_s - \frac{T_f + T_i}{2}\right) = \left(T_x - \frac{T_f + T_i}{2}\right) + (T_s - T_x)$,

therefore $\left(T_x - \frac{T_f + T_i}{2}\right) = \frac{q d}{0.03 k_f} \left(\frac{\mu}{w}\right)^{0.8} - (T_s - T_x)$,

so that heat exchanger area becomes

$$A_x = Aq \,/\, 1.307 \left(\frac{W}{A_x}\right)^{0.6} \left[\frac{q d}{0.03 k_f} \left(\frac{\mu_f}{w}\right)^{0.8} - (T_s - T_x)\right] ,$$

or

$$A_x^{0.4} = Aq \,/\, 1.307 \quad (W)^{0.6} \left[\frac{q d}{0.03 k_f} \left(\frac{\mu_f}{w}\right)^{0.8} - (T_s - T_x)\right] .$$

Evidently from this equation, the heat exchanger area, and hence weight, is minimized for a given total mass flow W when the local mass flow is as small as possible. This implies the largest possible number of circuits within the structural cooling system. The other two components affecting weight, the blower and its power supply, will be governed by total mass flow, W, and pressure drop in the system. Evidently, the minimum pressure loss within the structure for a given value of W is obtained by using the largest possible number of very short cooling circuits. A practical limit is considered to be reached when each square foot of cooled surface is fed individually with cooling vapor. This will certainly give an optimistic weight because the weight of internal ducting, which becomes large as the number of circuits is concerned, is neglected in the present work. If the system is shown to be impractical on this basis, therefore, the conclusion is sound.

In the equation for A_x, W is written as wA so that

$$A_x = Aq^{2.5} \Big/ \left[1.307 \, w^{0.6} \left(\frac{q d}{0.03 k_f} \left(\frac{\mu}{w}\right)^{0.8} - (T_s - T_x)\right)\right]^{2.5} ,$$

and heat exchanger weight, in pounds per square foot of cooled surface is

$$0.542 \, A_x / A .$$

The blower quoted previously from Reference 6, as an example of blower weight, was 2.25 lb for a mass flow of 2360 lb/hr. Pressure heads will always be small in the system under consideration, so that blower weight may be proportioned directly as mass flow.

[redacted]

[redacted]

Therefore, blower weight per unit area of cooled surface is

$$2.25/2360 \times W/A = 0.000953\ w .$$

The final step is to calculate the weight of the turbine necessary to drive the blower. Reference 11 gives a weight of 50 pounds for a 350-HP turbine. Proportioned on the basis of power, the turbine weight per unit area of cooled surface becomes: power/350 x 50/A = power/7A. The power required is $\frac{\text{total pressure drop} \times W}{3600 \times 550 \times \rho}$, so that it is necessary to calculate the pressure drop through both the structure and the heat exchanger.

From Reference 6, the pressure drop per foot of length in a rectangular duct is

$$\frac{\Delta P}{\Delta N} = 0.2155 \times 10^{-8} \frac{w}{\rho d^3} .$$

Since it is assumed that each square foot of surface is fed individually, then each duct is one foot long and the pressure drop becomes

$$\Delta P = 0.2155 \times 10^{-8} \frac{w}{\rho d^3} .$$

The net area of the heat exchanger (area between tubes) is proportioned from the net area of the reference exchanger on the basis of frontal area. Therefore, the net area is $0.1217/3.68 \times A_x$. The air velocity in the heat exchanger equals $\frac{W}{\rho A_x}$. The pressure drop in the heat exchanger is

$$\Delta P = 4F'' \frac{N_r}{2s} V^2 \rho = \frac{4 \times 0.171 \times 4 \times W^2}{64.4\ \rho A_x^2} = 0.0425 \frac{W^2}{\rho A_x^2} ,$$

(N_r is equal to 4 since the heat exchanger has 4 rows of tubes).
The total pressure drop, neglecting line and valve losses, is

$$0.2155 \times 10^{-8} \frac{w}{\rho d^3} + 0.0425 \frac{w^2 A^2}{\rho A_x^2} .$$

Therefore, turbine weight per unit area of surface is

$$\frac{w^2}{\rho^2 (7 \times 3600 \times 550)} \left(\frac{0.2155 \times 10^{-8}}{d^3} + 0.0425\, w \frac{A^2}{A_x^2} \right) .$$

Density is obtained both from the condition of specified pressure within the closed system and from the average temperature.

The equations given previously for heat exchanger, blower, and turbine weights must now be added and the total minimized with respect to mass flow, w. Apparently, this is not practical by analytical techniques, but it is accomplished rapidly by trial and error.

Aluminum Structure

q = 1000 BTU/hr ft^2

T_x = boiling temperature of water, which can be lowered to 100° F by using a boiler pressure of 5 psi

T_s = 200° F

c_p = 0.24 BTU/lb° F – intermediate coolant is air

μ_f = 0.0464

k_f = 0.0157 BTU-ft/ft^{2}hr° F

ρ = 0.023 lb/ft^2, based upon a system pressure of 5 psi and an average temperature of 120° F

[redacted]

[redacted]

Weight calculations were made over a range of values of mass flow, and the results are given in Table V-2. Values of heat transfer coefficients; average temperature differences between air, structure, and heat exchanger; air velocities; and pressure losses are shown in this table to demonstrate that values are reasonable.

Optimum equipment weight is obtained with an air mass flow of approximately 215 lb/hr. Air velocities in the structure and heat exchanger are reasonable and can be increased if advantageous to do so. These calculations were performed at a duct depth of 0.02 ft. Decreasing this depth tends to increase the heat transfer coefficient to the structure which permits a reduction in ΔT_s and a corresponding increase in ΔT_x The heat exchanger area may then be reduced. The following table indicates the results of varying duct depth at the optimum flow of 215 lb/hr.

d	h_s	h_x	T_s	T_x	A_x	V_s
0.028	14.22	32.0	70.2	29.8	1.05	93.1
0.020	19.92	68.10	50.2	49.8	0.294	134.5
*0.0175	22.80	81.6	43.9	56.1	0.218	155.8
0.0170	23.40	84.0	42.8	57.3	0.208	160.5
0.0165	24.15	85.6	41.4	58.6	0.198	165.2
0.0150	26.60	94.5	37.6	62.4	0.170	183.5

d	V_x	ΔP_s	ΔP_x	Blower Weight	Exchanger Weight	Turbine Weight	Σ Weight
				lb			
0.028	75.1	0.920	5.85	0.205	0.570	0.040	0.815
0.020	277.0	2.62	64.75	0.205	0.160	0.0491	0.414
*0.0175	379.0	3.94	114.5	0.205	0.118	0.0839	0.407
0.0170	397.0	4.30	124.0	0.205	0.113	0.0910	0.409
0.0165	398.5	4.70	162.2	0.205	0.107	0.1183	0.431
0.0150	490.0	6.30	182.0	0.205	0.0924	0.1343	0.432

* Optimum

Optimum duct depth is reached at approximately d = 0.0175 ft. At best conditions, therefore, equipment weight will be in the neighborhood of 0.407 lb/ft^2 of cooled surface. This does not account for the additional penalty imposed by ducting, reservoir, piping, and water pump. Of these items, the most sifnificant is ducting; if it is assumed that, at minimum, this ducting will be one sheet of material extending over the inside surface of the structure, say 0.015-in. thick, its weight becomes 0.216 lb/ft^2. Therefore, this system is substantially heavier than the duct water cooling so that it need not be considered further for use with an aluminum structure.

Titanium Structure

q = 700 BTU/hr ft^2

T_x = boiling temperature of water which in this case is set at 200° F by using a boiler pressure of 12 lb/in.^{2}. This permits the steam to be throttled into the structural cooling system at 5 lb/in.^{2}, and to serve as the intermediate coolant. A

[redacted]

[redacted]

gain is thus obtained from the superheating of the steam and also from the higher specific heat.

$T_s = 600°\,F$

Following the same process as described for the aluminum structure, it is found that minimum weight of mechanical equipment results when a circulating mass flow of 22 lb/hr ft^2 of steam is used. The combined weight of heat exchanger, turbine, and blower is 0.048 lb/ft^2. A weight for the sheet material that will form the inner surface of a cooling duct is again based upon a 0.015-in. thick sheet. This will now be titanium, and its weight becomes 0.352 lb/ft^2.

For one hour of flight and a heat flux to the titanium structure of 700 BTU/ft^2hr, the cooling water requirement is 700/1110 = 0.63 lb/ft^2, so that the total becomes 0.63 + 0.048 + 0.352 = 1.030 lb/ft^2. This value is slightly more than that for the direct, water-cooling system. In addition, it has the added penalty of a 600° F structural temperature. If the flight is for more than one hour, this cooling system could give the lighter weight, but a study of Section IX will show that a considerable weight advantage must be shown in the cooling system to compensate for the loss in the higher temperature structure.

Stainless Steel Structure

$q = 254$ BTU/hr ft^2

$T_s = 1000°\,F$

The boiling temperature of the water and the system pressures, are identical for the titanium structure. Again, following the same analytical process, the minimum weight of mechanical equipment occurs at a mass flow of 6 lb/hr ft^2. Combined weight of turbine, blower, and heat exchanger is 0.013 lb/ft^2. The weight of a 0.015-in. thick duct sheet of stainless steel is 0.61 lb/ft^2, and the cooling water required for a one-hour flight is 254/1110 = 0.23 lb/ft^2, giving a total weight of 0.84 lb/ft^2. Again, this is too close to the weight of the direct water-cooling system to compensate for the increase in structural temperature from 200° to 1000° F. A weight check can be made for any specific case, however, using the methods of Section IX.

(2) Indirect, Refrigeration-Type Cooling Systems

Assume that the circulating medium enters the structure at a temperature of T_j and leaves at a temperature of T_f. If the boiling temperature of the expendable coolant is T_B, the intermediate coolant must be compressed to a temperature sufficiently above T_B, so that when the added structural heat has been extracted, the expansion through the same ratio produces the temperature T_j. Then, assuming the unobtainable isentropic compressions and expansions, the temperature of the intermediate coolant after compression must be $T_B + (T_f - T_j)$. The required pressure ratio given by

$$P_2/P_1 = \left(T_2/T_1\right)^{\frac{\gamma}{\gamma-1}} ,$$

becomes

$$P_2/P_1 = \left[\frac{T_B + (T_f - T_j)}{T_f}\right]^{\frac{\gamma}{\gamma-1}} .$$

The total mass flow of intermediate coolant is

$$W = \frac{Aq}{(T_f - T_j)C_p} ,$$

where A is the total area to be cooled and q is the heat flux per unit area.

The weight of a turbine-compressor combination required to supply this quantity of air at the proper pressure ratio is extrapolated from the performance and weight of the J44 turbojet engine. It is realized that the final stages of compression would be at a much higher temperature than would occur in the engine, and that the wheels and compressor case would necessarily be

[redacted]

made from high-density alloys, but this weight would tend to be offset by the lack of combusters and exhaust nozzle. Extrapolation is performed by linear ratio of mass flows and pressure ratios.

Weight of J44 = 300 lb

Air consumption = 24 lb/sec at sea level

Pressure ratio = 2.5

Therefore, the weight of required compressor-turbine is

$$\frac{300}{24 \times 3600 \times 2.5} \times W \times \frac{P_2}{P_1} .$$

A study of this equation shows that its minimum value is reached when T_i equals 0° R and T_f is the maximum possible value. However, T_f is limited to some value slightly less than structural temperature, and T_i cannot be taken too low because the condition of infinite volume is approached. It is also found, however, that the weight equation is not particularly sensitive to T_i when the value is below 400° R, so that an arbitrary choice of T_i is easily made.

Beginning with sodium as the final heat sink, air as the intermediate fluid, and aluminum as the structural material, the conditions are

T_B = 1200° F = 1660° R

T_f = 150° F = 610° R (Allowing a margin below the structural temperature of 200° F)

γ = 1.4

T_i = 0° F = 460° R

q = 1000 BTU/ft^2 hr

Then, the turbine-compressor weight per unit of cooled area is

$$\frac{1}{720} \times \frac{1000}{0.24 \times 150} \times \left(\frac{18.10}{610}\right)^{3.5} = 0.0386\,(2.97)^{3.5} = 1.74 \text{ lb/ft}^2 .$$

To show the maximum benefit of the sodium-air cycle, assume one hour of flight, so that a flux of 1000 BTU/hr over a unit area requires approximately 0.90 lb of water per square foot, or 0.42 lb of sodium. Obviously, the saving in coolant is completely offset by the weight of turbine and compressor, and the system is of no value for use with an aluminum structure. Note also that the 1.74 lb/ft^2 does not include the weight of a heat exchanger.

Clearly, this argument can also be applied to the use of lithium as the final coolant since the entire saving of expendable coolant weight cannot equal the added weight of machinery. Increased pressure ratio would also be required since the boiling point of lithium is approximately 1900° F.

The same procedure is now applied to a titanium structure with a heat flux of 700 BTU/hr ft^2, a structural temperature of 600° F, and T_f of 550° F.

In selecting T_i, a wider range is now available because T_f is higher, but as $T_f - T_i$ is increased, the volumetric changes as the air passes through the system are increased and similarly with internal velocities. With the realization that internal velocities may be too high, a T_i value of 200° F will be taken. Then, weight of the required turbine-compressor per unit of cooled area will be

$$\frac{1}{720} \times \frac{700}{0.24 \times 350} \times \left(\frac{2010}{1010}\right)^{3.5} = 0.0116\,(1.99)^{3.5} = 0.129 \text{ lb/ft}^2 .$$

In this case, it also becomes necessary to calculate the heat exchanger weight to demonstrate that the system has no value.

Total heat to be transferred to the sodium is 700 BTU/ft^2 of cooled surface. Permissible temperature drop in the air equals 350° F, so that mass flow required through the exchanger

equals $700/(350 \times 0.24) = 8.3$ lb/hr ft^2. From the equation for heat transfer within the heat exchanger, $h_x A_x \Delta T = 700 \times 2000$, and $\Delta T = 350$, therefore $h_x A_x = 4000$.

In a previous part of this section, the following expression relating h, A_x, and the total mass flow W has been developed from an example heat exchanger:

$$h_x = 1.307 \, (W/A_x)^{0.6} \, .$$

Substituting a total mass flow for 2000 ft^2 of surface, and equating the two expressions for h_x gives

$$\frac{4000}{A_x} = 1.307 \left(\frac{8.3 \times 2000}{A_x} \right)^{0.6} \, .$$

Therefore,

$$A_x^{0.4} = \frac{4000}{1.307 (16{,}600)^{0.6}} = \frac{3061}{16{,}600^{0.6}} \, ,$$

so that

$$A_x = \frac{3061^{2.5}}{16{,}600^{1.5}} = 243 \text{ ft}^2 \, .$$

Again, from the previous text giving heat exchanger characteristics, the heat exchanger weight is equal to $(0.542 \times 243)/2000 = 0.066$ lb/ft^2 of cooled surface.

This weight is based upon an aluminum heat exchanger, but for use with boiling sodium a much higher temperature material is required. Heat exchanger weight will probably increase as the material density increases, since it can be assumed that minimum thicknesses are used in the example from which weights are taken. Then, the heat exchanger weight becomes $3 \times 0.066 = 0.198$ lb/ft^2.

Including an air duct which covers the entire structural surface, and assuming 0.015-in. thick titanium, gives an additional weight of 0.352 lb/ft^2. The total system weight is therefore $0.129 + 0.198 + 0.352 = 0.679$ lb/ft^2 of cooled surface. The weight of sodium for one hour of flight is $700/1000 \times 0.42 = 0.294$ lb/ft^2. Total weight for one-hour flight equals 0.973 lb/ft^2. Again, this weight is too close to that of the directly cooled aluminum structure to compensate for the increased structure weight of 600° F operation.

The use of lithium would show a useful weight reduction of approximately 0.22 lb/ft^2 for a one-hour flight, but at the cost of increased heat exchanger and compressor temperatures. In this case, the increased structure weight due to operation at 600° F becomes the deciding factor and this must be checked for each specific case by the methods of Section IX. It will generally be found, from Section IX, that even with a low loading of 1000 lb/in., it is not possible to construct a 600° F structure for a weight penalty of less than 0.25 lb/ft^2, so that the use of lithium does not appear to be justified in this application.

c. Direct, Open-Cycle Atmospheric Cooling

This cooling system has been described in Section V, B, where its most serious limitations are mentioned. These include the effects of unavoidable stagnation temperatures in the inlet duct and in the first nozzle stage of the turbine, and the more serious temperature condition which exists in the exit duct and in the final stages of the compressor. Other problems are the drag produced by the energy losses in the turbine, compressor, and intake; the difficulties of designing a supersonic compressor; and the weight and size of machinery.

[redacted]

Considering an example in which the structure is aluminum with a flux of 1000 BTU/ft^2 hr, and assuming a speed of only Mach 5.38, the stagnation temperature that is experienced in the intake duct and the first stages of the turbine is 2200° F. This temperature is beyond present capabilities, but may be possible in the future with coated molybdenum. The alternative, which is cooling, is still in an early stage when applied to rotating machinery.

With the best available diffuser designs, energy losses through the shocks in the intake are expected to be large at a Mach number of 5.0 with a deterioration of the situation as speeds increase. This loss appears, of course, as drag.

Assuming that by some means the air can be reduced in velocity through the turbine, and that the temperature can be maintained at ambient conditions (approximately 392° R), the permissible temperature rise through the structure is approximately 360° F.

For a heat flux of 1000 BTU/hr ft^2 over 2000 ft^2 of surface, a mass flow of 2000 x 1000/(0.24 x 360) = 23,000 lb/hr is required. The air enters the compressor at low velocity and a temperature of 350° F or 810° R, so that after accelerating this air to Mach 5.0, the final compressor blades and the exit duct experience boundary layer temperatures of 810 (1 + 0.2 x 5^2) = 4860° R or 4400° F. As explained in Section V, B, there is no relief from these temperatures by radiation, so that additional cooling is required.

The size, and therefore the weight, of the turbine-compressor unit is largely a function of the air volume to be handled, and assuming ambient pressure at 60,000 ft as applying through the system, the volumetric flow in the turbine is 23,000/(32.2 x 0.000224 x 3600) = 885 ft^3/sec. The J73-GE-3 turbojet engine weighing 3880 lb, takes a sea-level air flow of 142 lb/sec and has a frontal area of 9.96 ft^2. The mass flow is equivalent to 1850 ft^3/sec.

By comparison, it may be expected that the turbine-compressor for open-cycle atmospheric cooling at Mach 5.38 would be somewhat smaller and lighter than the J73, but after allowances are made for cooling, it may be expected that the unit will weigh at least 2000 lb. To this must be added the weight of ducting so that again direct water cooling is not only lighter and more simple, but occupies much less volume.

Sufficient information has been mentioned to show that direct atmospheric cooling is not suitable for use in high-speed aircraft structures. Additional details can be found in Reference 1.

d. Direct, Closed-Cycle Cooling - Atmosphere Used as Heat Sink

Two versions of this system have been described in Section V, B, depending upon whether the coolant merely circulates, experiencing a temperature rise in the hot areas of the structure, and a temperature reduction in the cooler areas, or whether it is compressed after passing through the structure so that heat may be dissipated at a higher temperature level than it is received.

The first of these two systems has not received serious consideration during this study for the cooling of primary structure because:

(1) Chordwise gradients of equilibrium temperature are generally too small, in the regions of primary structure, to make the system worthwhile.

(2) The structural temperature must be at least as high as the temperature of the heat dissipation area, and since this dissipation will invariably be by radiation alone, such temperatures must be at least 1000°to 1200° F. This reasoning presents a particularly strong argument against the system because, at temperatures where a useful amount of heat can be radiated, the structural weight penalty will be as great as the cost of direct water cooling.

The second system, which introduces compression and expansion of the working fluid into the cycle, can also be dismissed, for most applications, with minimum consideration. Since no other useful refrigerants have been found, assume that air is used as the working fluid, the structure is aluminum receiving the same flux of 1000 BTU/ft^2 hr as used in the previous

[redacted]

examples, and that heat is to be rejected at 1200° F. Then, the weight of the compressor-turbine unit is the same as developed for the refrigeration system using a sodium heat sink. This value is 1.74 lb/ft^2 which is much greater than the direct, water-cooling system, for one hour of flight.

If titanium structure is considered, operating at 600° F and receiving a flux of 700 BTU/ft^2 hr, the turbine-compressor weight is 0.129 lb/ft^2 and the weight of internal ducting is 0.352 lb/ft^2. The total weight of 0.481 lb/ft^2 does offer a slight possibility of producing the lightest system if structural loadings are very light, flight time is long, and sufficient radiating area can be found on the airframe. It should be noted that no weight has been added for the radiating area, although it will certainly be of high-density material and may be quite large.

3. Cooling Systems for Secondary Structure

With respect to structural cooling, secondary structure has been defined in Section V, D, as those areas where equilibrium temperatures are too high for the use of insulation and an external wall generally associated with it. The result is that the external surface must be cooled and, as can be seen from Section II, the heat fluxes are immediately very large, except when speeds are so low that cooling is unnecessary. This fact has two immediate and important consequences:

(1) With respect to the area involved, the actual coolant weight becomes relatively more important than is the case with primary structure, adding emphasis to the use of coolants with high heat capacity.

(2) Equilibrium temperatures are high so that more possibility exists for the direct use of coolants with high heat capacity.

It is possible, of course, to give consideration to each cooling system listed in Table V-1 and to calculate weights after applying each of these systems to the cooling of a typical high-flux area. The experience with the study of cooling systems for primary structure has shown, however, that direct convective cooling is simple and light when compared with the complexity and the machinery weight of indirect systems. In the cooling of primary structure, there is at least a potential advantage in the more complex systems since they permit the use of high-capacity expendable coolants having high boiling points. Direct cooling of the structure with these materials is not generally possible because equilibrium temperatures are too low, and the structural weight penalty due to high-temperature operation is large.

In the areas of high flux, however, direct cooling is possible, even with lithium, at speeds exceeding Mach 5.0. One other significant point is that if surface cooling is to be used, it should be done at the highest possible temperature, so that maximum advantage is taken of radiation from the surface as a means of dissipating heat. The structural weight penalty due to this high-temperature operation is now unimportant because of the limited size of such areas.

This latter point justifies some clarification in order that relative magnitudes can be appreciated. In one extreme example for a Mach 20 aircraft, a leading edge with a chord of only 6 inches and a length of approximately 30 feet required 800 pounds of lithium as a coolant, or approximately 8000 pounds of water. Obviously, the structural weight penalty of high-temperature operation is overshadowed completely by the saving in coolant.

Notwithstanding these arguments, a number of indirect cooling systems have been checked numerically for leading edge cooling, and the results are reported in Reference 1. A mercury refrigeration system was studied for an aircraft of only Mach 4.0 velocity, and the use of expendable coolant was avoided by radiating the heat from an area of the airframe normally at low temperature. The mercury was used to absorb heat from the leading edge, then compressed to a liquid with a corresponding temperature rise, and finally passed through the radiator. After giving up heat to the atmosphere by radiation, the mercury was cooled to a temperature below that of the structure by expansion, and then recirculated. This system gave a weight four times that of a water cooling system, assuming one hour of flight.

A similar system was studied in which cooling was accomplished without the use of refrigeration, by circulating molten aluminum from the high-temperature leading edge to a radiating area of the same temperature. Even when assuming operating temperatures of 2500° F, the weights become impractical.

A refrigeration system has been studied, Reference 1, in which sodium is used as a refrigerant, giving up heat to an expendable sink of lithium. This system was considered when it seemed impractical to use lithium directly because of corrosion, but the calculations show that large volumes would be required because of the high specific volume of sodium gas, and this indicates that the compressor would be too large for the aircraft.

The conclusion to be drawn is that for areas of large heat flux the most promising method of cooling is performed by evaporating an expendable coolant material directly at the surface. This leaves only film, transpiration, and convective cooling to be considered.

Film and transpiration cooling have been discussed in Section V, B, where it is explained that insufficient experimental work exists, particularly using a liquid as a coolant, to give comparative system weights. The expected reductions in heat transfer due to the flow of gas normal to the surface are large enough to justify the continuing development of this technique; if expectations can be realized, it is probable that this approach to the cooling of high-flux areas ultimately will prove the most efficient. A suggestion is made, in connection with transpiration cooling, that may give the maximum amount of cooling for the minimum expenditure of weight. This suggestion is to transpire the high-capacity metals, in the gaseous state, and thus obtain the advantages of both schemes.

Pending the development of a successful transpiration cooling system, therefore, direct cooling of the surface by convection is apparently the most efficient method and, obviously, the coolant with the highest heat capacity should be used if temperatures permit. In most applications above Mach 5.0, the use of lithium is possible; since lithium is both the most efficient and the most difficult coolant to use, some of its problems will be discussed.

To use the latent heat of lithium, structural temperatures in the regions of high heat flux will be of the order of 1800° to 2000° F, so that structural material requirements include not only strength and oxidation resistance at these temperatures, but also resistance to the corrosive effects of lithium. The subject of corrosion by liquid lithium is treated in detail in Reference 2, where it is shown that few materials are sufficiently resistant. The two most promising are pure iron, which has no structural strength at 1800° F, and molybdenum, which has useful strength in the temperature range required (see Section III). Also from Section III, molybdenum has good conductivity, a requirement in the successful transfer of large heat fluxes through the structural walls. No evidence is available on the corrosive effects of lithium vapor.

The major problem with the use of molybdenum as a structural material is its lack of resistance to oxidation. The problem is sufficiently acute to render the material unuseable in an oxidizing atmosphere at temperatures exceeding approximately 1000° F, unless protection is provided. Considerable developmental work has been and is still being done on protective coatings for molybdenum; one significant program is reported in Reference 13. The results reported in this reference show considerable promise and although it is still a large step from the coating of small laboratory specimens to the successful protection of airframe parts including fasteners, it seems reasonable to expect that this will ultimately be accomplished.

Also unknown at the present time (at least so far as the authors of this report are aware) are boiling heat-transfer characteristics of lithium. The subject, according to Reference 14, has not been dealt with on a theoretical basis and only over-all heat transfer tests have been made. It is significant to note, however, that Reference 2 reports a nonboiling heat transfer of 1 million BTU/ft^2 hr in a lithium-to-lithium heat exchanger at a flow rate not exceeding 3 gpm. In Table I-3 of Section I, Part III, the maximum flux on the leading edge of any vehicle, except the re-entry missile, is given as 2.23×10^6 BTU/ft^2 hr for a 1/2-in. diameter nose, and as 1.11×10^6 BTU/ft^2 hr for a 2-in. diameter nose. This suggests that lithium cooling will be capable of dealing with the most severe heating conditions, except for those on the re-entry missile.

[redacted]

REFERENCES

(1) Weinberg, M. I. and Norwich, E. J., "A Preliminary Investigation of Cooling Systems for Airframe Structures," Bell Aircraft Corporation, Report 02-941-037, October 1955.

(2) "Liquid Metals Handbook," AEC-Navy Report NAVEXOS P-733 (Rev), Second Edition, Revised, January 1954.

(3) "International Critical Tables," National Research Council, McGraw-Hill Book Company, 1933.

(4) Mellon, J. W., "Inorganic and Theoretical Chemistry," Longmans, Green and Company, September 1946.

(5) Hodgman, C. D., "Handbook of Chemistry and Physics," 31st Edition, Chemical Rubber Publishing Company, 1949.

(6) Rodert, L. A. and Jackson, R., "Preliminary Investigation and Design of an Air-Heated Wing for Lockheed 12A Airplane," NACA Advanced Restricted Report A-34, April 1942.

(7) McAdams, W. H., "Heat Transmission," Third Edition, McGraw-Hill Book Company, 1954.

(8) "Advanced Strategic Weapon System–Structures," Report D143-945, 013, Bell Aircraft Corporation, (Classified SECRET).

(9) Lynch, R. H. and Robinson, W., "Weight, Power and Space Requirements for Typical Cooling Systems Employing Heat Rejection to an Aircraft Fuel System," Ohio State University Project No. 269, Report No. 24a.

(10) Wood, G. P. and Brevoort, M. J., "Design, Selection and Installation of Aircraft Heat Exchangers," NACA Advanced Restricted Report 3G31, July 1943.

(11) "Specifications for Turbine Pump Assembly," Report 56-947-418, Bell Aircraft Corporation, June 1955.

(12) Keusch, R. G., "Effect of Supersonic Flight on Power Plant Installation Systems," Proceedings of the Symposium on the Thermal Barrier, American Society of Mechanical Engineers, 1954.

(13) Herzig, A. J. and Blanchard, J. R., "Protecting Molybdenum from Oxidation," Metal Progress, Volume 68, No. 4, October 1955, Pages 109-114.

(14) Jakob, M., "Heat Transfer," John Wiley and Sons, Volume I, 1949.

(15) Hancock, D. A., "The Cooling of a Supersonic Aircraft," Royal Aircraft Establishment Technical Note No. Mech. Eng. 147, April 1953.

(16) Stevens, E. D. and Fuechsal, K. M., "The Aerodynamic Heating Problem," WADC Technical Note WCRR53-215, June 1953.

(17) Adams, H. W., "Temperature Problems of Equipment in High-Speed Aircraft," Presented at the ASME Symposium on the Thermal Barrier, November-December 1954.

[redacted]

TABLE V-1

SUMMARY OF STRUCTURAL COOLING SYSTEMS

Type of System	Heat Sink Carried in Vehicle							Atmosphere Used as Heat Sink		
	Direct Open-Cycle Cooling				Indirect Open-Cycle Cooling		Endothermic Reactions	Direct Open-Cycle	Direct Closed Cycle	
System Mechanics	Film Cooling	Transpiration Cooling	Ablation Cooling	Convective Cooling	Circulation System	Refrigeration System		Convective Cooling	Circulation System	Refrigeration System
Method of heat absorption and dissipation.	Change of state in expended coolant. (Temperature rise only if fuel is used).				Temperature rise in working fluid. Change of state in expended fluid.	Temperature rise or change of state in working fluid. Change of state in expended fluid.	Chemical reaction.	Temperature rise in circulating air. Air expended.	Temperature rise in circulating fluid. Heat radiated and convected to atmosphere.	Temperature rise or change of state in working fluid. Heat radiated and convected to atmosphere.
Probable application	All types. High flux areas.	All types. High flux areas.	Expendable types. High flux areas. Short flight times.	All types. All areas.	All types.	All types.	All types. Short flight times.	All types. Low speed. Long flight times.	All types. High speed. High altitude. Long flight times.	Nonexpendable vehicles because of cost. Long flight times.
Structural temperature, set by:	Change-of-state temperature of available coolants.		Melting point of available materials.	Change-of-state temperature of available coolants.	Change-of-state temperature of expendable coolants.	Pressure-temperature relationships of available refrigerants.	Reaction temperature of available chemicals.	Material limits on turbines and exit ducts.	Arbitrarily set by flow rates and heat rejection area.	Pressure-temperature relationships of available refrigerants.
Internal power requirements.	Small	Small power, high pressure.	None	Small	Small	Large	None	None	Small	Large
Mechanical complexity.	Moderate	Moderate	None	Little	Little	Considerable	None	Considerable	Little	Considerable

TABLE V-2

EQUIPMENT WEIGHTS AT VARIOUS VALUES OF MASS FLOW

(Aluminum Alloy Structure, Circulating Air, Water Heat Sink)

Mass Flow (lb/hr)	Heat Transfer Coefficients		Average Temperature Differences (°F)		Heat Exchanger Area (ft^2)	Air Velocities (ft/sec)		Pressure Drops (psi)		Weight per Unit Cooled Area (lb/ft^2)			
w	h_s	h_x	ΔT_s	ΔT_x	A_x	V_s	V_x	ΔP_s	ΔP_x	Blower	Exchanger	Turbine	Total
115	12.25	5.86	81.9	18.1	9.4	67.8	4.38	1.29	0.019	0.110	5.10	0.0005	5.210
150	14.60	19.70	68.5	31.5	1.61	91.4	34.4	1.69	1.42	0.143	0.875	0.0015	1.020
175	15.45	29.50	64.7	35.3	0.960	107.0	67.5	1.77	4.85	0.167	0.522	0.0037	0.693
200	18.85	55.3	53.0	47.0	0.385	119.8	188.5	2.33	32.95	0.191	0.209	0.0230	0.423
210	19.00	60.55	52.6	47.4	0.348	131.0	228.0	2.54	45.00	0.200	0.190	0.0324	0.422
215	19.92	68.10	50.2	49.8	0.294	134.5	277.0	2.62	64.75	0.205	0.160	0.0491	0.414
225	20.25	75.6	48.9	51.1	0.259	141.5	330.0	2.74	89.00	0.215	0.141	0.0674	0.423

NOTES

SECTION VI

DETERMINATION OF THERMAL GRADIENTS, STRESSSES, AND DEFLECTIONS

By M.A. Brull, M.A. Goldberg, and W.H. Dukes

TABLE OF CONTENTS

NOMENCLATURE

A_n = Fourier coefficient

a = thermal diffusivity of structural material

b_s = web spacing in a multiweb beam

b_w = half-depth of multiweb beam

c_p = specific heat of structural material

E = Young modulus

$f_0 f_1 f_2$ = functions defined in Equation (15)

$G(x)$ = initial temperature

h = heat transfer coefficient

I_ξ = moment of inertia of beam cross-section about ξ axis

I_η = moment of inertia of beam cross-section about η axis

i, j = subscript denoting a specific element of the structure, or denoting the three coordinate directions

k = thermal conductivity of structural material

L = beam length

M = joint thermal resistance ratio

m = number of elements in skin

n = number of elements in web

P = tensile or compressive load

p = $2\left(\tau_s / b_s\right)$

Q = voltage scale for differential analyzer

q = heat flux

R = volume of body

r = $2\left(b_w / b_s\right)$

S = normal stress-carrying area of beam cross-section

ΔS_j = area of jth element of the structure

s = $\tau_w / 2\,\tau_s$

T = web temperature

T_{aw} = adiabatic wall temperature

t = skin temperature

U = dimensionless web temperature = T / T_{aw}

$\bar{U}$ = $Q\,U$

U_e = strain energy

u = dimensionless skin temperature = t / T_{aw}

$\bar{u}$ = $Q\,u$

NOMENCLATURE (cont)

V = dimensionless web temperature $= (T_{aw} - T)/T_{aw}$

v = dimensionless skin temperature $= (T_{aw} - t)/T_{aw}$

W = strain energy per unit volume

x = $\bar{x} \Big/ \frac{b_s}{2}$

$\bar{x}$ = coordinate along equivalent length of T section

x_i = Cartesian coordinates ($i = 1, 2, 3$)

α = coefficient of thermal expansion

γ_n, λ_n = eigenvalues

Δ = cubical dilatation = $\frac{1}{3} \epsilon_{ii} = \frac{1}{3} (\epsilon_{11} + \epsilon_{22} + \epsilon_{33})$

δ = $\frac{h}{k} \quad \frac{b_s}{2}$

ϵ_e = elastic strain

ϵ_t = thermal strain

ϵ_{ij} = Cartesian strain tensor

η, ξ = centroidal coordinates of any point on beam cross-section

Θ = first invariant of the stress tensor = $\frac{1}{3} \sigma_{ii} = \frac{1}{3} (\sigma_{11} + \sigma_{22} + \sigma_{33})$

θ = dimensionless time = $\dfrac{\alpha \bar{\theta}}{(b_s/2)^2}$

$\bar{\theta}$ = time

κ = time-scale for differential analyzer

ν = Poisson's ratio

σ = thermal stress

$\bar{\sigma}$ = dimensionless thermal stress = $\sigma \; / \; \alpha E T_{aw}$

σ_{ij} = Cartesian stress tensor

τ_s = skin thickness

τ_w = web thickness

$\Phi_n(x)$ = function defined in Equation (9)

$\phi_n(x)$ = function defined in Equation (8)

$\chi(x)$ = lateral deflection of beam

ζ = joint heat-transfer coefficient

SECTION VI

DETERMINATION OF THERMAL GRADIENTS, STRESSES, AND DEFLECTIONS

A. GENERAL

The presence of nonuniform temperature gradients within a structure will produce thermal stresses that may be of appreciable magnitude. These induced stresses must be considered in the structural design of high-speed vehicles subjected to aerodynamic heating.

Nonuniform temperature gradients arise from (1) nonuniform distribution of heat input from the boundary layer to the structure, and (2) nonuniform distribution of the heat capacity of the structure. While the thermal stresses due to (1) and (2) may be calculated by the same procedure, the method of determining the temperature distribution depends upon whether case (1) or case (2), or a combination of both, is encountered.

For a shell of uniform wall thickness, the temperature gradients are entirely due to the variations of heat input over the shell surface. In many such cases, the heat flux from the boundary layer is large when compared with the conductive heat flux within the structure so that the temperature distribution may be calculated to a good approximation by neglecting conduction and using the methods presented in Part I, Section 1.0 of this report.

When the heat capacity of the structure is not uniformly distributed, the temperature gradients depend upon the geometry of the structure and the thermal diffusivity of the material, as well as the heat input conditions. The temperature distribution is then the solution of a transient heat flow problem.

Presented in this section are methods for the calculation of transient temperature distribution due to case (2). Included are general procedures for the rapid determination of thermal stresses due to both types of nonuniform temperature gradients.

Analytical solutions are developed for determining the transient temperature distribution and thermal stresses in a typical structural element. A method of calculation using an electronic differential analyzer is also developed in terms of general dimensionless parameters. By using this method of automatic computation, calculations have been carried out for a wide range of values of the geometric and heat input parameters. The results of these calculations are presented in Part I, Section 3.0.

A general method of solution for the determination of thermal deflections is also presented.

B. GENERAL IDEAS ON THERMAL STRESSES

It is of interest to examine here the basic mechanism by which temperature gradients produce thermal stresses. While these concepts are generally well known, a brief review should help to make the present treatment self-contained and to justify some of the assumptions made in the subsequent analyses.

It is of course well known that heating a body will cause an expansion which, for a wide range of temperatures, is proportional to the temperature rise. When the temperature rise is not uniform, different elements of the body will tend to expand by different amounts and, in general, the requirement that the body remain continuous will conflict with the requirement that each element expand by an amount proportional to the local temperature rise. Thus, the various elements will exert upon

each other a restraining action resulting in continuous unique displacements at every point. This restraining action takes the form of a system of strains which cancels out all or part of the thermal expansions at every point (so as to ensure continuity), and which must therefore be accompanied by a corresponding system of self-equilibrating elastic or inelastic stresses. These stresses are the so-called thermal stresses. These concepts can be illustrated in a simple manner by considering a rod fixed at one end, as shown in Diagram VI-1, and subjected to a uniform temperature rise Δt.

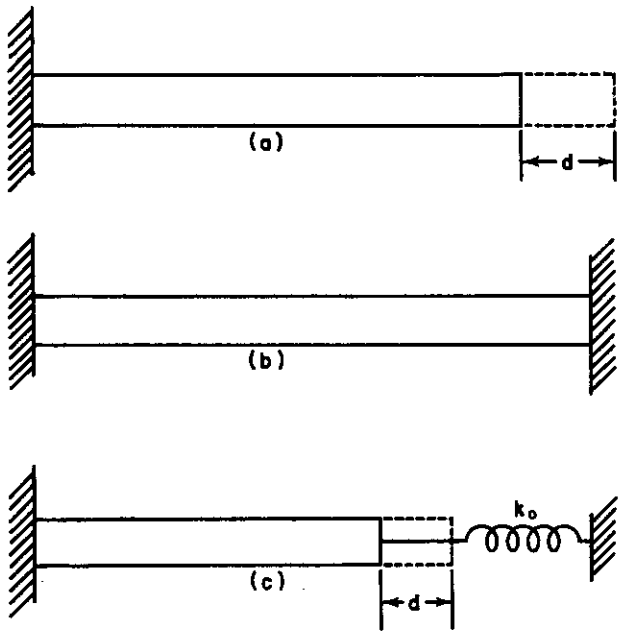

(a)

$d = \alpha L \Delta t \qquad \epsilon_e = 0$

$\sigma = 0$

(b)

$d = 0 \qquad \epsilon_e = -\alpha \Delta t$

$\sigma = -\alpha E \Delta t$ (COMPRESSION)

(c)

$$d = \frac{\alpha E L \Delta t}{E + \frac{L k_o}{A}}$$

$$\epsilon_e = -\left[\frac{\alpha L \Delta t}{L + (EA/k_o)}\right]$$

$$\sigma = \frac{-\alpha E L \Delta t}{L + (EA/k_o)} \quad \text{(COMPRESSION)}$$

Diagram VI-1.

In case (a), the rod is completely unrestrained against expansion so that a displacement equal to $\alpha L \Delta t$ takes place at the end, and no thermal stress is present. In case (b), the rod is completely restrained and no displacement takes place, but the thermal expansion is canceled by an elastic compressive strain equal to $-\alpha \Delta t$ which must therefore be accompanied by a compressive thermal stress equal to $-\alpha E \Delta t$. In case (c), the thermal expansion is allowed to take place partially; the total allowed displacement is now $\alpha L \Delta t - \frac{P}{k_o}$, where P is the force exerted by the spring and k_o is the spring constant. It follows from the equilibrium requirement that $\sigma = \frac{P}{A}$. Also, it is found that the actual displacement will be $\frac{\alpha E L \Delta t}{E + L k_o / A}$, so that there will exist an elastic compressive strain equal to $\frac{-\alpha L \Delta t}{L + (EA/k_o)}$ accompanied by a corresponding compressive stress equal to $-\frac{\alpha E L \Delta t}{L + (EA/k_o)}$. In the case of nonuniform heating, the situation can be thought of as analogous to case (c) of Diagram VI-1, except that the spring action is replaced by elastic restraint of the various elements on each other. It is clear then, that the extent of the restraint on a given region of the body will depend upon not only temperature differences between this region and adjacent ones, but also the geometry of the various elements. More accurately, it can be stated that the thermal stresses will depend upon the temperature gradient (the vector $\partial T / \partial x_i$). Also the temperature level influences these stresses because material properties generally are temperature-dependent, and the body will behave as a nonhomogeneous elastic or elasto-plastic medium.

For many practical cases, however, the temperature rise will be moderate so that it is permissible to assume that the material is elastic and to carry out thermal stress calculations using uniform elastic properties corresponding with the average temperature. The remainder of this section is devoted exclusively to thermal stresses in a homogeneous elastic structure. This problem has been formulated adequately within the scope of the classical theory of elasticity, and a

general treatment can be found in Reference 1. It can be shown that thermal stress effects can be accounted for by modifying the definition of the components of strain, and introducing a system of body and surface forces determined by the temperature distribution. Unfortunately, the solution of these problems usually leads to boundary value problems which rapidly become intractable for practical structures. However, it will be shown that, by adopting simplifying assumptions commonly made in engineering practice, useful approximate solutions can be obtained for thermal stresses and deformations in practical structures.

A number of investigations have considered thermal stresses induced by aerodynamic heating. The problem of solid and hollow wings has been treated in References 2 and 3, while Torda and Hoff (Reference 4) and Pohle and Oliver (Reference 5) have obtained solutions for the case of an I beam. Freudenthal (Reference 6) and Hilton (Reference 7) have considered cases where the material was inelastic.

C. IDEALIZATION OF THE BUILT-UP STRUCTURE

The study of thermal stresses in typical aircraft structures requires solutions applicable to multicell or skin-stringer construction. Typical wing structures of these types are shown in Diagram VI-2.

If it is assumed that the heat input to the structure does not vary widely along the chord, the temperature will vary as shown in (c) of Diagram VI-2, the lower temperature in the skin over each skin-web junction being due to the presence of the web which acts effectively as a heat sink.

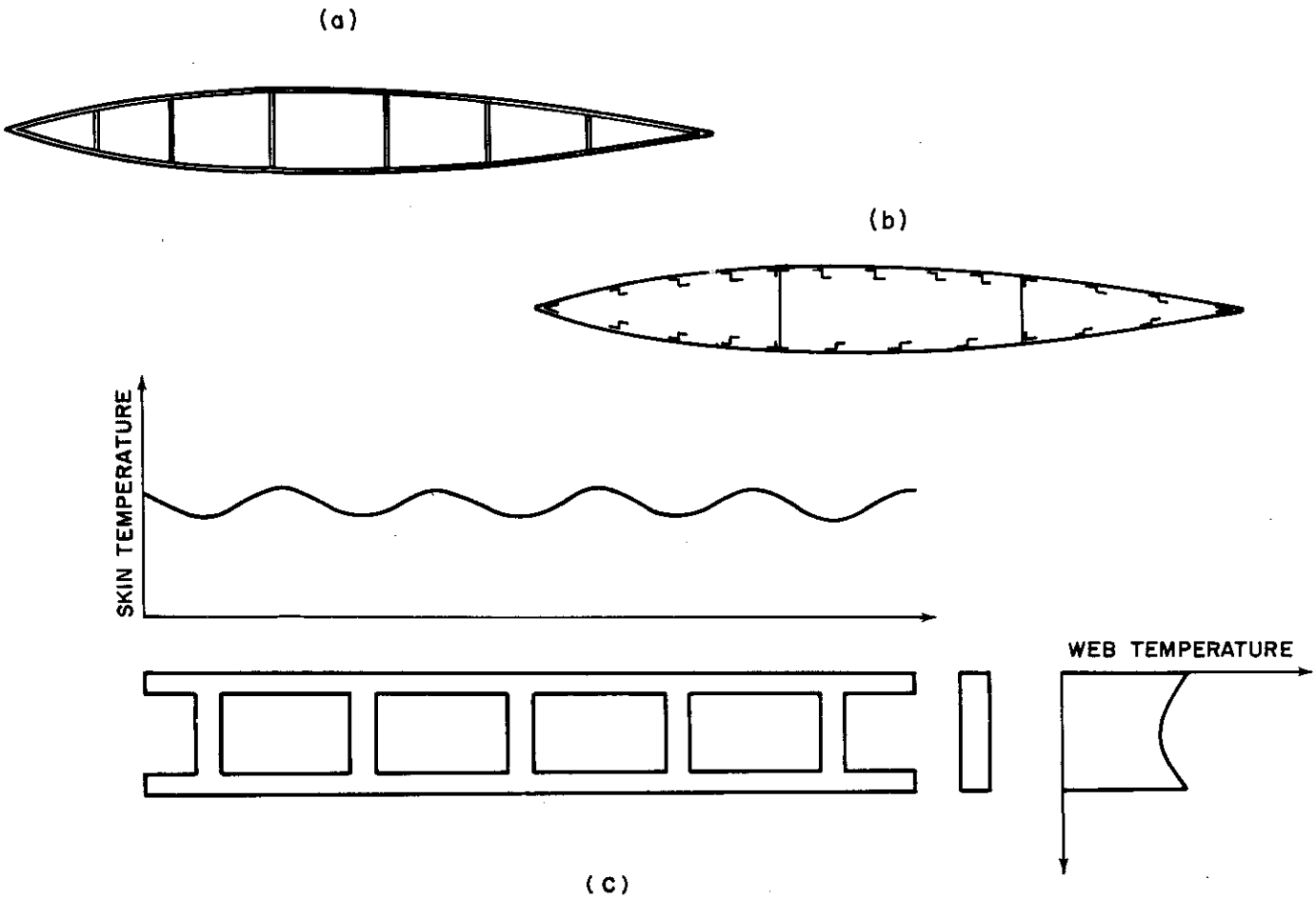

Diagram VI-2.

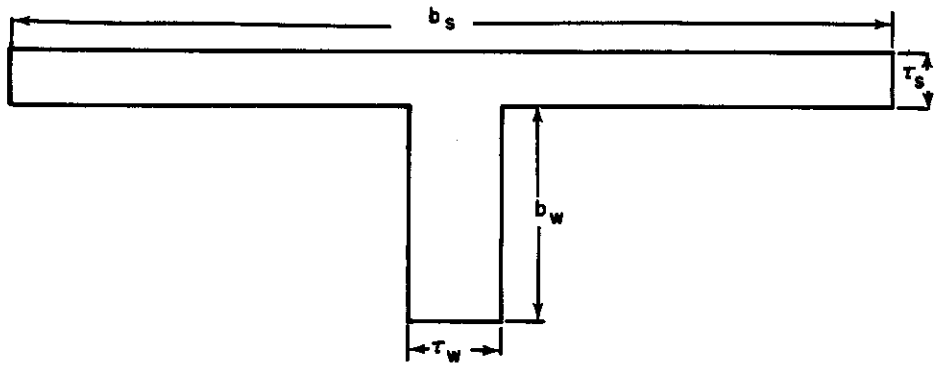

Diagram VI-3.

With such a variation in temperature along the skin and in the webs, it is always possible to determine positions along the skin and webs at which the rate of change of temperature vanishes. It is then permissible to isolate a section of the structure such as shown in Diagram VI-3, and to determine the temperature distribution in this isolated section. By treating the heat transfer problem in such a T section for a wide range of values of the geometrical proportions, it will be possible to use the results to determine temperature distributions in complete wing cross-sections. It is likely, however, that the position of the joints where the rate of change of temperature along the skin is zero will change with time, so that the procedure of isolating a T section is not strictly correct. However, this assumption probably will not introduce appreciable errors in the analysis if the webs are not spaced too closely.

Thus, reasonable approximations to the temperature distribution in a built-up structure can be obtained by solving the heat transfer problem for an isolated T section. It will be shown later that the solution for thermal stresses in a T section can also be used to calculate thermal stresses in a multiweb beam.

The problem of determining temperatures in a T section subjected to aerodynamic heating will be considered first.

D. REVIEW OF PREVIOUS WORK AND ASSUMPTIONS

Solutions for the transient temperature distribution in a T section subjected to aerodynamic heating have been obtained previously by several investigators (References 4, 5, 8, 9). It will be of interest here to state the assumptions of these investigators and to discuss their validity.

The following assumptions are most common:

(1) The only heat input to the structure takes place by forced convection from the boundary layer so that the heat flux into the structure is proportional to the difference between the adiabatic wall temperature and the surface temperature.

(2) There is no heat transfer between the structure and the air trapped inside the structure, so that all surfaces except that in contact with the boundary-layer can be considered insulated.

(3) The heat transfer coefficient and the adiabatic wall temperature are constant along the skin segment of the T section and do not vary with time.

(4) The skin thickness τ_s and web thickness τ_w are small compared with the web spacing b_s and web depth b_w so that temperature variations in the direction of these thicknesses may be neglected.

(5) The joint between the skin and web furnishes perfect contact, so that the heat transfer between the skin and web takes place by pure conduction.

Assumption (1) implies that the effects of solar radiation and radiation from the skin to the air are negligible. The effect of solar radiation has been considered and found negligible (Reference 10) for most practical cases. Radiation from the skin to the surrounding air is, in general, small at the lower temperatures; its effect becomes more significant as the skin temperature increases. However, it would take a large convective heat input to increase skin temperatures enough to cause substantial radiation effects. Since large heat transfer coefficients would cause the peak thermal stresses to occur early in the flight, it is likely that the effect of radiation would become appreciable only after the thermal stresses have reached their peak values. In extreme cases, where the skin temperature might be expected to reach high values early in the flight, it is most probable that an insulated structure would be used, so that calculations would be based upon an effective heat transfer coefficient between the insulation and the skin, and radiation phenomena would not enter. Thus, radiation from the skin to the air probably has little effect on the thermal stresses, and any errors due to this approximation would be conservative.

Assumption (2) implies that no heat can be transferred from the skin to the web through the air trapped within the structure. Solutions based upon this approximation will tend to predict higher skin temperatures and lower web temperatures than actually exist in the structure. As will be shown later, this would make the predicted thermal stresses higher than the actual stresses. In any case, the radiation from skin to web will most likely be small, for the same reasons as given previously under the discussion of assumption (1), while the free convection heat transfer from skin to web will give rise to a heat flux much smaller than the input due to aerodynamic heating. Thus, assumption (2) can be expected to give rise to small (if any) errors and, furthermore, this approximation will yield conservative values for thermal stresses.

Assumption (3) does not correspond with the actual physical situation since the heat transfer coefficient and boundary layer temperature depend upon the Reynolds number and will therefore vary with position along the aircraft. However, since only a small segment of the structure is considered in this analysis, it is permissible to assume that the heat input conditions are constant along the skin as long as the correct average heat input conditions are used for each T section. Thus, the variations in heat transfer coefficient and adiabatic wall temperature are represented by a series of steps. With this simplification, it is possible to obtain general thermal stress information and, in particular, to study the effects of structural configuration on the peak thermal stresses. Assumption (3) also implies the neglect of variations in heat input conditions with time. Again, this simplification does not correspond with the actual physical situation. However, it is necessary to reduce the complexity of the problem and to study the effect of variations in geometry. It will be shown later that solutions obtained under assumption (3) may be combined to account approximately for the effect of heat input variations with time.

Assumption (4) states that the temperature is constant through the thickness of the skin and webs of the structure. Since, for a practical aircraft structure, these thicknesses are always small compared with other dimensions, assumption (4) is perfectly justified.

Solutions based on assumption (5) are restricted to the case of a skin with integral stiffeners. In any other case, the riveted or bonded joint would introduce a thermal resistance that would tend to increase the skin temperature in the region of the skin-web junction and to decrease the web temperature. As a result, assumption (5) leads to the prediction of lower thermal stresses than actually would occur in a built-up T section. As will be shown later, these errors may be appreciable and it is desirable to avoid the use of assumption (5).

In Reference 4, Torda and Hoff present a solution of the T section problem based upon assumptions (1) through (5), and the additional assumption that the skin temperature is not affected by the presence of the web. Thus, they determine the skin temperature variation first by neglecting the heat flow into the web, and then they solve for the web temperature distribution considering the web as a rod with one end insulated; the temperature at the other end is prescribed equal to the skin temperature determined previously. This additional assumption leads to a simple solution, but it is correct only when the web area is small compared with the skin area and for the case of perfect joint conductivity. Thus, this solution is valid only if $b_w \tau_w << b_s \tau_s$, or, in terms of the dimensionless parameters, $\tau s << 1$. Practical structures will seldom satisfy this restriction and it is

also unlikely that the thin webs implied by this simplification would be used as integral stiffeners. Hence, this solution can only be used to obtain approximate values for the thermal stresses.

In Reference 5, Pohle and Oliver have obtained a solution, based upon assumptions (1) through (5), which is a refinement of the previous treatment since it accounts for heat conduction between the skin and web. The neglect of the joint thermal resistance for a built-up section is the only serious restriction of this solution. Pohle and Oliver have found, however, that their series solution converges slowly, and this characteristic makes it difficult to carry out a sufficient number of computations to study the effects of geometry changes.

In Reference 15, Seide and Taylor present a solution based upon assumption (1) through (4), with the additional assumption that the skin temperature is not affected by the skin-to-web heat flow. This solution is essentially a modification of the solution of Reference 4 taking into account the joint thermal resistance. Since this solution neglects the heat flow from the skin to the web, it is restricted to large values of joint thermal resistance and will, in general, predict higher skin stresses and lower web stresses than actually exist.

In Reference 8, Schuh presents a solution similar to that of Pohle and Oliver, and based upon the same assumptions. Schuh's results have the advantage of being presented in dimensionless form. However, to reduce the minimum number of parameters necessary, he assumes in the heat flow analysis that the skin segment is infinitely long compared with the web. As a result, the solution leads to lower skin stresses and higher web stresses than actually occur. Since the compressive thermal stresses in the skin are likely to be most important from a design standpoint, an accurate solution for these stresses would be desirable.

In Reference 9, Johnston considers various structural elements and used essentially the same formulation of the problem as Pohle and Oliver. He then reduces the problem further by separating the structure into small elements for which finite difference heat flow equations are written. This method unfortunately leads to tedious computations for each case considered and, as a result, is impractical for the purpose of a general study of the problem.

A complete study of the temperature distribution and thermal stresses in T sections has been carried out and the results are presented in this section of the report. To make these results applicable to the largest possible number of cases, the work has been developed entirely in terms of dimensionless parameters. Analytical solutions have been developed, based upon assumptions (1) through (4), but accounting for the effect of joint thermal resistance.

To carry out a parameter study, a lumped-parameter solution was developed leading to a set of simultaneous ordinary differential equations which may be solved conveniently with an electronic differential analyzer. Transient temperatures and thermal stresses were then calculated for a wide range of values of the geometric and heating parameters, as well as for several values of joint resistance. The results of this work are presented here and the details of the various solutions can be found in Reference 11.

E. ANALYTICAL SOLUTIONS FOR TRANSIENT TEMPERATURES

An analytical solution for the transient temperature distribution in a T section has been obtained under assumptions (1) through (4) listed in the previous section. The case of perfect joint conductivity will be considered first.

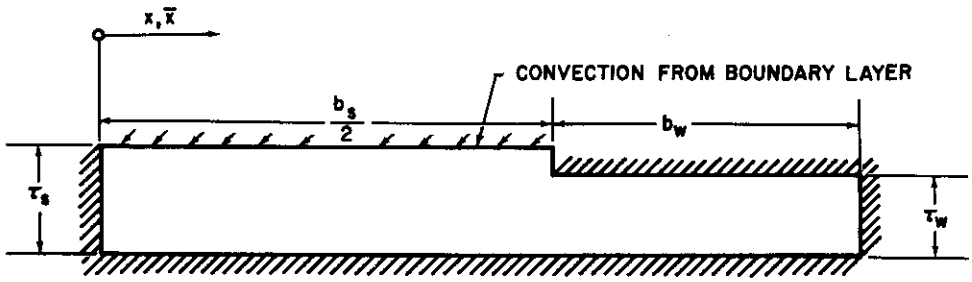

Diagram VI-4.

By virtue of assumption (4), the heat flow problem can be treated as one-dimensional conduction in a composite rod such as shown in Diagram VI-4. The segment $0 \le \bar{x} \le \left(\frac{b_s}{2}\right)$ represents the skin, and the region $\left(\frac{b_s}{2}\right) \le \bar{x} \le b_w + \left(\frac{b_s}{2}\right)$ represents the web.

Referring to Diagram VI-4, heat balance equations may be written for elements of the skin and web, and it is found that the temperatures $t(\bar{x}, \bar{\theta})$ and $T(\bar{x}, \bar{\theta})$ in the skin and web must satisfy the partial differential equations

$$\frac{\partial^2 t}{\partial \bar{x}^2} + \frac{h}{k\tau_s}\left(T_{aw} - t\right) = \frac{1}{a}\frac{\partial t}{\partial \bar{\theta}}; \quad 0 \le \bar{x} \le \frac{b_s}{2}, \tag{1}$$

$$\frac{\partial^2 T}{\partial \bar{x}^2} = \frac{1}{a}\frac{\partial T}{\partial \bar{\theta}}; \quad \left(\frac{b_s}{2}\right) \le \bar{x} \le b_w + \left(\frac{b_s}{2}\right). \tag{2}$$

The boundary and initial conditions appropriate to the rod shown in Diagram VI-4 are

$$\frac{\partial t}{\partial \bar{x}} = 0, \text{ at } \bar{x} = 0 \qquad \text{(end } \bar{x} = 0 \text{ insulated)}$$

$$\frac{\partial T}{\partial \bar{x}} = 0, \text{ at } \bar{x} = \frac{b_s}{2} + b_w \qquad \text{(end } \bar{x} = \frac{b_s}{2} + b_w \text{ insulated)}$$

$$t\left(\frac{b_s}{2}, \bar{\theta}\right) = T\left(\frac{b_s}{2}, \bar{\theta}\right) \qquad \text{(temperature continuous at skin-web junction)}$$

$$2\tau_s k \frac{\partial t}{\partial \bar{x}} = \tau_w k \frac{\partial T}{\partial \bar{x}}, \ \bar{x} = \frac{b_s}{2} \qquad \text{(heat flow into the web at the skin-web junction is equal to the heat flow from both skin segments)}$$

(3)

$$t(\bar{x}, 0) = G(x), \ 0 \le \bar{x} \le \frac{b_s}{2} \qquad \text{(initial temperature known throughout)} \tag{4}$$

$$T(\bar{x}, 0) = G(x), \ \frac{b_s}{2} \le \bar{x} \le \frac{b_s}{2} + b_w$$

It is convenient to define the following dimensionless quantities:

$$v(x,\theta) = \frac{T_{aw} - t}{T_{aw}}, \ V(x,\theta) = \frac{T_{aw} - T}{T_{aw}}, \ x = \frac{\bar{x}}{\left(\frac{b_s}{2}\right)}, \ \theta = \frac{a\,\bar{\theta}}{\left(\frac{b_s}{2}\right)^2}$$

$$\delta = \frac{h}{k}\frac{b_s}{2}, \ p = \frac{2\tau_s}{b_s}, \quad r = \frac{2b_w}{b_s}, \quad s = \frac{\tau_w}{2\tau_s}, \text{ and } \epsilon^2 = \frac{\delta}{p}.$$

Introducing these new variables in Equations (1) through (4) gives

$$\left.\begin{aligned} \frac{\partial^2 v}{\partial x^2} &= \frac{\partial v}{\partial \theta} + \epsilon^2 v, \quad 0 \le x \le 1 \\ \frac{\partial^2 V}{\partial x^2} &= \frac{\partial V}{\partial \theta}, \quad 1 \le x \le 1 + r \end{aligned}\right\}, \tag{5}$$

$$\left.\begin{aligned} &\frac{\partial v}{\partial x} = 0 && \text{at} \quad x = 0 \\ &\frac{\partial V}{\partial x} = 0 && \text{at} \quad x = 1+r \\ &v(1,\theta) = V(1,\theta) \\ &\frac{\partial v}{\partial x} = s\,\frac{\partial V}{\partial x} && \text{at} \quad x = 1 \end{aligned}\right\}, \text{ and} \tag{6}$$

$$\left.\begin{aligned} &v(x,0) = G(x) && 0 \le x \le 1 \\ &V(x,0) = G(x) && 1 \le x \le 1+r \end{aligned}\right\}. \tag{7}$$

The transient temperature distribution is therefore the solution of the boundary value problem defined by Equations (5), together with the boundary conditions (6) and the initial condition (7). The solution can be carried out conveniently by the technique of separation of variables. The details of this development are given in Reference 11.

The resulting solutions for $v(x,\theta)$ and $V(x,\theta)$ are

$$v(x,\theta) = \sum_{n=1}^{\infty} A_n e^{-\gamma_n^2 \theta} \phi_n(x), \text{ and} \tag{8}$$

$$V(x,\theta) = \sum_{n=1}^{\infty} A_n e^{-\gamma_n^2 \theta} \Phi_n(x), \tag{9}$$

where

$$\phi_n(x) = \cos \lambda_n x,$$

$$\Phi_n(x) = \frac{\cos\lambda_n}{\cos\gamma_n r} \cos \gamma_n (x - r - 1),$$

$$\gamma_n^2 = \lambda_n^2 + \epsilon^2,$$

and the characteristic numbers λ_n are the positive roots of the equation,

$$\lambda_n \tan \lambda_n = -\gamma_n \, s \tan \gamma_n \, r \; .$$

The constants A_n are the coefficients of the generalized Fourier series for $G(x)$ in terms of the characteristic functions $\psi_n(x)$ defined as

$$\psi_n(x) = \begin{cases} \phi_n(x) & 0 \le x \le 1 \\ \Phi_n(x) & 1 \le x \le 1+r \; . \end{cases}$$

The functions $\psi_n(x)$ can easily be shown to be orthogonal (Reference 11) in the interval $0 \le x \le 1+r$ with respect to the weighting function

$$g(x) = \begin{cases} 1, & 0 \le x \le 1 \\ S, & 1 \le x \le 1+r \end{cases},$$

thus

$$\int_0^{1+r} g(x)\,\psi_n(x)\,\psi_m(x)\,dx = 0, \quad \text{if } m \neq n \quad .$$

The coefficients A_n are then given by

$$A_n = 2\,\frac{\int_0^{1+r} g(x)G(x)\psi_n(x)\,dx}{\int_0^{1+r} g(x)\psi_n^2(x)\,dx} = 2\,\frac{\int_0^1 G(x)\phi_n\,dx + S\int_0^{1+r} G(x)\,\Phi_n(x)\,dx}{\int_0^1 \phi_n^2(x)\,dx + S\int_0^{1+r}\Phi_n^2(x)\,dx} \quad . \tag{10}$$

For the particular case where the initial temperature $G(x)$ is uniform,

$$v(x,0) = V(x,0) = Vo,$$

and the coefficients A_n are given by

$$A_n = \frac{2Vo}{\cos\lambda_n}\,\frac{\left(\frac{1}{\lambda_n} + \frac{\lambda_n}{\gamma_n^2}\right)\tan\lambda_n}{\left(\frac{1}{\lambda_n} + \frac{\lambda_n}{\gamma_n^2}\right)\tan\lambda_n + \frac{1}{\cos^2} + \frac{rs}{\cos^2\lambda_n r}} \quad .$$

If the case of joint thermal resistance is considered now, Equations (1), (2), and (4) will still apply, but the boundary conditions (3) must be modified. Barzelay (Reference 12) has shown that the effect of joint resistance is to make the skin-to-web heat transfer take place by a mechanism similar to convection. The heat flux between the skin and the web is then given by

$$q = \zeta\tau_w\left[t(1,\theta) - T(1,\theta)\right],$$

where ζ is a joint heat transfer coefficient which depends upon the characteristics of the joint. Some experimental information on proper values for ζ is available in Reference 12. With this modification, the boundary conditions (3) are now replaced by

$$2\tau_s k\,\frac{\partial t}{\partial \bar{x}} = -\zeta(t-T)\tau_w, \text{ at } \bar{x} = \frac{b_s}{2}$$

$$k\tau_w\,\frac{\partial t}{\partial \bar{x}} = -\zeta(t-T)\tau_w, \text{ at } \bar{x} = \frac{b_s}{2}.$$

The other boundary conditions remain the same. In terms of the dimensionless variables, the new boundary conditions are

$$\left.\begin{aligned} &\frac{\partial v}{\partial x} = 0, \text{ at } x = o \\ &\frac{\partial V}{\partial x} = 0, \text{ at } x = 1+r \\ &\frac{\partial v}{\partial x} = \beta s\left[V - v\right], \text{at } x = 1 \\ &\frac{\partial V}{\partial x} = \beta\left[V - v\right], \text{at } x = 1 \end{aligned}\right\}$$

The solution of Equations (5) with these new boundary conditions can be obtained by the same method as for the previous case; the result is

$$v(x,\theta)=\sum_{n=1}^{\infty} A_n e^{-\gamma_n^2\theta}\,\phi_n(x) \qquad V(x,\theta)=\sum_{n=1}^{\infty} A_n e^{-\gamma_n^2\theta}\,\Phi_n(x),$$

where $\phi_n(x)=\cos\lambda_n x$, $\Phi_n(x)=-\frac{\lambda_n}{\gamma_n s}\frac{\sin\lambda_n}{\sin\gamma_n r}\cos\gamma_n(x-r-1)$, $\gamma_n^2=\lambda_n^2+\xi^2$, $\beta=\frac{\zeta}{k}\frac{b_s}{2}$.

and the eigenvalues λ_n are the positive roots of the equation

$$\lambda_n\tan\lambda_n=-\frac{\beta\gamma_n s\tan\gamma_n r}{\beta-\gamma_n\tan\gamma_n r}.$$

The coefficients A_n are still given by equation (10), but the new expressions for $\phi_n(x)$ and $\Phi_n(x)$ must now be substituted in this expression.

For the case of uniform initial temperature, the coefficients A_n are given by

$$A_n=4v_o\frac{\left[\frac{1}{\lambda_n}+\frac{\lambda_n}{\gamma_n\sin\gamma_n r}\right]\sin\lambda_n}{\frac{1}{\sin^2\lambda_n}+\left[1-\frac{\lambda_n^2}{\beta}\right]\frac{1}{\lambda_n\tan\lambda_n}+\frac{\lambda_n^2}{\beta s}+\frac{\lambda_n^2 r}{s}\frac{1}{\sin^2\gamma_n r}}.$$

F. ANALYTICAL SOLUTION FOR THERMAL STRESSES

The normal thermal stresses will now be determined for a box structure such as shown in Diagram VI-2. To obtain a simple solution, the classical assumption that beam cross-sections remain plane is adopted; hence, the thermal stresses determined here apply to interior cross-sections of a long beam, sufficiently far from fixed or free ends. The temperature is assumed to be known as a function of θ,ξ,η where the ξ and η axes are the principal inertia axes of the cross-section (see Diagram VI-5).

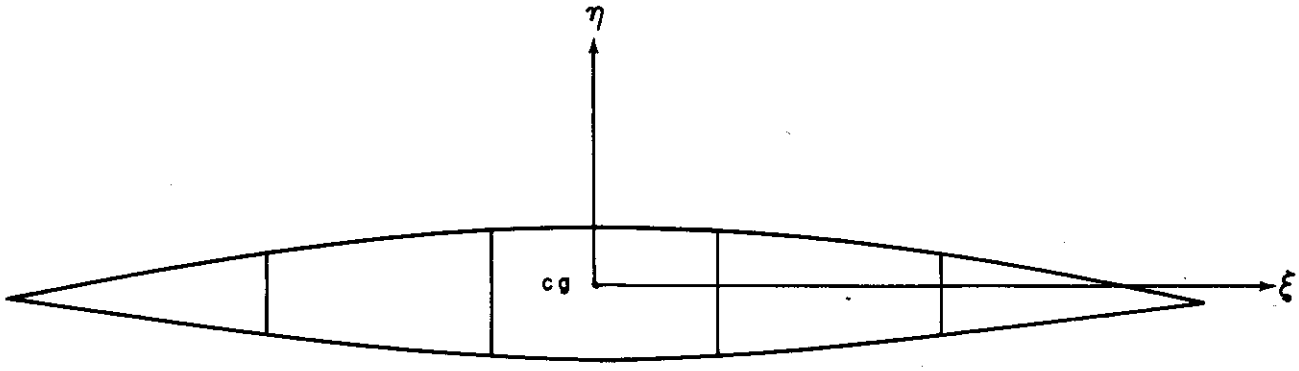

Diagram VI-5.

It can be shown (Reference 11) that, if cross-sections of the beam remain plane, the normal stress σ_n (positive when tensile) must be a function of the form

$$\sigma_n=-\alpha E\left[t(\xi,\eta,\theta)-T_{aw}f_o(\theta)-T_{aw}f_1(\theta)\xi-T_{aw}f_2(\theta)\eta\right]$$

where $f_0(\theta), f_1(\theta)$ and $f_2(\theta)$ are functions independent of ξ and η and must be determined for a particular structure. It is useful to define a dimensionless thermal stress given by

$$\bar{\sigma}_n = \frac{\sigma_n}{\alpha E T_{aw}} \quad . \tag{16}$$

It will be noted that $\bar{\sigma}_n = 1$ is the maximum thermal stress that could be reached in a structure subjected abruptly to a temperature rise T_{aw} The origin of temperature is taken here as the initial temperature of the structure.

From Equations (15) and (16), the dimensionless stress $\bar{\sigma}_n$ is obtained as

$$\bar{\sigma}_n = f_0 + f_1 \xi + f_2 \eta - u \quad . \tag{17}$$

The static equilibrium of the cross-section requires that

$$\begin{aligned} \int_s \bar{\sigma}_n \, dS &= 0, \\ \int_s \bar{\sigma}_n \eta \, dS &= 0, \text{ and} \\ \int_s \bar{\sigma} \xi \, dS &= 0, \end{aligned} \tag{18}$$

where the integrations are carried out over the normal stress-carrying area S Substituting Equation (17) in Equation (18) yields three expressions that can be solved for f_0, f_1, and f_2 . The result is

$$\begin{aligned} f_0(\theta) &= \frac{1}{S} \int_s u(\xi, \eta, \theta) \, dS \\ f_1(\theta) &= \frac{1}{I_\eta} \int_s \xi u(\xi, \eta, \theta) \, dS \text{ , and} \\ f_2(\theta) &= \frac{1}{I_\xi} \int_s \eta u(\xi, \eta, \theta) \, dS \text{ ,} \end{aligned} \tag{19}$$

where I_ξ and I_η are the moments of inertia of the cross-section about the ξ and η axes.

From Equations (17) and (19), the thermal stresses are then obtained as

$$\bar{\sigma}_n = \frac{1}{S} \int_s (\xi, \eta, \theta) \, dS - u(\xi, \eta, \theta) + \frac{\xi}{I_\eta} \int_s \xi u(\xi, \eta, \theta) \, dS + \frac{\eta}{I_\xi} \int_s \eta u(\xi, \eta, \theta) \, dS \quad .$$

This expression may now be written as

$$\bar{\sigma}_n = U_{ave} - U + \frac{M_{\eta t} \xi}{I_\eta} + \frac{M_{\xi t} \eta}{I_\xi} \quad , \tag{20}$$

where U_{ave} = average temperature over the cross-section area,

$M_{\eta t} = \int_s \xi u(\xi, \eta, \theta) \, dS$

= first moment of the temperature about the η axis (a "thermal moment" about the η axis), and

$$M_{\xi t} = \int_s \eta u(\xi,\eta,\theta)\,ds$$

= first moment of the temperature about the ξ axis (a "thermal moment" about the ξ axis).

It should be noted that when the temperature distribution is symmetric about the ξ or η axes, the third or fourth terms in Equation (20) vanish.

Equation (20) can be used to calculate the normal thermal stress at any point of the cross-section. It is also possible to calculate the shear flow in the various elements. However, it can be shown (Reference 11) that these shear flows are directly proportional to the rate of change of the temperature in the spanwise direction and this will usually be small. Hence, the thermal shear stresses can reasonably be expected to be small except in regions near the fixed or free ends of the beam where the present analysis does not apply.

G. NUMERICAL METHODS FOR THERMAL STRESS CALCULATION

Since, in practical cases, the temperature is usually obtained from numerical finite difference calculations or from some automatic computation device, it is convenient to obtain thermal stress expressions which can be computed numerically rather than by formal integration. This can easily be done by replacing the integrals in $U_{ave}, M_{\xi t}$, and $M_{\eta t}$ by finite summations. Thus, if the subscript i or j denotes a given element of the cross-section and there are m such elements, the quantities $U_{ave}, M_{\xi t}$, and $M_{\eta t}$ can be written

$$\left.\begin{aligned} U_{ave} &= \frac{1}{S}\sum_{j=1}^{m} u_j \Delta S_j \ , \\ M_{\xi t} &= \sum_{j=1}^{m} \eta_j u_j \Delta S_j \ , \text{ and} \\ M_{\eta t} &= \sum_{j=1}^{m} \xi_j u_j \Delta S_j \ , \end{aligned}\right\} \qquad (21)$$

where ξ_j and η_j are the coordinates of the centroid of the jth element of structure, U_j is the temperature, and ΔS_j is the area of the element. Then, from Equations (20) and (21), the thermal stress in the ith element is obtained as

$$\bar{\sigma}_{ni} = -u_i + \frac{1}{S}\sum_{j=1}^{m} u_j \Delta S_j + \frac{\xi_i}{I_\eta}\sum_{j=1}^{m} \xi_j u_j \Delta S_j + \frac{\eta_i}{I_\xi}\sum_{j=1}^{m} \eta_j u_j \Delta S_j \ . \qquad (22)$$

H. SOLUTION BY ELECTRONIC DIFFERENTIAL ANALYZER

The analytical solutions obtained in the previous sections are not convenient to use for carrying out large number of numerical calculations. For this reason, it is desirable to develop a formulation of the problem suitable for use in conjunction with modern high-speed computing facilities. The particular problem under consideration here could be adapted for the use of either digital or analogue equipment. While it is true that a high-speed digital computer will yield better accuracy since a large number of significant figures can be carried, the differential analyzer will afford the flexibility needed to investigate special limiting cases. In the present investigation, the heat input conditions are, at best, known only approximately and the greater accuracy of digital equipment would not increase the reliability of the results since the original data are not exact. For these reasons, the investigation described here was carried out using a REAC electronic differential analyzer. Since this type of computer can solve only systems of ordinary differential equations, the structure must be represented by a "lumped mass" system and heat balance equations must be written for each element. The T section is, therefore, divided into finite elements as shown in Diagram VI-6. The

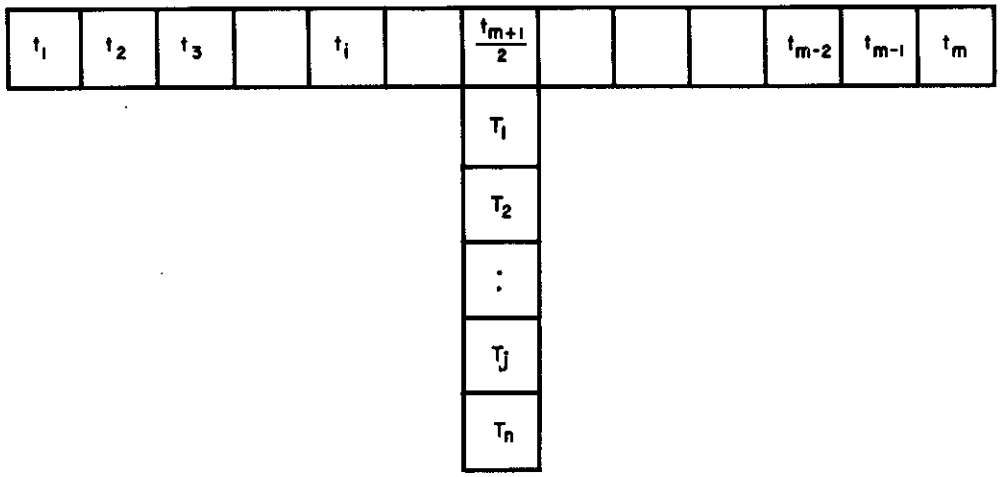

Diagram VI-6.

skin is divided into an odd number of elements, m, so that the $\left(\frac{m+1}{2}\right)$ element is above the skin-web junction. For convenience in deriving the heat balance equations, it is assumed that $\tau_w < \frac{b_s}{m}$, so that only one skin element is in contact with the web. This is not a severe restriction. The web is divided into n elements (n may be even or odd). Heat balance equations can be written for each skin and web element.

For a general skin element, the heat balance equation is

$$h\left(T_{aw}-t_i\right)\frac{b_s}{m}+mk\,\frac{\tau_s}{b_s}\left(t_{i-1}-2t_i+t_{i-1}\right)=wC_p\,\frac{b_s\tau_s}{m}\,\frac{dt_i}{d\bar{\theta}}\,,\left(i\neq 1,\,m,\,\frac{m+1}{2}\right)\,. \tag{23}$$

Equation (23) holds only for an interior skin element not in contact with the web. For these special skin elements, special equations must be written,

$$h\left(T_{aw}-t_i\right)\frac{b_s}{m}+mk\,\frac{\tau_s}{b_s}\left(t_2-t_1\right)=wC_p\,\frac{b_s t_s}{m}\,\frac{dt_i}{d\bar{\theta}}\,, \tag{24}$$

$$h\left(T_{aw}-t_m\right)\frac{b_s}{m}+mk\,\frac{\tau_s}{b_s}\left(t_{m-1}-t_m\right)=wC_p\,\frac{b_s T_s}{m}\,\frac{dt_m}{d\bar{\theta}}\,,\ \text{and} \tag{25}$$

$$h\left(T_{aw}-t_{\frac{m+1}{2}}\right)\frac{b_s}{m}+mk\,\frac{\tau_s}{b_s}\left(t_{\frac{m+1}{2}+1}-2t_{\frac{m+1}{2}}+t_{\frac{m+1}{2}-1}\right)+\xi\,\tau_w\left(T_i-t_{\frac{m+1}{2}}\right)=wC_p\,\frac{b_s\tau_s}{m}\,\frac{dt_{\frac{m+1}{2}}}{d\bar{\theta}}\,. \tag{26}$$

The last term on the left-hand side of Equation (26) accounts for the skin-to-web conduction.

For an interior web element, the heat balance equation is easily obtained as

$$nk\,\frac{\tau_w}{b_w}\left(T_{j+1}-2T_j+T_{j+1}\right)=wc_p\,\frac{b_w\tau_w}{n}\,\frac{dT_j}{d\bar{\theta}}\,,\ (j\neq 1,n)\,. \tag{27}$$

For the end elements of the web, the following special equations apply:

$$\xi\,\tau_w\left(t_{\frac{m+1}{2}}-T_1\right)+nk\,\frac{\tau_w}{b_w}\left(T_2-T_1\right)=wc_p\,\frac{b_w\tau_w}{n}\,\frac{dT_1}{d\bar{\theta}}\ \text{and} \tag{28}$$

$$nk\,\frac{\tau_w}{b_w}\left(T_{n-1}-T_n\right)=wC_p\,\frac{b_w\tau_w}{n}\,\frac{dT_n}{d\bar{\theta}}\,. \tag{29}$$

Introducing the dimensionless variables into Equations (23) through (29) gives

$$\frac{du_i}{d\theta} = \frac{\delta}{p}\left(1-u_i\right)+\frac{m^2}{4}\left(u_{i-1}-2u_i+u_{i+1}\right)\quad\left(i\neq 1,m,\frac{m+1}{2}\right)\quad, \tag{30}$$

$$\frac{du_1}{d\theta} = \frac{\delta}{p}\left(1-u_1\right)+\frac{m^2}{4}\left(u_2-u_1\right), \tag{31}$$

$$\frac{du_m}{d\theta} = \frac{\delta}{p}\left(1-u_m\right)+\frac{m^2}{4}\left(u_{m-1}-u_m\right), \tag{32}$$

$$\frac{du_{\frac{m+1}{2}}}{d\theta} = \frac{\delta}{p}\left(1-u_{\frac{m+1}{2}}\right)+\frac{m^2}{4}\left(u_{\frac{m+1}{2}+1}-2u_{\frac{m+1}{2}}+u_{\frac{m+1}{2}-1}\right)+\frac{2mns}{r+2nM}\left(U-u_{\frac{m+1}{2}}\right), \tag{33}$$

$$\frac{dU_j}{d\theta} = \frac{n^2}{r^2}\left(U_{j+1}-2U_j+U_{j-1}\right),\quad\left(j\neq 1,n\right)\quad, \tag{34}$$

$$\frac{dU_1}{d\theta} = \frac{n^2}{r^2}\left(U_2-U_1\right)+\frac{2n^2}{r(r+2nM)}\left(u_{\frac{m+1}{2}}-U_1\right), \text{ and} \tag{35}$$

$$\frac{dU_n}{d\theta} = \frac{n^2}{r^2}\left(U_{n-1}-U_n\right). \tag{36}$$

It should be noted that the dimensionless temperatures, u and U, used in these equations are defined differently than those used in the analytical solution. In Equations (33) and (35), the last term on the right-hand side represents the heat flow from the skin to the web. The effect of the joint resistance is contained in the factor M called resistance ratio which would be equal to zero for perfect conduction and would become infinite for a perfectly insulated joint. Practical values of M can be obtained from the work of Barzelay (Reference 12).

The calculations for the present investigation were carried out with $m=11$ and $n=4$. Since the independent variable on the computer is time, it is convenient to introduce in the heat balance equations a computer time variable which can be adjusted to speed up or slow down the solution. This is done by defining the computer time, θ^* as $\theta^*=\kappa\theta$, so that derivatives with respect to θ are now written as

$$\frac{du_i}{d\theta} = \frac{du_i}{d\theta^*}\,\frac{d\theta^*}{d\theta} = \kappa u'_i\quad. \tag{37}$$

Since the unknowns u_i and U_j appear as voltages in the computer circuit, it is also convenient to introduce a voltage scale so that full advantage can be taken of the computer voltage scale. Thus, since the dimensionless temperatures vary between zero and unity, the computer unknowns are chosen as

$$\left.\begin{aligned}\bar{u}_i &= Qu_i \text{ and}\\ \bar{U}_j &= QU_j\quad,\end{aligned}\right\} \tag{38}$$

where Q is the full-scale computer voltage. In the case considered, the temperature distribution is symmetric about the midplane of the web so that only 6 of the 11 skin elements need to be con-

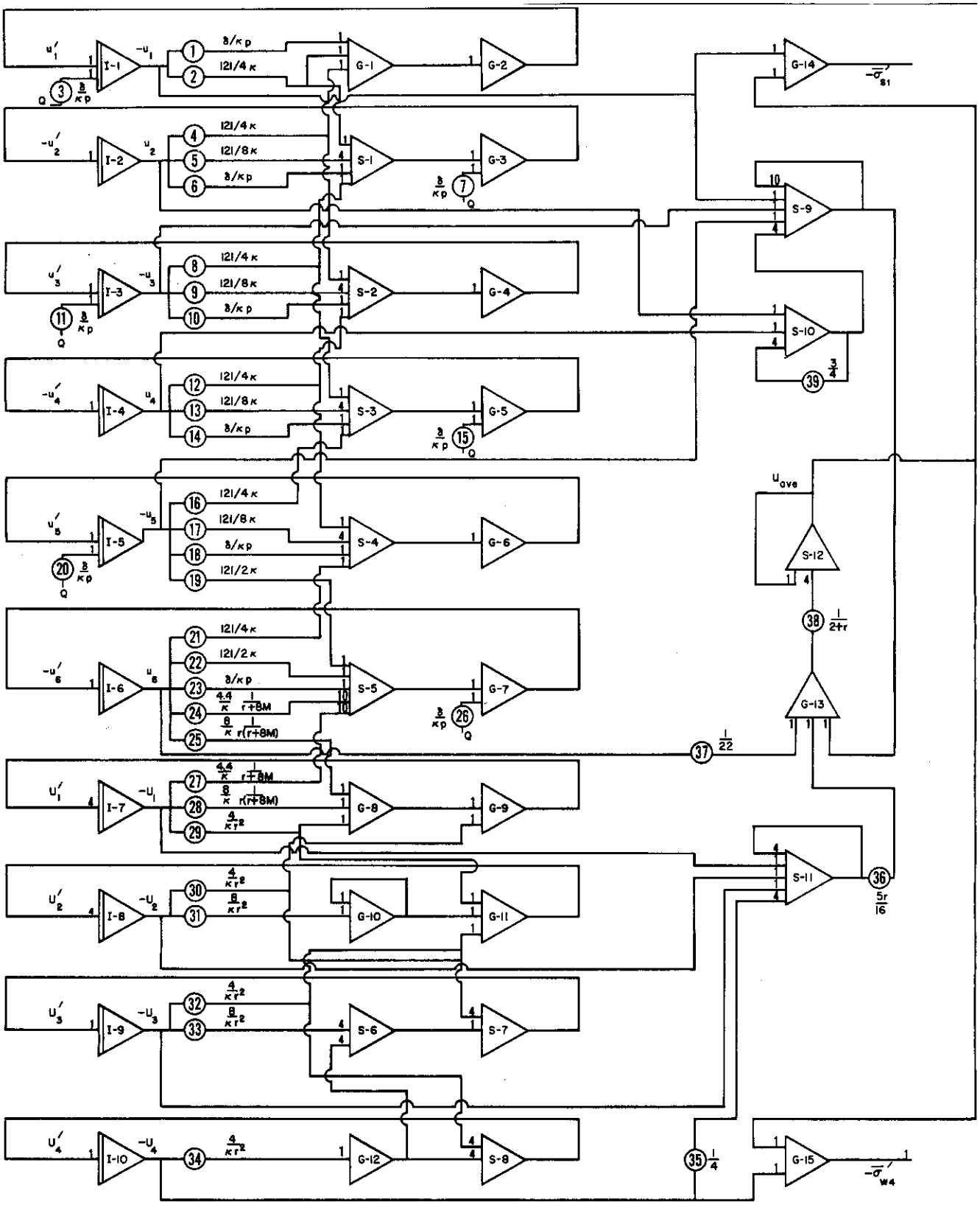
I-1
I-2
I-3
I-4
I-5
I-6
I-7
I-8
I-9
I-10
G-1
G-2
G-3
G-4
G-5
G-6
G-7
G-8
G-9
G-10
G-11
G-12
G-13
G-14
G-15
S-1
S-2
S-3
S-4
S-5
S-6
S-7
S-8
S-9
S-10
S-11
S-12
8/κp
121/4κ
121/8κ
121/2κ
u_ave
1/22
1/4
1/2+r
3/4
5r/16

Diagram VI-7.

sidered, and $t_1 = t_{11}, t_2 = t_{10}, t_3 = t_9$ ----, etc. In terms of the computer variables, the 10 simultaneous equations to be solved are

$$\bar{u}'_1 = \frac{\delta}{\kappa p}\left(Q - \bar{u}_1\right) + \frac{121}{4\kappa}\left(\bar{u}_2 - \bar{u}_1\right)$$

$$\bar{u}'_i = \frac{\delta}{\kappa p}\left(Q - \bar{u}_i\right) + \frac{121}{4\kappa}\left(\bar{u}_{i+1} - 2u_i + u_{i-1}\right), \left(i = 2,3,4,5\right)$$

$$\bar{u}'_6 = \frac{\delta}{\kappa p}\left(Q - \bar{u}_6\right) + \frac{121}{4\kappa}\left(\bar{u}_5 - \bar{u}_6\right) + \frac{88}{\kappa}\,\frac{s}{r+8M}\left(\bar{U}_1 - \bar{u}_6\right) \qquad (39)$$

$$\bar{U}'_1 = \frac{16}{\kappa r^2}\left(\bar{U}_2 - \bar{U}_1\right) + \frac{32}{\kappa}\,\frac{1}{r(r+8M)}\left(\bar{u}_6 - \bar{U}_1\right)$$

$$\bar{U}'_j = \frac{16}{\kappa r^2}\left(\bar{U}_{j+1} - 2\bar{U}_j + \bar{U}_{j-1}\right), \left(j = 2,3\right)$$

$$\bar{U}'_4 \quad \frac{16}{\kappa r^2}\left(\bar{U}_3 - \bar{U}_4\right).$$

The differential analyzer circuit for the solution of Equations (39) is shown in Diagram VI-7. The thermal stresses can also be calculated by means of the differential analyzer. In this investigation, these stresses were calculated at station 1 in the skin and at station 4 in the web corresponding with the maximum compressive and tensile stresses, respectively. The stresses were calculated assuming that the T section under consideration constitutes one-half of an I beam treated symmetrically through its upper and lower surfaces. Under these conditions, it is clear from Equation (22) that the thermal stresses are given by

$$\bar{\sigma}'_n = u_{ave} - u \,. \qquad (40)$$

For the case of a T section, the average temperature is obtained as

$$u_{ave} = \frac{1}{1+rs}\,\frac{1}{m}\sum_{i=1}^{m} u_i + \frac{1}{1+rs}\,\frac{1}{n}\sum_{j=1}^{h} U_j \,. \qquad (41)$$

The expressions on the right-hand side of both Equations (40) and (41) can easily be calculated simultaneously with the temperatures on the differential analyzer. This circuit is also shown in Diagram VI-7. The schematic representation of computer components used in Diagram VI-7 is as follows:

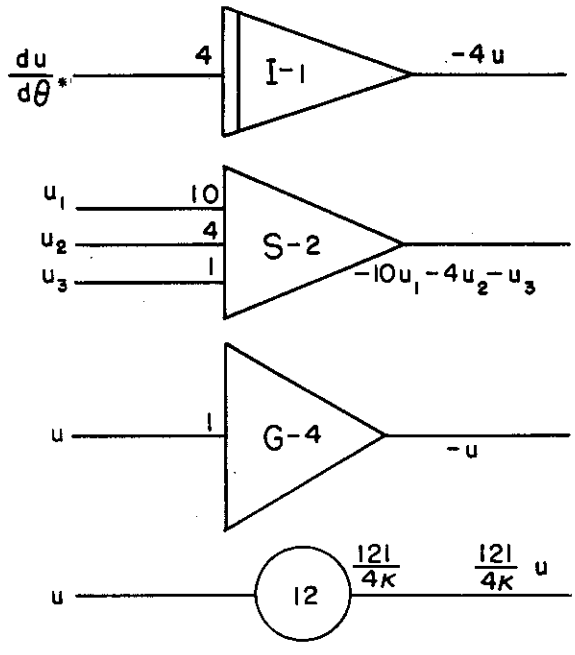

Integrator No. 1 with a 4-to-1 gain input connection. Input and output voltages shown.

Summer No. 2 with various inputs to obtain a linear combination.

Inverter No. 4.

Potentiometer No. 12 with setting of $\frac{121}{4\kappa}$ (note that $\frac{121}{4\kappa}$ must be smaller than unity).

The potentiometer settings for the circuit of Figure VI-7 are given in the table that follows.

Pot. No.	Setting	Pot. No.	Setting	Pot No.	Setting
1	$\delta/\kappa p$	14	$\delta/\kappa p$	27	$4.4/[\kappa(r+8M)]$
2	$121/4\kappa$	15	$\delta/\kappa p$	28	$8/[\kappa r(r+8M)]$
3	$\delta/\kappa p$	16	$121/4\kappa$	29	$4/\kappa r^2$
4	$121/4\kappa$	17	$121/8\kappa$	30	$4/\kappa r^2$
5	$121/8\kappa$	18	$\delta/\kappa p$	31	$8/\kappa r^2$
6	$\delta/\kappa p$	19	$121/2\kappa$	32	$4/\kappa r^2$
7	$\delta/\kappa p$	20	$\delta/\kappa p$	33	$8/\kappa r^2$
8	$121/4\kappa$	21	$121/4\kappa$	34	$4/\kappa r^2$
9	$121/8\kappa$	22	$121/2\kappa$	35	1/4
10	$\delta/\kappa p$	23	$\delta/\kappa p$	36	5r/16
11	$\delta/\kappa p$	24	$4.4/\kappa(r+8M)$	37	1/22
12	$121/4\kappa$	25	$8/\kappa r(r+8M)$	38	1/2+r
13	$121/8\kappa$	26	$\delta/\kappa p$	39	3/4

I. APPROXIMATE SOLUTION FOR THERMAL STRESSES IN A MULTIWEB CROSS-SECTION

The stresses calculated by means of the differential analyzer are obtained from Equation (30). This equation was derived by considering an isolated T section and assuming that it is the upper or lower half of an I beam heated symmetrically through its upper and lower surfaces. While, in general, this structural configuration does not correspond with the cases of most practical interest, the resulting stress data can easily be modified so as to apply to the case of a multiweb wing. This is done by assuming that the restraining effect of the surrounding structure on a given T section takes the form of a uniform tension or compression superposed on the stress distribution calculated for the isolated T section. Considering a multiweb cross-section as shown in Diagram VI-8, Equation (22) should be used to calculate the thermal stresses at any point. If the cross-section is divided into m elements, which are precisely the isolated T sections considered in the previous solution, the thermal stress at the centroid of the ith T section is given by

$$\bar{\sigma}_i = -u_i + \frac{1}{S}\sum_{j=1}^{m} u_{aj}\,\Delta S_i + \frac{\xi_i}{I_\eta}\sum_{j=1}^{m}\xi_j\,u_{aj}\Delta S_j + \frac{\eta_i}{I_\xi}\sum_{j=1}^{m}\eta_j\,u_{aj}\,\Delta S_j \quad , \qquad (42)$$

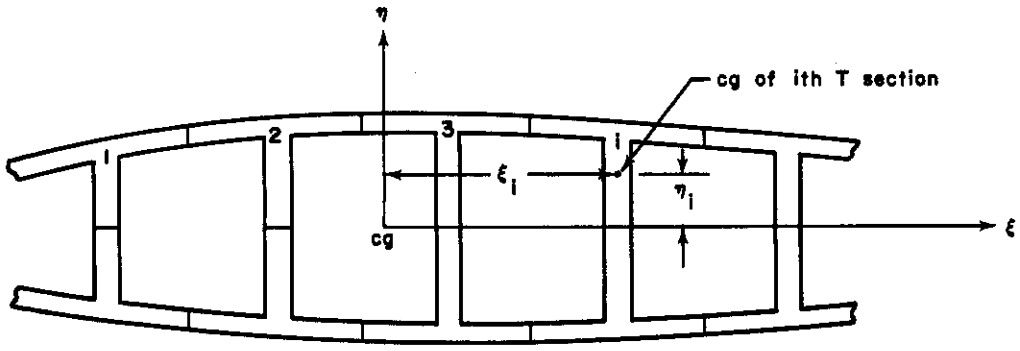

Diagram VI-8.

where u_{aj} is the average temperature of the jth T section and ξ_i, ξ_j, η_i, and η_j are the coordinates of the centroid of the ith or jth T section with respect to the centroid of the entire multicell cross-section. If the ith T section were isolated and unrestrained, the thermal stress at its centroid would be given by Equation (40) as

$$\bar{\sigma}'_i = u_{ai} - u_i \quad , \qquad (43)$$

and the restraint of the rest of the cross-section on the ith T section causes at the centroid of this section a stress increment $\Delta\bar{\sigma}_i$ given by

$\Delta\bar{\sigma}_i = \bar{\sigma}_i - \bar{\sigma}'_i$ and

$$\Delta\bar{\sigma}_i = -u_{ai} + \frac{1}{S}\sum_{j=1}^{m} u_{aj}\Delta S_j + \frac{\xi_i}{I_\eta}\sum_{j=1}^{m}\xi_j u_{aj}\Delta S_j + \frac{\eta_i}{I_\xi}\sum_{j=1}^{m}\eta_j u_{aj}\Delta S_j \quad . \qquad (44)$$

Equation (44) gives the uniform stress acting on the ith T section due to the restraint exerted by the rest of the multiweb cross-section.

The maximum total stresses in the skin and web of the ith T section are therefore given by

$$\bar{\sigma}_{si} = \bar{\sigma}'_{si} + \Delta\bar{\sigma}_i \quad \text{and}$$
$$\bar{\sigma}_{wi} = \bar{\sigma}'_{wi} + \Delta\bar{\sigma}_i \quad , \qquad (45)$$

where $\bar{\sigma}'_{si}$ and $\bar{\sigma}'_{wi}$ are the stresses calculated in the skin and web for the isolated T section. The values of $\bar{\sigma}_{si}$ and $\bar{\sigma}'_{wi}$ obtained from the differential analyzer can be determined from the charts of Reference 13.

In order to use Equation (44) to calculate the stress correction, it is necessary to use the stress and temperature charts of Reference 13 together with Equations (40) and (41). Inasmuch as this calculation will be lengthy, it is desirable to obtain an expression for the stress correction which depends only on geometry. This can be done if it is assumed that the heat transfer coefficient and boundary layer temperature do not vary widely along the chord or with time.

If this assumption is made, it can be shown (Reference 11) that the thermal stress correction is given by

$$\Delta\bar{\sigma}_i = -\frac{1}{1+r_i s_i} + \frac{1}{S}\sum_{j=1}^{m}\frac{1}{1+r_j s_j}\Delta S_j + \frac{\xi_i}{I_\eta}\sum_{j=1}^{m}\frac{1}{1+r_j s_j}\xi_j\Delta S_j + \frac{\eta_i}{I_\xi}\sum_{j=1}^{m}\frac{1}{1+r_j s_j}\eta_j\Delta S_j \quad . \qquad (46)$$

Equation (46) gives the stress correction in terms of the simple geometric parameters for the cross-section.

Note that, if all the T sections have the same geometry, r and s are the same for all T sections, and that in such a case

$$\Delta\bar{\sigma}_i = 0 \quad .$$

This result should be expected since, for a similar geometry, the heat conduction process takes place similarly for all T sections regardless of absolute size; therefore, the average temperature at any instant would be the same for all the sections, so that no restraint would be incurred.

J. THERMAL STRESSES IN FUSELAGE RINGS

The temperature gradients calculated by the afore-mentioned methods apply within a close approximation to a T section used as a fuselage ring (Diagram VI-9), provided that the depth b_w

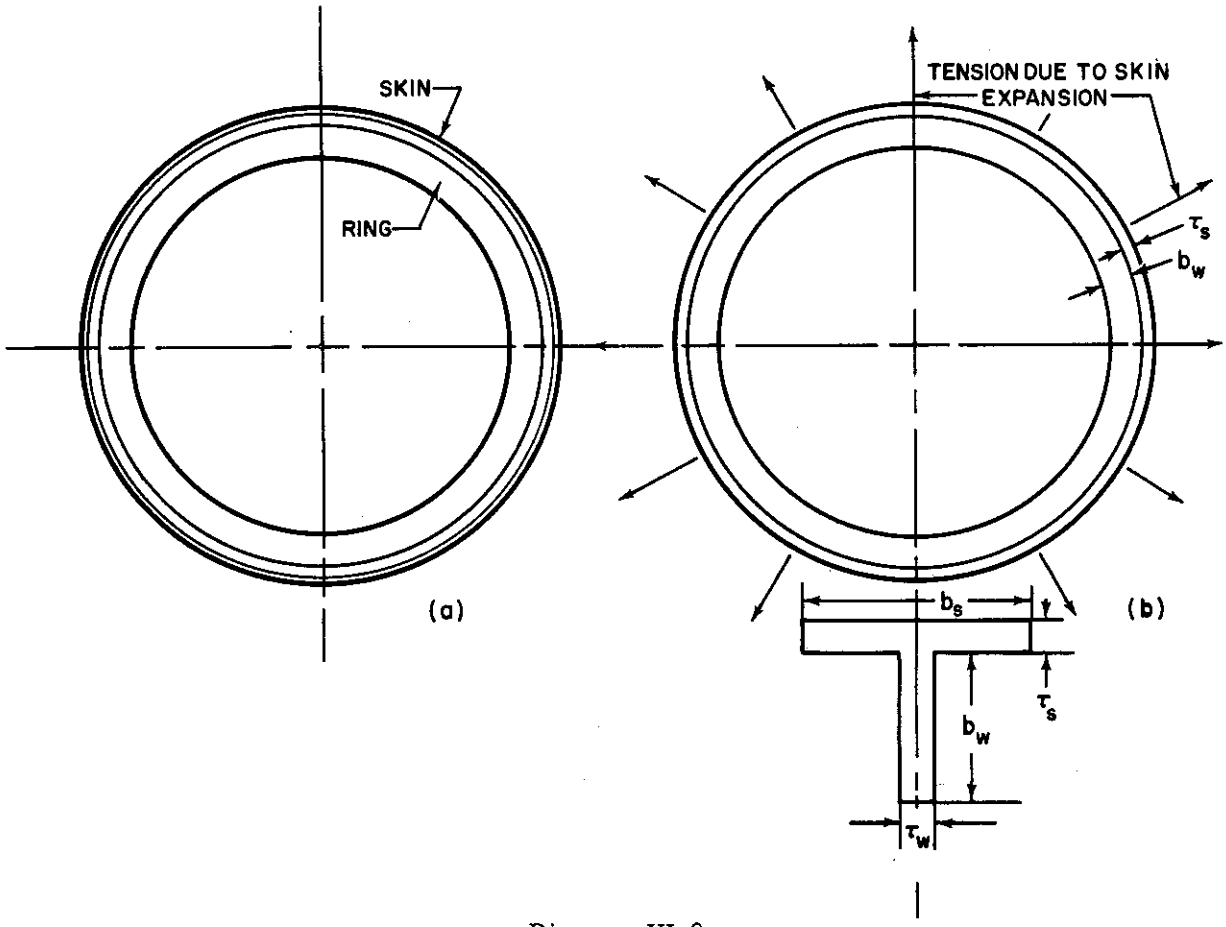

Diagram VI-9.

is small compared with the radius of the ring. It can also be shown that the stresses calculated by Equation (40) and plotted in Reference 13 are a close approximation to the values of stress for a ring. This is due to the fact that the ring is free to expand radially but cannot distort. It is true that the skin around a given ring would be at a higher temperature than the ring, and would therefore tend to expand more and exert a radial tension on the ring; however, the skin area is always smaller than the ring area so that this effect can be neglected. The important stresses in this case are the hoop compression stresses in the skin which can be computed easily by assuming that the skin is restrained against radial expansion.

K. LIMITING CASES

Two limiting cases of interest will be considered here. The case of an infinite heat transfer coefficient, $\frac{\delta}{p} \to \infty$ and the case of an infinite joint resistance, $M \to \infty$ Referring to Equations (39), it can be shown that, for $\frac{\delta}{p} \to \infty$ the dimensionless skin temperature would initially increase to unity as the heat is applied, while the web temperature would be zero. Then, from Equation (41), the average temperature would be $u_a = \frac{1}{1+r+s}$, so that, for an isolated T section, the stresses in the skin and the web would be

$$\left.\begin{aligned} \bar{\sigma}'_s &= -\frac{r\,s}{1+r\,s} \quad \text{and} \\ \bar{\sigma}'_w &= \frac{1}{1+r\,s} \quad . \end{aligned}\right\} \tag{47}$$

In this case, the maximum thermal stresses would occur immediately upon application of the hot boundary layer.

For the case of $M \to \infty$ the skin temperature approaches unity while the web temperature remains constant and equal to zero. Thus, in such a case, the maximum thermal stresses would again be given by Equation (47), but this time the peak values are approached asymptotically with time.

It is of interest to note that the case of $M \to \infty$ has been simulated on the differential analyzer and that the computer results were within 1% of the theoretically predicted values. This illustrates the accuracy as well as the flexibility of the electronic differential analyzer. The investigation of such limiting cases would have been difficult to perform with a digital machine.

L. EFFECT OF VARIABLE ADIABATIC WALL TEMPERATURE

The temperature and thermal stresses obtained by the use of the differential analyzer apply only to the case of a constant adiabatic wall temperature and a constant heat transfer coefficient. The treatment of the more general case of variable heat input conditions is considerably more difficult and, from an analytical standpoint, is practically impossible. The differential analyzer circuit considered previously can be applied to this case if the dimensionless temperatures, u_i are defined as

$$u_i = u / T_{aw}^* \quad , \tag{48}$$

where T_{aw}^* is now the average value of T_{aw} and will be chosen as a reference. Since the heating conditions are now time-dependent, the terms involving the input voltage Q and the heat transfer parameter $\frac{\delta}{p}$ must now be varied with time. This could be done with suitable function generator equipment. However, for such cases, the use of finite difference equations in conjunction with a digital computer may be a more convenient method of solution.

In some instances, it is permissible to consider the heat transfer coefficient as constant while allowing the boundary layer temperature to vary. In such a case, it can be shown (Reference 11) that the temperature curves obtained from the circuit previously mentioned can be used to obtain the correct structural temperatures.

The calculation is performed in a step-by-step procedure, applying the computer solution over small time increments $\Delta\theta$.

If t_j is the temperature at the end of the jth time increment at some point of the structure, and T_b^j is the boundary layer temperature during that interval of time, it can be shown that T_j may be obtained from

$$t^j = T_o + \left(T_b^i - T_o\right) u(\theta) + \left(T_b^2 - T_b'\right) u\left[\theta - \Delta\theta\right] + \left(T_b^3 - T_b^2\right) u\left[\theta - 2\Delta\theta\right]$$
$$+ \text{------} + \left(T_b^j - T_b^{j-1}\right) u\left[\theta - (j-1)\Delta\theta\right] \quad . \tag{49}$$

In Equation (49), $u(\theta)$ is the dimensionless temperature at some point as obtained from the differential analyzer solution with constant boundary layer temperature. It is clear from Equation (49) that the variation of the boundary layer temperature introduces no essential complication, since it simply requires the superposition of solutions obtained for constant boundary layer temperatures. This is to be expected because the problem is linear. Thus, the term $\left(T_b^i - T_o\right) u(\theta)$ is the temperature rise corresponding with a value of T_{aw} equal to $T_b' T_o$ applied starting at $\theta = 0$. The next term, $\left(T_b^2 - T_b'\right) u\left[\theta - \Delta\theta\right]$ is the temperature rise produced by a value of T_{aw} equal to $T_b^2 - T_b'$ for a time interval $\theta - \Delta\theta$. In fact, Equation (49) is a finite difference representation

of the well-known Duhamel formula which, for this case, would be written $t(\theta) = T_o + \int_0^\theta \frac{dT_b}{d\theta'} u(\theta-\theta')\, d\theta'$, where θ' is a dummy time variable. A simple graphical procedure for this computation is presented in Reference 13.

M. NUMERICAL SOLUTION BY FINITE DIFFERENCES

Although the present investigation was based primarily upon the use of an electronic differential analyzer, it is of interest also to present finite difference equations which can be used to perform hand computations for isolated cases, or to establish a program for automatic digital computation. Finite difference equations can be obtained easily by replacing the derivatives in Equations (30) through (36) by finite difference quantities. Thus, the quantity $\frac{du_i}{d\theta}$ is now written $\frac{\Delta u_i}{\Delta\theta}$ or $\frac{u_i - u_i}{\Delta\theta}$ where u_i and u_i denote the temperature in element i at the beginning and at the end of the time interval $\Delta\theta$.

With these modifications, Equations (30) through (36) become

$$\Delta u_i = \left\{\frac{\delta}{p}(1-u_i) + \frac{m^2}{4}(u_{i+1} - 2u_i + u_{i-1})\right\}\Delta\theta \quad (i \neq 1, m, \tfrac{m+1}{2}),$$

$$\Delta u_1 = \left\{\frac{\delta}{p}(1-u_1) + \frac{m^2}{4}(u_2 - u_1)\right\}\Delta\theta,$$

$$\Delta u_m = \left\{\frac{\delta}{p}(1-u_m) + \frac{m^2}{4}(u_{m-1} - u_m)\right\}\Delta\theta,$$

$$\Delta u_{\frac{m+1}{2}} = \left\{\frac{\delta}{p}\left(1 - u_{\frac{m+1}{2}}\right) + \frac{m^2}{4}\left(u_{\frac{m+1}{2}+1} - 2u_{\frac{m+1}{2}} - u_{\frac{m+1}{2}-1}\right) + \frac{2Mns}{r+2nM}\left(U_1 - u_{\frac{m+1}{2}}\right)\right\}\Delta\theta, \qquad (50)$$

$$\Delta U_1 = \left\{\frac{n^2}{r^2}(U_2 - U_1) + \frac{2n^2}{r(r+2nM)}\left(u_{\frac{m+1}{2}} - U_1\right)\right\}\Delta\theta,$$

$$\Delta U_j = \left\{\frac{n^2}{r^2}(U_{j+1} - 2U_j + U_{j-1})\right\}\Delta\theta \quad (j \neq 1, n), \text{ and}$$

$$\Delta U_n = \left\{\frac{n^2}{r^2}(U_{n-1} - U_n)\right\}\Delta\theta.$$

A common procedure in solving finite difference equations, such as Equation (50), is to substitute in the right-hand side the initial values u_i^o of all the unknown quantities. The disadvantage of the procedure is that, since the unknown temperatures are actually varying, serious inaccuracies are introduced into the solution if the time increment $\Delta\theta$ as chosen is too large. Although the limitation of a small $\Delta\theta$ is not important if the calculation is carried out on a high-speed digital machine, it can seriously hamper hand computation. A refinement of this method, developed in Reference 3, was found to give good accuracy with much larger values of $\Delta\theta$ The development of this method for application to the present problem can be found in Reference 11.

N. THERMAL DEFLECTIONS

The presence of thermal gradients within a structure may, in certain cases, result in appreciable deformations. Since these deformations may have considerable influence on aeroelastic phenomena, such as control effectiveness or panel flutter, it is of interest to present methods for their determination. The classical strain energy method will therefore be extended to include thermal effects. In order to present general methods of analysis, the following development is carried out for a three-dimensional elastic body. The results can then be simplified easily for particular cases. It is convenient to utilize Cartesian tensor notation.

The space coordinates x, y, z are now denoted by $x_i\ (i = 1, 2, 3)$, and the components of stress are denoted by σ_{ij} where the first subscript indicates the normal to the plane in which the

stress acts and the second subscript denotes the direction of a given component. The summation convention applies throughout the following development. Thus, whenever a subscript is repeated in a single term, a summation must be carried out over all the values of the subscript. For instance, $a_{ij}x_i$ implies summation over j, that is $a_{ij}x_j = a_{i1}x_1 + a_{i2}x_2 + a_{i3}x_3$, or in the same manner $\dfrac{\partial \sigma_{ij}}{\partial x_j} = \dfrac{\partial \sigma_{i1}}{\partial x_1} + \dfrac{\partial \sigma_{i2}}{\partial x_2} + \dfrac{\partial \sigma_{i3}}{\partial x_3}$.

The basic elasticity relations needed to develop strain energy expressions including thermal strain are developed in References 1 and 14 and are listed as follows:

$$\left.\begin{aligned} \epsilon_{ij} &= \frac{1+\nu}{E}\sigma_{ij} - \frac{\nu}{E}\delta_{ij}\Theta + \alpha T \delta_{ij} \quad \text{or} \\ \sigma_{ij} &= \frac{E}{1+\nu}\epsilon_{ij} + \frac{\nu E}{(1+\nu)(1-2\nu)}\Delta\,\delta_{ij} - \frac{\alpha E T}{1-2\nu}\delta_{ij}; \end{aligned}\right\} \quad \text{(Stress – strain relations)} \quad (51)$$

$$\epsilon_{ij} = \frac{1}{2}\left(\frac{\partial u_i}{\partial x_j} + \frac{\partial u_j}{\partial x_i}\right) . \quad \text{(Strain – displacement relations)} \quad (52)$$

The strain energy function (strain energy density) is defined as

$$W = \frac{1}{2}\sigma_{ij}\epsilon_{ij} . \quad (53)$$

This function can be expressed in terms of either stresses or strains by using Equations (51); thus,

$$W = \frac{1}{2}\left[\frac{1+\nu}{E}\sigma_{ij}\sigma_{ij} - \frac{\nu}{E}\Theta^2 + \alpha T \Theta\right] . \quad (54)$$

Equation (54) can be written in expanded form with the following result:

$$W = \frac{1}{2}\left\{\frac{1}{E}\left(\sigma_{11}^2 + \sigma_{22}^2 + \sigma_{33}^2\right) + \frac{2(1+\nu)}{E}\left(\sigma_{12}^2 + \sigma_{23}^2 + \sigma_{31}^2\right) - \frac{2\nu}{E}\left(\sigma_{11}\sigma_{22} + \sigma_{22}\sigma_{33} + \sigma_{33}\sigma_{11}\right) + \left(\sigma_{11} + \sigma_{22} + \sigma_{33}\right)\alpha T\right\} . \quad (56)$$

The total strain energy for a body occupying region R is then given by

$$U_e = \int_R W \, dR .$$

Making use of Equations (55) and (56), and the theorem of Castigliano, it is now possible to obtain expressions for thermal deflection in various types of structures. As a simple example, equations for the thermal deflections of cantilever beams will be developed here. The beam is shown in Diagram VI-10 together with the coordinate system adopted. The beam cross-sections are assumed symmetric about the y and z axes which are therefore principal flexural axes. The x axis passes through the centroid of all cross-sections. For simplicity, the temperature is assumed constant with y and, hence, there is no deflection in the y direction. If the simple beam theory is assumed to apply in the present case, the stress components are

$$\sigma_{11} = \sigma_x ,$$
$$\sigma_{22} = \sigma_{33} = 0 ,$$
$$\sigma_{13} = \sigma_{31} = \sigma_{xz} , \text{ and}$$
$$\sigma_{12} = \sigma_{21} = \sigma_{23} = \sigma_{32} = 0 .$$

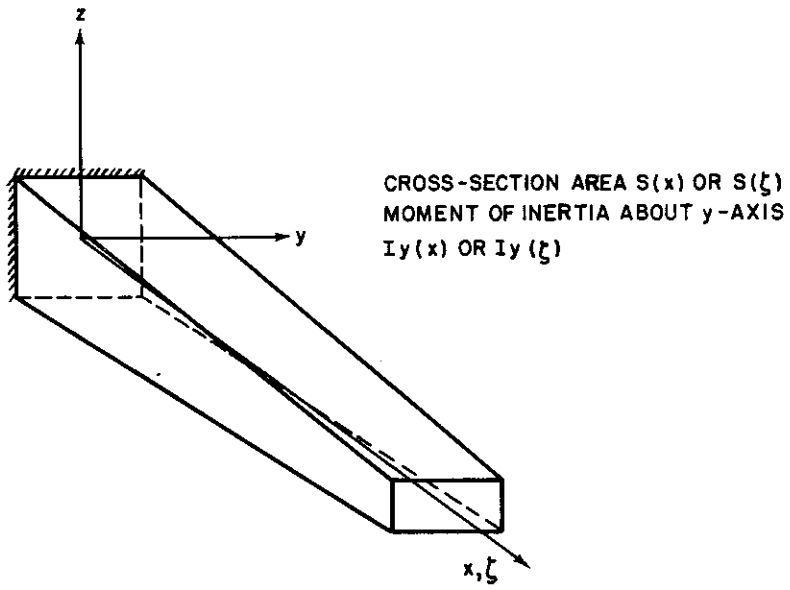

Diagram VI-10.

Then, from Equations (55) and (56), the strain energy expression for the beam is obtained as

$$U_e = \frac{1}{2} \int_0^L \int_S \left\{ \frac{1}{E} \sigma_x^2 + \frac{2(1+\nu)}{E} \sigma_{xz}^2 + \sigma_x \alpha T \right\} dS \; dx \; . \tag{57}$$

If, in addition to these simplifications, the effect of shear deformation is neglected, the strain energy expression further reduces to

$$U_e = \frac{1}{2} \int_0^L \int_S \left[\frac{1}{E} \sigma_x^2 + \sigma_x \alpha T \right] dS \; dx \; . \tag{58}$$

The lateral deflection of the beam can be calculated by applying the theorem of Castigliano to Equation (58). The result of this is easily shown (Reference 11) to be

$$X(x) = -\frac{a}{2} \int_0^x \frac{x-\zeta}{I_y(\zeta)} \int_S T(\zeta, z) \, dA \, d\zeta \; , \tag{59}$$

where $X(x)$ is the lateral deflection and ζ is a dummy variable in the x direction.

[redacted]

REFERENCES

(1) Timoshenko, S. and Goodier, J. N., "Theory of Elasticity," 2nd Edition, McGraw-Hill Book Company, New York, 1951.

(2) Kaye, J., et al., "Thermal Stresses and Deflections in Supersonic Aircraft Wings," Air Force Technical Report No. 5786, 1949.

(3) Durham, F. F. and Brull, M. A., "Thermal Stresses in Supersonic Wings," Air Force Technical Report No. 6351, Part II, 1950.

(4) Torda, P. and Hoff, N. J., "Aerodynamic Heating and Thermal Stresses," Proceedings of the Third Anglo-American Conference at Brighton, England, 1951, Page 103.

(5) Pohle, F. V. and Oliver, H., "Temperature Distribution and Thermal Stresses in a Model Supersonic Wing," Journal of the Aeronautical Sciences, January 1954, Vol. 21, No. 1, Page 8.

(6) Freudeuthal, A. M., "On Inelastic Thermal Stresses in Flight Structures," Journal of the Aeronautical Sciences, November 1954, Vol. 21, No. 11.

(7) Hilton, H. H., "Thermal Stresses in Thick-Walled Cylinders Exhibiting Temperature-Dependent Visco-Elastic Properties of the Kelvin Type," Proceedings of the Second U. S. National Congress of Applied Mechanics, Ann Arbor, Michigan, June 1954, Page 547.

(8) Schuh, H., "Transient Temperature Distribution and Thermal Stresses in a Skin-Shear Web Configuration at High-Speed Flight for a Wide Range of Parameters," KTH Aero Rapport F1 161, Stockholm, September 1954.

(9) Johnson, G. S., "Aerodynamic Heating for Structural Design," Bell Aircraft Corporation, Report 02-941-003, June 1954.

(10) Allen, H. F. and Brull, M. A., "A Study of Special and Unusual Conditions Affecting the Structural Design and Testing of High-Speed Aircraft and Missiles," Final Report, Air Force Contract No. AF33(038)-12235, University of Michigan, 1952.

(11) Brull, M. A., Dukes, W. H., and Goldberg, M. A., "Thermal Stresses in Stiffened Structures," Bell Aircraft Corporation, Report 02-984-033, December 1955.

(12) Barzelay, M. E. and Boisson, J. C., "Investigation of Stresses Due to Thermal Gradients in Typical Aircraft Structures," NACA S1 K06, January 1952.

(13) Bell Aircraft Corporation, "Structural Design for Aerodynamic Heating," Wright Air Development Center, Technical Report No. 55-305, Part I, 1955.

(14) Sokolnikoff, J. S., "Mathematical Theory of Elasticity," McGraw-Hill Book Company, 1946.

(15) Seide, P. and Taylor, E. C., "Thermal Stresses in Thick Skin Multicell Wing Structures," Northrop Aircraft, Inc., Report No. NAI-54-482, July 1954.

[redacted]

NOTES

SECTION VII

STRENGTH ANALYSIS OF HIGH-SPEED-STRUCTURES

By P.P. Bijlaard, R.E. Wong, M.A. Goldberg,
and W.H. Dukes

TABLE OF CONTENTS

LIST OF ILLUSTRATIONS

NOMENCLATURE

A = cross-sectional area of column or shell (in. ^{2}), or a constant defining a creep curve

A_r = cross-sectional area of shell stiffening ring (in. ^{2})

a = mean radius of a shell, semimajor axis of elliptical tank end, or length of a plate element (in.)

B = constant defining a creep curve

b = plate width, distance between flange centers in an H-section column, semiminor axis of an elliptical tank end, column width at any point in the cross-section (in.)

b' = width of a column cross-section at ordinate y' (in.)

C = buckling coefficient for cylinders

ΔC = incremental cylinder buckling coefficient due to pressure

$\overline{\Delta C}$ = incremental cylinder buckling coefficient representing longitudinal tension due to pressure

C_f = ring stiffness coefficient for shell stiffening rings

D = shell diameter (in.)

D_f = flexural rigidity of plate (lb-in. ^{2})

D_i = inside diameter of shell (in.)

d = depth of column cross-section (in.)

E = Young's modulus (psi)

E_{sx}, E_{sy} = average secant moduli in a plate in the x and y directions, respectively (psi)

E_T = tangent modulus (psi)

E_l = effective elastic modulus defining a creep law (psi)

e = eccentricity of an ellipse = $\sqrt{(a^2-b^2)/a^2}$

f_i = initial deflection of a column divided by column depth

f_j = $f_i/(1-\bar{\sigma}/\sigma_E)$

h = distance between flanges of an idealized H section (in.)

I = moment of inertia of column or ring (in. ^{4})

K = buckling coefficient for a plate element; constant defining a creep law

K_k = stress factor for a tank end of a particular elliptical ratio k

k = elliptical ratio for tank end = a/b

L = a constant based on elliptical ratio

L_r = ring spacing for a ring stiffened shell (in.)

$\mathscr{l}$ = pin-ended column length or shell length (in.); stringer length between ribs (in.)

M = bending moment in shell; internal moment in a column due to buckling deformation (in. -lb)

m = exponent in viscosity term of a creep law

P = $\sigma_E/(\sigma_E-\bar{\sigma})$

NOMENCLATURE (cont)

P_u = ultimate total load of a plate subjected to a nonuniform applied load (lb)

$\overline{P_u}$ = ultimate external load of a plate subjected to a uniform thermal load (lb)

ΔP_u = ultimate externally applied load on a plate carrying the nonuniform thermal stress σ_{xt} (in.)

ΔP_{ui} = ultimate externally applied load on a plate carrying the uniform thermal stress σ_{xtu} (lb)

ΔP_{uL} = ultimate externally applied load on a plate carrying the uniform thermal stress $\overline{\sigma}_{xt}$ (lb)

p = internal pressure (psi)

$\bar{p}$ = $\frac{p}{E}\left(\frac{a}{t}\right)^2$ = dimensionless pressure parameter

R = radius at center of dome (in.)

r = radius of curvature (in.)

S_l, S_L = areas under the stress curve for a plate

ΔT = temperature difference between two points (° F)

t = plate or shell thickness (in.)

t_d = thickness of tank dome (in.)

t_e = effective thickness of tank end (in.)

t_k = thickness of tank knuckle (in.)

t_y = effective thickness of shell including rings = $t + A_r/L$ (in.)

V = volume of shell ($in.^3$)

W = weight (lb)

W_t = work done by variable edge stress during plate buckling

W_u = work done by stress σ_{xu} during plate buckling

w = plate deflection normal to its plane (in.)

w_o = maximum value of w

x = coordinate of a point in the plane of a plate (in.)

y = coordinate of a point in the plane of a plate; distance across column cross-section, measured from neutral axis (in.)

y' = distance measured across cross-section from one extreme fiber (in.)

y_l = distance of neutral axis from origin of y' (in.)

α = slope of the line: $\log \epsilon_p$ against $\log \theta$ with constant stress; material coefficient of expansion (in./in.° F)

β = slope of the line σ against $\log \epsilon_p$ for constant time; the ratio a/b

δ = shortening of elemental strip of a plate during buckling

δ_o = initial deflection of a column (in.)

NOMENCLATURE (cont)

ϵ = strain (in./in.)

ϵ_1, ϵ_3 = strains at extreme fibers (in./in.)

ϵ' = bending strains produced by the deformation at buckling (in./in.)

ϵ_p = plastic strain (in./in.)

η = plasticity coefficient

θ = time

θ_{cr} = critical time for column buckling

λ = viscosity coefficient in a creep law

μ = Poisson's ratio

ρ = radius of gyration of a column (in.) or material density ($lb/in.^3$)

σ = stress (psi)

$\bar{\sigma}$ = average compression stress applied to a column (psi)

σ' = bending stress produced by the deformation at buckling (psi)

σ_{cr} = critical buckling stress for a compressive element (psi)

σ_{cy} = material yield stress (psi)

σ_E = Euler Stress for a column (psi)

$\bar{\sigma}_{mx}\ \bar{\sigma}_{my}$ = maximum membrane stress in the x and y directions respectively, due to stretching of a plate during buckling, with nonuniform applied stress (psi)

$\sigma_{mxu}\ \sigma_{myu}$ = membrane stresses in the x and y directions respectively, due to stretching of a plate during buckling with uniform applied stress (psi)

$\bar{\sigma}_{mxu}\ \bar{\sigma}_{myu}$ = maximum values of σ_{mxu} and σ_{myu}

$\sigma_x\ \sigma_y$ = stresses in the x and y directions respectively (psi)

σ_{xe} = edge stress in a plate after buckling (psi)

σ_{xn} = nonuniform edge stress applied to a plate (psi)

$\bar{\sigma}_{xn}$ = maximum value of σ_{xn}

σ_{xp} = postbuckling stress of a plate (psi)

σ_{xt} = nonuniform thermal stress applied to a plate (psi)

$\bar{\sigma}_{xt}$ = maximum value of σ_{xt}

σ_{xta} = average value of σ_{xt}

σ_{xtu} = uniform thermal stress applied to a plate (psi)

σ_{xu} = uniform compressive stress applied to a plate (psi)

σ_{ULT} = average ultimate stress in a plate (psi)

τ_{cr} = critical value of time parameter

[redacted]

SECTION VII

STRENGTH ANALYSIS OF HIGH-SPEED STRUCTURES

A. GENERAL

As defined in the Introduction of the report, the objectives of this study include the compilation and development of methods for analysis of high-speed structures, and the discussion of many methods of structural design for high-speed aircraft. It is the intent of this section of the report to satisfy the first of these objectives with particular regard to the analysis of unprotected structures, and also to provide data for the discussion of structural design at elevated temperatures that follows in Part III. This section only collects and presents the analytical methods and no conclusions or implications are drawn from the results.

While the methods given herein are needed for the stress analysis of high-temperature structures, they are also the means by which the optimum design stress values given in Section IX are translated into structural proportions and sizes.

In this section, Parts B and C are devoted to the elevated temperature analysis of conventional structural elements such as columns and plates; the effects of elevated temperature are considered in Part B, and the effects of temperature gradients are covered in Part C. Part D is concerned specifically with the design of integral and nonintegral pressure vessels which, for reasons explained later, are sufficiently important to justify a special part of this section.

Structural metallic materials exhibit two important effects when exposed to temperature, and these effects must be considered in the design of all elements that operate at temperature. The first effect, an immediate reduction of strength and stiffness when heat is applied, is discussed in the first portion of Part B. Here it is shown how this effect is included in the design of tension members, columns, and plates. It is shown also that such structural elements may be analyzed by utilizing the theories developed for use at room-temperature. The main contribution of this work is in the convenient graphical results (see Part I) which include the elevated temperature material properties.

The second significant effect of elevated temperature is the time during which loads are sustained. The second portion of Part B is concerned with methods for the design of structural elements subjected to both elevated temperature and long-time loading. Again, graphical results greatly facilitate the practical application of these methods.

The work of Section VI shows that the relative rates of temperature buildup in the outer skin of a vehicle, and the diffusion of heat with the structural interior, may be such that significant gradients are developed throughout the structural members. Section VI also gives methods of calculating the stresses produced by these temperature gradients. Part C of this section contains a discussion on the inclusion of thermal stresses into the stress analysis of structures, and methods are given for predicting the allowable strength of compression elements when thermal stresses are present. Wherever possible the results are presented in graphical form to simplify and speed their use in design. However, the problem is too complex in some cases for such general treatment and, at least for the present, only methods are given.

In the study of structural elements subjected to both applied loads and thermal loads, only the effects of temperature on the material properties have been included. Generally, at the temperatures and stress levels which will lead to efficient design, the total time of application of design loads must extend into a number of hours before the effects of time become appreciable on the material characteristics. Thermal stresses, however, are usually transient effects and peak values may prevail for only a few seconds during each flight so that it is impractical to consider "long-time" thermal stresses.

[redacted]

The significance of pressure vessels in the structure of hypersonic aircraft has been explained in Section I. For speeds beyond approximately Mach 3.0, it is expected that all ground-launched vehicles will require large boosters in which almost all the structure will be a pressure vessel. The importance of weight alone, therefore, justifies careful consideration of the design of such vessels, but the pressure vessel has two other characteristics which emphasize the need for close study. Because of its symmetry and uniformity, the pressure vessel is more amenable to optimization than is the case with many structures. Consequently, the results of optimization studies can generally be incorporated without excessive modification by such practical considerations as edge distances, bend radii, rivet sizes, and minimum thicknesses. These factors, although small and very detailed, are the reasons why elaborate analytical structural optimization studies are often severely limited when applied to practice, and why much of the "art" still remains in good structural design.

The second characteristic of pressure vessels to justify a more-than-usually detailed study of the structural design is the fact that high stress levels are carried continuously. The principal operating loads (pressure) are not subject to the wide fluctuations such as inertial effects that occur in the remainder of the airframe. It is, therefore, economical from a weight standpoint to design so that the normal operating pressure load develops a stress approaching yield. Low-cycle fatigue thus becomes a significant factor because of the high stress level, and stress concentrations and discontinuities should be minimized. These considerations are doubly important to pressure vessel design because the biaxial state of stress does not permit the usual amount of yielding before failure, and also because pressurized gas is usually contained so that large amounts of energy are available to convert a small failure into complete disintegration of the vessel.

Considerable theoretical and experimental design work on pressure vessels of the quality required for airframe construction, has been accomplished. The simple membrane formulas are found in any textbook, and References 14 and 26 consider the local bending effects at the discontinuity between the shell and the heads. Stability under external pressures is discussed in References 27 through 31, and Reference 16 covers the case where the vessel is an integral tank, with internal pressure and body bending or compressive loads. Reference 12, representing an accumulation of many years of practical experience with pressure vessels, establishes the design and testing criteria that may be used safely.

Among the problems that are not covered in the literature is the case where a vessel is an integral part of the body and is stabilized against compressive buckling both by internal pressure and by internal ring stiffeners. Such a case may arise when the body bending moments are large so that it is not economical to use an unstiffened shell. In these circumstances, the problem is better considered as a ring-stiffened cylinder with pressure providing additional stabilization since the rings will generally be the principal stabilizing agent. Methods for predicting the compression instability of such a structure are given in this section together with optimization of proportions for a given loading condition. The optimization work is included here, rather than in Sections VIII and IX, because it optimizes structural proportions only for a given material and temperature, while Sections VIII and IX also optimize the material and its operating temperature.

As an aid to pressure vessel design, formulas are given in this section for the rapid prediction of weight and the preliminary design of airframes. Although the results of these methods are mathematically simple, they represent an accumulation of much experience in establishing safe proof-stress levels and in identifying which items of the tank control the design and the weight.

All previous work on pressure vessel design for aircraft, including the items described previously, has been done for room-temperature or low-temperature applications. In applying pressure vessels to elevated temperature structures, the first consideration is not the elevated temperature strength of the tank, but rather the limiting temperatures for the contents of the tank or for the vapors or gases remaining after the propellants are expended. The final item in this section discusses these questions and advances the conclusion that, generally, propellant tanks should not be subjected to high temperatures, but must be protected. Values are given to substantiate this conclusion, and, as a result, no additional work has been done on elevated temperature pressure vessels.

[redacted]

B. ANALYSIS OF TEMPERATURE EFFECTS

1. Short-Time Loading

The metallurgical response of various materials to elevated temperature and the resulting changes in mechanical properties under loads applied for a short time are discussed fully in Section III; values of the mechanical properties are presented graphically in Section 2.0 of Part I.

The term "short-time loading" infers a loading time sufficiently short that material properties do not change significantly during the time of load application. This is almost invariably the case for any single application of the critical loads found in airframe structures, with the possible exception of pressure loads in propellant tanks and pressurized compartments. If the material properties do not change during load application, the effects of elevated temperature can be dealt with by means of the analytical methods developed for room-temperature structures, using the stress-strain curve appropriate for the material in its new condition.

a. Tension Members

In the design of tension members for short-time loading, the material properties can be taken directly from the curves of Section 2.0, Part I, for the appropriate temperature.

b. Columns

For the design of stable section columns, the modified Euler formula is used in which the tangent modulus replaces the elastic modulus when the elastic limit is exceeded. Column curves developed in this basis are given in Section 4.0 of Part I, with the tangent moduli taken from Section 2.0.

c. Plates and Shells

A comprehensive method of treating the elastic and plastic buckling of plate elements is presented in References 1 and 2 in which the buckling stress is given by

$$\sigma_{cr} = \left\{ \left(K\pi^2 \eta E\right) \Big/ \left[12\left(1-\mu^2\right)\right] \right\} \quad (t/b)^2 ,$$

where η is a plasticity coefficient which incorporates all the effects of nonlinearity of the stress-strain relationship of the material, and is a complex function of the tangent and secant moduli. Expressions and curves for the calculation of η for various loading conditions and structural geometries are given in Reference 2.

Based upon the afore-mentioned formula, compression buckling curves for long plates subjected to short-time loading at elevated temperatures are given in Section 4.0 of Part I, considering a variety of materials and temperatures. Values of η for these curves have been calculated with the curves presented in Reference 2, and with the material properties given in Section 2.0 of Part I. Similarly, the values of E and μ appropriate for the particular material and temperature under consideration are taken from Section 2.0, Part I.

2. Long-Time Loading

As discussed in Section III, materials exposed to elevated temperatures for extended periods of time exhibit further reduced mechanical properties under short-time loading. When the loading is sustained, the yield and ultimate strengths may be reduced still further. Materials subjected to long-time loading may show a continuous increase in strain under constant load at stress levels which, under short-time loading, are in the elastic range. This characteristic of a material is known as creep, and its extent is a function of load intensity and temperature. If the load is maintained long enough, materials can fail in tension generally after considerable strain and at a lower stress than under short-time loading; this phenomenon is known as stress rupture. Numerical values of creep strain and stress rupture for various materials and temperatures are presented in Section 2.0 of Part I.

[redacted]

[redacted]

Methods of analysis for predicting the strength of structures in compression and under long-time loading are complex and have received considerable attention, particularly the creep buckling of columns. Failure in creep can also be defined to occur from aerodynamic considerations when the distortions of the structure exceed a certain amount. The analysis of portions of structure loaded in tension has not received much analytical treatment. Therefore, it is only the approaches to such treatments that are given herein.

While the subsequent discussions and methods of analyses are based upon a constant temperature and loading condition, in the practical airframe there is a frequency-time-loading-temperature spectrum peculiar to each aircraft and mission. As discussed in Section III, it may be possible with some materials and temperature levels to represent the actual spectrum by an equivalent constant load-temperature condition. If sufficient test data are not available with which to do this, it is suggested that an arbitrary conservative constant condition be established for preliminary design, and that material and structural element tests then be conducted in the laboratory to verify the assumption.

a. Tension Members

The effects of creep in tension members is analogous to the effects of yielding at room temperature. The creep strain at failure, moreover, is a function of whether the structure is monolithic, or is perforated by rivets or bolts attaching ribs or frames to the external skin.

Consider a solid wing of essentially rectangular cross-section, uniformly heated and unperforated. Under a given loading at which creep occurs, the stress distribution through a cross-section will, in time, change FROM A TRIANGULAR ONE TO A CURVED ONE, ALMOST IDENTICAL TO THAT BELONGING TO A STRESS-STRAIN CURVE AS GIVEN BY THE PERTINENT ISOCHRONOUS CURVE. If the stress level is essentially constant along most of the span, an exhorbitant tip deflection results for a maximum fiber strain of 1%. Failure in this case would be represented by an intolerable airload redistribution and/or the loss of stability and control.

In hollow, monolithic structure, failure due to creep should prove to be based upon the same criteria. If the structure is subject to shear lag, creep like yielding, as explained in Reference 39, should reduce the shear lag and the structure should assume a more uniform stress distribution.

Extending the analyses and test results of perforated materials at room temperature given in Reference 39 which show that built-up riveted structures fail at small values of gross strain, this type of construction subject to material creep at elevated temperatures should fail by stress rupture at low values of gross strain and through a row of perforations. For these structures, therefore, stress rupture is likely to be the design criteria rather than permanent distortion of the structure.

From the preceding discussions, it appears that, in the selection of materials for airframes subjected to long times at load, the type of structure must be considered along with a detailed study of permissible distortions.

One other effect of creep that should be considered in the design of tension members is its action at stress concentrations, such as rivet holes. Some test results are available on the creep strength of riveted joints in Reference 20.

Theoretical consideration has been given to the influence of creep on the concentrations that occur around each rivet in the general area of a stringer-stiffened skin panel under tension. Evidently, the highly stressed material fibers will creep more rapidly than those away from the concentration, and the resulting deformation will relieve the high stresses and tend to make the general stress distribution more uniform. This effect, similar to that of plastic deformation, is somewhat more pronounced than would follow from considering the pertinent isochronous curve as the stress-strain diagram of the material. Also, this creep effect occurs with stresses below the so-called elastic limit.

From these arguments it seems that creep at stress concentrations is a relieving agent and can be ignored. However, before this can be applied safely to design, some study must be given not only to the actual strains involved, since stress rupture may occur, but also to the residual stresses remaining after removal of load, due to permanent deformations. These residual

[redacted]

stresses may be significant in reducing the fatigue life of a tension member that experiences elevated temperature and prolonged and repeated loading.

As mentioned previously, there is no evidence of theoretical work on this subject, but it is evident that the problem is one that requires extensive experimental work to obtain reliable results. Until such work is undertaken, no conclusions can be made.

b. Compression Members

Before considering the design of compression members for long-time loading, it is necessary to explain the significance of creep when applied to unstable compression elements, as well as to explain isochronous or time-dependent stress-strain curves.

Consider a compression element operating under constantly applied load and at a uniform elevated temperature, with the conditions such that the material creeps at a rate which increases with the local intensity of loading. If a small initial eccentricity exists, so that the structural element is subjected to a small bending moment in addition to the compression loads, then the resulting stress gradient will cause varying amounts of creep across the section. Higher creep rates at the more highly stressed fibers cause an increase of eccentricity with time, until a value of deflection is reached at which the element fails. Thus, as a result of the creep phenomenon, a structure carrying a constant compression load will fail if the load is sustained for sufficient time.

In the analysis of creep buckling of structural elements, it will be convenient, as shown in the discussions that follow, to use the creep data in the form of isochronous stress-strain curves. Creep data are generally obtained by performing tests in which a constant load is applied to the test specimen, and strain is measured periodically. The results become a graphic plot of strain against time for various values of stress. By suitable cross-plotting, however, this information can be presented as stress against strain in which all points associated with the same time are connected, giving a constant time curve. The resulting curves, representing stress against strain for a constant time and temperature, are called isochronous stress-strain curves. It should be noted that, despite their importance in analysis, isochronous stress-strain curves have no physical basis and cannot be reproduced in a test.

Brief consideration will show that the creep buckling problem is complex because of its mathematical nonlinearity and because of the arbitrary nature of creep characteristics of materials. It is not surprising that various approaches to the solution of this problem have been made by a number of authors. These methods are summarized briefly in the following, together with the relative merits of each method and comparisons with test results where available.

c. Columns

The most simple and generalized method is presented in Reference 3. The authors of Reference 3 consider columns, with a given initial crookedness at a given temperature, which must sustain a compressive load during a given time. It is shown that the compressive load which this column will sustain during the given time can be determined conservatively by the following method.

Instead of the actual column, Reference 3 considers a column with the same initial crookedness and consisting of a noncreeping material with a stress-strain diagram equal to the isochronous stress-strain diagram for the material of the actual column and for the given temperature and time. The ultimate load of the column being considered is determined by assuming that the initial deflection has a sinusoidal shape and that this same shape is maintained for the additional deflections, in the manner explained in Reference 4, pages 51 through 63. The ultimate load so determined gives a conservative approximation for the load that the actual column can sustain at the given temperature during the given time. The test results are in good agreement with the calculations of Reference 3.

The authors of Reference 3 conclude that the tangent modulus load

$$\sigma_{cr} = \frac{\pi^2 E_T}{(\ell/\rho)^2} ,$$

where E_T is obtained from the isochronous stress-strain diagram, is a good approximation, but that this should be checked. This check is not performed in Reference 3, but it is a simple matter to calculate the tangent modulus loads from their isochronous stress-strain curves. The results are as follows:

350° F, 200 hours

σ_{cr} (psi x 10^{-3})	E_T from Figure 4, Reference 3 (psi x 10^{-3})	$\ell/\rho = \pi\sqrt{\frac{E_T}{\sigma_{cr}}}$
7.2	2700	61
6	5500	95
5	6600	114

450° F, 200 hours

σ_{cr}	E_T from Figure 5, Reference 3	$\ell/\rho = \pi\sqrt{\frac{E_T}{\sigma_{cr}}}$
3	3700	110
2	5700	168

Plotting the results for 350° and 450° F in Reference 3, Figures 7 and 9 respectively, the values for 350° F are exactly on the curve through the test points. Those for 450° F are a maximum of 30% above the experimental values. Also, the (eccentric) loads computed in Reference 3 are approximately 15% above the test points. However, the calculations and tests were made with an initial eccentricity of $\ell/1200$, so it seems probable that tests without applied eccentricities would be in good agreement with the computed tangent modulus values from the isochronous-stress-strain curves.

Additional confirmation of the isochronous tangent modulus method for predicting creep buckling of columns is provided by the test results included in Reference 9. This reference gives column creep curves for 7075-T6 aluminum alloy plotted against a time-temperature parameter. Selecting two extreme values of this parameter, 16 and 20, Figure VII-1 shows creep buckling stresses against ℓ/ρ as taken from Reference 9, and also as calculated by the isochronous tangent modulus method. Material properties for the calculated values were taken from Section 2.0 of Part I where, it should be noted, creep data are also plotted against the same time-temperature parameter as used in Reference 9. The curves of Figure VII-1 show conservatism in the isochronous tangent moduli method.

Kempner's Method

The method of Kempner is given in Reference 5. From Equation (1) of Reference 5, it is assumed that

$$\frac{d\epsilon}{d\theta} = \frac{1}{E_1}\frac{d\sigma}{d\theta} + \frac{1}{\lambda}\sigma^m . \qquad (1)$$

In a conventional creep test, σ is constant. Hence, from Equation (1), with $\sigma = \sigma_0$,

$$d\epsilon = \frac{1}{E_1} d\sigma_0 + \frac{1}{\lambda}\sigma_0^m \, d\theta \text{ , and}$$

$$\epsilon = \frac{1}{E_1}\sigma_0 + \frac{1}{\lambda}\sigma_0^m \theta + C . \qquad (2)$$

At $\theta = 0$, $\epsilon = \epsilon_0 = \sigma_0/E_1$, so that from Equation (2),

$$\epsilon_0 = \frac{1}{E_1}\sigma_0 + C = \frac{1}{E_1}\sigma_0$$

and $C = 0$. Hence, Equation (2) becomes

$$\epsilon = \frac{1}{E_1}\sigma_0 + \frac{1}{\lambda}\sigma_0^m\theta\,; \quad \text{also,} \tag{3}$$

$$\epsilon_0 = \frac{1}{E_1}\sigma_0\,. \tag{4}$$

Dividing Equation (3) by Equation (4),

$$\frac{\epsilon}{\epsilon_0} = 1 + \frac{E_1}{\lambda}\sigma_0^{m-1}\theta\,, \tag{5}$$

which is identical with Equation (2) of Reference 5. From Equation (3) the creep curves for stresses $\sigma_0=\sigma_1$ and $\sigma_0=\sigma_2$ are assumed to be straight lines in the $\epsilon - \theta$ diagram:

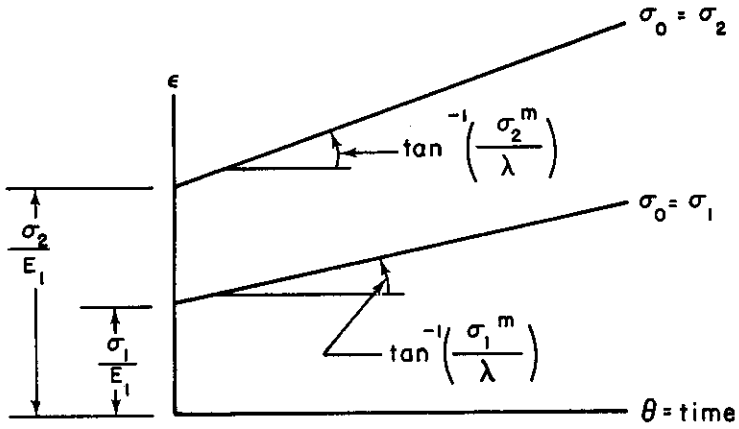

If the creep curves can actually be approximated by such straight lines, E_1 is determined by the ordinates at $\theta = 0$, which are σ_1/E_1 and σ_2/E_1, for $\sigma_0=\sigma_1$ and $\sigma_0=\sigma_2$, respectively. The tangents of the slope angles of the straight lines are, from Equation (3), σ_1^m/λ and σ_2^m/λ, for $\sigma_0 = \sigma_1$ and $\sigma_0 = \sigma_2$, respectively. If

$$\left.\begin{aligned} \frac{\sigma_1^m}{\lambda} &= P \\ \frac{\sigma_2^m}{\lambda} &= Q \end{aligned}\right\}, \tag{6}$$

where P and Q are measured from the creep curves,

$$\left(\frac{\sigma_1}{\sigma_2}\right)^m = \frac{P}{Q}\,,$$

or

$$m \log\frac{\sigma_1}{\sigma_2} = \log\frac{P}{Q}\,,$$

so that

$$m = \frac{\log(P/Q)}{\log(\sigma_1/\sigma_2)}\,. \tag{7}$$

[redacted]

To find better values for m, curves for other stresses, $\sigma_0 = \sigma_3$, $\sigma_0 = \sigma_4$, etc., should be considered. It is then found from Equation (6) that

$$\lambda = \sigma_1^m / P \quad \text{or} \quad \lambda = \sigma_2^m / Q \ . \tag{8}$$

With known values for E_1, m, and λ, one calculates that $\sigma_E = \dfrac{\pi^2 E_1 I}{A \ell^2}$. (9)

Assuming that f_i equals the initial deflection of an unloaded column divided by h, where h is the depth of the column, then

$$f_j = \frac{f_i}{1 - \dfrac{\bar{\sigma}}{\sigma_E}} \ ,$$

where σ_E is given by Equation (9), and $\bar{\sigma}$ is the average compressive stress assumed in the column. With m and f_j, one finds from Figures 4 through 6 of Reference 5 a value for τ_{cr}, where

$$\tau_{cr} = \frac{E_1 (2\bar{\sigma})^m}{4\lambda \left(\sigma_E - \bar{\sigma}\right)} \theta_{cr} \ ,$$

so that the critical time is

$$\theta_{cr} = \frac{4\lambda \left(\sigma_E - \bar{\sigma}\right)}{E_1 (2\bar{\sigma})^m} \tau_{cr} \tag{10}$$

Libove's Method

The method of Libove is given in References 6 and 7 for H columns and rectangular columns, respectively. This method applies to materials with creep curves that are straight if plotted in a $\log \epsilon_p - \log \theta$ diagram. Such a creep curve is shown in Reference 8 for 75S-T6 at 600° F. These creep curves are also straight lines in the $\sigma - \log \epsilon_p$ diagram. Here, ϵ_p represents: plastic strain equals total strain minus elastic strain. In this case, the total strain is given as

$$\epsilon = \frac{\sigma}{E} + A e^{B\sigma} \theta^K \ , \tag{11}$$

or

$$\epsilon_p = \epsilon - \frac{\sigma}{E} = A e^{B\sigma} \theta^K \ . \tag{12}$$

The constants A, B, and K can be derived from the creep tests. From Equation (12),

$$\log \epsilon_p = \log A e^{B\sigma} + K \log \theta \ , \tag{13}$$

so that K is found from the lines in the sketch as

$$K = \tan \alpha \ , \tag{14}$$

[redacted]

[redacted]

where α is the slope angle of the lines for constant σ. Further from Equation (12),

$$\log \epsilon_p = \log A\theta^K + \log e^{B\sigma}$$

$$= \log A\theta^K + B\sigma \ ,$$

or

$$\sigma = -\frac{1}{B} \log A\theta^K + \frac{1}{B} \log \epsilon_p \ .$$

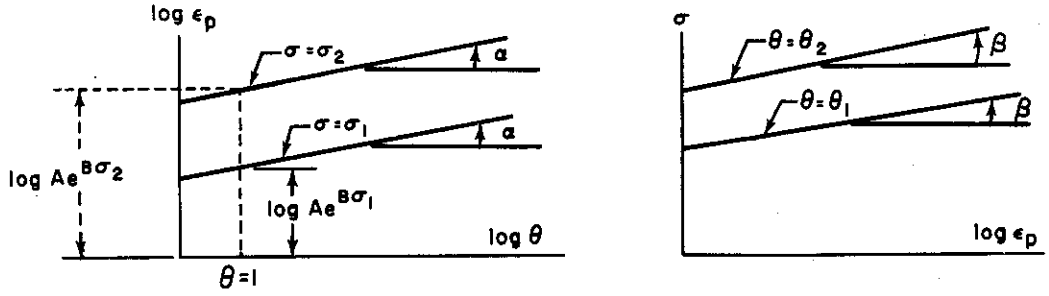

Hence, from the lines for constant time θ in this sketch, $\frac{1}{B} = \tan \beta$, so that

$$B = \cot \beta \ . \qquad (15)$$

Finally, from Equation (13), for $\theta = 1$ or $\log \theta = 0$,

$$\log \epsilon_p = \log Ae^{B\sigma} \ ,$$

so that $A = \dfrac{(\epsilon_p)_{\theta=1}}{e^{B\sigma_1}}$

or $A = \dfrac{(\epsilon_p)_{\theta=1}}{e^{B\sigma_2}}$ (16)

for $\sigma = \sigma_1$, or $\sigma = \sigma_2$, respectively, where B is given by Equation (15).

After calculating A, B, and K from Equations (14) through (16), and assuming an initial deflection δ_0 and an average stress $\bar{\sigma}$, the Euler stress for the column is calculated using E for the given temperature

$$\sigma_E = \frac{\pi^2 E}{(\ell/\rho)^2} \ .$$

If the column is of the H section type, then, from Reference 6,

$$\gamma_R / \gamma_L = e^{-(B/K)\left[\sigma_L(o) - \sigma_R(o)\right]}$$

where

$$\sigma_L(o) - \sigma_R(o) = 4\bar{\sigma} \frac{\delta_0}{b} \frac{\sigma_E}{(\sigma_E - \bar{\sigma})}$$

[redacted]

and b is the distance between the centers of the column flanges. With this value of γ_R / γ_L and the value of K from Figure 5 of Reference 6, the value of $\theta_{cr} \gamma_L$ is found where

$$\gamma_L = \left(\frac{AEB}{2K} \frac{\bar{\sigma}}{\sigma_E - \bar{\sigma}} \right)^{1/K} e^{(B/K)} \sigma_L(o) \quad \text{and}$$

$$\sigma_L(o) = \bar{\sigma} \left[1 + 2 \frac{\delta_o}{b} \left(\frac{\sigma_E}{\sigma_E - \bar{\sigma}} \right) \right] ;$$

hence,

$$\theta_{cr} = \frac{\gamma_L \theta_{cr}}{\gamma_L} .$$

For a rectangular column as considered in Reference 7,

$$S = e^{-\frac{6B\bar{\sigma}}{K} \frac{\delta_o}{b} \frac{\sigma_E}{\sigma_E - \bar{\sigma}}} .$$

Replacing the label γ_R / γ_L in Figure 5 of Reference 6 by S, and replacing the label $\gamma_L \theta_{cr}$ by $\left(\frac{3P}{4} - \frac{1}{2} \right)^{1/K} S^{-1/2} \theta'_{cr}$, with S and K one then finds from Figure 5 of Reference 6 the value of

$\left(\frac{3P}{4} - \frac{1}{2} \right)^{1/K} S^{-1/2} \theta'_{cr}$, where $P = \frac{\sigma_E}{\sigma_E - \bar{\sigma}}$ and $\theta'_{cr} = \theta_{cr} \left(\frac{AEB}{K} \right)^{1/K} e^{B\bar{\sigma}/K}$,

so that θ_{cr} can be calculated since all other values are known.

Evidently, the methods of Kempner and Libove, while more refined and having better physical basis than the isochronous tangent modulus method, are more complicated. Moreover, they lack generality since it is necessary to specify initial deflection, a factor which is usually unknown. In the case of Libove's method, the results are a function of the cross-sectional shape. Furthermore, both methods are applicable only to materials of which the creep characteristics approach those given by Equations ( ) or ( ). These methods are therefore suitable for detailed analysis, but are not appropriate for the simple generalizations required in the present work, or for preliminary design generally. It is questionable whether available creep data, particularly for the materials that will be used at higher temperatures, is sufficiently complete and accurate to justify the use of complex creep buckling formulas.

It is proposed, therefore, that the loads a column can sustain, under specified conditions of temperature and time, should be determined as the tangent modulus loads using the isochronous curves as stress-strain curves. Column curves computed as these tangent modulus loads are given in Section 4.0 of Part I for a range of materials and temperatures. These curves have been calculated using the creep data of Section 2.0, Part I.

d. Plates and Shells

A search of available literature has revealed no work on the creep buckling of plates and shells which parallels methods of Kempner and Libove for columns. However, if the isochronous stress-strain curve method is satisfactory for column design, then it seems likely that this technique can also be applied to creep buckling of plates and shells. Methods for predicting plate buckling when stresses exceed the elastic limit (that is, when the stress-strain curve becomes nonlinear), are given in References 1 and 2. It is proposed that these methods be applied to creep

buckling by calculating the plasticity coefficients, η, using secant and tangent moduli from the isochronous stress-strain curves.

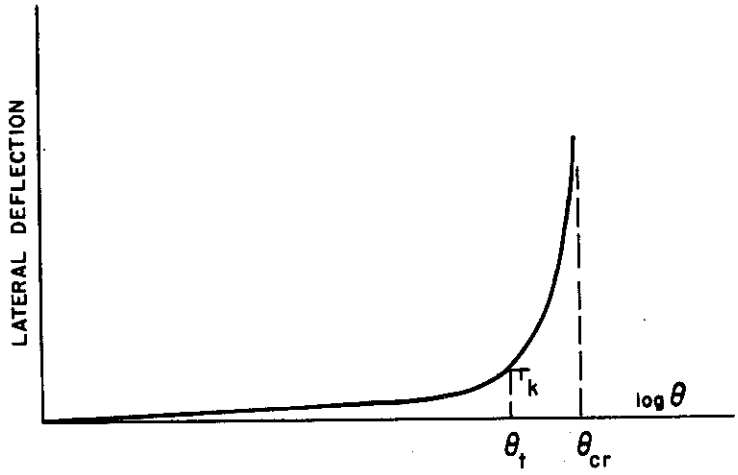

Since this computation neglects the membrane stresses that occur at greater plate deflections, these creep buckling loads would actually apply to, say, the "top of the knee" of the time-deflection curve. That is, the creep buckling load at a given temperature and for a given time interval of, say, 10 hours, would apply to the load under which the deflection would reach the "top of the knee" T_k in the preceding sketch after $\theta = \theta_t = 10$ hours. To find the ultimate load under which the plate fails after a given time, say, θ_{cr} hours, the membrane stresses must be taken into account. This can be done by considering again the pertinent isochronous curve as the stress-strain diagram. Hence, for simply supported plates with unloaded edges that are not held straight in the plane of the plate, the ultimate creep load is given by Equation (2) in Figure 5 of Reference 22, which in Figure 31 of Reference 11 is shown to be in excellent agreement with recent test data, so that

$$\sigma_{ULT} = \sqrt{\sigma_{cr}\ \sigma_{cy}} - 0.25\ \sigma_{cr} \ ,$$

where σ_{cr} is determined from the isochronous curves as explained previously. If σ_{ULT} is lower than σ_{cr}, which occurs if $\sigma_{cr} > 0.64\ \sigma_{cy}$, σ_{cr} determines the ultimate load.

If the edges of the simply supported plate are held straight in the plane of the plate, Equation (64), derived in the present section, applies for the ultimate load, so that

$$\sigma_{ULT} = \sigma_{cy} - 1/2\ \sigma_{cr} \left[-0.545 + \sqrt{1.54\ \frac{\sigma_{cy}}{\sigma_{cr}} - 0.0865} \right]^2 .$$

Similarly, for simply supported flanges or cruciform sections, for H sections, and Z sections or channels, the graphs and formulas in Figure 18 of Reference 35 can be used. With the present notations the formula for H beams is

$$\sigma_{ULT} = 0.80\ \left(\sigma_{cr}\ \sigma_{cy}^4\right)^{1/5} \ ,$$

and that for Z beams and channels is

$$\sigma_{ULT} = 0.77\ \left(\sigma_{cr}\ \sigma_{cy}^4\right)^{1/5} .$$

[redacted]

In these cases also, the governing ultimate stress is either σ_{ULT} or σ_{cr}, whichever is the smaller.

Plate buckling curves, giving σ_{cr} have been prepared in the manner discussed previously, and are included in Section 4.0 of Part I based upon the creep data of Section 2.0 of Part I.

C. ANALYSIS OF TEMPERATURE GRADIENT EFFECTS

1. Temperature Gradients in Columns

Consider a column having a cross-section as shown in the following sketch and subjected to a linear temperature gradient across the section. The temperature distribution is constant along the column. If the column is built in at the ends, or if it is continuous over a number of supports so that complete end restraint is provided by symmetry, then the expansions due to temperature are resisted by moments at the ends. Since the thermal strains are constant at all points along the column and the end moments produce a constant internal moment at all points along the column, the thermal strains are cancelled and the column remains straight. It is assumed that the thermal stresses are produced only by the restraint against end rotation and that the general expansion of the column is unrestrained. This is typical of a wing skin panel where the complete panel would be unrestrained against a general spanwise expansion appropriate for the average temperature, but where the local expansions due to gradients across the sections of individual stringers are prevented by continuity of the stringers across the ribs.

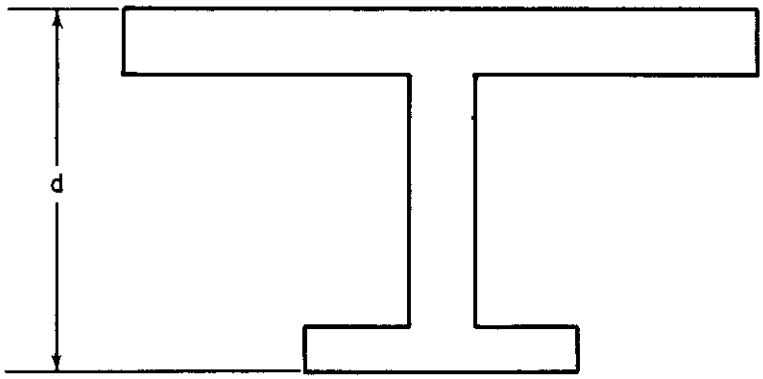

For internal stringers, the moments above the ribs are approximately equal if the stringers are initially straight and continuous over many ribs with equal spacing, and if the temperature gradient does not vary along the length of the stringers and is equal for all stringers. Thus, the end rotations caused by the temperature gradient are cancelled, and the stringers remain straight until the buckling load is reached. For stringers located at the ends of the panel (such as near the wing tip), unless the stringer ends are clamped, the moments above the supports will not be equal, and some initial deflections will occur. Therefore, Reference 11 considers (1) the case of a column with no initial deflection from temperature gradient, and (2) the case of a pin-ended column with initial deflection from temperature gradient. Stringers located near the ends fall between these two cases; the closer this problem is to the first case, the more the extreme ends of the stringers are restrained against rotation. Reference 11 also presents the case of an elastically restrained column with a temperature gradient.

This section of the report considers only the initially straight column. The pertinent buckling stresses for various materials have been computed and are presented for this case in Section 4.0 of Part I. Since the other cases of end restraint effects have not been evaluated, these results may seem to lack conservatism when applied to end bay stringers without rotational end restraints. On the other hand, a small rotational end restraint can cancel the influence of eccentricity, as can be seen from the graphs in Figures 24 and 25 of Reference 36.

[redacted]

Since, with the assumption of initial straightness, the thermal stresses do not result in incipient buckling, the only consequence is their addition to the applied stress. Thus, it follows that the applied external load at which the elastic limit is exceeded in a particular fiber is modified by the presence of thermal stress. The problem is therefore reduced to the buckling of a column in which the material characteristics vary across the column cross-section, and this variation is dependent upon the distribution of thermal stress and temperature.

The problem is treated here by using the Euler buckling formula, but including an effective stiffness. The most convenient procedure for using the solution is that of assuming a known strain distribution which leads directly to an average stress. An effective stiffness is then calculated, and finally the required ℓ/ρ to make the average stress a critical value. While this procedure is not convenient for the direct analysis of a given column, it has been used satisfactorily for the production of design curves.

Before buckling, the conditions in the column are as follows:

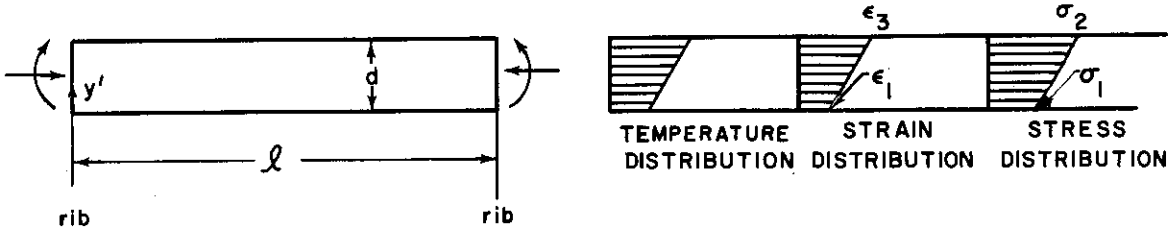

AVERAGE STRESS $\bar{\sigma} = \frac{1}{A}\int_0^d \sigma b' dy' = \frac{1}{A}\int_{\epsilon_1}^{\epsilon_3} \sigma b' \frac{dy'}{d\epsilon} d\epsilon$, AND ASSUMING $\frac{dy'}{d\epsilon}$ = CONSTANT = $\frac{\Delta y'}{\Delta \epsilon}$,

$$\bar{\sigma} = \frac{1}{A\left(\frac{\Delta\epsilon}{\Delta y'}\right)} \int_{\epsilon_1}^{\epsilon_3} b'\sigma d\epsilon = \frac{d}{A(\epsilon_3 - \epsilon_1)} \int_{\epsilon_1}^{\epsilon_3} b'\sigma d\epsilon.$$

At incipient buckling the infinitely small deflection of the column superimposes a new system of strains on the previous system due to flexure of the cross-section. This strain is accompanied by stresses which give rise to a pure bending moment that controls the tendency to buckle. IDENTIFY THAT PART OF THE EXTRA STRAINS AND STRESSES WHICH CAUSES THE PURE BENDING MOMENT AS ϵ' AND σ', RESPECTIVELY.

Note that σ' and ϵ' are only infinitely small increments over and above the strains and stresses due to the applied load and the thermal effects. Since from Shanley's concept, Reference 19, the stress increases at all points, THE INCREMENTS σ' AND ϵ' CAN BE RELATED to the stress through the tangent modulus. Therefore,

$$\sigma' = \frac{d\sigma}{d\epsilon}\ \epsilon' = E_T\ \epsilon' \quad .$$

Since ϵ' is the strain due to flexure, then ϵ' equals y/r, where y is measured from the "neutral axis" for the superimposed stresses σ' and r is the local radius of curvature of this axis.

Total load due to σ' is therefore equal to $\int_0^d b'\sigma' dy$ equals zero. But σ' equals $E_T \epsilon'$ and ϵ' equals $\frac{y}{r}$, hence $\int_0^d \frac{b'}{r} E_T\ y\ dy$ equals zero.

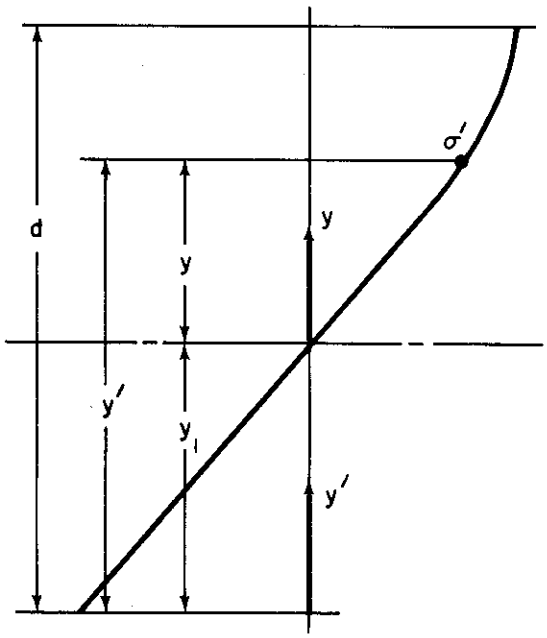

Adding the term $\int_o^d \frac{b'}{r} E_T y_1 dy$ to both sides gives

$$\int_o^d \frac{b'}{r} E_T (y + y_1) dy = y_1 \int_o^d \frac{b'}{r} E_T dy ,$$

where y_1 determines the position of the "neutral axis." But $(y + y_1)$ equals y' and dy equals dy', and r is a constant. Therefore,

$$y_1 = \frac{\int_o^d b' E_T y' dy'}{\int_o^d b' E_T dy'} .$$

This is equivalent to taking moments of area in the usual manner, but "weighting" the area as the local value of tangent modulus.

Now, the internal moment due to the stresses σ' is

$$M = \int_{-y_1}^{d-y_1} b' y \sigma' dy = \int_{-y_1}^{d-y_1} b' y \epsilon' E_T dy = \frac{1}{r} \int_{-y_1}^{d-y_1} b' y^2 E_T dy .$$

If the column were of a material having uniform and perfectly elastic mechanical properties denoted by E then the internal bending moment would be related to the stiffness and the radius of curvature by the equation $M = EI/r$.

Therefore, if an effective stiffness for the column with thermal stresses is assumed, the preceding equation gives

$$M = (EI)_{EFF}/r .$$

Equating the two expressions for M gives

$$(EI)_{EFF} = \int_{-y_1}^{d-y_1} b' y^2 E_T dy \quad \text{or}$$

$$(EI)_{EFF} = \int_o^d b'(y' - y_1)^2 E_T dy' .$$

These results are equivalent to those derived in Reference 38 where, for a hinged column, the residual stresses at room temperature are so distributed that the column remains straight. For the case in question, the column is held straight by the end moments.

The procedure for analyzing the column can now be outlined. Assume a value of strain ϵ_1 at one extreme fiber. From the given temperature distribution and the coefficient of expansion of the material, calculate the strain at all other points across the section. Using stress-strain curves for the material at each temperature encountered, compute the stresses σ and the tangent moduli E_T at all points across the section. Calculate the average stress

$$\bar{\sigma} = \frac{d}{A(\epsilon_3 - \epsilon_1)} \int_{\epsilon_1}^{\epsilon_3} b' \sigma \, d\epsilon \, .$$

Calculate the position of the neutral axis from

$$y_1 = \frac{\int_0^d b' E_T y' dy'}{\int_0^d b' E_T dy'} \, .$$

Calculate the effective stiffness from

$$(EI)_{EFF} = \int_0^d b'(y' - y_1)^2 E_T \, dy' \, .$$

Now, assuming that the average stress becomes the critical stress, calculate the necessary value of ℓ/ρ from

$$(\ell/\rho)^2 = \pi^2 (EI)_{EFF} / I \sigma_{cr} \, .$$

This process can be repeated for various assumed values of ϵ_1 and the resulting values of σ_{cr} or $\bar{\sigma}$, and ℓ/ρ can be plotted as a column curve.

In Section 4.0 of Part I, the results of these calculations are presented for a wide range of materials, temperature gradients, and section shapes. To reduce the work involved in the large number of calculations, the steps just described were set into an IBM automatic digital computer. The computer was equipped with a magnetic memory drum into which were fed the material properties of stress and tangent modulus for values of strain and temperature. The program was then arranged so that the machine could effectively read the material property curves for the values required.

2. Temperature Gradients and Thermal Stresses in Plates

The presence of temperature gradients in a stiffened shell structure produces thermal stresses in the skin which may affect both the buckling and ultimate load-carrying ability of the plate element. A number of conditions may be recognized. If the hot skin panels are bounded on all sides by cooler stiffening structure, such as may be the case with rib and stringer stiffening, then compressive thermal stresses are produced in both directions; that is, the thermal stresses are biaxial. In a multiweb wing, the rib restraint is lacking over most of the area and thermal stresses are likely to be present only in the spanwise direction. Finally the thermal stress applied to a skin panel generally will not be constant across the panel because of temperature variations which are due to the presence of the stiffening structure.

In the work that follows, the effect of the total load from thermal stresses and applied load is considered. The thermal stresses at incipient plate buckling are those occuring in the flat plate when its temperature varies and/or is different from that of the ribs and stringers. It is assumed that the temperature in the skin (plate) does not vary in the direction of its thickness.

At the ultimate load a given variation in temperature will cause relatively smaller thermal stresses σ_{xt} (curve 3 for σ_{xt} in Figure VII-8) in the plate than at incipient buckling, because the extensional rigidity of the plate is diminished owing to large plastic deformations, especially along

the edges. The decrease of the direct stress from thermal and applied loads with respect to those at the edges, due to the finite plate deflections, is given by the tensile membrane stresses σ_{mx} (Figure VII-8) which reduce the stresses σ_x from curve 4 to those of curve 2.

The problem discussed here is dealt with in the following three subsections: (1) equivalent uniform loading for the buckling of simply supported and clamped plates under nonuniform edge loading, (2) reduction of the ultimate load under nonuniform edge stresses to that under uniform loading, and (3) ultimate load for a plate under uniform biaxial stress.

a. Equivalent Load for Buckling

In this subsection, it will be shown that a nonuniform edge loading can be reduced to an equivalent uniform loading.

As shown in Reference 10, the buckling mode shapes for plates are affected primarily by the edge support and are insensitive to the stress distribution. Therefore, excellent accuracy may be obtained by assuming that the deflection modes in the case of variable edge loading are of the same form as in the case of uniform loading. The method of solution for variable edge loading is then to determine an equivalent uniform loading which would exert the same external work as the true loading.

For a simply supported plate, the deflection is given by

$$w = w_o \sin \frac{\pi}{a} x \sin \frac{\pi}{b} y \tag{17}$$

and the work done by a uniform loading σ_{xu} is

$$W_u = \frac{t}{2} \int_0^a \int_0^b \sigma_{xu} \left(\frac{\partial w}{\partial x}\right)^2 dx\,dy$$

$$= \frac{t}{2} \int_0^a \int_0^b \sigma_{xu} \left(\frac{\pi}{a}\right)^2 w_o^2 \cos^2 \frac{\pi}{a} x \sin^2 \frac{\pi}{b} y\,dx\,dy \cdot$$

Since the loading is uniform, σ_{xu} is a constant and this expression may be integrated with the result

$$W_u = \frac{\pi^2}{8} t \sigma_{xu} w_o^2 \frac{b}{a} \cdot \tag{18}$$

Assuming that, in the case of variable edge loading, the deflection is also of the form of Equation (17), the work done by the variable edge load is given by

$$W_t = \frac{t}{2} \int_0^a \int_0^b \sigma_{xn} \left(\frac{\pi}{a}\right)^2 w_o^2 \cos^2 \frac{\pi}{a} x \sin^2 \frac{\pi}{b} y\,dx\,dy ,$$

or performing the integration with respect to x,

$$W_t = \frac{\pi^2}{4} \frac{t w_o^2}{a} \int_0^b \sigma_{xn} \sin^2 \frac{\pi y}{b} dy \cdot \tag{19}$$

The equivalent uniform loading σ_{xu} is now obtained by setting W_t equal to W_u. Thus, making use of Equations (18) and (19) gives

$$\sigma_{xu} = \frac{2}{b} \int_0^b \sigma_{xn} \sin^2 \frac{\pi y}{b} dy \cdot \tag{20}$$

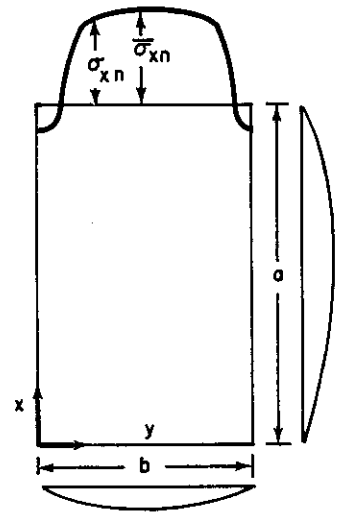

Equation (20) gives the equivalent uniform loading corresponding with the true stress distribution σ_{xn}. If σ_{xn} is not known in analytical form, the integration can be performed numerically. If the stresses σ_{xn} are not within the elastic range, the plastic reduction factor η may be calculated by assuming that the stresses are everywhere equal to $\bar{\sigma}_{xn}$, the maximum value of σ_{xn}. Similarly, for a nonuniform edge load σ_{yn} in the y direction, the equivalent uniform load is

$$\sigma_{yu} = \frac{2}{a} \int_0^a \sigma_{yn} \sin^2 \frac{\pi x}{a} \, dx \, . \tag{21}$$

In the case of a plate with clamped edges, the deflection mode may be assumed as

$$w = w_o \sin \frac{\pi x}{a} \sin^2 \frac{\pi y}{b} \, , \tag{22}$$

so that the work due to uniform loading is

$$W_u = \frac{3}{32} \pi^2 t w_o^2 \frac{b}{a} \sigma_{xu} \, , \tag{23}$$

while the work done by the true loading is given by

$$W_t = \frac{\pi^2}{4} t w_o^2 \frac{1}{a} \int_0^b \sigma_{xn} \sin^4 \frac{\pi y}{b} \, dy \, . \tag{24}$$

The condition W_t equals W_u then yields the equivalent uniform loading as

$$\sigma_{xu} = \frac{8}{3b} \int_0^b \sigma_{xn} \sin^4 \frac{\pi y}{b} \, dy \, . \tag{25}$$

Similarly, the equivalent uniform load for nonuniform loading in the y direction can be calculated using the same method, Equation (21), as for a simply supported plate.

b. Post-Buckling Load and for Simply Supported Plates

For the case of a uniformly distributed thermal stress, the stress distribution at failure would be as shown by curve (1) of Figure VII-8. The stress at the edge would be equal to the yield stress σ_{cy}, while the stress at the center would be equal to the difference between the yield stress σ_{cy} and the maximum membrane stress $\bar{\sigma}_{mxu}$ due to the stretching of the center strip of the plate caused by the lateral deflection. If a thermal stress distribution is considered, such as shown by curve (3) of Figure VII-8, the superposition of this thermal stress σ_{xt} and the uniform stress due to external load would give rise to a stress distribution such as shown by curve (4), if there were no buckling. However, when the plate buckles, strips of the plate in the x direction will experience an extension caused by the lateral deflection. The true stress distribution will then be

the result of superposition of curve (4) with the proper distribution of membrane stresses. The result will be a stress distribution such as that shown by curve (2) of Figure VII-8. Areas S_1 and S_2 represent the change in stress distribution with respect to curve (1) due to the variations in thermal stress. If these two areas were equal, the ultimate load would then be equal for both the case of variable thermal stress and the case of constant thermal stress. It can be shown, however, that S_1 must be smaller than S_2. There are two reasons for this:

(1) Since area S_1 represents stresses which are located closer to the center strips of the plate, the stresses will do more work during the deflection than will the stresses corresponding to the area S_2. This is because the quantity

$$\sin^2 \frac{\pi y}{b}$$

of Equation (19) will increase towards the center of the plate.

(2) The extensional membrane stress at the center of the plate is now $\bar{\sigma}_{mx}$ instead of $\bar{\sigma}_{mxu}$ as shown in Figure VII-8. It then follows that the deflection of the plate will be larger so that the plastic buckling reduction factor η for variable thermal stress is smaller than that for uniform thermal stress.

It follows that $S_1 < S_2$ and hence the ultimate load for the case of variable thermal stress is smaller than for the case of uniform thermal stress.

If the plate were subjected to only a uniformly applied external load, as shown in Equation (51), the ultimate load could be calculated as (Reference 11)

$$\bar{P}_u = bt \left(\sigma_{cy} - \frac{1}{2} \bar{\sigma}_{mxu}\right) . \tag{26}$$

For the case of variable thermal stresses, due to the previous arguments, the total ultimate load P_u must be smaller than in the case of constant thermal stresses. In the case of variable thermal stresses, the total thermal load is $t\int_0^b \sigma_{xt}\, dy$, so that the ultimate externally applied load for variable thermal stress must satisfy the inequality

$$\Delta P_u < \bar{P}_u - t \int_0^b \sigma_{xt}\, dy . \tag{27}$$

If the thermal stress were uniformly distributed and of magnitude $\bar{\sigma}_{xt}$ equal to the maximum value of the variable thermal stress, the ultimate externally applied load would be

$$\Delta P_{uL} = \bar{P}_u - bt\, \bar{\sigma}_{xt} . \tag{28}$$

In the actual case with variable thermal stress, the stresses are everywhere smaller than, or at most equal to, $\bar{\sigma}_{xt}$. It therefore follows that the true applied ultimate load ΔP_u must be greater than ΔP_{uL} of Equation (28). It is then clear that Equations (27) and (28) define upper and lower bounds for P_u. This may be expressed

$$\bar{P}_u - bt\, \bar{\sigma}_{xt} < \Delta P_u < \bar{P}_u - t\int_0^b \sigma_{xt}\, dy . \tag{29}$$

Since an exact calculation of the ultimate externally applied load, ΔP_u, would be complex, if at all possible, it seems logical to assume that ΔP_u will be the mean between the upper and lower bounds defined by Equation (29). It is therefore expressed as

$$\Delta P_u = \frac{1}{2}\left[\bar{P}_u - bt\,\bar{\sigma}_{xt} + \bar{P}_u - t\int_0^b \sigma_{xt}\, dy\right] , \tag{30}$$

and the total ultimate load, which is the sum of ΔP_u and the thermal load, becomes

$$P_u = \bar{P}_u - \frac{1}{2}\left[bt\,\bar{\sigma}_{xt} - t\int_0^b \sigma_{xt}\,dy\right] \tag{31}$$

or

$$P_u = \bar{P}_u - \frac{1}{2}\,bt\left[\bar{\sigma}_{xt} - \sigma_{xta}\right] \quad , \tag{32}$$

where σ_{xta} is the average value of the thermal stress over the plate, defined as

$$\sigma_{xta} = \frac{1}{b}\int_0^b \sigma_{xt}\,dy \quad .$$

The effect of variable edge loading σ_x on the buckling and ultimate loads of flat plates may now be accounted for by using Equations (20) and (32), respectively. Similar formulas for similar distributions apply for σ_y. It seems sufficiently accurate, at the ultimate load as well, to replace a varying edge stress, σ_{yn} equals σ_{yt}, by a uniform stress from Equation (21). The problem of determining the strength of flat panels in the presence of thermal stresses is, therefore, reduced to the determination of buckling and ultimate load due to a uniform edge loading.

Methods for the calculation of critical stresses for flat plates under compressive loading are available in Reference 4, and the determination of ultimate load of plates under uniform edge loading is given in the following.

Although the preceding considerations were based upon uniaxial loading, the same methods of accommodating nonuniform thermal stress distributions are valid for biaxial conditions. The case of biaxial loading is of most interest for aerodynamic heating analysis since it represents the case of a hot skin panel attached to cold ribs and stringers. Accordingly, the development of ultimate loads for a panel under uniform thermal and applied edge loadings, as given in the following, is done for the biaxial case. Similarly, Reference 4, quoted previously for critical stresses of plates subjected to uniform edge loading, also gives the biaxial case. Critical stresses in the plastic range can be calculated by using Equation (23) of Reference 1.

c. Ultimate Load of Plates Under Uniform Biaxial Edge Loading

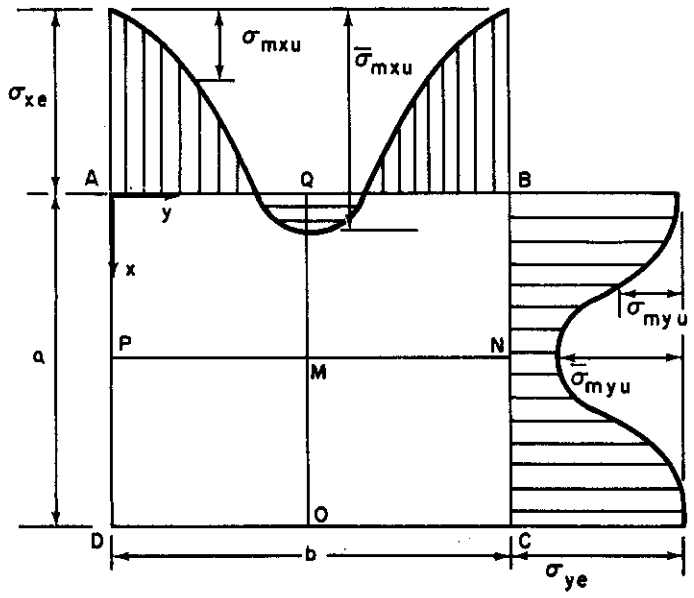

[redacted]

Consider a plate, HAVING UNLOADED SIDES SIMPLY SUPPORTED AND HELD STRAIGHT IN THE PLANE OF THE PLANE OF THE PLATE, that is compressed in the x direction. When the skin becomes hotter than the ribs and stringers, compressive thermal stresses will be superimposed in the x and y directions. This will substantially lower the critical stress, σ_{cr}, for incipient buckling, but the ultimate stress may still be high and, for thin plates, higher than the critical stress without thermal stresses.

A formula for the ultimate stress in the x direction with stresses imposed in the y direction was derived in Reference 11, and the main features of this development are given in the following. As shown in Reference 10, up to deflections of the order of magnitude of the thickness t it is sufficiently accurate to assume that the plate bends in the shape

$$w = w_o \sin \frac{\pi}{a} x \sin \frac{\pi}{b} y \cdot \tag{33}$$

Using Equation (33), the deflecting forces per unit surface caused by stresses σ_x and σ_y are

$$D_x = -t\sigma_x \partial^2 w / \partial y^2 = \frac{\pi^2}{a^2} w_o t \sigma_x \quad \text{and} \tag{34}$$

$$D_y = -t\sigma_y \partial^2 w / \partial y^2 = \frac{\pi^2}{b^2} w_o t \sigma_y \cdot \tag{35}$$

Hence, at any point, the deflecting force caused by a stress σ_y is $(a/b)^2$ times that from a stress σ_x, so that a uniformly distributed stress σ_y is equivalent to a uniformly distributed stress

$$(\sigma_x)_u = \beta^2 \sigma_y \ , \tag{36}$$

where $$\beta = a/b \cdot \tag{37}$$

Since the x strips between AD and BC (such as QO) deflect, while the edge strips AD and BC do not, the former strips become longer than the latter (since the nodal lines AB and DC remain straight). This causes tensile membrane stresses σ_{mxu} to be superimposed. In the elastic range, the membrane stresses are given by (see Reference 10)

$$\sigma_{mxu} = \bar{\sigma}_{mxu} \sin^2 \frac{\pi}{b} y \cdot \tag{38}$$

It can be shown (Reference 11) that the same distribution of membrane stress may be assumed to hold in the plastic range. It may also be shown that these membrane stresses cause deflecting forces that are equivalent to those from a uniform stress σ_{xu} given by (Reference 10)

$$(\sigma_x)_{ux} = \frac{3}{4} \bar{\sigma}_{mxu} \cdot \tag{39}$$

In the same manner, from Equation (36), the membrane stresses σ_{myu} are equivalent to a uniform stress equal to

$$(\sigma_x)_{uy} = \frac{3}{4} \beta^2 \bar{\sigma}_{myu} . \tag{40}$$

The total load acting on the plate will therefore be equivalent to a uniformly distributed stress $(\sigma_x)_u$ obtained by adding to the edge stress, σ_{xe}, the contributions given in Equations (36), (39), and (40). Thus

$$(\sigma_x)_u = \sigma_{xe} - \frac{3}{4} \bar{\sigma}_{mxu} + \beta^2 \sigma_{ye} - \frac{3}{4} \beta^2 \bar{\sigma}_{myu} \cdot \tag{41}$$

[redacted]

The membrane stress $\bar{\sigma}_{mxu}$ is induced by the elongation of the strip QO which is given by

$$\delta = \frac{1}{2} \int_0^a \left(\frac{\partial w}{\partial x}\right)^2 dx = \frac{\pi^2}{4a} w_o^2 , \tag{42}$$

so that the difference between the average stresses in the strips AD and QO is

$$\epsilon_{xm} = \delta/a = \frac{\pi^2}{4} \left(\frac{w_o}{a}\right)^2 . \tag{43}$$

FROM THE ASSUMPTION THAT σ_x DOES NOT VARY IN THE x DIRECTION AND THAT POISSON'S RATIO DOES NOT INFLUENCE THE DISTRIBUTION OF THE DIRECT STRESSES, (AN ASSUMPTION PROVEN CORRECT IN THE ELASTIC RANGE IN REFERENCE 10,) ONE OBTAINS

$$\bar{\sigma}_{mxu} = E_{sx} \epsilon_{xm} = \frac{\pi^2}{4} E_{sx} \left(\frac{w_o}{a}\right)^2 , \tag{44}$$

where E_{sx} is the average secant modulus to be used. Similarly, assuming the edges AD and BC to remain straight in the plane of the plate,

$$\bar{\sigma}_{myu} = E_{sy} \epsilon_{ym} = \frac{\pi^2}{4} E_{sy} \left(\frac{w_o}{b}\right)^2 . \tag{45}$$

Hence,

$$\bar{\sigma}_{myu} = \frac{E_{sy}}{E_{sx}} \left(\frac{a}{b}\right)^2 \bar{\sigma}_{mxu} = \frac{E_{sy}}{E_{sx}} \beta^2 \bar{\sigma}_{mxu} . \tag{46}$$

At incipient buckling, the restraining forces due to the flexural rigidity of the plate are just in equilibrium with the deflecting forces caused by the buckling stresses $\sigma_x = \eta \sigma_{cr}$, where, from page 329 of Reference 4,

$$\sigma_{cr} = \left(\beta + \frac{1}{\beta}\right)^2 \frac{\pi^2 \bar{D}}{b^2 t} \tag{47}$$

and η is the plastic reduction factor.

As explained in Reference 10, with a finite deflection, these restraining forces will be in equilibrium with the deflecting forces when these forces reach the value equivalent to a uniformly distributed load σ_x equal to $\eta \sigma_{cr}$, Hence, from Equation (41),

$$(\sigma_x)_u = \eta \sigma_{cr} , \tag{48}$$

WHERE η IS THE PLASTIC REDUCTION FACTOR WITH THE ACTUAL FINITE DEFLECTION w_o. HENCE, FROM EQUATIONS (41), (46), AND (48),

$$\sigma_{xe} - \frac{3}{4} \bar{\sigma}_{mxu} + \beta^2 \sigma_{ye} - \frac{3}{4} \beta^2 \frac{E_{sy}}{E_{sx}} \bar{\sigma}_{mxu} = \eta \sigma_{cr} , \tag{49}$$

so that

$$\bar{\sigma}_{mxu} = \frac{\sigma_{xe} + \beta^2 \sigma_{ye} - \eta \sigma_{cr}}{3/4 \left(1 + \beta^4 E_{sy} / E_{sx}\right)} . \tag{50}$$

[redacted]

Then, from the preceeding figure and Equation (38), the post buckling stress is

$$\sigma_{xp} = \sigma_{xe} - \int_0^b \sigma_{mxu}\, dy = \sigma_{xe} - \frac{1}{2}\,\bar{\sigma}_{mxu} \quad . \tag{51}$$

Equations (50) and (51) show that the post-buckling stress σ_{xp} depends upon $\beta = a/b$. In general, the value of β corresponding to minimum σ_{xp} will decrease as the deflection increases. However, as explained in Reference 11, the plate will not be free to change its wavelength continuously because, at a certain wavelength, the buckles will "freeze."

This process can be illustrated by considering a long plate for which any wavelength would satisfy the boundary conditions. For such a plate, the plastic deformation due to the compressive and bending stresses will cause permanent buckles, so that after a certain stress has been reached, the wavelength becomes fixed. As a first approximation, it may be assumed, as further explained in Reference 11, that at the ultimate load $\beta = a/b$ is about equal to unity. In that case, E_{sy}/E_{sx} may also be taken as unity. For uniaxial compression without temperature stresses, the ultimate load is a function of the yield stress σ_{cy} and the critical stress σ_{cr}. From References 21 and 22 for the case of simply supported edges that are not held straight (and where $\sigma_y = 0$), the ultimate load is found experimentally as

$$\sigma_{ULT} = \frac{b_e}{b}\,\sigma_{cy} = \sqrt{\sigma_{cr}\,\sigma_{cy}} - 0.25\,\sigma_{cr}. \tag{52}$$

Assuming accordingly that in the present case the ultimate load is reached when the edge stresses σ_{xe} reach the yield stress, so that in Equation (50)

$$\beta = 1, \quad E_{sy}/E_{sx} = 1, \text{ and } \sigma_{xe} = \sigma_{cy},$$

this equation becomes

$$\bar{\sigma}_{mxu} = 2/3\,(\sigma_{cy} + \sigma_{ye} - \eta\,\sigma_{cr}). \tag{53}$$

As shown in Reference 11 for a given case, η can be calculated from the deformations of the plate. Since this calculation is intricate, a direct formula was derived for η and this proved to be in excellent agreement with the more exact calculation. From Reference 23, it is found that, for the conditions of loading assumed in Equation (52), the membrane stresses σ_{mxu} and σ_{myu} are equivalent to a uniform stress

$$(\sigma_x)_u = 0.848\,\bar{\sigma}_{mxu} \tag{54}$$

In that case, since the equivalent loading should be equal to $\eta\sigma_{cr}$, setting $\sigma_{xe} = \sigma_{cy}$ gives the relation

$$\sigma_{cy} - 0.848\,\bar{\sigma}_{mxu} = \eta\,\sigma_{cr}, \quad \text{or} \tag{55}$$

$$\bar{\sigma}_{mxu} = 1.18\,\sigma_{cy} - 1.18\,\eta\,\sigma_{cr} \tag{56}$$

[redacted]

Since Equation (51) also applies here, with $\sigma_{xp} = \sigma_{ULT}$ and $\sigma_{xe} = \sigma_{cy}$,

$$\sigma_{ULT} = \sigma_{cy} - 1/2\ \bar{\sigma}_{mxu} = 0.41\ \sigma_{cy} + 0.59\ \eta\ \sigma_{cr} \quad \text{and} \tag{57}$$

$$\eta = 1.7\ \frac{\sigma_{ULT}}{\sigma_{cr}} - 0.7\ \frac{\sigma_{cy}}{\sigma_{cr}} \cdot \tag{58}$$

Insertion of σ_{ULT} from Equation (52) gives

$$\eta = 1.7 \sqrt{\frac{\sigma_{cy}}{\sigma_{cr}}} - 0.425 - 0.7\ \frac{\sigma_{cy}}{\sigma_{cr}} \cdot \tag{59}$$

To apply this formula to other cases it should be understood that η depends on the deflection of the plate, which causes the difference in stress σ_{mxu} between the edge strips AD and BC on the one hand and the center strip OQ on the other hand. Hence, as explained more fully in Reference 11, η is actually a function of $\bar{\sigma}_{mxu}$ and σ_{cr} Therefore, η should be expressed in terms of these variables. From Equation (55),

$$\frac{\sigma_{cy}}{\sigma_{cr}} = 0.848\ \frac{\bar{\sigma}_{mxu}}{\sigma_{cr}} + \eta \cdot \tag{60}$$

Inserting this into Equation (59), one obtains

$$\eta = 0.25 - 0.35\ \frac{\bar{\sigma}_{mxu}}{\sigma_{cr}} + 0.71 \sqrt{\frac{\bar{\sigma}_{mxu}}{\sigma_{cr}}} \cdot \tag{61}$$

Using this formula for η in Reference 11, the ultimate stress was calculated for the case of a simply supported plate with its edges held straight (in the plane of the plate) and compressed in the longitudinal direction. The expression for ultimate stress is then

$$\sigma_{ULT} = \sigma_{cy} - 1/2\ \bar{\sigma}_{mxu}\ , \tag{62}$$

where $\bar{\sigma}_{mxu}$ follows from

$$\frac{\bar{\sigma}_{mxu}}{\sigma_{cr}} = \left[-0.545 + \sqrt{1.54\ \frac{\sigma_{cy}}{\sigma_{cr}} - 0.0865} \right]^2 \cdot \tag{63}$$

As shown in Reference 11, this formula is in good agreement with available test results. If temperature stresses are present so that Equation (53) applies, insertion of Equation (61) gives

$$\frac{\bar{\sigma}_{mxu}}{\sigma_{cr}} = \frac{2}{3} \left(\frac{\sigma_{cy}}{\sigma_{cr}} + \frac{\sigma_{ye}}{\sigma_{cr}} - 0.25 + 0.35\ \frac{\bar{\sigma}_{mxu}}{\sigma_{cr}} - 0.71 \sqrt{\frac{\bar{\sigma}_{mxu}}{\sigma_{cr}}} \right) \cdot$$

Solving for $\bar{\sigma}_{mxu} / \sigma_{cr}$, one obtains

$$\frac{\bar{\sigma}_{mxu}}{\sigma_{cr}} = \left[-0.308 + \sqrt{0.87 \left(\frac{\sigma_{cy}}{\sigma_{cr}} + \frac{\sigma_{ye}}{\sigma_{cr}} \right) - 0.1225} \right]^2 \cdot \tag{64}$$

[redacted]

The value of σ_{ULT} is found by inserting this into Equation (62). The ultimate load becomes

$$\bar{P}_u = b t \sigma_{ULT} \cdot \tag{65}$$

In all these formulas, σ_{cr} is given by Equation (47).

As calculated in a similar way, from Reference 11 for a plate where the edges parallel with the x axis are clamped, the ultimate load is

$$\bar{P}_u = b t \left(0.595 \sigma_{cy} - 0.24 \sigma_{ye} \right) \cdot \tag{66}$$

In Reference 11, formulas are also given for determining the effective width of the skin after it has buckled, for stringer panels as well as multiweb beams. In all these cases, the contributions σ_{xt} and σ_{yt} of the thermal stresses, which at the ultimate load will be smaller than at the critical load, are assumed to be known. Hence, P_u from Equation (32), and also the externally applied load $P_u - b t \sigma_{xtq}$, can be calculated. Also in Reference 11, a formula has been derived for the critical stress of stringer panels under biaxial loading.

D. PROPELLANT TANK DESIGN

1. Propellant Tank Weights

To derive expressions for the weights of nonintegral propellant tanks as a function of pressure, capacity, and material, a design criterion is needed because structural weight must depend upon the stress level for which the material is to operate. A suitable set of criteria for the design and testing of pressure vessels, for use in both manned and unmanned vehicles, has been formulated and is detailed in Reference 12. The stress level at proof pressure, as defined in Reference 12, is used for the development of the weight expressions which follow.

a. Weight of Cylindrical Shells

When the cylindrical portion of a pressure vessel is at a sufficient distance from the ends, the maximum stress at the internal surface due to internal pressure is represented to a sufficiently accurate degree by the well-known hoop membrane formula

$$\sigma = \frac{p a}{t} \cdot$$

Rewriting in terms of the diameter and solving for thickness gives

$$t = \frac{p D_i}{2\sigma - p} \cdot$$

The weight of the cylindrical shell is

$$W = \pi \left(D_i + t \right) \ell \rho t$$

and the volume is

$$V = \pi D_i^2 \ell / 4 \quad ,$$

so that

$$W/V = 4 \left(D_i + t \right) \rho t / D_i^2 \cdot$$

[redacted]

Substituting for t in terms of the stress gives

$$W/V = 8\rho\sigma p/\left(2\sigma - p\right)^2$$

or, to a close approximation when p is relatively small in comparison with 2σ,

$$W/V = 2\rho p/\sigma \quad .$$

Evidently, from this equation, the shell weight of a cylindrical vessel of given volume is independent of the length and diameter of the shell, so that for a given capacity the weight does not depend upon the number and size of the tanks in which the volume is contained. However, it is obvious that the weight of such items as tank ends, internal baffles, and support structure must be included before a realistic weight comparison can be made.

The maximum stress experienced by a pressure vessel should occur during the proof pressure test that is performed on each article before acceptance. Thus, it is reasonable to use the proof pressure and the corresponding stress as the bases for weight estimation. Reference 12 has shown that the amount of volumetric set for a given vessel, when the water displacement method is used in pressure testing, is a linear function of the material strain. Furthermore, it recommends that the total volumetric set at proof pressure should not exceed 0.1% of the original volume of the vessel. It was established analytically that a 0.1% volumetric set would correspond with a permanent material strain of 0.0005 in./in. Moreover, Reference 13 shows that for a pressure vessel having a biaxial stress condition of 2 to 1, the permanent strain of the material occurs in the hoop direction only. Thus, it is valid to base the weight estimation on the hoop membrane formula, and the stresses used, in conjunction with proof pressure, should be those corresponding with a permanent strain of 0.0005 in./in. AS DETERMINED FROM A BIAXIAL STRESS-STRAIN CURVE.

b. Weight of Elliptical Ends

In designing the ends of a pressure vessel, the analysis is usually divided into two parts: knuckle region and dome region. In the region of the knuckle, there exists a circumferential compressive stress of such a magnitude that failure may occur due to instability; in the dome area, the tensile stress is the governing factor. Furthermore, analysis shows (Reference 14) that the length of this knuckle region is approximately one-fourth of the radius of the cylindrical shell. Therefore, the weight can be closely approximated by assuming an equivalent end thickness equal to the average thickness of the knuckle and dome.

From Reference 14, it can be concluded that the state of stress existing at the junction of the knuckle and the dome is much less than that existing in the critical portion of the knuckle and at the center of the dome. Hence, the allowable stresses used in the determination of thickness of knuckle and dome should be those of the base metal and not of the weld, if welding is done in the junction of knuckle and dome.

Reference 15 has translated the analytical work of Reference 14 into design charts which make the actual design of pressure vessel ends an easy task.

The maximum stress in the knuckle region can be expressed as

$$\sigma = K_k \, pa/t_k \quad .$$

Maximum stress in the dome region is:

$$\sigma = pR/2t_d = kpa/2t_d \text{ , since } R = ka \quad .$$

[redacted]

Solving these equations for t_k and t_d and taking the average value gives an effective end thickness as

$$t_e = \frac{pa}{2\sigma}\left(K_k + \frac{k}{2}\right) .$$

The surface area of an ellipse equals

$$2\pi a^2 + \frac{\pi b^2}{e} \ln\left(\frac{1+e}{1+e}\right) ,$$

where

$$e = \sqrt{\frac{a^2 - b^2}{a^2}} = \sqrt{1 - \frac{1}{k^2}}$$

Substituting the value of e in the expression for area and multiplying by an effective thickness t_e and a material density ρ gives the weight of the end as

$$W = \pi a^3 \rho \frac{p}{2\sigma}\left(K_k + \frac{k}{2}\right)\frac{L}{k} ,$$

where

$$L = 2k + \frac{1}{\sqrt{k^2-1}} \ln\left(\frac{k + \sqrt{k^2-1}}{k - \sqrt{k^2-1}}\right) .$$

The volume of an ellipse is

$$V = \frac{4}{3}\pi\frac{a^3}{k} , \text{ so that } \frac{W}{V} = \frac{3}{8}\frac{\rho p}{\sigma}\left(K_k + \frac{k}{2}\right) L .$$

Values of L for various k ratios are

$k = 2$; $L = 5.518$
$k = 3$; $L = 7.250$
$k = 4$; $L = 12.103$

From Reference 15, the stress factors are

$k = 2$; $K_k = 1.086$
$k = 3$; $K_k = 2.85$
$k = 4$; $K_k = 4.90$

With the above values of L and K_k substitution into the equation for W/V gives:

For $k = 2$,

$$W/V = 4.32\, \rho p/\sigma .$$

For $k = 3$,

$$W/V = 11.80\, \rho p/\sigma .$$

For $k = 4$,

$$W/V = 31.35\, \rho p/\sigma .$$

[redacted]

c. Weight of Spherical Pressure Vessels

For a spherical pressure vessel under internal pressure, the formula for the maximum stress is represented to a sufficiently accurate degree by

$$\sigma = \frac{p\,(D_i + t)}{4t} \quad ,$$

or

$$t = \frac{p\,D_i}{4\sigma - p} \quad .$$

Weight of a sphere is

$$W = \pi t \rho \left(D_i + t\right)^2 \quad , \quad \text{and}$$

volume of a sphere is

$$V = \frac{1}{6} \pi D_i^3 \quad ,$$

so that

$$\frac{W}{V} = \frac{96 \rho p \sigma^2}{(4\sigma - p)^3} \quad .$$

Or again, as an approximation, assuming p as small when compared with 4σ,

$$W/V = 1.5\, \rho p / \sigma \quad .$$

Therefore, it is shown that the spherical vessel weighs 75% of that for only the shell of the cylindrical vessel operating at the same stress level.

Reference 12 has shown analytically that 0.1% volumetric set at proof pressure corresponds with a material permanent strain of 0.0003 in./in. AS DETERMINED FROM A BIAXIAL STRESS-STRAIN CURVE for a spherical vessel.

Charts of the formulas for weight-to-volume ratio for cylindrical and spherical vessels, and elliptical ends, are given in Section 5.0 of Part I for a variety of materials. The following table shows the materials included in these curves together with the RECOMMENDED PROOF PRESSURES.

[redacted]

Material	Condition	Density ($lb/in.^3$)	Ultimate Tensile Strength (psi)	Recommended Proof Pressure Stress Cylinders (psi)	Recommended Proof Pressure Stress Spheres (psi)
18-8 SS	Annealed	0.286	75,000	28,000	26,000
18-8 SS	1/4-hard	0.286	125,000	60,000	56,000
17-7 PH	FA (formed & aged)	0.276	170,000	112,000	100,000
4130, 4140, 4340	Normalized	0.283	90,000	67,000	65,000
4130, 4140, 4340	Heat-treated	0.283	140,000	118,000	115,000
Cor-Ten	Cold-rolled	0.284	70,000	48,000	45,000
403, 410 SS	Heat-treated	0.280	180,000	126,000	120,000
K-Monel	Age-hardened after welding	0.306	134,500	80,000	77,000
6061 Aluminum	Welded in T4, aged to T6	0.098	38,000	28,800 (for cylinder) 32,600 (for head)	28,800
Titanium	Pure-annealed	0.163	100,000	70,000	66,000

2. Buckling Strength of Pressurized Ring-Stiffened Shells

The buckling strength of a cylinder under axial compression is given by

$$\sigma_{cr} = C \eta E t / a \quad , \tag{67}$$

where the coefficient C depends upon the length-to-radius and the radius-to-thickness ratios, and upon the end conditions of the cylinder. Values of this coefficient have been determined by tests; however, these tests were not carried to small values of these ratios. With the use of ring-stiffened cylinders, it seems likely that the spacing of the rings can be sufficiently close that the theoretical small deflection theory values of C equals 0.605 can be attained.

The plasticity coefficient η is added to include the effect of buckling beyond the elastic limit, and values for unstiffened shells are given in Reference 2. Because more suitable data are not available, it is proposed that these values of η be used throughout, irrespective of whether the cylinder is pressurized or unpressurized.

In Reference 18, the buckling coefficients C for unpressurized cylinders are computed and shown to be, for a dimensional range of

$$20 \geq \frac{L}{a}\sqrt{\frac{a}{t}} \geq 1.7,$$

$$C = 0.2 + 3.6 \left(20 - \frac{L}{a}\sqrt{\frac{a}{t}}\right)^4 \times 10^{-6}. \tag{68}$$

[redacted]

For long shells when

$$\frac{L}{a}\sqrt{\frac{a}{t}} > 20, \quad C = 0.2,$$

and for short shells when

$$\frac{L}{a}\sqrt{\frac{a}{t}} \leq 1.7, \quad C \geq 0.605 .$$

In applying the critical stress formula (Equation 67) to pressurized cylinders, it is convenient to add an incremental buckling coefficient, ΔC to account for the stabilizing effect of the internal pressure. Values for ΔC for long, unstiffened cylinders have been determined by experiment, as reported in References 16 and 17, and are presented in Figure 5.3-1, Part I, as a function of the pressure parameter

$$\bar{p} = \frac{p}{E}\left(\frac{a}{t}\right)^2 .$$

It is noted that the applied stress should be reduced by the longitudinal tension stress $\frac{pa}{2t}$.

It may be more convenient, however, to compare the gross applied stress with a critical stress which includes the longitudinal stress due to internal pressure. In this case, the "fore-tension" stress can be represented by an additional incremental buckling coefficient, $\overline{\Delta C}$, which is equal to $\frac{\bar{p}}{2}$ since

$$\overline{\Delta C}\, E \frac{t}{a} = \frac{pa}{2t} \quad \text{and}$$

$$\overline{\Delta C} = \frac{1}{2}\frac{p}{E}\left(\frac{a}{t}\right)^2 .$$

The critical stress is then

$$\sigma_{cr} = (C + \Delta C + \overline{\Delta C})\, \eta E \frac{t}{a} .$$

Reference 38 determines buckling coefficients for short, pressurized cylinders in the range of $\frac{L}{a}\sqrt{\frac{a}{t}}$ from 1.7 to 20 by assuming the fourth-degree curve (Equation 68) to exist between these two geometric limits. The buckling coefficients $(C + \Delta C)$ are taken at 0.605 for the lower limit, while those for the upper limit are determined from Figure 5.3-1, Part I. Curves for various values of $\bar{p}$ are determined in this manner and appear in Figure 5.3-2, Part I.

In both Figures 5.3-1 and 5.3-2, Part I, the upper limit for $C+\Delta C$ is shown not to exceed 0.605, the value of the buckling coefficient of long, unpressurized cylinders as determined by the small deflection analysis. It may be proven by subsequent tests that this value can be exceeded. On the other hand, when cylinders are short, the internal pressure may prove to have a destabilizing influence and maximum values may be less than 0.605.

3. Optimum Proportions of Pressurized Ring-Stiffened Shells

In Section VIII, methods are developed by which maximum stress levels attainable under compression loading may be determined for various types of structures and materials at various temperature levels. It has not been possible to apply this general treatment to the case of ring-stiffened

shells, or ring- and pressure-stabilized shells, but some method of selecting optimum proportions for such structures is desirable even if it is restricted to a single previously selected material and temperature. In fact, if such a method is made available, it seems reasonable that the material and operating temperature should be selected from the optimum curves of Section IX for unstiffened cylinders, and that the method should then be applied to determine optimum proportions of stabilization.

Such a method is presented in the following, and typical results for one particular combination of material, temperature, and pressure are given in Figure VII-2. The method is developed first for ring-stabilized unpressurized shells and is then extended to the pressurized condition by the use of buckling coefficients taken from the previous part of this section.

a. Weight-Strength Analysis of Ring-Stiffened Shells

The method is presented, in condensed form, as follows; full details can be found in Reference 18.

For a ring-stiffened shell, two modes of instability are possible: general instability in which both shell and rings buckle, and panel instability which involves only buckling of the shell between rings.

The case of general instability has been treated by Timoshenko in Reference 4, Pages 470 to 473. By the use of small deflection theory, the critical stress is shown to be

$$\sigma_{cr} = 0.605\, E\, \frac{t}{a} \sqrt{\frac{t_y}{t}} \quad ,$$

where $t_y = t + A_r/L_r$.

From experimental results, it is known that the assumption of small deflections is not valid for an unstiffened shell. In fact, such an assumption yields results that lack conservatism. When rings are added, however, the shell remains round, and it may be assumed that the small deflection theory applies for general instability.

Actually, the case of bending rather than axial compression must be considered, and analogous to the case of an unstiffened shell (Reference 4), it is assumed that the buckling stress during bending is 30% higher. Hence, for a shell subjected to bending, the critical stress for general instability is

$$\sigma_{cr} = 0.786\, \eta\, E\, \frac{t}{a} \sqrt{\frac{t_y}{t}} \quad ,$$

where η, the plastic reduction factor, has been added to account for buckling beyond the elastic limit. The flexural rigidity required to prevent general instability of the rings is assumed to be determined by Shanley's coefficient C_f, Reference 25, and from page 71 of this reference a value of 1/16,000 is taken. Then, from Equation 3.5 of the same reference, the ring stiffness is

$$(EI)_r = C_f \frac{MD^2}{L_r} \quad .$$

From page 78 of Reference 25, the moment of inertia of the ring may be written as $5.24\, A_r^2$, so that

$$A_r^2 = C_f \frac{MD^2}{5.24\, L_r E} \quad .$$

[redacted]

By proper substitutions the average cross-sectional area of the shell can be obtained as

$$A = \pi D t + \frac{0.00345 \pi D^2 M^{1/2}}{E^{1/2} L_r^{3/2}} .$$

Considering now the local instability between rings, the work of Reference 18 can be used, and this gives

$$\sigma_{cr} = 1.3 \eta C E t/a = 2.6 \eta C E t/D ,$$

where the 1.3 factor has been included to cover the condition of bending, and C is given by the following.

For $\frac{L}{a}\sqrt{\frac{a}{t}} \geq 20$, $C = 0.2$.

For $20 \geq \frac{L}{a}\sqrt{\frac{a}{t}} \geq 1.7$, $C = 0.2 + 3.6\left(20 - \frac{L}{a}\sqrt{\frac{a}{t}}\right)^4 \times 10^{-6}$.

For $\frac{L}{a}\sqrt{\frac{a}{t}} \leq 1.7$, $C = 0.1\left[\left(\frac{L}{a}\sqrt{\frac{a}{t}}\right)^2 + \frac{9}{\left(\frac{L}{a}\right)^2\left(\frac{a}{t}\right)}\right]$.

The bending moment taken by the shell, based upon local instability, is

$$M = \pi D^2 t \sigma_{cr}/4 = 0.65 \pi \eta C E t^2 D .$$

Using this equation to calculate t, and inserting in the equation for A, gives

$$\frac{A}{M^{2/3}} = \frac{1}{\left(\frac{M}{D^3}\right)^{1/6}}\left[\frac{2.2}{(\eta C)^{1/2}} + 0.0108\left(\frac{D}{L}\right)^{3/2}\right]\frac{1}{E^{1/2}} .$$

To express $\frac{A}{M^{2/3}}$ as a function only of $\frac{M}{D^3}$, C and $\frac{L}{a}\sqrt{\frac{a}{t}}$ must be expressed in the form

$$\frac{L}{a}\sqrt{\frac{a}{t}} = \frac{L}{D}\sqrt{\frac{2D}{t}} .$$

From the expression for M, it can be shown that

$$t/D = \left(M/D^3\right)^{1/2}\frac{1}{\left(0.65 \pi \eta C E\right)^{1/2}} ,$$

so that

$$\frac{L}{a}\sqrt{\frac{a}{t}} = 1.68 \eta^{1/4}\frac{L}{D}\left(\frac{CE}{M/D^3}\right)^{1/4} .$$

[redacted]

[redacted]

Substituting into the expressions for C and solving for L/D gives, for $\frac{L}{a}\sqrt{\frac{a}{t}}$ between 1.7 and 20,

$$\frac{L}{D} = 11.9 \left(\frac{M/D^3}{\eta C E}\right)^{1/4} \left[1 - 1.15 \left(C - 0.2\right)^{1/4}\right] .$$

If C exceeds 0.605 so that $\frac{L}{a}\sqrt{\frac{a}{t}}$ is smaller than 1.7, then

$$\frac{L}{D} = \left(\frac{M/D^3}{\eta E C}\right)^{1/4} \frac{1}{\left[1.565\, C \pm \left(2.45 C^2 - 0.881\right)^{1/2}\right]^{1/2}} .$$

Also from the expression for

$$\sigma_{cr}, \; C = \frac{\sigma_{cr}}{2.6\, \eta E\, t/D}$$

Substituting for t/D gives

$$C = \frac{\sigma_{cr}^2}{3.3\, \eta E \left(M/D^3\right)} .$$

With these equations and assuming a value of σ_{cr}, C may be calculated. Then, using the appropriate formula for $\frac{L}{D}$, $\frac{A}{M^{2/3}}$ may be calculated for each assumed value of $\frac{M}{D^3}$. By trial and error and choosing various values of σ_{cr}, the minimum value of $\frac{A}{M^{2/3}}$ is found for each value of $\frac{M}{D^3}$. It will be found that the total cylinder weight as expressed by $\frac{A}{M^{2/3}}$ is quite sensitive to the choice of σ_{cr} and, therefore, converges rapidly to a minimum value.

Calculations made in Reference 18 show that for the range of values of $\frac{M}{D^3}$ of practical importance, $8 > \left(\frac{M}{D^3}\right)^{\frac{1}{3}} > 2$, it is not econimical to allow higher stresses than those corresponding to a C value of 0.6. As already shown, the C value for general instability is higher than 0.605. Consequently, for all practical cases, general instability will not be governing and is not considered further.

Reference 18 also demonstrates that the torsional stiffness of open section rings has a small effect on the cylinder buckling stress, and also that it is not econimical to use rings with closed cross-sections.

b. Weight-Strength Analysis of Pressure-Stiffened and Ring-Stiffened Shells

As shown in Reference 38, if the cylinder is pressure stabilized the aforementioned formulas can be used. However, after calculating C for the assumed value of σ_{cr} and the given value of $\frac{M}{D^3}$, a value of $\frac{L}{a}\sqrt{\frac{a}{t}}$ is obtained from Figure 5.3-2 of Part I, and this value is used to calculate $\frac{L}{D}$. Then, $\frac{A}{M^{2/3}}$ is calculated as before. At high values of $\frac{M}{D^3}$, the cylinders may become critical in tension.

[redacted]

c. Presentation of Results

It is evident from this work that extensive calculations are required to produce curves giving optimum proportions for ring-stabilized and pressure-stabilized shells, including a range of materials, temperatures, pressures, and values of $\frac{M}{D^3}$. Such calculations have been performed only for 24S-T aluminum alloy at room temperature with two pressure values of $\bar{p} = 0$ and $\bar{p} = \frac{p}{E}\left(\frac{a}{t}\right)^2 = 0.40$. In the latter case, a failing tensile stress of 50,000 psi was assumed. These results are shown in Figure V11-2 where a curve for an unstiffened shell is also included. From this figure, it is evident that a maximum weight saving of approximately 20% can be realized by the addition of rings to an unpressurized shell.

4. Temperature Limitations For Propellant Tanks

Before extending the design and analysis of pressurized propellant tanks to elevated temperatures, it will be profitable to examine temperature limits that may be placed on such tanks for reasons other than structural; it is reasonable to expect that the association of high-temperature structures and highly potent propellants involves certain hazards. This subject, one of many associated with high-speed flight, has not yet received comprehensive study. This is due to the lack of sufficient time, or because of the need for experimental work. The potential problems are outlined in the following where sufficient numerical values are given to show the undesirability of operating propellant tanks at elevated temperature.

Temperature limitations for propellant tanks may be necessary because of limits imposed by the propellant, and/or limits imposed for safe operation with a partly empty tank.

Any limitations imposed by the requirements of the propellant can be expected to apply automatically to the tank itself, while the tank is full. Heat transfer rates that are possible into liquids are high and, in most practical cases, it will be impossible to raise the wall temperature more than a few degrees above that of the contained liquid. Because of the heat capacity of a large volume of propellant, it is possible that temperature limitations may not require structural countermeasures as the propellant is often expended before its temperature can rise appreciably. Under these conditions, the tank wall above the propellant level will generally experience a rapid increase in temperature and may, therefore, present a hazard because of its close proximity to the remaining propellant. This condition may require protection of the tank wall from the direct effects of aerodynamic heating, and, of course, such protection applies after boost when the tanks are empty.

Chief among the effects of temperature on fuels and oxidizers is the increase of vapor pressure and, hence, the increase of internal tank pressure, if the liquids are not to boil away. With rocket power plants, the choice of accepting a weight penalty by loss due to boiling, perhaps for structural simplification, is not usually open, since a boiling liquid will cause cavitation in the propellant pumps. This condition is not permissible because it causes overspeeding of the pumps, and results in irregular propellant flow to the thrust chambers with a disturbance of the combustion and a breakdown in thrust chamber cooling. Figures VII-3 through VII-7 give vapor pressures over a range of temperatures for some principal fuels and oxidizers. In almost all cases, pressures exceeding 250 psi are attained below 500° F.

Minimum tank pressure is that necessary to supply propellants to the pumps at the required flow rate, and to overcome pressure losses in such areas as pipes and valves. Any pressure above this minimum that may be required to prevent boiling due to heat input represents an increased tank weight that can be readily computed from the tables of Section 5.0, Part I. On the basis of past experience, typical minimum pressure values range from 25 to 50 psi. Since the tank weight is proportional to pressure, it is evident from Figures VII-3 through VII-7 that only a few degrees of propellant temperature rise can be permitted if tank weights are not to be increased many times. Note also that higher working pressures involve increased weights in lines, fittings, pumps, and motors.

It will be evident that, if heating conditions are sufficiently severe or prolonged so that some protection of the propellants is necessary, the resulting tank temperatures will be within the range of aluminum. Large tank diameters are beneficial since they present the least heated surface area for a given volume and, consequently, for a given heat capacity.

These arguments apply primarily to tanks supplying propellants for rocket engines, where the large flow requirements and correspondingly large pumping powers require centrifugal pumps. For the much smaller fuel requirements of the gas turbine, pumps that are less troubled by cavitation can be used and excess heat into the fuel tank can be absorbed by fuel boil off. Weight optimization then becomes necessary between fuel boil off loss, tank weight due to pressure, and heat protection weight.

The second important effect of operating propellants at elevated temperatures is the accelerated corrosion rate that occurs, particularly with oxidizers. The importance of corrosion is a function of the life expectancy of the tanks. For nonexpendable aircraft, the decision to allow propellants to reach high temperatures may well specify the type of material through the provision for corrosion. An extensive test program, reported in Reference 32, gives data from which material selections may be made and shows generally the temperature limitations imposed by corrosion. Two examples will suffice to show the significance of this problem. Aluminum 6061-T6 immersed in white fuming nitric acid, for instance, has a corrosion rate at 160° F that is 3100 times that at room temperature; for type 347 stainless steel, this ratio is approximately 4 times. This high corrosion rate introduces difficulties such as decreased effective metal area and mechanical properties, and possible corrosion products in the solid or sludge form which may result in malfunction of the entire power plant system.

One further limit to the operation of propellants at high temperature arises from thermal decomposition, this being especially critical in the case of white fuming nitric acid. References 33 and 34 give decomposition data for both red and white fuming nitric acid.

If the propellant capacity of the tank is large, or the powered flight time is short, so that propellant temperatures do not rise sufficiently to make the aforementioned limitations of importance, then consideration must be given to the condition of the tank wall after it becomes dry. Typical values of heat flux during boost are given in Section II. Here, it is apparent that, even at moderate supersonic speeds, the flux is sufficient to increase the tank wall temperature rapidly if heat protection is not provided.

The thermal stresses that may result in the tank shell due to rapid temperature rise are discussed elsewhere as they are common to all structural elements. In this section of the report, consideration will be given only to the special effects that are caused by the presence of propellants.

Among these problems, a group of considerable significance arises from the possibility of the cool propellant splashing or surging onto the hot wall of the dry area of the tank. When this occurs, all the difficulties of propellants at high temperatures discussed previously arise in an acute form, together with a local condition of thermal shock in the tank wall.

Regardless of the tank pressure, if the tank wall is at high temperature, the splashed fuel will be boiled, and perhaps decomposed, until the heat contained in the local area of skin is removed. If the tank is, say, 70 to 80% full when this occurs, the volume of vapor produced could require a large relief valve if tank design pressures are not to be exceeded.

The thermal shock of the tank wall as a result of local quenching may produce surface spalling, or fatigue cracking, and similar effects of thermal shock, but it will certainly produce thermal stresses. If a small area is quenched in the center of a large hot plate, circumferential and radial stresses are produced having the magnitude

$$\frac{\alpha E \Delta T}{(1-\mu)}.$$

Both the radial and circumferential stresses are tension.

For steel, where ΔT, the temperature difference between the hot wall and the liquid, may be 600° F for a fuel tank or even 1100° F for a liquid oxygen tank, yield stresses can be exceeded when thermal stresses are combined with pressure stresses.

[redacted]

With α = 8×10^{-6} in./in.
E = 25×10^{6} psi
ΔT = 1100° and 600° F
Stress = 314,000 and 171,400 psi, respectively

Although the implications of local yielding of a tank wall require further study, possible results are (1) precipitation of buckling if the tank is integral and carries compressive loads; (2) panel flutter if a wave is produced in the external surface; (3) stress redistribution and concentration if the tank is nonintegral and subject only to tension stresses, since the residual compressive stresses following yielding tend to make the local area characteristic of a "hole;" and (4) fatigue effects that follow from the stress concentrations and the yielding.

From this discussion, it is evident that the problems arising from fuel splashing on a hot tank wall are not amenable to analysis, and confirmation of their significance must await tests. In the meantime, the potential difficulties are sufficiently serious to justify protecting propellants from the effects of aerodynamic heating.

There is one other result of a propellant tank having a hot wall above the liquid level and a cold wall below that deserves consideration. It is the case of a large booster in which longitudinal accelerations maintain the propellant level approximately normal to the tank axis. A steel tank, with a wall thickness of 0.08 inch and containing liquid oxygen, may have a temperature which varies from -300° to +1000° F in a longitudinal distance of approximately 12 inches. With a nominal diameter of 4 feet, the tank wall would develop an eccentricity of $4 \times 12 \times 1300 \times 8 \times 10^{-6}/2 = 0.25$ inch due to the different diameters at the two extreme temperatures. If the tank is integral and carrying compression stresses due to bending moments or engine thrusts, such an initial eccentricity may precipitate early buckling. This is another problem that requires experimental checking before a decision regarding its importance can be made.

[redacted]

[redacted]

REFERENCES

(1) Bijlaard, P. P., "Theory and Tests on the Plastic Stability of Plates and Shells," I. A. S. Journal, September 1949, Vol. 16, No. 9, page 529.

(2) Krivetsky, A., "Plasticity Coefficients for the Plastic Buckling of Plates and Shells," I. A. S. Journal, June 1955, Vol. 22, No. 6, page 432.

(3) Carlson, R. L. and Schwope, A. D., "A Method for Estimating Allowable Load Capacities of Columns Subject to Creep," Proceedings Second U. S. National Congress of Applied Mechanics, 1954, pages 563 through 568.

(4) Timoshenko, S., "Theory of Elastic Stability," 1936.

(5) Kempner, J. and Patel, H. A., "Creep Buckling of Columns," NACA TN 3138, January 1954.

(6) Libove, C., "Creep Buckling of Columns," Journal of Aeronautical Sciences, July 1952, pages 459 through 467.

(7) Libove, C., "Creep Buckling Analysis of Rectangular-Section Columns," NACA TN 2956, June 1953.

(8) Jackson, L. R., Schwope, A. D., and Shaber, F. R., "Stress-Strain-Time Properties of Some Aircraft Materials;" Shanley, F., "Weight-Strength Analysis of Aircraft Structures," 1952, pages 307 through 322, Figures 17-5 and 17-6.

(9) Mathauser, E. E. and Brooks, W. A., "An Investigation of the Creep Life-Time of 75S-T6 Aluminum Alloy Columns," NACA TN 3204, July 1954.

(10) Bijlaard, P. P., "Determination of the Effective Width of Plates With Small Deviations From Flatness by the Method of Split Rigidities," Proceedings of the First U. S. National Congress of Applied Mechanics, Chicago, 1951, pages 357 through 362.

(11) Bijlaard, P. P., "Buckling in the Presence of Thermal Stresses," Bell Aircraft Corporation Report (unpublished).

(12) Schnitt, A., "Proposal for Pressure Vessel Design and Testing Criteria and Discussion," Bell Aircraft Corporation, Report 02-947-004, 21 February 1951.

(13) Wong, R. E., "Progress Report on Pressure Vessel Development-1, Analytical Method for Predicting the Proportional Limit, Yield, and Ultimate Stresses for a Cylindrical Pressure Vessel," Bell Aircraft Corporation, Report 56-941-007, 20 July 1950.

(14) Coates, W. M., "The State of Stress in Full Heads of Pressure Vessels," Transactions of the ASME, Vol. 52, No. 22, September - December 1930.

(15) Rattinger, I., "Design Charts for the Elastic Stress Distribution in Pressure Vessels with Elliptical Heads," Bell Aircraft Corporation, Report 02-984-016, 1 October 1954.

(16) Lo, H., Crate, H., and Schwartz, E. B., "Buckling of Thin-Walled Cylinder Under Axial Compression and Internal Pressure," NACA TN 2021.

(17) Rafel, N. "Effect of Normal Pressure on the Critical Compressive Stress of Curved Sheet," NACA Wartime Report, Restricted Bulletin 2K01, November 1942.

(18) Bijlaard, P. P., "Weight-Strength Analysis of Ring Stiffened Shells," Bell Aircraft Corporation, Report 02-984-030, August 1954.

(19) Shanley, F., "Weight-Strength Analysis of Aircraft Structures," The Rand Corporation, First Edition, McGraw-Hill Book Company, Inc., 1952.

(20) Mordfin, L., "Creep and Creep-Rupture Characteristics of Some Riveted and Spot-Welded Lap Joints," NACA TN 3412, June 1955.

(21) Bleich, F., "Buckling Strength of Metal Structures," 1952, page 478.

[redacted]

(22) Winter, G., "Performance of Compressive Plates as Parts of Structural Members," Engineering Structures Supplement, Academic Press, New York, pages 179 through 185.

(23) Bijlaard, P. P. and Fisher, G. P., "Column Strength of H Sections and Square Tubes in Post-Buckling Range of Component Plates," NACA TN 2994, August 1953.

(24) Bijlaard, P. P., "Buckling of a Cylindrical Shell Compressed in the Axial Direction and Clamped at the Loaded Edges," Bell Aircraft Corporation, Report 02-984-026, 2 September 1954.

(25) Shanley, F., "Weight-Strength Analysis of Aircraft Structures," McGraw-Hill Book Company, Inc., 1952.

(26) Timoshenko, S., "Theory of Plates and Shells," McGraw-Hill Book Company, Inc., 1940.

(27) Sturm, R. G., "A Study of the Collapsing Pressure of Thin-Walled Cylinders," University of Illinois, Engineering Experiment Station Bulletin, Series No. 329, 11 November 1941.

(28) Saunders, H. E. and Windenburg, D. F., "Strength of Thin Cylindrical Shells Under External Pressure," Transactions of ASME, Vol. 53, APM-53-17a, 1931.

(29) Windenburg, D. F. and Trilling, C., "Collapse by Instability of Thin Cylindrical Shells Under External Pressure," Transactions of ASME, Vol. 56, 1934.

(30) Bijlaard, P. P., "Buckling Under External Pressure of Cylindrical Shells Evenly Stiffened by Rings Only," Bell Aircraft Corporation, Report 02-941-002, 21 May 1952.

(31) Wong, R. E., "Design Charts for the Buckling of Cylindrical Shells Stiffened by Rings Under External Pressure," Bell Aircraft Corporation, Report 02-948-010, 1 December 1953.

(32) Kinsley, E. J., "Corrosion Test Program No. 1," Bell Aircraft Laboratory Report 51-106, August 1952.

(33) Heubusch, H. P., "The Decomposition of Red Fuming Nitric Acid," Bell Aircraft Corporation, Report D127-945-039, 19 November 1951.

(34) Heubusch, H. P., "The Decomposition of White Fuming Nitric Acid," Bell Aircraft Corporation, Report D127-945-038, 29 October 1951.

(35) Stowell, E. Z., Heimerl, G. J., Libove, C., and Lundquist, E. E., "Buckling Stresses for Flat Plates and Sections," Transactions ASCE, Vol. 117, 1952, pages 545 through 575.

(36) Bijlaard, P. P., Fisher, G. P., and Winter, G., "Eccentrically Loaded, End Restrained Columns," Transactions ASCE, Vol. 120, 1955, pages 1070 through 1115.

(37) Osgood, W. R., "The Effect of Residual Stresses on Column Strength," Proceedings First U. S. National Congress of Applied Mechanics, 1951, pages 415 through 418.

(38) Bijlaard, P. P. and Wong, R. E., "Weight-Strength Analysis of Pressure Vessels and Influence of Internal Pressure on Ring-Stiffened Shells," Bell Aircraft Corporation, Report 02-984-031, June 1955.

(39) Koegler, R. K. and Schnitt, A., "The Effects of Yielding and Perforations on a Wing Tension Surface," I. A. S. Journal, October 1943, Vol. 10, No. 8, pages 273 through 284.

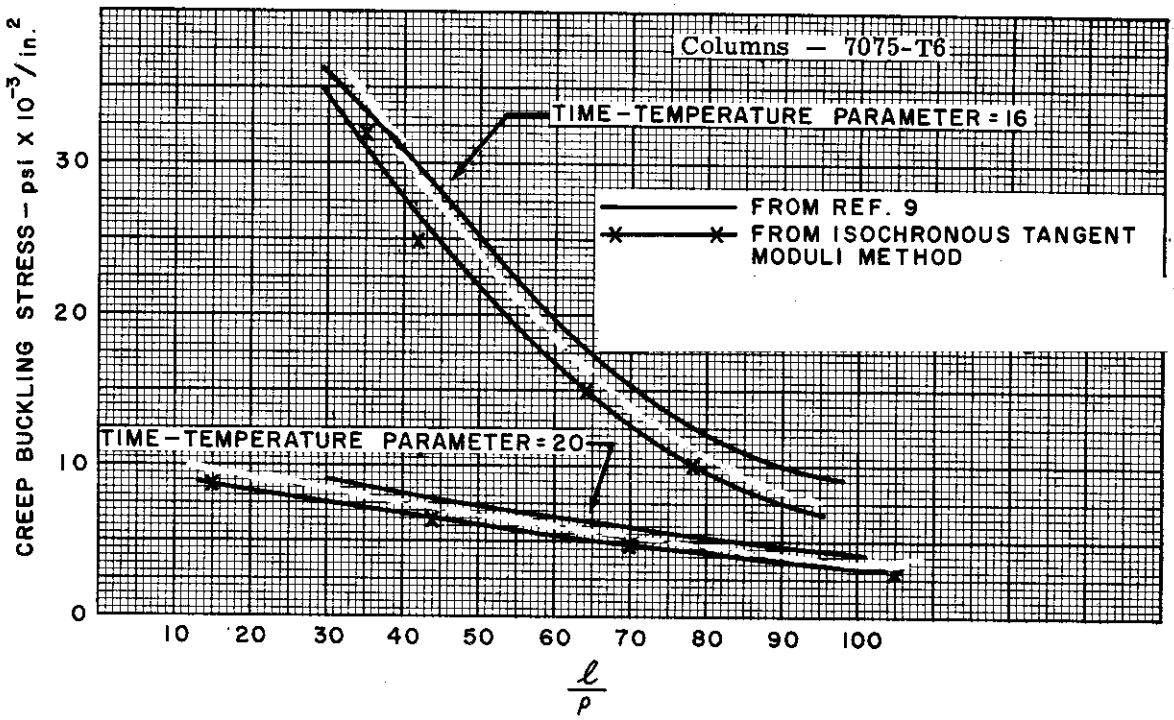

Figure VII-1. Creep Buckling — Comparison Between Test Results and Isochronous Tangent Moduli Method

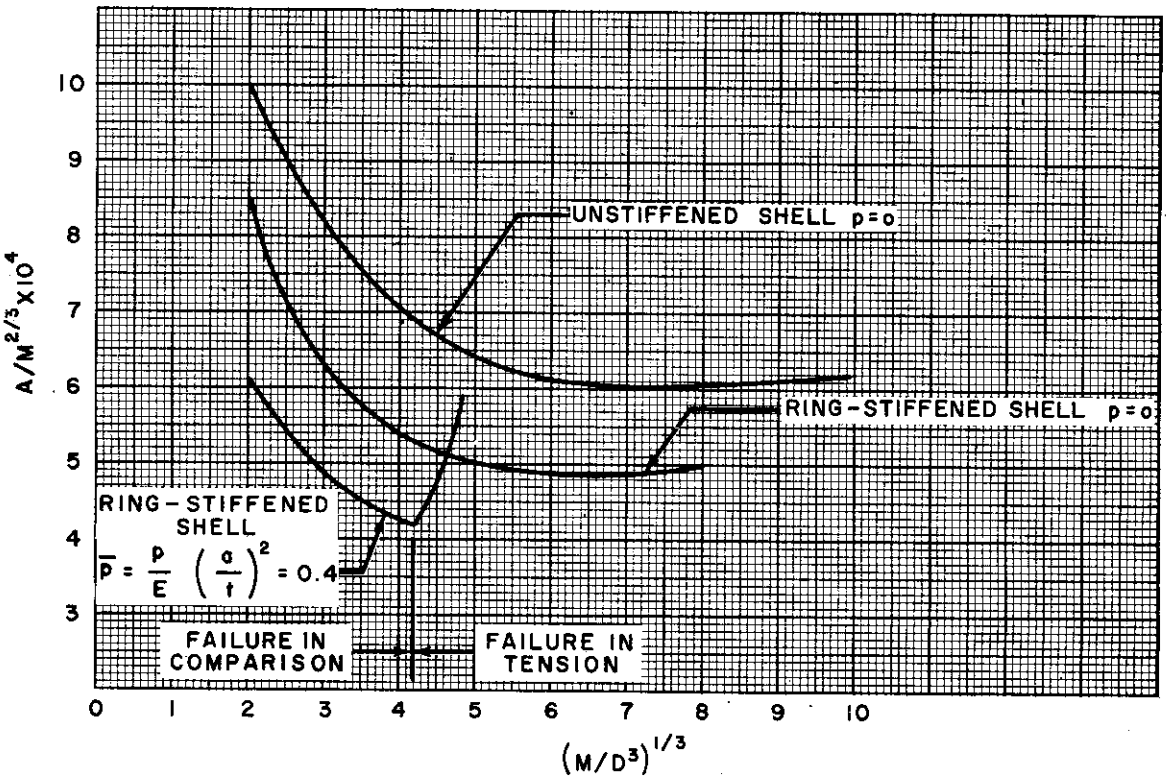

Figure VII-2. Weight Comparison for 24S-T Cylinders at Room Temperature

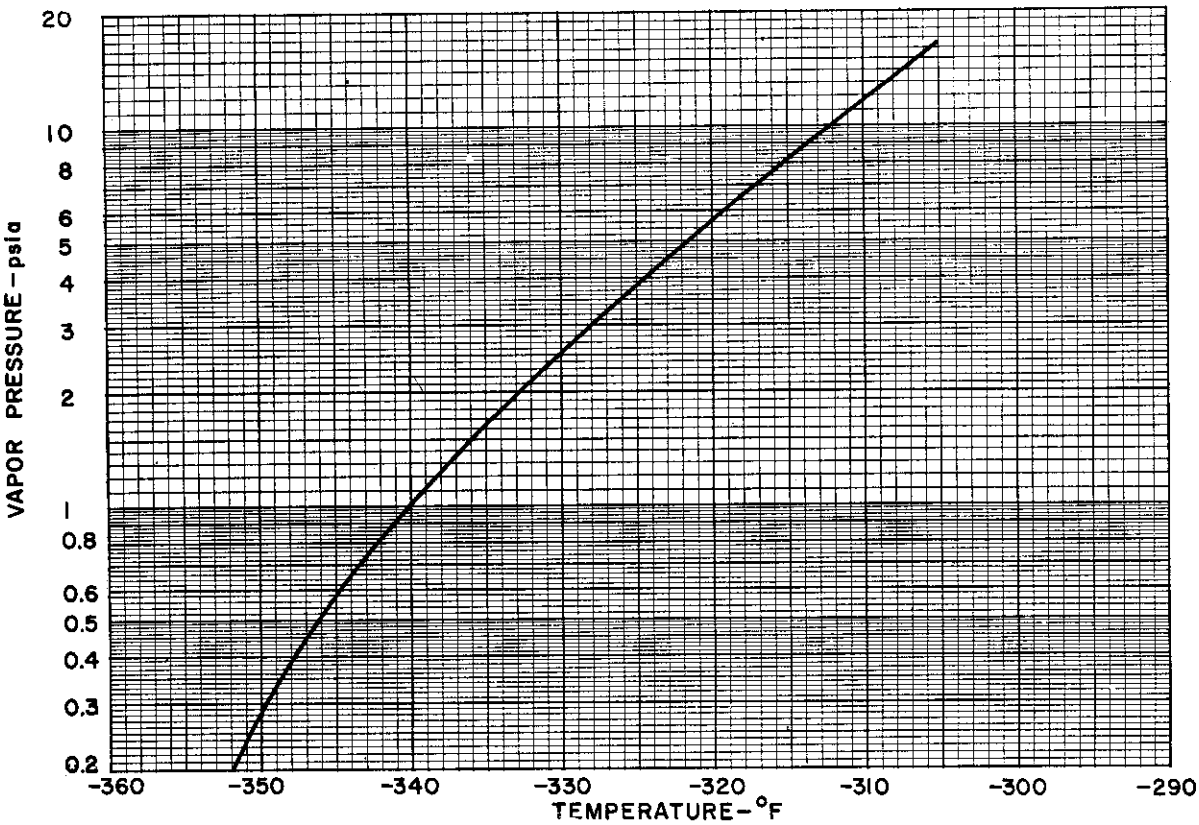

Figure VII-3. Vapor Pressure vs. Temperature with Fluorine as Oxidizer

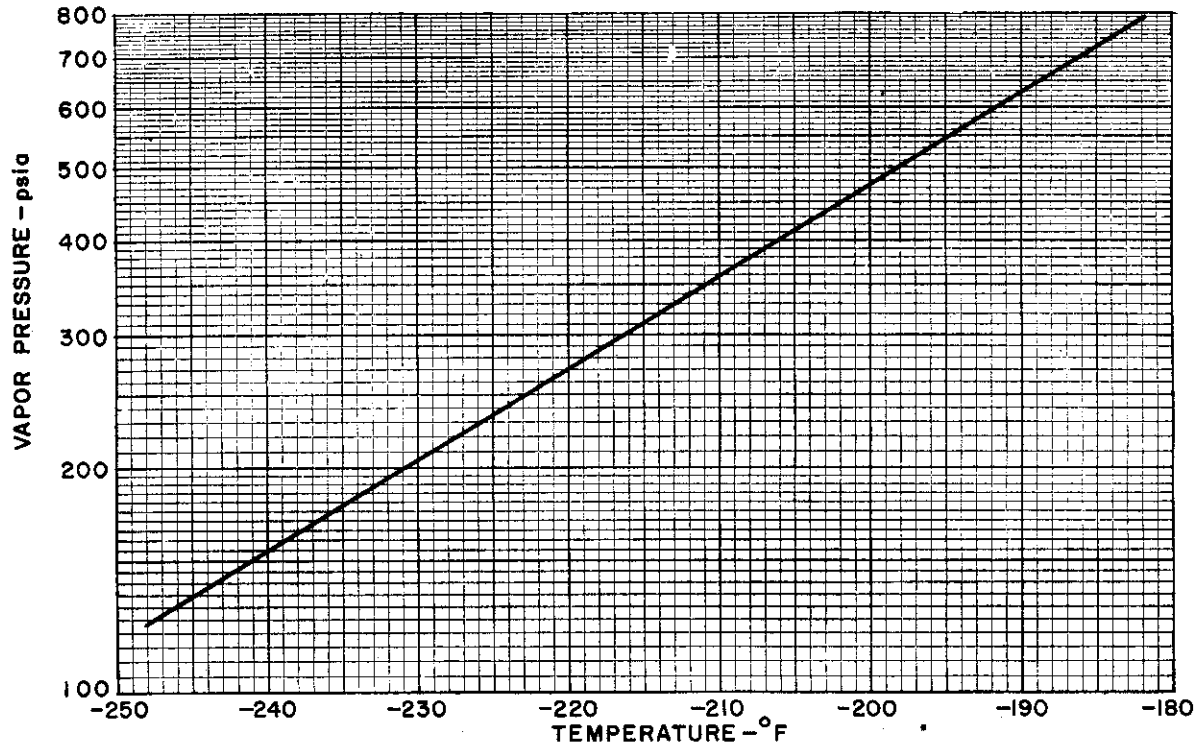

Figure VII-4. Vapor Pressure vs. Temperature with Liquid Oxygen as Oxidizer

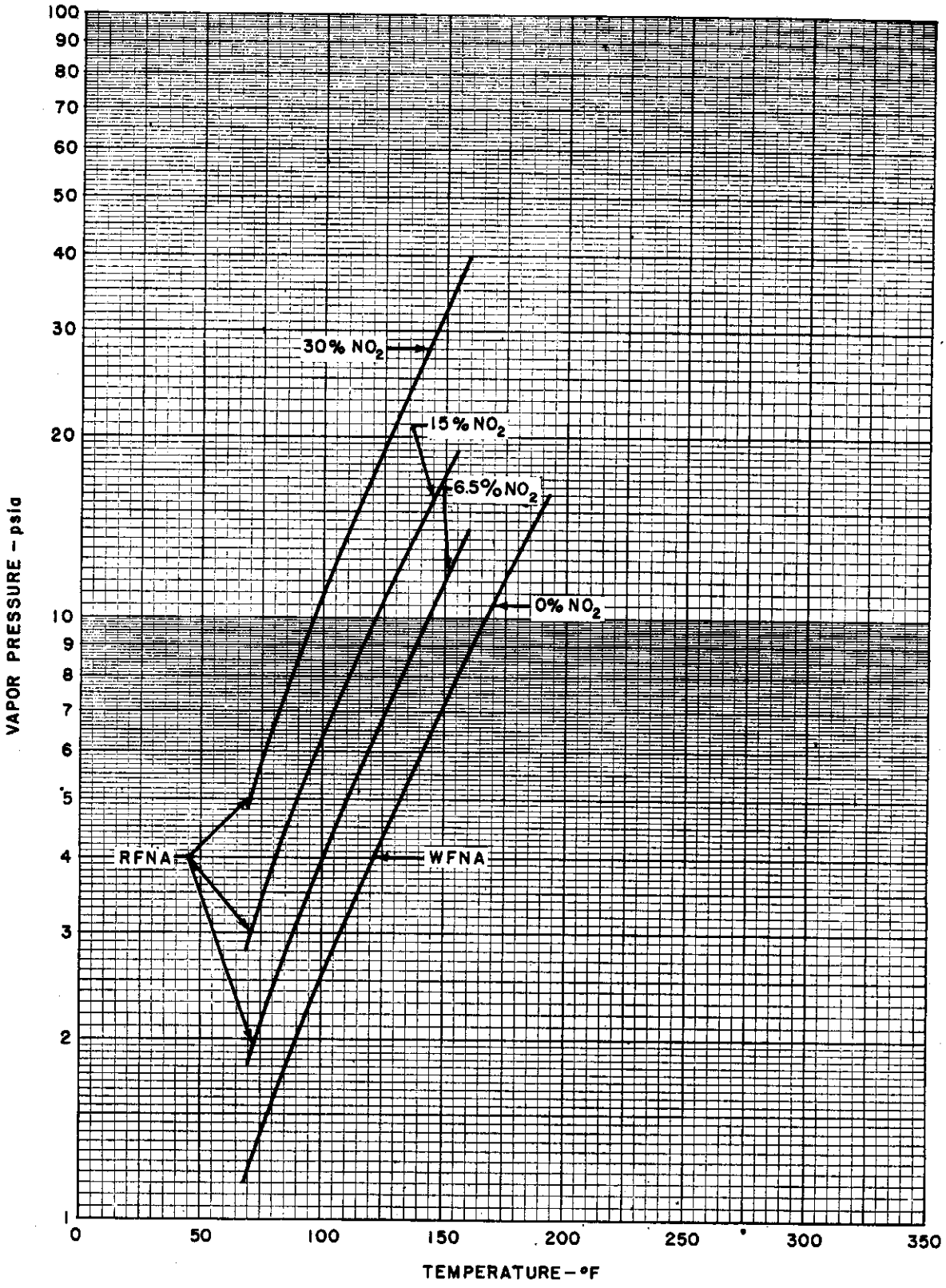

Figure VII-5. Vapor Pressures vs. Temperature with Red and White Fuming Nitric Acid as Oxidizers

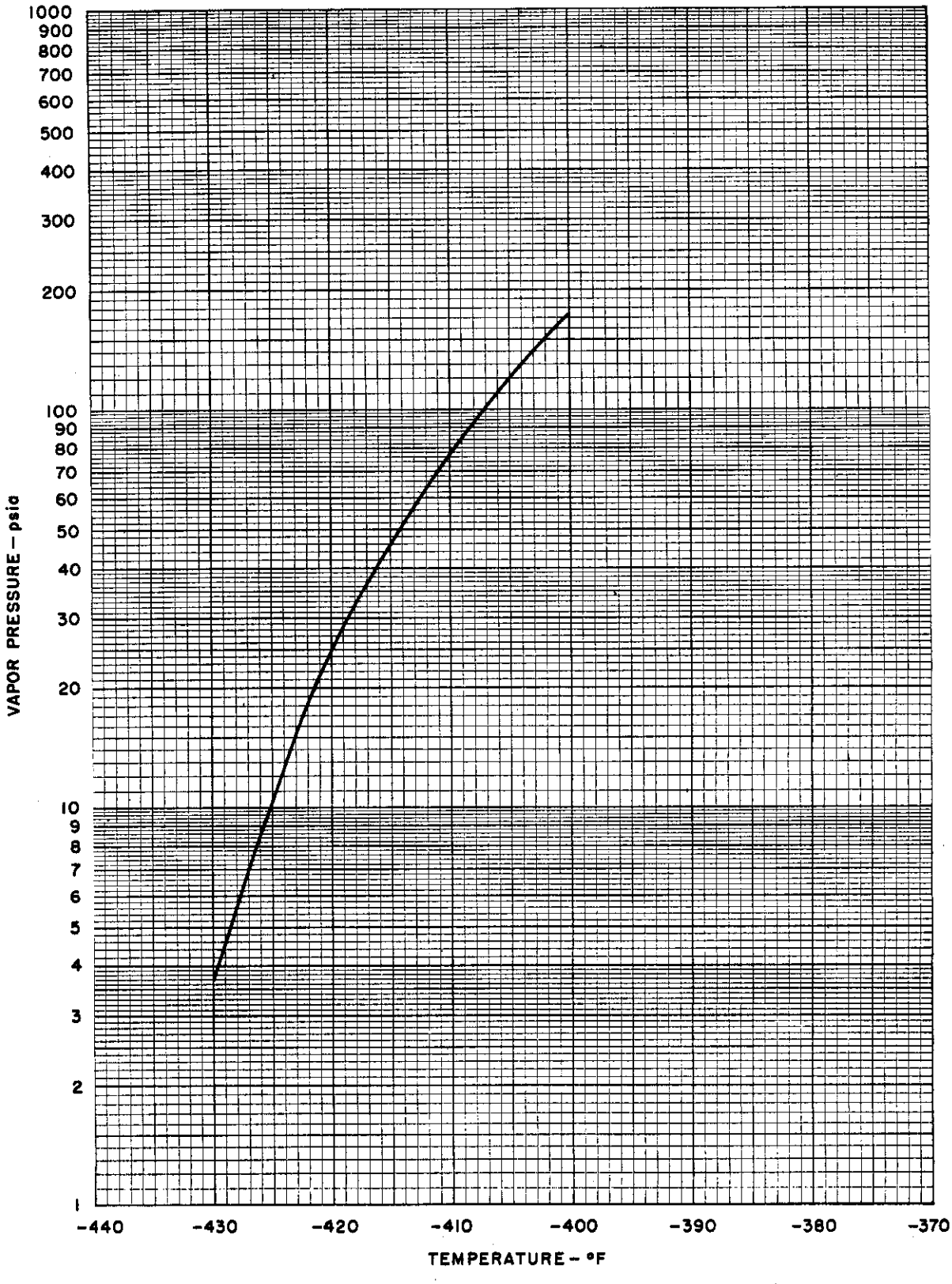

Figure VII-6. Vapor Pressure vs. Temperature with Liquid Hydrogen as Fuel

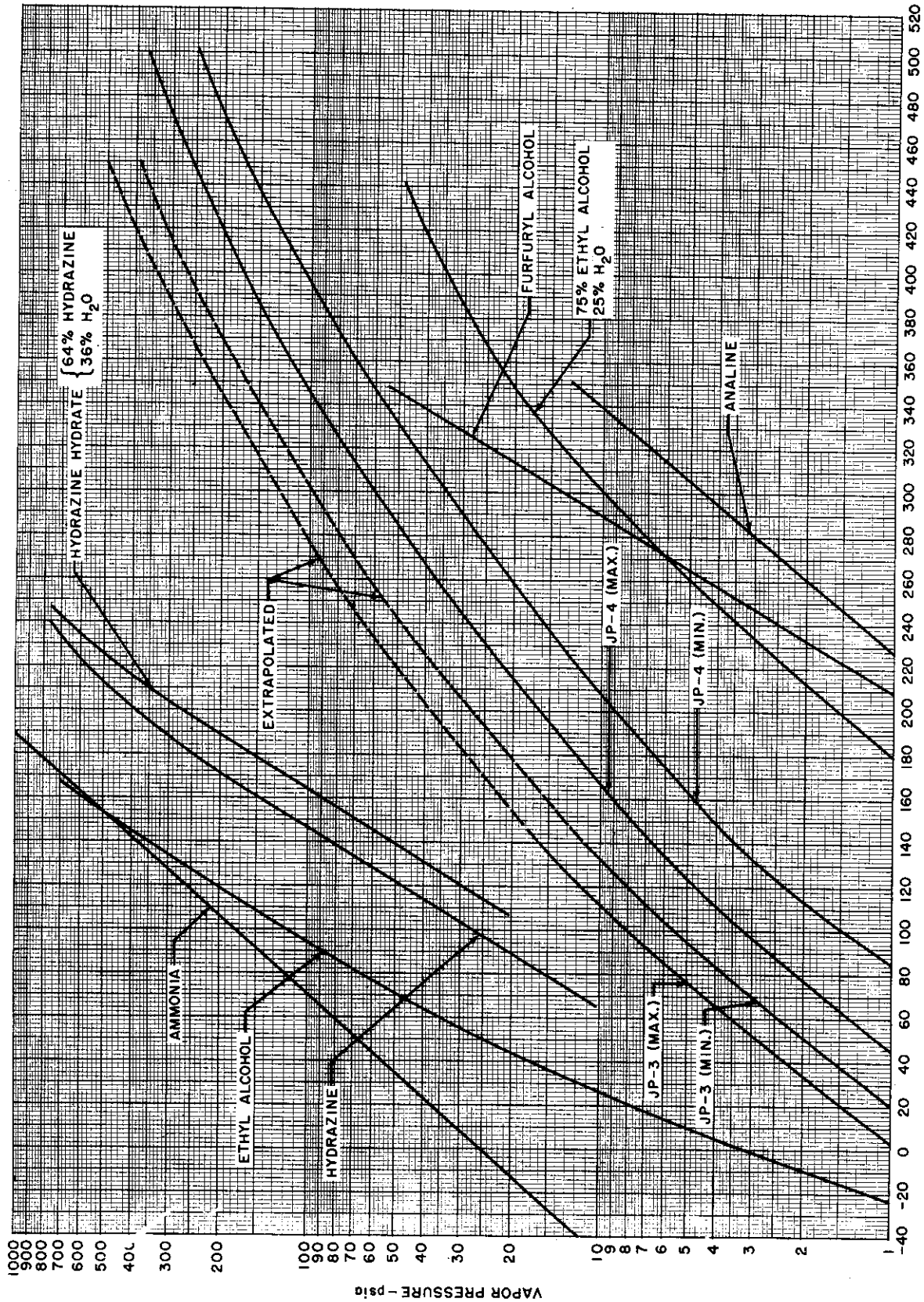

Figure VII-7. Vapor Pressures vs. Temperature with Various Fuels

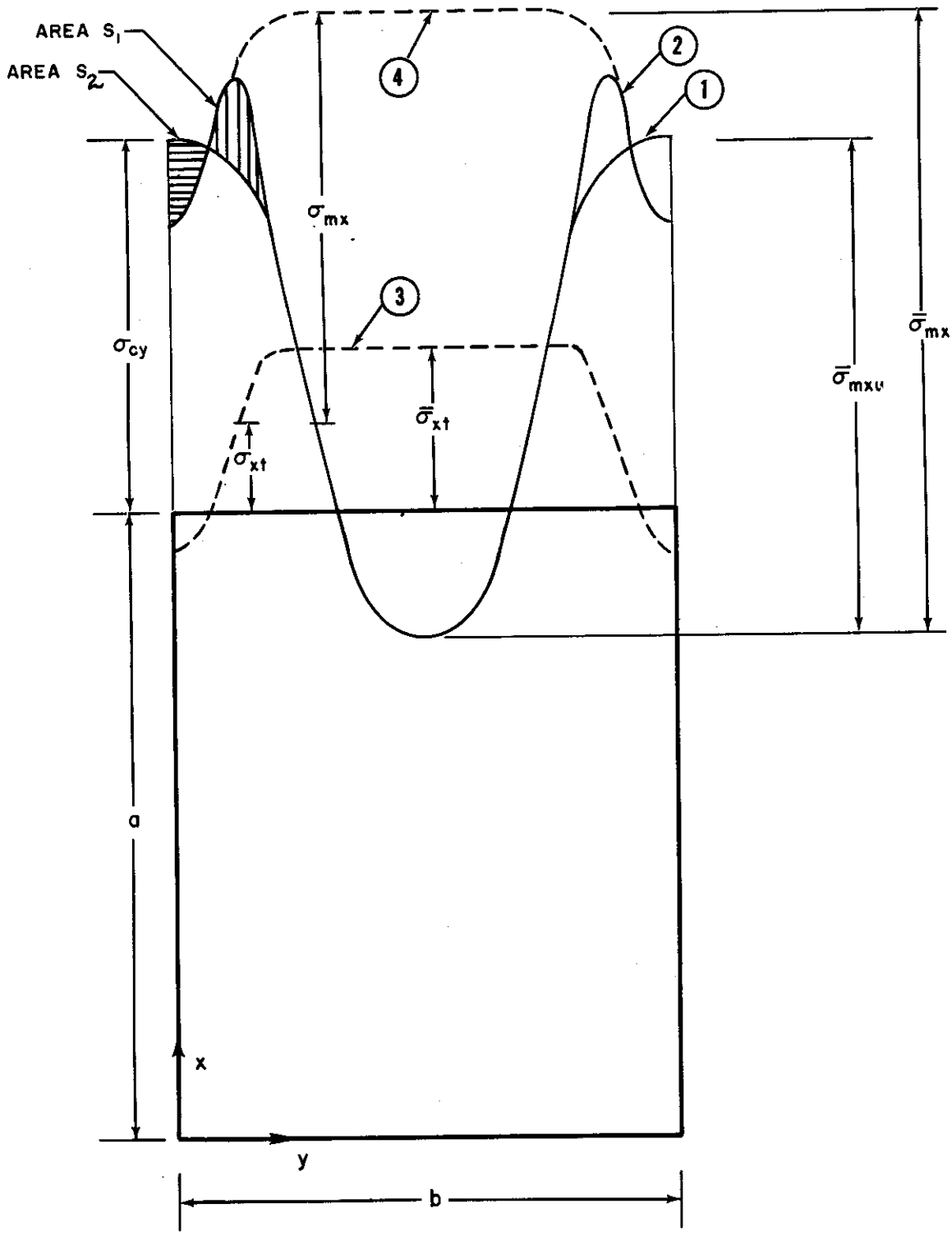

Figure VII-8. Stresses in Plate at Ultimate Load

SECTION VIII

SELECTION OF COMPARISON PARAMETERS

By A. Schnitt, M.A. Brull, and H.S.Wolco

TABLE OF CONTENTS

NOMENCLATURE

b = width of skin panel

c = structural chord for multiweb beam

c_s = specific heat of structural material

D = diameter of cylindrical shell

E = Young's modulus

E_s = secant modulus

E_t = tangent modulus

h = structural depth for multiweb beams

h_e = heat transfer coefficient

K = plate buckling coefficient for single-skin panel

k_i = thermal conductivity of insulation

k_3 = shape factor in wide-column buckling equation

L = distance between rings for ring-stiffened cylindrical shells

L_o = effective column length

M = total bending moment

M_c = moment carried by the covers of a multiweb

M_w = moment carried by the webs of a multiweb

q = edge loading per inch of chord

R = load distribution factor for multiweb beams

$r = \dfrac{t_s}{t_s + t_i}$ ratio of structural material thickness to total wall thickness

S = loading parameter defined in Equation (29)

T_{aw} = adiabatic wall temperature

T_i = initial temperature of the structure

T_o = equilibrium wall temperature

T_R = temperature ratio defined as $= (T_o - T_i)/(T_o - T_s)$

T_s = operating temperature specified for a given insulated structure

t = wall thickness for cylindrical shells

$\bar{t}$ = average structural thickness for a wide column

t_e = effective thickness for protected structures

t_i = thickness of insulation

t_s = skin thickness

t_w = web thickness

w_i = insulation weight

w_p = weight per unit wetted area of protective system

NOMENCLATURE (cont)

w_1 = weight per unit wetted area of outer wall and supporting structure

w_2 = coolant weight

w_3 = weight per unit wetted area of pumping and valving equipment

y = distance from neutral axis of a beam

η = plasticity coefficient

θ = time

θ_F = duration of flight

ν = Poisson's ratio

ρ, ρ_s = density of structural material

ρ_i = density of insulation material

σ = stress

[redacted]

SECTION VIII

SELECTION OF COMPARISON PARAMETERS

A. GENERAL

This section of the report presents methods of comparison between materials used in structural design which will serve as a guide in selecting material, structural configuration, and protective equipment (if any) for a given vehicle. The results of these analyses have been used in Section IX as a basis for comparing structural efficiencies, and also in Part III in the treatment of preliminary structural design problems.

In the past, the choice of structural material and configuration has presented no major difficulties because a great deal of theoretical and experimental information is available by which to optimize aluminum structures. For operation at room temperatures, it can be shown (References 1 and 2) that material and configuration can be selected purely on the basis of loading and size. The prospect of operation at elevated temperatures, however, introduces the additional factors of temperature and time-of-loading at temperature.

It is realized that in only a few special cases will aircraft be subject to the simplified conditions of constant temperature and short-time loading, or constant temperature and long-time loading. However, as explained previously, comparisons will be made only on these simplified bases. It is anticipated that the results of present and future research will yield methods by which the true load-temperature-time relations may be accounted for (see Sections I and III). The comparison parameters developed in this section can then be used in conjunction with properly defined temperature and time variables.

It should be noted also that the optimum design parameters developed here do not account for thermal stresses. Comparison between materials may be made on the basis of total loading which includes both thermally induced loading and applied loading. The determination of buckling and ultimate applied load can then be carried out by the methods of Sections VI and VII.

Many investigators have compared materials for elevated temperature operation on the basis of the ratio of yield-strength to density. While this procedure is more adequate for elements loaded in tension only, it is entirely inadequate for compression structures; in addition, this method does not consider the possibility of protecting the structure by insulation or cooling, or both.

Recently, other investigators have extended the comparison to simple columns and simply supported plates. Although these comparisons do represent an improvement over the strength-density criterion, they do not incorporate all the basic factors which should enter into consideration. These are: type of structure (such as wide column or multiweb), loading, size, operating temperature or heat input conditions, and time of loading at temperature.

To make a fair comparison between materials, it is necessary to consider optimized structures of different materials, but designed for the same ultimate load and environmental conditions. A logical parameter to use for this comparison is the stress-to-density ratio $\left(\frac{\sigma}{\rho}\right)$ for optimum structural proportions.

It can be shown that this quantity varies inversely with structural weight so that for a given ULTIMATE LOAD AND FIXED OVERALL DIMENSIONS, maximum $\frac{\sigma}{\rho}$ corresponds with minimum weight-strength. With insulated or cooled structures, it is possible, as will be shown later, to use an effective stress-to-density ratio $\left(\frac{\sigma}{\rho}\right)_e$ which includes the weight due to protective devices, so that a direct comparison of protected and unprotected structures is obtained.

[redacted]

For flights of appreciable duration, it is possible to compare material, as the basis of equal operating temperature, since it is likely that a steady-state condition will be reached. However, for flights of very short duration, the comparison between materials should be made on the basis of identical heat input conditions, so that the thermal properties of the various materials will determine the actual operating temperature. Parameters for both types of comparisons are developed here.

B. COMPARISON BASED UPON STEADY-STATE TEMPERATURE

A logical comparison between materials and structures for operation at elevated temperature requires consideration of all factors mentioned previously. Obviously, a series of optimum stress curves must be obtained for various materials and structural configurations over a wide range of operating temperatures.

As stated previously, some optimum design information is available for room-temperature operation. For example, Reference 3 presents optimum stress curves as a function of loading for optimum wide columns of 24S-T and 75S-T aluminum. Since each curve is the result of a large number of tests, the work necessary to obtain similar data for different materials over a wide range of temperatures and exposure times would be formidable. For this reason, considerable research would be avoided if a method were developed by which one could transform optimum stress curves for a given material at room temperature into the corresponding optimum stress curve for another material at a different temperature. Younger (Reference 4) has proposed a graphical method of performing such a transformation for wide-column optimum stress curves. Although this attempt represents a most important step in the right direction, some of the assumptions made in the development invalidate the results, especially when the transformation is used between materials having widely different moduli. A different procedure, based on less restrictive assumptions, has been developed and is presented for three basic types of structural configurations: wide columns, multiweb beams, and unstiffened cylinders. Similar methods could be developed also for other types of structures.

1. Development of the Transformation Laws for Optimum Stress Curves

a. Wide Columns

The optimum design of wide columns has been considered by Shanley (Reference 5) and Micks (Reference 6). Micks has shown, for such elements, that minimum weight-strength occurs when the local buckling stress for each element of the panel is equal to the column buckling stress.

For wide columns, the buckling stress is given by (see Reference 5)

$$\sigma = \pi^{\frac{2}{3}} E_t^{\frac{1}{3}} k_3^{\frac{2}{3}} (q/L_o)^{\frac{2}{3}}, \tag{1}$$

where E_t = tangent modulus,

$k_3 = r_t / \bar{t}$ = shape factor,

r_t = radius of gyration of column cross-section,

$\bar{t}$ = average thickness of cross-section,

q = load per inch width, and

L_o = effective column length.

The buckling stress for a single skin panel is

$$\sigma = K \eta E \left(\frac{t_s}{b}\right)^2, \tag{2}$$

where η = plasticity coefficient,

E = Young's modulus,

t_s = skin thickness, and

b = width of skin panel

Micks (Reference 6) has shown that the shape factor k_3 in Equation (1) may be expressed as a function of the quantity $(t_s/b)^2$ only. Since the buckling stress of a skin panel and the buckling stress of the entire element are assumed equal for optimized wide columns, the quantity $(t_s/b)^2$ entering into the definition of k_3 (Equation (26) of Reference 6) can be expressed in terms of stress as

$$\left(\frac{t_s}{b}\right)^2 = \frac{1}{K}\left(\frac{\sigma}{\eta E}\right). \tag{3}$$

Therefore, for optimum wide columns, the shape factor k_3 is determined only by the value of the quantity $(\frac{\sigma}{\eta E})$ and is the same for all materials for a given value of $(\frac{\sigma}{\eta E})$ This property leads to a simple method of obtaining optimum stress curves for any material from the corresponding curve for another material. The procedure is as follows.

Given an optimum stress curve of σ vs. q/L_o for a specific material, the quantity $(\frac{\sigma}{\eta E})$ is calculated by taking values of σ and determining the coefficient η (Reference 7 and 8). The only information required is the stress-strain curve for the material in question. For the same value of stress σ, the shape factor k_3 can be determined from the optimum curve by

$$k_3 = \frac{\sigma^{\frac{3}{2}}}{\pi E_t^{1/2}(q/L_o)}. \tag{4}$$

The shape factor k_3 is then plotted as a function of $\left(\frac{\sigma}{\eta E}\right)$ and, according to the afore-mentioned remarks, this curve represents a universal relationship valid for all materials. To produce an optimum stress curve for a given material, values of σ are assumed and the corresponding values of E_t and η are obtained from the stress-strain curve of the material and Reference 8. It is then possible to calculate the quantity $\left(\frac{\sigma}{\eta E}\right)$ corresponding with the assumed stress values, and k_3 can then be read from the universal curve. The values of q/L_o corresponding with the assumed stress values for optimum columns of the new material can then be calculated from

$$\frac{q}{L_o} = \frac{\sigma^{3/2}}{\pi E_t^{1/2} k_3}. \tag{5}$$

The resulting curve of σ vs. q/L_o for the new material is the optimum stress curve for wide columns of the new material.

b. Multiweb Beams

The determination of optimum proportions for multiweb beams has been investigated by Gerard (Reference 9). In this paper, the optimization criterion was obtained from the assumption that minimum weight-strength is attained when buckling of the top cover and the webs occurs at the same stress. Gerard only considers buckling of the webs under pure bending and neglects forced crippling. Failure by forced crippling may occur when the webs of the beam are formed channels so that the attachments between the skin and webs are not in the plane of the webs. In such cases, the webs act as an elastic, rather than a rigid, restraint and the assumption of simple support is violated. As a result, the optimum ratio of web thickness to cover thickness predicted by this method will probably be somewhat lower than the true value in cases where the failure is likely to be due to forced crippling. This observation has been confirmed by theoretical and experimental work performed at the Bell Aircraft Corporation (Reference 12) and at the NACA (Reference 10). In view of these assumptions, the optimum curves presented here apply to multiweb beams where the forced crippling mode is not present. Integral construction, which is currently in wide use, satisfies this requirement.

The buckling stress for the top cover is given by

$$\sigma_c = \frac{4\pi^2 \eta E}{12(1-\nu^2)} \left(\frac{t_s}{b}\right)^2 , \tag{6}$$

while the web buckling stress is

$$\sigma_w = \frac{25\pi^2 \eta_w E}{12(1-\nu^2)} \left(\frac{t_w}{h}\right)^2 , \tag{7}$$

where σ_c = top cover buckling stress,

σ_w = web buckling stress,

t_s = top cover thickness,

t_w = web thickness,

b = width of one cell,

h = height of beam,

η = plasticity coefficient for skin, and

η_w = plasticity coefficient for webs.

If it is assumed that $\eta = \eta_w$, equating σ_c and σ_w according to the optimization criterion yields the relation

$$\frac{t_w}{t_s} = \frac{2}{5} \frac{h}{b} . \tag{8}$$

To find the optimum number of cells for a given beam, an expression for the solidity (the ratio of material area to total enclosed area of the cross-section) is written in terms of the number of cells, n, and differentiated with respect to n. The solidity is given by (see Reference 9)

$$S = \left[\frac{12(1-\nu^2)q}{4\pi^2 \eta E c}\right]\left[n^{-2/3}\left(\frac{c}{h}\right) + \frac{2}{5}(n+1)n^{1/3}\left(\frac{h}{c}\right)\right], \tag{9}$$

where $q = \sigma_c t_s$ = loading in top cover,

c = structural chord, and

n = number of cells.

It should be noted that the first factor on the right-hand side of Equation (9) depends only upon loading, structural chord, and material properties, so that the optimum number of cells can be obtained by differentiating the second factor and equating the result to zero. The result of this operation is

$$n^2 + \frac{1}{4}n - \frac{5}{4}\left(\frac{c}{h}\right)^2 = 0 ,$$

the solution of which is the optimum number of cells. This solution is given approximately by

$$n_o = -\frac{1}{8} + \left(\frac{5}{4}\right)^{1/2}\left(\frac{c}{h}\right) \tag{10}$$

from which it follows that the ratio of cell width to cell depth is

$$\left(\frac{b}{h}\right)_o = \left(\frac{4}{5}\right)^{1/2}\left[1 + \frac{1}{8n_o}\right] \tag{11}$$

or

$$\left(\frac{b}{h}\right)_o \approx 1 . \tag{12}$$

Equations (8), (10), and (11) completely determine the optimum proportions of multiweb beams regardless of material. To develop a method of transformation applicable to the optimum stress curves for such beams, it is necessary to derive a universal relationship between the loading and some material parameter which will hold for all materials. This can be done as follows.

The moment carried by the webs is given by

$$M_w = (n+1)\int_{-h/2}^{h/2} \sigma_w\, y\, t_w\, dY , \tag{13}$$

while the moment carried by the cover plates is

$$M_c = \sigma_c t_s c h = n\sigma_c t_s b h . \tag{14}$$

If the nonlinearity of stress distribution due to plastic bending is neglected, the stress at any point of the cross-section is

$$\sigma = \frac{My}{\frac{1}{12}(n+1)t_w h^3 + \frac{1}{2}nh^2 t_s b} . \tag{15}$$

Substituting Equation (15) in Equations (13) and (14) gives, after some simplification,

$$M_c = \frac{M}{1+R} \quad \text{and}$$
$$M_w = \frac{RM}{1+R} , \tag{16}$$

where

$$R = \frac{1}{6}\left(\frac{n+1}{n}\right)\left(\frac{t_w}{t_s}\right)\left(\frac{h}{b}\right) . \tag{17}$$

Using Equations (8), (10), and (11) in Equation (17) gives the value of R for the optimum configuration as

$$R_o = \frac{1}{960}\left(\frac{h}{c}\right)^2 + \frac{1}{8\sqrt{5}}\left(\frac{h}{c}\right) + \frac{1}{12} .$$

For thin wings, the first and second terms of this expression are small compared with the last. Since multiweb construction is likely to be used only for such wings, the optimum value of R may be taken as

$$R_o = \frac{1}{12} , \tag{18}$$

from which it is seen that in a multiweb beam of optimized proportions, the covers will carry about 90% of the moment.

By use of Equations (15), (16), and (17), the cover stress can be expressed, in terms of the external moment, thus

$$\sigma_c = M \frac{h/2}{\frac{1}{12}(n+1)t_w h^3 + \frac{1}{2} n t_s h^2 b} = \frac{M}{(1+R_o)t_s hc} .$$

This last expression may be written

$$\sigma_c = \frac{M}{(1+R_o)\frac{t_s}{b} hcb} = \frac{M}{(1+R_o)\left(\frac{t_s}{b}\right)h^2 c} .$$

Finally, substituting for $\left(t_s/b\right)$ from Equation (6) yields the relation

$$\sigma_c \left(\frac{\sigma_c}{\eta E}\right)^{1/2} = \frac{1}{1+R_o}\left[\frac{4\pi^2}{12(1-\nu^2)}\right]^{1/2} \frac{M}{h^2 c} . \qquad (19)$$

Equation (19) is a relation between the material parameter $\sigma_c\left(\frac{\sigma_c}{\eta E}\right)^{1/2}$ and the structural index $\frac{M}{h^2 c} = \frac{q}{h}$, which holds for all optimum multiweb beams. Since the proportions do not enter into this expression, if two multiweb beams of different materials are designed for the same ultimate bending moment, they must fail at the same value of the parameter $\sigma_c\left(\sigma_c/\eta E\right)^{1/2}$. It is possible to obtain theoretical optimum stress curves by using Equation (19) with the proper value of R_o given by Equation (18). Since Equation (19) gives a universal relation between $\left(M/h^2 c\right)$ and $\sigma_c\left(\sigma_c/\eta E\right)^{1/2}$, an optimum stress curve for a specific material can be obtained by plotting for the material in question a curve of σ_c vs. $\sigma_c\left(\sigma_c/\eta E\right)^{1/2}$ for which the only information needed is a stress-strain curve (the value of η to be used is that for flat plates in compression, Reference 7). From Equation (19) and this curve, it is then possible to obtain an optimum stress curve for the material in question.

Owing to the assumptions made in the development of Equation (19), it may be advantageous to use experimental information in obtaining the universal curve of $\sigma_c\left(\frac{\sigma_c}{\eta E}\right)^{1/2}$ vs. $\frac{M}{h^2 c}$. This could easily be done if an optimum stress curve for multiweb beams of a specific material were available. This optimum stress curve determined experimentally can easily be replotted as a curve of $\sigma_c\left(\frac{\sigma_c}{\eta E}\right)^{1/2}$ vs. $\frac{M}{h^2 c}$ using the stress-strain curve for the given material. This new curve could then apply to optimized beams of any material. The use of an experimental curve as the starting point of the transformation should help to minimize any errors introduced by the neglect of forced crippling and plastic bending effects.

[redacted]

c. Unstiffened Cylinders

In the case of long unstiffened cylinders, the optimization is accomplished by making the maximum bending stress equal to the buckling stress of the cylinder in bending. The buckling stress for cylinders is given by (Reference 13)

$$\sigma = 2.6\, c\eta E\left(\frac{t}{D}\right), \tag{20}$$

where σ = critical buckling stress,

c = buckling coefficient,

t = wall thickness, and

D = shell diameter.

If the nonlinearity of stress distribution is again neglected, the bending stress and structural index $\frac{M}{D^3}$ are related by

$$\frac{M}{D^3} = \frac{\pi}{4}\frac{\sigma}{(D/t)}\,. \tag{21}$$

Substituting for D/t in Equation (21) by use of Equation (20) yields the relation

$$\sigma\left(\frac{\sigma}{\eta E}\right) = \frac{10.4}{\pi}\, c\, \frac{M}{D^3}\,. \tag{22}$$

Since the buckling coefficient c is a constant, Equation (22) then takes the form of a universal relation satisfied by all optimum cylinders having the same structural index.

For cylinders, a parameter that furnishes a direct comparison of structural weight for various materials is the quantity $\left(\rho A/M^{2/3}\right)$ (Reference 1), which is given by the equation

$$\rho\frac{A}{M^{2/3}} = 4\left(\frac{M}{D^3}\right)^{1/3}\frac{1}{\sigma/\rho}\,. \tag{23}$$

Equations (22) and (23) may now be used to transform optimum curves for cylinders. Such optimum curves are given in References 1 and 11 for 24S-T aluminum cylinders at room temperature.

2. Comparison of Materials

By employing the methods developed previously, it is possible to obtain optimum stress curves for any material as long as a stress-strain curve is available. It is a simple matter to present these curves as structural efficiency σ/ρ versus structural index so that a direct comparison of materials is possible. For short exposure times under load, the short-time stress-strain curves are used in performing the transformation. It is then possible to plot optimum stress curves for various materials at different temperatures. The information can be summarized by superposing these curves and presenting optimum envelopes so that, for a given loading and temperature, the most efficient material and the optimum stress-density ratio are immediately determined. It is then possible to determine optimum structural weight.

When the exposure time under loading is appreciable, creep effects may become significant. For such cases a new family of optimum stress curves can be obtained by using isochronous stress-strain curves, in terms of the Larson-Miller parameter, as a basis for performing the transformations. The resulting optimum envelopes are then plotted for various values of the Larson-Miller parameter rather than for various temperatures. These new optimum envelopes may then be used to verify and, if necessary, modify the material choice made with the short-time optimum envelopes, by considering the life expectancy of the entire vehicle under a given loading.

[redacted]

[redacted]

3. Method of Comparison Between Protected and Unprotected Structures

In many practical cases, the use of protective equipment such as insulation and cooling may result in a more efficient structure because it will permit the use of a material that is lighter, but possesses less resistance to heat. With the use of insulation or cooling, such materials would operate near room-temperature conditions, so that the advantage of their high stress-to-density ratio would be realized. It is clear, however, that the insulation or cooling system weight must be included in the comparison between protected and unprotected structures. Thus, it is necessary to define a structural efficiency parameter that will account for the weight penalty that is due to the protective equipment. This is developed as follows.

It is convenient to define the quantities

$\left(\frac{\sigma}{\rho}\right)_e$ = effective structural efficiency,

t_e = effective structural thickness defined so that the weight per unit area is $\rho_s t_e$, and

ρ_s = density of structural material.

In the following development, the quantity $\left(\sigma/\rho\right)_s$ will denote the structural efficiency of the material at the structural operating temperature for which the protection device is designed. For any structure, protected or not, the stress-density ratio can be related to the edge loading q by the equation

$$\frac{\sigma}{\rho} = \frac{q}{\rho t} , \tag{24}$$

so that for the structure operating at a given temperature

$$\left(\frac{\sigma}{\rho}\right)_s = \frac{q}{\rho_s t_s} . \tag{25}$$

If the structure is protected, the total weight per unit wetted area is $\rho_s t_e$, instead of $\rho_s t_s$, so that the effective efficiency is

$$\left(\frac{\sigma}{\rho}\right)_e = \frac{q}{\rho_s t_e} = \left(\frac{q}{\rho_s t_s}\right)\left(\frac{t_s}{t_e}\right) ,$$

and, from Equation (25),

$$\left(\frac{\sigma}{\rho}\right)_e = \left(\frac{\sigma}{\rho}\right)_s \left(\frac{t_s}{t_e}\right) . \tag{26}$$

It is obvious from Equation (26) that the factor $\left(t_s/t_e\right)$ represents the reduction of structural efficiency due to the weight of the protective equipment.

The weight per unit wetted area for the protected structure is $\rho_s t_e = \rho_s t_s + w_p$, where w_p is the weight per unit wetted area of the protective device. This relation may be written

$$\frac{t_e}{t_s} = 1 + \frac{w_p}{\rho_s t_s} . \tag{27}$$

[redacted]

The structural thickness t_s may be expressed in terms of the edge loading q and the stress σ,

thus, $t_s = \frac{q}{\sigma}$, and hence

$$\rho_s t_s = \frac{q}{(\sigma/\rho)_s} .$$

Substituting this expression in Equation (27) gives

$$\frac{t_s}{t_e} = \frac{1}{1 + S w_p} , \tag{28}$$

where $$S = \frac{(\sigma/\rho)_s}{q} . \tag{29}$$

The value of the parameter S may be expressed in more convenient form for the various types of structural elements. Thus, for wide columns, S may be written as

$$S = \frac{(\sigma/\rho)_s}{(q/L_o)L_o} . \tag{30}$$

This form is more convenient to deal with since L_o can easily be estimated as a function of (q/L_o). In general, L_o may vary from about 10 inches for the higher values of (q/L_o) to 20 inches for the lower values of (q/L_o). For multiweb beams, S may be expressed as

$$S = \frac{(\sigma/\rho)_s}{(q/h)h} = \frac{(\sigma/\rho)_s}{(M/h^2 c)h} , \tag{31}$$

and S can therefore be determined for any given case since the beam thickness h is usually fixed.

From Equations (26) and (28), the effective value of structural efficiency is obtained as

$$\left(\frac{\sigma}{\rho}\right)_e = \left(\frac{\sigma}{\rho}\right)_s \frac{1}{1 + S w_p} . \tag{32}$$

To complete the method of comparison between unprotected and protected structure, a means of estimating w_p must be devised. It has been shown in Sections IV and V of the report that the most practical types of protective devices are insulation with outer skin, and insulation with outer skin construction and water cooling. For this reason, the method of estimating w_p will be developed only for these two types of protective equipment.

a. Insulation with Outer Skin

The weight of insulation necessary to maintain a given temperature T_s is given by

$$w_p = w_i + \rho_i t_i$$

or $$w_p = w_i + \frac{1 - r}{r} \rho_i t_s , \tag{33}$$

where w_l = weight per unit wetted area of the outer skin and the associated supporting structure. This quantity can be taken as constant and equal to 1 lb/ft^2 for insulation thicknesses up to 4 in.;

ρ_i = density of the insulation;

t_i = thickness of insulation;

t_s = structural thickness; and

$$r = \frac{t_s}{t_s + t_i} .$$

The results of Section V indicate that, if the heat capacity of the insulation is assumed small compared with that of the structure, the quantity $(1-r)/r$ can be expressed as

$$\frac{1-r}{r} = \frac{k_i \theta_F}{\rho_s c_s t_s^2 \ln T_R} , \tag{34}$$

where k_i = thermal conductivity of the insulation,

c_s = specific heat of the structural material,

θ_F = exposure time for the flight considered,

$$T_R = \frac{T_o - T_i}{T_o - T_s} ,$$

T_o = equilibrium outer wall temperature,

T_i = initial structure temperature, and

T_s = maximum allowable operating temperature for the structure.

Substituting Equation (34) in Equation (33), and remembering that $\rho_s t_s = 1/S$, gives

$$\frac{t_s}{t_e} = \frac{1}{1 + S w_p} = \frac{1}{1 + S\left[\frac{\rho_i k_i}{c_s} \frac{S\theta_F}{\ln T_R} + w_l\right]} . \tag{35}$$

Typical calculations show that, for efficient insulating materials, the major part of the weight penalty is due to the outer skin, so that a good approximation to (t_s/t_e) is

$$\frac{t_s}{t_e} = \frac{1}{1 + S w_l} . \tag{36}$$

However, the insulation thickness may, for some cases, exceed a practical limiting value, so that it may be necessary to cool the structure to reduce this thickness. For this reason, the required thickness of insulation should always be computed as a check on the practicality of the system. The required insulation thickness is given by

$$t_i = \frac{k_i}{c_s} \frac{S\theta_F}{\ln T_R} . \tag{37}$$

b. Insulation with Outer Skin and Water Cooling

For the case of an insulated and cooled structure, it can be shown (Section V) that the protective system weight is

$$w_p = w_1 + w_3 + w_i + w_2$$

$$w_p = w_1 + w_3 + \rho_i t_i + \frac{k_i}{t_i} \frac{T_o - T_s}{1000} \theta_F \ , \tag{38}$$

where w_1 = weight per unit wetted area of outer skin structure

w_2 = coolant weight = $\frac{k_i}{t_i} \frac{T_o - T_s}{1000} \theta_F$,

w_3 = weight per unit wetted area of the pumping and valving equipment, and

w_i = insulation weight = $\rho_i t_i$.

The other variables in Equation (38) have been defined previously.

Study of typical water cooling systems has shown (Section V) that the weight of pumping and valving equipment contributes only a small amount to the weight per unit wetted area. Hence, w_3 will be neglected in the subsequent development. It is of interest to determine the optimum distribution of insulation and water weights. This is accomplished by differentiating Equation (38) with respect to t_i, and setting the result equal to zero. The optimum insulation thickness is then found to be

$$t_i = \left[\left(\frac{k_i}{\rho_i} \right) \frac{T_o - T_s}{1000} \theta_F \right]^{1/2} . \tag{39}$$

Substituting this value of t_i in Equation (38) gives

$$w_p = w_1 + 2 \sqrt{\frac{\rho_i k_i (T_o - T_s)}{1000} \theta_F} . \tag{40}$$

An optimum is achieved when the weight of insulating material and the weight of coolant (in this case water) are equal. It may, however, be necessary in some cases to use nonoptimum distribution in order to limit the thickness of insulation given by Equation (39) to a practical value.

From Equations (28) and (40), it is now possible to obtain the value of $\frac{t_s}{t_e}$ for an insulated and cooled structure, thus

$$\frac{t_s}{t_e} = \frac{1}{1 + S \left[w_1 + 2 \sqrt{\frac{\rho_i k_i (T_o - T_s) \theta_F}{1000}} \right]} . \tag{41}$$

It is of interest to determine the value of the various parameters for which the weight of insulation system will be equal to that of a system with both cooling and insulation.

From Equations (33), (34), and (40), it is found that the two systems have equal weight when the following equation is satisfied:

$$\frac{\rho_i k_i}{c_s} \frac{S \theta_F}{\ln T_R} = 2 \sqrt{\frac{\rho_i k_i (T_o - T_s) \theta_F}{1000}} .$$

[redacted]

A critical value of the parameter S can then be obtained as

$$S^* = 2c_s \sqrt{\frac{T_o - T_s}{1000 \rho_i k_i \theta_F}} \ln T_R \cdot \qquad (42)$$

Note that if $S < S^*$, the system with insulation only is the lightest, while for $S > S^*$, insulation and cooling should be used. As noted previously, these considerations may be limited by the necessary thickness of insulation.

In making the choice of structure and material for a particular case, the value of S^* may be calculated from Equation (42) and the value of S is known for the structure under consideration. Then, t_s / t_e is calculated from either Equation (35) or (41), depending upon whether S is greater or smaller than S^*. At this point, the insulation thickness t_i should be calculated. The thickness of insulation will cause the structural depth of the wing to decrease and, as a result, the loading index will be higher for the protected structure than for the unprotected one. The value of $(\sigma/\rho)_s$ for this new loading can be obtained for the assumed operating temperature from the optimum stress curves, and $(\sigma/\rho)_e$ can then be calculated from Equation (32).

The value of $(\sigma/\rho)_e$ should be compared with the value of (σ/ρ) obtained from the optimum envelope corresponding with the assumed equilibrium temperature T_o.

4. Conclusions

The methods developed here should prove useful in preliminary structural design for aerodynamic heating since they provide a simple means of comparing the structural efficiencies of materials and protected or unprotected structures.

Although the effect of thermal stresses has not been included in this development, the influence of these stresses on the choice of material and type of structure (whether protected or not) can be estimated easily. In general, protected structures will experience practically no thermal stresses, while unprotected elements will experience a substantial increase in effective loading due to thermal stress. Therefore, it appears logical to make the comparison between protected and unprotected structures at constant loading. This, in effect, amounts to assuming that the loading increase due to thermal stresses is approximately equal to the loading increase due to decreasing the wing thickness in order to accommodate the insulation thickness. Thus, a comparison between protected and unprotected structure can be made for a constant value of the loading index, so that the structural efficiency (σ/ρ) will be inversely proportional to the structural weight.

C. COMPARISONS BASED UPON TRANSIENT HEAT INPUT CONDITIONS

For flights of very short duration, the heat input conditions and the thermal properties of the structural material determine the transient temperatures in the structure. It is clear, then, that for such flights, comparison between materials based upon the same operating temperature would not give an accurate picture of their relative efficiencies. An appropriate comparison in such cases would be one based upon identical heat input conditions, and taking into account the differences in thermal properties of various materials so that the transient operating temperature would be adjusted automatically according to the thermal properties of the various materials.

Parameters for such transient heat flow comparisons may be developed by carrying out the solution of a simple heat flow problem.

Consider a structural member of width b and thickness t, as shown in the following diagram, subjected to uniform aerodynamic heating from a boundary layer at temperature T_{aw}.

[redacted]

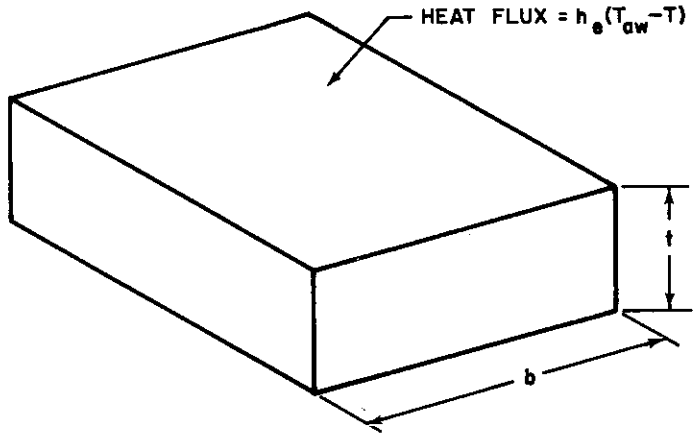

The heat balance for a unit area of the element of this diagram requires that the temperature of the member satisfy the equation

$$\frac{dT}{d\theta} = \frac{h_e}{\rho c_s t}(T_{aw}-T), \tag{43}$$

where T = temperature of member,

T_{aw} = adiabatic wall temperature,

ρ = density of material,

c_s = specific heat of material,

h_e = heat transfer coefficient,

t = thickness of member, and

θ = time.

The solution of Equation (43) is easily obtained as

$$T = T_{aw} - (T_{aw}-T_i)e^{-\frac{h_e}{\rho c_s t}\theta}, \tag{44}$$

where T_i is the initial temperature of the structure. Equation (44) may be written in the form

$$\ln \frac{T_{aw}-T_i}{T_{aw}-T} = \frac{h_e}{\rho c_s t}\,\theta\,,$$

and, remembering that the material thickness t is related to the stress and the loading by the expression $t = q/\sigma$, this expression becomes

$$\ln \frac{T_{aw}-T_i}{T_{aw}-T} = \left(\frac{h_e\theta}{q}\right)\left(\frac{1}{c_s}\right)\left(\frac{\sigma}{\rho}\right),$$

which may be written

$$\frac{\sigma/\rho}{c_s \ln \frac{T_{aw}-T_i}{T_{aw}-T}} = \frac{q}{h_e\theta}\,. \tag{45}$$

For the purpose of making simple comparisons between materials, it will be sufficient to consider only tensile or stable compression members. Under these conditions, the working stress can be taken as the compressive or tensile yield strength of the materials in question, and Equation (45) becomes

$$\frac{\sigma_Y/\rho}{c_s \ln \frac{T_{aw} - T_i}{T_{aw} - T}} = \frac{q}{h_e \theta} , \tag{46}$$

where σ_Y is the yield strength of the material.

It should be noted that the right-hand side of Equation (46) contains only quantities which depend upon the heating and loading conditions, while the left-hand side contains the material parameters. It is possible to plot the quantity $\frac{c_s}{\sigma_Y/\rho} \ln \frac{T_{aw} - T_i}{T_{aw} - T}$ against the temperature T for various materials if T_{aw} is given. In view of Equation (46), these curves may be considered as the relations between $q/h_e\theta$ and T at constant values of T_{aw} for various materials. Then, to compare materials under identical heating and loading conditions, the quantity $q/h_e\theta$ is calculated for the given flight conditions. Operating temperatures for the various materials under consideration may be obtained from the curves mentioned previously. The comparison is then made by considering the value of σ_Y/ρ for each material at the operating temperature that was determined. It is possible, by this procedure, to plot a family of envelopes giving the relation between σ_Y/ρ and $q/h_e\theta$ for various values of T_{aw}. These curves make possible a rapid choice of material for given transient heating conditions. The quantity $q/h_e\theta$ has the dimensions of temperature so that the transient heating envelopes just mentioned are completely analogous to the yield stress-to-density ratio versus temperature curve, and for the comparison of tensile materials at a steady-state temperature. The only difference is that the additional variable T_{aw} has been introduced so that there is now a family of envelopes rather than a single curve.

It should be noted that this procedure can be used in conjunction with optimum stress curves for wide columns or multiweb beams to compare such elements under identical transient heat input conditions. For such cases, the new optimum envelopes would have the quantity $q/h_e\theta$ as a parameter instead of the operating temperature; since there is the additional variable T_{aw}, a family of optimum envelopes for each value of $q/h_e\theta$ would result.

REFERENCES

(1) Shanley, F. R., "Weight-Strength Analysis of Aircraft Structures," 1st Edition, McGraw-Hill Book Company, Inc., 1952.

(2) Gerard, G., "Minimum Weight Analysis of Compression Structures," Interscience Publishers, New York (to be published).

(3) Dow, N. F. and Hickman, W. A., "Design Charts for Flat Compression Panels Having Longitudinal Extruded Y-Section Stiffeners and Comparison with Panels Having Formed Z-Section Stiffeners," NACA TN 1389, 1947.

(4) Younger, D. C., "The Development of Optimum Design Envelope Curves of Sheet-Stiffener Compression Panels Having Hat, Z, or Y-Section Stiffeners for Various Materials and Temperature Environments," Proceedings of the First Midwestern Conference on Solid Mechanics, University of Illinois, 1953, Page 5.

(5) Shanley, F. R., "Principles of Structural Design for Minimum Weight," Journal of the Aeronautical Sciences, Vol. 16, No. 3, March 1949, Page 133.

(6) Micks, W. R., "A Method of Estimating the Compressive Strength of Optimum Sheet-Stiffener Panels for Arbitrary Material Properties, Skin Thickness and Stiffener Shape," Journal of the Aeronautical Sciences, Vol. 20, No. 10, October 1953, Page 705.

(7) Bijlaard, P. P., "Theory and Test on the Plastic Stability of Plates and Shells," Journal of the Aeronautical Sciences, Vol. 16, No. 9, September 1949, Page 529.

(8) Krivetsky, A., "Plasticity Coefficients for the Plastic Buckling of Plates and Shells," Journal of the Aeronautical Sciences, Vol. 22, No. 6, June 1955, Page 432.

(9) Gerard, G., "Optimum Number of Webs Required for a Multicell Box Under Bending," Journal of the Aeronautical Sciences, Vol. 15, No. 1, January 1948, Page 53.

(10) Pride, R. A. and Anderson, M. S., "Experimental Investigation of the Pure Bending Strength of 75S-T6 Aluminum Alloy Multiweb Beams with Formed Channel Webs," NACA TN 3082, 1954.

(11) Bijlaard, P. P. and Wong, R. E., "Weight-Strength Analysis of Pressure Vessels and Influence of Pressure on Ring-Stiffened Shells," Bell Aircraft Corporation, Report 02-984-031, June 1955.

(12) Bijlaard, P. P. and Johnston, G. S., "Compressive Buckling of Plates Due to Forced Crippling of the Stiffeners," Sherman M. Fairchild Publication Fund, Paper No. FF-8, Institute of the Aeronautical Sciences, January 1953.

(13) Bijlaard, P. P., "Weight-Strength Analysis of Ring-Stiffened Shells," Bell Aircraft Corporation, Report 02-984-030, 1955.

[redacted]AL

SECTION IX

RELATIVE STRUCTURAL EFFICIENCIES

By M.A. Brull and H.S. Wolko

[redacted]L

[redacted]

TABLE OF CONTENTS

[redacted]

[redacted]

LIST OF ILLUSTRATIONS

[redacted]

NOMENCLATURE

c = structural chord

c_s = heat capacity of structural material

h = structural thickness of beam

h_e = heat transfer coefficient

k_i = thermal conductivity of insulation material

L_o = effective column length

M = bending moment

q = loading per unit of chord length

T_{aw} = adiabatic wall temperature

T_o = equilibrium temperature

T_s = structural temperature

t = structural thickness

t_c = effective thickness for insulated structure

t_i = insulation thickness

t_s = skin thickness

t_w = web thickness

w = unit structural weight

w_c = compression cover weight

w_i = insulation weight

w_p = total unit weight of protective device

w_w = web weight

w_1 = outer wall weight

w_2 = coolant weight

R_w = ratio of structural weight at elevated temperature to room-temperature structural weight

θ = time

ρ = density

ρ_i = density of insulation material

ρ_s = density of structural material

σ = stress

σ_u = ultimate strength

σ_y = yield strength

$\left(\frac{\sigma}{\rho}\right)_e$ = effective stress-to-density ratio for protected structures

$\left(\frac{\sigma}{\rho}\right)_s$ = stress-to-density ratio for structural material maintained at $T=T_s$

SECTION IX

RELATIVE STRUCTURAL EFFICIENCIES

A. GENERAL

In this section, the methods developed in Section VIII are used to determine optimum stress curves for a number of structural configurations, materials, and load-time-temperature conditions. The application of these results to the choice of structural configuration, material, and protective equipment is illustrated by means of typical examples. The weight penalty due to thermal effects is computed as a function of temperature for a hypothetical aircraft.

B. DETERMINATION OF THE OPTIMUM CURVES

Optimum stress curves for wide columns, multiweb beams, and unstiffened cylinders have been derived by using the transformation laws developed in Section VIII. The following materials have been selected because their mechanical properties appear most promising:

2024-T3 Aluminum Alloy - Clad	C-110M Titanium Alloy
7075-76 Aluminum Alloy	17-7 PH Stainless Steel
FSI-H24 Magnesium Alloy	Inconel X Nickel-Base Alloy

Two cases of load-temperature history were considered: constant-temperature, short-time loading; and constant-temperature, long-time loading. In addition, yield-strength-density ratio curves have been determined for the same materials, for the case of short-time loading and transient temperature.

The optimum stress curves for short-time loading were developed using the short-time stress-strain curves for the various materials, while the long-time loading curves are based upon isochronous stress-strain curves and are presented in terms of the Larson-Miller parameter

$$\lambda = (T_s + 460)(20 + \log\theta)10^{-3} \qquad (1)$$

where T_s = structural temperature (° F) and θ = time (hr). It is realized that the cases of constant-temperature, long-time loading do not represent the conditions to which most vehicles will be subjected. However, recent results (see Section III) indicate that the true load-temperature history of a given aircraft may, in time, be accounted for by properly defining an equivalent constant-temperature, long-time loading condition. Therefore, it is anticipated for future aircraft that the short-time ultimate-loading condition will be used to make the initial choice of configuration and material, and that some equivalent long-time constant-loading condition will then be used to verify and, if necessary, to modify the initial design.

1. Wide Columns

Optimum stress curves for wide columns were calculated by applying the transformation procedure developed in Section VIII to the optimum stress curve determined experimentally at the NACA for 75S-T6 Y-stiffened panels. This experimental curve is presented in Reference 1. In this manner, short-time optimum stress curves were obtained for the six materials mentioned previously for a range of temperatures appropriate to each material. The information contained in these individual curves was then summarized and is presented in the form of optimum envelopes in Figure IX-1. The procedure was repeated for the case of long-time loading; in this case, the optimum curves are in terms of the Larson-Miller parameter rather than the temperature. For reasons which will become apparent later, it is necessary to present individual curves rather than envelopes for long-time loading. These curves are presented in Figures IX-2 through IX-6. Envelope curves for long-time loading are presented in Figure IX-7, for the sake of completeness.

[redacted]

2. Multiweb Beams

For the case of multiweb beams, little experimental information is available on optimum stress. Reference 2 presents some data on this subject, but the tests were carried out only for a restricted range of loading index and the values chosen are in the range where it is unlikely that multiweb beams will prove efficient. For this reason, the optimum stress curves for multiweb beams were obtained by using the theoretical relation developed in Section VIII. Thus, the universal optimum-stress-structural-index relationship is that given by Equation (19) of Section VIII. As for wide columns, the short-time optimum stress information is presented in the form of envelope curves of $\frac{\sigma}{\rho}$ as a function of the loading index $\frac{M}{h^2 c} = \frac{q}{h}$ for a range of temperature. These optimum envelopes are presented in Figures IX-8 and IX-9; the figures are identical except the abscissa scale of Figure IX-9 is constructed to show the range of loading for which it is advantageous to use stainless steel. The individual optimum curves for long-time loading are presented in Figures IX-10 through IX-14, and the long-time optimum envelopes are presented in Figure IX-15.

3. Unstiffened Cylinders

For unstiffened cylinders, the optimum stress curves were obtained by applying the transformation of Section VIII to Figure 2.14 of Reference 3. As before, the results of these calculations are presented in the form of optimum envelopes for short-time loading in Figure IX-16, while the individual optimum curves for long-time loading are presented in Figures IX-17 through IX-21. The long-time loading envelopes are shown in Figure IX-22.

4. Transient Conditions

As explained in Section VIII, it is necessary, for flights of very short duration, to make material comparisons on the basis of identical heat input rather than equal temperatures. For such cases, it is necessary to produce curves of stress-to-density ratio as a function of the heat input parameter $\frac{q}{h_e \theta}$ These curves are obtained by using Equation (45) of Section VIII. For simplicity, the study of transient conditions was limited to stable compression elements, and material comparisons were made on the basis of compressive-yield-strength-to-density ratio. Curves representing this ratio versus temperature are presented in Figure IX-23. By applying Equation (46) of Section VIII, these curves were transformed into optimum stress envelopes plotted against the heat input parameter $\frac{q}{h_e \theta}$ for various values of the adiabatic wall temperature T_{aw}. The curves are presented in Figure IX-24 for adiabatic wall temperatures of 800°, 1200°, and 1600° F.

C. USE OF THE OPTIMUM CURVES

The optimum stress curves mentioned previously may be used to advantage in selecting structural configuration and material for a given aircraft. As will be shown, it is also possible to determine the life expectancy of a given design under specified load and temperature conditions.

The data obtained from the optimum curves may also be used to compute structural weights. In general, the computation of structural weight requires consideration of compression material, tensile material, shear material, miscellaneous weight increments due to such items as attachments. The optimum curves presented in this section furnish the information necessary to determine the weight of the various members. Thus, for wide columns, the average thickness of the column is given by

$$t = \frac{q}{\sigma} = \frac{\left(\frac{q}{L_o}\right) L_o}{\sigma}, \tag{2}$$

so that the weight per unit area is

$$w = \rho t = \frac{\left(\frac{q}{L_o}\right) L_o}{\left(\frac{\sigma}{\rho}\right)}. \tag{3}$$

[redacted]

For multiweb beams, the skin thickness is obtained from the expression

$$t_s = \frac{\left(M_e/h^2c\right)h}{\sigma} = \left(\frac{q_c/h}{\sigma}\right)h \ , \tag{4}$$

and, according to the development in Section VIII, the web thickness is obtained from

$$\frac{t_w}{t_s} = 0.4 \ . \tag{5}$$

With the skin and web thicknesses known, it is possible to calculate the weight of the compression cover and the webs. The weight of the tension cover is then obtained from the ultimate tensile strength of the material. Curves of ultimate tensile strength versus temperature are given in Figure IX-25. For cylinders, the weight may be calculated from Equation (23) of Section VIII.

In the case of insulated or cooled structures, the effective optimum-stress-density ratio was defined as

$$\left(\frac{\sigma}{\rho}\right)_e = \left(\frac{\sigma}{\rho}\right)_s \frac{t_s}{t_e} \ , \tag{6}$$

where $\left(\frac{\sigma}{\rho}\right)_s$ is the stress-to-density ratio for the structural material at its true operating temperature for which the insulation is designed, and t_e is the equivalent thickness designed so that the weight of the structure is $\rho_s t_e$. Since $\left(\frac{\sigma}{\rho}\right)_s$ and $\frac{t_s}{t_e}$ are known, it is easy to solve for t_e and t_s so that the weight may be determined by the methods discussed previously. Examples of the use of the various optimum envelopes are given in the following.

1. Selection of the Most Efficient Material for an Unprotected Structure

The proper use of the optimum stress envelopes is best illustrated by means of typical examples.

(1) Consider a wide column of length $L_o = 15$ in. subjected to a loading of 2200 lb/in. and operating at an equilibrium temperature of 600° F. With these data, the structural index is obtained as

$$\frac{q}{L_o} = \frac{2200}{15} = 147 \text{ lb/in.}^2 \ .$$

From Figure IX-1, for $\frac{q}{L_o} = 147$, it can be seen that with a temperature of 600° F, the most efficient material is C-110M titanium alloy, and the optimum stress-to-density ratio is

The weight of the element would then be

$$w = \frac{q}{\sigma/\rho} = \frac{(2200)(144)}{(25.5)(10^4)} = 1.24 \text{ lb/ft}^2 \ .$$

(2) Consider a multiweb beam with a chord of 200 in. and a thickness ratio of 5%. If the ultimate moment is 20×10^6 lb-in. at a temperature of 400° F, select the most efficient material and determine the optimum stress. For the conditions given, the structural index is

$$\frac{M}{h^2c} = \frac{20 \times 10^6}{(10)^2(200)} = 10^3 \text{ lb/in.}^2 \ .$$

From Figure IX-8, it can be seen that for $\frac{M}{h^2c} = 10^3 \text{ lb/in.}^2$ and T = 400° F, the most efficient material to use is 2024-T3 aluminum alloy, and that the optimum stress is given by

$$\frac{\sigma}{\rho} = 29 \times 10^4 \text{ in.} \ ,$$

[redacted]

so that the top cover should be designed to buckle at 29,000 lb/in.^{2}. The weight of the top cover per unit area would then be

$$w_c = \rho t_s = \frac{q}{\sigma/\rho} = \frac{(10)(10^3)(144)}{(29)(10^4)} = 4.95\ \text{lb/ft}^2 .$$

It can be shown (see Section VIII) that the total weight of a multiweb beam, including the web weight but without the weight of the tension cover, is 1.4 times the weight of the top cover. Hence, for the present case, the weight of the compression cover and webs is

$$w = (1.4)(4.95) = 6.93\ \text{lb/ft}^2 .$$

(3) Consider an unstiffened cylinder of 72-in. diameter and subjected to a moment of 45×10^6 in.-lb at a temperature of 600° F. Select the most efficient material, and find the ratio of diameter to wall thickness and the weight per unit axial length. From the aforementioned data, the structural index is obtained as

$$\left(\frac{M}{D^3}\right)^{\frac{1}{3}} = \left[\frac{45 \times 10^6}{(72)^3}\right]^{\frac{1}{3}} = 4.9\ (\text{lb/in.}^2)^{\frac{1}{3}} .$$

From Figure IX-16 with $\left(\frac{M}{D^3}\right)^{\frac{1}{3}}$ and T=600°F, it is found that the most efficient material is C-110M titanium alloy, and that the optimum stress is obtained from $\frac{\sigma}{\rho} = 20.5 \times 10^4$ in.

From Equation (22) of Section VIII, $\frac{D}{t}$ is given by $\frac{D}{t} = \frac{\pi}{4}\frac{\sigma}{M/D^3} = \frac{\pi}{4}\frac{(20.5)(10^4)(0.16)}{(4.9)^3} = 218$.

The wall thickness is therefore $t = \frac{D}{D/t} = \frac{72}{218} = 0.33$ in.

The weight per foot of axial length is then easily obtained as $w = \pi D t_p = 143$ lb/ft.

(4) As a final example, the method of selection of structural configuration, as well as material, will be illustrated for a hypothetical wing. The following data are assumed:

Ultimate moment	$M = 16 \times 10^6$ in.lb.
Wing thickness	$h = 7$ in.
Structural thickness ratio	$h/c = 0.05$
Equilibrium temperature	$T = 800°$ F

The structural chord is found to be $c = \frac{h}{h/c} = 140$ in. Wide-column construction will be considered first. The compression loading per inch of chord is

$$q = \frac{M}{hc} = \frac{16 \times 10^6}{(7)(140)} = 16{,}300\ \text{lb/in.}$$

Since this loading is high, the desired column length is taken to be $L_o = 12$ in. The structural index for wide columns would then be

$$\frac{q}{L_o} = 1360\ \text{lb/in.}^2 .$$

From Figure IX-1, the best wide-column material for $\frac{q}{L_o} = 1360$ lb/in.^{2} and T=800°F is found to be 17-7 PH stainless steel with $\frac{\sigma}{\rho} = 38 \times 10^4$ in. The weight of compression cover per foot of span is therefore

$$w_c = \frac{qc}{\sigma/\rho} = \frac{(16{,}300)(140)(12)}{(38)(10^4)} = 72\ \text{lb/ft} .$$

[redacted]

The unit weight of tension cover is obtained by assuming that the effective stress in the tension cover is 90% of the ultimate stress. Then, from Figure IX-25, for 17-7 PH at 800° F, the value of $0.9\frac{\sigma_u}{\rho}$ is found to be $0.9\frac{\sigma_u}{\rho} = 44.5 \times 10^4$ in.,

so that the weight per unit span of tension cover is

$$w_t = \frac{(12)(140)(16{,}300)}{(44.5)(10^4)} = 62 \text{ lb/ft}.$$

It is reasonable to assume that the weight of the ribs is about 22% of the cover weight, so that the total weight per foot of span is

$$w = 1.22\,(w_c + w_t) = 164 \text{ lb/ft}.$$

Multiweb construction will now be considered. In this case, the structural index is

$$\frac{M}{h^2 c} = \frac{q}{h} = 2330 \text{ lb/in.}^2.$$

From Figure IX-8, with $\frac{M}{h^2 c} = 2330$ lb/in.^{2} and $T = 800°$ F it is seen that the most efficient material is C-110M titanium alloy with $\frac{\sigma}{\rho} = 32 \times 10^4$ in. The weight of the compression cover per foot of span is therefore

$$w_c = (12)(140)\,\frac{16{,}300}{(32)(10^4)} = 85.5 \text{ lb/ft}.$$

As shown in Section VIII, the weight of the webs is 40% of the top cover weight, so that

$$w_w = (0.4)(85.5) = 34.2 \text{ lb/ft}.$$

The weight of the tension cover is the same as in the previous case, so that the total weight per foot of span is

$$w = w_c + w_w + w_t = 181.7 \text{ lb/ft}.$$

It is seen that, for the present case, wide column stainless steel construction is indicated. It should be noted that the structural depth of the wing was assumed the same for both types of construction. Since, according to Reference 4, the skin material for optimum wide columns would constitute about 40% of the total panel material, it is probable that the structural depth will be different for the two types of structure, so that the value of q would not be the same for both structures. However, the simplification introduced by taking equal values of h for both cases should not introduce appreciable errors in these comparative calculations.

2. Comparison Between Unprotected and Protected Structures

Comparisons between protected and unprotected structures may be made by the methods of Section VIII. These methods also furnish a systematic means of selecting the protective system. The procedure can best be illustrated by means of an example. The structure of example (4) in the preceding will be considered.

Calculations carried out for specific cases have shown that, in general, if insulation or cooling is used, it is advantageous to provide enough protection so that the aluminum alloys may be employed as structural materials. Therefore, the only case considered here is that of an insulated structure with 7075-T6 aluminum alloy as the structural material, and the protective system is designed so that the structure operates at a temperature of 200° F. The duration of the flight is assumed to be 0.5 hours. The case of wide-column construction will be considered first. For 7075-T6 at 200° F and with $\frac{q}{L_o} = 1360$ lb/in.^{2} the optimum stress-density ratio is obtained from Figure IX-26 as $\left(\frac{\sigma}{\rho}\right)_s = 61 \times 10^4$.

[redacted]

From Equation (29) of Section VIII, the parameter S is calculated as

$$S = \frac{(\sigma/\rho)_s}{q} = 37.4 \text{ in.}^2/\text{lb.}$$

The alternate protective systems considered here for the inner structure are thermoflex insulation, or thermoflex insulation and water cooling. It is assumed that the temperature of the insulation is the mean between the equilibrium temperature and the structural temperature. For thermoflex insulation at 500° F and a density ρ_i of 3 lb/ft^3, the conductivity if taken from Part I, Section 2.0, of this report as

$$k_i = 0.55 \frac{\text{BTU-in.}}{\text{ft}^2 \text{hr °F}} .$$

From the same source, the specific heat of 7075-T6 is $c_s = 0.23$ BTU/lb°F.

Hence, from equation (42) of Section VIII, the value of S^* is determined as

$$S^* = (2)(0.23)\left[\frac{(600)(12)^5}{(1000)(0.55)(3)(0.5)}\right]^{\frac{1}{2}} \ln(1.16) = 29.2 \text{ in.}^2/\text{lb.}$$

It is then seen that $S > S^*$, so that according to the conclusions of Section VIII, insulation and cooling should be used. Then, according to equation (40) of Section VIII, the weight of the protective system is

$$w_p = w_i + 2\sqrt{\frac{\rho_i \, k_i \, (T_o - T_s)\, \theta_F}{1000}} .$$

Where w_i is the weight of outer skin taken as 1 lb/ft^2,

$$w_p = \frac{1}{144} + 2\sqrt{\frac{(3)(0.55)(600)(0.5)}{(1000)(12)^5}} = 0.00977 \text{ lb/in.}^2 .$$

It should be noted that the insulation thickness required may be calculated from equation (39) of Section VIII. In the present case, this is found to be $t_i = 0.07$ in. Substituting the values of w_p and S determined previously in equation (28) of Section VIII gives

$$\frac{t_s}{t_e} = \frac{1}{1+Sw_p} = \frac{1}{1+(37.4)(0.0098)} = 0.734 .$$

Hence, the efficiency of the insulated structure is calculated as

$$\left(\frac{\sigma}{\rho}\right)_e = \left(\frac{\sigma}{\rho}\right)_s \left(\frac{t_s}{t_e}\right) = 44.7 \times 10^4 \text{ in.}$$

For unprotected wide-column construction, the efficiency was

$$\frac{\sigma}{\rho} = 38 \times 10^4 \text{ in.} \quad ;$$

therefore, the use of a cooled and insulated structure will result in decreasing the structural weight by a factor equal to $\frac{38}{44.7} = 0.85$. The protected wide-column structure will have a weight per unit span of

$$w = (0.85)(164) = 139.5 \text{ lb/ft.}$$

This weight saving of 15% is considered significant and a protected structure would be recommended.

Since the unit weights of wide-column and multiweb structures were not very different for the unprotected structure, it is of interest to determine the efficiency of a protected multiweb, since the multiweb might benefit more from insulation and cooling than the wide column.

[redacted]

From Figure IX-27, for an optimum 7075-T6 multiweb operating at 200° F with $\frac{M}{h^2 c} = 2330$ lb/in^2, it is found that the structural efficiency is $\left(\frac{\sigma}{\rho}\right)_s = 55.25 \times 10^4$ in., so that S is now given by

$$S = \frac{55.25 \times 10^4}{16,300} = 33.9 \text{ in.}^2/\text{lb.}$$

Since the value of S is still greater than S^*, the insulated and cooled system will be used. The weight of the protective system is then unchanged so that the ratio of structural thickness to effective thickness is

$$\frac{t_s}{t_e} = \frac{1}{1+(33.9)(0.0098)} = 0.75 .$$

The efficiency of the protected multiweb is, therefore,

$$\left(\frac{\sigma}{\rho}\right)_e = \left(\frac{\sigma}{\rho}\right)_s \frac{t_s}{t_e} = (55.25)(10^4)(0.75) = 41.5 \times 10^4 \text{ in.}$$

Since the efficiency for the unprotected multiweb was $\sigma/\rho = 32 \times 10^4$, the weight per foot of span for the insulated and cooled multiweb is

$$w = (181.7)\frac{32}{41.5} = 140 \text{ lb/ft.}$$

As can be seen, a weight decrease of 23% is realized by insulating the multiweb so that for the insulated and cooled structure, the wide column and multiweb constructions have equal weight. The choice of structure for such a case would then probably be made on the basis of stiffness and torsional rigidity. It should be pointed out here that, when different types of unprotected structures give rise to unit weights which are not very different, it is advisable to consider insulation or cooling for each type since one type of construction may experience more beneficial effects from insulation and cooling than another. In the preceding example, for instance, the weight reduction due to insulation was 15% for wide panel construction and 23% for multiweb construction.

3. Life-Strength Considerations

In previous examples, sample design problems have been carried out on the basis of short-time ultimate loading. These considerations are not sufficient, however, to ensure structural integrity if the vehicle is expected to operate at elevated temperature for significant periods of time. In such cases, creep and relaxation effects may cause an appreciable loss of strength for a given life expectancy, or may limit the life of the vehicle under specified loading and temperature conditions. It is, therefore, of interest to determine the expected life of a given structure under long-time loading. As explained previously, optimum stress curves based upon isochronous stress-strain relations were developed for this purpose. Since these curves are in terms of the Larson-Miller parameter, λ, the problem of determining the life expectancy of an aircraft for a given temperature and loading is then equivalent to determining the permissible value of λ for a given geometry. For any optimized structural member, all the proportions are determined in terms of a single reference thickness; therefore, structures having the same reference thickness have the same geometry. The reference thickness is given by

$$t = \frac{q}{(\sigma/\rho)\rho} ,$$

so that, for a given material, radial lines through the origin of the optimum stress curves represent lines of constant geometry. This property furnishes a simple method for determining the life expectancy of a given vehicle.

Referring to Figure IX-28, the curves represent optimum stress for a given type of construction in terms of the Larson-Miller parameter λ. It is assumed that the material and type of construction have been chosen previously on the basis of short-time ultimate loading. Point A of Figure IX-28 represents the chosen design. That is, the structural index corresponding with point A is the ultimate loading value, and the $\frac{\sigma}{\rho}$ corresponding to point A is the value for the structure and material chosen. Then, the line OA of Figure IX-28 represents the actual structure and material selected. For any loading, the allowable value of λ is determined by the line OA. In Figure IX-28, point B represents the loading in level flight, and point C gives the allowable value of λ.

The determination of life expectancy will now be carried out for a hypothetical structure. Assume that a multiweb beam is designed for a short-time ultimate loading index of $\frac{M}{h^2 c} = 1000$, and a temperature of 400°F; then, according to Figure IX-8, the most efficient material would be 2024-T3 aluminum alloy with $\frac{\sigma}{\rho} = 29 \times 10^4$. This point is plotted on Figure IX-11 and a radial line is drawn from the origin to this point. If it is assumed that the ultimate load factor is 1.67, the level-flight loading is $\frac{M}{h^2 c} = 600$. It is then clear from Figure IX-11 that the allowable value of λ is 17.5. The life expectancy determined from

$$\log \theta = \frac{17,500}{860} - 20 = 0.4,$$

so that the allowable life for the given level-flight loading is 2.5 hours.

4. Transient Conditions

As an example of the use of the transient heating stress curves, consider the problem that follows.

Select the most efficient material for a vehicle subjected to a loading of $q = 15,000$ lb/in. and a heat transfer coefficient of $h_e = 10 \text{ BTU/ft}^2 \text{hr°F}$ for 3 minutes. For these values, the transient heating parameter is determined as

$$\frac{q}{h_e \theta} = \frac{(15,000)(12)}{(10)(778)(0.05)} = 463 \text{ °F}.$$

From Figure IX-24, it is found that: for $T_{aw} = 800$°F, the most efficient compressive material is 7075-T6; for $T_{aw} = 1200$° F, the best material is 17-7 PH; and for $T_{aw} = 1600$° F, the material selected is Inconel X.

D. WEIGHT PENALTY DUE TO ELEVATED TEMPERATURE OPERATION

It is of interest to determine the weight penalty caused by elevated temperature for a given structure and loading. The methods developed in Section VIII and the optimum stress curves presented in this section furnish all the information necessary to perform the computations. These calculations have been carried out for two specific cases and the results are shown in Figures IX-29 and IX-30. The figures present curves of the ratio of structural weight at elevated temperature to the room temperature structural weight as a function of equilibrium temperature. The calculations were carried out for a multiweb beam. Loading indexes of $\frac{M}{h^2 c} = 600 \text{ lb/in.}^2$ and $\frac{M}{h^2 c} = 2400 \text{ lb/in.}^2$ were assumed. For a beam of 7-in. thickness, these values would correspond to compressive loadings of 4200 lb/in. and 16,800 lb/in., respectively. The duration of flight was assumed to be 0.5 hours. Detailed computations are summarized in the following tables.

[redacted]

CASE 1. $\frac{M}{h^2 c}$ = 600 lb/in.^{2}, h = 7 in., θ_f = 0.5 hr.
The insulation used was thermoflex with a density of 3 lb/ft^3.

Unprotected Structure									
T_o (°F)	Room Temp.	200	300	400	600	800	1200	1400	
Material	Mg	Mg	Mg	2024	Ti	Ti	Inconel X	Inconel X	From Figure IX-8.
(σ/ρ) 10^{-4} (in.)	30	28	26	22	15	14.5	10	9.5	
R_w	1.00	1.07	1.15	1.36	2.0	2.07	3.0	3.16	
Protected Structure									
	Structure is designed with magnesium maintained at 200°F. From Figure IX-8, $(\sigma/\rho)_s = 28 \times 10^4$, $S = \frac{(\sigma/\rho)_s}{q} = 66.6$ in.^{2}/lb.								
	T_o (°F)		300	400	600	800	1200	1400	
	S^* (in.^{2}/lb)		62.2	51.5	40.0	33.4	27.1	24.0	Equation (42), Section VIII.
	S		>S*	>S*	>S*	>S*	>S*	>S*	
Protective System — Insulation plus Water Cooling									
$(w_2 + w_i)$(lb/in.^{2})		0.00115	0.00163	0.00230	0.00281	0.00363	0.00398		Equation (40), Section VIII.
t_1 (in.)		0.331	0.469	0.662	0.810	1.045	1.15		Equation (39), Section VIII.
w_p (lb/in.^{2})		0.00810	0.00858	0.00925	0.00976	0.01058	0.01093		Equation (40), Section VIII.
t_s/t_e		0.65	0.636	0.618	0.606	0.587	0.578		Equation (28), Section VIII.
$(\sigma/\rho)_e \times 10^{-4}$		18.2	17.8	17.3	17.0	16.4	16.2		Equation (26), Section VIII.
R_w		1.65	1.685	1.735	1.765	1.830	1.850		

[redacted]

CASE 2. $\frac{M}{h^2 c} = 2400$ lb/in.^{2}, $h = 7$ in., $\theta_f = 0.5$ hr.

The insulation used was thermoflex with a density of 3 lb/ft^3.

Unprotected Structure									
T_o (°F)	Room Temp.	200	300	400	600	800	1200	1400	
Material	7075	7075	7075	7075	Ti	Ti	Inconel X	Inconel X	From Figure IX-8.
$(\sigma/\rho)\,10^{-4}$ (in.)	57.5	56.0	50.5	40.0	34.5	32.3	25.5	23.3	
R_w	1.0	1.025	1.14	1.44	1.665	1.78	2.25	2.58	
Protected Structure									
	Structure is designed with 7075-T6 maintained at 200°F. From Figure IX-8, $\left(\frac{\sigma}{\rho}\right)_s = 56 \times 10^4$, $S = \frac{56 \times 10^4}{16800} = 33.3$ in.^{2}/lb.								
	T_o (°F)		300	400	600	800	1200	1400	
	S^* (in.^{2}/lb)		55	45.5	35.4	29.6	24.0	21.2	Equation (42), Section VIII.
	S		<S*	<S*	<S*	>S*	>S*	>S*	
Protective System	Insulation				Insulation plus Water Cooling				
w_i or $(w_2 + w_i)$ (lb/in.^{2})	0.00069	0.00118	0.00214		0.00281	0.00363	0.00398		Equations (37) and (40), Section VIII.
t_i (in.)	0.398	0.680	1.23		0.81	1.05	1.15		For insulation only, t_i from Equation (37), Section VIII. For insulation and cooling, t_i from Equation (39), Section VIII.
w_p (lb/in.^{2})	0.00764	0.00813	0.00909		0.00976	0.01058	0.01093		
t_s/t_e	0.798	0.788	0.768		0.755	0.74	0.733		
$(\sigma/\rho)_e \times 10^{-4}$	44.7	44.2	43.0		42.3	41.5	41.0		
R_w	1.285	1.30	1.335		1.36	1.385	1.40		

[redacted]

Examination of Figures IX-29 and IX-30 reveals that, for an unprotected structure, the weight penalty rises rapidly with increasing temperature. The use of insulation and cooling is found to be very beneficial and permits a reduction in weight penalty of 40 to 70%. While the use of protective devices is profitable for the highly loaded structure, such devices are somewhat less advantageous but still indicated for the lightly loaded structure. Similar calculations could easily be carried out for wide-column construction and for other loadings and exposure times. It should be noted that the weight penalty as calculated here does not account for thermal stresses. The presence of such stresses may increase the weight of the unprotected structure while leaving the protected structure unaltered. The thermal stress increments are, however, assumed to be offset by the fact that the structural thickness was not modified for insulated structures.

The weight penalty increases rather slowly with equilibrium temperature for protected structures because adding insulation or coolant results in small weight increases, so that most of the protective device weight is in the outer skin and its supporting structure. For temperatures exceeding 1600°F, the weight of the outer skin will probably start to increase since this is the upper limit for efficient operation of Inconel X. It is clear, however, that the weight of the unprotected structure would still increase much faster than the weight of the outer skin. The major limitations on the use of insulation and water cooling appear to be the insulation thickness and the volume of water; for the cases considered here, the insulation thickness did not exceed 1.23 inches (see Tables IX-1 and IX-2). For extreme cases, where the volume of water may become large, cooling with liquid metals such as lithium should be considered.

E. CONCLUSIONS

The optimum stress curves presented in this section, and the methods of comparison between structures and material based upon these curves, should prove useful for preliminary structural design in the presence of aerodynamic heating. In particular, these results provide systematic and logical procedures for narrowing down the scope of preliminary design investigations while ensuring that an optimum, or near-optimum, choice of material and configuration will be made. Furthermore, the design of insulation and cooling systems is incorporated directly into the structural design problem so that the optimization may be carried out for the entire structural system.

The characteristics of the optimum design curves show that material comparisons based upon compressive yield stress (Reference 5) are not adequate because, for typical structural configurations, the attainable working stress approaches the compressive yield only for high loading. In addition, comparisons based upon simple column or plate buckling (Reference 6) include no optimization, so that conclusions based upon these comparisons may lead to erroneous choice of material or configuration.

As a final remark, it should be pointed out that the optimum stress curves presented here may be used to obtain an indication of the desirable mechanical properties which should be developed in new alloys intended for aircraft use.

[redacted]

[redacted]

REFERENCES

(1) Dow, N. F. and Hickman, W. A., "Design Charts for Flat Compression Panels Having Longitudinal Extruded Y Section Stiffeners and Comparison With Panels Having Formed Z Section Stiffeners," NACA TN 1389, August 1947.

(2) Pride, R. A. and Anderson, M. S., "Experimental Investigation of the Pure Bending Strength of 75S-T6 Aluminum Alloy Multiweb Beams With Formed Channel Webs," NACA TN 3082, 1954.

(3) Shanley, F. R., "Weight-Strength Analysis of Aircraft Structures," McGraw-Hill Book Company, Inc., New York, 1952.

(4) Micks, W. R., "A Method of Estimating the Compressive Strength of Optimum Sheet-Stiffener Panels for Arbitrary Material Properties, Skin Thickness, and Stiffener Shapes," Journal of the Aeronautical Sciences, Vol. 20, No. 10, October 1953, Page 705.

(5) Heimerl, G. J. and Hughes, P. J., "Structural Efficiencies of Various Aluminum, Titanium, and Steel Alloys at Elevated Temperatures," NACA TN 2975, 1953.

(6) Heimerl, G. J. and Barrett, P. F., "A Structural-Efficiency Evaluation of Titanium at Normal and Elevated Temperatures," NACA TN 2269, 1951.

[redacted]

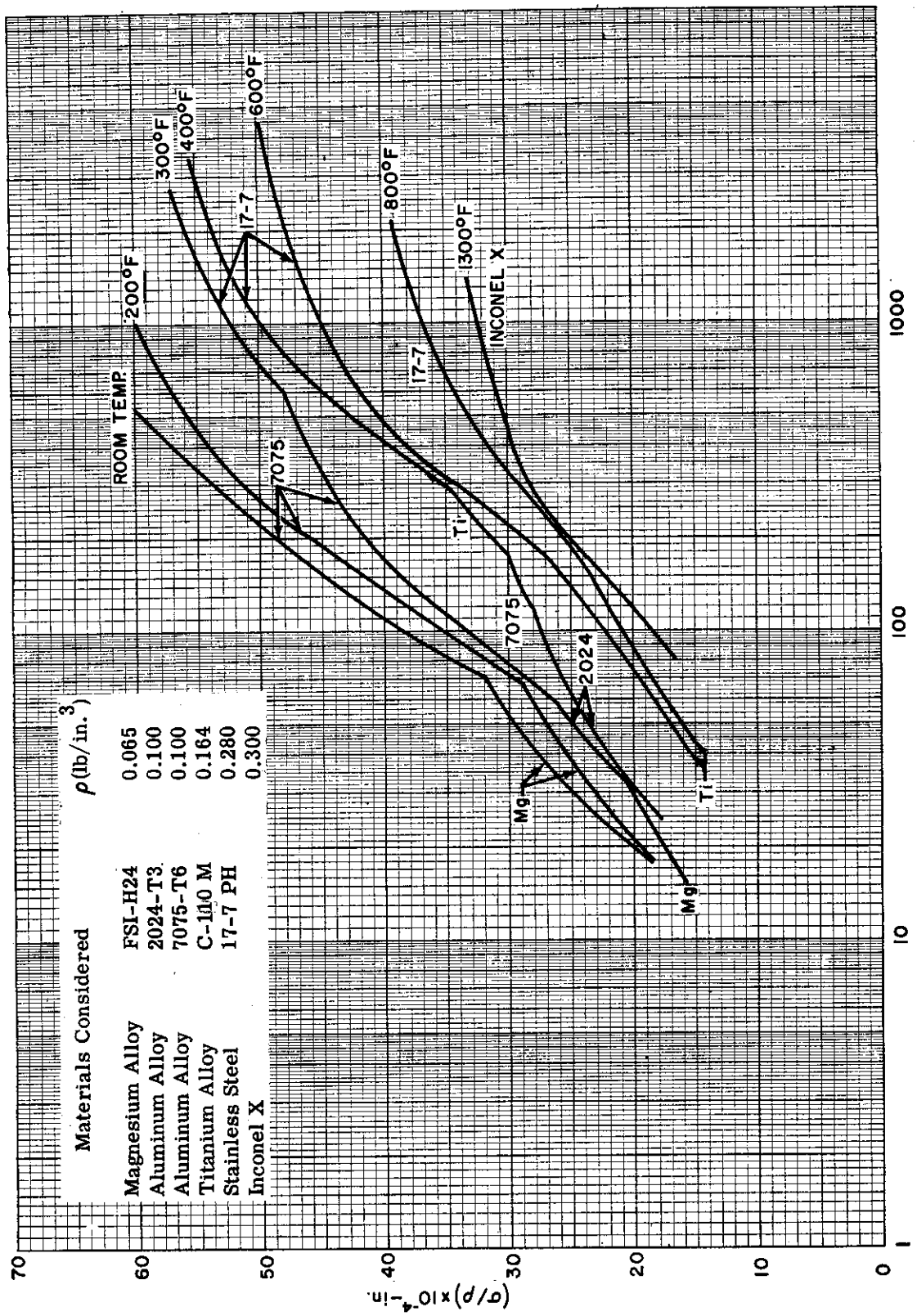

Figure IX-1. Optimum Stress Envelopes for Wide Columns, Short-time Loading

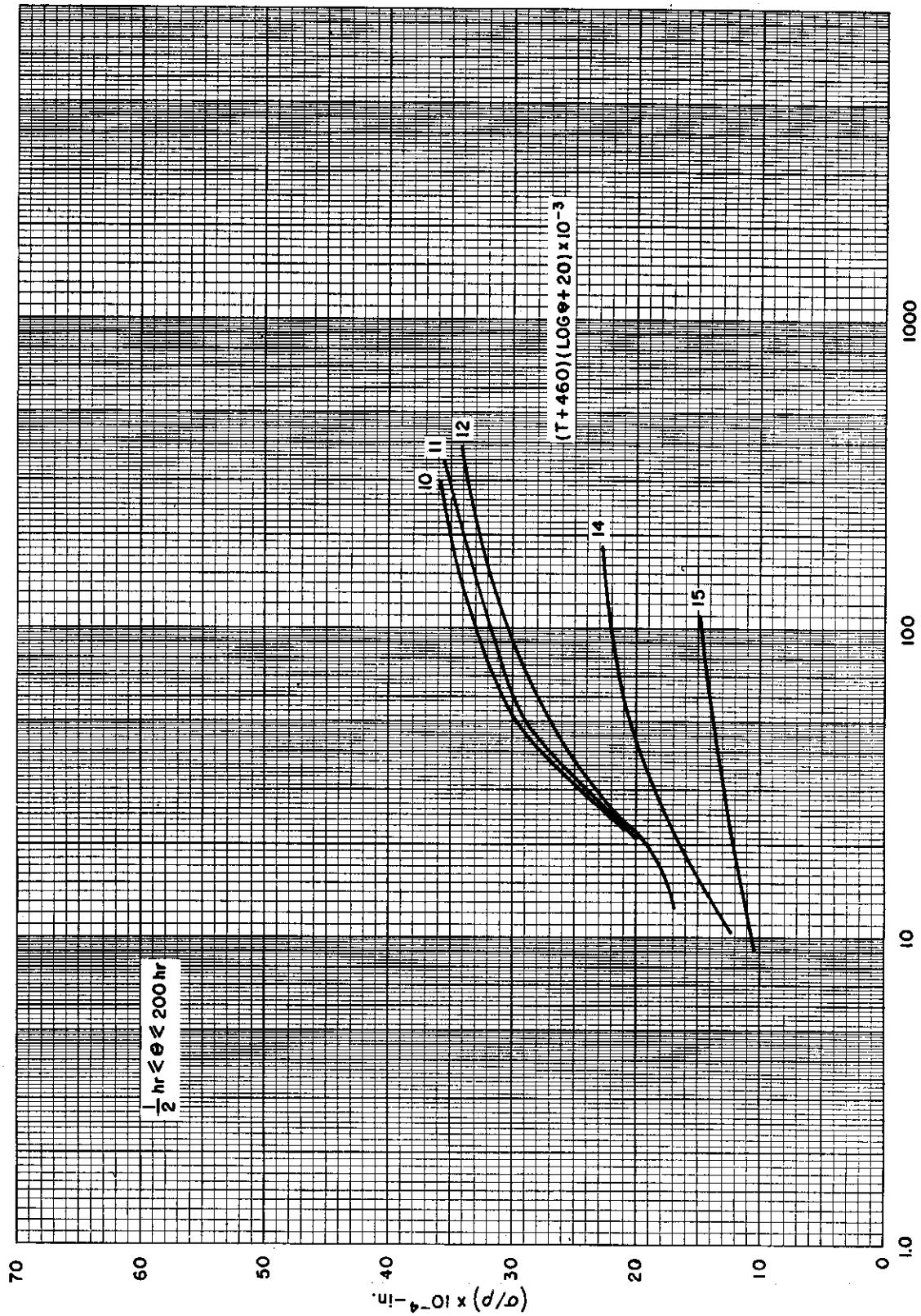

Figure IX-2. Optimum Stress Curves for Magnesium Wide Columns, Long-time Loading

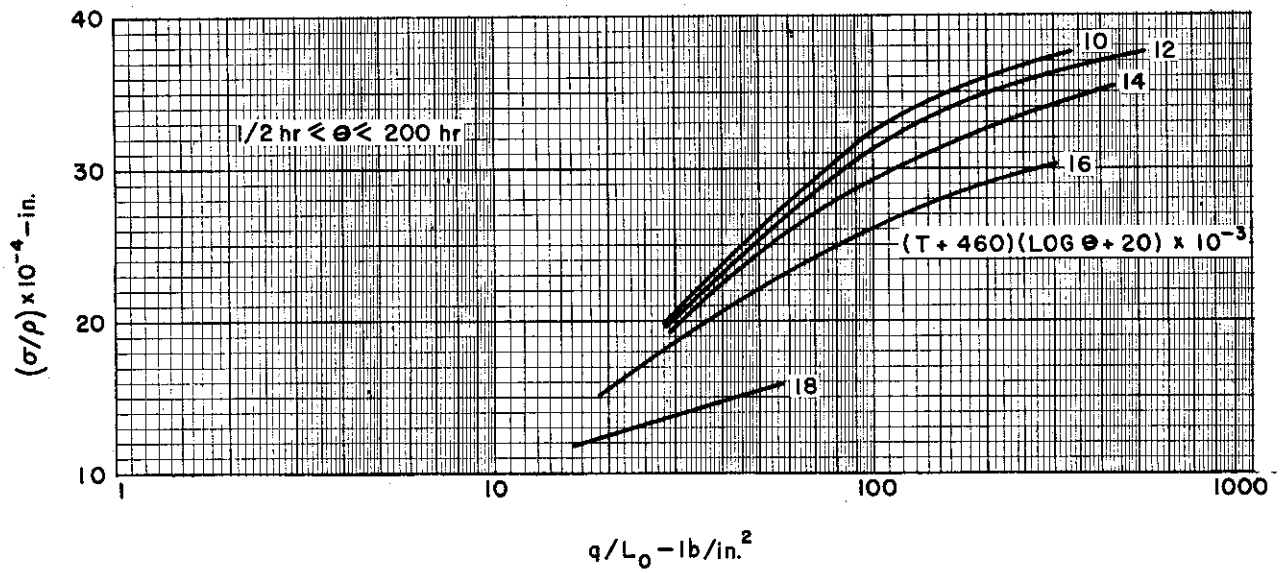

Figure IX-3. Optimum Stress Curves for 2024 Aluminum Wide Columns, Long-time Loading

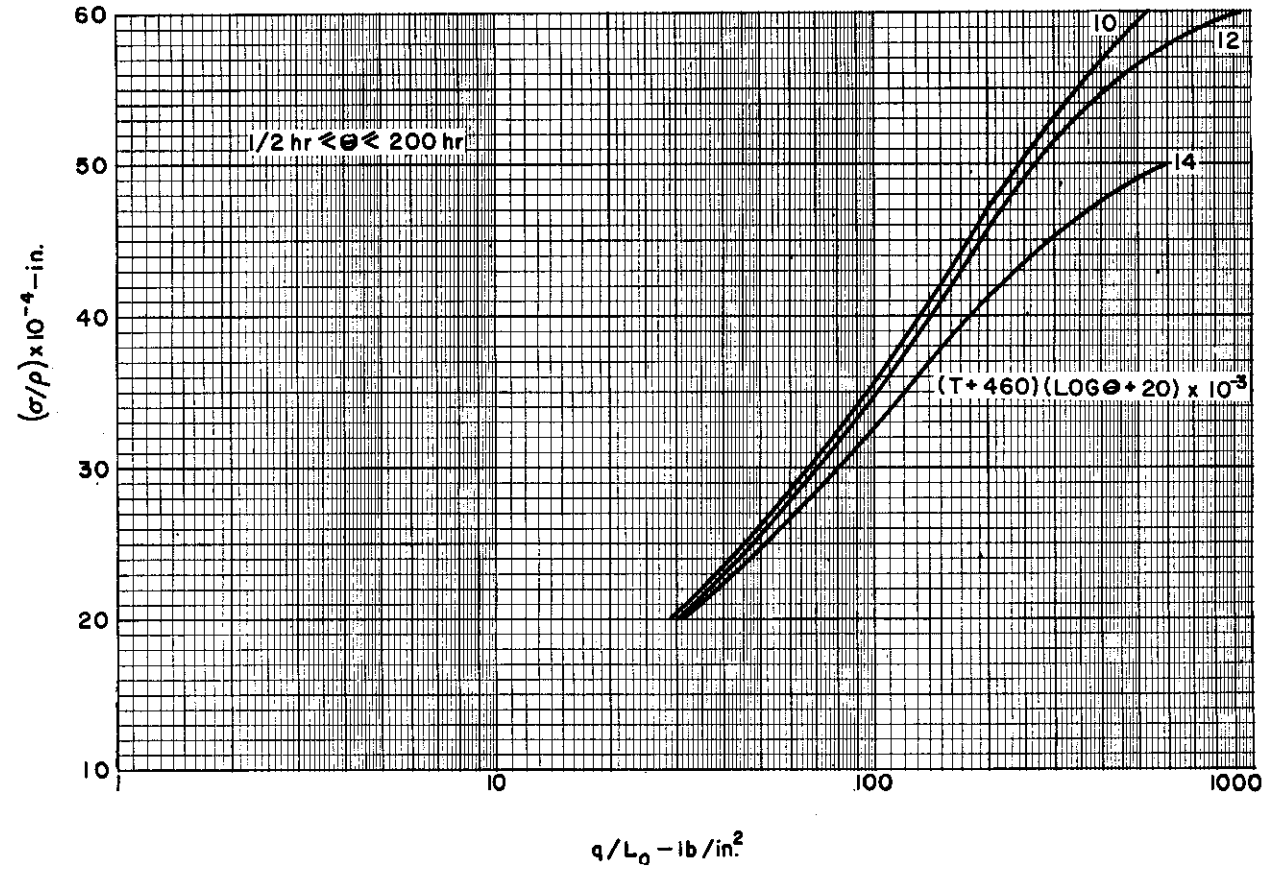

Figure IX-4. Optimum Stress Curves for 7075 Aluminum Wide Columns, Long-time Loading

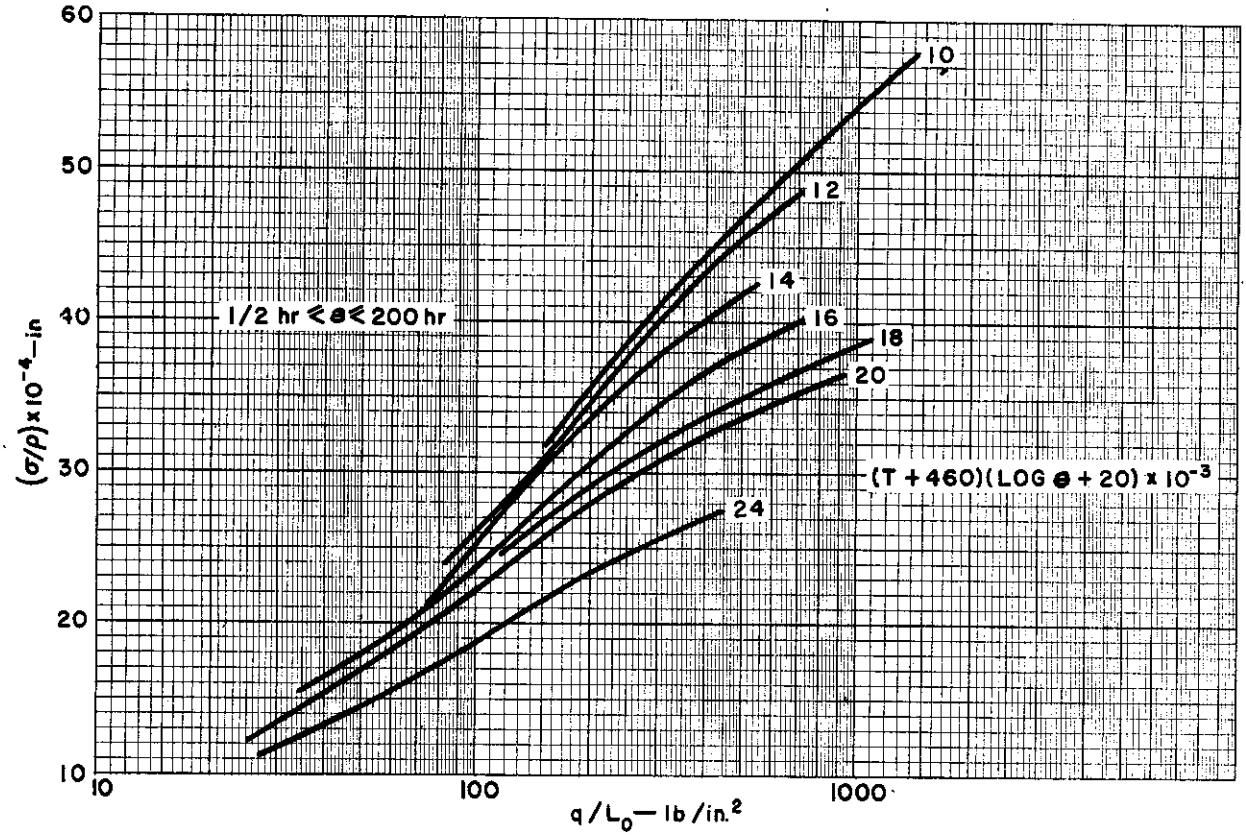

Figure IX-5. Optimum Stress Curves for Titanium Wide Columns, Long-time Loading

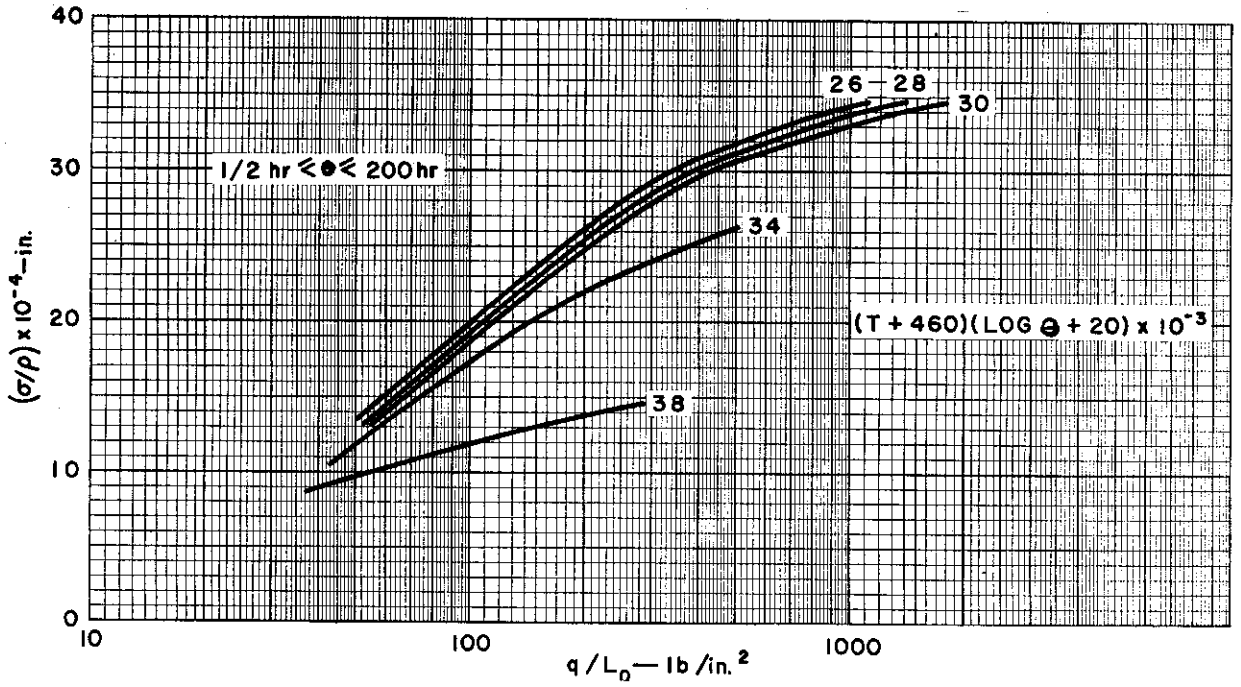

Figure IX-6. Optimum Stress Curves for Inconel X Wide Columns, Long-time Loading

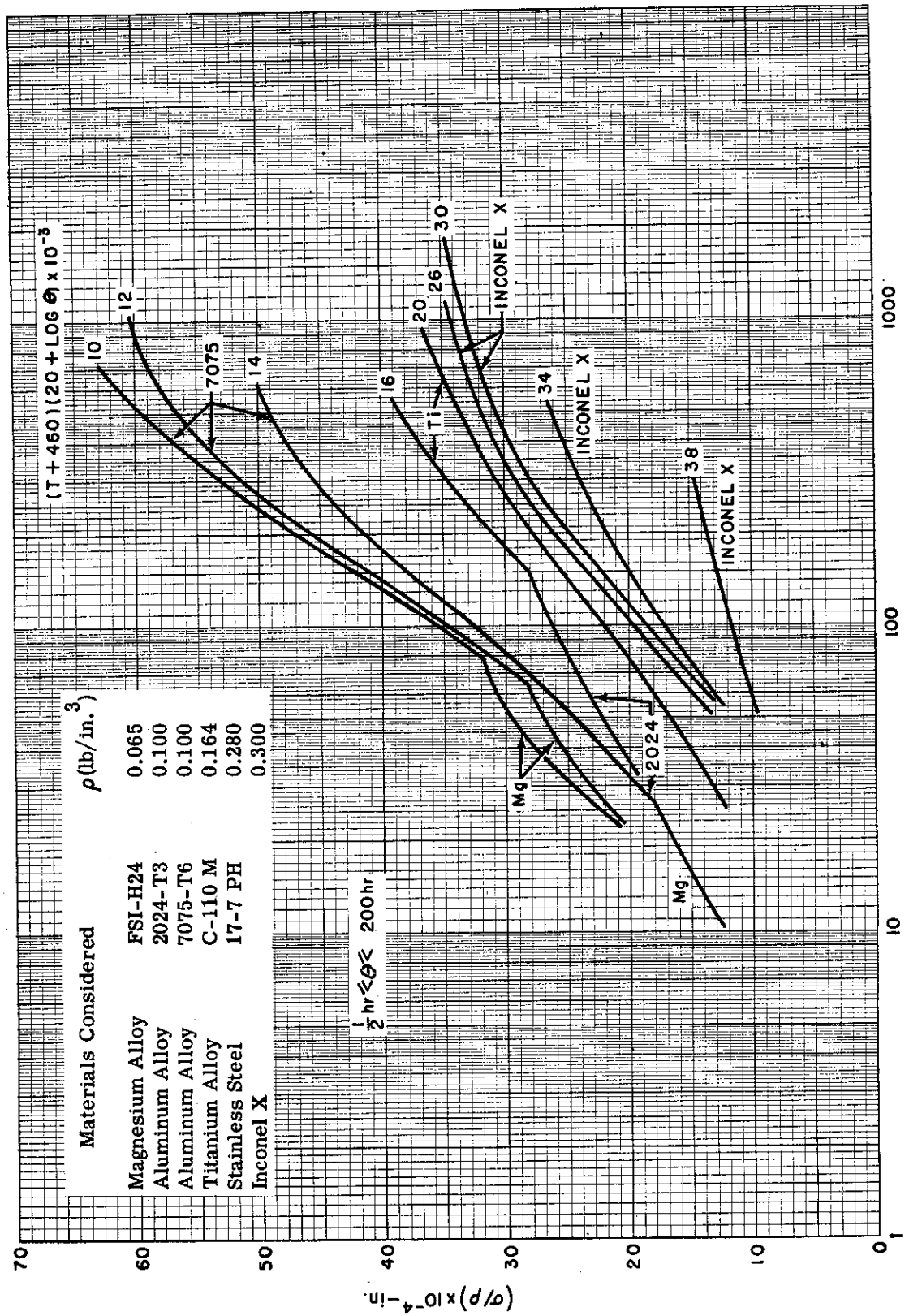

Figure IX-7. Optimum Stress Envelopes for Wide Columns, Long-time Loading

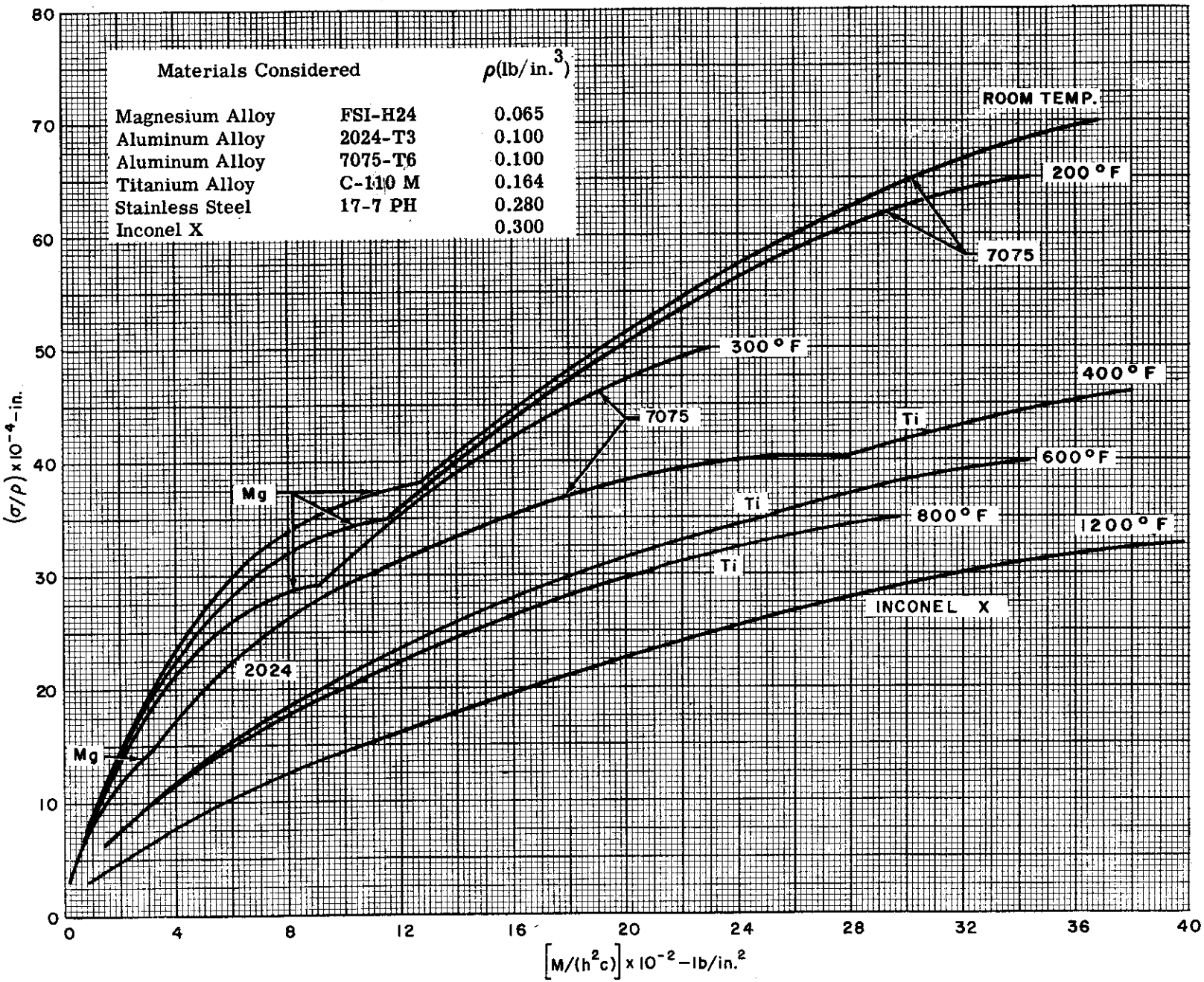

Figure IX-8. Optimum Stress Envelopes for Multiweb Beams, Short-time Loading

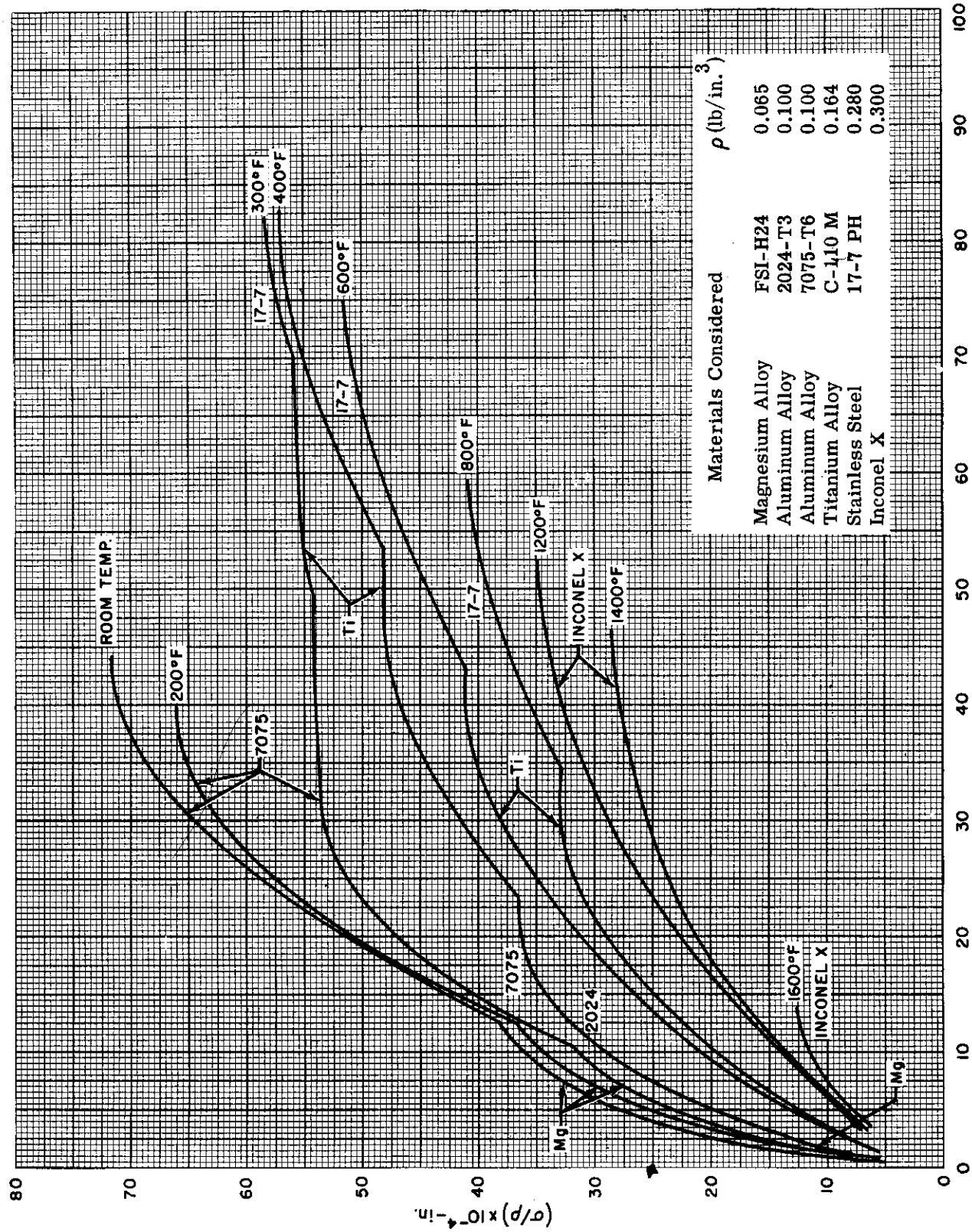

Figure IX-9. Optimum Stress Envelopes for Multiweb Beams, Short-time Loading

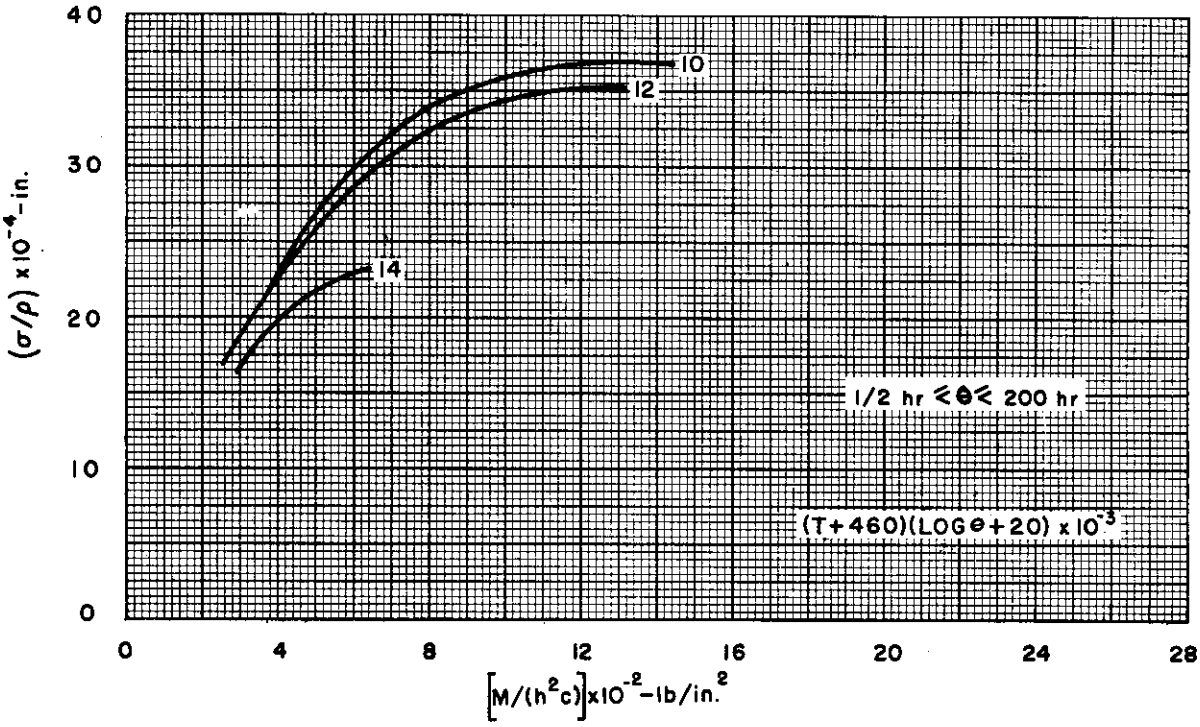

Figure IX-10. Optimum Stress Curves for Magnesium Multiweb Beams, Long-time Loading

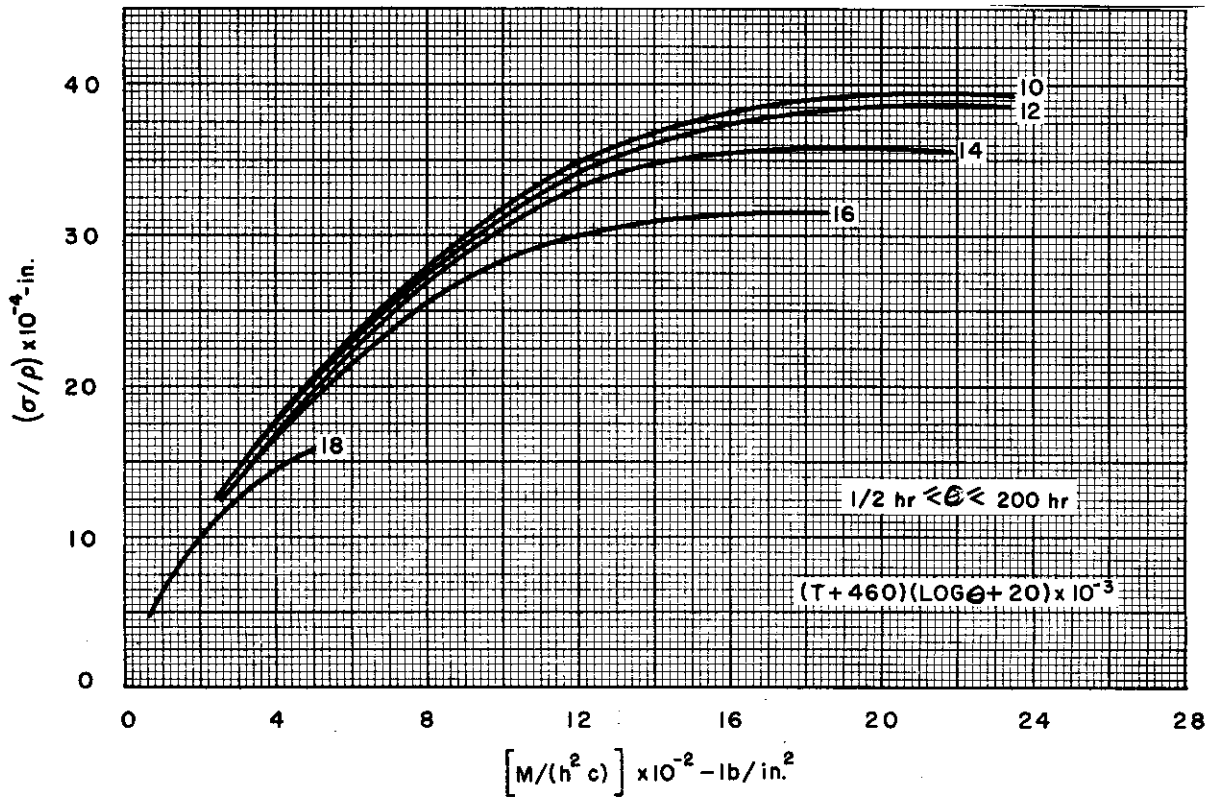

Figure IX-11. Optimum Stress Curves for 2024 Aluminum Multiweb Beams, Long-time Loading

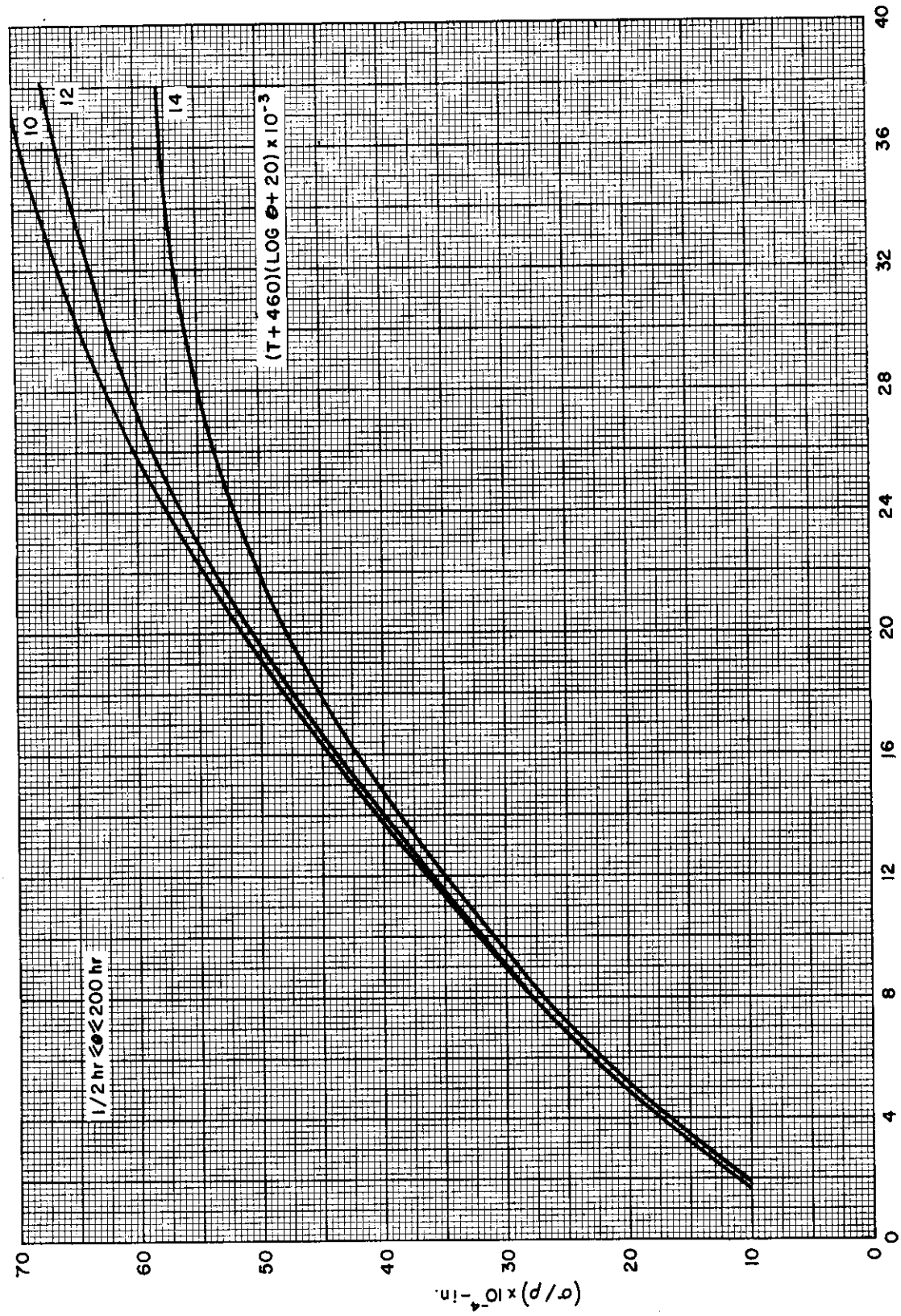

Figure IX-12. Optimum Stress Curves for 7075 Aluminum Multiweb Beams, Long-time Loading

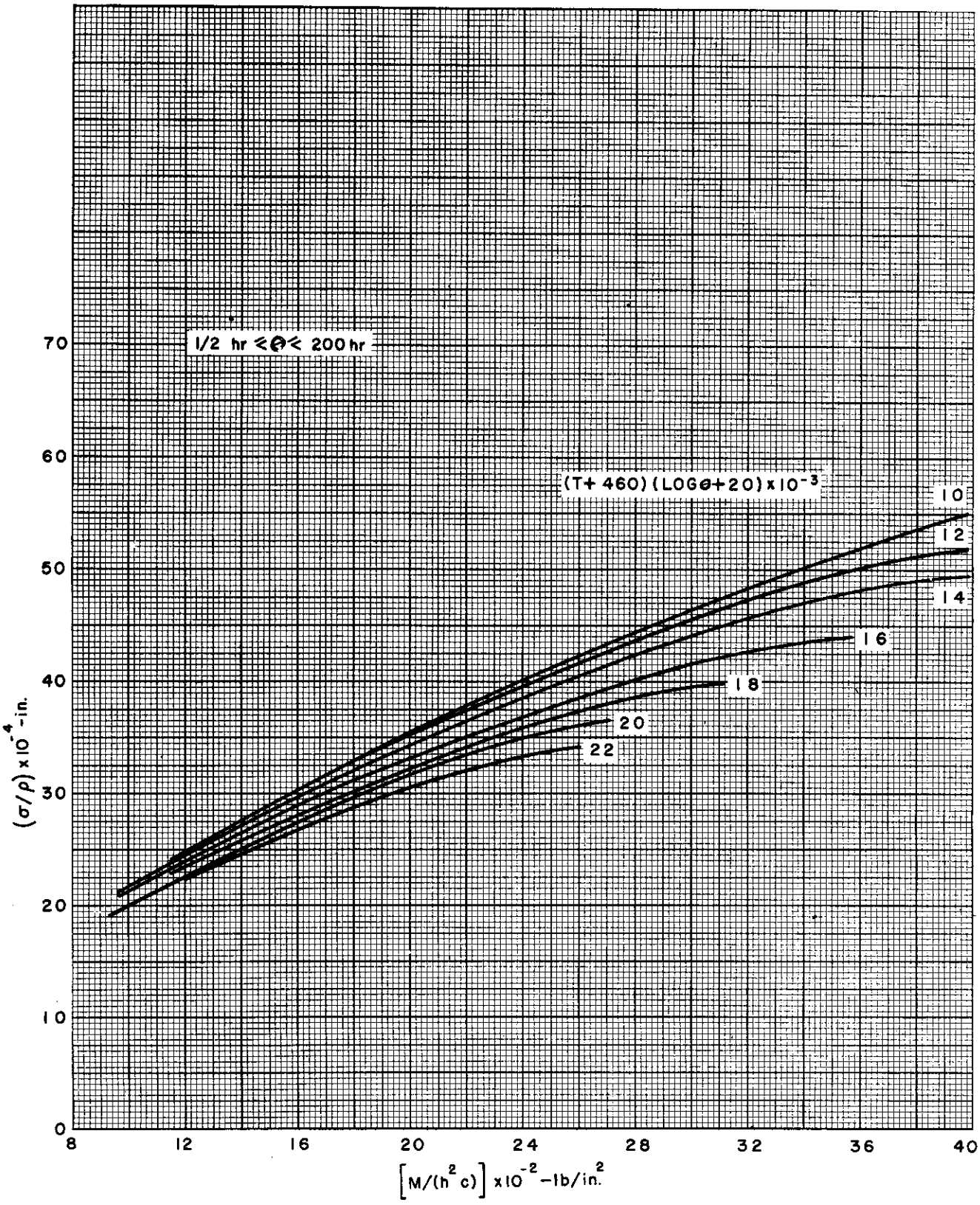

Figure IX-13. Optimum Stress Curves for Titanium Multiweb Beams, Long-time Loading

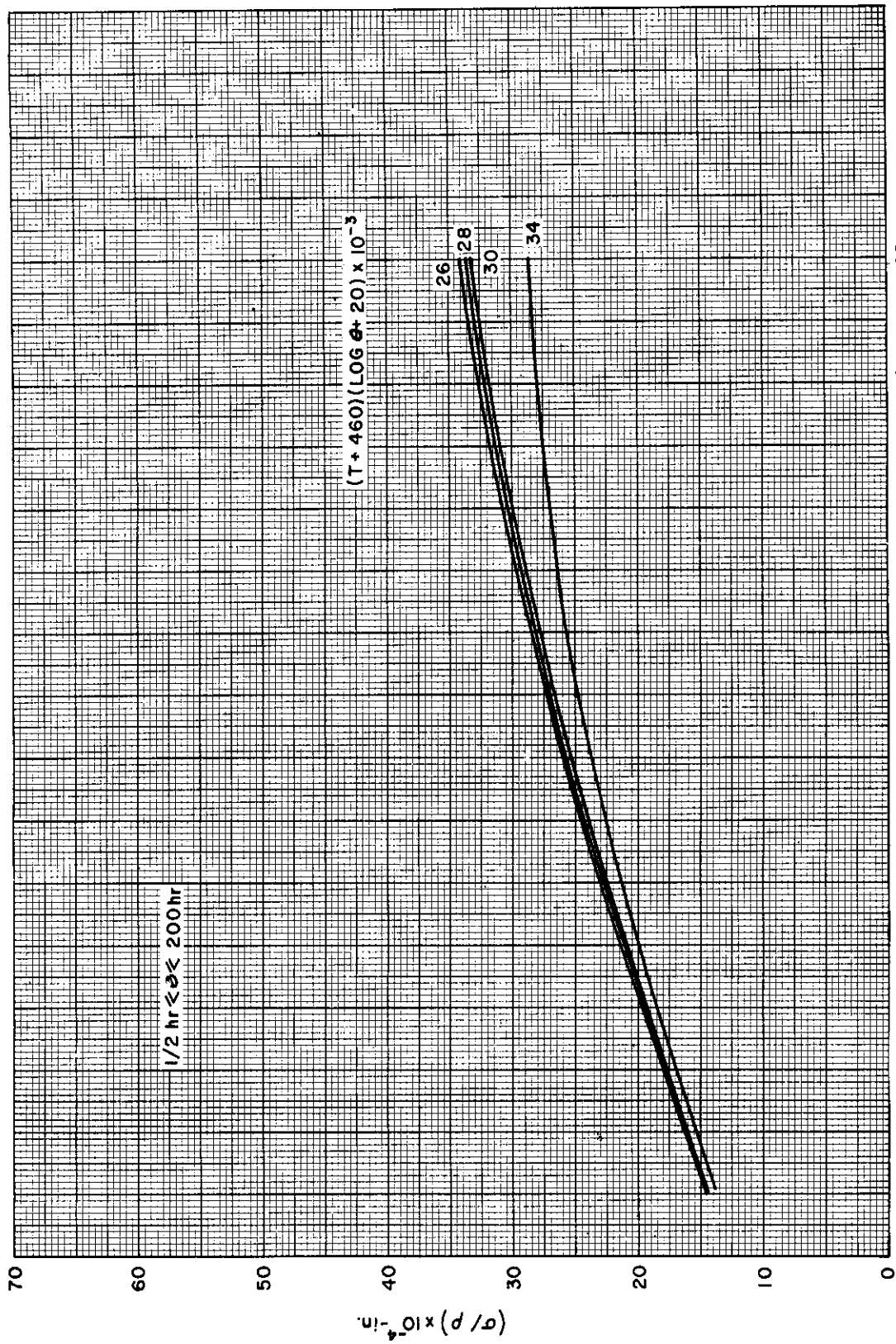

Figure IX-14. Optimum Stress Curves for Inconel X Multiweb Beams, Long-time Loading

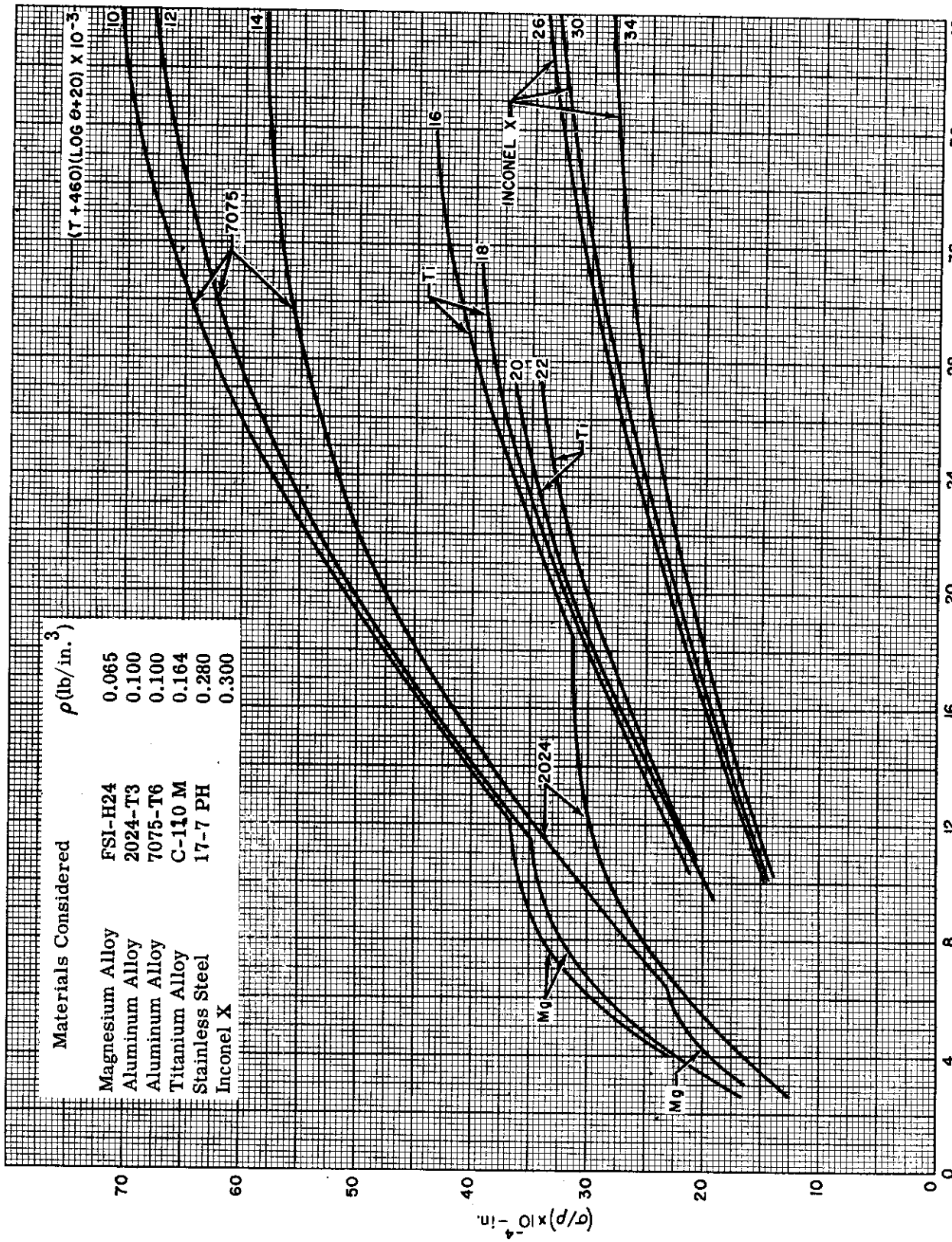

Figure IX-15. Optimum Stress Envelopes for Multiweb Beams, Long-time Loading

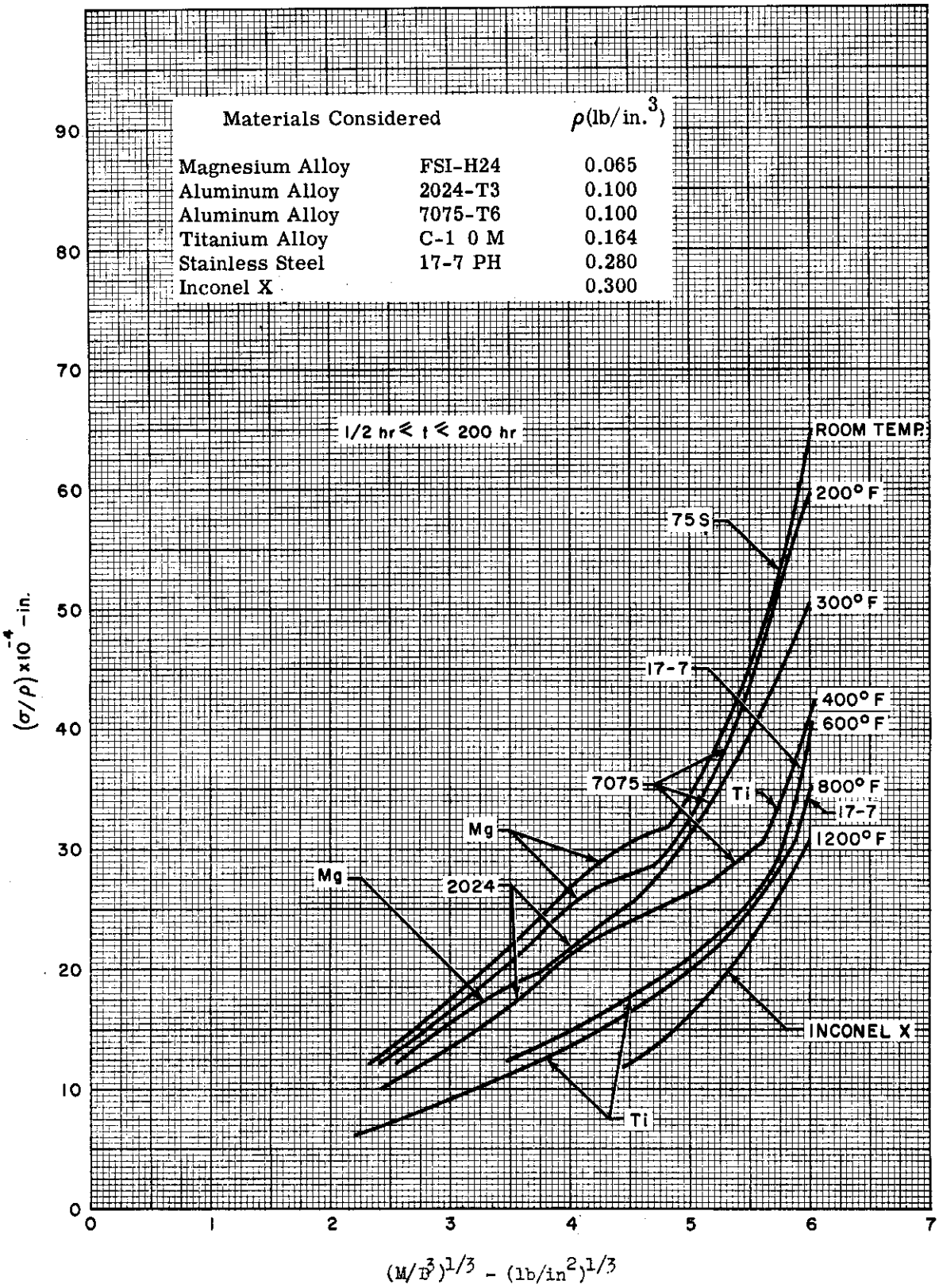

Figure IX-16. Optimum Stress Envelopes for Unstiffened Cylinders, Short-time Loading

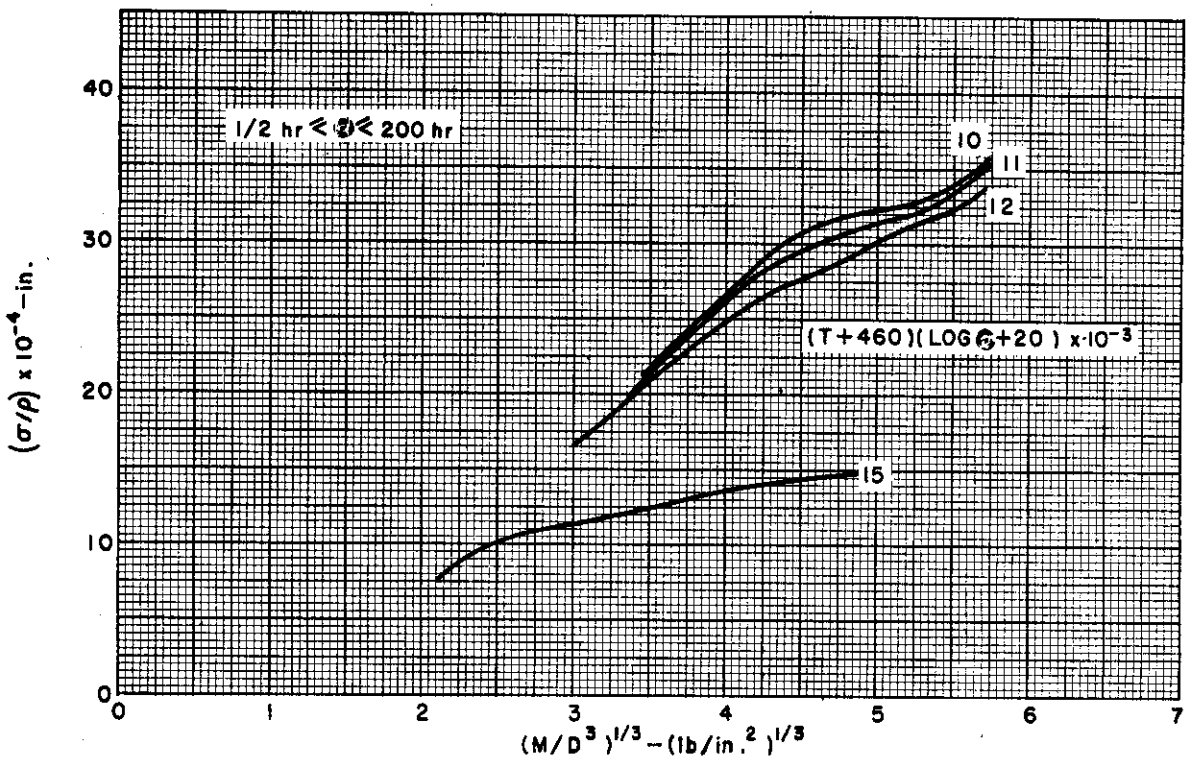

Figure IX-17. Optimum Stress Curves for Magnesium Unstiffened Cylinders, Long-time Loading

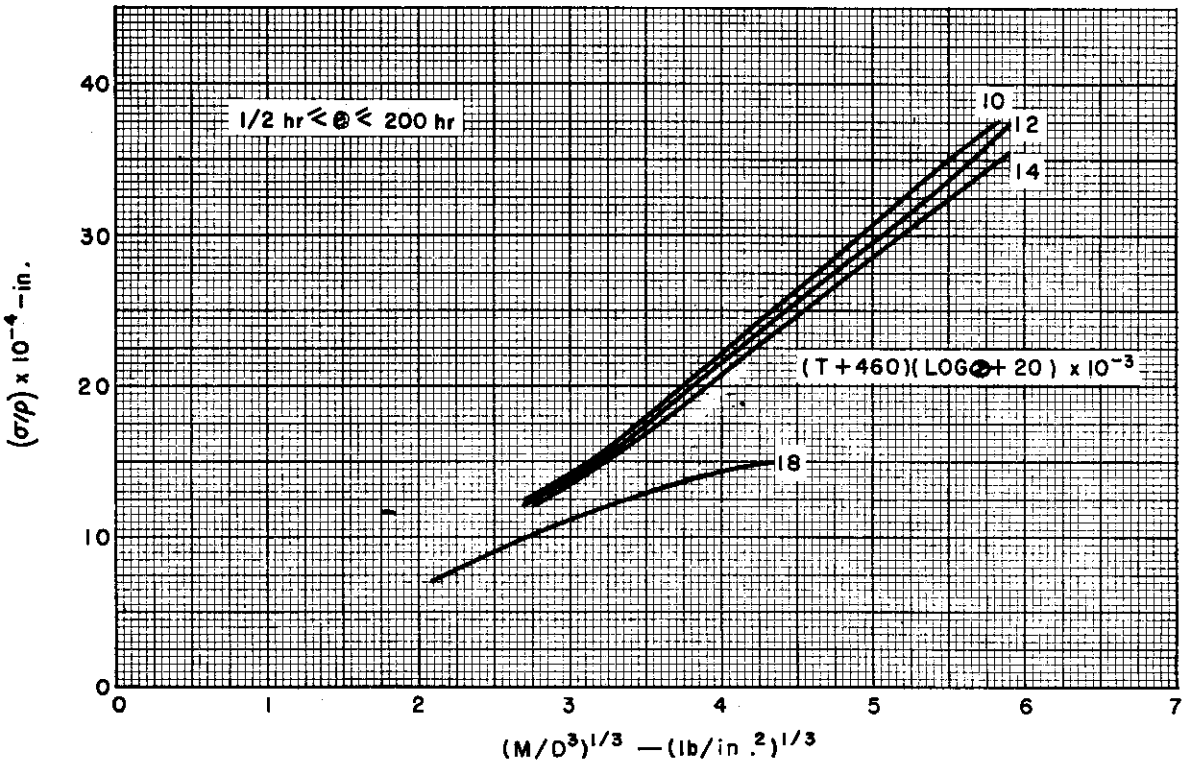

Figure IX-18. Optimum Stress Curves for 2024 Aluminum Unstiffened Cylinders, Long-time Loading

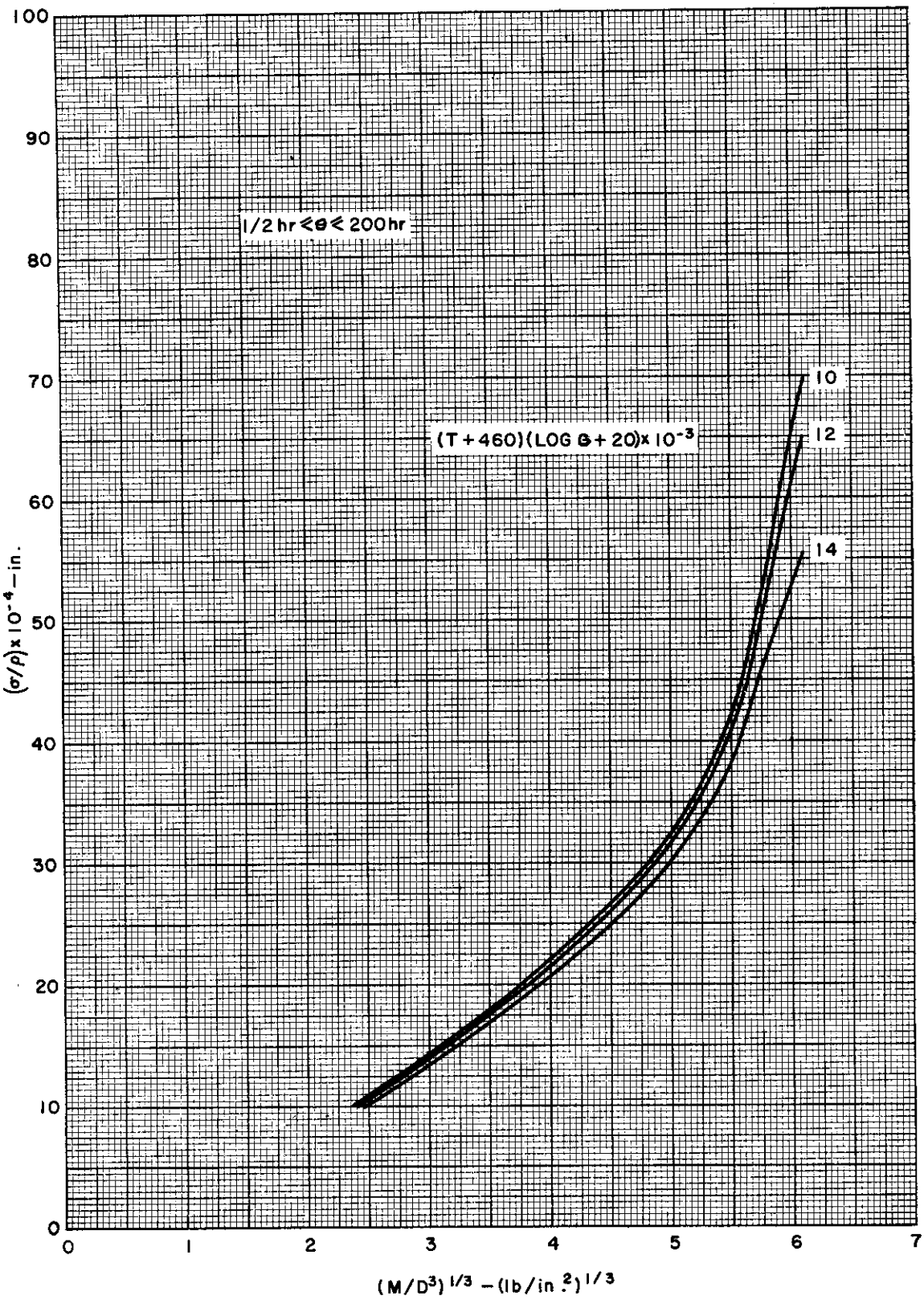

Figure IX-19. Optimum Stress Curves for 7075 Aluminum Unstiffened Cylinders, Long-time Loading

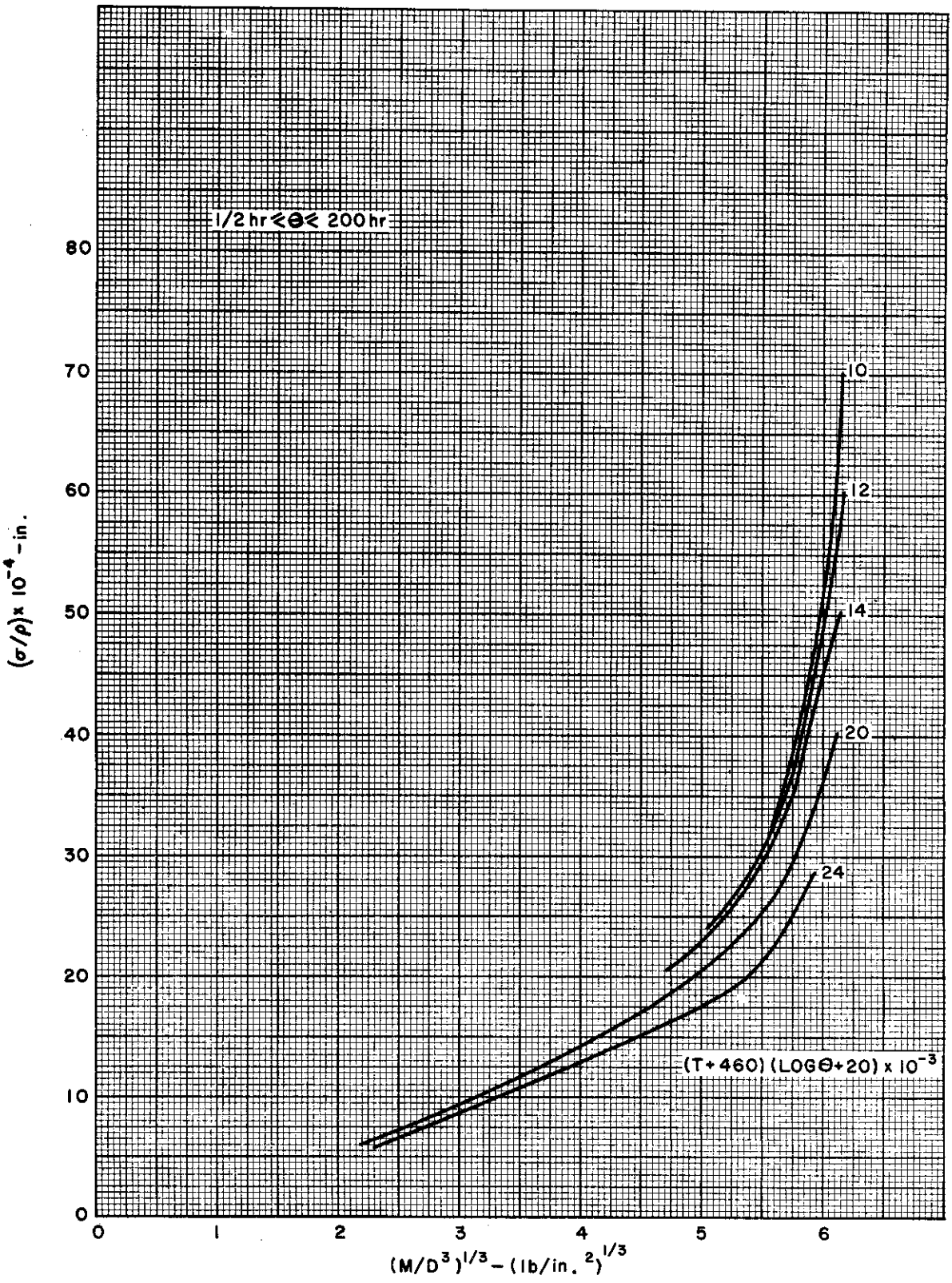

Figure IX-20. Optimum Stress Curves for Titanium Unstiffened Cylinders, Long-time Loading

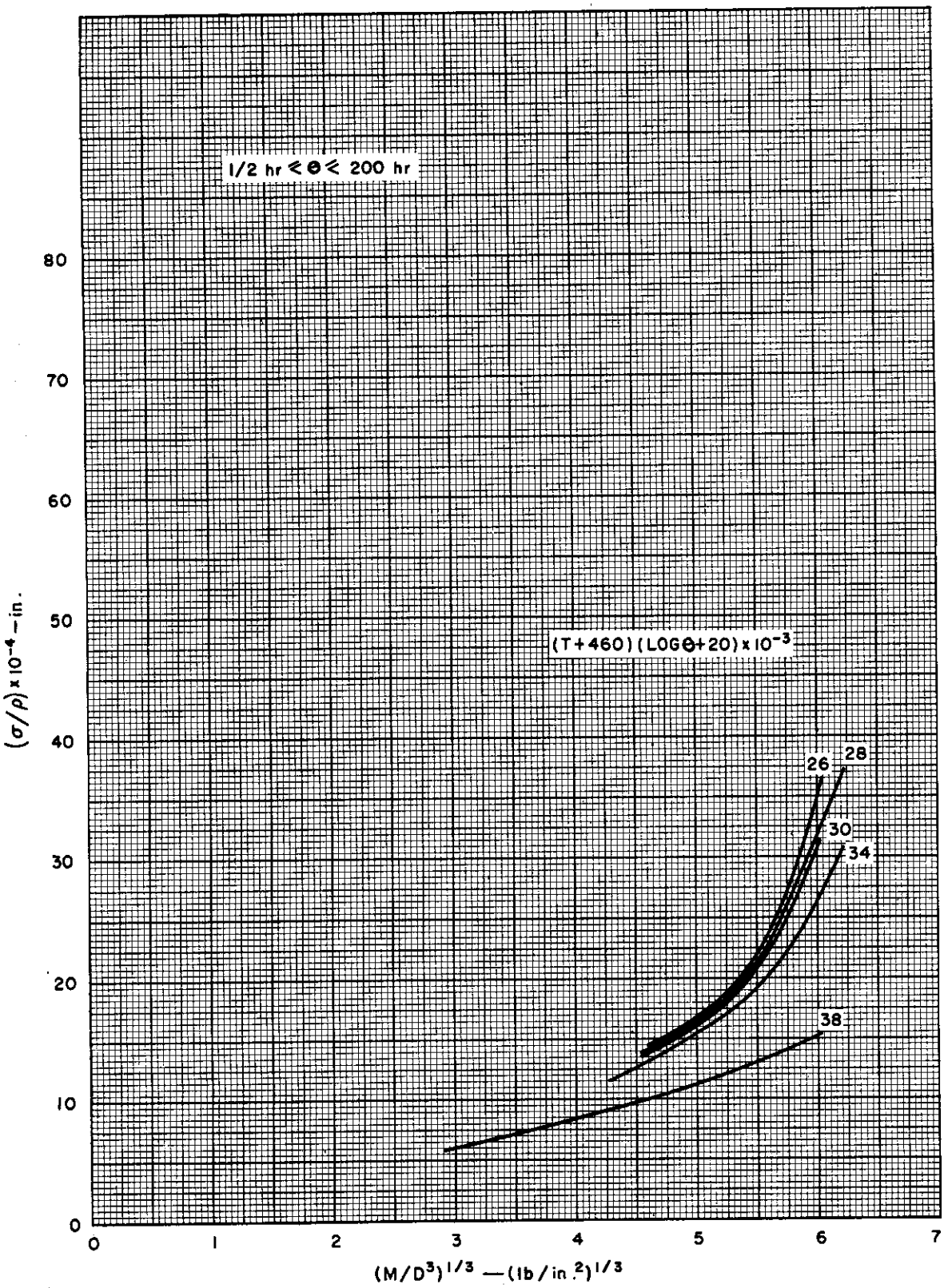

Figure IX-21. Optimum Stress Curves for Inconel X Unstiffened Cylinders, Long-time Loading

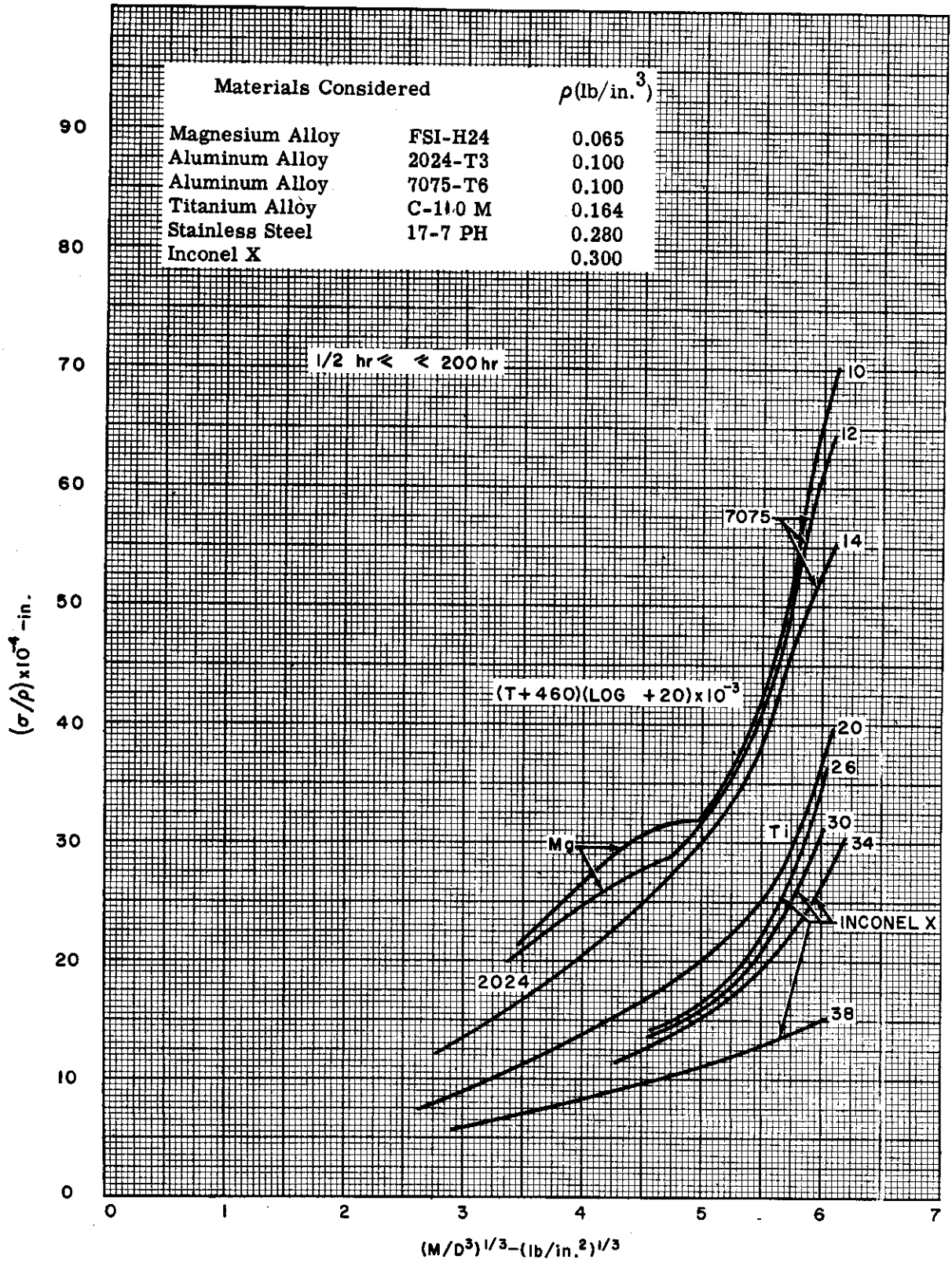

Figure IX-22. Optimum Stress Envelopes for Unstiffened Cylinders, Long-time Loading

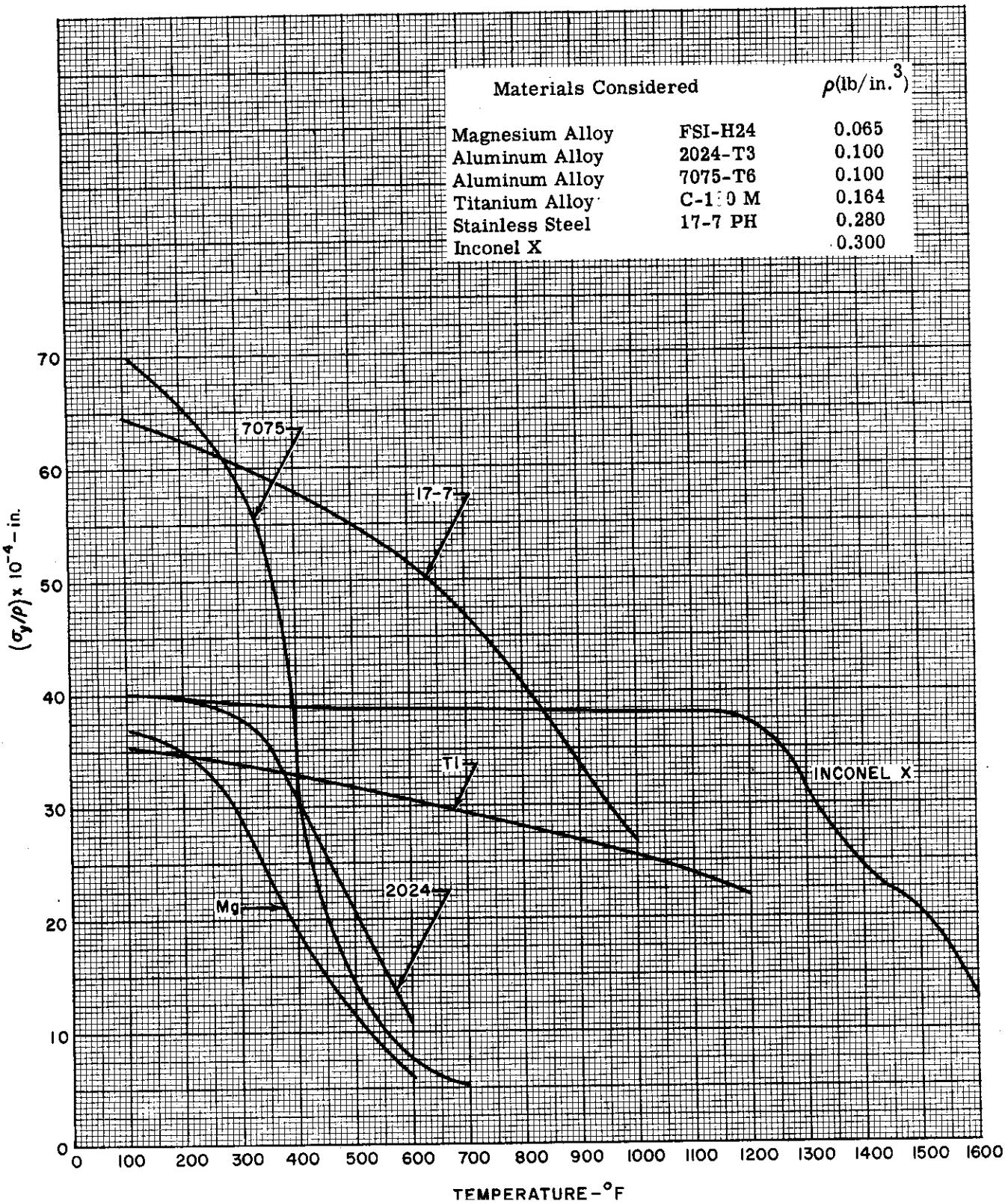

Figure IX-23. Variation of Compressive Yield Stress with Temperature for Various Materials

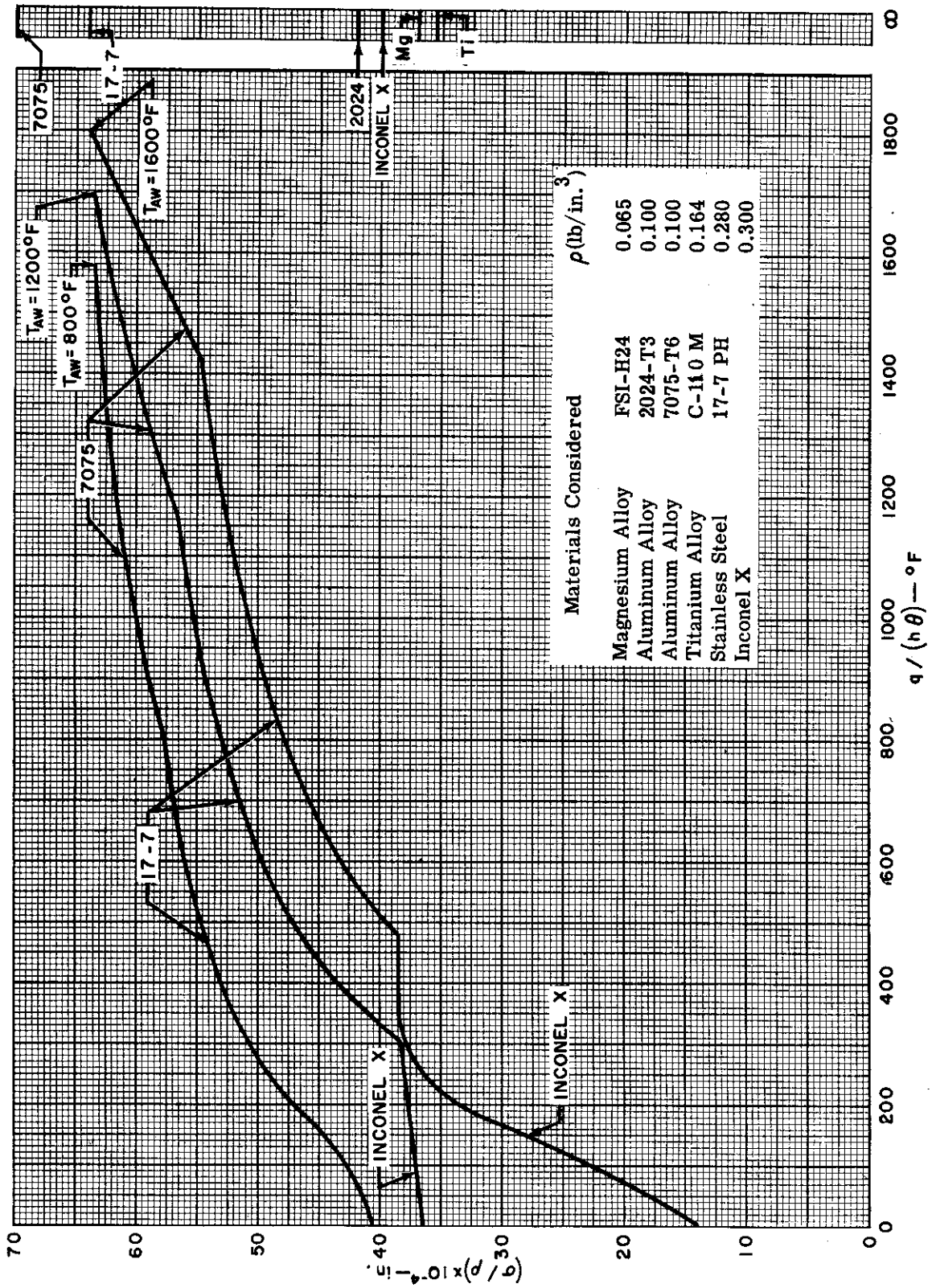

Figure IX-24. Structural Efficiency Under Transient Heating Conditions

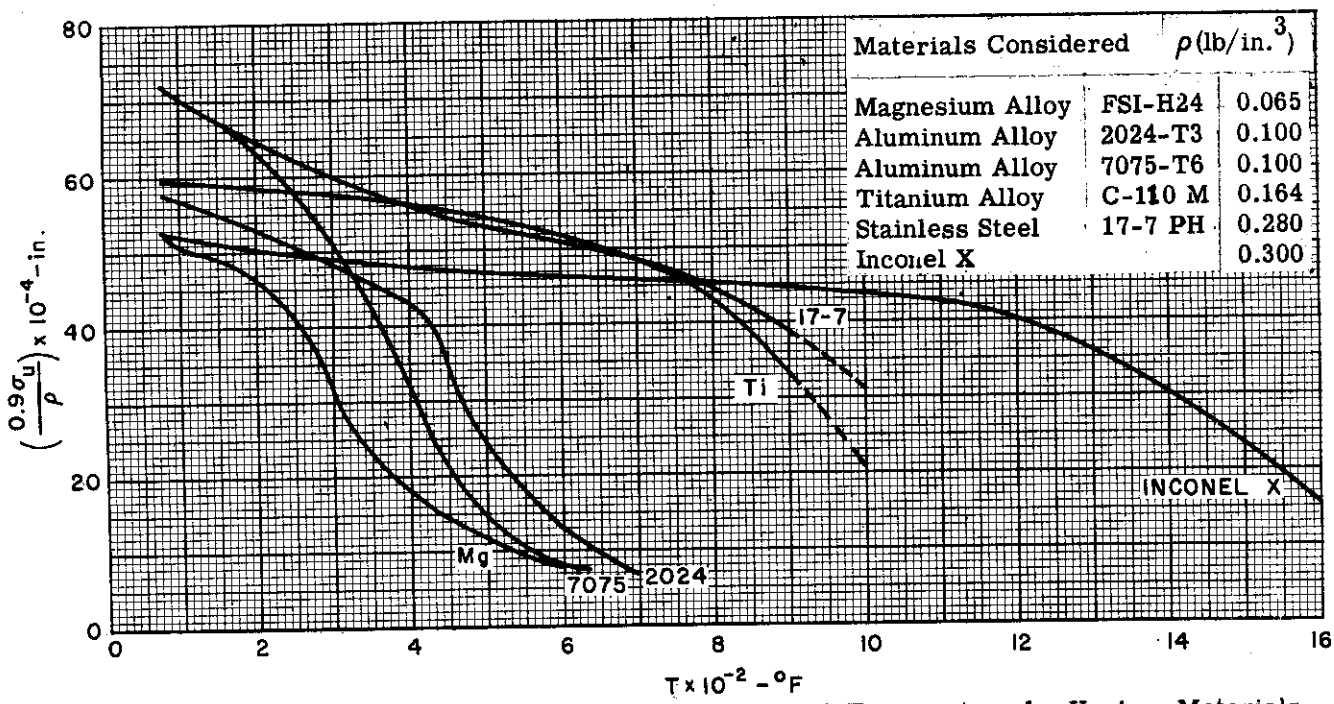

Figure IX-25. Variation of Ultimate Tensile Strength With Temperature for Various Materials

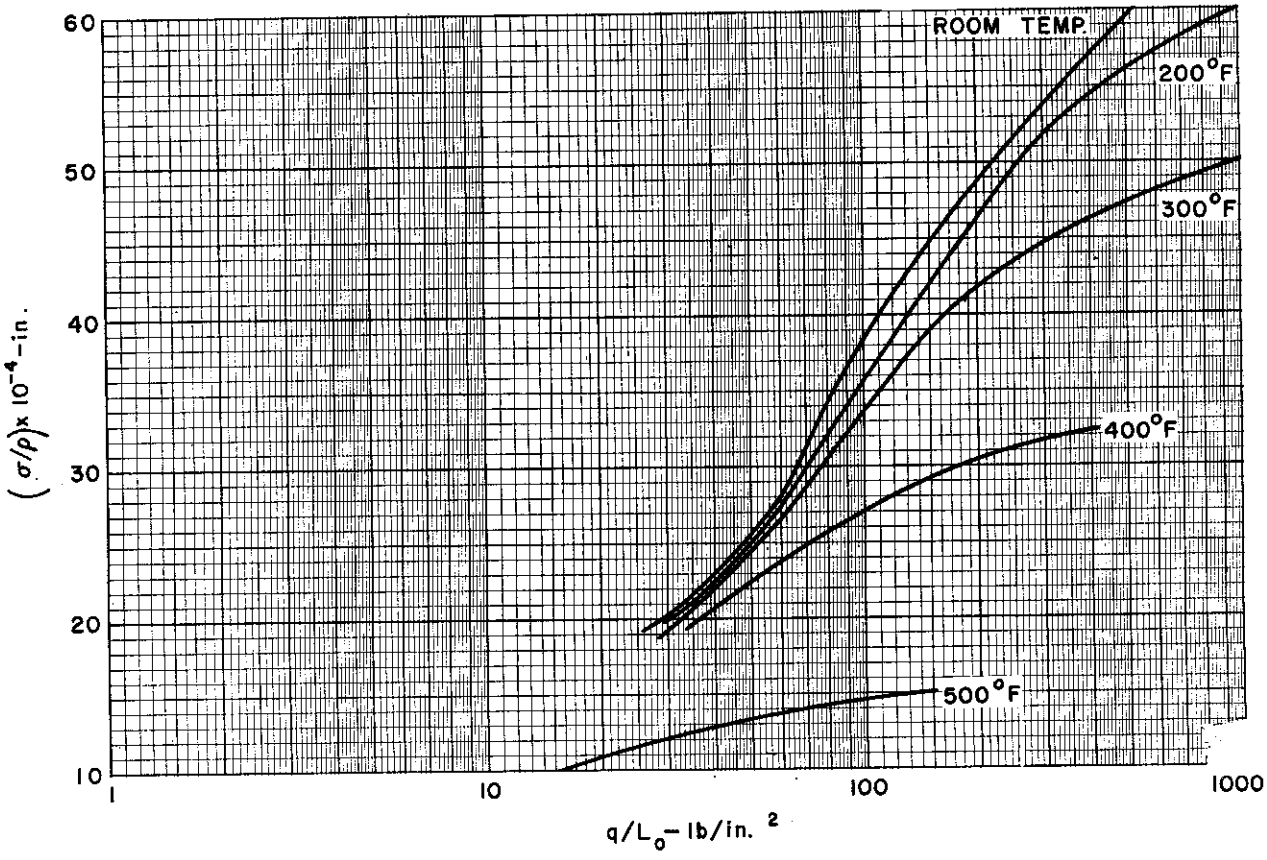

Figure IX-26. Optimum Stress Curves for 7075 Aluminum Wide Columns, Short-time Loading

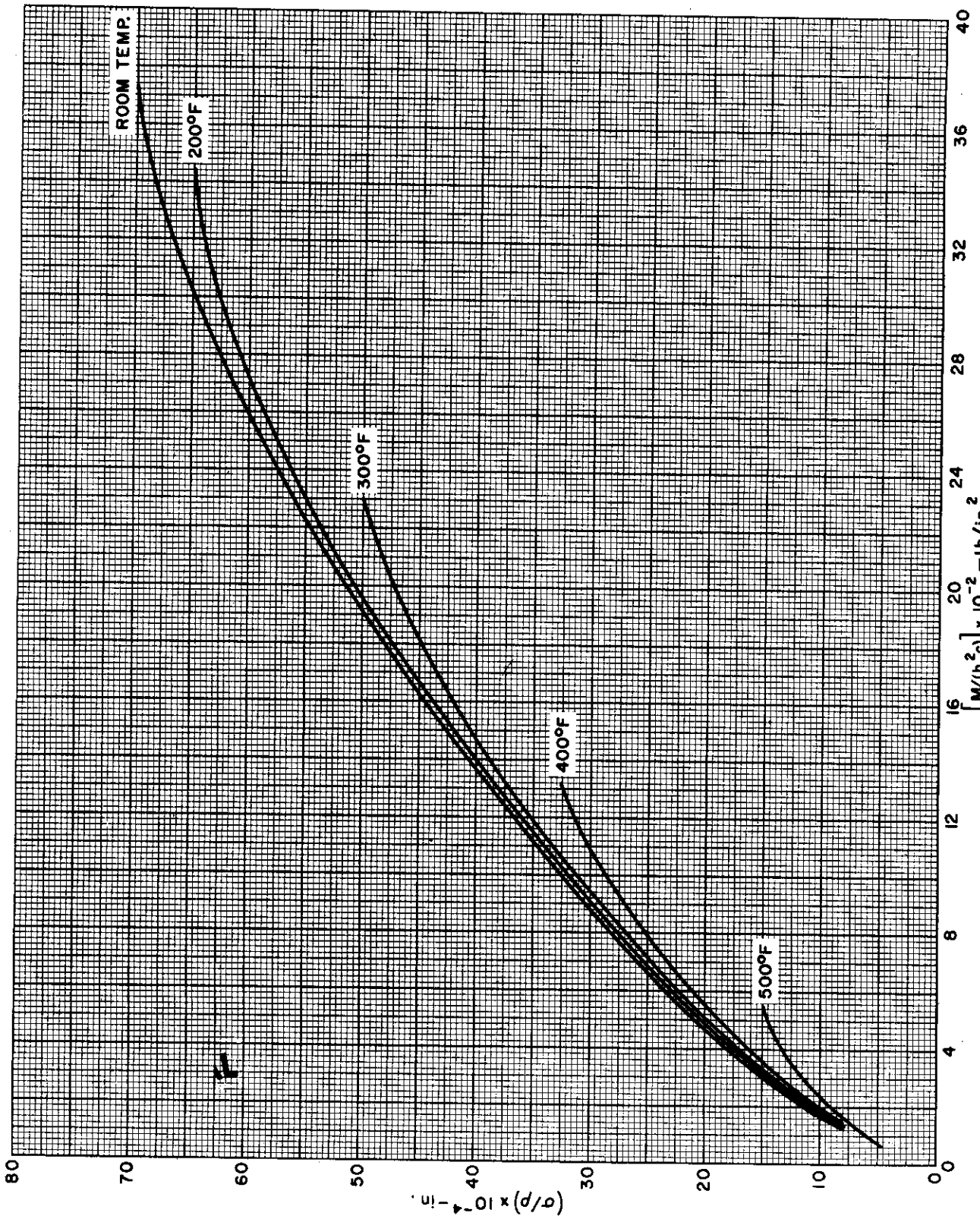

Figure IX-27. Optimum Stress Curves for 7075 Aluminum Multiweb Beams, Short-time Loading

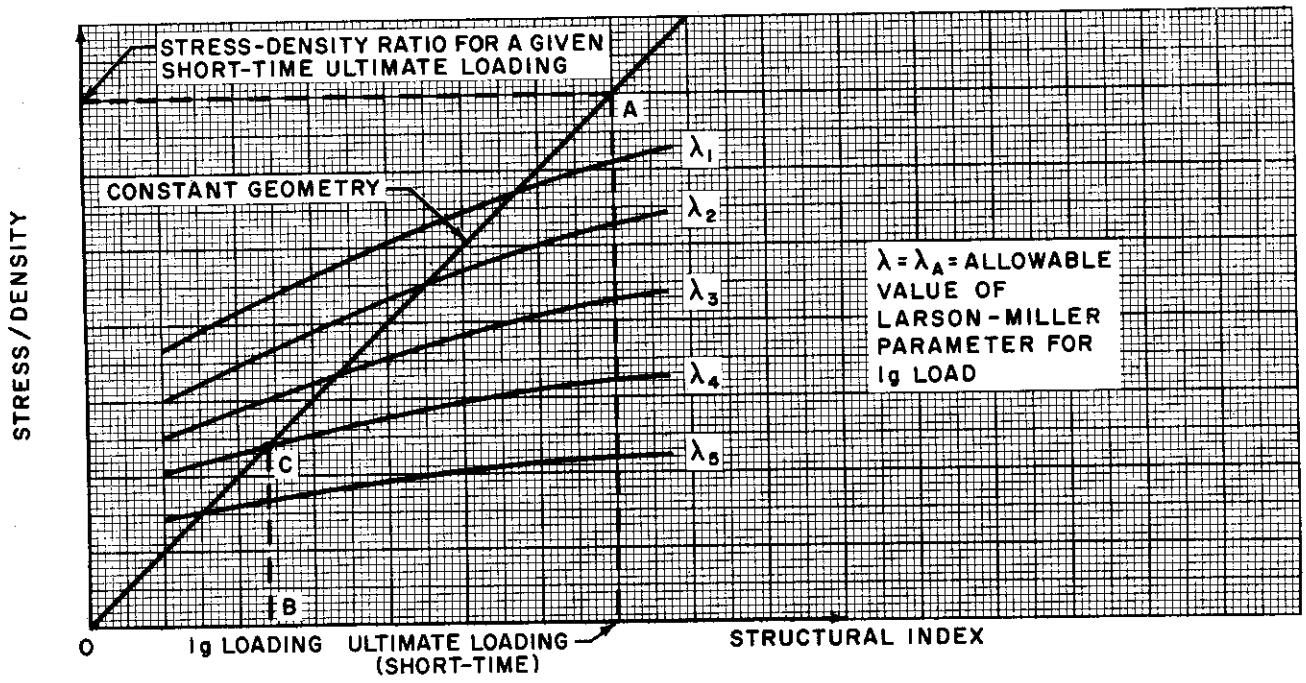

Figure IX-28. Determination of Life for a Given Strength

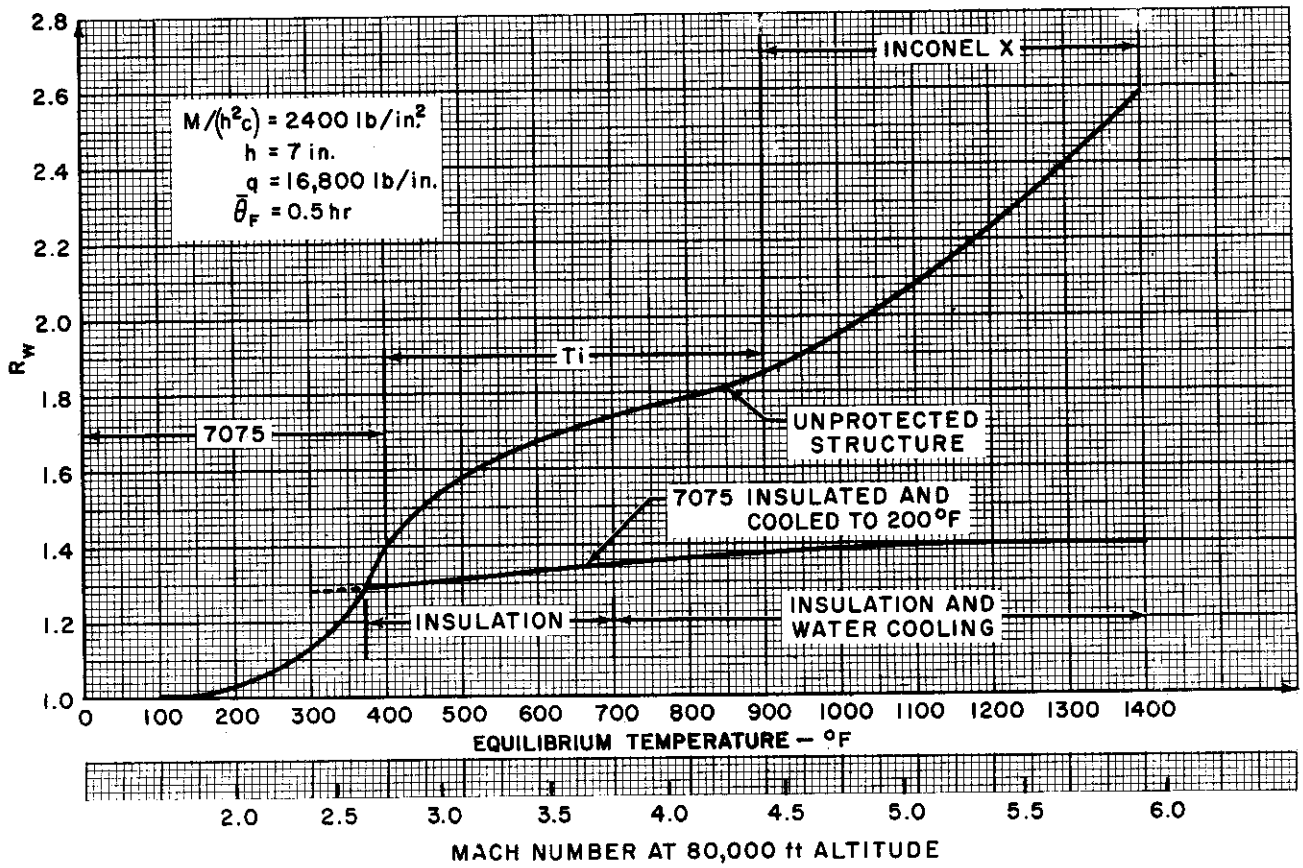

Figure IX-29. Variation of Weight Penalty Due to Aerodynamic Heating With Temperature

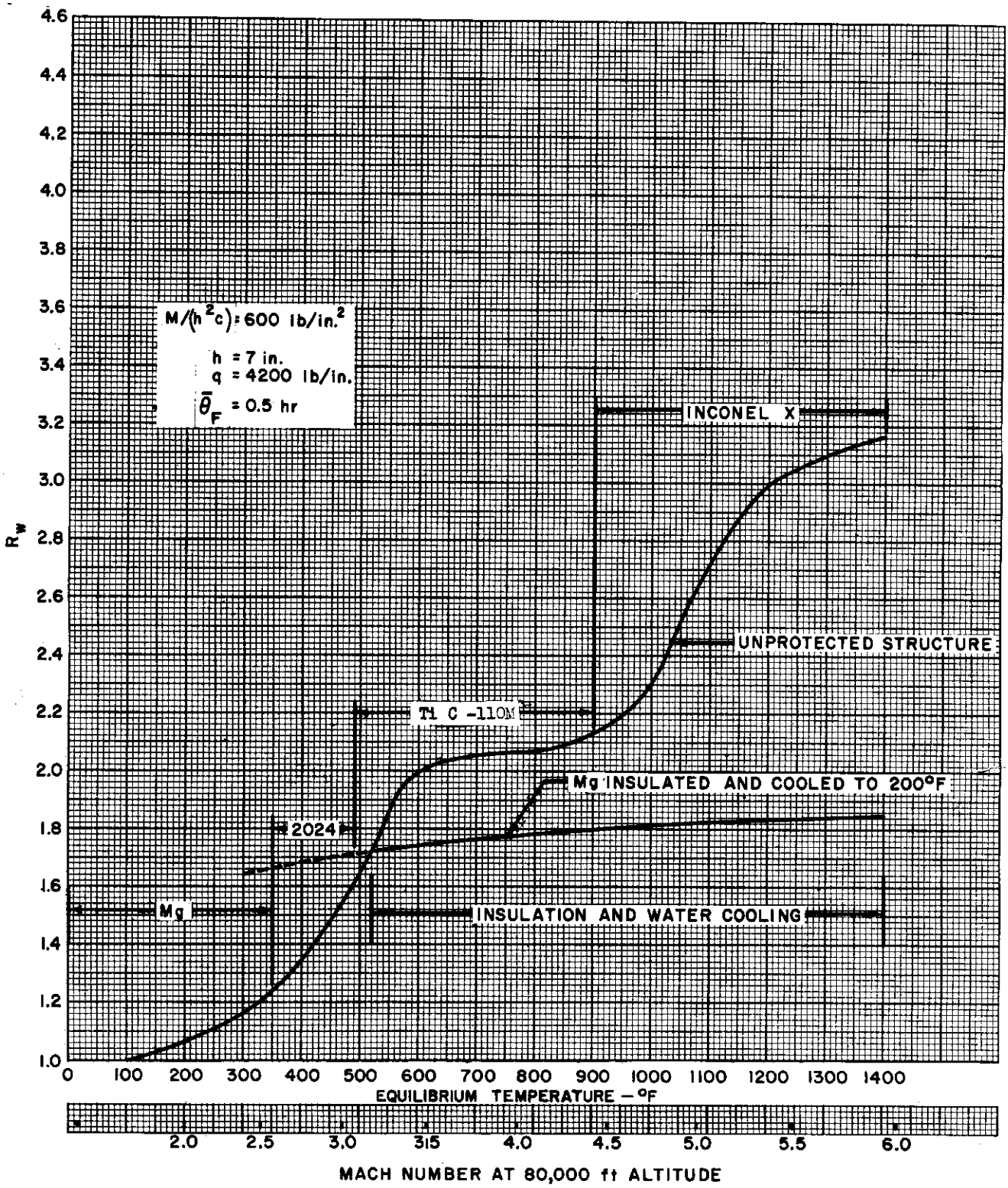

Figure IX-30. Variation of Weight Penalty Due to Aerodynamic Heating With Temperature

NOTES